

**MOLECULAR CLONING, HETEROLOGOUS EXPRESSION, AND
STEADY-STATE KINETICS OF *CAMPYLOBACTER JEJUNI*
PERIPLASMIC NITRATE REDUCTASE**

by

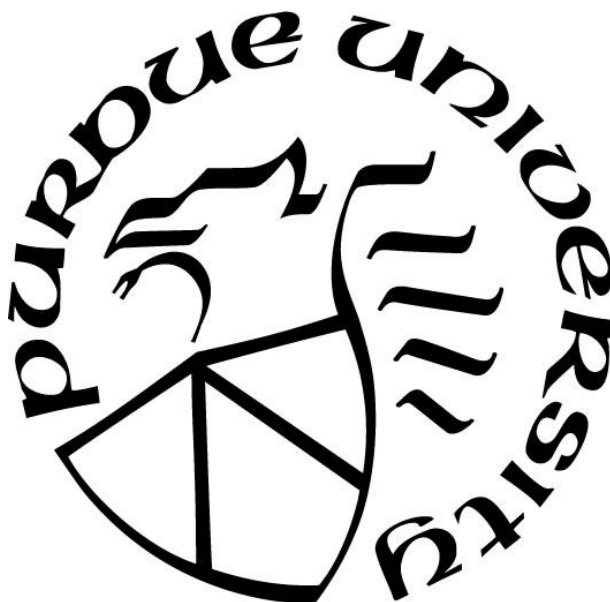
Breeanna Mintmier

A Dissertation

Submitted to the Faculty of Purdue University

In Partial Fulfillment of the Requirements for the degree of

Doctor of Philosophy



Chemistry and Chemical Biology

Indianapolis, Indiana

August 2020

THE PURDUE UNIVERSITY GRADUATE SCHOOL
STATEMENT OF COMMITTEE APPROVAL

Dr. Partha Basu, Chair

Department of Chemistry and Chemical Biology

Dr. Millie Georgiadis

Department of Chemistry and Chemical Biology

Dr. Frédérique Deiss

Department of Chemistry and Chemical Biology

Dr. Robert Minto

Department of Chemistry and Chemical Biology

Approved by:

Dr. Eric Long

Dedicated to my father, my hero.

ACKNOWLEDGMENTS

The work presented in this dissertation would not have been possible without the support of a vast network of individuals. First, I would like to acknowledge my advisor, Dr. Partha Basu. Thank you for giving me the opportunity to work on this project and for your continual support and guidance on both a professional and personal level. I would also like to thank my undergraduate research advisor Dr. John Ford (IUP) and my inorganic chemistry instructor Dr. Charles Lake for sparking my interest in research, helping me grow as a scientist, and encouraging me to pursue graduate school. In addition, I would like to thank my committee members from Duquesne University for their constructive criticism, support, and guidance. I especially want to thank my thesis committee members at IUPUI for assisting in an easy transition from Duquesne University to IUPUI and for their support in the presentation and evaluation of this thesis project.

The members of the Basu Research Group both past and present have provided me with lasting friendships and constant support. Specifically, I would like to thank my predecessor on the Nap project, Dr. Courtney Sparacino-Watkins. Courtney has graciously answered many emails when I first started and even proceeded to give me in person training. Dr. John Thomas was responsible for most of my initial training and was a constant source of support. Thanks for the laughs and great memories, John. I especially want to acknowledge Dr. Sara Dille without whom I would not have survived graduate school. Thank you, Sara, for being my friend and for the constant support during all the defense and personal battles I have faced in the past seven years. Thank you for pushing me to be a better scientist, for helping me grow as a person. Special thanks to Dr. Jennifer McGarry who has helped me as an enzymologist and biochemist. I am so thankful to you Jen for joining our group and helping me to learn better technique especially with the kinetics experiments as well as helping me to increase my knowledge and become a better scientist. Additionally, I want to thank fellow graduate student Kyle Colston for his constant support both in and outside of the lab. I wish you plenty of success in the future on your own projects. Finally, I have mentored several undergraduates and one high school student who have assisted me in one way or another with common laboratory tasks (most often growing cultures) that has my life easier. I am very grateful for their assistance and patience.

Several faculty members from both Duquesne University and IUPUI have welcomed me into their laboratories to use instruments or for trouble shooting experiments in the expression and

purification of the NapA enzyme. As such, I would like to thank Dr. Peter Castric (Duquesne University), Dr. Joseph McCormick (Duquesne University), Dr. John Stolz (Duquesne University), Dr. Mike Cascio (Duquesne University), Dr. Mike (IUPUI), and Dr. Millie Georgiadis (IUPUI). Funding for this project is gratefully acknowledged from the NIH, Duquesne University, and the IUPUI School of Science.

I have had the great opportunity to work with many fantastic collaborators, several of whom have graciously welcomed me into their laboratories to learn new techniques or use their instruments and facilities. I would like to thank Drs Tracey Palmer and Frank Sargent (Newcastle University in the UK) for supplying useful plasmids, gene constructs, and cell strains, Dr. Maissa Gaye (Boston University) for initial mass spectrometric analysis of NapA when we first arrived at IUPUI, Dr. A. Andy Pacheco (University of Wisconsin Milwaukee) for the use of his glovebox for initial NapA kinetics, Dr. Ian Webb (IUPUI) and Dr. Jared Shaw (Formerly DOE) for assistance in intact mass spectrometry, Dr. Oliver Einsle (University of Freiburg) for trouble shooting crystal growth of NapA for future X-ray crystallography experiments, Dr. Daniel Bain (University of Pittsburgh) for assistance in ICP-MS measurements, and finally Drs Martin Kirk and Jing Yang (University of New Mexico) for X-ray spectroscopy measurements.

In addition to faculty, I would like to thank the both the staff and graduate student communities of both Duquesne University and IUPUI for their support and friendship. For instrument maintenance and equipment assistance, I would like to acknowledge Dan Bodner (Duquesne University), Patricia Beddow (Formerly IUPUI), and Anne Shanahan (IUPUI). I would like to thank Kitty O'Doherty, Beverly Hewitt, and Lynn Gerrard for their patience and assistance in many ventures and the abundant bookkeeping measures that they have provided to assist me as a graduate student at IUPUI. I especially want to thank Kitty and Beverly in addition to Jim Crase and Wai Ping Kam for all of their help in making the move from Duquesne University to IUPUI as smooth as possible. Many graduate students have assisted me in my graduate journey with advice both scientific and personal as well as helping me practice for defenses and presentations. I want to specially thank Dr. Joseph Sallmen for assisting me in trouble shooting the cloning of the nap genes, Dr. Tara Kennedy for her assistance in electroporation, Dr. Kim Rosmus for her fantastic advice and assistance in preparing for defenses, Dr. Meghan McCleod for advice, friendship, and assistance with adjusting to life at IUPUI, and finally to Dr. Alex Latta for great advice, many

enlightening conversations, and assistance with the research experimentation and formal presentation of research (both oral and written).

Finally, I would like to acknowledge my family. I want to thank my family for their constant support throughout my time in graduate school. I am so grateful for your love and understanding while I devoted most of my time and attention to attaining this degree. Specifically, I want to thank my dad for his sacrifice both home and abroad. I have been blessed to receive a completely free undergraduate education thanks to the GI Bill and your gracious sacrifice. I am who I am today because of you. Thank you so much for giving me the opportunity to pursue my dreams. I would like to thank my sisters for their constant support. Thank you, Alli, for being the one I could lean on in my dark times. Thank you, Laura, for providing me with my first experiences teaching which have significantly helped me maintain my patience with struggling students and helped me identify flaws in my own methods.

TABLE OF CONTENTS

LIST OF TABLES	12
LIST OF FIGURES	14
LIST OF ABBREVIATIONS	23
ABSTRACT.....	26
CHAPTER 1. INTRODUCTION	27
1.1 Molybdenum Enzymes	27
1.2 Moco Biosynthesis.....	29
1.3 Significance of Molybdenum Enzymes	31
1.4 The Challenge: Obtaining Active Soluble Recombinant Molybdenum Enzymes.....	32
1.4.1 Production of Soluble Molybdenum Enzymes	32
1.4.2 Active versus Inactive Molybdenum Enzymes	33
1.4.2.1 Effective Methods for Moco Synthesis and Incorporation.....	34
1.4.2.1a Homologous versus Heterologous Expression Systems	34
1.4.2.1b Optimization of Expression Conditions.....	37
1.4.2.1c Boosting Moco Biosynthesis.....	39
1.4.2.1d Moco Reconstitution.....	40
1.4.2.2 Metal Loading.....	41
1.4.2.3 Modification of the Molybdenum center.....	42
1.4.2.4 Incorporation of Additional Prosthetic Groups	44
1.4.2.4a Iron-Sulfur Cluster Containing Molybdopterin Enzymes.....	46
1.4.2.4b Heme Containing Molybdopterin Enzymes.....	48
1.4.2.4c Flavin-Containing Molybdopterin Enzymes.....	49
1.4.2.5 Redox Enzyme Maturation Proteins (REMP)	51
1.4.3 Transport of Molybdenum Enzymes	52
1.5 The Chosen Molybdenum Enzyme for Study.....	56
1.6 Objectives and Project Outline	57
CHAPTER 2. MOLECULAR CLONING, EXPRESSION, AND PURIFICATION OF PERIPLASMIC NITRATE REDUCTASE.....	122
2.1 Introduction.....	122

2.2	Materials and Methods.....	131
2.2.1	Molecular Cloning of the <i>C. jejuni nap</i> Genes	132
2.2.2	Bacterial Strains and Growth Conditions	133
2.2.3	Expression Optimization Experiments	134
2.2.3.1	IPTG Optimization	134
2.2.3.2	Glucose Optimization	135
2.2.3.3	Optimization of Induction Temperature	135
2.2.3.4	Optimization of Induction Time	135
2.2.3.5	Optimized IPTG Method	136
2.2.3.6	Auto-induction Method	136
2.2.4	Anaerobic versus Aerobic Expression Comparison	136
2.2.5	Purification Optimization Experiments	137
2.2.5.1	IMAC Spin Columns	137
2.2.5.2	Addition of Protease inhibitors:.....	137
2.2.5.3	Periplasmic Isolation	138
2.2.5.4	Affinity Chromatography	139
2.2.5.5	Size Exclusion Chromatography	139
2.2.5.6	Final Optimized Protocol for Purification of Recombinant <i>C. jejuni</i> NapA	140
2.2.6	SDS-PAGE	140
2.2.7	Activity Assays	141
2.2.8	Mass Spectrometry	141
2.2.8.1	Digested Peptide Analysis	141
2.2.8.2	Intact Protein Analysis by Ion Mobility Mass Spectrometry	142
2.2.8.3	Metal Analysis by Inductively Coupled Plasma Mass Spectrometry (ICP-MS)	143
2.3	Results.....	143
2.3.1	Optimizing NapA Expression.....	144
2.3.2	Anaerobic Expression of NapA	149
2.3.3	Optimizing NapA Purification.....	150
2.3.3.1	Periplasmic Isolation	151
2.3.3.2	Addition of Protease Inhibitors.....	152
2.3.3.3	Affinity Chromatography	153

2.3.3.4	Size Exclusion Chromatography	154
2.3.3.5	Optimized NapA Purification	157
2.3.3.6	Molecular Size Determination of NapA	157
2.4	Discussion	159
2.5	Summary	164
CHAPTER 3. ACTIVITY AND CHARACTERIZATION OF RECOMBINANT PERIPLASMIC NITRATE REDUCTASE		165
3.1	Introduction	165
3.2	Materials and Methods for Biochemical Characterization of NapA	168
3.2.1	UV-Vis Spectroscopy	168
3.2.2	Protein Concentration Determination	168
3.2.3	Mass Spectrometry	168
3.2.4	Metal Analysis	168
3.2.5	Enzyme Kinetics	169
3.2.6	Homology Model	169
3.3	Results	170
3.3.1	NapA Characterization	170
3.3.2	Nitrate Reductase Activity of NapA	171
3.3.3	The pH Effect on <i>C. jejuni</i> NapA Activity	172
3.4	Discussion	174
3.5	Summary	179
CHAPTER 4. THE MOLYBDENUM CENTER AND ACTIVE SITE OF PERIPLASMIC NITRATE REDUCTASE		180
4.1	Introduction	180
4.2	Materials and Methods	184
4.2.1	Protein Concentration Determination	184
4.2.2	SDS-PAGE	184
4.2.3	Metal Analysis	184
4.2.4	Enzyme Kinetics	184
4.2.5	Tobacco Etch Virus (TEV) Protease Cleavage	185
4.2.6	X-ray Absorption Spectroscopy (XAS)	185

4.3	Results.....	186
4.3.1	The Influence of NaCl and Sulfate on <i>C. jejuni</i> NapA Activity.....	186
4.3.2	Impact of the His-tag on Metal Loading and Nitrate Reductase Activity	189
4.3.3	XAS of Recombinant <i>C. jejuni</i> NapA	190
4.4	Discussion.....	196
4.5	Summary.....	202
CHAPTER 5. ROLE OF THE MOLYBDENUM-COORDINATING RESIDUE IN PERIPLASMIC NITRATE REDUCTASE.....		204
5.1	Introduction.....	204
5.2	Materials and Methods.....	206
5.2.1	Protein Concentration Determination	206
5.2.2	SDS-PAGE	206
5.2.3	Metal Analysis	206
5.2.4	UV-Vis Spectroscopy	206
5.2.5	Site-Directed Mutagenesis.....	211
5.2.6	Production and Purification of Recombinant Proteins	211
5.2.7	Steady-State Kinetics.....	212
5.3	Results.....	212
5.3.1	Variants of NapA and their Characterization	212
5.3.2	Steady-State Kinetics of NapA Variants using Nitrate as a Substrate.....	215
5.3.3	TMAO and DMSO Reductase Activity.....	215
5.3.4	Nitrate Activity Dependence on pH	217
5.4	Discussion.....	219
5.4.1	Nitrate Reduction by the C176 Nap Variants	219
5.4.2	Alternative Substrates of the C176 Nap Variants.....	221
5.4.3	Implications of Mo Ligand Exchange in Energetics	224
5.4.4	The Impact of pH on Nitrate Reduction Catalyzed by the C176 NapA Variants....	230
5.5	Summary.....	235
CHAPTER 6. CONCLUSIONS.....		237
6.1	Overview and Conclusions	237
6.2	Significance.....	243

6.3 Future Work	244
APPENDIX A. BUFFERS	248
APPENDIX B. MOLECULAR CLONING RECIPES AND METHODS	251
APPENDIX C. ADDITIONAL PROTOCOLS	259
APPENDIX D. SEQUENCING AND MASS SPECTROMETRIC CONFIRMATION OF PERIPLASMIC NITRATE REDUCTASE PROTEINS	262
APPENDIX E. PERIPLASMIC NITRATE REDUCTASE ACTIVITY AS A FUNCTION OF TIME	282
APPENDIX F. PRELIMINARY INVESTIGATION OF ARSENITE ACTIVITY	283
APPENDIX G. MUTATION OF A CRITICAL LYSINE RESIDUE IN THE ELECTRON TRANSFER PATHWAY OF PERIPLASIMC NITRATE REDUCTASE	285
REFERENCES	292

LIST OF TABLES

Table 1.1: Expression parameters for recombinant eukaryotic XO family enzymes.	60
Table 1.2: Expression parameters for recombinant eukaryotic SO family enzymes.	62
Table 1.3: Expression parameters for recombinant prokaryotic XO family enzymes.	64
Table 1.4: Expression parameters for recombinant prokaryotic SO family enzymes.	66
Table 1.5: Expression parameters for recombinant prokaryotic DMSOR family enzymes.	67
Table 1.6: Purification parameters for recombinant eukaryotic XO family enzymes.	73
Table 1.7: Purification parameters for recombinant eukaryotic SO family enzymes.	75
Table 1.8: Purification parameters for recombinant prokaryotic XO family enzymes.	77
Table 1.9: Purification parameters for recombinant prokaryotic SO family enzymes.	79
Table 1.10: Purification parameters for recombinant prokaryotic DMSOR family enzymes.	80
Table 1.11: Kinetic parameters for eukaryotic XO family of enzymes.	85
Table 1.12: Kinetic parameters for eukaryotic SO family of enzymes.	93
Table 1.13: Kinetic parameters for prokaryotic XO family of enzymes.	105
Table 1.14: Kinetic parameters for prokaryotic SO family of enzymes.	110
Table 1.15: Kinetic parameters for DMSOR family of enzymes.	111
Table 1.16: Known REMP chaperones for molybdopterin enzymes.	120
Table 2.1: Summary of plasmids and oligonucleotides used in the cloning of <i>C. jejuni napALD</i>	133
Table 3.1: Kinetic parameters reported for NapA (A) or NapAB (AB) in various organisms using the methyl/benzyl viologen solution assay.	173
Table 3.2: Kinetic parameters reported for recombinant <i>C. jejuni</i> NapA at various pH.	176
Table 4.1: Kinetic parameters reported for recombinant <i>C. jejuni</i> NapA in the prescence of various NaCl concentrations.	187
Table 4.2: EXAFS fits for as-isolated <i>C. jejuni</i> NapA (35.5 mg/mL) XAS data. The data were fit in k space in a k range of 2.4-12 with R range of 1.15-3. E ₀ =20016 eV. Mo-S phase correction applied. Fits 8-9 are the best fits analyzed and are depicted in Figure 4.11.	191
Table 4.3: EXAFS fits for as-isolated <i>C. jejuni</i> NapA treated with 450 mM NaCl XAS data. The data were fit in k space in a k range of 2.4-12 with R range of 1.15-3. E ₀ =20016 eV. Mo-S phase correction applied. Fits 5-6 are the best fits analyzed and are depicted in Figure 4.13.	195

Table 5.1: Reported variations of the molybdenum-coordinating residue in various mononuclear molybdenum enzymes.	207
Table 5.2: Summary of plasmids and oligonucleotides used in this study.	211
Table 5.3: Metal analysis of <i>C. jejuni</i> NapA variants.....	213
Table 5.4: Kinetic parameters of <i>C. jejuni</i> NapA and C176S/D/A variants compared to similar DMSOR family enzymes.....	214
Table 5.5: Kinetic parameters for NapA variants at various pH conditions.....	218
Table 5.6: Calculated $\Delta\Delta G_b$ and $\Delta\Delta G_b^\ddagger$ values comparing the effects of mutation and substrate for the enzyme-substrate complex and the enzyme-bound transition state, respectively.....	228

LIST OF FIGURES

Figure 1.1: A) The general structure of the molybdenum cofactor (Moco). B) First coordination spheres of the Mo center in the three mononuclear molybdenum enzyme families: xanthine oxidase (XO) family, sulfite oxidase (SO) family, and dimethyl sulfoxide reductase (DMSOR) family. 28

Figure 1.2: The bacterial biosynthetic pathway of Moco. Enzymes are colored in blue; co-substrates are colored in green. End products for various families are denoted by the box arrow. 30

Figure 1.3: Common prosthetic groups in molybdopterin enzymes. A) iron sulfur clusters: [2Fe2S] on the left, [3Fe4S] in the center, and [4Fe4S] on the right; B) heme groups: heme B on the left and heme C on the right; C) flavin groups: FMN on the left and FAD on the right. 45

Figure 1.4: The proposed roles of the REMP chaperone in molybdenum enzyme maturation. A) Degradation prevention: REMP binds target enzyme preventing proteolysis. B) Enzyme maturation: Stabilizing enzyme target enabling proper protein folding (top pathway) and/or assisting in cofactor insertion (bottom pathway). C) Moco sulfuration: Interaction with a sulfurase enables the REMP to transfer sulfur to moco before insertion into the target protein (top pathway) or the REMP itself has both a sulfurase domain and a Moco binding domain and generates the sulfur that is transferred to moco (bottom pathway). D) Enzyme translocation and complex assembly: The REMP is involved in targeting the delivery of the enzyme to form a complex and may assist in assembly of the complex (left) or the REMP targets the TAT machinery for protein translocation into the periplasm (right). Green oval is the target molybdenum enzyme, N = N-terminus, C = C-terminus, purple dot represents Moco, orange circle labelled S represents sulfur, orange diamond represents an iron sulfur cluster, and RR represents the TAT leader sequence. 50

Figure 1.5: A general scheme of the SecT pathway where unfolded peptides are transported across the membrane to be folded in the periplasm. N = N-terminus, C = C-terminus, and green diamond is the properly folded target protein. 53

Figure 1.6: A general scheme of the TAT pathway where peptides are folded in the cytoplasm and cofactors are inserted before the mature folded enzyme is transported across the membrane into the periplasm. Green oval is the target molybdenum enzyme, N = N-terminus, C = C-terminus, purple dot represents Moco, orange diamond represents an iron sulfur cluster, and RR represents the TAT leader sequence. 54

Figure 1.7: The currently proposed first Mo coordination sphere in *Cupriavidus necator* Nap. Left panel, the crystal structure of *C. necator* NapAB (PDB 3ML1); right panel, the line drawing schematic of the first Mo coordination sphere in *Cupriavidus necator* NapA. 57

Figure 1.8: The proposed coordination environment of *C. jeuni* NapA (at the top) with the native coordinating Cys (red) where X is unassigned and may be a sulfido or an oxo group. Below the arrows are the three proposed variants that will be created by site directed mutagenesis: the Ser variant (blue), the Asp variant (green) and the Ala variant (magenta). 58

Figure 2.1: Diagram of the biological nitrogen cycle. Reactions are color coded by process.... 122

Figure 2.2: Nitrate reductase classification flow chart. Nitrate reductases are divided into four general categories: eukaryotic nitrate reductases (Euk-NR), periplasmic nitrate reductases (Nap), respiratory nitrate reductases (Nar), and assimilatory nitrate reductases (Nas)..... 124

Figure 2.3: The operon structures of *nap* A) between Proteobacterial classes and B) within Epsilonproteobacteria. From the top down in A) *S. barnesii* (ϵ), *D. desulfuricans* (δ), *E. coli* (γ), *C. necator* (β), and *R. sphaeroides* (α). From the top down in B) *S. barnesii* SES-3, *H. felis* ATCC 49179, *N. salsuginis* DSM 16511, *A. butzleri* JV22, *H. cetorum* MIT 007128, *C. jejuni* 51494, *Sulfurimonas* sp. AST-10, *H. heilmannii* ASB 1.4. Genes are labelled by subunit letter and color coded by subunit. X is a hypothetical protein that is not a confirmed component of the *nap* operon. The dashed lines between genes represents the various amounts of DNA that separates the *nap* genes in that genome..... 125

Figure 2.4: Amino acid sequence alignment of NapA from *Desulfovibrio desulfuricans* (Dd), *Campylobacter jejuni* (Cj), *E. coli* (Ec), *Rhodobacter sphaeroides* (Rs), and *Cuprividicus necator* (Cn). The highly conserved residues are highlighted in grey and important residues are in color. The cysteines coordinating the [4Fe4S] cluster are green and the Mo-coordinating cysteine is highlighted in yellow. Two residues proposed to be critical for the NapAB interface by reference [308] are highlighted in red..... 129

Figure 2.5: Plasmid map of pBM10C. Construct pBM10C contains the *C. jejuni napLD* genes inserted between the NcoI and EcoRI endonuclease sites and the *C. jejuni* His-tagged *napA* gene inserted between the NdeI and XhoI endonuclease sites of the pRSF-Duet-1 expression vector. 132

Figure 2.6: SDS-PAGE gel of enriched NapA (~108 kDa) samples where NapA was expressed under various IPTG concentrations. Lane 1-NapA expressed in the prescence of 0 mM IPTG, Lane 2- NapA expressed in the prescence of 1 mM IPTG, Lane 3- PageRuler Plus prestained protein ladder (kDa), Lane 4- NapA expressed in the prescence of 10 mM IPTG, Lane 5- NapA expressed in the prescence of 100 mM IPTG. The ~ 108-kDa NapA bands are denoted by the red arrow and the ~12 kDa NapD bands are denoted by the blue arrow. 144

Figure 2.7: SDS-PAGE gel of enriched NapA (~108 kDa) samples where NapA was expressed under various conditions testing for leaky expression. Lane 1-Empty *E. coli* K12 strain expressed as a negative control, Lane 2- NapA expressed in the prescence of 0 mM IPTG and 0% (w/v) glucose, Lane 3- NapA expressed in the prescence of 1 mM IPTG and 0% (w/v) glucose, Lane 4- NapA expressed in the prescence of 0 mM IPTG and 1% (w/v) glucose, Lane 5- NapA expressed in the prescence of 1 mM IPTG and 1% (w/v) glucose, Lane 6- PageRuler Plus prestained protein ladder (kDa). The ~ 108-kDa NapA bands are denoted by the red arrowhead and the ~12 kDa NapD bands are denoted by the blue arrow. 145

Figure 2.8: SDS-PAGE gel of enriched NapA (~108 kDa) samples where NapA was expressed under various glucose concentrations. Lane 1-NapA expressed in the prescence of 0.5% (w/v) glucose, Lane 2- NapA expressed in the prescence of 1% (w/v) glucose, Lane 3- PageRuler Plus prestained rotein ladder (kDa), Lane 4- NapA expressed in the prescence of 2% (w/v) glucose, Lane 5- NapA expressed in the prescence of 4% (w/v) glucose. The ~ 108-kDa NapA bands are denoted by the red arrow and the ~12 kDa NapD bands are denoted by the blue arrow..... 146

Figure 2.9: Left panel: SDS-PAGE gel of enriched NapA (~108 kDa) samples where NapA was expressed under various IPTG concentrations in the prescence of 0.5% (w/v) glucose. Lane 1- NapA expressed in the prescence of 0.1 mM IPTG, Lane 2- PageRuler Plus prestained protein ladder (kDa), Lane 3- NapA expressed in the prescence of 1 mM IPTG, Lane 4- NapA expressed in the prescence of 10 mM IPTG, Lane 5- NapA expressed in the prescence of 100 mM IPTG. The ~ 108-kDa NapA bands are denoted by the red arrow and the ~12 kDa NapD bands are denoted by the blue arrow. Right panel: NapA expression plotted as a function of the logarithmic IPTG concentration. NapA expression decreases with increasing IPTG concentration..... 146

Figure 2.10: SDS-PAGE gel of enriched NapA (~108 kDa) samples where NapA was expressed at various temperatures. Lane 1- PageRuler Plus prestained protein ladder (kDa), Lane 2- NapA expressed at 16°C, Lane 3- NapA expressed at room temperature (~24°C), Lane 4- NapA expressed at 37°C, Lane 5- NapA expressed at 42°C. The ~ 108-kDa NapA bands are denoted by the red arrow and the ~12 kDa NapD bands are denoted by the blue arrow. 148

Figure 2.11: SDS-PAGE gel of enriched NapA (~108 kDa) samples where NapA was expressed at various induction times. Lane 1- NapA expressed for 2 h, Lane 2- NapA expressed for 4 h, Lane 3- NapA expressed for 6 h, Lane 4- PageRuler Plus prestained protein ladder (kDa) Lane 5- NapA expressed for 8 h, Lane 6- NapA expressed for 12 h, Lane 7- NapA expressed for 16 h, Lane 8- NapA expressed for 20 h, Lane 9- NapA expressed for 24 h. The ~ 108-kDa NapA bands are denoted by the red arrow and the ~12 kDa NapD bands are denoted by the blue arrow..... 148

Figure 2.12: Traditional induction versus auto-induction. Lane 1- PageRuler Plus prestained protein ladder (kDa), Lane 2- NapA expressed by the optimized traditional induction method, Lane 3- NapA expressed by auto-induction. The ~ 108-kDa NapA bands are denoted by the red arrow and the ~12 kDa NapD bands are denoted by the blue arrow..... 149

Figure 2.13: SDS-PAGE of anaerobically expressed NapA versus aerobically expressed NapA. Lane 1- NapA aerobically expressed for 24 h with agitation, Lane 2- NapA aerobically expressed for 48 h with agitaiton, Lane 3- NapA anaerobically expressed for 24 h without agitation, Lane 4- NapA anaerobically expressed for 48 h without agitation, Lane 5- NapA anaerobically expressed for 24 h with agitation, Lane 6- NapA anaerobically expressed for 48 h with agitation, Lane 7- PageRuler Plus prestained protein ladder (kDa). The ~ 108-kDa NapA bands are denoted by the red arrow and the ~12 kDa NapD bands are denoted by the blue arrow. 150

Figure 2.14: SDS-PAGE of periplasmic isolated NapA with various methods. Lane 1- NapA from sonicated control containing both cytoplasmic and periplasmic proteins, Lane 2- NapA isolated from method #1, Lane 3- NapA isolated from method #2, Lane 4- NapA isolated from method #3, Lane 5- PageRuler Plus prestained protein ladder (kDa), Lane 6- NapA isolated from method #4. The ~ 108-kDa NapA bands are denoted by the red arrow and the ~12 kDa NapD bands are denoted by the blue arrow. 151

Figure 2.15: SDS-PAGE of NapA purified in the prescence and absence of protease inhibitors. Lane 1- PageRuler Plus prestained protein ladder (kDa), Lane 2- NapA purified in the absence of the protease inhibitor cocktail and PMSF, Lane 3- NapA purified in the prescence of the protease inhibitor cocktail and the absence of PMSF, Lane 4- NapA purified in the absence of the protease inhibitor cocktail and the prescence of PMSF. The ~ 108-kDa NapA bands are denoted by the red arrow and the ~12 kDa NapD bands are denoted by the blue arrow. 152

Figure 2.16: SDS-PAGE of NapA purification utilizing a linear imidazole gradient during the affinity chromatography step. A) Lane 1-clarified lysate, Lane 2-His-trap column flow through (non-binding proteins), Lane 3-washing with buffer A (wwbA) fraction #1, Lane 4-wwbA fraction #2, Lane 5- PageRuler Plus prestained protein ladder (kDa), Lane 6- linear imidazole gradient (lig) fraction # 12, Lane 7- lig fraction # 15, Lane 8- lig fraction # 19, Lane 9- lig fraction # 24. B) Lane 1- lig fraction # 34, Lane 2- lig fraction # 36, Lane 3- lig fraction # 37, Lane 4- lig fraction # 38, Lane 5- lig fraction # 39, Lane 6- lig fraction # 40, Lane 7- lig fraction # 41, Lane 8- PageRuler Plus prestained protein ladder (kDa), Lane 9- lig fraction # 42. The ~ 108-kDa NapA bands are denoted by the red arrow and the ~12 kDa NapD bands are denoted by the blue arrow..... 153

Figure 2.17: SDS-PAGE of NapA purified by a step gradient during the affinity chromatography step. A) Lane 1- clarified lysate, Lane 2-His-trap column flow through (non-binding proteins), Lane 3- PageRuler Plus prestained protein ladder (kDa), Lane 4- 20 mM imidazole wash step, Lane 5- 50 mM imidazole wash step, Lane 6- His-trap fraction #1-3, Lane 7- His-trap fraction #7-9. B) Lane 1- His-trap fraction #22, Lane 2- His-trap fraction #23, Lane 3- His-trap fraction #24, Lane 4- PageRuler Plus prestained protein ladder (kDa), Lane 5- His-trap fraction #25, Lane 6- His-trap fraction #26, Lane 7- His-trap fraction #27. The ~ 108-kDa NapA bands are denoted by the red arrow and the ~12 kDa NapD bands are denoted by the blue arrow. NapD is faint and running at the dye front. 154

Figure 2.18: SDS-PAGE examples of Size Exclusion Chromatography (SEC) fractions. A) SEC resulted in a single peak. Lane 1- SEC fraction # 9, Lane 2- SEC fraction # 10, Lane 3- SEC fraction # 11, Lane 4- SEC fraction # 12, Lane 5- SEC fraction # 13, Lane 6- SEC fraction # 14, Lane 7- PageRuler Plus prestained protein ladder (kDa), Lane 8- Pure NapA. B) SEC resulted in two peaks. Lane 1- SEC peak #1 (eluted first), Lane 2- SEC peak #2 (eluted second), Lane 3- PageRuler Plus prestained protein ladder (kDa). The ~ 108-kDa NapA bands are denoted by the red arrow and the ~12 kDa NapD bands are denoted by the blue arrow. 155

Figure 2.19: Example chromatograms of NapA as-isolated samples during SEC on the HiPrep 16/60 Sephacryl S-200 column when the two peaks are resolved differently at a flow rate of 0.2 mL/min. A) Native NapA isolated 11-7-17. B) Native NapA isolated 12-9-17. C) Native NapA isolated 3-23-18. D) Native NapA isolated 5-16-18. 156

Figure 2.20: SDS-PAGE of NapA purified via the optimized protocol previously published [329]. Lane 1- PageRuler Plus prestained protein ladder (kDa), Lane 2- Pure NapA. The ~ 108-kDa NapA band is denoted by the red arrow and the ~12 kDa NapD band is denoted by the blue arrow... 156

Figure 2.21: Mass spectrometry coverage map of *C. jejuni* NapA overexpressed in *E. coli* K12. The identified peptides are highlighted in red. A 73% coverage was obtained..... 157

Figure 2.22: Size exclusion chromatography calibration for molecular weight determination. A) chromatogram of the eluted NapA peak. B) calibration curve for the Superdex-200 column at flow rate of 0.5 mL/min. 158

Figure 2.23: Intact mass spectrum of as-isolated NapA revealing the prescence of a NapAD complex. This spectrum is the isolated m/z 5533 peak representing the complex and its CID fragments. Free NapA and free NapD were obtained with CID of the NapAD complex peak at ~100 V of collisional energy. Data was collected by Dr. Jared Shaw and the data analyzed by Dr. Ian Webb and Dr. Jennifer McGarry. 159

Figure 3.1: Interface of <i>R. sphaeroides</i> NapAB (PDB 1OGY) with NapA in pink and NapB in cyan. The essential residues reported by Simpson <i>et al.</i> [308] are highlighted as E47 in green, S772 in orange, and R83 in dark red. The image was created with Chimera and Corel Draw.....	167
Figure 3.2: UV-Vis spectrum of as-isolated <i>C. jejuni</i> NapA in 50 mM HEPES pH 7.0.....	170
Figure 3.3: The electrostatic potential plots for NapA showing the active site face of (a) <i>D. desulfuricans</i> , (b) <i>E. coli</i> , (c) <i>R. sphaeroides</i> and (d) <i>C. jejuni</i> , <i>D. desulfuricans</i> , <i>E. coli</i> and <i>R. sphaeroides</i> (PDB codes 2NAP, 2NYA, and 1OGY, respectively) structure data were downloaded from PDB.org database. Comparison of the electrostatic maps reveals that NapA from <i>C. jejuni</i> is the most basic, as indicated by the blue color, while <i>R. sphaeroides</i> is the most acidic (red). <i>D. desulfuricans</i> and <i>E. coli</i> electrostatic potential maps are intermediate. The NapA structures were aligned and the electrostatic potentials were calculated in Pymol (–10 kT = red; 10 kT = blue; 0 kT = white).....	171
Figure 3.4: Steady-state kinetic analysis using the Michaelis-Menten model of the reduction of nitrate by <i>C. jejuni</i> NapA. The solid lines represent Michaelis-Menten fit. The data was analyzed, and the graph produced in Origin. This kinetics curve was reproduced by at least ten biological replicates. Each curve contained three technical replicates for each substrate concentration. ...	172
Figure 3.5: The effect of pH on <i>C. jejuni</i> NapA nitrate reductase activity with respect to A) k_{cat} , B) K_M , and C) k_{cat}/K_M . <i>C. jejuni</i> NapA has a pH optimum of 7.4 but is most efficient at pH 7. ...	172
Figure 3.6: Observed pattern in the velocity of nitrate reduction at excess $[NO_3^-]$ by NapA at A) pH 6.0 (inset shows the extended concentration range tested) B) pH 7.0. The observed decline in velocity depicted in (B) has been observed at excess $[NO_3^-]$ in all pH conditions investigated except pH 6.0 (A).	173
Figure 3.7: Proposed mechanism for substrate inhibition of <i>R. sphaeroides</i> NapAB. A second nitrate molecule binds in a reversible process in the active site preventing the regeneration of the reduced free enzyme state and reversibly inactivating the enzyme.....	177
Figure 3.8: Electrostatic charges of the active site pockets of A) <i>C. jejuni</i> NapA and B) <i>R. sphaeroides</i> NapAB (PDB 1OGY). The electrostatic potentials were calculated in Chimera using the APBS plugin (–10 kT = red; 10 kT = blue; 0 kT = white).....	179
Figure 4.1: Homology model of <i>C. jejuni</i> NapA created in MOE by Courtney Sparacino-Watkins [329]. Full model depicted in the right panel and a zoomed in view of the molybdenum center in the upper left panel. The first coordination sphere of molybdenum is depicted as a line drawing in the lower left panel. The terminal ligand in the sixth position is unassigned in <i>C. jejuni</i> NapA and may be occupied by either an oxygen or a sulfur atom.	180
Figure 4.2: Diagram of the Nap enzyme complex depicting electron transfer in Nap and the possible roles of chaperones, NapD and NapL, in the maturation and transport of NapA. Q represents the quinone pool and question marks represent unclear mechanisms.	181
Figure 4.3: The proposed OAT mechanism for Nap where Mo is coordinated by a terminal oxo ligand in which NO_3^- binds to the five-coordinate Mo-center via one oxygen atom to give a six-coordinate center. NO_3^- is reduced to nitrite and oxygen is transferred to Mo, becoming a terminal oxo group of the oxidized Mo(VI) center. The resting Mo(IV) state is regenerated by reduction of the Mo via protonation of the Mo=O to water leading to its dissociation.	183

Figure 4.4: The sulfur shift mechanism as proposed in reference [375]. The initial resting state of the enzyme is proposed to have a Mo—S- as opposed to the Mo=S moiety. Thus, the terminal sulfido group can undergo internal redox with the cysteine sulfur forming a disulfide bond. The disulfide bond has been proposed to form in the presence of substrate, with migration of the cysteine S from Mo in the sulfur shift. Nitrate binds to the vacant site on the Mo center, transfers an oxygen atom to the Mo, and product nitrite is released. The resting state is then regenerated by proton-coupled electron transfer, the formation and departure of a water molecule, and the internal redox of the terminal sulfide with cysteine sulfur. 183

Figure 4.5: The impact of NaCl on the nitrate reductase activity of *C. jejuni* NapA with respect to A) k_{cat} and B) K_M . The ionic strength ranged from 0.13 M in the 0 M NaCl sample to 1.13 M in the 1.0 M NaCl sample. 187

Figure 4.6: Lineweaver-Burke plot of the inhibition of *C. jejuni* NapA by sulfate. Nitrate reduction rates of *C. jejuni* NapA in the presence of 0 mM sulfate, 0.1 mM sulfate, and 1 mM sulfate are depicted by the black squares, red circles, and the blue triangles, respectively. The data of all three conditions is within error of each other resulting in three lines that are essentially the same suggesting sulfate is not an inhibitor of *C. jejuni* NapA. Curvature of the data may suggest a small impact, but this impact is minimal and may be beyond the detection limit of the enzyme assay. 188

Figure 4.7: SDS-PAGE gel of TEV cleaved NapA. Lane 1- PageRuler Plus prestained protein ladder (kDa), Lane 2-TEV protease + NapA reaction mixture, Lane 3-NapA cleaved by TEV protease and purified by a second run on the HisTrap column, Lane 4-TEV protease + bound His-tagged NapA + contaminant proteins eluted from the HisTrap column after TEV cleavage. The NapA band at ~108-kDa is denoted by the green arrow and the NapD band is denoted by the blue arrow. Bands below the NapA band in lanes 2 and 4 are affinity column contaminants normally removed by SEC. 188

Figure 4.8: UV-Vis spectrum of as-isolated *C. jejuni* NapA cleaved by TEV protease in 50 mM HEPES pH 7.0. 189

Figure 4.9: Steady-state kinetic analysis using the Michaelis-Menten model of the reduction of nitrate by *C. jejuni* NapA with the His-tag cleaved by TEV protease. The solid line represents the Michaelis-Menten fit. The data was analyzed, and the graph produced in Origin. This kinetic curve was reproduced by at least ten biological replicates. Each curve contained three technical replicates for each substrate concentration. 190

Figure 4.10: XANES spectra of two batches of WT *C. jejuni* NapA at 49 mg/mL (isolated November 2018) and 35.5 mg/mL (isolated June 2019). A) the Mo K-edge of WT NapA isolated in November 2018 in blue (edge energy of 20013.68 eV) and WT NapA isolated in June 2019 in red (edge energy of 20012.12 eV). B) XANES spectra of the 35.5-mg/mL NapA sample isolated in June 2019 compared to the reference Mo foil. NapA sample is in red, Mo foil is in black, and sodium molybdate is in green. 193

Figure 4.11: EXAFS Spectra for WT NapA (isolated June 2019, 35.5 mg/mL sample). A) WT NapA fit to 1 Mo=O + 5 Mo-S + 0.9 Mo-O active site model. Top panel is the Fourier transform of EXAFS data and the bottom panel is the k-space data. B) WT NapA fit to 1 Mo=O + 5 Mo-S +

1.2 Mo-O active site model. Top panel is the Fourier transform of EXAFS data and the bottom panel is the k-space data. Experimental data is the black line and the fit is the red line. 193

Figure 4.12: XANES spectra of two batches of WT *C. jejuni* NapA treated with 450 mM NaCl. A) Full XANES spectra depicting the difference in oscillation patterns of WT NapA (red) and NaCl-treated NapA (blue). B) the Mo K-edge of WT NapA isolated in June 2019 in blue (edge energy of 20012.12 eV) and WT NapA treated with NaCl in red (edge energy of 20015.24 eV). C) XANES spectra of the NaCl-treated NapA sample compared to the reference Mo foil. NaCl-treated NapA sample is in blue, Mo foil is in black, and sodium molybdate is in green. 194

Figure 4.13: EXAFS Spectra for WT NapA treated with 450 mM NaCl. A) NaCl-treated WT NapA fit to 1 Mo=O + 2 Mo-S (long) + 3 Mo-S (short) active site model. Top panel is the Fourier transform of EXAFS data and the bottom panel is the k-space data. B) NaCl-treated WT NapA fit to 1 Mo=O + 3 Mo-S (long) + 2 Mo-S (short) active site model. Top panel is the Fourier transform of EXAFS data and the bottom panel is the k-space data. Experimental data is the black line and the fit is the red line. 196

Figure 4.14: Crystal structure of sulfite oxidase (PDB 2A99, 42% identity with *C. jejuni* NapA) with chloride ion bound in the active site. Molybdenum ion depicted as aqua sphere, chloride ion as green sphere, W204 in cyan, and R190 in magenta. Image visualized in Chimera. 197

Figure 5.1: A) a partial structure of Moco as in Nap, consists of the Mo metal coordinated by two molybdopterin (MPT) molecules (only one is displayed here). The Mo metal is coordinated to four dithiolene sulfurs that are appended to a pyranopterin heterocycle. The generic R group is guanine dinucleotide in Nap. (B) The first coordination sphere of Mo in several members of the DMSOR family. 204

Figure 5.2: Purity and integrity of C176 NapA variants. SDS-PAGE of A) native *C. jejuni* NapA, B) C176S NapA, C) C176D NapA, and D) C176A NapA. The NapA variants are ~108 kDa. 213

Figure 5.3: UV-Visible Spectra of the C176 NapA variants in 50 mM HEPES pH 7.00. 213

Figure 5.4: Steady-state kinetic data following the Michaelis-Menten model using nitrate as a substrate for (A) native *C. jejuni* NapA (B) C176S *C. jejuni* NapA variant (C) C176D *C. jejuni* NapA variant. These kinetics curves were reproduced by at least four biological replicates. Each data point in the curves contained three technical replicates for each substrate concentration. . 214

Figure 5.5: Steady-state kinetic data following the Michaelis-Menten model using TMAO as a substrate for native *C. jejuni* NapA (black squares) and C176S NapA (red circles). These kinetics curves were reproduced by one biological replicate. Each data point contained three technical replicates for each substrate concentration. 216

Figure 5.6: Steady-state kinetic data using DMSO as a substrate for C176D NapA fit to the Michaelis-Menten model. This kinetics curve was reproduced by at least five biological replicates. Each data point contained three technical replicates for each substrate concentration. 216

Figure 5.7: The pH profile for the NapA variants with nitrate as substrate. Top panel: native NapA pH dependence of A) k_{cat} , B) K_M , and C) k_{cat}/K_M . Middle panel: C176S NapA pH dependence of D) k_{cat} , E) K_M , and F) k_{cat}/K_M . Bottom panel: C176D NapA pH dependence of G) k_{cat} , H) K_M , and I) k_{cat}/K_M 217

Figure 5.8: Chemical structures of the substrates explored in this study with nitrate on the left, TMAO in the center, and DMSO on the right. 221

Figure 5.9: Influential tyrosine in DMSOR. Chimera image of the DMSOR crystal structure PDB 4DMR depicting the molybdopterin active site with bound DMSO molecule and influential Tyr 114 in green..... 222

Figure 5.10: Proposed interaction of the Asp ligand with bound DMSO compared to a Cys ligand at the active site in NapA variants. The native Nap interaction with DMSO is shown in the left panel and C176D NapA interaction is shown in the right panel. It is unclear if DMSO binds in native NapA but DMSO is not turned over. C176D NapA can stabilize DMSO binding to molybdenum through a proposed electrostatic interaction between the partially positive sulfur atom in DMSO and the partially negative carboxylate oxygen atom. The stabilized enzyme-substrate complex in the C176D variant enable DMSO turnover. 224

Figure 5.11: Catalytic scheme proposed for *C. jejuni* NapA. The reduced molybdenum (IV) state of the enzyme (denoted E) binds reversibly to substrate nitrate (denoted S) in the first step forming the ES complex where nitrate is coordinated to the Mo(IV) metal center. As catalysis proceeds, the O-N bond weakens and the Mo=O bond begins to form in the proposed transition state (denoted $[ES^\ddagger]$). Nitrate is reduced to nitrite transferring an oxygen atom to the oxidized Mo(VI) center (denoted E^0). The enzyme is regenerated from the oxidized E^0 state to the fully reduced E state in two proton coupled electron transfer steps with an intermediate Mo(V) state of the enzyme denoted E^0_{red} . The terminal oxo moiety transferred from the original substrate is protonated to produce water. Water diffuses from the active site enabling another substrate molecule to bind to the fully reduced Mo(IV) state (E). 225

Figure 5.12: Schematic diagrams depicting energy changes due to the effect of mutation or substrate. The activation energy of nitrate reduction calculated from k_{cat}/K_M is ΔG_T^\ddagger and is composed of two terms: the energetically unfavorable term ΔG_0^\ddagger , which represents the activation energy of the chemical steps where bonds are broken and created (i.e. for k_{cat}), and the energetically favorable term ΔG_b , which represents the realization of binding energy (i.e. from the K_D or estimated from K_M). (A) Diagram comparing the reaction of native NapA enzyme, E, with substrate nitrate to the reaction of C176S/D variant enzymes, E_M , with substrate nitrate. (B) Diagram comparing the reaction of the C176S NapA, ($C^{176S}E$) and C176D NapA ($C^{176D}E$) with substrate nitrate. (C) Diagram comparing the reaction of the E and $C^{176S}E$ with substrate TMAO. (D) Diagram comparing the reaction of the E with substrates nitrate and TMAO. (E) Diagram comparing the reaction of the $C^{176S}E$ with substrates nitrate and TMAO (F) Diagram comparing the reaction of the $C^{176D}E$ with substrates nitrate and DMSO. 226

Figure 5.13: The double logarithmic plot of $\log(k_{cat})$ vs pH for nitrate reduction by A) native NapA, B) C176S NapA, C) C176D NapA represents the pH dependence of the turnover number, k_{cat} , for each of the C176 Nap variants. The data in (A) was fit to equation (3) in the text and revealed two catalytically important ionizations in NapA with pK_a of 5.44 and 9.38. The data in (B) and (C) did not converge to equation (3) and thus were fit to higher polynomials to qualitatively determine information about the catalytically important ionizations in the C176S/D variants. Based on the shape of the fitted curve, the C176S/D variants are proposed to form products from multiple protonic states of the ES complex..... 232

Figure 5.14: Diagrams of the enzyme equations involved in the protonation states of the NapA enzyme. The free enzyme and enzyme-substrate complex have in a simplified form three protonation forms representing protonation of residues that are catalytically important. The biomolecule can be fully deprotonated, monoprotated, or diprotated: A) where only one protonated state, i.e. the monoprotated state (EHS^-), is catalytically active and B) where two protonic states, i.e. the monoprotated (EHS^-) and the fully deprotonated (ES^{2-}) states, produce products..... 233

LIST OF ABBREVIATIONS

[2Fe2S]	two iron two sulfur cluster
[3Fe4S]	three iron four sulfur cluster
[4Fe4S]	four iron four sulfur cluster
Aio	arsenite oxidase
ALA	δ -aminolevulinic acid
AlaS	δ -aminolevulinic acid synthase
ANO	adenosine- ¹ N-oxide
ANRA	assimilatory nitrate reduction to ammonia
AO	aldehyde oxidase
ATP	adenosine triphosphate
AU	absorbance unit
BSOR	biotin sulfoxide reductase
ccm	cytochrome <i>c</i> maturation
CIA	cytosolic iron-sulfur protein assembly
CID	collision-induced dissociation
CO	carbon monoxide
CoA	coenzyme A
cPMP	cyclic pyranopterin monophosphate
DFT	density functional theory
DMS	dimethyl sulfide
DMSO	dimethyl sulfoxide
DMSOR	dimethyl sulfoxide reductase
DNA	deoxyribonucleic acid
DNRA	dissimilatory nitrate reduction to ammonia
DTT	dithiothreitol
EDTA	ethylenediaminetetraacetic acid
EPR	electron paramagnetic resonance spectroscopy
Euk-NR	eukaryotic nitrate reductase
EXAFS	extended x-ray absorption fine structure
FAD	flavin adenine dinucleotide
FDH	formate dehydrogenase
FDR	false discovery rate
FMN	flavin mononucleotide
FNR	fumarate-nitrate reduction transcription factor
$\Delta\Delta G_b$	change in the binding energy of the enzyme and substrate
$\Delta\Delta G_b^\ddagger$	change in the binding energy of the enzyme and transition state
ΔG_0^\ddagger	activation energy of chemical steps where bonds are broken & created
ΔG_b	binding energy as a result of enzyme and substrate forming a complex
ΔG_T^\ddagger	activation energy for nitrate reduction by NapA
GH	glycine-histidine
GI	gastrointestinal

GIT	gastrointestinal tract
GMP	guanosine monophosphate
GST	glutathione S-transferase
GTP	guanosine triphosphate
HCD	higher-energy collisional dissociation
HEPES	2-[4-(2-hydroxyethyl)piperazin-1-yl]ethanesulfonic acid
HMB	hydroxymethylbilane
hMCD	human molybdenum cofactor deficiency
hSO	human sulfite oxidase
ICPMS	inductively coupled plasma mass spectrometry
IMAC	immobilized metal ion affinity chromatography
IPTG	isopropyl- β -D-thiogalactopyranoside
ISC	iron-sulfur cluster assembly
<i>lac</i>	lactose operon
LB	Luria-Bertani broth
lig	Linear imidazole gradient
LUCA	last universal common ancestor
mARC	mitochondrial amidoxime reducing component
MCD	molybdopterin cytosine dinucleotide
MGD	molybdopterin guanine dinucleotide
Moco	molybdenum cofactor
MPT	molybdopterin
MV	methyl viologen
NAD ⁺	oxidized nicotinamide adenine dinucleotide
NADH	reduced nicotinamide adenine dinucleotide
Nap	periplasmic nitrate reductase
Nar	respiratory nitrate reductase
Nas	assimilatory nitrate reductase
NiR	nitrite reductase
NO	nitric oxide
NO ₂ ⁻	nitrite
NO ₃ ⁻	nitrate
NR	nitrate reductase
OAT	oxygen atom transfer
OD	optical density
PBG	porphobilinogen
Pcr	perchlorate reductase
PCR	polymerase chain reaction
PDT	pyranopterin
PFV	protein film voltammetry
PMSF	phenylmethylsulfonyl fluoride
REMP	redox enzyme maturation protein
RNA	ribonucleic acid
SDS-PAGE	sodium dodecyl sulfate polyacrylamide gel electrophoresis
SEC	size exclusion chromatography

SecT	secreation translocase
SO	sulfite oxidase
SSM	secondary structure matching
SSRL	Stanford synchrotron radiation light source
SUF	sulfur mobilization
TAT	twin arginine translocase
TB	terrific broth
TEV	tobacco etch virus
TMA	trimethyl amine
TMAO	trimethyl amine N-oxide
TMAOR	trimethyl amine N-oxide reductase
U	selenocysteine
UV-Vis	ultraviolet-visible spectroscopy
Vmax	maximal velocity
WD	tyrptophan-aspartate
wwbA	Washing with buffer A
XANES	x-ray absorption near edge structure
XAS	x-ray absorption spectroscopy
XDH	xanthine dehydrogenase
XO	xanthine oxidase

ABSTRACT

Mononuclear molybdenum enzymes catalyze a variety of reactions that are essential in the cycling of nitrogen, carbon, arsenic, and sulfur. For decades, the structure and function of these crucial enzymes have been investigated to develop a fundamental knowledge for this vast family of enzymes and the chemistries they catalyze. The dimethyl sulfoxide reductase (DMSOR) family is the most diverse family of molybdoenzymes and, the members of this family catalyze a myriad of reactions that are important in microbial life processes. Periplasmic nitrate reductase (Nap) is an important member of the DMSO reductase family that catalyzes the reduction of nitrate (NO_3^-) to nitrite (NO_2^-), and yet the physiological role of Nap is not completely clear. Enzymes in this family can transform multiple substrates; however, quantitative information about the substrate preference is sparse and more importantly, the reasons for the substrate selectivity are not clear. Substrate specificity is proposed to be tuned by the ligands coordinating the molybdenum atom in the active site. As such, periplasmic nitrate reductase is utilized as a vehicle to understand the substrate preference and delineate the mechanistic underpinning of these differences. To this end, NapA from *Campylobacter jejuni* has been heterologously overexpressed, and a series of variants, where the molybdenum-coordinating cysteine has been replaced with another amino acid, has been produced. The kinetic and biochemical properties of these variants will be discussed and compared with those of the native enzyme, providing quantitative information to understand the function.

CHAPTER 1. INTRODUCTION

A version of this chapter has been published as cited by reference [1]. Adapted by permission from Springer Nature Customer Service Centre GmbH: Springer Nature, Journal of Biological Inorganic Chemistry, Copyright Liscence 4844410164166.

1.1 Molybdenum Enzymes

Molybdenum (Mo) is an essential nutrient for life on earth. Over 50 enzymes have been discovered with molybdenum at their active sites. Often these molybdenum-containing enzymes also require pterin and catalyze a variety of reactions that are essential for all forms of life. The catalytically competent Mo-center is formed by coordination from one or two equivalents of pyranopterin (PDT), also known as molybdopterin (MPT), through chelation with its cis-sulfur donors. Pterin refers to a member of the pteridine family of bicyclic *N*-heterocycles consisting of a pyrimidine ring is joined at the 5,6-position to a pyrazine ring where the pteridine is substituted by an amino group at position 2 and a keto group at position 4 [2]. Pterins are abundant in biology and are mainly involved in roles such as pigments, one-carbon transfer cofactors and redox cofactors. As a component of MPT pterin is involved in the redox role of this cofactor [2]. Once formed, the Mo-bound MPT is then referred to as the molybdenum cofactor (Moco) [3] (Figure 1.1A). Mononuclear molybdenum enzymes are classified based on the structure and coordination of Moco. The most common classification lists three main families: the xanthine oxidase (XO), sulfite oxidase (SO), and dimethyl sulfoxide reductase (DMSOR) families (Figure 1.1B) [4-7].

For members of the XO family, the molybdenum is coordinated by one molybdopterin monophosphate or molybdopterin cytosine dinucleotide (MCD) molecule. Remaining coordination sites are occupied with oxygen, sulfur or selenium ligands supporting a square pyramidal geometry [5]. As a common feature of this family, the Moco does not have any covalent attachment to the polypeptide. The MPT component of Moco is stabilized in the pocket by hydrogen-bonding interactions [4]. The hydrogen-bonding interactions and the conformation of the pterin have been utilized to predict the redox state of the MPT molecule [8].

An interesting case occurs in carbon monoxide (CO) dehydrogenase from *Oligotropha carboxidovorans*, where the molybdenum atom is coordinated by a bridging sulfur atom that is

also attached to a copper atom. The Cu-center is additionally coordinated by a cysteine residue from the polypeptide [9]. Mechanistically, members of the XO family catalyze the oxidative hydroxylation of aldehydes and aromatic heterocycles through the transformation of a C-H bond into a C-OH moiety that subsequently tautomerizes to a C=O unit [10].

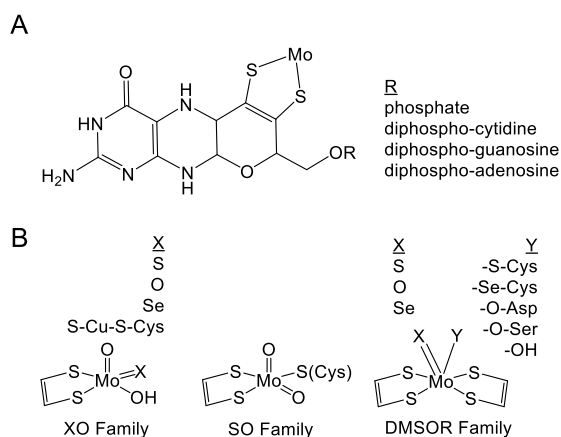


Figure 1.1: A) The general structure of the molybdenum cofactor (Moco). B) First coordination spheres of the Mo center in the three mononuclear molybdenum enzyme families: xanthine oxidase (XO) family, sulfite oxidase (SO) family, and dimethyl sulfoxide reductase (DMSOR) family.

In the case of the SO family, the molybdenum is coordinated by a sulfur atom from an equatorial cysteine in the polypeptide backbone. The molybdenum is also coordinated by the dithiolene from the PDT, and an oxo group at the apical site. In the oxidized state, the fifth position belongs to a terminal oxo group occupying an equatorial position in a distorted square-pyramidal geometry [10]. In the reduced state of the enzyme, this terminal oxo group is replaced by either a hydroxy group or a water molecule.

Members of this family catalyze important reactions in many forms of life. The mammalian SO catalyzes the last reaction in the degradation of amino acids such as cysteine or methionine and plays an important role in detoxification of sulfite into the sulfate anion [11, 12], while another member of the SO family, eukaryotic nitrate reductase (Euk-NR), catalyzes the assimilation of nitrate in plants, algae and fungi [11, 12]. A relatively new member of the SO family, the mitochondrial amidoxime reducing component, mARC, catalyzes the reduction of *N*-hydroxylated compounds such as benzamidoxime and pentamidine monoamidoxime, among others [13].

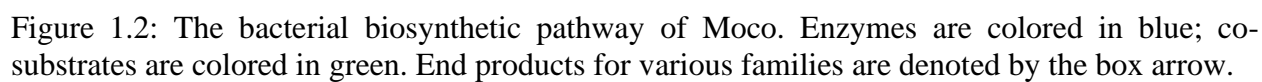
Recently, it has been demonstrated that mARC can reduce nitrite to nitric oxide (NO), thus suggesting its potential importance in cardiovascular health [14].

The DMSOR family is by far the most diverse family of all the pterin-containing mononuclear molybdenum enzymes [15]. Even though similarities exist in the overall folds, significant variations exist in the coordination sphere of the metal as well as amino acids around the enzyme's catalytic pocket [10]. The molybdenum is always coordinated by four sulfurs from the two dithiolene groups of two PDT molecules. The fifth position of coordination is usually filled by an oxygen or sulfur from amino acid side chains, while the sixth and final position comes from oxygen (oxo or hydroxy) or sulfur (sulfido) atoms [6, 10]. The metal usually adopts a distorted trigonal prismatic geometry [6].

The DMSOR family includes DMSOR, trimethylamine *N*-oxide reductase (TMAOR), biotin sulfoxide reductase (BSOR), nitrate reductase (NR), formate dehydrogenase (FDH) and more. These can be further categorized; for example, bacterial NRs come in three forms: assimilatory nitrate reductase (Nas), respiratory nitrate reductase (Nar), and periplasmic nitrate reductase (Nap) [12, 16]. The NRs reduce nitrate; however, their Mo coordination spheres differ, underscoring the diversity in the DMSOR family. Both the SO and DMSOR families catalyze oxygen atom transfer (OAT) reactions.

1.2 Moco Biosynthesis

Although the reactions of pterin-containing molybdenum enzymes vary, all the Moco enzymes synthesize the cofactor in essentially the same way across species. The biosynthesis of the complex cofactor Moco has at least four steps: (1) GTP is converted to a stable intermediate, cyclic pyranopterin monophosphate (cPMP). (2) cPMP is converted to PDT via the addition of sulfur to create a cis-dithiolene ligand. (3) The cyclic phosphate ring is opened. (4) Molybdenum is inserted into the dithiolene unit first by an adenylation reaction with ATP followed by metal insertion. At this stage, the presumed dioxo-molybdenum is converted to the requisite Mo-center (Figure 1.2). In SO it is a dioxo-Mo center and in XO it is an oxo-thio Mo center. In most bacteria and archaea, once the molybdenum is inserted into the PDT forming the Moco, further maturation is achieved by adding a nucleotide such as guanosine or cytosine forming the molybdopterin guanine dinucleotide (MGD) or the molybdopterin cytosine dinucleotide (MCD) forms of Moco respectively [2, 17, 18]. Once Moco is transported and incorporated into the respective apoproteins



further coordination can occur by protein-based ligands [17]. The molecular pathways for Moco biosynthesis are largely conserved in bacterial, archaeal, and eukaryotic systems [3, 18-21]. In humans, deficiencies in any of the Moco biosynthesis enzymes due to genetic mutations can cause simultaneous loss of sulfite oxidase, xanthine oxidoreductase and aldehyde oxidase activities, causing serious physiological disorders including death at an early age [3, 11, 22].

1.3 Significance of Molybdenum Enzymes

The MPT is recognized to be present in the last universal common ancestor (LUCA) of bacteria and archaea, underscoring its importance for the origin of life [23]. Molybdenum enzymes are indispensable in all forms of life as they catalyze essential reactions in life processes such as respiration, detoxification, assimilation, and catabolism [17]. All forms of life, whether eukaryotic, prokaryotic, or archaeal have at least one moco-containing enzyme. Moco enzymes involved in the respiratory electron transfer chain provide ecological diversity enabling bacteria to respire under numerous conditions including: highly oxidizing and reducing environments, extremes of high and low temperatures, high alkalinity and acidity, and even in the presence of highly toxic chemicals. These enzymes catalyze vital reactions from the cycling of C, S, N, Se, and As [4].

In humans, Moco-deficiency is a lethal autosomal recessive disease that causes severe physiological disorders leading to death. Human Molybdenum Cofactor Deficiency (hMCD) results in complete loss of SO, XO and AO activities and is mainly caused by the deficiency of SO that protects the brain from elevated levels of toxic sulfite [3]. There are three types of hMCD (types A, B and C) resulting from mutations in the conserved Moco biosynthetic pathway in humans. In most patients, the *MOCS1* gene product, involved in production of cPMP, a precursor of MPT, is defective. Patients exhibit progressive neurological damage leading to early childhood death [24]. The Type A hMCD has been treated in humans using repeated injections of cPMP [25]. Type B and Type C hMCD are caused by defects in downstream *MOCS2/MOCS3*, and gephyrin genes, respectively, [24] and no treatment has been reported.

Given the importance of the molybdenum enzymes in nature, significant efforts have been directed toward obtaining large quantities (> 30 mg/L culture) of these enzymes to study this fascinating family of enzymes. Overexpression studies carried out on bacterial hosts have been the primary way to produce active molybdenum enzymes. Yet, the set of conditions for overexpressing any type of recombinant protein are not the same for every enzyme [26]. Given the complexity of

the biosynthetic pathway and the large size of these enzyme complexes (Nap for example is composed of 4 enzyme components with a combined size of ~200-kDa), many challenges had to be addressed to ensure the production of active enzyme. A summary of the heterologous and homologous expression studies is discussed in the following sections to illuminate underlying patterns and challenges that have been reported to date.

1.4 The Challenge: Obtaining Active Soluble Recombinant Molybdenum Enzymes

Large quantities (>50 mg/mL) of the active enzyme are often required for spectroscopic and structural analysis. In the past, this limited studies to sources where higher quantities of the native enzyme could be harvested (i.e., chicken liver and spinach). Development of homologous and heterologous expression systems in both bacterial (i.e., *E. coli*) and eukaryotic (i.e., yeast) have facilitated the production of substantial quantities of the desired protein. For moco-containing proteins, the optimal expression system requires a cost-effective host that multiplies rapidly, is easy to handle in the laboratory [27], and possesses the machinery to overexpress the recombinant protein in an active soluble state [28]. The three common concerns for recombinant molybdenum enzymes are 1) the production of soluble protein, 2) the activation of protein (i.e., cofactor insertion, posttranslational modifications, etc.), and 3) transport (i.e., to or across membranes). These challenges will be discussed in detail in the sections below in the context of the expression systems developed in the last few decades.

1.4.1 Production of Soluble Molybdenum Enzymes

At high temperatures ($\geq 37^{\circ}\text{C}$), inclusion bodies form during the expression of BSOR [29] and SO [30]. Formation of inclusion bodies can be prevented in several ways; including expression at lower temperatures (15-30°C) [31, 32], coexpression with soluble fusion tags such as maltose-binding protein [26], or coexpression with molecular chaperones that aid in the folding of the translated product [33]. Pollock and Barber [29] reduced inclusion body formation by lowering the expression temperature and decreasing the growth period. Even under the optimized conditions, only 2–3% of the total soluble protein contained the recombinant BSOR while 8–10% of the pellet fraction contained insoluble BSOR [29]. D’Errico *et al.* were also able to reduce inclusion body formation by reducing the induction temperature from 37°C to 22°C, although

quantitation of the amount of enzyme still lost in the insoluble fraction was not reported [30]. In some cases, the recombinant protein requires accessory proteins to correctly fold into an active state [33]. The coexpression of Moco delivery proteins allows the target proteins to be acquired with an intact and active cofactor. Cofactor addition can stabilize the recombinant target protein and increase the overall yield [34]. Such chaperones will be discussed in further detail in Section 1.4.2.5 *Redox Enzyme Maturation Proteins (REMP)*.

Caution must be taken when choosing an expression strain as not all expression strains are suitable for molybdenum enzymes. For example, Pinske *et al.* reported that *E. coli* BL21(DE3) strain does not possess the genes required for the molybdate transport system (mod operon) or the molybdenum-responsive transcriptional regulator (ModE) [27]. This renders the strain to be impractical for the expression of Mo enzymes [27]. Selecting expression strains is discussed in Section 1.4.2.1a *Homologous versus Heterologous*. In addition to the expression conditions, the expression medium is important in protein production. Supplementation of the media with key nutrients, i.e. molybdenum, is beneficial for optimal production of molybdopterin holoenzymes.

1.4.2 Active versus Inactive Molybdenum Enzymes

Expression strains should be able to perform any necessary activation processes, such as cofactor insertion, chemical modifications, or post-translational modifications. In the case of molybdenum enzymes, metal cofactor synthesis is a necessity to obtain active recombinant protein [27]. Sambrook *et al.* suggested that the optimization of recombinant expression should be determined empirically [26]. Using different host strains, expression systems, and amendments will eventually aid in the establishment of the optimal conditions for the expression of the target protein [26]. The major concern for molybdenum enzyme production is balancing increased production without reducing activity. A comprehensive list of molybdenum enzyme recombinant expression systems is provided in Tables 1.1-1.15. Due to the complex cofactor, there are many challenges in achieving optimal cofactor synthesis, metal loading, multi prosthetic group loading, modifications to the Mo center, cofactor activation, and proper protein folding. These challenges are discussed in detail in the sections below.

1.4.2.1 Effective Methods for Moco Synthesis and Incorporation

A major difficulty in the overexpression of mononuclear molybdenum enzymes is the synthesis and full incorporation of the molybdenum cofactor. Outside of the protein environment Moco readily degrades under aerobic conditions and is stable for ~90 minutes under anoxic conditions [35]. Although there have been attempts to synthesize the cofactor in vitro [36-44], there has not been a complete and unprotected analog to reconstitute the apoenzyme. Several strategies to achieve holoenzyme production have been employed while using the cell to biosynthesize Moco. This aspect has been covered in detail in recent reviews [19, 45, 46]. The most common methods to increase holoenzyme production include supplementation of molybdenum, using specialized strains that boost specific components of the cofactor biosynthesis, cofactor reconstitution, optimized expression conditions (e.g., lower temperatures and longer growth times), and the inclusion of chaperone proteins in the expression system. The former will be discussed below in Sections *1.4.2.1a-1.4.2.1d* and the latter will be discussed in Section *1.4.2.5*.

1.4.2.1a Homologous versus Heterologous Expression Systems

The choice of overexpression host that produces the target protein is important, especially for enzymes with complex cofactors such as Moco. The expression host must have the machinery required to properly fold the protein and insert the cofactors. Leimkühler *et al.* [47-49] studied the homologous expression of xanthine dehydrogenase (XDH) in *Rhodobacter capsulatus* where the enzyme was expressed in strains unable to transport molybdenum. Expression of XDH without the necessary molybdenum transport system genes resulted in inactive protein [48]. It was concluded that the insertion of the cofactor into the enzyme seems to proceed only when all the components of the Moco biosynthetic pathway are present [48].

Unsuccessful expression systems with absent components were noted by Pinske *et al.* [27] as well as Yang and coworkers [50]. Pinske *et al.* [27] subsequently discovered the reason *E. coli* BL21 (DE3) strain is not suitable, specifically, the *mod* genes are absent. These *MOD* genes encode for the molybdate transporter as well as key transcriptional regulator, ModE. Although these defects severely reduce mature molybdopterin enzyme production, the supplementation of the media with excess molybdate permits the production of molybdopterin enzymes with limited cofactor incorporation. In this case, molybdate is nonspecifically transported by the sulfate ABC

type transport system [27]. Pinske determined *E. coli* BL21 (DE3) to be naturally devoid of molybdenum-dependent FDH and NR activity. Upon the addition of a plasmid containing the *fnr* gene and media supplementation with molybdate, formate-dependent hydrogen production and NR activity could be restored, however, to only 25–30% of an *E. coli* K12 strain. The FDH activity observed was determined to be the result of FDH-H. FDH-N activity could not be restored even in the presence of the *fnr* gene and molybdate. The addition of ModE could only partially restore the activities of both FDH enzymes [27].

Despite the deficiencies of *E. coli* BL21 (DE3), many groups were able to supplement and express active Moco enzymes (Tables 1.1-1.10) [30, 51-59]; however, few report the Mo content or show Mo content variability. For example, Pollock *et al.* [55] reported a Mo content of 44% in spinach NR expressed in *E. coli* BL21 (DE3). However, Hilton *et al.* [54] reported 66-87% Mo incorporation in *Rhodobacter sphaeroides* DMSOR expressed in *E. coli* BL21. Nevertheless, the most common expression system is *E. coli*, and there are *E. coli* strains that do not suffer the same deficiencies as the *E. coli* BL21 strain. For example, *E. coli* K12 derived strains have been successfully used to overexpress mature molybdopterin enzymes (Tables 1.1-1.10) [14, 60-91]. D'Errico *et al.* [30] expressed *D. radiodurans* SO in both *E. coli* BL21 and *E. coli* TP1000. A higher yield of protein was observed in the *E. coli* BL21 strain but more active protein was isolated from *E. coli* TP1000 [30]. Initially, Hilton *et al.* showed no expression of DMSOR in *E. coli* BL21 (DE3) due to formation of insoluble and inactive protein [92], but they reported an expression system with *E. coli* BL21 (DE3) cells using an IPTG-inducible pET system where the *R. sphaeroides* leader sequence was removed. The cells were grown at low temperatures for 24 hours to allow for proper cofactor insertion [54]. They obtained ~1 mg of pure protein per 5 liters of cell culture or a 31% yield of active protein.

Multiple successful homologous and heterologous molybdopterin enzyme expression systems have been reported (Tables 1.1-1.5). The benefit of using a homologous system lies in the complex differences between organisms. For example, NRs that reduce nitrate to nitrite, are categorized in bacteria as Nas, Nar, and Nap as mentioned previously. All three of which have specific chaperones in addition to the general Moco biosynthetic machinery. These chaperones can be organism specific or even strain specific. Therefore, a homologous system is preferred because it conveniently has all the native partners necessary to properly produce the enzyme. The challenge is in the convenience of engineering the system to produce the protein target under the desired

conditions. Some systems are easier to manipulate than others. For instance, *Cupriavidus necator* (previously classified as *Alcaligenes eutrophus* as well as *Ralstonia eutropha*) Nap is located on the 450 kb mega plasmid pHG1 and not in the organism's chromosomal DNA [93]. This genetic locus permits easy manipulation of the Nap genes for overexpression and mutagenesis compared to Nar genes located on a chromosome [93]. However, if the growth requirements of the organism are impacted by such manipulations, then complications may arise. If protein variants are to be investigated, then there must be additional manipulations to the native protein structure. Such manipulations could impact the synthesis of the variant, which may lead to diminishing the production of necessary protein partners downstream in the operon or negatively impacting the growth of the organism. These issues may be overcome, and thus homologous expression is preferred.

The benefits of heterologous systems are the abundant opportunities that exist to streamline the expression process. *E. coli*, for example, has a fast doubling time, is easy to culture, and has the Moco biosynthetic machinery. The difficulties lie in the organism's codon preferences. *E. coli* uses a preferred set of codons when translating RNA transcripts into protein and this set of codons may differ from some organisms. Such codon differences could result in mistranslations during protein synthesis. Although codon optimized constructs can be produced, it may not always be applicable. There can also be protein folding issues if *E. coli* does not contain the proper chaperone or scaffolds necessary for the target enzyme. All such complications are specific to heterologous systems and should be addressed during design and optimization. For instance, *Saccharomyces cerevisiae* lacks the genes necessary for Moco biosynthesis and, thus, eukaryotic nitrate reductase (Euk-NR) could not be expressed in the yeast host [94]. Utilizing *E. coli* as a heterologous host may result in some unexpected issues as observed by Pinske [27]. In addition, Hilton and colleagues reported differences in the expression of *R. sphaeroides* DMSOR in *E. coli* depending on the sequence of the twin-arginine translocase (TAT) signal peptide on the N-terminus of the DMSOR gene. The importance of the leader sequence is discussed in Section 1.4.3 *Transport of Molybdenum Enzymes* [54].

Successful expression of active Moco enzymes in a heterologous system has been accomplished with members of the SO family (Tables 1.2, 1.4, 1.7, 1.9). These enzymes contain a form of Moco that often does not rely on native REMPs for the maturation of the target Moco enzyme. For example, human SO (hSO) has successfully been expressed in *E. coli*, with high Mo

incorporation [57, 67, 68, 95, 96] (Table 1.7). The XO and DMSOR families are more complicated because these enzymes contain modified forms of Moco, i.e., sulfurated or nucleotide-containing forms (Figures 1.1-1.2). However, heterologous systems have been successful in producing active Moco enzymes (Tables 1.1-1.15). The benefit of coexpressing the target enzyme with its specific chaperone is discussed in Section 1.4.2.5 *Redox Enzyme Maturation Proteins (REMP)*.

Although homologous systems seem to show the most success, the production of active protein has not always been straightforward. Only a handful of homologous systems reported Mo incorporation (Tables 1.6-1.10) where the Mo incorporation ranged from 25 to 66%. Thus, there is no guarantee that any expression system will work as designed, and optimizations should be made to obtain the desired quantities of active protein.

1.4.2.1b *Optimization of Expression Conditions*

The optimization of the expression medium can greatly influence the yield of protein. Temple *et al.* [57] optimized the recombinant expression of hSO and their parameters have been adapted by subsequent expression work not only for SO but for other eukaryotic molybdenum enzymes expressed in *E. coli* as well [55]. Temple *et al.* identified the potential of expression in TP1000 *E. coli* cells (discussed in Section 1.4.2.1c), while also exploring the effects of molybdate and IPTG concentration on active protein. A nine-fold increase in yield was reported when the IPTG concentration was decreased while simultaneously increasing the induction time. In an attempt to keep inclusion bodies from forming, expression temperature was reduced from 37°C to 30°C, the induction time was increased from 6 hours to 18 hours, and the optimal IPTG concentration for maximum yield of active protein was found to be 20 μ M compared to the standard IPTG concentration of 100 μ M [57]. The improved conditions for expression and purification resulted in ~15 mg of protein per liter of cell culture, which is impressive for recombinant eukaryotic molybdenum enzyme expression in a bacterial host.

As previously mentioned, BSOR, which has a more complex bis-MGD form of Moco, formed inclusion bodies [29]. Pollock *et al.* [29] improved the heterologous expression of *R. sphaeroides* BSOR in *E. coli* by expressing the protein in JM109 cells, at room temperature and only for four hours ensuring the presence of viable cells before lysis. The yield was ~ 1 mg of pure protein per 8 liters of cells [29]. Utilizing the same expression vector and *E. coli* strain as Pollock [29], Temple *et al.* optimized BSOR expression significantly improving protein yield [72].

Utilizing anaerobic expression conditions while lowering the amount of IPTG and increasing the growth period produced 46 mg of the purified enzyme from 40 liters with 26% recovery and 120-fold increase in purity [72]. Overall, their yield was 1.15 mg of protein/L of culture, approximately ten times more than previously achieved, but still less than their hSO yields [57]. This considerable yield coupled with a high Mo incorporation of ~88% enabled them to study the Mo center of BSOR with both electron paramagnetic resonance spectroscopy (EPR) and X-ray absorption spectroscopy (XAS) [72].

Johnson and Rajagopalan [97] expanded upon Temple and coworkers' procedure [72] for homologous expression of *E. coli* BSOR, by homologously expressing TMAOR from *E. coli*. Problems with the DE3 lysogen were identified and the expression vector was switched to pTrc99A, which does not depend on the T7 polymerase but instead relies on the native *E. coli* polymerase. From this expression system, 1.3-2.1 mg of TMAOR per liter of cell culture was obtained with 30-66% Moco incorporation [97]. By using Temple and coworkers' [72] strategies, Johnson *et al.* [97] successfully established a system for overexpression of TMAOR that resulted in active protein of 0.3 mg/g, cells which was a 600% increase in yield compared to the native isolation.

Optimizing strains can also reduce inclusion body formation and boost recombinant protein production. Arsenate reductase was overexpressed by Malasarn *et al.* [98] using methods similar to the expression of SO by Temple [57]; however, the *E. coli* C43 strain for toxic membrane protein expression was used. Like Temple *et al.*, they expressed at a lower temperature and for a longer duration which allowed the isolation of soluble holoprotein. Protein yield was not reported; however, they observed 1.35 mol of Mo per mol of enzyme suggesting high cofactor incorporation, assuming reported contents are exclusively from the cofactor [98].

The idea of slowing down expression seems to be a common theme as low temperatures and longer growth times produce more active enzyme (see Tables 1.1-1.15). The use of media additives to slowly turn on expression was applied during the heterologous expression of *Ralstonia sp.* S22 arsenite oxidase in *E. coli* [99]. In that study, the cells were grown in an auto-inducing medium with small amounts (0.5% (w/v)) of glucose and lactose [98]. The medium slows the expression, allowing for growth at 37°C without the risk of inclusion body formation [100]. Arsenite oxidation was confirmed via in-gel assays, but only unitless kinetic parameters were reported [99]. Soon after, Warelow *et al.* overexpressed *Rhizobium sp.* NT-26 arsenite oxidase in *E. coli* [62]. They

examined both aerobic and anaerobic conditions using *E. coli* strains DH5 α , JM109, and BL21. The highest yield resulted from a DH5 α host grown aerobically in rich medium. This system achieved 1.1 mg/L yield of protein, 83% of which was fully incorporated with molybdenum [62].

Sabaty *et al.* overexpressed *R. sphaeroides* YedY in both *E. coli* and *R. sphaeroides* [101]. *R. sphaeroides* was determined to be the better host by comparing the amount of active enzyme and the specific activity of recombinant protein under various conditions. As a periplasmic protein, the YedY leader sequence is important for maturation purposes. Regardless of whether the leader sequence was present or not, *R. sphaeroides* was the better host due to its ability to produce the highest quantities of active enzyme when compared to *E. coli*. Still, others were not able to obtain large amounts of active enzyme even after optimizations. Hartmann *et al.* [88] expressed and characterized *R. capsulatus* oxygen tolerant and NAD⁺ dependent FDH of the *fdsGBACD* operon. A 39% molybdenum incorporation was reported despite modifying expression and purification conditions. However, kinetic data consistent with previously isolated FDHs was recorded suggesting the oxygen tolerant FDH was comparable to formerly studied FDHs (both FDH-H and FDH-N). It appears that the path to active protein is more complicated in some systems. This is probably a result of the limited knowledge about the organism specific Moco machinery.

1.4.2.1c Boosting Moco Biosynthesis

In addition to media amendments and expression conditions, attempts have been made to boost Moco synthesis in a deficient host. The most notable achievement is the use of *E. coli* TP1000 cells as the expression strain. The TP1000 strain was developed by Palmer *et al.* by inserting a kanamycin resistance cassette in place of the *mobA* and *mobB* genes, which are responsible for modifying MPT by conjugation with guanosine monophosphate (GMP) (Figure 1.2) [102]. This modified version of the cofactor, MGD, is widely present in the DMSOR family of molybdenum enzymes. Eukaryotic molybdenum enzymes do not have the dinucleotide and only require MPT for Moco biosynthesis. Therefore, by inhibiting the conversion of MPT to MGD, there is an increase of Moco insertion into recombinant eukaryotic protein [57, 102]. With the use of the *E. coli* TP1000 strain specifically and the optimization of hSO expression reported by Temple *et al.* [57], Temple was able to procure 5-15 mg of active protein per liter of culture. Incorporation of Moco was optimized to almost 80%, which has been a significant improvement from previous attempts to express eukaryotic molybdenum enzymes. Comparing *E. coli* TP1000

to the common host *E. coli* BL21, D'Errico *et al.* noted [30] that *Deinococcus radiodurans* SO expressed at a higher yield of protein in the *E. coli* BL21 strain. Although TP1000 produced less total protein, the protein obtained from this *E. coli* strain was more active than that isolated from the *E. coli* BL21 strain [30].

Several groups have successfully utilized the Moco expression strain TP1000 which boosts the production and incorporation of the MPT form of Moco [13, 30, 55, 103-124]. Palmer also created the plasmid pTPR1 (unpublished) that carries the *moa* genes so that proteins involved in the biosynthesis of Moco are also overexpressed. This plasmid has been used in the production of mARC by Sparacino *et al.* [14]. These methods work well for the eukaryotic enzymes; however, the bacterial Moco has more variability in its structure posing additional challenges. This is particularly true for the DMSOR family that has the molybdenum center coordinated by two MPT molecules. Due to the addition of nucleotides to the MPT molecules in many DMSOR family enzymes, the benefits of the TP1000 strain are less clear. There is a need for a similar strain that boosts the different nucleotide versions of MPT (i.e. MGD and MCD). Despite the lack of an optimized expression strain, DMSOR enzymes and prokaryotic XO/SO enzymes have still been produced in reasonable yields in the active form (Tables 1.8-1.10).

1.4.2.1d Moco Reconstitution

There has been a shift from producing holoenzyme *in vivo* to reconstituting the apoenzyme with Moco. Truong and coworkers heterologously expressed the first Euk-NR in a yeast host, *S. cerevisiae*, although the protein was inactive and the yield was low [94]. They suggested the inactivity of the enzyme is due to the lack of Moco. This proved to be true when Zhang *et al.* reported that, unlike the *Pichia* yeasts, *S. cerevisiae* does not contain the Moco biosynthetic machinery [125]. Despite this predicament, Truong *et al.* demonstrated that apoprotein can be produced. The apoprotein was reconstituted with a low amount of Moco by Truong *et al.* that restored some activity to the NR protein using complementation and Moco from milk XO. Even though the Moco domain was incomplete, the authors reported catalytic NADH:cytochrome *c* reductase activity. The yeast host was proven capable of correctly inserting the prosthetic groups FAD and cytochrome b-557 and correctly folding these domains [94].

In addition to complementing Moco from another enzyme, several groups started using the biosynthetic precursors and enzymes to reconstitute the target enzyme. Utilizing a system that

increased DMSOR yields to 3.4 mg/L culture with 83% Mo enrichment, Temple *et al.* demonstrated that MobA, MPT, guanosine triphosphate (GTP), and MgCl₂ are required and sufficient for the activation of DMSOR recombinantly purified from *mobAB(-)* and *mobA(-)* strains [64]. Leimkühler and Rajagopalan were also able to reconstitute inactive hSO by incubating Moco-free hSO with cPMP, MPT synthase and molybdate [109]. Recently, this approach was expanded by Kaufmann *et al.* [126] who reported the extraction of an intact bis-MGD form of the cofactor from FDH (*fds* operon). The extracted FDH bis-MGD cofactor is stable outside of the protein environment for up to 90 min under anoxic conditions. Kaufmann reconstituted apo-TMAOR with the extracted FDH cofactor to restore activity similar to the anaerobically expressed and purified holoenzyme [126]. Similarly, Kaufmann was also able to reconstitute apo-TMAOR with Moco extracted from XDH to produce an active TMAOR enzyme. A caveat to this method of reconstitution is efficiency, as the ratio of apoenzyme to the reconstituted enzyme is still high.

1.4.2.2 Metal Loading

Metal loading is an important factor in the biosynthetic scheme because Moco is only inserted into the target protein after the cofactor synthesis is complete. As mentioned, the expression strain must have all the components necessary to create the cofactor. In the case of *E. coli* BL21 (DE3), crucial components are missing. Such strains are less valuable for the expression of catalytically active redox enzymes such as NR or XO [27]. Leimkühler *et al.* expressed XDH in a mutant strain without *moeA*, an important Moco biosynthetic gene responsible for inserting molybdate into MPT and reported purification of inactive XDH [48]. This is consistent with Pinske's [27] and Yang's [50] observations of the *E. coli* BL21 (DE3) expression strain. Interestingly, supplementation of high molybdate concentrations revived the activity of XDH but not the bis-MGD containing enzymes, NR and DMSOR [48].

Proper metal loading is heavily influenced by REMPs as was observed in the heterologous expression of *Comamonas acidovorans* XDH in *E. coli* [69] and in *Pseudomonas aeruginosa* [127]. *C. acidovorans* XdhAB in the presence of *P. aeruginosa* XdhC had high metal loading in both expression systems, while *C. acidovorans* XdhAB in the absence of *P. aeruginosa* XdhC had significantly lower Mo incorporation (Table 1.8) [69, 127]. The exact roles of the REMPs and the benefits of coexpressing them are discussed in Section 1.4.2.5.

In addition to difficulties in proper metal loading, there is also the risk of losing metal during purification especially if a His-tag is used. His-tags are known for stripping metals from proteins [128] and causing additional problems with protein characterization [55, 101]. Temple *et al.* demonstrated the effect of the His-tag on the purification of SO [57]. The untagged SO had higher molybdenum incorporation (80%) than the His-SO (62%) (Table 1.7). Kinetic parameters were not significantly different: untagged SO had a K_M of 10.4 μ M while His-SO had a K_M of 12.1 μ M (Table 1.12) [57]. Other than metal stripping, the His-tag did not appear to interfere with catalysis. Pollock *et al.* [55] also reported Mo loss due to the His-tag. A comparison of His-tagged and GST-tagged Euk-NR from spinach revealed Mo incorporation of 44% and 93%, respectively [55]. Despite the potential metal stripping by the His-tag, many molybdopterin enzymes have been purified with non-cleavable His-tags and still retained over 50% Mo incorporation (Tables 1.6-1.10). Ivanov *et al.* [127] and Yu *et al.* [129] reported Mo incorporation of nearly 90% for XO family enzymes. In contrast, Sabaty *et al.* demonstrated a C-terminal His-tag was detrimental to the activity and yield of YedY although metal stripping was not discussed. Through modeling studies, it was suggested that the addition of a hydrophilic affinity tag may destabilize the terminal hydrophobic residues and impair YedY folding and activity [101]. Sabaty *et al.* successfully engineered a TEV cleavable His-tag between the TAT leader sequence and the YedY sequence that improved expression of active enzyme (Table 1.1) [101]. The effect of the His-tag is enzyme specific and does not appear to strip Mo or impact activity in every case.

1.4.2.3 Modification of the Molybdenum center

Moco is created in the same general biosynthetic pathway (Figure 1.2) in most organisms. At the end of the biosynthetic path, Moco is modified for its specific target protein before being inserted into that target. For example, the Moco-oxo core is modified to Moco-sulfido as in XO. The enzyme, XO, is only active when Moco is sulfurated, which is typically conducted by Moco sulfurase. Yamaguchi and coworkers expressed XO in *E. coli* JM109 cells at 30°C with low IPTG concentration (0.05 mM) and reported that 80% of the expressed enzyme was inactive due to the presence of desulpho- and demolybdo- forms (Mo incorporation was 36%). The need to coexpress the human XO with the human Moco sulfurase gene and/or chaperone XdhC is a potential approach to offset the low activity [66]. In an attempt to increase sulfuration as well as active

protein produced, Moco sulfurase was supplemented during expression with mixed results [104-106].

Schumann *et al.* [106] attempted to overcome the problem of low Mo incorporation and low sulfuration when expressing eukaryotic AO in prokaryotic hosts. They coexpressed the mouse AO with a Moco sulfurase in *E. coli* TP1000 and expressed the cells at a temperature of 30°C for 24 hours. Their approach proved to be successful, as there was a 50% higher level of the terminal sulfido ligand of Mo, although only 20% of the purified enzyme was in the catalytically active form [106]. It was expected that enzymatic activity linearly correlates with the level of terminal sulfido ligand present in Mo, which is not the case. The difference in observed activity may be interpreted as either the need for optimizing the expression conditions, the inability of prokaryotic hosts to process the cofactor properly, or enzymatic handling as the enzyme is expected to be oxygen sensitive. The recombinant enzyme displayed K_M values close to the K_M of the native mouse enzyme previously published. However, the recombinant enzyme was only 20% as active as the natively isolated enzyme with respect to several aldehydes including benzaldehyde. Later they were able to increase the active form to 30% in purified proteins [105].

Hartmann and coworkers [104] also coexpressed human AO and human Moco sulfurase; however, an analysis showed no increase in the levels of sulfurated Mo-MPT. The authors isolated the target protein in a low yield which they suggest is influenced by the difference in codon usage between humans and *E. coli*. They concluded that when heterologous expression systems are used the terminal sulfido ligand is problematic. Loss of the terminal sulfido ligand is the main issue when attempting to obtain a fully active mammalian Mo enzyme. Only 30% of the isolated protein was in the active form. While 60% of the isolated protein did contain Mo, only half of the Mo containing enzyme included the terminal sulfur ligand to the Mo-MPT [104].

In the DMSOR family, where Mo is coordinated by two MPT groups, there is variation in the reports of the terminal 6th ligand. DMSOR contains an oxo group in this position while Nap [130], FDH [90], and TMAOR [126] have a sulfido terminal ligand not an oxo-group. In recent studies of TMAOR [126], the terminal ligand was determined to be dependent on expression and purification conditions. Kaufmann *et al.* compared the TMAOR enzyme expressed aerobically and purified aerobically (+O₂^{exp}/+O₂^{pur}) to enzyme expressed anaerobically and purified aerobically (-O₂^{exp}/+O₂^{pur}) and to enzyme expressed anaerobically and purified anaerobically (-O₂^{exp}/-O₂^{pur}). They concluded that aerobic conditions oxidize the bis-MGD cofactor resulting in an oxo group

instead of the natural sulfido ligand. While both forms are active, the oxo containing aerobically obtained enzyme was only ~5% as active (as judged by the specific activity values) as the sulfido containing anaerobically obtained enzyme [126].

In addition to the terminal ligand, Moco is also modified by ligation of the protein to the metal center during the insertion process. Little is known about the insertion process, except that it may be more specialized by specific chaperones for individual target enzymes [131]. In the XO and DMSOR families, Moco is modified at the MPT phosphate group by nucleotide addition and these families are suspected to have a dedicated chaperone that inserts Moco into the enzyme. For example, TorD is the dedicated chaperone for the catalytic subunit TorA of TMAOR that is predicted to be involved in Moco insertion [132, 133]. The SO family has the unmodified MPT form of Moco and thus is believed to not require a dedicated chaperone [19]. It is postulated that MoeA, another protein in the biosynthetic pathway, may be able to directly insert the MPT form of Moco into the target enzyme [134]. These chaperones will be discussed in more detail in Section 1.4.2.5. While it is believed that the target protein is partially unfolded until Moco is inserted, the mechanism by which Moco is transferred and coordinated by the protein has not been completely elucidated. Mutagenesis experiments [54, 67, 135] informed that Moco can still be incorporated into the target enzyme even without the coordinating residue present. Therefore, it is logical to assume that amino acid residue coordination occurs after Moco insertion. An intact first Mo coordination sphere is essential for the full activity of each of these enzymes.

1.4.2.4 Incorporation of Additional Prosthetic Groups

The expression host must synthesize and insert not only Moco but also the other prosthetic groups that the multitude of molybdenum enzymes and their electron transfer partners rely on. Among these groups are iron-sulfur clusters, hemes, and flavins (Figure 1.3). The addition of these prosthetic groups adds another layer of complexity to the various processes the host must be able to perform to produce active molybdenum enzymes. Due to a large number of catalytic ligands of Euk-NR (FAD, *b*-type cytochrome and Moco), for instance, the complete enzyme complex has not been expressed in *E. coli* [55]. Pollock *et al.* were able to successfully express the Moco domain of spinach Euk-NR by adapting Temple and coworkers' protocol [57] for hSO expression in *E. coli* TP1000 cells. Barbier and coworkers [136] created a simplified Euk-NR fragment of the yeast *Pichia angusta* NR denoted S-NaR1. The protein was expressed in large quantities by fermentation

in yeast *Pichia pastoris*. This expression system was easier to produce and purify an active NR segment that is more stable than the holo-NR due to its smaller size and low complexity with Moco as its only cofactor.

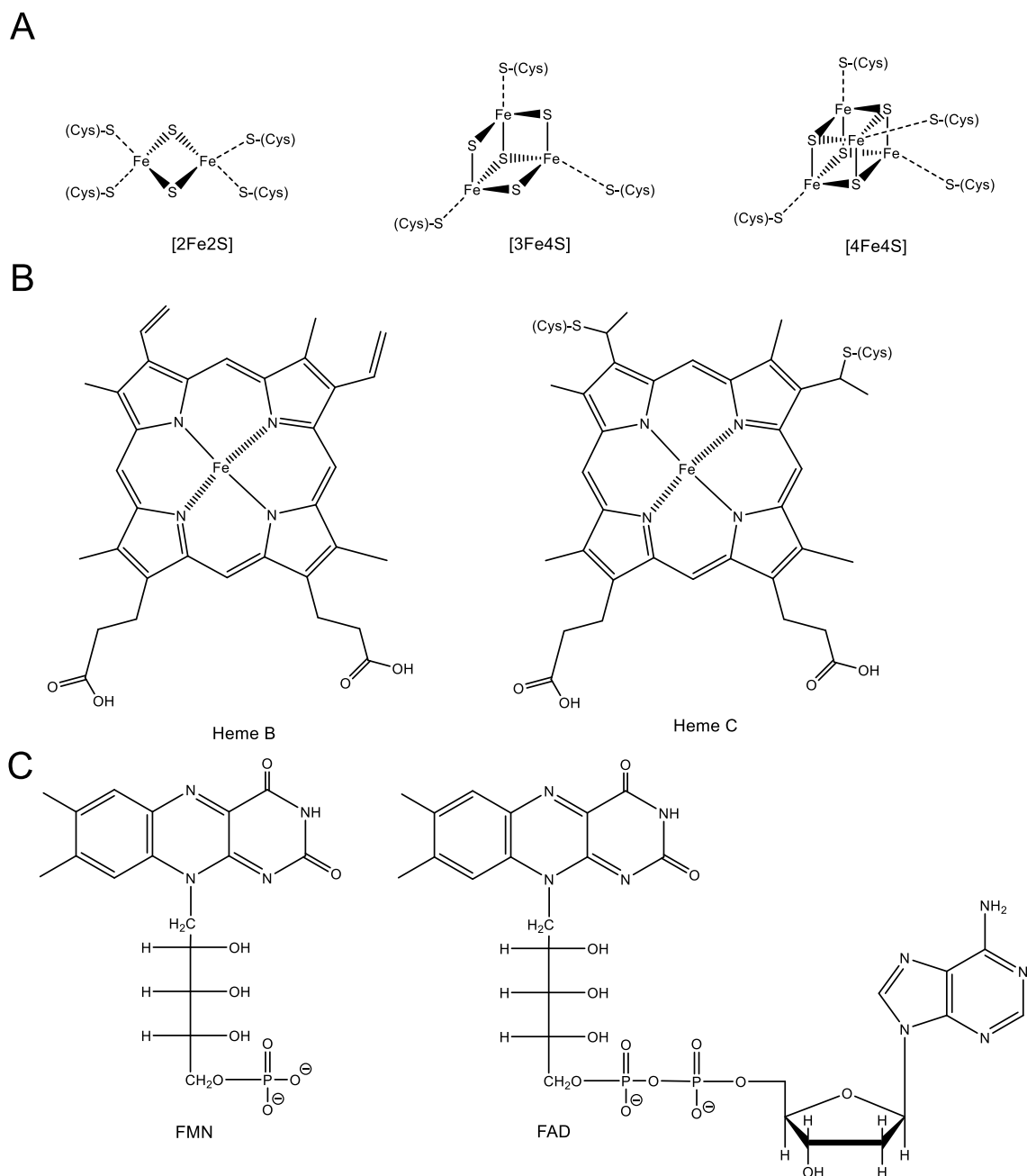


Figure 1.3: Common prosthetic groups in molybdopterin enzymes. A) iron sulfur clusters: [2Fe2S] on the left, [3Fe4S] in the center, and [4Fe4S] on the right; B) heme groups: heme B on the left and heme C on the right; C) flavin groups: FMN on the left and FAD on the right.

Studying molybdopterin enzyme systems in pieces as was completed for Euk-NR reveals valuable information. However, a full picture can only be obtained once all the components are functioning in concert. To better equip the desired expression systems, a greater understanding of the synthesis and the players involved in the production pathways for the other prosthetic groups that exist in Moco enzymes is necessary.

1.4.2.4a Iron-Sulfur Cluster Containing Molybdopterin Enzymes

The most common prosthetic group in Moco enzymes is the iron-sulfur cluster. Three forms of iron-sulfur clusters are found in Mo enzymes, namely [2Fe2S], [3Fe4S], and [4Fe4S] (Figure 1.3A). The same general pathway can produce all three forms. In bacteria, iron-sulfur clusters are assembled by the iron-sulfur cluster assembly (ISC) machinery and/or the sulfur mobilization (SUF) system. Eukaryotes have ISC and SUF homologs in addition to their own cytosolic iron-sulfur protein assembly (CIA) machinery [137-139].

The initial step of iron-sulfur cluster assembly in prokaryotes involves an L-cysteine desulfurase (IscS and SufS, respectively) that activates sulfur. L-cysteine donates the sulfur group to the protein creating L-alanine and a protein-bound persulfide intermediate. In the ISC pathway, IscS interacts with its scaffold protein IscU, where iron and sulfur are assembled into [2Fe2S] or [4Fe4S] clusters [138, 140-142]. Agar *et al.* reported sequential cluster assembly with the initial IscU product containing one [2Fe2S]²⁺ cluster per dimer. Then converting to a form containing two [2Fe2S]²⁺ clusters per dimer and finally to a form that contains one [4Fe4S]²⁺ cluster per dimer [142]. Both cluster types are reductively labile in IscU and are degraded within minutes upon exposure to air. The ISC pathway, IscU and IscS proteins, in particular, have been widely conserved [142].

Additionally, other ISC interacting partners have been reported including ferredoxin, HscA, HscB, IscA, CyaY, and IscX [140, 141]. Ferredoxin is a [2Fe-2S] cluster-containing protein likely involved in electron-transfer to reduce S⁰ to S²⁻ during cluster assembly. HscA and HscB are chaperones that interact with IscU facilitating cluster transfer to apo-protein targets. IscA binds iron or an iron-sulfur cluster, although the exact role is unknown [141]. The involvement of CyaY and IscX is controversial [140], and a trafficking role has been proposed for IscX. However, direct evidence has been lacking [141].

In the SUF pathway, the L-cysteine desulfurase SufS interacts with the sulfur acceptor protein SufE. SufE enhances SufS activity. SufB most likely accepts the sulfur from SufE then together with SufC and SufD, iron-sulfur clusters are assembled on SufB [138, 140]. The SufBCD complex serves as a scaffold for the assembly of a transient iron-sulfur cluster akin to IscU [141]. Once the clusters are produced, they can then, in turn, be transferred from the scaffold protein complex to the target proteins.

In the eukaryotic CIA pathway, sulfur is not obtained via a dedicated cysteine desulfurase. Instead, the CIA relies on the mitochondrial export of a sulfur-containing compound, 'X-S', the identity of which is currently unknown. The compound X-S has been suggested to be glutathione-complexed to an iron-sulfur cluster [138]. The iron-sulfur clusters are assembled into the tetrameric complex formed between proteins CFD1 and NBP35, which acts as a scaffold complex bridging the clusters between the CFD1 and NBP35 subunits [138].

Heterologous production of iron-sulfur containing enzymes in *E. coli* is hindered by low expression level, protein degradation, insufficient cluster assembly, and cluster degradation. The biggest challenge for iron-sulfur containing Moco enzyme production is the degradation of the cluster. Iron-sulfur clusters degrade in air readily. While adding a reducing agent, such as dithiothreitol (DTT), to enzyme buffers does help, it cannot prevent oxidation over time. Preferably, the enzymes should be purified anaerobically under an inert atmosphere [143]. Some groups have now benefitted from boosting iron-sulfur assembly by the addition of plasmids, such as pRKISC plasmid, that contain the *E. coli isc* locus [143-145]. Furthermore, there are reports to reconstitute iron-sulfur clusters both semi-enzymatically and chemically [137, 146-148].

Chemical reconstitution requires a thiol-specific reductant, an iron source, a sulfide salt, and a reconstitution buffer (50 mM Tris-HCl pH 8.0–8.3, 0–150 mM NaCl, 0%–10% glycerol, supplemented with the thiol-specific reductant). Reconstitution begins with a reduction of the apoenzyme, then 2-8-fold excess of Fe is added and incubated for 5 minutes followed by addition of the sulfide salt (at the same concentration as Fe). The reaction mixture incubates for another 2-3 hours before excess Fe and sulfide are removed with a desalting column [137]. For example, Sjuts *et al.* [147] chemically reconstituted the [4Fe4S] clusters in the reductive dehalogenase PceA by first reducing apoenzyme with 2% β -mercaptoethanol for 1 h under strictly anaerobic conditions. Then, Na₂S and FeCl₃ were slowly added to a final concentration of 150 μ M each and

reconstitution was carried out for 16 h at 4°C with gentle shaking before dialysis was used to remove excess salt [147].

However, the sulfide salts used in chemical reconstitution are often contaminated by oxidation products of sulfur. Additionally, the reaction rate is more easily controlled in a semi-enzymatic method where the concentration of the desulfurase enzyme can be easily modified and thus sulfide production is easily controlled. The semi-enzymatic method of reconstitution is similar to chemical reconstitution except this method slowly releases sulfide from cysteine using a cysteine desulfurase. The apoenzyme is treated with Fe, DTT, cysteine, and the desulfurase enzyme where sulfide is transferred to the enzyme from cysteine, and DTT mediates the reductive release of sulfide from the desulfurase [137]. For instance, Wachnowsky *et al.* [148] semi-enzymatically reconstituted the [2Fe2S] cluster in human enzyme BOLA3 where 200 μ M BOLA3 was mixed with 2 μ M of the desulfurase NifS, 5 mM DTT, 0.6 mM Fe³⁺, and 0.6 mM L-cysteine. The reaction was incubated for 1 hour before excess salt was removed via a PD-10 desalting column [148].

1.4.2.4b Heme Containing Molybdopterin Enzymes

Along with iron-sulfur clusters, Moco enzymes can contain Fe in the form of heme prosthetic groups. There are two main forms of heme in Moco enzymes, *b*-type and *c*-type hemes (Figure 1.3B). The *b*-type heme is the parent heme molecule of all other hemes [138]. It consists of the basic unmodified tetrapyrrole ring with an iron center. The *c*-type heme is covalently attached to the protein backbone through two thioether linkages at the C3 and C8 atoms via the thiol side chain of cysteine residues [138].

The core pathway of heme synthesis consists of two distinct mechanisms to synthesize the precursor δ -aminolevulinic acid (ALA): First, through the condensation of succinyl coenzyme A (CoA) and glycine by δ -aminolevulinic acid synthase (AlaS) or through the second mechanism utilizing the C₅ skeleton of a tRNA-bound glutamate to generate ALA in a two-step reaction [149]. Most organisms have the following steps conserved for the most part where porphobilinogen synthase creates porphobilinogen (PBG) from two ALA molecules, hydroxymethylbilane synthase produces hydroxymethylbilane (HMB) from PBG, and uroporphyrinogen synthase forms the heme precursor uroporphyrinogen III [149].

The major challenge for the expression of heme-containing Moco enzymes is obtaining high quantities of the holoenzyme. To address the issue of low heme production/incorporation, two primary approaches have been adopted [150-152]. The first is to supplement the media with heme or heme precursors. For example, supplementation of the media with ALA boosts heme production [151]. The second is the engineering of the host strain to enhance intracellular heme production. For example, the *ccm* (cytochrome *c* maturation) gene cassette can be overexpressed with *c*-type heme proteins to boost ligation into the target protein [152].

1.4.2.4c Flavin-Containing Molybdopterin Enzymes

Moco enzymes can also contain flavin prosthetic groups mainly in the form of flavin mononucleotide (FMN) and flavin adenine dinucleotide (FAD) (Figure 1.3C). Both flavins are produced from the precursor riboflavin [153-155]. Although some microorganisms can synthesize riboflavin, animals and other microorganisms must obtain it from their diets. All organisms, including animals, utilize riboflavin in the cell in the formation of FAD and FMN cofactors to be used in various enzymes [154].

In bacteria, riboflavin is synthesized from GTP by GTP cyclohydrolase II which removes C-8 from GTP, producing formate; the enzyme also removes pyrophosphate. The next two steps are the deamination of the amino group at position 2 and the reduction of the ribosyl side chain to ribityl. The resulting pyrimidine precursor is then converted to a pteridine compound followed by condensation with 3,4-dihydroxy-2-butanone 4-phosphate. The final step is catalyzed by riboflavin synthase which involves the exchange of a 4-carbon unit from one molecule of 6,7-dimethyl-8-ribityllumazine to another, thus transforming one of them into riboflavin and the other one into 5-amino-6-ribitylamino-2,4(1H,3H)-pyrimidinedione [154]. Riboflavin is converted into FMN by riboflavin kinase where FMN is produced by phosphorylation of 5' position of the ribityl chain [153-155]. FMN is then converted into FAD by FAD synthase, which catalyzes the transfer of an adenylyl moiety from ATP to FMN [153-155].

Overexpression of flavin-containing Moco enzymes can be optimized by the substitution of native promoters with stronger recombinant promoters upstream of key flavin synthesis genes in the host genome. These substitutions make it possible to obtain strains with a high activity of riboflavin kinase and FAD synthetase. This boosted expression will ensure the accumulation of one or both flavin nucleotides. Additionally, the hydrolysis of FMN to riboflavin can be prevented

by supplementing with a higher level of phosphate or using other inhibitors of nonspecific acid and alkaline phosphatases. However, a better solution might be to eliminate the genes encoding the enzymes that hydrolyze FMN and FAD altogether [155].

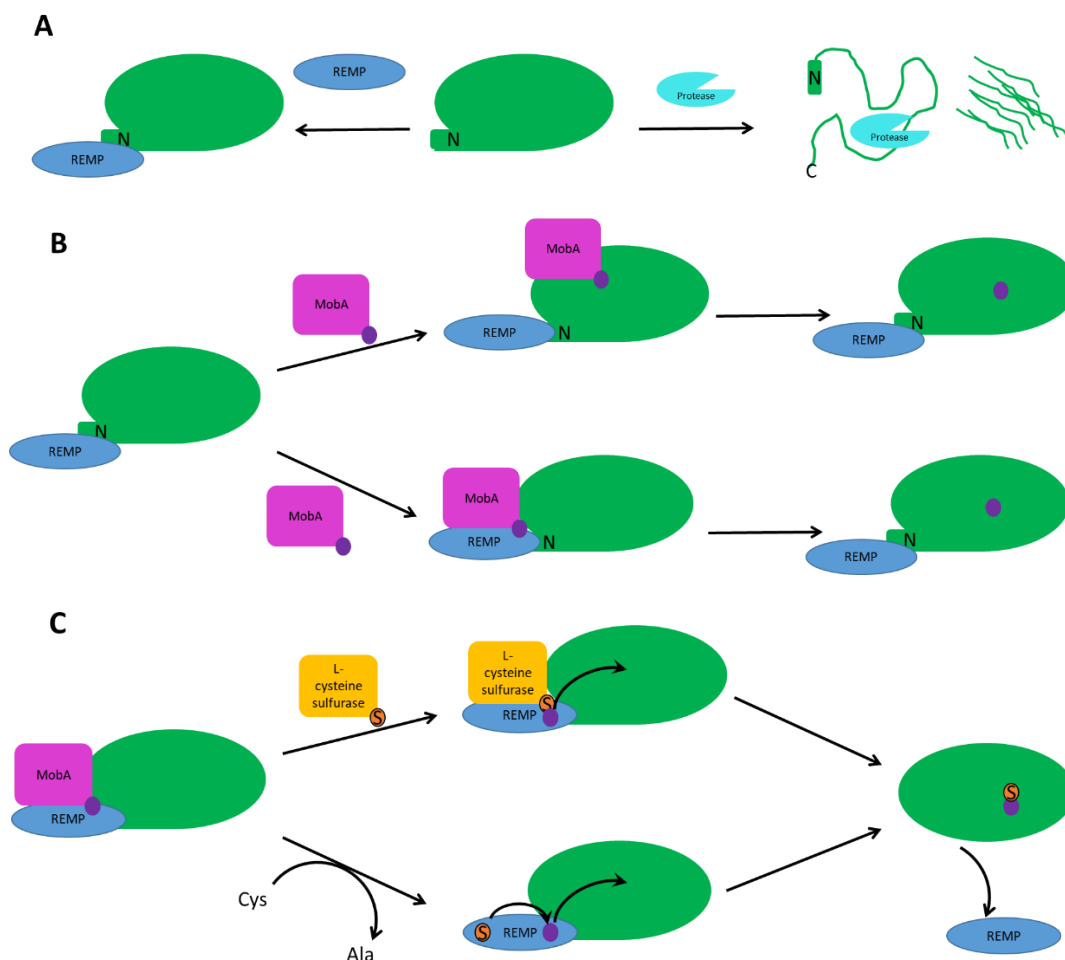
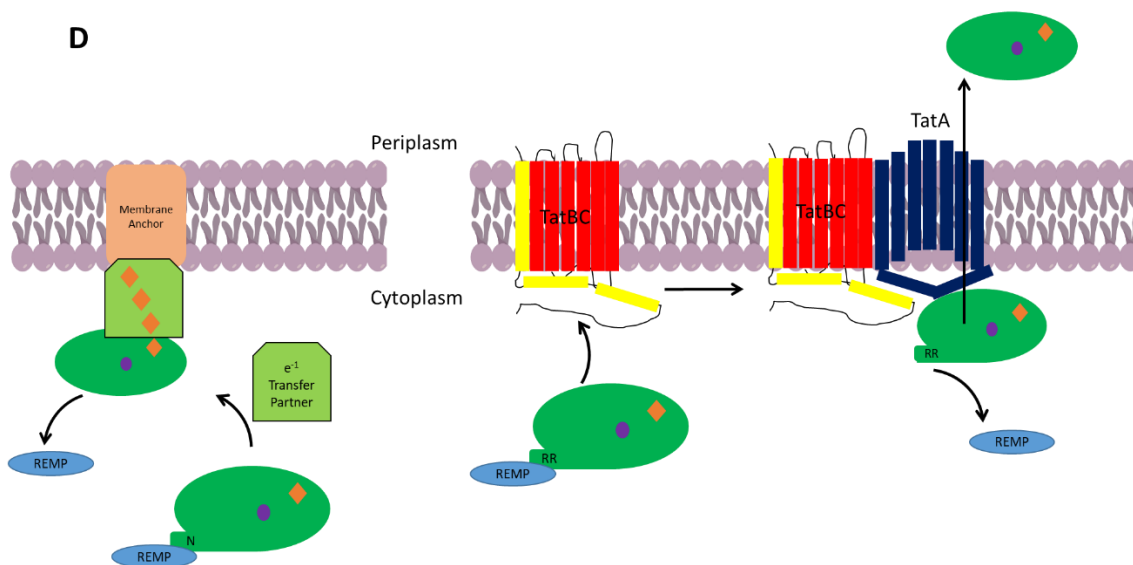


Figure 1.4: The proposed roles of the REMP chaperone in molybdenum enzyme maturation. A) Degradation prevention: REMP binds target enzyme preventing proteolysis. B) Enzyme maturation: Stabilizing enzyme target enabling proper protein folding (top pathway) and/or assisting in cofactor insertion (bottom pathway). C) Moco sulfuration: Interaction with a sulfurase enables the REMP to transfer sulfur to moco before insertion into the target protein (top pathway) or the REMP itself has both a sulfurase domain and a Moco binding domain and generates the sulfur that is transferred to moco (bottom pathway). D) Enzyme translocation and complex assembly: The REMP is involved in targeting the delivery of the enzyme to form a complex and may assist in assembly of the complex (left) or the REMP targets the TAT machinery for protein translocation into the periplasm (right). Green oval is the target molybdenum enzyme, N = N-terminus, C = C-terminus, purple dot represents Moco, orange circle labelled S represents sulfur, orange diamond represents an iron sulfur cluster, and RR represents the TAT leader sequence.

Figure 1.4 continued.



1.4.2.5 Redox Enzyme Maturation Proteins (REMP)

Biosynthetic pathways outlined several important steps in creating mature and active pterin molybdenum enzymes. There are several dedicated chaperones (Table 1.16) in the redox enzyme maturation protein (REMP) family of proteins that assist in the maturation of specific molybdenum enzymes [156]. The most studied REMPs are part of the TorD sub-family and include members such as NarJ, TorD, and DmsD [156]. The TorD sub-family shows a high α -helix content, a cytoplasmic location, a molecular weight between 18-25kda, and an acidic pI [131]. Generally, the REMPs are involved in the maturation of molybdenum enzymes through stabilization, degradation prevention, Moco/cofactor insertion, and/or final translocation to the membrane (Figure 1.4). The importance of the REMP chaperones in overexpression is system dependent. If the host has a similar chaperone that can carry out the role, then the target's specific chaperone may not be needed. However, several systems need the target enzyme to be coexpressed with the chaperone to retrieve active enzyme. The effect of XdhC, for example, on the expression of XDH has been evaluated extensively [48, 49, 69, 116-119, 127]. The Leimkühler group [47-49] studied the homologous expression of XDH in *R. capsulatus*, and it was determined that XdhC seems to have a role in the insertion of Moco after sulfuration [48]. A *nifH* promoter activated under anaerobic conditions in the presence of a nitrogen source was engineered to be upstream to the *xdhABC* genes [47]. The engineered plasmid was transformed into different *R. capsulatus* strains. In an XdhC

mutant, evidence was provided for XdhC as a chaperone protein that is likely to be involved in the insertion of MPT and/or folding of XDH [49]. The active XDH enzyme is only produced in the presence of XdhC [49].

Similarly, Böhmer *et al.* [89] used Hartmann's methods [88] to investigate the role of FDH chaperone protein FdsC. FdsC binds bis-MGD and interacts with catalytic subunit, FdsA, and Moco biosynthesis protein, MobA. It is suggested that FdsC is a scaffold protein that aids in the insertion of Moco into FdsA [89]. Furthermore, Oresnik *et al.* expressed DMSOR in *E. coli* C41 DE3 at 37°C for 8 hours. GST purified DmsA was used to study the role of the chaperone DmsD. DmsD was determined to bind the TAT leader sequence of DmsA and is suggested to be an escort protein for the translocation of DmsA [157].

Several REMPs have been shown to bind the twin-arginine translocase (TAT) leader sequence of their dedicated targets including TorD, DmsD, and NapD [156, 158-160]. These REMPs have similar proposed roles in prohibiting translocation before maturation, cofactor insertion, TAT proofreading and/or escorting the matured enzyme to the TAT machinery [156]. The TAT translocation process is discussed in Section 1.4.3 *Transport of Molybdenum Enzymes*. Some expression systems such as the homologous *E. coli* expression system, rely on the host's natural REMP production. The host already makes a normal amount of the chaperones, so they are present but not overexpressed. Therefore, the REMP could still complete its role and create active protein in these systems (Tables 1.1-1.10).

Other systems may overexpress the whole operon or use the REMP homologs in the host. As stated, *C. necator* Nap is located on the 450-kb mega plasmid pHG1 and not in the organism's chromosomal DNA which, permits easy manipulation of the Nap genes for overexpression [93]. The entire operon is present, and a *C. necator nap* mutant can easily be the host for overexpression without impacting necessary REMPs since the entire operon is present on the overexpression plasmid. However, heterologous systems may need to overexpress the REMPs in addition to the target enzyme. Further studies are needed to fully understand the roles of REMPs and the interactions in these specific expression systems.

1.4.3 Transport of Molybdenum Enzymes

Molybdenum enzymes are found in various locations including in the cytoplasm, the periplasmic space, and integrated into the membrane. The expression of the cytoplasmic enzymes

in the cytoplasm is usually desirable due to high protein yields and ease of access via common lysis procedures [26]. Many molybdenum enzymes are associated with the membrane which may add additional challenges for isolation. The addition of an artificial signal sequence to send the recombinant protein to the periplasm has been an effective method in the isolation of recombinant proteins [161]. There are several natural periplasmic molybdenum enzymes as well including TMAOR, DMSOR, Nap, periplasmic AO, etc. For these reasons transport of Mo enzymes, whether for the function or simply to streamline isolation, is an essential capability the host requires for successful expression.

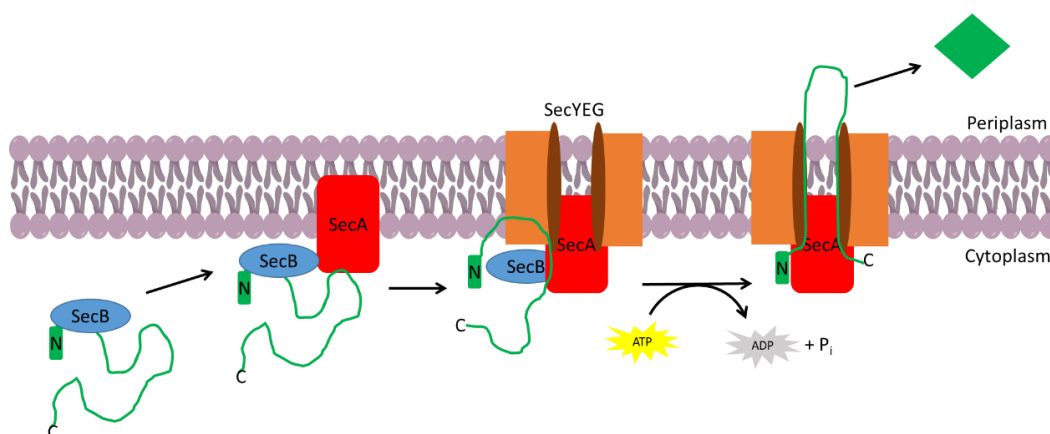


Figure 1.5: A general scheme of the SecT pathway where unfolded peptides are transported across the membrane to be folded in the periplasm. N = N-terminus, C = C-terminus, and green diamond is the properly folded target protein.

Transport of recombinant proteins to the periplasm follows host secretion pathways. Two common pathways used in *E. coli* and bacterial hosts are the well-documented secretion (SecT) translocase pathway (Figure 1.5) and the twin-arginine translocase (TAT) pathway (Figure 1.6) [162-164]. Periplasmic recombinant protein isolation has several advantages, including a lower number of protein contaminants in the periplasm, as well as the presence of an authentic N-terminus in the target protein and decreased proteolysis [165]. The SecT pathway transports unfolded protein via recognition of a periplasmic leader sequence that usually has 10 to 20 mostly hydrophobic amino acids at the amino-terminus [165]. The leader sequence is cleaved upon translocation and the protein folded in the periplasmic space. The TAT system is independent of the SecT translocase and is capable of secreting folded proteins that contain a twin-arginine motif

near the amino-terminal [165]. The efficiency of the periplasmic secretion of recombinant proteins depends on the host strain, signal sequence, and the type of protein to be secreted [165].

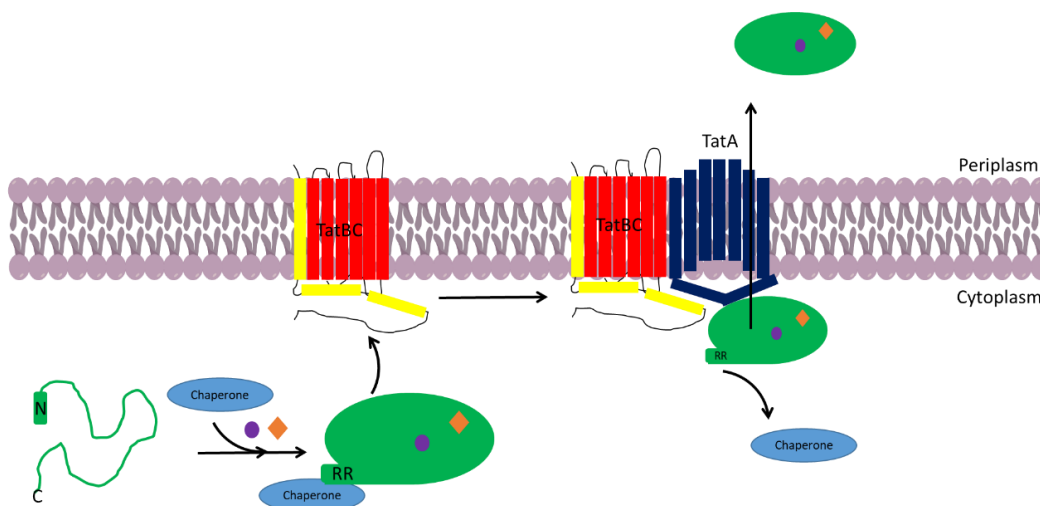


Figure 1.6: A general scheme of the TAT pathway where peptides are folded in the cytoplasm and cofactors are inserted before the mature folded enzyme is transported across the membrane into the periplasm. Green oval is the target molybdenum enzyme, N = N-terminus, C = C-terminus, purple dot represents Moco, orange diamond represents an iron sulfur cluster, and RR represents the TAT leader sequence.

Molybdenum enzymes that are naturally secreted into the periplasm rely mostly on the TAT system (Figure 1.6). Such enzymes are complex and require multiple cofactors to be inserted before translocation. As such, quite a few homologous expression cases have been reported where periplasmic isolation is utilized when purifying the enzyme from its natural organism [61, 63, 70, 71, 101, 130, 166-171]. There have been limited instances where heterologously expressed enzymes have been isolated from the periplasm or any obstacles with the TAT systems of a non-natural host have been mentioned. TAT processing is prevalent in many bacterial species; however, the signal peptides recognized by the TAT machinery seem to be species specific. Hilton *et al.* expressed inactive *R. sphaeroides* DMSOR in *E. coli* which suggests that differences in the signal sequence between the two organisms may prohibit protein maturation and translocation processes [92]. Investigations of the impact of the signal peptide were conducted by comparing enzyme devoid of a signal peptide to the enzyme that had either the *E. coli* or the *R. sphaeroides* signal peptide [54]. *R. sphaeroides* DMSOR expressed with the highest activity when no signal peptide was present suggesting that *E. coli* indeed had difficulties recognizing the *R. sphaeroides*

signal. Interestingly, the *E. coli* signal peptide was not enough for the TAT processing to proceed efficiently, perhaps due to the absence of a necessary *R. sphaeroides* TAT chaperone. Sabaty *et al.* observed different results when investigating the TAT signal peptide of YedY [101]. For YedY, expression of the enzyme without the signal peptide results in inactive insoluble protein. The *R. sphaeroides* signal was necessary for heterologous expression in *E. coli* which differs from Hilton's observations. They suggested the signal sequence's role in maturation can differ between enzymes and is most likely species dependent.

Protein signal peptides and translocation are a definite factor to keep in mind when designing an expression system of periplasmic Mo enzymes. Signal peptides are commonly composed of three distinct components. The positively charged n-region on the N-terminus approximately 1–5 residues long, a central hydrophobic region (h-region) approximately 7–15 residues long, and a c-region on the end of the peptide closer to the C-terminus that is approximately 3–7 residues long make up a signal peptide. The cleavage site for the signal peptidase is located in the c-region [172]. It is impossible to predict the optimal signal peptide for the overexpression of a specific target protein. However, *in silico* analysis has progressed to speculate a few trends such that good-performing signal peptides have a higher charge/length ratio in the n-region and have a much higher proportion of coils [172].

Besides being required for translocation by the respective protein translocases, signal peptides also impact the biosynthesis, folding, and stability of the respective target proteins [161]. Typically, the recombinant protein is expressed at high levels which can lead to saturation of the translocase machinery resulting in very low recombinant protein yields, or, in extreme cases, the desired target proteins were not secreted at all [161, 173]. It is conceivable that in a non-physiological situation the processing of transportation across the membrane is responsible (e.g. by saturation of the signal peptidase that cleaves the leader sequence) [174]. Furthermore, overexpression of a translocation-incompatible substrate (e.g., proteins containing a non-optimal secretion tag) can be toxic for hosts such as *E. coli* [175].

Protein secretion in heterologous systems is a complex process that may face several obstacles such as incomplete translocation, insufficient capacity of the export machinery, and proteolytic degradation. It has been reported that protein size as well as the amino acid composition of the leader peptide and of the target protein may influence secretion efficiency. An optimum rate of translation to achieve high-level secretion of heterologous proteins may also be important as

observed by secretion diminishing severely at higher rates [176]. This effect is most often caused by a limited secretion capacity of the host transport machinery, which may result in the excess recombinant protein accumulating in inclusion bodies. Therefore, it is important to optimize the expression level by carefully balancing the promoter strength and plasmid replication levels. In addition, the coexpression of the translocation components may increase transport capacity. Competition from native proteins transported by the host system can cause a severe production bottleneck in any system. Low protein translation rates will prevent saturation of the transport machinery, which may be beneficial in the TAT pathway as it is less efficient and slower than the SecT pathway with transit times in the order of a few minutes compared to a few seconds. Additionally, the energy cost of translocation by the TAT pathway may be excessive for high-level secretion and may explain its inherent low capacity [176]. In the past few years, it has become increasingly clear that an optimally designed signal peptide has to be identified in order to ensure that the respective host's translocation machinery will allow the best possible protein secretion yields [161].

1.5 The Chosen Molybdenum Enzyme for Study

For this venture, periplasmic nitrate reductase has been chosen to investigate the chemistry and mechanism surrounding Moco in order to determine any common themes between the members of this diverse class of enzymes. Specifically, the implications of molybdenum coordination on activity in enzymes from the DMSOR family has been explored. Periplasmic nitrate reductase, Nap, is an excellent candidate to explore how exchanging the ligands of the Mo center impact activity. There is ambiguity and controversy already in the assignment of Nap's first coordination sphere, particularly the terminal ligand. Nap has a Mo center coordinated by four sulfurs from the two MPT ligands in addition to the coordinating amino acid Cys as the fifth ligand and a sixth ligand that is controversially assigned as a sulfido group (Figure 1.7). Thus, Nap can be used to probe both the coordinating residue and the terminal ligand controversy of sulfido vs oxo as the sixth ligand. Only a handful of Nap enzymes have been over expressed and kinetically analyzed (Table 1.15).

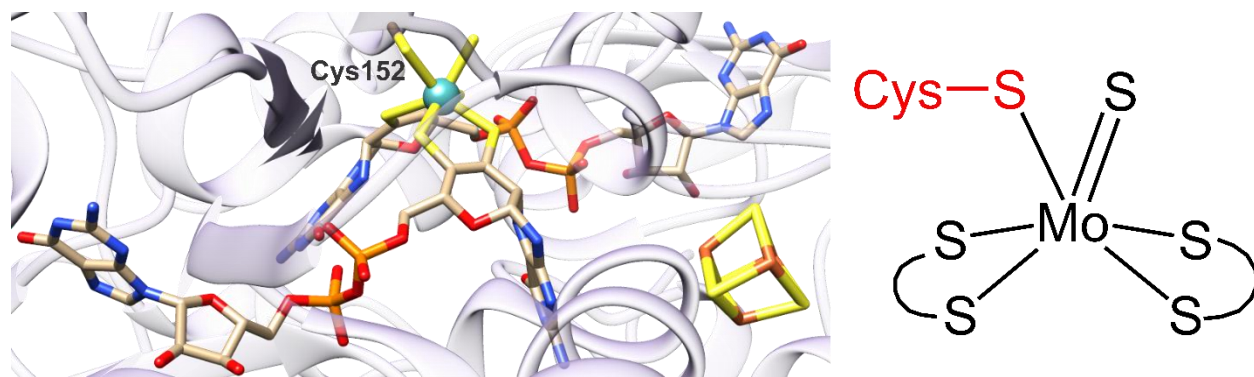


Figure 1.7: The currently proposed first Mo coordination sphere in *Cupriavidus necator* Nap. Left panel, the crystal structure of *C. necator* NapAB (PDB 3ML1); right panel, the line drawing schematic of the first Mo coordination sphere in *Cupriavidus necator* NapA.

Furthermore, Nap was chosen for the broad impact of nitrate and nitrate reductase on the physiology of microbes, health, and the environment. Nap is a significant player in the electron transport chains and respiration pathways of many microbes including several notable pathogens. Nap catalyzes the reduction of nitrate to nitrite at its molybdenum center in a two-electron process. *Epsilonproteobacteria* contain the largest predicted Nap and yet no *Epsilonproteobacterial* Nap have been isolated. *Campylobacter jejuni* Nap will be isolated as a representative *Epsilonproteobacteria* as it also has a significant impact on health. Nitrate reduction has been shown to impact the pathogenicity (i.e. increase the virulence) of several enteric pathogens including *Salmonella*, *E. coli*, and *Campylobacter*. Thus, there is significant interest in the area of nitrate reduction, specifically in *Campylobacter jejuni*.

1.6 Objectives and Project Outline

With various modifications of the coordination site of molybdenum, members of the DMSOR family catalyze a variety of reactions with the same Moco foundation (Figure 1.1A) [4]. The DMSOR family of enzymes vary in the first coordination sphere of the molybdenum active site (Figure 1.1B), e.g., respiratory nitrate reductase, NarG, has an aspartate instead of a cysteine coordinating to the molybdenum center. Such differences at the molybdenum center consequently have mechanistic repercussions. The diversity of the coordinating amino acid led to the hypothesis that these diversities in the coordination sphere set a preference for the substrate transformation. The diversity exists primarily in two ligands of the the Mo center in the DMSOR family of

enzymes (Figure 1.1B). Specifically, the fifth ligand representing the amino acid ligand and the sixth ligand representing the terminal position. The fifth ligand varies between Cys, SeCys, Ser, Asp, or a hydroxyl ligand while the sixth ligand varies between a sulfur, oxygen, or selenium atom [15].

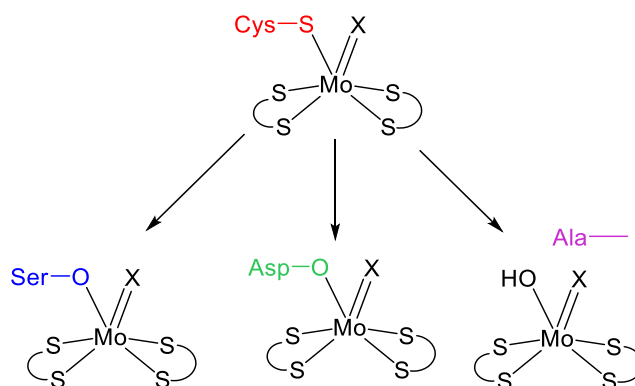


Figure 1.8: The proposed coordination environment of *C. jejuni* NapA (at the top) with the native coordinating Cys (red) where X is unassigned and may be a sulfido or an oxo group. Below the arrows are the three proposed variants that will be created by site directed mutagenesis: the Ser variant (blue), the Asp variant (green) and the Ala variant (magenta).

The objective of this study is to use periplasmic nitrate reductase (Nap) as a vehicle to understand the substrate preference and delineate the mechanistic underpinning of these differences. Specifically, the goal is to develop a fundamental understanding as to how these perturbations at the molybdenum center influence the function of specific members of the DMSOR family. *Campylobacter jejuni* Nap catalytic subunit NapA has been chosen as the molecular platform that can be utilized to test the putative tailored reactivity of the Moco center. The specific aims for this study are 1) clone, heterologously express, and biochemically characterize *C. jejuni* NapA, and 2) determine substrate selectivity by the members of the DMSOR family using wild-type recombinant NapA as a model where the coordinating cysteine residue will be exchanged for a serine, aspartate, and alanine (Figure 1.8). The catalytic activity of these variants under steady-state conditions will be determined using spectrophotometric assays with substrates NO_3^- , DMSO, and TMAO. This foundational information will help develop a better understanding of the reactivity of the DMSOR family and increase the knowledge of nitrate reduction in *Epsilonproteobacteria* specifically in *C. jejuni*. *Epsilonproteobacteria* are of interest because this class of bacteria can respire on nitrate with Nap as the only NR expressed. Additionally,

Epsilonproteobacteria is a highly conserved subclade of NapA enzymes with a sequence identity of 60% or greater [16].

The molecular cloning, expression, and isolation of *C. jejuni* NapA will be presented in Chapter 2. The biochemical characterization and nitrate steady-state kinetics of the native NapA enzyme in context of *C. jejuni* physiology will be presented in Chapter 3. The structure and function of the molybdenum center in the NapA active site will be discussed in Chapter 4. The mutagenesis studies for production and characterization of the coordinating residue variants will be presented in Chapter 5. Chapter 6 will summarize the results of each aim and discuss the impact of this study on the current understanding of molybdenum enzymes and nitrate reduction in *Epsilonproteobacteria*, specifically in the context of *C. jejuni*.

Table 1.1: Expression parameters for recombinant eukaryotic XO family enzymes.

<u>Protein Expressed</u>	<u>Expression System</u>	<u>Plasmid System</u>	<u>Expression Medium</u>	<u>Inducer</u>	<u>Inducer Concentration (mM)</u>	<u>OD600 at Induction</u>	<u>Induction Time (hours)</u>	<u>Induction Temperature (°C)</u>	<u>Amendments</u>	<u>Ref.</u>
<i>A. thaliana</i> AO	<i>E. coli</i> BL21 (DE3) pLysS	pEX5-CT/TOPO TA	N/M ^a	IPTG	1	N/M ^a	24	18	N/M ^a	[58]
<i>A. thaliana</i> AO	<i>Pichia pastoris</i>	pPICZC	BMGY medium	methanol	0.50 ^m	N/M ^a	0-48	30	l	[177]
<i>A. thaliana</i> AO	<i>Pichia pastoris</i>	N/M	BMMY	methanol	0.50 ^m	2-3	10	28	l	[178]
<i>A. thaliana</i> AO	<i>Pichia pastoris</i>	pPICZC	BMGY medium	methanol	0.50 ^m	N/M ^a	0-48	30	l	[179]
<i>D. melanogaster</i> AO	<i>E. coli</i> TP1000	pTrcHis	N/M ^a	N/M ^a	N/M ^a	N/M ^a	N/M ^a	N/M ^a	N/M ^a	[107]
Human AO	<i>E. coli</i> TP1000	pQE-30 Xa	TB	IPTG	1	0.4	72	RT ⁿ	f	[103]
Human AO	<i>E. coli</i> TP1000	pQE-30 Xa	LB	IPTG	0.020	N/M ^a	24	30	b	[104]
Human AO	<i>E. coli</i> TP1000	pTrcHis (using codon optimized AO gene)	LB	IPTG	0.020	N/M ^a	24	30	b	[180]
Monkey AO	<i>E. coli</i> M15	pQE-30Xa/pQE-60	LB	IPTG	1	0.5-0.6	72	22	h	[181]
Monkey AO	<i>E. coli</i> M15	pQE-30 Xa	LB	IPTG	1	0.6	72	22	N/M ^a	[182]
Chimeric monkey-rat AO	<i>E. coli</i> M15	pQE-30 Xa	LB	IPTG	1	0.5-0.6	72	22	i	[183]
Monkey and Rabbit AO	<i>E. coli</i> M15	pQE-30Xa	N/M ^a	N/M ^a	N/M ^a	N/M ^a	N/M ^a	N/M ^a	N/M ^a	[184]
Mouse AO	<i>E. coli</i> BL21	pCW	TB	IPTG	1	1	60	22	i	[59]
Mouse AO	Human (HEK293), mouse (HC11)	pCMVβ	Dulbecco's modified Eagle's medium/RP MI 1640	N/M ^a	N/M ^a	N/M ^a	48 ^a	N/M ^a	j	[185]
Mouse AO	HEK293	pBluescript	N/M ^a	N/M ^a	N/M ^a	N/M ^a	N/M ^a	N/M ^a	N/M ^a	[186]
Mouse AO	<i>E. coli</i> TP1000	pTrcHis	LB	IPTG	0.020	N/M ^a	24	30	b	[106]
Mouse AO	<i>E. coli</i> TP1000	pTrcHis	LB	IPTG	10000	N/M ^a	24	30	b	[105]
Mouse AO	mouse (HC11)	pCMVβ	RPMI 1640	N/M ^a	N/M ^a	N/M ^a	48	N/M ^a	j	[187]
Pig Liver AO	<i>E. coli</i> M15	pQE-30 Xa	TB	IPTG	1	0.4	72	37	k	[188]
Rat AO	<i>E. coli</i> M15	pQE-30 Xa	LB	IPTG	1	0.5-0.6	72	22	i	[189]
<i>Arabidopsis thaliana</i> XO	<i>Pichia pastoris</i> KM71 mutants	pPICZA	BMGY	methanol	0.50 ^m	2.0-3.0	16-20	30	f	[190]
Bovine XO	Sf9 insect cells-baculovirus	pJVP10Z	IPL41	N/M ^a	N/M ^a	N/M ^a	48	27	c	[191]

Table 1.1 Continued

<u>Protein Expressed</u>	<u>Expression System</u>	<u>Plasmid System</u>	<u>Expression Medium</u>	<u>Inducer</u>	<u>Inducer Concentration (mM)</u>	<u>OD600 at Induction</u>	<u>Induction Time (hours)</u>	<u>Induction Temperature (°C)</u>	<u>Amendments</u>	<u>Ref.</u>
<i>Drosophila melanogaster</i> XO	<i>Aspergillus nidulans</i>	pGPT-pyrG1	modified minimal media	maltose	N/M ^a	N/M ^a	20	25	N/M ^a	[192]
Human XO	<i>E. coli</i> JM109	pTrc99a	LB	IPTG	0.05	o	N/M ^a	30	b	[66]
Human XO	COS-1 cells	Svpoly vector	N/M ^a	N/M ^a	N/M ^a	N/M ^a	N/M ^a	N/M ^a	N/M ^a	[193]
Human XO	<i>E. coli</i> BL21 derivatives	pET3a	N/M ^a	N/M ^a	N/M ^a	N/M ^a	N/M ^a	N/M ^a	N/M ^a	[194]
Mouse XO	HC11-C24 & MDA-MB-231 cells	pCMV-Myc	RPMI 1640	N/M ^a	N/M ^a	N/M ^a	N/M ^a	37	e	[195]
Porcine XO	<i>Spodoptera frugiperda</i> (Sf9)	pFastBac (baculovirus)	Grace's insect medium	N/M ^a	N/M ^a	N/M ^a	N/M ^a	27	d	[196]
Rat XO	Sf9 insect cells-baculovirus	pJVP10Z	IPL41	N/M ^a	N/M ^a	N/M ^a	48	27	c	[197]
Rat XO	<i>Spodoptera frugiperda</i> (Sf9)	pJVP10Z/AcNPV virus	IPL41	N/M ^a	N/M ^a	N/M ^a	48	27	c	[198]

a) N/M- Not mentioned; b) 1 mM molybdate; c) 8.3% FBS, 10 μ M riboflavin, 10 μ M guanosine, 80 μ M FeSO₄, 0.5 mM Na₂MoO₄; d) 10% FBS, 10 mM riboflavin, 10 mM guanosine, 80 mM FeSO₄, 0.5 mM Na₂MoO₄; e) 2 mM L-glutamine, 2 g/L NaHCO₃, pH 7.4, 1X of antibiotic /antimycotic solution, 5 ug/ml insulin, 10% FBS; f) 1% yeast extract, 2% peptone, 100 mM potassium phosphate, pH 6.0, 1.34% yeast nitrogen base without amino acids, 0.04% biotin, 1% glycerol; g) 1 g/ml riboflavin, and 50 M Na₂MoO₄, 250 μ l of trace element solution; h) 1 g/ml riboflavin, and 50 M Na₂MoO₄, 250 μ l of trace element solution; i) ATP (1 mM), riboflavin (3 mM), and Na₂MoO₄ (50 mM); j) 10% fetal calf serum, 5 mg/ml insulin, and 10 ng/ml epidermal growth factor; k) 250 ml of trace element solution containing 2.7 g of FeCl₃·6H₂O, 0.2 g of ZnCl₂·4H₂O, 0.2 g of CoCl₂·6H₂O, 0.2 g Na₂MoO₄·2H₂O, 0.2 g of CaCl₂·H₂O, 0.1 g of CuCl₂, 0.05 g of H₃BO₃, and 10 ml of concentrated HCl autoclaved in a total volume of 100 ml of double-distilled H₂O, 1 mg/ml riboflavin, and an additional 50 mM sodium molybdate; l) 1% yeast extract, 2% peptone, 100 mM potassium phosphate (pH 6.0), 1.34% yeast nitrogen base with ammonium sulfate, 4x10⁻⁵% biotin, 0.3 mM sodium molybdate; m) inducer concentration in units of (v/v) %; n) RT- room temperature; o) Induction initiated at mid-log phase.

Table 1.2: Expression parameters for recombinant eukaryotic SO family enzymes.

<u>Protein Expressed</u>	<u>Expression System</u>	<u>Plasmid System</u>	<u>Expression Medium</u>	<u>Inducer</u>	<u>Inducer Concentration (mM)</u>	<u>OD600 at Induction</u>	<u>Induction Time (hours)</u>	<u>Induction Temperature (°C)</u>	<u>Amendments</u>	<u>Ref.</u>
<i>Chlamydomonas reinhardtii</i> crARC	<i>E. coli</i> TP1000	pQE80	LB	IPTG	0.01	0.1 ^l	36	22	k	[199]
<i>A. thaliana</i> mARC2	<i>E. coli</i> TP1000	pQE80	LB	IPTG	0.015	0.1	20	22	e	[115]
Human mARC1	<i>E. coli</i> TP1000	pQE80	LB	IPTG	0.015-0.030	0.1	20	22	e	[13]
Human mARC1 & mARC2	<i>E. coli</i> TP1000	pQE80	LB	IPTG	0.015	0.1	20	22	e	[113]
Human mARC1 & mARC2	<i>E. coli</i> TP1000	pQE80	LB	IPTG	0.015-0.030	0.1	20	22	e	[114]
Human mARC1 & mARC2	<i>E. coli</i> SHuffle pLysS pTPR1/HEK 293	pET28a	TB	IPTG	1	0.8	30	20	e	[14]
Human mARC1 & mARC2	<i>E. coli</i> TP1000	pQE80	LB	IPTG	0.015	0.1	20	22	e	[200]
Human mARC1 & mARC2	<i>E. coli</i> TP1000	pQE80	LB	IPTG	0.015	0.1	20	22	e	[201]
<i>A. thaliana</i> NR	<i>Pichia pastoris</i>	pHILD2	MM medium	methanol	124 ^g	~2	24	N/M ^a	h	[202]
<i>A. thaliana</i> NR	<i>Pichia pastoris</i>	pHILD2	MM medium	methanol	247	10	72	N/M ^a	i	[203]
<i>A. thaliana</i> NR	<i>Pichia pastoris</i>	pHILD3	MM medium	methanol	247	10	72	30	i	[204]
Maize (<i>Zea mays</i>) NR (Mo domain)	<i>Pichia pastoris</i>	pPICZ-A	glycerol minimal media	methanol	N/M ^a	N/M ^a	N/M ^a	30	N/M ^a	[205]
<i>Phytophthora infestans</i> NR	<i>Aspergillus nidulans</i>	pTZ19 U	N/M ^a	N/M ^a	N/M ^a	N/M ^a	N/M ^a	N/M ^a	N/M ^a	[206]
<i>Pichia angusta</i> (yeast) NR	<i>Pichia pastoris</i>	pPICZ-b	MGY	methanol	N/M ^a	N/M ^a	24	30	N/M ^a	[136]
<i>P. angusta</i> (yeast) NR	<i>Pichia pastoris</i>	pPICZ-B	MGY	methanol	N/M ^a	N/M ^a	24	30	N/M ^a	[207]
<i>P. angusta</i> (yeast) NR	<i>Pichia pastoris</i>	N/M ^a	N/M ^a	N/M ^a	N/M ^a	N/M ^a	N/M ^a	N/M ^a	N/M ^a	[208]
Spinach (<i>Spinacia oleracea</i>) NR (Mo domain)	<i>E. coli</i> BL21 (DE3) codon plus, DH5a, JM109, TP1000	pGEX-5x-1/pET28a(+)	LB	IPTG	0.02	1	16-18	30	e	[55]
Spinach (<i>S. oleracea</i>) NR (Mo domain)	<i>Pichia pastoris</i>	pHIL-D2	glycerol minimal media	methanol	N/M ^a	N/M ^a	N/M ^a	30	N/M ^a	[205]
<i>Arabidopsis thaliana</i> SO	<i>E. coli</i> TP1000	pQE-80	YT	IPTG	0.1	0.08	20-24	30	e	[112]

Table 1.2 Continued

<u>Protein Expressed</u>	<u>Expression System</u>	<u>Plasmid System</u>	<u>Expression Medium</u>	<u>Inducer</u>	<u>Inducer Concentration (mM)</u>	<u>OD600 at Induction</u>	<u>Induction Time (hours)</u>	<u>Induction Temperature (°C)</u>	<u>Amendments</u>	<u>Ref.</u>
<i>A. thaliana</i> SO	<i>E. coli</i> M15/TP1000	pQE-60/pQE80	YT medium	IPTG	0.1	N/M ^a	24	22	e	[209]
Human SO	<i>E. coli</i> BL21 (DE3), DH5 α , MC4100, TP1000	pTrcdel, pTrcHis (created)	LB	IPTG	0.02-0.167	1	16-18	30	e	[57]
Human SO	<i>E. coli</i> TP1000	pTrcHis	LB	IPTG	0.02-0.167	1	16-18	30	e	[109]
Human SO	<i>E. coli</i> TP1000	pTrcHis	LB	IPTG	0.02-0.167	1	16-18	30	e	[110]
Human SO	<i>E. coli</i> TP1000	pTrcHis	LB	IPTG	0.02-0.167	1	16-18	30	e	[111]
Human SO	<i>E. coli</i> TP1000	pQE80L	N/M ^a	IPTG	0.1	0.5	15	30	N/M ^a	[210]
Human SO	<i>E. coli</i> M15	pQE-30	N/M ^a	IPTG	1	N/M ^a	4-5	N/M ^a	N/M ^a	[211]
Human SO	<i>E. coli</i> DH5-a.	pPROK1	LB	IPTG	0.4	N/M ^a	6	37	c	[67]
Human SO	<i>E. coli</i> DH5a	pPROK1	N/M ^a	IPTG	N/M ^a	N/M ^a	N/M ^a	N/M ^a	N/M ^a	[68]
Human SO	<i>E. coli</i> TP1000	pQE-80L	N/M ^a	IPTG	0.1	N/M ^a	48	24	f	[212]
Human SO R160Q	<i>E. coli</i>	pRG118	LB	IPTG	1	N/M ^a	5	37	b	[95]
Maize (<i>Zea mays</i>) SO	<i>E. coli</i> BL21 (DE3) pLysS	pET-30a	N/M ^a	IPTG	0.1	N/M ^a	N/M ^a	N/M ^a	N/M ^a	[56]
Mouse SO	<i>E. coli</i> TP1000	pQE80	N/M	IPTG	0.1	N/M ^a	48	25	d	[108]
Rat SO	<i>E. coli</i> JM 109	pPROK1	LB	IPTG	1	N/M ^a	5	37	b	[96]
Rat SO	<i>E. coli</i> DH5 α	pPROK1	LB	IPTG	0.4	N/M ^a	6	37	c	[67]

a) N/M- Not mentioned; b) 5 μ M Hemin, 50 μ M Na₂MoO₄; c) 5 mL Antifoam A, 50 μ M Na₂MoO₄; d) 150 mM molybdate; e) 1 mM molybdate; f) 500 μ M molybdate; g) calculated from % (v/v) or % (w/v) ; h) 1.34% yeast nitrogen base with ammonium sulfate, 1% glycerol, and 4 x 10⁻⁵ % biotin; i) 2.8% (w/v) yeast nitrogen base with ammonium sulfate, 100 mM potassium phosphate, pH 6.0, 4 X 10⁻⁵ % biotin, 0.2 mM sodium molybdate; j) 70% (w/v) Difco yeast nitrogen base w/o amino acids, 2 % (w/v) glucose, 50 mg tryptophan/L; k) 0.1 mM molybdate; l) OD at 550 nm.

Table 1.3: Expression parameters for recombinant prokaryotic XO family enzymes.

<u>Protein Expressed</u>	<u>Expression System</u>	<u>Plasmid System</u>	<u>Expression Medium</u>	<u>Inducer</u>	<u>Inducer Concentration (mM)</u>	<u>OD600 at Induction</u>	<u>Induction Time (hours)</u>	<u>Induction Temperature (°C)</u>	<u>Amendments</u>	<u>Ref.</u>
<i>E. coli</i> AO	<i>E. coli</i> TP1000	pTrcHis	LB	IPTG	0.01	N/M ^a	24	22	b	[120]
<i>E. coli</i> AO	<i>E. coli</i> TP1000	pTrcHis	LB	IPTG	0.01	N/M ^a	24	22	h	[213]
<i>methylobacillus</i> sp. KY4400 AO	<i>E. coli</i> XL1-blue, JM109	pUC118/pBlu escript II	N/M ^a	N/M ^a	N/M ^a	N/M ^a	N/M ^a	N/M ^a	N/M ^a	[214]
<i>Pyrococcus furiosus</i> AO	<i>Caldicellulosiruptor bescii</i> JWC8018	pDCW89/pE T24a fusion	LOD medium	Anaerobic growth	N/M ^a	N/M ^a	m	75	g	[215]
<i>Brevundimonas diminuta</i> 7 Isoquinoline 1-oxidoreductase	<i>P. putida</i> KT2440, <i>P. putida</i> 86	pJB653	mineral salts medium	benzoate & 3-methylbenzoate	8, 2	N/M ^a	16-20	N/M ^a	i	[216]
<i>Ochrobactrum</i> sp. SJY1 nicotinic hydroxylase	<i>P. putida</i> KT2440	pME6032	LB	IPTG	0.5	0.8	12	25	N/M ^a	[129]
<i>P. putida</i> KT2440 nicotinate dehydrogenase	<i>P. entomophila</i> L48	pJB866/pRS ETB	LB	m-toluic acid	~15mM	0.1	12	30	i	[50]
<i>P. putida</i> KT2440 nicotinate dehydrogenase	<i>Pseudomonas fluorescens</i> R2f/ <i>Pseudomonas</i> sp. DSM6412	pBBR1MCS-5	LB	N/M ^a	N/M ^a	N/M ^a	N/M ^a	30	N/M ^a	[217]
<i>Burkholderia</i> sp. CT39-3 piperonal oxidase	<i>Burkholderia</i> sp. CT39-3	pBBR1MCS2	2 × YT	IPTG	1	N/M ^a	72	28	N/M ^a	[218]
<i>Arthrobacter ilicis</i> Ru ^{61a} quinaldine 4-oxidase	<i>P. putida</i> KT2440	pJB653	mineral salts medium	2-methylbenzoate	2	0.8-1.2	N/M ^a	N/M ^a	N/M ^a	[219]
<i>Pseudomonas putida</i> 86 quinoline 2-oxidoreductase	<i>P. putida</i> KT2440 and 86-1 Δqor	pJB653	mineral salts medium	2-methylbenzoate	2	0.7–1.0 (OD at 550nm)	N/M ^a	30	j	[220]
<i>P. putida</i> 86 quinoline 2-oxidoreductase	<i>P. putida</i> mt-2 KT2440	pCIB 119	mineral salts medium	N/M ^a	N/M ^a	N/M ^a	N/M ^a	30	k	[221]
<i>Comamonas acidovorans</i> XDH	<i>E. coli</i> JM109 (DE3)	pET23a(+)	LB	N/M	N/M ^a	N/M ^a	16	21	e	[69]
<i>C. acidovorans</i> XDH	<i>Pseudomonas aeruginosa</i>	pUCP-Nde	LB	IPTG	1	0.8-1	4.0-5.0	37	f	[127]
<i>R. capsulatus</i> XDH	<i>E. coli</i> TP1000	pTrcHis	LB	IPTG	0.02	1	18-20	30	b	[116]
<i>R. capsulatus</i> XDH	<i>E. coli</i> TP1000	pTrcHis	LB	IPTG	0.02	1	18-20	30	b	[222]
<i>R. capsulatus</i> XDH	<i>E. coli</i> TP1000	pTrcHis	LB	IPTG	0.02	1	18-20	30	b	[117]
<i>R. capsulatus</i> XDH	<i>E. coli</i> TP1000	pTrcHis	LB	IPTG	0.02	1	18-20	30	b	[118]
<i>R. capsulatus</i> XDH	<i>E. coli</i> TP1000	pTrcHis	LB	IPTG	0.02	1	18-20	30	b	[119]
<i>R. capsulatus</i> XDH	<i>R. capsulatus</i>	pPHU231	RCV	Anaerobic growth under nitrogen	N/M ^a	N/M ^a	40	N/M ^a	c	[47]

Table 1.3 Continued

<u>Protein Expressed</u>	<u>Expression System</u>	<u>Plasmid System</u>	<u>Expression Medium</u>	<u>Inducer</u>	<u>Inducer Concentration (mM)</u>	<u>OD600 at Induction</u>	<u>Induction Time (hours)</u>	<u>Induction Temperature (°C)</u>	<u>Amendments</u>	<u>Ref.</u>
<i>R. capsulatus</i> XDH	<i>R. capsulatus</i> WT & <i>moeA</i> mutant	pPHU231	RCV	Anaerobic growth under nitrogen	N/M ^a	N/M ^a	40	N/M ^a	d	[48]
<i>R. capsulatus</i> XDH	<i>E. coli</i> TP1000	pPHU231	RCV	Anaerobic growth under nitrogen	N/M ^a	N/M ^a	40	N/M ^a	c	[223]
<i>R. capsulatus</i> XDH	<i>R. capsulatus</i> (<i>xdhC</i> mutant)	pPHU231	RCV	Anaerobic growth under nitrogen	N/M ^a	N/M ^a	40	N/M ^a	d	[49]

a) N/M- Not mentioned; b) 1 mM molybdate c) 10 mM Ammonium; d) 10 mM Serine; e) 1 mM guanosine and 0.25 mM sodium molybdate; f) 0.25 mM molybdate g) 1µM cellobiose and 1µM sodium molybdate and/or tungstate; h) 2 mM molybdate i) various carbon sources; j) 1 g/L ammonium sulfate, 8 mM benzoate; k) 1 mM catechol; l) 50 mM nicotinic acid; m) induced at late exponential phase.

Table 1.4: Expression parameters for recombinant prokaryotic SO family enzymes.

<u>Protein Expressed</u>	<u>Expression system</u>	<u>Plasmid System</u>	<u>Expression Medium</u>	<u>Inducer</u>	<u>Inducer Concentration (mM)</u>	<u>OD600 at Induction</u>	<u>Induction Time (hours)</u>	<u>Induction Temperature (°C)</u>	<u>Amendments</u>	<u>Ref.</u>
<i>Deinococcus radiodurans</i> SO	<i>E. coli</i> BL21-CodonPlus(DE3)-RIL/ TP1000	pET28c/pTRc99A	LB	IPTG	1	1	16	22	N/M ^a	[224]
<i>Sinorhizobium meliloti</i> SorT	<i>E. coli</i> TP1000	pProex	LB	IPTG	0.25	0.8	d	30	b	[122]
<i>Starkeya novella</i> sulphite:cytochrome c oxidoreductase	<i>R. capsulatus</i>	pRK415/dor promoter	RCV medium	DMSO	60	N/M ^a	18-20	N/M ^a	b	[171]
<i>Thermus thermophilus</i> AT62 SO	<i>E. coli</i> TP1000	pQE-60	LB	IPTG	1	0.6	6	22	b	[121]
<i>T. thermophilus</i> HB8 SO	<i>E. coli</i> TP1000	pQE-60	LB	IPTG	1	0.5	3	22	b	[123]
<i>E. coli</i> YedY	<i>E. coli</i> JM109	pMSYZ3	TB	IPTG	0.1	0.8	12	30	b	[70]
<i>E. coli</i> HB101 YedYZ	<i>E. coli</i> HB101 or SJB20	pMS119EH	TB	IPTG	0.1	0.8	12	30	c	[71]
<i>E. coli</i> YedY	<i>E. coli</i> TP1000	pTrcHis	LB	IPTG	0.02	N/M ^a	24	30	b	[124]
<i>R. sphaeroides</i> YedY	<i>R. sphaeroides</i> , <i>E. coli</i> BL21 DE3	pBBR1MCS-2, pIND4, pET-TEV, pMS742	LB/hutner media	IPTG	1	0.6	d	16	N/M ^a	[101]

a) N/M- Not mentioned; b) 1 mM molybdate; c) 0.003% (w/v) metal ions mixture, 1 mM molybdate; d) Induced overnight, exact induction time not reported.

Table 1.5: Expression parameters for recombinant prokaryotic DMSOR family enzymes.

<u>Protein Expressed</u>	<u>Expression system</u>	<u>Plasmid System</u>	<u>Expression Medium</u>	<u>Inducer</u>	<u>Inducer Concentration (mM)</u>	<u>OD600 at Induction</u>	<u>Induction Time (hours)</u>	<u>Induction Temperature (°C)</u>	<u>Amendments</u>	<u>Ref.</u>
<i>A. faecalis</i> Aio	<i>E. coli</i> DH5a	pPROEX-HTb	LB	IPTG	0.04	N/M ^a	24	21	b	[80]
<i>Ralstonia</i> sp. S22 Aio	<i>E. coli</i> C43 (DE3) cyo-	pET-28a	ZYM-5052 (auto-inducing medium)	Medium	Medium	N/M ^a	16-20	37	b	[99]
<i>Rhizobium</i> sp. NT-26 Aio	<i>E. coli</i> DH5a	pPROEX-HTb	LB	IPTG	0.04	N/M ^a	24	21	b	[80]
<i>Rhizobium</i> sp. NT-26 Aio	<i>E. coli</i> (DH5a, JM109 pir, RK4353, C43)	pPROEX-HTb	LB	IPTG	0.04	N/M ^a	24	21	b	[62]
<i>Rhizobium</i> sp. str. NT-26 Aio	<i>E. coli</i> DH5a	pPROEX-HTb	LB	IPTG	0.04	N/M ^a	24	21	b	[81]
<i>Rhizobium</i> sp. str. NT-26 Aio	<i>E. coli</i> DH5a	pPROEX-HTb	LB	IPTG	0.04	N/M ^a	24	21	b	[82]
<i>Shewanella</i> sp. strain ANA-3 Arr	<i>E. coli</i> C43	pET32 derivatives	LB	IPTG	0.04	1	18	RT ^x	g	[98]
<i>Shewanella</i> sp. strain ANA-3 Arr	<i>Shewanella</i> sp. strain ANA-3	pET15b/pBAD18-kan	TB	L-arabinose	20	2.5	4	30	h	[225]
<i>E. coli</i> BSOR	<i>E. coli</i>	pUC9	N/M ^a	N/M ^a	N/M ^a	N/M ^a	N/M ^a	N/M ^a	N/M ^a	[74]
<i>R. sphaeroides</i> BSOR	<i>E. coli</i> JM109	pGEX-5X-2	M9ZB	IPTG	0.04	1	24	RT ^x	b	[72]
<i>R. sphaeroides</i> BSOR	<i>E. coli</i> JM109, ΔMu29	FLAG*Shift 12c	LB	IPTG	2	0.2	0.5-3/4-6	37/24	N/M ^a	[73]
<i>R. sphaeroides</i> BSOR	<i>E. coli</i> JM109	pGEX-5X-2	LB	IPTG	0.1	0.8	4	24	b	[29]
<i>R. sphaeroides</i> BSOR	<i>E. coli</i> JM110	pGEX-5X-3	LB	IPTG	0.1	0.8	4	24	b	[135]
<i>Sterolibacterium denitrificans</i> steroid C-25 dehydrogenase	<i>Thauera aromatica</i> K172	pI21016	phosphate-buffered medium	IPTG	1	0.7	30	48	v	[226]
<i>E. coli</i> DMSOR	<i>E. coli</i> K38	pTZ18R	LB	Heat	w	N/M ^a	22	30	N/M ^a	[65]
<i>E. coli</i> DMSOR	<i>E. coli</i> C41 (DE3)	pTZ19R/pTZGEX	LB	IPTG	1	0.5	8	37	N/M ^a	[157]
<i>E. coli</i> DMSOR	<i>E. coli</i> CC118	pBR322/pTZ18R/pJBS633	peptone/fumara te media	N/M ^a	N/M ^a	N/M ^a	N/M ^a	30 or 37	d	[227]
<i>E. coli</i> DMSOR	<i>E. coli</i> HB101	pBR322	glycerol-fumarate minimal medium	N/M ^a	N/M ^a	N/M ^a	48	37	N/M ^a	[228]

Table 1.5 Continued

<u>Protein Expressed</u>	<u>Expression system</u>	<u>Plasmid System</u>	<u>Expression Medium</u>	<u>Inducer</u>	<u>Inducer Concentration (mM)</u>	<u>OD600 at Induction</u>	<u>Induction Time (hours)</u>	<u>Induction Temperature (°C)</u>	<u>Amendments</u>	<u>Ref.</u>
<i>E. coli</i> DMSOR	<i>E. coli</i> Dss301	pBR322	glycerol-DMSO min. med., glycerol-fumarate min. med., or glucose-peptone-fumarate rich med.	N/M ^a	N/M ^a	N/M ^a	18-48	N/M ^a	N/M ^a	[229]
<i>E. coli</i> DMSOR	<i>E. coli</i> HB101(moc o insertion mutant)	pBR322	minimal glycerol/fumara te media	N/M ^a	N/M ^a	N/M ^a	48	37	N/M ^a	[75]
<i>E. coli</i> DMSOR	<i>E. coli</i> K12 derivatives	pRS415 put in chromosome	Luria broth	N/M ^a	N/M ^a	N/M ^a	N/M ^a	30 or 37	e	[230]
<i>E. coli</i> DMSOR	<i>E. coli</i> HB101 and DSS301	pBR322	glycerol-DMSO min. med., glycerol-fumarate min. med.	N/M ^a	N/M ^a	N/M ^a	24-48	37	N/M ^a	[77]
<i>E. coli</i> DMSOR	<i>E. coli</i> HB101, RK5208	pBR322	glycerol-DMSO min. media or glycerol-fumarate min. media	N/M ^a	N/M ^a	N/M ^a	48, 72	37, 23	N/M ^a	[76]
<i>E. coli</i> DMSOR	<i>E. coli</i> HB101	pBR322	glycerol-fumarate minimal medium	N/M ^a	N/M ^a	N/M ^a	N/M ^a	N/M ^a	N/M ^a	[78]
<i>R. capsulatus</i> DMSOR	<i>Rhodobacte r capsulatus</i>	pUC19/pJP5603	RCV media	N/M ^a	N/M ^a	N/M ^a	N/M ^a	N/M ^a	N/M ^a	[166]
<i>R. sphaeroides</i> DMSOR	<i>Escherichia coli</i> BL21(DE3)	pET-29, pET-28	M9ZB	IPTG	0.08 ^y	N/M ^a	24	RT ^x	c	[54]
<i>R. sphaeroides</i> DMSOR	<i>E. coli</i> MC4100	pTrc 99 A	M9ZB	IPTG	0.005	1	20-24	RT ^x	b	[64]
<i>R. sphaeroides</i> DMSOR	<i>E. coli</i> BL21 DE3	pET-29	N/M	IPTG	N/M ^a	N/M ^a	N/M ^a	N/M ^a	N/M ^a	[92]
<i>C. glutamicum</i> ATCC 13032 FDH	<i>C. glutamicum</i> Δcg0618	pEKEx2	CGXII medium	IPTG	0.7	1.5	4	30	q	[231]
<i>Desulfovibrio vulgaris</i> FDH	<i>Desulfovibri o vulgaris</i>	pUC19	<i>D. vulgaris</i> liquid medium	N/M ^a	N/M ^a	N/M ^a	N/M ^a	30	s	[232]

Table 1.5 Continued

<u>Protein Expressed</u>	<u>Expression system</u>	<u>Plasmid System</u>	<u>Expression Medium</u>	<u>Inducer</u>	<u>Inducer Concentration (mM)</u>	<u>OD600 at Induction</u>	<u>Induction Time (hours)</u>	<u>Induction Temperature (°C)</u>	<u>Amendments</u>	<u>Ref.</u>
<i>E. coli</i> strain JG0205 FDH	<i>E. coli</i> JG0205 Δ fdhf	pTrc99a	TGYEP	IPTG	0.1	ae	ad	30	r	[233]
<i>E. coli</i> FDH	<i>E. coli</i> JG0205 Δ fdhf	pTrc99a	TGYEP	IPTG	0.1	ae	ad	30	r	[234]
<i>E. coli</i> FDH	<i>E. coli</i> JW3863 (Δ fdol)	pBR322, pUC19	LB	N/M ^a	N/M ^a	N/M ^a	N/M ^a	30	N/M ^a	[232]
<i>E. coli</i> FDH	<i>E. coli</i>	pACYC184	N/M ^a	N/M ^a	N/M ^a	N/M ^a	N/M ^a	N/M ^a	N/M ^a	[235]
<i>E. coli</i> FDH	<i>E. coli</i> K-12	pGEM3(grew slow), pACYC184	TYG medium	Heat	N/M ^a	N/M ^a	N/M ^a	N/M ^a	N/M ^a	[60]
<i>Methanobacterium formicicum</i> FDH	<i>E. coli</i>	pBR322	M9 medium	ag	N/M ^a	N/M ^a	3	40	t	[236]
<i>R. capsulatus</i> FDH	<i>E. coli</i> MC1061	pTrcHis	LB	IPTG	0.02	N/M ^a	24	30	b	[88]
<i>R. capsulatus</i> FDH	<i>E. coli</i> MC1061	pTrcHis	LB	IPTG	0.02	N/M ^a	24	30	b	[91]
<i>R. capsulatus</i> FDH	<i>E. coli</i> MC1061	pTrcHis	LB	IPTG	0.02	N/M ^a	24	30	b	[90]
<i>R. capsulatus</i> FDH	<i>E. coli</i> MC1061	pTrcHis (FdsC) pACYduet-1 (FdsGBA, FdsD)	LB	IPTG	0.02	N/M ^a	24	30	b	[89]
<i>Wolinella succinogenes</i> FDH	<i>E. coli</i>	pBluescript IISK	LB	N/M ^a	N/M ^a	N/M ^a	N/M ^a	37	N/M ^a	[237]
<i>Methanosarcina barkeri</i> Formylmethanofuran dehydrogenase	<i>E. coli</i> BL21 (DE3)	pBluescript SK ⁺ , pET-17b	M9	IPTG	0.1	0.7 ^{af}	1-1.5	37	u	[52]
<i>Methanobacterium thermoautotrophicum</i> Formylmethanofuran dehydrogenase (W)	<i>E. coli</i> BL21 (DE3)	pCR TM II	M9	IPTG	0.2	0.5 ^{af}	1-1.5	37	u	[51]
<i>C. necator</i> Nap	<i>C. necator</i>	pCM62	gluconate mineral medium	N/M ^a	N/M ^a	N/M ^a	N/M ^a	30	j	[130]
<i>C. necator</i> Nap	<i>C. necator</i>	pVK102 (Knauf et al 1982), pBluescript SK ⁺	gluconate mineral medium	N/M ^a	N/M ^a	N/M ^a	N/M ^a	30	j	[170]

Table 1.5 Continued

<u>Protein Expressed</u>	<u>Expression system</u>	<u>Plasmid System</u>	<u>Expression Medium</u>	<u>Inducer</u>	<u>Inducer Concentration (mM)</u>	<u>OD600 at Induction</u>	<u>Induction Time (hours)</u>	<u>Induction Temperature (°C)</u>	<u>Amendments</u>	<u>Ref.</u>
<i>C. necator</i> Nap	<i>C. necator</i>	pVK102 (Knauf et al 1982), pT7-5, pBluescript SK+	gluconate mineral medium	N/M ^a	N/M ^a	N/M ^a	N/M ^a	30	N/M ^a	[93]
<i>E. coli</i> Nap	<i>E. coli</i> K12 strain LCB2048	pJG460	GN	N/M ^a	N/M ^a	N/M ^a	ad	37	i	[61]
<i>E. coli</i> Nap	<i>E. coli</i> K12 derivatives	pBR322	LB	N/M ^a	N/M ^a	N/M ^a	N/M ^a	N/M ^a	N/M ^a	[169]
<i>R. sphaeroides</i> Nap	<i>R. sphaeroides nap</i> mutant MS523	pRK415	LB	N/M ^a	N/M ^a	N/M ^a	N/M ^a	37	N/M ^a	[167]
<i>R. sphaeroides</i> Nap	<i>Rhodobacter sphaeroides</i>	pMS617 (ref 3)	Hutner medium	N/M ^a	N/M ^a	N/M ^a	24	30	N/M ^a	[168]
<i>Synechococcus</i> sp. strain PCC 7942 NR (narB)	<i>Escherichia coli</i> DH5α	pTrc99A	LB	IPTG	1	N/M ^a	6-7	37	N/M ^a	[83]
<i>Synechococcus</i> sp. strain PCC 7942 NR (narB)	<i>Escherichia coli</i> DH5α	pTrc99A	LB	IPTG	1	0.6	3	37	N/M ^a	[84]
<i>E. coli</i> NarGHI	<i>E. coli</i> LCB79	pJF119EH (Fürste et al. 1986)	Terrific Broth	IPTG	0.2	N/M ^a	ad	30	N/M ^a	[238]
<i>E. coli</i> NarGHI	<i>E. coli</i> LCB2048	pJF119EH (Fürste et al. 1986)	2TY medium	IPTG	0.2	N/M ^a	N/M ^a	37	k	[85]
<i>E. coli</i> NarGHI	<i>E. coli</i> LCB2048	pJF119EH (Fürste et al. 1986)	TB	IPTG	0.2	N/M ^a	N/M ^a	30	N/M ^a	[86]
<i>E. coli</i> NarGHI	<i>E. coli</i> JCB4023, LCB3514, LCB3515, LCB3766	pJF119EH (Fürste et al. 1986)	minimal medium	IPTG	0.2	0.1	N/M ^a	37	l	[239]
<i>E. coli</i> NarGHI	<i>E. coli</i> JCB4023	pJF119EH (Fürste et al. 1986)	M9 minimal medium	N/M ^a	N/M ^a	N/M ^a	N/M ^a	N/M ^a	m	[240]
<i>E. coli</i> NarGHI	<i>E. coli</i> JCB4023	pJF119EH (Fürste et al. 1986)	TB	IPTG	0.2	N/M ^a	N/M ^a	37	N/M ^a	[241]

Table 1.5 Continued

<u>Protein Expressed</u>	<u>Expression system</u>	<u>Plasmid System</u>	<u>Expression Medium</u>	<u>Inducer</u>	<u>Inducer Concentration (mM)</u>	<u>OD600 at Induction</u>	<u>Induction Time (hours)</u>	<u>Induction Temperature (°C)</u>	<u>Amendments</u>	<u>Ref.</u>
<i>E. coli</i> NarGHI	<i>E. coli</i> LCB79, LCB162A, LCB162B	pJF119EH (Fürste <i>et al.</i> 1986)	basal medium	IPTG	0.2	N/M ^a	N/M ^a	N/M ^a	n	[242]
<i>E. coli</i> NarGHI	<i>E. coli</i> LCB79	pJF119EH (Fürste <i>et al.</i> 1986)	2TY medium	IPTG	0.2	N/M ^a	N/M ^a	37	k	[243]
<i>E. coli</i> NarGHI	<i>E. coli</i> LCB3064	pJF119EH (Fürste <i>et al.</i> 1986)	TB	IPTG	0.2	N/M ^a	N/M ^a	37	N/M ^a	[244]
<i>E. coli</i> NarGHI	<i>E. coli</i> LCB79	pJF119EH (Fürste <i>et al.</i> 1986)	growth medium: 12 g L-1 tryptone, 24 g L-1 yeast extract, 5 g L-1 NaCl, 4 mL L-1 glycerol	IPTG	1	2	10-11	30	p	[245]
<i>E. coli</i> NarGHI	<i>E. coli</i> LCB79	pJF119EH (Fürste <i>et al.</i> 1986)	2TY medium	IPTG	0.2	N/M ^a	N/M ^a	37	k	[246]
<i>E. coli</i> NarGHJI	<i>E. coli</i> LCB 2048	pACYC184	basal medium	nitrate	16	N/M ^a	N/M ^a	N/M ^a	o	[247]
<i>E. coli</i> NarGYWV	<i>E. coli</i> LCB 2048	pJF119EH (Fürste <i>et al.</i> 1986)	basal medium	nitrate	16	N/M ^a	N/M ^a	N/M ^a	o	[87]
<i>E. coli</i> NR-A & Z (Nar)	<i>E. coli</i> LCB79	pJF119EH (Fürste <i>et al.</i> 1986), pBR322	N/M ^a	N/M ^a	N/M ^a	N/M ^a	N/M ^a	N/M ^a	N/M ^a	[248]
<i>E. coli</i> NR-Z	<i>E. coli</i> LCB79	pLCB14	basal medium	nitrate	16	N/M ^a	N/M ^a	N/M ^a	o	[249]
<i>B. megaterium</i> NCT-2 Nas	<i>E. coli</i> BL21 (DE3), Transetta (DE3)	pETDuet	LB	IPTG	0.1	0.8	10	20	N/M ^a	[53]
<i>E. coli</i> TMAOR	<i>E. coli</i> RK4353	pET-29a(+)/pET-28a(+)/pTrc 99 A	M9ZB	IPTG	0.01 ^z , 0.04 ^{aa}	1	24	RT ^x	b	[97]
<i>E. coli</i> TMAOR	<i>E. coli</i> MC4100	miniMu repiicon MudII4042	minimal medium	lactose	~5.8	N/M ^a	N/M ^a	N/M ^a	N/M ^a	[63]
<i>E. coli</i> TMAOR	<i>E. coli</i> BW25113	pJF119EH	N/M ^a	IPTG	0.02 ^{ab} , 0.07 ^{ac}	N/M ^a	24 ^{ab} , 30 ^{ac}	30 ^{ab} , 37 ^{ac}	f	[126]

Table 1.5 Continued

<u>Protein Expressed</u>	<u>Expression system</u>	<u>Plasmid System</u>	<u>Expression Medium</u>	<u>Inducer</u>	<u>Inducer Concentration (mM)</u>	<u>OD600 at Induction</u>	<u>Induction Time (hours)</u>	<u>Induction Temperature (°C)</u>	<u>Amendments</u>	<u>Ref.</u>
<i>Haemophilus influenzae</i> TMAOR	<i>E. coli</i> DH5a	pPROEX-HTb	LB	IPTG	0.1	0.6-0.8	ad	30	b	[79]

a) N/M- Not mentioned; b) 1 mM molybdate c) tested addition of pLysE, 0.5 mM molybdate, 40 mM fumaric acid; d) 10 µg/ml thiamine; e) multiple electron acceptors tested; f) 1 mM molybdate, and 7 mM TMAO; g) 20 mM lactate, 1 mM molybdate, 14 mM DMSO; h) 4 mL/L glycerol, 5 mM MgSO₄, 200 µM molybdate, 0.2 g/L ferric ammonium citrate; i) 0.4% glycerol and 20 mM potassium nitrate; j) 0.4% (w/v) fructose as carbon source and 0.2% ammonium chloride (w/v) as nitrogen source; k) 2 g/L glucose; l) either [methyl-2H] methionine (35 mM, isotope purity 98%, Cambridge Isotope Laboratories, Inc), l-lysine-ε-¹⁵N-2HCl (136 mM, isotope purity 98%, euriso-top), or l-histidine-d-¹⁵N-HCl-H₂O (142 mM; isotope purity 98%, eurisotop); m) Mohr salt (10 µM), Na₉₈MoO₄ (5 µM, isotope purity ~98% Oak Ridge National Laboratory, US), and with NH₄Cl (18.7 mM); n) 1 g/L nitrate, 2 g/L glucose, 1 µM molybdate; o) 1-2 g/L glucose, 1 µM molybdate; p) 0.1 mM molybdate; q) Formate; r) 0.4% glucose, 1 mM molybdate, 10 µM Na₂SeO₃ and 15 mM sodium formate; s) 0.5 g K₂HPO₄, 2.0 g MgSO₄·7H₂O, 1.0 g Na₂SO₄, 1.0 g NH₄Cl, 0.1 g CaCl₂·2H₂O, 1.0 g yeast extract, 1.0 mg sodium resazurin, 3.3 g 60% sodium lactate and 0.1 g L ascorbic acid in 1 L water, with pH adjusted to 7.8; t) 0.1% Tryptone, 0.01% yeast extract; u) amino acids 0.01%; v) benzoate; w) Heated at 42°C for 30 min to induce expression; x) RT- room temperature; y) Induced with 1 mM IPTG for expression tests and optimized at 0.08 mM; z) pTrc expression vector; aa) pET expression vector; ab) aerobic expression; ac) anaerobic expression; ad) Induced overnight, exact induction time not reported; ae) Induced at mid sponential phase; af) OD at 578 nm; ag) Heated to 30 to 40°C to induce expression.

Table 1.6: Purification parameters for recombinant eukaryotic XO family enzymes.

Enzyme	Homogenization	Lysis Amendments	Purification Procedures	Protein Yield (g/L)	Molybdenum Incorporation	Chaperones	Chaperone function	Ref.
<i>A. thaliana</i> AO	N/M ^a	N/M ^a	m	N/M ^a	N/M ^a	N/M ^a	N/M ^a	[58]
<i>A. thaliana</i> AO	vigorous mixing with glass beads	1 mM EDTA, and 5% glycerol, containing protease inhibitors	n	N/M ^a	N/M ^a	ABA3	acts as a Moco sulfurase	[177]
<i>A. thaliana</i> AO	French press	200 mM NaCl, 0.2 mM phenylmethylsulfonyl fluoride, and 5 % glycerol	o	N/M ^a	N/M ^a	N/M ^a	N/M ^a	[178]
<i>A. thaliana</i> AO	vigorous mixing with glass beads	1 mM EDTA, and 5% glycerol, containing protease inhibitors	n	N/M ^a	N/M ^a	N/M ^a	N/M ^a	[179]
<i>D. melanogaster</i> AO	N/M ^a	N/M ^a	p	N/M ^a	N/M ^a	N/M ^a	N/M ^a	[107]
Human AO	sonication	lysozyme (5 mg/ml), MgCl ₂ (28.6 ug/ml), RNase (10 ug/ml), DNase (10ug/mL)	h	7.4x10 ⁻⁴ -2.2x10 ⁻³	N/M ^a	N/M ^a	N/M ^a	[103]
Human AO	cell disruptor	N/M ^a	g	0.00009 ^r , 0.0011 ^s	55.2 ± 8.41% ^r , 66.4 ± 6.58% ^s	N/M ^a	N/M ^a	[180]
Human AO	cell disruptor	N/M ^a	i	0.00005	60%	Moco sulfurase	catalyzes the generation of the sulfurylated form of MoCo	[104]
Monkey AO	solubilized with QIAexpressionist	N/M ^a	h	N/M ^a	N/M ^a	N/M ^a	N/M ^a	[181]
Monkey AO	QIAexpressionist (QIAGEN)	N/M ^a	h	N/M ^a	N/M ^a	N/M ^a	N/M ^a	[182]
Monkey and Rabbit AO	N/M ^a	N/M ^a	h	N/M ^a	N/M ^a	N/M ^a	N/M ^a	[184]
chimeric monkey and rat AO	QIAexpressionist (QIAGEN)	N/M ^a	h	N/M ^a	N/M ^a	N/M ^a	N/M ^a	[183]
Mouse AO	cell disruptor	1mM EDTA and 0.5mM PMSF	j	3.3x10 ⁻⁵	N/M ^a	N/M ^a	N/M ^a	[59]
Mouse AO	N/M ^a	N/M ^a	c	N/M ^a	N/M ^a	N/M ^a	N/M ^a	[185]
Mouse AO	N/M ^a	N/M ^a	c	N/M ^a	N/M ^a	N/M ^a	N/M ^a	[186]
Mouse AO	French press	N/M ^a	k	8.3x10 ⁶	70%	Moco sulfurase	catalyzes the generation of the sulfurylated form of MoCo	[106]
Mouse AO	cell disruptor	DNase I and lysozyme (1 mg/l)	l	0.008	58%	Moco sulfurase	catalyzes the generation of the sulfurylated form of MoCo	[105]
Mouse AO	N/M ^a	N/M ^a	c	N/M ^a	N/M ^a	N/M ^a	N/M ^a	[187]
Porcine AO	spheroplast isolation/sonication	Lysozyme 0.25 mg/ml, 6 mM magnesium acetate, 20% glycerol (v/v), and 0.1 mM dithiothreitol	q	N/M ^a	N/M ^a	N/M ^a	N/M ^a	[188]
Rat AO	QIAexpressionist	N/M ^a	h	N/M ^a	N/M ^a	N/M ^a	N/M ^a	[189]

Table 1.6 Continued

<u>Enzyme</u>	<u>Homogenization</u>	<u>Lysis Amendments</u>	<u>Purification Procedures</u>	<u>Protein Yield (g/L)</u>	<u>Molybdenum Incorporation</u>	<u>Chaperones</u>	<u>Chaperone function</u>	<u>Ref.</u>
<i>Arabidopsis thaliana</i> XO	vortexing with glass beads/french press	0.5mM EDTA, 200 mM NaCl, 0.2 mM phenylmethylsulfonyl fluoride, and 5% glycerol	g	N/M ^a	N/M ^a	N/M ^a	N/M ^a	[190]
Bovine XDH	Potter Teflon-glass homogenizer	50 mM Tris-HCl buffer, pH 8.5, 0.4 mM EDTA and 1 mM PMSF	e	N/M ^a	N/M ^a	N/M ^a	N/M ^a	[191]
<i>Drosophila melanogaster</i> XO	blender	50 mM borax, 1 mM EDTA, Tris/HCl pH 9.2, Sigma protease-inhibitor cocktail	d	6.25x10 ⁻⁵	N/M ^a	N/M ^a	N/M ^a	[192]
Human XO	sonication	0.5mM EDTA, 0.2mM PMSF, 0.5 mg/ml of lysozyme	b	N/M ^a	36%	N/M ^a	N/M ^a	[66]
Human XO	sonication	0.5mM dithiothreitol, 1mM EDTA, 5ug/ml leupeptin, 0.1uM pepstatin, 1mM PMSF	c	N/M ^a	N/M ^a	N/M ^a	N/M ^a	[193]
Human XO	N/M ^a	N/M ^a	c	N/M ^a	N/M ^a	N/M ^a	N/M ^a	[194]
Porcine XO	N/M ^a	N/M ^a	f	N/M ^a	N/M ^a	N/M ^a	N/M ^a	[196]
Rat XO	Potter Teflon-glass homogenizer	50 mM Tris-HCl buffer, pH 8.5, 0.4 mM EDTA and 1 mM PMSF	e	0.00015	10%	N/M ^a	N/M ^a	[197]
Rat XO	Potter Teflon-glass homogenizer	50 mM Tris-HCl buffer, pH 8.5, 0.4 mM EDTA and 1 mM PMSF	e	N/M ^a	N/M ^a	N/M ^a	N/M ^a	[198]

a) N/M- Not mentioned; b) anion exchange chromatography, hydroxyapatite chromatography, size exclusion chromatography; c) not purified, analyzed lysates or crude protein extracts, or focused on microbiological or genetic studies; d) ammonium sulfate precipitation; dialysis; hydrophobic affinity chromatography; dialysis; ion exchange chromatography; e) anion exchange chromatography, Centricon 100 micro-concentrator (Amicon), hydroxyapatite chromatography, size exclusion chromatography, folate affinity chromatography; f) Membrane and Cytosol Protein Extraction Kit (Beyotime, Jiangsu, China); g) Immobilized Metal Affinity Chromatography (IMAC), anion exchange chromatography, size exclusion chromatography; h) IMAC; i) IMAC, PD-10 (buffer exchange/desalting) columns, anion exchange chromatography, size exclusion chromatography; j) Immobilized dye affinity chromatography, dialysis, benzamidine-Sepharose chromatography (removal of proteases, thrombin); k) IMAC, dialysis, size exclusion chromatography, benzamidine-Sepharose chromatography (removal of proteases, thrombin); l) IMAC, PD10 (buffer exchange/desalting) columns, thrombin cleavage, size exclusion chromatography; m) failed attempts at purification with and without a Histag; n) ammonium sulfate (0-55% saturation), dialysis, heat-treated (60°C, 3 min) to remove excess contaminating proteins; o) IMAC, anion exchange chromatography; p) IMAC, size exclusion chromatography; q) IMAC, dialysis; r) Native gene expressed; s) codon-optimized gene expressed.

Table 1.7: Purification parameters for recombinant eukaryotic SO family enzymes.

<u>Enzyme</u>	<u>Homogenization</u>	<u>Lysis Amendments</u>	<u>Purification Procedures</u>	<u>Protein Yield (g/L)</u>	<u>Molybdenum Incorporation</u>	<u>Chaperones</u>	<u>Chaperone function</u>	<u>Ref.</u>
Chlamydomonas reinhardtii crARC	N/M ^a	N/M ^a	t	N/M ^a	N/M ^a	N/M ^a	N/M ^a	[199]
<i>A. thaliana</i> mARC2	french press/sonication	N/M ^a	h	N/M ^a	N/M ^a	N/M ^a	N/M ^a	[115]
human mARC1 & mARC2	french press/sonication	N/M ^a	h	0.01-0.015	45% ^v , 37% ^w	N/M ^a	N/M ^a	[113]
human mARC1 & mARC2	N/M ^a	N/M ^a	h	0.01	60% ^v , 80% ^w	N/M ^a	N/M ^a	[14]
human mARC1	french press/sonication	N/M ^a	h	N/M ^a	80%	N/M ^a	N/M ^a	[13]
human mARC1 & mARC2	french press/sonication	N/M ^a	h	N/M ^a	30%	N/M ^a	N/M ^a	[114]
human mARC1 & mARC3	french press/sonication	N/M ^a	h	N/M ^a	N/M ^a	N/M ^a	N/M ^a	[200]
human mARC1 & mARC2	french press/sonication	N/M ^a	h	N/M ^a	N/M ^a	N/M ^a	N/M ^a	[201]
<i>A. thaliana</i> NR	vortexed ~5min with glass beads	10mM MgCl ₂ , 1mM EDTA, 5mM DTT, 0.1% Triton X-100, and proteinase inhibitors (0.4 pg/mL leupeptin and 1 pg/mL pepstatin)	q	N/M ^a	N/M ^a	N/M ^a	N/M ^a	[202]
<i>A. thaliana</i> NR	bead beater	1 mM EDTA, and 5% (v/v) glycerol	o	11.60 ^u	N/M ^a	N/M ^a	N/M ^a	[203]
<i>A. thaliana</i> NR	continuous-flow Dyno Mill model KDL filled with glass beads	N/M ^a	o	N/M ^a	20%	N/M ^a	N/M ^a	[204]
Maize NR (Mo domain)	Bead-Beater and 0.5-mm glass beads/continuous flow Dyno Mill model KDL	N/M ^a	p	0.032	N/M ^a	N/M ^a	N/M ^a	[205]
<i>P. angusta</i> NR (S-NaR1)	0.5mm beads in bead beater	N/M ^a	h	~30 ^u	N/M ^a	N/M ^a	N/M ^a	[136]
<i>P. angusta</i> NR Mo fragment	0.5mm beads in bead beater	N/M ^a	s	N/M ^a	N/M ^a	N/M ^a	N/M ^a	[207]
<i>P. angusta</i> NR	0.5mm beads in bead beater	N/M ^a	h	N/M ^a	N/M ^a	N/M ^a	N/M ^a	[208]
spinach NR (Mo domain-GST)	sonication	DTT (10 mM), aprotinin (0.1 mg/ml), EDTA (1mM), PMSF (0.1 mM), and sodium molybdate (1 mM)	m	~0.014	93%	N/M ^a	N/M ^a	[55]
spinach NR (Mo domain-His)	sonication	DTT (10 mM), aprotinin (0.1 mg/ml), EDTA (1mM), PMSF (0.1 mM), and sodium molybdate (1 mM)	n	0.014	44%	N/M ^a	N/M ^a	[55]
spinach NR (Mo domain)	Bead-Beater and 0.5-mm glass beads/continuous flow Dyno Mill model KDL	N/M ^a	o	0.42	N/M ^a	N/M ^a	N/M ^a	[205]
Tobacco NR	vortex-mixing in the presence of glass beads	10% (w/v) glycerol, 1mM-EDTA, 1 /uM Na ₂ MoO ₄ , 0.01mM-FAD, 2mM-2-mercapto-ethanol, 1mM phenylmethanesulphonyl fluoride	r	0.05 ^u	N/M ^a	N/M ^a	N/M ^a	[94]
<i>A. thaliana</i> SO	N/M ^a	N/M ^a	j	N/M ^a	N/M ^a	N/M ^a	N/M ^a	[209]
<i>A. thaliana</i> SO	French pressure cell.	N/M ^a	k	N/M ^a	N/M ^a	N/M ^a	N/M ^a	[112]

Table 1.7 Continued

<u>Enzyme</u>	<u>Homogenization</u>	<u>Lysis Amendments</u>	<u>Purification Procedures</u>	<u>Protein Yield (g/L)</u>	<u>Molybdenum Incorporation</u>	<u>Chaperones</u>	<u>Chaperone function</u>	<u>Ref.</u>
human SO	Microfluidics M110L Microfluidizer Processor	0.5 mM EDTA and 0.1 mg/ml phenylmethylsulfonylfluoride.	b	0.0039-0.0056	80-90%	N/M ^a	N/M ^a	[57]
human His-SO	Microfluidics M110L Microfluidizer Processor	0.5 mM EDTA and 0.1 mg/ml phenylmethylsulfonylfluoride.	c	0.0152	62%	N/M ^a	N/M ^a	[57]
human SO	Microfluidics M110L Microfluidizer Processor	0.5 mM EDTA and 0.1 mg/ml phenylmethylsulfonylfluoride.	b	N/M ^a	N/M ^a	N/M ^a	N/M ^a	[109]
human His-SO	Microfluidics M110L Microfluidizer Processor	0.5 mM EDTA and 0.1 mg/ml phenylmethylsulfonylfluoride.	c	N/M ^a	N/M ^a	N/M ^a	N/M ^a	[109]
human SO	Microfluidics M110L Microfluidizer Processor	0.5 mM EDTA and 0.1 mg/ml phenylmethylsulfonylfluoride.	d	N/M ^a	N/M ^a	N/M ^a	N/M ^a	[110]
human SO	Microfluidics M110L Microfluidizer Processor	0.5 mM EDTA and 0.1 mg/ml phenylmethylsulfonylfluoride.	d	N/M ^a	N/M ^a	N/M ^a	N/M ^a	[111]
human SO	sonication	N/M ^a	e	N/M ^a	N/M ^a	N/M ^a	N/M ^a	[211]
human SO	French pressure cell.	0.5 mM EDTA and 0.1 mg/ml phenylmethylsulfonylfluoride.	f	N/M ^a	76%	N/M ^a	N/M ^a	[67]
human SO	N/M ^a	N/M ^a	g	N/M ^a	80%	N/M ^a	N/M ^a	[68]
human SO	N/M ^a	N/M ^a	h	N/M ^a	N/M ^a	N/M ^a	N/M ^a	[210]
human SO	N/M ^a	N/M ^a	i	N/M ^a	N/M ^a	N/M ^a	N/M ^a	[212]
human SO R160Q	N/M ^a	N/M ^a	g	N/M ^a	91%	N/M ^a	N/M ^a	[95]
mouse SO	N/M ^a	N/M ^a	i	N/M ^a	N/M ^a	N/M ^a	N/M ^a	[108]
rat SO	N/M ^a	N/M ^a	g	N/M ^a	100%	N/M ^a	N/M ^a	[96]
rat SO	French pressure cell.	0.5 mM EDTA and 0.1 mg/ml phenylmethylsulfonylfluoride.	f	N/M ^a	N/M ^a	N/M ^a	N/M ^a	[67]
<i>Zea mays</i> SO	N/M ^a	N/M ^a	l	N/M ^a	N/M ^a	N/M ^a	N/M ^a	[56]

a) N/M- Not mentioned; b) Streptomycin sulfate treatment, ammonium sulfate precipitation, anion exchange chromatography, hydrophobic interaction chromatography; c) Streptomycin sulfate treatment, ammonium sulfate precipitation, IMAC, dialysis; d) Streptomycin sulfate treatment, ammonium sulfate precipitation, anion exchange chromatography, hydrophobic interaction chromatography, size exclusion chromatography; e) QIAexpress kit (Qiagen) for IMAC (Ni-NTA spin column); f) Streptomycin sulfate treatment, ammonium sulfate precipitation, G-25 Sepharose (buffer exchange/desalting) column, anion exchange chromatography, hydrophobic interaction chromatography; g) ammonium sulfate precipitation, heat treated, acetone fractionation, dialysis, anion exchange chromatography, size exclusion chromatography; h) IMAC; i) IMAC, anion exchange chromatography; j) IMAC, dialysis; k) IMAC, PD10 (buffer exchange/desalting) columns, anion exchange chromatography, size exclusion chromatography; l) nickel chelate affinity purification kit (Sangon Co., Shanghai, China); m) glutathione-agarose affinity matrix, Factor Xa cleavage, anion-exchange chromatography, size exclusion chromatography; n) IMAC, size exclusion chromatography; o) ammonium sulfate precipitation, affinity chromatography; p) immunoaffinity chromatography; q) not purified, studied cell extracts or desalted extracts; r) ammonium sulfate precipitation; s) IMAC, dialysis, anion-exchange chromatography, size exclusion chromatography; t) IMAC, PD10 (buffer exchange/desalting) column; u) in percent yield; v) mARC1; w) mARC2.

Table 1.8: Purification parameters for recombinant prokaryotic XO family enzymes.

<u>Enzyme</u>	<u>Homogenization</u>	<u>Lysis Amendments</u>	<u>Purification Procedures</u>	<u>Protein Yield (g/L)</u>	<u>Molybdenum Incorporation</u>	<u>Chaperones</u>	<u>Chaperone function</u>	<u>Ref.</u>
<i>E. coli</i> AO	TS Series Benchtop cell disruptor	DNaseI (1 ug/mL).	i	0.0018	58%	YagQ	incorporation of Moco	[120]
<i>E. coli</i> AO	TS Series Benchtop cell disruptor	DNaseI (1 ug/mL).	i	N/M ^a	N/M ^a	N/M ^a	N/M ^a	[213]
<i>Pyrococcus furiosus</i> tungsten AO	sonication	1 mg/mL lysozyme	j	N/M ^a	N/M ^a	N/M ^a	N/M ^a	[215]
<i>Brevundimonas diminuta</i> 7 Isoquinoline 1-oxidoreductase	ultrasonication	N/M ^a	k	N/M ^a	N/M ^a	N/M ^a	N/M ^a	[216]
<i>Ochrobactrum</i> sp. SJY1 nicotine hydroxylase	N/M ^a	N/M ^a	n	N/M ^a	~100%	N/M ^a	N/M ^a	[129]
<i>P. putida</i> KT2440 nicotinate dehydrogenase	ultrasound	10uM PMSF	k	N/M ^a	N/M ^a	N/M ^a	N/M ^a	[50]
<i>Pseudomonas putida</i> KT2440 nicotinate dehydrogenase	N/M ^a	N/M ^a	k	N/M ^a	N/M ^a	N/M ^a	N/M ^a	[217]
<i>Burkholderia</i> sp. CT39-3 piperonal oxidase	sonication	N/M ^a	n	N/M ^a	55%	N/M ^a	N/M ^a	[218]
<i>Arthrobacter ilicis</i> Ru ^{61a} quinaldine 4-oxidase	sonication	10 M phenylmethylsulfonyl fluoride, and 1.25 units/ml benzonnuclease	m	0.00014	N/M ^a	ORF1	proposed to be homolog of XdhC	[219]
<i>P. putida</i> 86 quinoline 2-oxidoreductase	French press/sonication	10 uM phenylmethanesulfonylfluoride, and 0.05 uL/mL Benzonnuclease	l	43-66°	50%	N/M ^a	N/M ^a	[220]
<i>P. putida</i> 86 quinoline 2-oxidoreductase	N/M ^a	N/M ^a	k	N/M ^a	N/M ^a	N/M ^a	N/M ^a	[221]
<i>C. acidovorans</i> XDH	lysozyme & sonication	0.1 mg/mL lysozyme, 1 mM EDTA, 2 mM 2-mercaptoethanol	h	0.00216 ^p	11-16% ^p , 100% ^q	XdhC'	successful MPT incorporation	[69]
<i>C. acidovorans</i> XDH	lysozyme & french press & sonication	0.1 mg/mL lysozyme, 1mM EDTA, and 2mM mercaptoethanol	h	0.056 ^q	24% ^p , 89% ^q	XdhC'	successful MPT incorporation	[127]
<i>R. capsulatus</i> XDH	French press	DNase I	b	0.0125	70%	XdhC	sulfuration of moco	[117]
<i>R. capsulatus</i> XDH	French press	DNase I	c	N/M ^a	80% (sulfurated)	XdhC	N/M ^a	[119]
<i>R. capsulatus</i> XDH	French press	DNase I	b	N/M ^a	N/M ^a	XdhC	N/M ^a	[118]
<i>R. capsulatus</i> XDH	french press	1 mM EDTA, and 2.5 mM dithiothreitol	d	N/M ^a	0-3% (in xdhC mutant)	XdhC	facilitating the insertion of MPT and/or folding of XDH during or after cofactor insertion	[48]

Table 1.8 Continued

<u>Enzyme</u>	<u>Homogenization</u>	<u>Lysis Amendments</u>	<u>Purification Procedures</u>	<u>Protein Yield (g/L)</u>	<u>Molybdenum Incorporation</u>	<u>Chaperones</u>	<u>Chaperone function</u>	<u>Ref.</u>
<i>R. capsulatus</i> XDH	french press	1 mM EDTA, and 2.5 mM dithiothreitol	e	25°	N/M ^a	N/M ^a	N/M ^a	[47]
<i>R. capsulatus</i> XDH	french press	1 mM EDTA, and 2.5 mM dithiothreitol	f	N/M ^a	N/M ^a	XdhC	N/M ^a	[49]
<i>R. capsulatus</i> XDH	passages through a 112 uM interaction chamber	DNaseI	b	0.008	N/M ^a	XdhC	N/M ^a	[116]
<i>R. capsulatus</i> XDH	passages through a 112 uM interaction chamber	DNaseI	b	N/M ^a	68.28 ± 7.15 %	N/M ^a	N/M ^a	[222]
<i>R. capsulatus</i> XDH	french press	1 mM EDTA, and 2.5 mM dithiothreitol	g	N/M ^a	N/M ^a	N/M ^a	N/M ^a	[223]

a) N/M- Not mentioned; b) IMAC, dialysis, anion exchange chromatography, hydrophobic interaction chromatography; c) IMAC, dialysis, anion exchange chromatography, affinity chromatography, PD-10 (buffer exchange/desalting) column; d) ammonium sulfate precipitation, dialysis, ion exchange chromatography; e) ammonium sulfate precipitation, dialysis, ion exchange chromatography, hydrophobic interaction chromatography; f) ammonium sulfate precipitation, dialysis, electrophoresis gel column; g) IMAC, anion exchange chromatography, affinity chromatography; h) anion exchange chromatography, IMAC, size exclusion chromatography; i) IMAC, dialysis or PD10 (buffer exchange/desalting) column anion exchange chromatography, size exclusion chromatography; j) anion exchange chromatography; k) not purified, studied crude cell extracts; l) ammonium sulfate fractionation, hydrophobic interaction chromatography, anion exchange chromatography; m) ammonium sulfate precipitation, hydrophobic interaction chromatography, size exclusion chromatography, anion exchange chromatography; n) IMAC; o) in percent yield; p) Expressed as complex with AB subunits; q) Expressed as complex with ABC subunits; r) Form *P. aeruginosa*.

Table 1.9: Purification parameters for recombinant prokaryotic SO family enzymes.

<u>Enzyme</u>	<u>Homogenization</u>	<u>Lysis Amendments</u>	<u>Purification Procedures</u>	<u>Protein Yield (g/L)</u>	<u>Molybdenum Incorporation</u>	<u>Chaperones</u>	<u>Chaperone function</u>	<u>Ref.</u>
<i>D. radiodurans</i> SO	ultrasonic treatment	0.7 mM phenylmethylsulfonyl fluoride	c	N/M ^a	N/M ^a	N/M ^a	N/M ^a	[224]
<i>S. meliloti</i> SorT	french press	N/M ^a	d	0.015	69%	N/M ^a	N/M ^a	[122]
<i>S. novella</i> sulphite:cytochrome c oxidoreductase	french press/Periplasmic isolation	N/M ^a	b	0.00025	63%	N/M ^a	N/M ^a	[171]
<i>T. thermophilus</i> AT62 SO	french press	N/M ^a	c	N/M ^a	N/M ^a	N/M ^a	N/M ^a	[121]
<i>T. thermophilus</i> HB8 SO	chemical lysis	5% (vol/vol) CellLytic reagent, 1 mg/ml lysozyme 50 ug/ml DNase I	e	N/M ^a	N/M ^a	N/M ^a	N/M ^a	[123]
<i>E. coli</i> YedY	periplasmic isolation by osmotic shock	0.4 mM phenylmethylsulfonyl fluoride, 5 mM EDTA	f	~0.1 ⁱ	N/M ^a	N/M ^a	N/M ^a	[70]
<i>E. coli</i> HB101 YedYZ	periplasmic isolation/french press	1 mM EDTA, 0.2 mM phenylmethylsulfonyl fluoride (PMSF), and 20% (w/v) sucrose	g	0.01	N/M ^a	N/M ^a	N/M ^a	[71]
<i>E. coli</i> YedY	Cell Disrupter	N/M ^a	e	N/M ^a	N/M ^a	N/M ^a	N/M ^a	[124]
<i>R. sphaeroides</i> YedY	periplasmic isolation, cell disruptor	1 mg/ml lysozyme	h	N/M ^a	N/M ^a	Unknown REMP, GroEL, Trigger Factor	protection from proteolysis before Moco is inserted, folding/stabilization	[101]

a) N/M- Not mentioned; b) anion exchange chromatography, ammonium sulfate precipitation, hydrophobic interaction chromatography, dialysis, size exclusion chromatography; c) IMAC, dialysis; d) IMAC, desalting column, Size exclusion chromatography; e) IMAC, Size exclusion chromatography; f) IMAC, anion exchange chromatography, size exclusion chromatography; g) periplasmic isolation, IMAC; h) IMAC, size exclusion chromatography, TEV cleavage; i) in units of mg protein/g of cells.

Table 1.10: Purification parameters for recombinant prokaryotic DMSOR family enzymes.

<u>Enzyme</u>	<u>Homogenization</u>	<u>Lysis Amendments</u>	<u>Purification Procedures</u>	<u>Protein Yield (g/L)</u>	<u>Molybdenum Incorporation</u>	<u>Chaperones</u>	<u>Chaperone function</u>	<u>Ref.</u>
<i>A. faecalis</i> Aio	french press	N/M ^a	ad	N/M ^a	N/M ^a	N/M ^a	N/M ^a	[80]
<i>Ralstonia</i> sp. S22 Aio	french press	N/M ^a	w	N/M ^a	N/M ^a	N/M ^a	N/M ^a	[99]
<i>Rhizobium</i> sp. NT-26 Aio	french press	N/M ^a	ad	0.0011	83.10%	N/M ^a	N/M ^a	[62]
<i>Rhizobium</i> sp. NT-26 Aio	french press	N/M ^a	ad	N/M ^a	N/M ^a	N/M ^a	N/M ^a	[81]
<i>Rhizobium</i> sp. NT-26 Aio	french press	N/M ^a	ad	N/M ^a	N/M ^a	N/M ^a	N/M ^a	[82]
<i>Rhizobium</i> sp. NT-26 Aio	french press	N/M ^a	ad	N/M ^a	N/M ^a	N/M ^a	N/M ^a	[80]
<i>Shewanella</i> sp. ANA-3 Arr	chemical lysis/centrifugation	protease inhibitor cocktail, CellLytic powder	ae	N/M ^a	135%	N/M ^a	N/M ^a	[98]
<i>Shewanella</i> sp. ANA-3 Arr	EDTA and lysozyme treatment	ULTRA protease inhibitor, MgCl ₂ and CaCl ₂ , DNase I	af	0.005	95%	N/M ^a	N/M ^a	[225]
<i>E. coli</i> BSOR	N/M ^a	N/M ^a	c	N/M ^a	N/M ^a	N/M ^a	N/M ^a	[74]
<i>R. sphaeroides</i> BSOR	Microfluidics M110L microfluidizer	N/M ^a	b	0.00115	88%	N/M ^a	N/M ^a	[72]
<i>R. sphaeroides</i> BSOR	sonication	dithiothreitol (10 mM), sodium molybdate (1 mM), aprotinin (0.1 mg/ml), EDTA (1 mM), and PMSF (0.1 mM)	b	1.25x10 ⁻⁴	N/M ^a	N/M ^a	N/M ^a	[29]
<i>R. sphaeroides</i> BSOR	sonication	0.1mM PMSF	d	N/M ^a	N/M ^a	N/M ^a	N/M ^a	[73]
<i>R. sphaeroides</i> BSOR	sonication	dithiothreitol (10 mM), sodium molybdate (1 mM), aprotinin (0.1 mg/ml), EDTA (1 mM), and PMSF (0.1 mM)	b	N/M ^a	N/M ^a	N/M ^a	N/M ^a	[135]
<i>S. denitrificans</i> steroid C-25 dehydrogenase	french press	0.1 mg DNase I, 1 mM dithiothreitol (DTT), and 0.02% (wt/vol) Tween 20	aj	1.32-2.04 ^{ao}	50-80%	SdhD	proposed role in folding/Moc o insertion binds TAT seq, escorts protein for translocation	[226]
<i>E. coli</i> DMSOR	french press	2 mM EDTA, 2 mM DTT, 0.1 mM PMSF	f	N/M ^a	N/M ^a	DmsD		[157]
<i>E. coli</i> DMSOR	N/M ^a	N/M ^a	g	N/M ^a	N/M ^a	N/M ^a	N/M ^a	[65]
<i>E. coli</i> DMSOR	French pressure cell, differential centrifugation	0.2 mM PMSF	g	N/M ^a	N/M ^a	N/M ^a	N/M ^a	[77]
<i>E. coli</i> DMSOR	french press	5 mM EDTA, 200 pg/ml PMSF	j	N/M ^a	N/M ^a	N/M ^a	N/M ^a	[227]
<i>E. coli</i> DMSOR	French pressure cell lysis and differential centrifugation	0.2 mM PMSF	g	N/M ^a	N/M ^a	N/M ^a	N/M ^a	[228]

Table 1.10 Continued

<u>Enzyme</u>	<u>Homogenization</u>	<u>Lysis Amendments</u>	<u>Purification Procedures</u>	<u>Protein Yield (g/L)</u>	<u>Molybdenum Incorporation</u>	<u>Chaperones</u>	<u>Chaperone function</u>	<u>Ref.</u>
<i>E. coli</i> DMSOR	French pressure cell lysis and differential centrifugation	0.2 mM PMSF	g	N/M ^a	N/M ^a	N/M ^a	N/M ^a	[229]
<i>E. coli</i> DMSOR	French pressure cell	2mM PMSF, 10 pg/mL DNase, 10 pg/mL RNase, and 40 mM MgCl	k	N/M ^a	N/M ^a	N/M ^a	N/M ^a	[75]
<i>E. coli</i> DMSOR	N/M ^a	N/M ^a	N/M ^a	N/M ^a	N/M ^a	N/M ^a	N/M ^a	[230]
<i>E. coli</i> DMSOR	French pressure cell, differential centrifugation	0.2 mM phenylmethylsulfonyl fluoride	l	N/M ^a	26%	N/M ^a	N/M ^a	[76]
<i>E. coli</i> DMSOR	French pressure cell	2mM PMSF, 10 pg/mL DNase, 10 pg/mL RNase, and 40 mM MgCl	k	N/M ^a	N/M ^a	N/M ^a	N/M ^a	[78]
<i>R. capsulatus</i> DMSOR	periplasmic isolation	0.5M sucrose, 1.5mM EDTA	h	N/M ^a	N/M ^a	N/M ^a	N/M ^a	[166]
<i>R. sphaeroides</i> DMSOR	freezing method	5 mg of DNase I	i	0.0002	66-87%	N/M ^a	N/M ^a	[54]
<i>R. sphaeroides</i> DMSOR	Microfluidics M110L Microfluidizer Processor	N/M ^a	e	0.0034	83%	MobAB	roles in cofactor insertion	[64]
<i>R. sphaeroides</i> DMSOR	N/M ^a	N/M ^a	g	N/M ^a	N/M ^a	N/M ^a	N/M ^a	[92]
<i>C. glutamicum</i> ATCC 13032 FDH	french press	protease inhibitor tablet	d	N/M ^a	N/M ^a	FdhD	accessory protein; acts as a sulfur transferase between a desulfurase and FdhF possibly	[231]
<i>D. vulgaris</i> formate dehydrogenase	chemical lysis/centrifugation	7 U/ml DNase, 250 mg lysozyme, 0.1% Triton X-100, and 5 mM MgCl ₂	f	N/M ^a	N/M ^a	FdhDE	maturation processing	[232]
<i>E. coli</i> FDH	cell disrupter	N/M ^a	ag	N/M ^a	N/M ^a	N/M ^a	N/M ^a	[233]
<i>E. coli</i> FDH	cell disrupter	N/M ^a	ag	N/M ^a	N/M ^a	N/M ^a	N/M ^a	[234]
<i>E. coli</i> FDH	chemical lysis/centrifugation	6 U/ml DNase, 250 mg lysozyme, 0.1% Triton X-100, and 5 mM MgCl ₂	f	N/M ^a	N/M ^a	N/M ^a	N/M ^a	[232]
<i>E. coli</i> FDH	french press	N/M ^a	g	N/M ^a	N/M ^a	N/M ^a	N/M ^a	[60]
<i>E. coli</i> FDH	N/M ^a	N/M ^a	g	N/M ^a	N/M ^a	N/M ^a	N/M ^a	[235]
<i>M. formicicum</i> FDH	N/M ^a	N/M ^a	ah	N/M ^a	N/M ^a	N/M ^a	N/M ^a	[236]
<i>R. capsulatus</i> FDH	cell disruptor/sonication	N/M ^a	p	0.006	39%	FdsC and FdsD	FdsD influences Moco insertion, FdsC has a role in the sulfuration of bis-MGD	[88]
<i>R. capsulatus</i> FDH	cell disruptor/sonication	N/M ^a	p	N/M ^a	39%	N/M ^a	N/M ^a	[91]

Table 1.10 Continued

<u>Enzyme</u>	<u>Homogenization</u>	<u>Lysis Amendments</u>	<u>Purification Procedures</u>	<u>Protein Yield (g/L)</u>	<u>Molybdenum Incorporation</u>	<u>Chaperones</u>	<u>Chaperone function</u>	<u>Ref.</u>
<i>R. capsulatus</i> FDH	cell disruptor/sonication	N/M ^a	p	N/M ^a	N/M ^a	FdsC	insertion of the sulfido group into Moco	[90]
<i>R. capsulatus</i> FDH (FdsC chaperone)	cell disruptor/sonication	N/M ^a	p	0.002-0.005	N/M ^a	FdsC and FdsD	FdsC might act as a platform connecting bis-MGD biosynthesis and its insertion into the target	[89]
<i>W. succinogenes</i> FDH	N/M ^a	N/M ^a	g	N/M ^a	N/M ^a	N/M ^a	N/M ^a	[237]
<i>M. barkeri</i> Formylmethanofuran dehydrogenase	boiling in SDS buffer	N/M ^a	ai	N/M ^a	N/M ^a	FmdE	possible NarJ like role	[52]
<i>m. thermoautotrophicum</i> Formylmethanofuran dehydrogenase (W)	boiling in SDS buffer	N/M ^a	g	N/M ^a	N/M ^a	N/M ^a	N/M ^a	[51]
<i>C. necator</i> Nap	periplasmic extraction	N/M ^a	u	N/M ^a	N/M ^a	N/M ^a	N/M ^a	[130]
<i>C. necator</i> Nap	periplasmic extraction	N/M ^a	v	N/M ^a	N/M ^a	N/M ^a	N/M ^a	[170]
<i>C. necator</i> Nap	sonication	N/M ^a	h	N/M ^a	N/M ^a	N/M ^a	N/M ^a	[93]
<i>E. coli</i> Nap	periplasmic extraction	N/M ^a	s	2x10 ⁻⁵ -5x10 ⁻⁵	N/M ^a	N/M ^a	N/M ^a	[61]
<i>E. coli</i> Nap	periplasmic isolation/french press	N/M ^a	t	N/M ^a	N/M ^a	N/M ^a	N/M ^a	[169]
<i>R. sphaeroides</i> Nap	periplasmic isolation/french press	N/M	q	0.001	N/M ^a	N/M ^a	N/M ^a	[167]
<i>R. sphaeroides</i> Nap	periplasmic extraction	1 mg/ml lysozyme	r	0.001	N/M ^a	N/M ^a	N/M ^a	[168]
<i>Synechococcus</i> sp. strain PCC 7942 NR (narB)	ultrasonic treatment/French Press	PMSF, aminocaproic acid and benzamidine at 1 mM	ac	N/M ^a	109%	N/M ^a	N/M ^a	[83]
<i>Synechococcus</i> sp. strain PCC 7942 NR (narB)	french press	N/M ^a	w	N/M ^a	120%	N/M ^a	N/M ^a	[84]
<i>E. coli</i> NarGHI	Emulsiflex C3 microfluidizer	0.2mM phenylmethylsulfonyl fluoride	g	N/M ^a	N/M ^a	N/M ^a	N/M ^a	[238]
<i>E. coli</i> NarGHI	French press cell lysis and differential centrifugation	N/M ^a	g	N/M ^a	N/M ^a	N/M ^a	N/M ^a	[239]
<i>E. coli</i> NarGHI	N/M ^a	EDTA 1 mM	d	N/M ^a	N/M ^a	N/M ^a	N/M ^a	[240]

Table 1.10 Continued

<u>Enzyme</u>	<u>Homogenization</u>	<u>Lysis Amendments</u>	<u>Purification Procedures</u>	<u>Protein Yield (g/L)</u>	<u>Molybdenum Incorporation</u>	<u>Chaperones</u>	<u>Chaperone function</u>	<u>Ref.</u>
<i>E. coli</i> NarGHI	N/M ^a	N/M ^a	d	N/M ^a	N/M ^a	N/M ^a	N/M ^a	[241]
<i>E. coli</i> NarGHI	french press	0.2 mM PMSF	x	N/M ^a	N/M ^a	NarJ	role in activating the $\alpha\beta$ (NarGNarH) complex	[243]
<i>E. coli</i> NarGHI	french press	0.2 mM PMSF	x	N/M ^a	N/M ^a	NarJ	N/M ^a	[246]
<i>E. coli</i> NarGHI	N/M ^a	N/M ^a	y	N/M ^a	N/M ^a	N/M ^a	N/M ^a	[85]
<i>E. coli</i> NarGHI	French press cell lysis and differential centrifugation	5 mM EDTA, 0.2 mM PMSF	g	N/M ^a	N/M ^a	N/M ^a	N/M ^a	[86]
<i>E. coli</i> NarGHI	french press	N/M ^a	x	N/M ^a	N/M ^a	NarJ	N/M ^a	[242]
<i>E. coli</i> NarGHI	French press cell lysis and differential centrifugation	N/M ^a	g	N/M ^a	N/M ^a	N/M ^a	N/M ^a	[244]
<i>E. coli</i> NarGHI	French press cell lysis and differential centrifugation	N/M ^a	z	N/M ^a	N/M ^a	N/M ^a	N/M ^a	[245]
<i>E. coli</i> NarGHJI	French press	1 mM benzamidine-HCl	aa	11 ^{an}	N/M ^a	NarJ/NarI	NarI-attachment of the complex to the membrane, NarJ-complex activation	[247]
<i>E. coli</i> NarGYWV	French press	1 mM benzamidine-HCl	ab	13.2 ^{an}	N/M ^a	NarW/NarV	N/M ^a	[87]
<i>E. coli</i> NR- Z	French press	1 mM benzamidine-HCl	g	N/M ^a	N/M ^a	N/M ^a	N/M ^a	[249]
<i>E. coli</i> NR-A & Z (Nar)	N/M ^a	N/M ^a	x	N/M ^a	36%	N/M ^a	N/M ^a	[248]
<i>B. megaterium</i> NCT-2 Nas	AH-1500 high pressure homogenizer	N/M ^a	d	N/M ^a	N/M ^a	N/M ^a	N/M ^a	[53]
<i>E. coli</i> TMAOR	Microfluidics M110L Microfluidizer Processor	10 ug/ml DNase I	m	0.0013	30-66%	N/M ^a	N/M ^a	[97]
<i>E. coli</i> TMAOR	periplasmic extraction	N/M ^a	n	N/M ^a	N/M ^a	N/M ^a	N/M ^a	[63]
<i>E. coli</i> TMAOR	sonication	N/M ^a	o	N/M ^a	34% ^{ak} , 97% ^{al} , 96% ^{am}	TorD	binds TAT seq, escorts protein for translocation, involved in cofactor insertion	[126]

Table 1.10 Continued

<u>Enzyme</u>	<u>Homogenization</u>	<u>Lysis Amendments</u>	<u>Purification Procedures</u>	<u>Protein Yield (g/L)</u>	<u>Molybdenum Incorporation</u>	<u>Chaperones</u>	<u>Chaperone function</u>	<u>Ref.</u>
<i>H. influenzae</i> TMAOR	French press	5% glycerol, 1mM Pefabloc SC	p	0.0014	53%	N/M ^a	N/M ^a	[79]

a) N/M- Not mentioned; b) glutathione-agarose affinity chromatography, anion exchange chromatography, size exclusion chromatography, Factor Xa proteolysis; c) cloning study, no expression/purification; d) affinity chromatography; e) IMAC, hydrophobic chromatography, ultrafiltration; f) affinity chromatography, dialysis; g) no purification, studies on whole cells, cell extracts and/or isolated membranes; h) ammonium sulfate precipitation, hydrophobic chromatography, ultrafiltration, size exclusion chromatography, ion exchange chromatography; i) extract heat treatment, IMAC, hydrophobic chromatography, ultrafiltration; j) size exclusion chromatography; k) extraction with detergent, anion exchange chromatography, size exclusion chromatography; l) purified from membranes by detergent extraction, anion-exchange chromatography; m) extract heat treatment, IMAC, anion exchange chromatography, size exclusion chromatography, dialysis; n) periplasmic extraction, anion exchange chromatography, native page, active band was cut out and the protein was electroeluted using a Bio-Trap apparatus; o) IMAC (Ni-NTA), purification was conducted comparing aerobically and anaerobically isolated enzyme; p) IMAC, size exclusion chromatography, PD-10 desalting column; q) periplasmic extraction, IMAC; r) periplasmic extraction, affinity chromatography, size exclusion chromatography; s) periplasmic isolation, anion exchange chromatography, hydrophobic interaction chromatography, size exclusion chromatography; t) periplasmic extraction, dialysis; u) periplasmic extraction, dialysis, cation exchange chromatography, size exclusion chromatography; v) periplasmic extraction; w) affinity chromatography, size exclusion chromatography; x) heat treatment, anion exchange chromatography, dialysis; y) membrane purification, detergent extraction, anion exchange chromatography, size exclusion chromatography; z) Enriched inner membrane vesicles were prepared from crude membranes by sucrose step centrifugation, purified enzyme by anion exchange chromatography; aa) ammonium sulfate precipitation, anion exchange chromatography, size exclusion chromatography, immunoprecipitation, dialysis; ab) detergent solubilization, anion exchange chromatography, dialysis, size exclusion chromatography; ac) ammonium sulfate precipitation, DEAE chromatography, G-25 (buffer exchange/desalting) column, affinity chromatography, size exclusion chromatography initially. Then routinely purified by ammonium sulfate and anti-NarB antibodies affinity chromatography, hydrophobic interaction chromatography; ad) affinity and size exclusion chromatography, His-tag encoded by the vector was removed using rTEV; ae) IMAC, U of Prescission protease tag cleavage, glutathione-affinity chromatography, size exclusion chromatography; af) IMAC, TEV cleavage, ammonium sulfate precipitation, hydrophobic interaction chromatography, size exclusion chromatography; ag) hydrophobic interaction chromatography, anion exchange chromatography, size exclusion chromatography; ah) crude extract studies or partially purified by anion exchange chromatography; ai) only the ferredoxin unit was purified not the moco unit; aj) anion exchange chromatography under anaerobic conditions, affinity chromatography; ak) aerobic expression and purification; al) anaerobic expression and aerobic purification; am) anaerobic expression and anaerobic purification; an) in percent yield; ao) in units of mg protein/g of cells.

Table 1.11: Kinetic parameters for eukaryotic XO family of enzymes.

Enzyme ^a	K _m (μM)	K _{cat} (min ⁻¹)	Specific Activity (μmol subs/min/mg)	pH	Substrate	Assay Description	Ref.
<i>A. thaliana</i> rAO homolog 1	N/M ^b	N/M ^b	0.558 ± 0.030	7.4	indole-3-carbaldehyde	l	[178]
<i>A. thaliana</i> rAO homolog 3	N/M ^b	N/M ^b	0.635 ± 0.060	7.4	abscisic aldehyde	l	[178]
<i>A. thaliana</i> rAO homolog 1 (+ DPI inhibitor)	N/M ^b	N/M ^b	0.004 ± 0.001	7.4	indole-3-carbaldehyde	l	[178]
<i>A. thaliana</i> rAO homolog 3 (+ DPI inhibitor)	N/M ^b	N/M ^b	0.100 ± 0.008	7.4	abscisic aldehyde	l	[178]
<i>A. thaliana</i> rAO homolog 1 (+ KCN inhibitor)	N/M ^b	N/M ^b	ND ^e	7.4	indole-3-carbaldehyde	l	[178]
<i>A. thaliana</i> rAO homolog 3 (+ KCN inhibitor)	N/M ^b	N/M ^b	ND ^e	7.4	abscisic aldehyde	l	[178]
<i>A. thaliana</i> rAO homolog 1	N/M ^b	N/M ^b	0.515 ± 0.023	7.4	abscisic aldehyde	l	[178]
<i>A. thaliana</i> rAO homolog 1	N/M ^b	N/M ^b	0.110 ± 0.0535	7.4	Benzaldehyde	l	[178]
<i>A. thaliana</i> rAO homolog 1	N/M ^b	N/M ^b	0.093 ± 0.024	7.4	heptaldehyde	l	[178]
<i>A. thaliana</i> rAO homolog 3	N/M ^b	N/M ^b	0.517 ± 0.029	7.4	heptaldehyde	l	[178]
<i>A. thaliana</i> rAO homolog 3	N/M ^b	N/M ^b	0.204 ± 0.039	7.4	indole-3-carbaldehyde	l	[178]
<i>A. thaliana</i> rAO homolog 3	N/M ^b	N/M ^b	0.146 ± 0.060	7.4	Benzaldehyde	l	[178]
<i>A. thaliana</i> rAO homolog 3	N/M ^b	N/M ^b	0.530 ± 0.052	7.4	NADH	m	[178]
<i>A. thaliana</i> rAO homolog 1	N/M ^b	N/M ^b	0.215 ± 0.043	7.4	NADH	m	[178]
<i>A. thaliana</i> rAO homolog 4	23.8	5712	0.072 ^c	7.0	Benzaldehyde	o	[58]
<i>A. thaliana</i> rAO homolog 4	58.1	15234	0.192 ^c	7.0	NAD ⁺	o	[58]
<i>A. thaliana</i> rAO homolog 4	2070	114240	90.06 ^c	7.0	Indole-3-acetaldehyde	o	[58]
<i>A. thaliana</i> rAO homolog 4	103.9	26190	0.33 ^c	7.0	Cinnamaldehyde	o	[58]
<i>A. thaliana</i> rAOα	14	N/M ^b	0.0071	7.5	Heptaldehyde	l	[179]
<i>A. thaliana</i> rAOα	19	N/M ^b	0.0080	7.5	Protocatechualdehyde	o	[179]
<i>A. thaliana</i> rAOα	0.74	N/M ^b	0.017	7.5	Benzaldehyde	o	[179]
<i>A. thaliana</i> rAOα	ND ^e	N/M ^b	ND ^e	7.5	Naphthaldehyde	o	[179]
<i>A. thaliana</i> rAOα	4.4	N/M ^b	0.0069	7.5	Indole-3-aldehyde	o	[179]
<i>A. thaliana</i> rAOα	39	N/M ^b	0.0073	7.5	Indole-3-acetaldehyde	o	[179]
<i>A. thaliana</i> rAOα	20	N/M ^b	0.0038	7.5	Cinnamaldehyde	l	[179]
<i>A. thaliana</i> rAOα	22	N/M ^b	0.038	7.5	Citral	l	[179]
<i>A. thaliana</i> rAOγ	57	N/M ^b	0.024	7.5	Heptaldehyde	l	[179]
<i>A. thaliana</i> rAOγ	ND ^e	N/M ^b	ND ^e	7.5	Protocatechualdehyde	o	[179]
<i>A. thaliana</i> rAOγ	7.7	N/M ^b	0.0087	7.5	Benzaldehyde	o	[179]
<i>A. thaliana</i> rAOγ	0.33	N/M ^b	0.065	7.5	Naphthaldehyde	o	[179]
<i>A. thaliana</i> rAOγ	ND ^e	N/M ^b	ND ^e	7.5	Indole-3-aldehyde	o	[179]
<i>A. thaliana</i> rAOγ	ND ^e	N/M ^b	ND ^e	7.5	Indole-3-acetaldehyde	o	[179]
<i>A. thaliana</i> rAOγ	410	N/M ^b	0.020	7.5	Cinnamaldehyde	l	[179]
<i>A. thaliana</i> rAOγ	ND ^e	N/M ^b	ND ^e	7.5	Citral	l	[179]
Human rAO	293	N/M ^b	8.1 ^c	7.4	6-substituted Quinazoline (R=OCH ₃)	p	[103]
Human rAO	142	N/M ^b	1.32 ^c	7.4	6-substituted Quinazoline (R=CH ₃)	p	[103]
Human rAO	399	N/M ^b	14.4 ^c	7.4	6-substituted Quinazoline (R=H)	p	[103]
Human rAO	27	N/M ^b	6.78 ^c	7.4	6-substituted Quinazoline (R=Cl)	p	[103]
Human rAO	IA ^g	IA ^g	IA ^g	7.4	6-substituted Quinazoline (R=NO ₂)	p	[103]

Table 1.11 Continued

<u>Enzyme^a</u>	<u>K_m (μM)</u>	<u>K_{cat} (min⁻¹)</u>	<u>Specific Activity (μmol subs/min/mg)</u>	<u>pH</u>	<u>Substrate</u>	<u>Assay Description</u>	<u>Ref.</u>
Bovine XO	85	N/M ^b	0.54 ^c	7.4	6-substituted Quinazoline (R=OCH ₃)	p	[103]
Bovine XO	56	N/M ^b	7.26 ^c	7.4	6-substituted Quinazoline (R=CH ₃)	p	[103]
Bovine XO	31	N/M ^b	1.02 ^c	7.4	6-substituted Quinazoline (R=H)	p	[103]
Bovine XO	11	N/M ^b	9.84 ^c	7.4	6-substituted Quinazoline (R=Cl)	p	[103]
Bovine XO	u	u	u	7.4	6-substituted Quinazoline (R=NO ₂)	p	[103]
Human rAO, codon optimized, chemically sulfurated	15.91 ± 2.9	306.5 ± 11.7	1.4591 ± 0.1705	8.0	Phenanthridine	q	[180]
Human rAO, codon optimized, chemically sulfurated	24.85 ± 3.5	220.5 ± 5.6	1.4591 ± 0.1705	8.0	Phenanthridine	r	[180]
Human rAO, codon optimized, chemically sulfurated	1.8 ± 0.5	27.5 ± 5.0	1.4591 ± 0.1705	8.0	Phenanthridine	l	[180]
Human rAO, codon optimized, chemically sulfurated	196.2 ± 10.8	271.7 ± 13.9	1.4591 ± 0.1705	8.0	Phthalazine	r	[180]
Human rAO, codon optimized, chemically sulfurated	22.14 ± 4.1	27.4 ± 3.7	1.4591 ± 0.1705	8.0	Phthalazine	l	[180]
Human rAO, codon optimized, chemically sulfurated	80.16 ± 8.4	187.8 ± 13.9	1.4591 ± 0.1705	8.0	Benzaldehyde	r	[180]
Human rAO, codon optimized, chemically sulfurated	12.1 ± 2.7	56.9 ± 8.6	1.4591 ± 0.1705	8.0	Benzaldehyde	l	[180]
Human rAO, original sequence, chemically sulfurated	26.53 ± 6.5	284.8 ± 11.3	1.5167 ± 0.1827	8.0	Phenanthridine	q	[180]
Human rAO, original sequence, chemically sulfurated	25.5 ± 4.8	292.1 ± 15.8	1.5167 ± 0.1827	8.0	Phenanthridine	r	[180]
Human rAO, original sequence, chemically sulfurated	0.78 ± 0.1	26.8 ± 1.4	1.5167 ± 0.1827	8.0	Phenanthridine	l	[180]
Human rAO, original sequence, chemically sulfurated	125.7 ± 4.1	223.3 ± 10.6	1.5167 ± 0.1827	8.0	Phthalazine	r	[180]
Human rAO, original sequence, chemically sulfurated	8.96 ± 0.8	31.62 ± 3.9	1.5167 ± 0.1827	8.0	Phthalazine	l	[180]
Human rAO, original sequence, chemically sulfurated	45.18 ± 6.2	203.7 ± 12.1	1.5167 ± 0.1827	8.0	Benzaldehyde	r	[180]
Human rAO, original sequence, chemically sulfurated	4.6 ± 0.3	29.8 ± 1.1	1.5167 ± 0.1827	8.0	Benzaldehyde	l	[180]
Human rAO, S1271L, chemically sulfurated	12.03 ± 0.9	233.36 ± 13.6	1.1321 ± 0.1553	8.0	Phenanthridine	q	[180]
Human rAO, S1271L, chemically sulfurated	15.98 ± 3.9	124.96 ± 2.5	1.1321 ± 0.1553	8.0	Phenanthridine	r	[180]
Human rAO, S1271L, chemically sulfurated	1.56 ± 0.1	15.65 ± 1.3	1.1321 ± 0.1553	8.0	Phenanthridine	l	[180]
Human rAO, S1271L, chemically sulfurated	177.4 ± 12.4	175.6 ± 8.2	1.1321 ± 0.1553	8.0	Phthalazine	r	[180]
Human rAO, S1271L, chemically sulfurated	12.16 ± 0.8	17.44 ± 0.7	1.1321 ± 0.1553	8.0	Phthalazine	l	[180]

Table 1.11 Continued

<u>Enzyme^a</u>	<u>K_m (μM)</u>	<u>K_{cat} (min⁻¹)</u>	<u>Specific Activity (μmol subs/min/mg)</u>	<u>pH</u>	<u>Substrate</u>	<u>Assay Description</u>	<u>Ref.</u>
Human rAO, S1271L, chemically sulfurated	67.8 ± 10.9	95.7 ± 5.2	1.1321 ± 0.1553	8.0	Benzaldehyde	r	[180]
Human rAO, S1271L, chemically sulfurated	7.83 ± 0.7	15.46 ± 1.2	1.1321 ± 0.1553	8.0	Benzaldehyde	l	[180]
Human rAO, codon optimized, no additional sulfuration	N/M ^b	N/M ^b	0.1414 ± 0.0298	8.0	Phenanthridine	q	[180]
Human rAO, original sequence, no additional sulfuration	N/M ^b	N/M ^b	0.1136 ± 0.0341	8.0	Phenanthridine	q	[180]
Human rAO, S1271L, no additional sulfuration	N/M ^b	N/M ^b	0.1267 ± 0.0210	8.0	Phenanthridine	q	[180]
Human rAO	7.1 ± 0.6	6.4 ± 0.1	N/M ^b	7.5	Benzaldehyde	l	[104]
Human rAO R802C	7.6 ± 1.9	5.3 ± 0.3	N/M ^b	7.5	Benzaldehyde	l	[104]
Human rAO R921H	6.3 ± 1.2	1.7 ± 0.1	N/M ^b	7.5	Benzaldehyde	l	[104]
Human rAO N1135S	6.7 ± 2.8	6.2 ± 0.3	N/M ^b	7.5	Benzaldehyde	l	[104]
Human rAO H1297R	5.2 ± 1.8	6.4 ± 0.3	N/M ^b	7.5	Benzaldehyde	l	[104]
Human rAO	1.3 ± 0.3	5.6 ± 0.2	N/M ^b	7.5	Phthalazine	l	[104]
Human rAO R802C	0.9 ± 0.3	5.2 ± 0.3	N/M ^b	7.5	Phthalazine	l	[104]
Human rAO R921H	1.6 ± 0.3	2.4 ± 0.1	N/M ^b	7.5	Phthalazine	l	[104]
Human rAO N1135S	1.2 ± 0.1	7.2 ± 0.1	N/M ^b	7.5	Phthalazine	l	[104]
Human rAO H1297R	1.3 ± 0.2	5.4 ± 0.1	N/M ^b	7.5	Phthalazine	l	[104]
Human rAO	3.9 ± 0.8	12.2 ± 0.5	N/M ^b	7.5	Phenanthridine	l	[104]
Human rAO R802C	4.4 ± 0.4	10.2 ± 0.2	N/M ^b	7.5	Phenanthridine	l	[104]
Human rAO R921H	ND ^e	ND ^e	N/M ^b	7.5	Phenanthridine	l	[104]
Human rAO N1135S	6.1 ± 1.0	32.6 ± 1.1	N/M ^b	7.5	Phenanthridine	l	[104]
Human rAO H1297R	4.1 ± 0.7	31.5 ± 1.0	N/M ^b	7.5	Phenanthridine	l	[104]
Human rAO	5.2 ± 0.7	5.6 ± 0.1	N/M ^b	7.5	Chloroquinazolinone	l	[104]
Human rAO R802C	4.7 ± 0.7	5.4 ± 0.2	N/M ^b	7.5	Chloroquinazolinone	l	[104]
Human rAO R921H	4.5 ± 0.8	3.6 ± 0.1	N/M ^b	7.5	Chloroquinazolinone	l	[104]
Human rAO N1135S	4.1 ± 0.5	6.5 ± 0.1	N/M ^b	7.5	Chloroquinazolinone	l	[104]
Human rAO H1297R	5.8 ± 0.5	6.7 ± 0.2	N/M ^b	7.5	Chloroquinazolinone	l	[104]
Monkey rAO (high affinity form)	2.70 ± 0.32	N/M ^b	0.0000582 ± 0.00000770 ^c	N/M ^b	(S)-RS-8359	i	[182]
Monkey rAO (low affinity form)	75.4 ± 16.2	N/M ^b	0.000287 ± 0.00000560 ^c	N/M ^b	(S)-RS-8359	i	[182]
Monkey AO (high affinity form)	3.63 ± 0.34	N/M ^b	0.000644 ± 0.0000476 ^c	N/M ^b	(S)-RS-8359	i	[182]
Monkey AO (low affinity form)	61.8 ± 3.45	N/M ^b	0.003454 ± 0.000642 ^c	N/M ^b	(S)-RS-8359	i	[182]
Rat rAO	23.8 ± 5.56	N/M ^b	0.0000898 ± 0.0000145 ^c	N/M ^b	(S)-RS-8359	i	[182]
Rat AO	90	N/M ^b	0.000333 ^c	7.4	(S)-RS-8359	i	[182, 250]
Monkey rAO (WT)	10.9 ± 2.19	N/M ^b	0.00722 ± 0.00173 ^c	7.4	(S)-RS-8359	o	[184]
Rabbit rAO (WT)	147 ± 14.6	N/M ^b	0.00360 ± 0.00150 ^c	7.4	(S)-RS-8359	o	[184]
Monkey Rabbit rAO Chimera 1	26.5 ± 16.4	N/M ^b	0.00168 ± 0.000266 ^c	7.4	(S)-RS-8359	o	[184]
Monkey Rabbit rAO Chimera 2	126 ± 24.7	N/M ^b	0.00332 ± 0.000296 ^c	7.4	(S)-RS-8359	o	[184]
Monkey Rabbit rAO Chimera 3	30.1 ± 8.88	N/M ^b	0.00285 ± 0.000755 ^c	7.4	(S)-RS-8359	o	[184]
Monkey Rabbit rAO Chimera 4	68.3 ± 10.2	N/M ^b	0.00362 ± 0.000469 ^c	7.4	(S)-RS-8359	o	[184]
Monkey Rabbit rAO Chimera 5	9.62 ± 1.85	N/M ^b	0.00310 ± 0.00124 ^c	7.4	(S)-RS-8359	o	[184]
Monkey Rabbit rAO Chimera 6	68.7 ± 13.8	N/M ^b	0.0143 ± 0.00424 ^c	7.4	(S)-RS-8359	o	[184]
Monkey Rabbit rAO Chimera 7	36.9 ± 3.25	N/M ^b	0.00652 ± 0.00197 ^c	7.4	(S)-RS-8359	o	[184]

Table 1.11 Continued

<u>Enzyme^a</u>	<u>K_m (μM)</u>	<u>K_{cat} (min⁻¹)</u>	<u>Specific Activity (μmol subs/min/mg)</u>	<u>pH</u>	<u>Substrate</u>	<u>Assay Description</u>	<u>Ref.</u>
Monkey Rabbit rAO Chimera 8	162 ± 23.7	N/M ^b	0.0101 ± 0.00196 ^c	7.4	(S)-RS-8359	o	[184]
Monkey rAO (WT)	ND ^e	N/M ^b	ND ^e	7.4	Cinchonidine	o	[184]
Rabbit rAO (WT)	7.40 ± 1.19	N/M ^b	0.156 ± 0.0558 ^c	7.4	Cinchonidine	o	[184]
Monkey Rabbit rAO Chimera 1	ND ^e	N/M ^b	ND ^e	7.4	Cinchonidine	o	[184]
Monkey Rabbit rAO Chimera 2	16.3 ± 8.85	N/M ^b	0.219 ± 0.151 ^c	7.4	Cinchonidine	o	[184]
Monkey Rabbit rAO Chimera 3	ND ^e	N/M ^b	ND ^e	7.4	Cinchonidine	o	[184]
Monkey Rabbit rAO Chimera 4	15.9 ± 1.31	N/M ^b	0.293 ± 0.0333 ^c	7.4	Cinchonidine	o	[184]
Monkey Rabbit rAO Chimera 5	ND ^e	N/M ^b	ND ^e	7.4	Cinchonidine	o	[184]
Monkey Rabbit rAO Chimera 6	ND ^e	N/M ^b	ND ^e	7.4	Cinchonidine	o	[184]
Monkey Rabbit rAO Chimera 7	ND ^e	N/M ^b	ND ^e	7.4	Cinchonidine	o	[184]
Monkey Rabbit rAO Chimera 8	23.6 ± 2.29	N/M ^b	0.185 ± 0.0422 ^c	7.4	Cinchonidine	o	[184]
Monkey rAO K1004Q	ND ^e	N/M ^b	ND ^e	7.4	Cinchonidine	o	[184]
Monkey rAO M1009I	ND ^e	N/M ^b	ND ^e	7.4	Cinchonidine	o	[184]
Monkey rAO A1023Y	ND ^e	N/M ^b	ND ^e	7.4	Cinchonidine	o	[184]
Monkey rAO I1032V	ND ^e	N/M ^b	ND ^e	7.4	Cinchonidine	o	[184]
Monkey rAO K1004Q, K1005R	ND ^e	N/M ^b	ND ^e	7.4	Cinchonidine	o	[184]
Monkey rAO K1004Q, K1005R, M1009I, V1010I	ND ^e	N/M ^b	ND ^e	7.4	Cinchonidine	o	[184]
Monkey rAO K1004Q, K1005R, M1009I, V1010I, R1021V, A1023Y	ND ^e	N/M ^b	ND ^e	7.4	Cinchonidine	o	[184]
Monkey rAO K1004Q, K1005R, M1009I, V1010I, R1021V, A1023Y, I1032V	ND ^e	N/M ^b	ND ^e	7.4	Cinchonidine	o	[184]
Monkey rAO K1004Q, K1005R, M1009I, V1010I, R1021V, A1023Y, I1032V, G1064K, I1067M	ND ^e	N/M ^b	ND ^e	7.4	Cinchonidine	o	[184]
Monkey rAO A1083T, V1085A	N/M ^a	N/M ^b	0.148 ± 0.00354	7.4	Cinchonidine	o	[184]
Monkey rAO K1004Q	36.6 ± 15.8	N/M ^b	0.00848 ± 0.00571 ^c	7.4	(S)-RS-8359	o	[184]
Monkey rAO M1009I	27.0 ± 3.13	N/M ^b	0.00720 ± 0.00205 ^c	7.4	(S)-RS-8359	o	[184]
Monkey rAO A1023Y	26.4 ± 15.9	N/M ^b	0.00309 ± 0.000892 ^c	7.4	(S)-RS-8359	o	[184]
Monkey rAO I1032V	33.4 ± 7.01	N/M ^b	0.00698 ± 0.00517 ^c	7.4	(S)-RS-8359	o	[184]
Monkey rAO K1004Q, K1005R	36.0 ± 0.867	N/M ^b	0.0117 ± 0.000333 ^c	7.4	(S)-RS-8359	o	[184]
Monkey rAO K1004Q, K1005R, M1009I, V1010I	52.1 ± 8.00	N/M ^b	0.00271 ± 0.00168 ^c	7.4	(S)-RS-8359	o	[184]
Monkey rAO K1004Q, K1005R, M1009I, V1010I, R1021V, A1023Y	96.5 ± 2.40	N/M ^b	0.000870 ± 0.000307 ^c	7.4	(S)-RS-8359	o	[184]
Monkey rAO K1004Q, K1005R, M1009I, V1010I, R1021V, A1023Y, I1032V	24.4 ± 1.53	N/M ^b	0.00395 ± 0.000314 ^c	7.4	(S)-RS-8359	o	[184]
Monkey rAO K1004Q, K1005R, M1009I, V1010I, R1021V, A1023Y, I1032V, G1064K, I1067M	15.7 ± 0.268	N/M ^b	0.00338 ± 0.000173 ^c	7.4	(S)-RS-8359	o	[184]
Monkey rAO A1083T, V1085A	128 ± 10.8	N/M ^b	0.0132 ± 0.0000930 ^c	7.4	(S)-RS-8359	o	[184]
Monkey rAO A1083T	ND ^e	N/M ^b	ND ^e	7.4	Cinchonidine	o	[184]
Monkey rAO V1085A	12.0 ± 2.44	N/M ^b	0.124 ± 0.00607 ^c	7.4	Cinchonidine	o	[184]
Rabbit rAO A1081V	ND ^e	N/M ^b	ND ^e	7.4	Cinchonidine	o	[184]

Table 1.11 Continued

Enzyme ^a	K _m (μM)	K _{cat} (min ⁻¹)	Specific Activity (μmol subs/min/mg)	pH	Substrate	Assay Description	Ref.
Monkey rAO A1083T	20.7 ± 1.23	N/M ^b	0.00306 ± 0.000516 ^c	7.4	(S)-RS-8359	o	[184]
Monkey rAO V1085A	131 ± 3.61	N/M ^b	0.0113 ± 0.00122 ^c	7.4	(S)-RS-8359	o	[184]
Rabbit rAO A1081V	35.2 ± 1.26	N/M ^b	0.00723 ± 0.000974 ^c	7.4	(S)-RS-8359	o	[184]
Monkey rAO (high affinity)	3.51 ± 1.00	N/M ^b	0.00196 ± 0.000262	6.0	(S)-RS-8359	r	[183]
Monkey rAO (low affinity)	16.4 ± 0.891	N/M ^b	0.00488 ± 0.000231 ^c	6.0	(S)-RS-8359	r	[183]
Rat rAO	52.8 ± 8.67	N/M ^b	0.00256 ± 0.000334 ^c	6.0	(S)-RS-8359	r	[183]
Monkey (iron sulfur/FAD domain)/ Rat (moco domain) chimeric rAO	36.3 ± 1.63	N/M ^b	0.00510 ± 0.000556 ^c	6.0	(S)-RS-8359	r	[183]
Rat (iron sulfur/FAD domain)/ Monkey (moco domain) chimeric rAO (high affinity)	4.43 ± 1.23	N/M ^b	0.000921 ± 0.000272 ^c	6.0	(S)-RS-8359	r	[183]
Rat (iron sulfur/FAD domain)/ Monkey (moco domain) chimeric rAO (low affinity)	17.1 ± 1.29	N/M ^b	0.00238 ± 0.000735 ^c	6.0	(S)-RS-8359	r	[183]
Mouse rAO	3.8 ± 0.4	N/M ^b	0.807 ± 0.079 ^c	7.8	Retinaldehyde	h	[59]
Rabbit Liver AO	8	N/M ^b	0.496 ^c	7.8	Retinaldehyde	h	[59]
Negative control strain empty pCMV	N/M ^b	N/M ^b	0.0239 ± 0.0068	7.0	Phenathridine	q	[185]
Mouse rAO	N/M ^b	N/M ^b	0.0507 ± 0.0053	7.0	Phenathridine	q	[185]
Mouse rAO homolog 2	N/M ^b	N/M ^b	0.0492 ± 0.0090	7.0	Phenathridine	q	[185]
Mouse rAO	97.7 ± 21.5	317.6 ± 28.5	0.00115	7.5	benzaldehyde	l	[106]
Mouse rAO V806E	634.5 ± 76.4	151.0 ± 20.8	N/M ^b	7.5	benzaldehyde	l	[106]
Mouse rAO M884R	7130 ± 2580	76.4 ± 17.8	N/M ^b	7.5	benzaldehyde	l	[106]
Mouse rAO V806E/M884R	ND ^e	ND ^e	N/M ^b	7.5	benzaldehyde	l	[106]
Mouse rAO E1265Q	ND ^e	ND ^e	N/M ^b	7.5	benzaldehyde	l	[106]
Mouse rAO	11.4 ± 4.0	128.1 ± 13.0	N/M ^b	7.5	phthalazine	l	[106]
Mouse rAO V806E	28.55 ± 0.35	103.0 ± 1.0	N/M ^b	7.5	phthalazine	l	[106]
Mouse rAO M884R	ND ^e	ND ^e	N/M ^b	7.5	phthalazine	l	[106]
Mouse rAO V806E/M884R	ND ^e	ND ^e	N/M ^b	7.5	phthalazine	l	[106]
Mouse rAO E1265Q	ND ^e	ND ^e	N/M ^b	7.5	phthalazine	l	[106]
Mouse rAO	55.8 ± 8.8	49.5 ± 8.7	N/M ^b	7.5	Retinaldehyde	l	[106]
Mouse rAO V806E	22.2 ± 2.8	13.9 ± 2.4	N/M ^b	7.5	Retinaldehyde	l	[106]
Mouse rAO M884R	7.5 ± 2.0	1.3 ± 0.4	N/M ^b	7.5	Retinaldehyde	l	[106]
Mouse rAO V806E/M884R	ND ^e	ND ^e	N/M ^b	7.5	Retinaldehyde	l	[106]
Mouse rAO E1265Q	ND ^e	ND ^e	N/M ^b	7.5	Retinaldehyde	l	[106]
Mouse rAO	17500 ± 4900	519.9 ± 112.3	N/M ^b	7.5	acetaldehyde	l	[106]
Mouse rAO V806E	52900 ± 17800	160.6 ± 38.1	N/M ^b	7.5	acetaldehyde	l	[106]
Mouse rAO M884R	ND ^e	ND ^e	N/M ^b	7.5	acetaldehyde	l	[106]
Mouse rAO V806E/M884R	ND ^e	ND ^e	N/M ^b	7.5	acetaldehyde	l	[106]
Mouse rAO E1265Q	ND ^e	ND ^e	N/M ^b	7.5	acetaldehyde	l	[106]
Mouse rAO	ND ^e	ND ^e	N/M ^b	7.5	xanthine	l	[106]
Mouse rAO V806E	ND ^e	ND ^e	N/M ^b	7.5	xanthine	l	[106]
Mouse rAO M884R	ND ^e	ND ^e	N/M ^b	7.5	xanthine	l	[106]
Mouse rAO V806E/M884R	ND ^e	ND ^e	N/M ^b	7.5	xanthine	l	[106]
Mouse rAO E1265Q	ND ^e	ND ^e	N/M ^b	7.5	xanthine	l	[106]
Mouse rAO	ND ^e	ND ^e	N/M ^b	7.5	hypoxanthine	l	[106]
Mouse rAO V806E	ND ^e	ND ^e	N/M ^b	7.5	hypoxanthine	l	[106]

Table 1.11 Continued

Enzyme ^a	K _m (μM)	K _{cat} (min ⁻¹)	Specific Activity (μmol subs/min/mg)	pH	Substrate	Assay Description	Ref.
Mouse rAO M884R	ND ^e	ND ^e	N/M ^b	7.5	hypoxanthine	l	[106]
Mouse rAO V806E/M884R	ND ^e	ND ^e	N/M ^b	7.5	hypoxanthine	l	[106]
Mouse rAO E1265Q	ND ^e	ND ^e	N/M ^b	7.5	hypoxanthine	l	[106]
Mouse AO	13 ± 6	130 ± 8	N/M ^b	8.0	Benzaldehyde	r	[105]
Mouse AO	29 ± 8	384 ± 40	N/M ^b	8.0	Butyraldehyde	r	[105]
Mouse AO	173 ± 18	1279 ± 55	N/M ^b	8.0	2-OH-pyrimidine	r	[105]
Mouse rAO	20 ± 6	44 ± 2	0.000207	8.0	Benzaldehyde	r	[105]
Mouse rAO	26 ± 5	140 ± 10	N/M ^b	8.0	Butyraldehyde	r	[105]
Mouse rAO	97 ± 11	413 ± 16	N/M ^b	8.0	2-OH-pyrimidine	r	[105]
Pig liver rAO	4.36 ± 0.56	8.47 ± 0.03	2.88252 ± 0.01132 ^c	7.4	Quinocetone	l	[188]
Pig liver rAO	2.96 ± 0.51	3.75 ± 0.16	1.27645 ± 0.06213 ^c	7.4	Mequindox	l	[188]
Pig liver rAO	3.16 ± 0.48	1.36 ± 0.06	0.4635 ± 0.020 ^c	7.4	Cyadox	l	[188]
Pig liver rAO	8.76 ± 1.21	646.62 ± 58.35	19.380 ± 1.75050 ^c	7.4	benzaldehyde	l	[188]
Pig liver rAO G1019T	1.90 ± 0.233	809.37 ± 76.12	24.270 ± 2.28365 ^c	7.4	benzaldehyde	l	[188]
Pig liver rAO G1019A	6.42 ± 0.759	743.52 ± 83.25	22.290 ± 2.49753 ^c	7.4	benzaldehyde	l	[188]
Pig liver rAO G1019D	10.60 ± 2.04	304.34 ± 39.83	9.120 ± 1.19426 ^c	7.4	benzaldehyde	l	[188]
Pig liver rAO G1019E	15.73 ± 3.97	372 ± 45.26	11.160 ± 1.35781 ^c	7.4	benzaldehyde	l	[188]
Pig liver rAO G1019K	13.80 ± 2.64	341 ± 31.67	10.230 ± 0.95015 ^c	7.4	benzaldehyde	l	[188]
Donryu rat rAO ultrarapid metabolizer strain (110Gly, 852Val)	16.0 ± 2.40	N/M ^b	0.00126 ± 0.00026 ^c	6.0	(S)-RS-8359	i	[189]
Donryu rat rAO Mut-1 strain (110Gly, 852Ala)	62.4 ± 6.98	N/M ^b	0.00120 ± 0.00032 ^c	6.0	(S)-RS-8359	i	[189]
Donryu rat rAO Mut-2 strain (110Ser, 852Val)	44.3 ± 5.34	N/M ^b	0.00036 ± 0.00009 ^c	6.0	(S)-RS-8359	i	[189]
Donryu rat rAO poor metabolizer strain (110Ser, 852Ala)	36.4 ± 4.54	N/M ^b	0.00032 ± 0.00010 ^c	6.0	(S)-RS-8359	i	[189]
Bovine Milk XO (XO activity)	37.7 ± 0.6	906 ± 12	N/M ^b	8.5	Oxygen	j	[191]
Bovine Milk XO (XDH activity)	111.0 ± 5.3	150 ± 6	N/M ^b	8.5	Oxygen	j	[191]
Bovine Milk XO (XO activity)	ND ^e	ND ^e	N/M ^b	8.5	NAD ⁺	m	[191]
Bovine Milk XO (XDH activity)	20.8 ± 2.2	738 ± 72	N/M ^b	8.5	NAD ⁺	m	[191]
Bovine rXDH W336A (as isolated)	44.5 ± 0.8	906 ± 18	N/M ^b	8.5	Oxygen	j	[191]
Bovine rXDH W336A (DTT Treated)	48.6 ± 3.0	690 ± 42	N/M ^b	8.5	Oxygen	j	[191]
Bovine rXDH W336A (as isolated)	ND ^e	ND ^e	N/M ^b	8.5	NAD ⁺	m	[191]
Bovine rXDH W336A (DTT Treated)	18.2 ± 0.2	198 ± 12	N/M ^b	8.5	NAD ⁺	m	[191]
Bovine rXDH R427Q (as isolated)	73.5 ± 4.6	960 ± 60	N/M ^b	8.5	Oxygen	j	[191]
Bovine rXDH R427Q (DTT Treated)	66.6 ± 1.5	660 ± 12	N/M ^b	8.5	Oxygen	j	[191]
Bovine rXDH R427Q (as isolated)	ND ^e	ND ^e	N/M ^b	8.5	NAD ⁺	m	[191]
Bovine rXDH R427Q (DTT Treated)	28.5 ± 1.8	342 ± 24	N/M ^b	8.5	NAD ⁺	m	[191]
Bovine rXDH R335A (as isolated)	42.9 ± 0.8	900 ± 24	N/M ^b	8.5	Oxygen	j	[191]
Bovine rXDH R335A (DTT Treated)	40.6 ± 0.9	366 ± 6	N/M ^b	8.5	Oxygen	j	[191]
Bovine rXDH R335A (as isolated)	ND ^e	ND ^e	N/M ^b	8.5	NAD ⁺	m	[191]
Bovine rXDH R335A (DTT Treated)	23.5 ± 1.1	372 ± 18	N/M ^b	8.5	NAD ⁺	m	[191]
<i>Drosophila melanogaster</i> XO	29 ± 6	1500 ± 120 ^d	N/M ^b	8.0	xanthine	m	[192, 251]
<i>Drosophila melanogaster</i> XO	29 ± 6	1920 ± 180	N/M ^b	8.0	xanthine	n	[192, 251]

Table 1.11 Continued

<u>Enzyme^a</u>	<u>K_m (μM)</u>	<u>K_{cat} (min⁻¹)</u>	<u>Specific Activity (μmol subs/min/mg)</u>	<u>pH</u>	<u>Substrate</u>	<u>Assay Description</u>	<u>Ref.</u>
<i>D. melanogaster</i> rXO	32 ± 2	1200 ± 120 ^d	N/M ^b	8.0	xanthine	m	[192]
<i>D. melanogaster</i> rXO	32 ± 2	1860 ± 18	N/M ^b	8.0	xanthine	n	[192]
<i>D. melanogaster</i> rXO	N/M ^b	660 ± 120 ^d	N/M ^b	8.0	Acetaldehyde	m	[192]
Human rXO	8.8 ± 0.60	1100 ± 52	N/M ^b	8.5	Xanthine	j	[66]
E803V Human rXO	72 ± 10	81 ± 7.2	N/M ^b	8.5	Xanthine	j	[66]
R881M Human rXO	NA ^f	NA ^f	NA ^f	8.5	Xanthine	j	[66]
Human rXO	1.7 ± 0.02	1800 ± 130	N/M ^b	8.5	Hypoxanthine	k	[66]
E803V Human rXO	NA ^f	NA ^f	NA ^f	8.5	Hypoxanthine	k	[66]
R881M Human rXO	21 ± 1.5	20 ± 1.4	N/M ^b	8.5	Hypoxanthine	k	[66]
Over Expressed Human rXO	39 ± 2.0	270 ± 50	N/M ^b	8.5	benzaldehyde	l	[66]
E803V Human rXO	6.2 ± 0.61	130 ± 9.0	N/M ^b	8.5	benzaldehyde	l	[66]
R881M Human rXO	18 ± 1.5	730 ± 60	N/M ^b	8.5	benzaldehyde	l	[66]
Human rXO	29 ± 1.5	330 ± 50	N/M ^b	8.5	p- (Dimethylamino)cinnamaldehyde	l	[66]
E803V Human rXO	0.32 ± 0.091	14 ± 0.70	N/M ^b	8.5	p- (Dimethylamino)cinnamaldehyde	l	[66]
R881M Human rXO	20 ± 0.90	300 ± 25	N/M ^b	8.5	p- (Dimethylamino)cinnamaldehyde	l	[66]
Human Liver XO	N/M ^b	~270 ⁿ	1.8	6.8	xanthine	j	[66, 252]
Bovine XO	N/M ^b	~1000	N/M ^b	8.5	xanthine	j	[66, 253]
Human rXO	N/M ^b	N/M ^b	0.000277 ± 0.000054	N/M ^b	Xanthine	o	[193]
Porcine rXO	21.69 ± 2.27	1137.6 ± 4.2 ^d	7.74 ± 0.03 ^c	7.4	xanthine	o	[196]
Porcine rXO G47A	24.13 ± 1.71	1162.8 ± 1.2 ^d	7.91 ± 0.01 ^c	7.4	xanthine	o	[196]
Porcine rXO N352A	22.70 ± 0.65	1130.4 ± 4.2 ^d	7.69 ± 0.03 ^c	7.4	xanthine	o	[196]
Porcine rXO S360P	64.28 ± 1.00	415.8 ± 4.2 ^d	2.83 ± 0.03 ^c	7.4	xanthine	o	[196]
Porcine rXO R427E	23.24 ± 0.90	1138.8 ± 6 ^d	7.75 ± 0.04 ^c	7.4	xanthine	o	[196]
Porcine rXO D430H	21.30 ± 0.59	1098 ± 4.2 ^d	7.47 ± 0.03 ^c	7.4	xanthine	o	[196]
Porcine rXO D431A	21.72 ± 0.74	1252.2 ± 7.2 ^d	8.52 ± 0.05 ^c	7.4	xanthine	o	[196]
Porcine rXO S1227A	50.80 ± 3.04	579 ± 9 ^d	3.94 ± 0.06 ^c	7.4	xanthine	o	[196]
Porcine rXO K1230A	39.25 ± 1.73	591 ± 4.2 ^d	4.02 ± 0.03 ^c	7.4	xanthine	o	[196]
Porcine rXO	58.20 ± 5.76	196.8 ± 7.2 ^d	1.34 ± 0.05 ^c	7.4	cyadox	o	[196]
Porcine rXO G47A	65.68 ± 4.42	207 ± 4.2 ^d	1.41 ± 0.03 ^c	7.4	cyadox	o	[196]
Porcine rXO N352A	60.10 ± 12.59	189.6 ± 26.4 ^d	1.29 ± 0.18 ^c	7.4	cyadox	o	[196]
Porcine rXO S360P	93.53 ± 8.15	114.6 ± 6 ^d	0.78 ± 0.04 ^c	7.4	cyadox	o	[196]
Porcine rXO R427E	20.86 ± 0.90	210 ± 7.2 ^d	1.43 ± 0.05 ^c	7.4	cyadox	o	[196]
Porcine rXO D430H	64.68 ± 3.52	144 ± 4.2 ^d	0.98 ± 0.03 ^c	7.4	cyadox	o	[196]
Porcine rXO D431A	61.29 ± 0.53	223.2 ± 1.2 ^d	1.52 ± 0.01 ^c	7.4	cyadox	o	[196]
Porcine rXO S1227A	148.20 ± 14.21	118.8 ± 7.2 ^d	0.81 ± 0.05 ^c	7.4	cyadox	o	[196]
Porcine rXO K1230A	162.89 ± 15.50	129.6 ± 12 ^d	0.88 ± 0.08 ^c	7.4	cyadox	o	[196]

Table 1.11 Continued

<u>Enzyme^a</u>	<u>K_m (μM)</u>	<u>K_{cat} (min⁻¹)</u>	<u>Specific Activity (μmol subs/min/mg)</u>	<u>pH</u>	<u>Substrate</u>	<u>Assay Description</u>	<u>Ref.</u>
Rat XO	1.8	N/M ^b	1030 ⁱ	7.8	xanthine	l	[198, 254]
Rat XO	46	N/M ^b	1030 ⁱ	7.8	oxygen	j	[198, 254]
Rat rXO (DTT treated)	1.3	N/M ^b	810 ⁱ	7.8	xanthine	s	[198]
Rat rXO (DTT treated)	8.5	N/M ^b	810 ⁱ	7.8	NAD ⁺	s	[198]
Rat rXO (DTT treated)	2.8	N/M ^b	270 ⁱ	7.8	xanthine	j	[198]
Rat rXO (DTT treated)	260	N/M ^b	270 ⁱ	7.8	oxygen	j	[198]
Rat rXO C535A+C992R	2.0 ± 0.1	N/M ^b	433 ± 14	7.8	xanthine	s	[198]
Rat rXO C535A+C992R	14.2 ± 0.8	N/M ^b	433 ± 14	7.8	NAD ⁺	s	[198]
Rat rXO C535A+C992R	2.96 ± 0.2	N/M ^b	585±6	7.8	xanthine	j	[198]
Rat rXO C535A+C992R	47.7 ± 6.5	N/M ^b	585±6	7.8	oxygen	j	[198]
Rat rXO C535A+C992R (DTT treated)	1.5 ± 0.2	N/M ^b	751 ± 15	7.8	xanthine	s	[198]
Rat rXO C535A+C992R (DTT treated)	10.7 ± 0.5	N/M ^b	751 ± 15	7.8	NAD ⁺	s	[198]
Rat rXO C535A+C992R (DTT treated)	2.8 ± 0.1	N/M ^b	267±6	7.8	xanthine	j	[198]
Rat rXO C535A+C992R (DTT treated)	153.0 ± 0.6	N/M ^b	267±6	7.8	oxygen	j	[198]
Rat rXO C525A+C992R+C1316S	1.7 ± 0.1	N/M ^b	730 ± 5	7.8	xanthine	s	[198]
Rat rXO C525A+C992R+C1316S	12.9 ± 0.4	N/M ^b	730 ± 5	7.8	NAD ⁺	s	[198]
Rat rXO C525A+C992R+C1316S	2.8 ± 0.1	N/M ^b	250±11	7.8	xanthine	j	[198]
Rat rXO C525A+C992R+C1316S	150.0 ± 12	N/M ^b	250±11	7.8	oxygen	j	[198]
Rat rXO C535A+C992R+C1324S	2.0 ± 0.1	N/M ^b	782 ± 10	7.8	xanthine	s	[198]
Rat rXO C535A+C992R+C1324S	13.4 ± 0.6	N/M ^b	782 ± 10	7.8	NAD ⁺	s	[198]
Rat rXO C535A+C992R+C1324S	2.9 ± 0.2	N/M ^b	275±5.5	7.8	xanthine	j	[198]
Rat rXO C535A+C992R+C1324S	205.0 ± 14	N/M ^b	275±5.5	7.8	oxygen	j	[198]

a) r- recombinant; b) N/M- Not mentioned; c) specific activity is reported as V_{max} ; d) value was calculated from data reported; e) ND- not detected; f) NA- negligible activity; g) IA- inactive; h) Conversion of trans retinaldehyde to trans retinoic acid using N'-methylnicotinamide as electron acceptor; i) Oxidation of (S)-RS-8359 using potassium ferrocyanide as electron acceptor. Product formation monitored by HPLC; j) Oxidation of xanthine to uric acid by measuring increase change in absorbance at 295 nm; k) Oxidation of hypoxanthine by measuring increase change in absorbance at 285 nm; l) Monitored the reduction of electron acceptor 2,6-dichlorophenolindophenol (DCPIP) at 600nm; m) Monitored the reduction of electron acceptor NAD⁺ to NADH at 340nm; n) Monitored the reduction of cytochrome c at 550nm utilizing electron mediator PMS/PES; o) monitored product formation by HPLC; p) Oxidation of quinazolines was monitored absorbance change at 270 nm; q) Monitored product formation of phenanthridone at 321-2 nm with molecular oxygen as the electron acceptor; r) Monitored the reduction of electron acceptor ferricyanide at 420nm; s) Monitored the formation of NADH fluorescence at 460nm emission when excited at 340nm; t) in mol product/min/mol FAD; u) active but parameters not determined.

Table 1.12: Kinetic parameters for eukaryotic SO family of enzymes.

Enzyme ^a	K _m (μM)	K _{cat} (min ⁻¹)	Specific Activity (μmol subs/min/mg)	pH	Substrate	Assay Description	Ref.
<i>Chlamydomonas reinhardtii</i> rcrARC	N/M ^b	N/M ^b	24.53 ± 3.68 ^d	6.5	benzamidoxime	k	[199]
Human rmARC1	110 ± 40	N/M ^b	0.4243 ± 0.0269 ^c	6.0	Benzamidoxime	k	[113]
Human rmARC2	270 ± 80	N/M ^b	0.4197 ± 0.0274 ^c	6.0	Benzamidoxime	k	[113]
Human rmARC1	520 ± 140	N/M ^b	0.5354 ± 0.0389 ^c	6.0	N-Hydroxy-cytosine	k	[113]
Human rmARC2	1520 ± 280	N/M ^b	0.2198 ± 0.0148 ^c	6.0	N-Hydroxy-cytosine	k	[113]
Human rmARC1	180 ± 5	N/M ^b	0.0342 ± 0.0024 ^c	6.0	Benzamidoxime	k	[114]
Human rmARC2	830 ± 170	N/M ^b	0.307 ± 0.022 ^c	6.0	Benzamidoxime	k	[114]
Human rmARC1	86 ± 13	N/M ^b	0.0555 ± 0.017 ^c	6.0	Nω-hydroxy-L-arginine	k	[114]
Human rmARC2	3000 ± 300	N/M ^b	0.373 ± 0.020 ^c	6.0	Nω-hydroxy-L-arginine	k	[114]
Human rmARC1	272 ± 60	N/M ^b	0.0431 ± 0.0028 ^c	6.0	Nω-hydroxy-Nδ-methyl-L-arginine	k	[114]
Human rmARC2	3700 ± 400	N/M ^b	0.0365 ± 0.0023 ^c	6.0	Nω-hydroxy-Nδ-methyl-L-arginine	k	[114]
Human rmARC1 (whole complex)	N/M ^b	N/M ^b	0.0343 ± 0.0009	6.0	Benzamidoxime	k	[114]
Human rmARC1 (without cyt b ₅)	N/M ^b	N/M ^b	0.0154 ± 0.0023	6.0	Benzamidoxime	k	[114]
Human rmARC1 (without cyt b ₅ reductase)	N/M ^b	N/M ^b	0.0016 ± 0.0002	6.0	Benzamidoxime	k	[114]
Human rmARC1 complex (without mARC1)	N/M ^b	N/M ^b	0.0022 ± 0.0004	6.0	Benzamidoxime	k	[114]
Human rmARC1 (only mARC1)	N/M ^b	N/M ^b	0.0022 ± 0.0004	6.0	Benzamidoxime	k	[114]
Human rmARC1 (without NADH)	N/M ^b	N/M ^b	0.0002 ± 0.0001	6.0	Benzamidoxime	k	[114]
Human rmARC2 (whole complex)	N/M ^b	N/M ^b	0.0907 ± 0.0056	6.0	Benzamidoxime	k	[114]
Human rmARC2 (without cyt b ₅)	N/M ^b	N/M ^b	0.0009 ± 0.0001	6.0	Benzamidoxime	k	[114]
Human rmARC2 (without cyt b ₅ reductase)	N/M ^b	N/M ^b	0.0012 ± 0.0002	6.0	Benzamidoxime	k	[114]
Human rmARC2 complex (without mARC2)	N/M ^b	N/M ^b	0.0003 ± 0.0001	6.0	Benzamidoxime	k	[114]
Human rmARC2 (only mARC2)	N/M ^b	N/M ^b	0.0002 ± 0.0001	6.0	Benzamidoxime	k	[114]
Human rmARC2 (without NADH)	N/M ^b	N/M ^b	0.0001 ± 0.0001	6.0	Benzamidoxime	k	[114]
Human rmARC1 (whole complex)	N/M ^b	N/M ^b	0.0391 ± 0.0014	6.0	Nω-hydroxy-L-arginine	k	[114]

Table 1.12 Continued

<u>Enzyme^a</u>	<u>K_m (μM)</u>	<u>K_{cat} (min⁻¹)</u>	<u>Specific Activity (μmol subs/min/mg)</u>	<u>pH</u>	<u>Substrate</u>	<u>Assay Description</u>	<u>Ref.</u>
Human rmARC1 (without cyt b ₅)	N/M ^b	N/M ^b	0.0115 ± 0.0027	6.0	Nω-hydroxy-L- arginine	k	[114]
Human rmARC1 (without cyt b ₅ reductase)	N/M ^b	N/M ^b	0.0016 ± 0.0003	6.0	Nω-hydroxy-L- arginine	k	[114]
Human rmARC1 complex (without mARC1)	N/M ^b	N/M ^b	0.0012 ± 0.0011	6.0	Nω-hydroxy-L- arginine	k	[114]
Human rmARC1 (only mARC1)	N/M ^b	N/M ^b	0.0018 ± 0.0004	6.0	Nω-hydroxy-L- arginine	k	[114]
Human rmARC1 (without NADH)	N/M ^b	N/M ^b	0.0005 ± 0.0005	6.0	Nω-hydroxy-L- arginine	k	[114]
Human rmARC2 (whole complex)	N/M ^b	N/M ^b	0.0568 ± 0.005	6.0	Nω-hydroxy-L- arginine	k	[114]
Human rmARC2 (without cyt b ₅)	N/M ^b	N/M ^b	0.0017 ± 0.0017	6.0	Nω-hydroxy-L- arginine	k	[114]
Human rmARC2 (without cyt b ₅ reductase)	N/M ^b	N/M ^b	0.0010 ± 0.0004	6.0	Nω-hydroxy-L- arginine	k	[114]
Human rmARC2 complex (without mARC2)	N/M ^b	N/M ^b	0.0001 ± 0.0001	6.0	Nω-hydroxy-L- arginine	k	[114]
Human rmARC2 (only mARC2)	N/M ^b	N/M ^b	0.0 ± 0.0	6.0	Nω-hydroxy-L- arginine	k	[114]
Human rmARC2 (without NADH)	N/M ^b	N/M ^b	0.0001 ± 0.0001	6.0	Nω-hydroxy-L- arginine	k	[114]
Human rmARC1 (whole complex)	N/M ^b	N/M ^b	0.0206 ± 0.0009	6.0	Nω-hydroxy-Nδ- methyl-L-arginine	k	[114]
Human rmARC1 (without cyt b ₅)	N/M ^b	N/M ^b	0.0089 ± 0.0002	6.0	Nω-hydroxy-Nδ- methyl-L-arginine	k	[114]
Human rmARC1 (without cyt b ₅ reductase)	N/M ^b	N/M ^b	0.0007 ± 0.0002	6.0	Nω-hydroxy-Nδ- methyl-L-arginine	k	[114]
Human rmARC1 complex (without mARC1)	N/M ^b	N/M ^b	0.0005 ± 0.0005	6.0	Nω-hydroxy-Nδ- methyl-L-arginine	k	[114]
Human rmARC1 (only mARC1)	N/M ^b	N/M ^b	0.0016 ± 0.0003	6.0	Nω-hydroxy-Nδ- methyl-L-arginine	k	[114]
Human rmARC1 (without NADH)	N/M ^b	N/M ^b	0.0001 ± 0.0001	6.0	Nω-hydroxy-Nδ- methyl-L-arginine	k	[114]
Human rmARC2 (whole complex)	N/M ^b	N/M ^b	0.0077 ± 0.0004	6.0	Nω-hydroxy-Nδ- methyl-L-arginine	k	[114]
Human rmARC2 (without cyt b ₅)	N/M ^b	N/M ^b	0.0002 ± 0.0002	6.0	Nω-hydroxy-Nδ- methyl-L-arginine	k	[114]

Table 1.12 Continued

Enzyme ^a	K _m (μM)	K _{cat} (min ⁻¹)	Specific Activity (μmol subs/min/mg)	pH	Substrate	Assay Description	Ref.
Human rmARC2 (without cyt b ₅ reductase)	N/M ^b	N/M ^b	0.0007 ± 0.0003	6.0	Nω-hydroxy-Nδ- methyl-L-arginine	k	[114]
Human rmARC2 complex (without mARC2)	N/M ^b	N/M ^b	0.0002 ± 0.0002	6.0	Nω-hydroxy-Nδ- methyl-L-arginine	k	[114]
Human rmARC2 (only mARC2)	N/M ^b	N/M ^b	0.0003 ± 0.0003	6.0	Nω-hydroxy-Nδ- methyl-L-arginine	k	[114]
Human rmARC2 (without NADH)	N/M ^b	N/M ^b	0.0001 ± 0.0001	6.0	Nω-hydroxy-Nδ- methyl-L-arginine	k	[114]
Human rmARC1 (dithionite reduced)	636 ± 139	N/M ^b	0.138 ^c	7.4	Nitrite	q	[14]
Human rmARC2 (dithionite reduced)	204 ± 84.4	N/M ^b	0.198 ^c	7.4	Nitrite	q	[14]
Human rmARC1 (in presence of NADH, CYB5, CYB5R)	6.5	N/M ^b	24.8 ^{c, x}	7.4	NADH	q	[14]
Human rmARC1 (in presence of NADH, CYB5, CYB5R)	0.08	N/M ^b	22.8 ^{c, x}	7.4	CYB5	q	[14]
Human rmARC1 (in presence of NADH, CYB5, CYB5R)	0.007	N/M ^b	25.6 ^{c, x}	7.4	CYB5R	q	[14]
Human rmARC1 (in presence of NADH, CYB5, CYB5R)	9500 ± 1500	6	3.60 ^{c, x}	7.4	Nitrite	q	[14]
Human rmARC1 C273A (in presence of NADH, CYB5, CYB5R)	ND ^e	~0	<0.0006	7.4	Nitrite	q	[14]
Human rmARC2 (in presence of NADH, CYB5, CYB5R)	ND ^e	~0	<0.0006	7.4	Nitrite	q	[14]
Human rmARC1 (- MoO ₄ ²⁻)	N/M ^b	N/M ^b	2.7 ± 0.2	6.0	Nitrate	k	[13]
Human rmARC1 (+MoO ₄ ²⁻)	N/M ^b	N/M ^b	3.2 ± 0.3	6.0	Nitrate	k	[13]
Human rmARC1 (in presence of NADH, CYB5, CYB5R)	N/M ^b	N/M ^b	0.00130 ± 0.00043	6.0	benzamidoxime	k	[13]
Human rmARC1 (in presence of CYB5, CYB5R)	N/M ^b	N/M ^b	ND ^e	6.0	benzamidoxime	k	[13]
Human rmARC1 (in presence of NADH, CYB5R)	N/M ^b	N/M ^b	0.00023 ± 0.00	6.0	benzamidoxime	k	[13]

Table 1.12 Continued

<u>Enzyme^a</u>	<u>K_m (μM)</u>	<u>K_{cat} (min⁻¹)</u>	<u>Specific Activity (μmol subs/min/mg)</u>	<u>pH</u>	<u>Substrate</u>	<u>Assay Description</u>	<u>Ref.</u>
Human rmARC1 (in presence of NADH, CYB5)	N/M ^b	N/M ^b	0.00020 ± 0.00	6.0	benzamidoxime	k	[13]
NADH, CYB5, CYB5R without rmARC1	N/M ^b	N/M ^b	22.0 ± 0.3 ^y	6.0	benzamidoxime	k	[13]
Human rmARC1	N/M ^b	N/M ^b	ND ^e	6.0	benzamidoxime	k	[13]
Human rmARC1 (in presence of NADH, CYB5, CYB5R)	N/M ^b	N/M ^b	0.00659 ± 0.00035	6.0	Pentamidine monoamidoxime	k	[13]
Human rmARC1 (in presence of NADH, CYB5, CYB5R)	N/M ^b	N/M ^b	0.00056 ± 0.00004	6.0	Pentamidine diamidoxime (reduced to Pentamidine monoamidoxime)	k	[13]
Human rmARC1 (in presence of NADH, CYB5, CYB5R)	N/M ^b	N/M ^b	0.00049 ± 0.00012	6.0	Pentamidine diamidoxime (reduced to Pentamidine)	k	[13]
Human rmARC1 (in presence of NADH, CYB5, CYB5R)	N/M ^b	N/M ^b	0.00431 ± 0.001	6.0	Diminazene diamidoxime (reduced to Diminazene monoamidoxime)	k	[13]
Human rmARC1 (in presence of NADH, CYB5, CYB5R)	N/M ^b	N/M ^b	0.00005 ± 0.00002	6.0	Diminazene diamidoxime (reduced to Diminazene)	k	[13]
Human rmARC1 (in presence of NADH, CYB5, CYB5R)	N/M ^b	N/M ^b	0.00048 ± 0.00001	6.0	N- hydroxymelagatran	k	[13]
Human rmARC1 (in presence of NADH, CYB5, CYB5R)	N/M ^b	N/M ^b	0.02042 ± 0.00456	6.0	guanoxaben	k	[13]
Human rmARC1 (in presence of NADH, CYB5, CYB5R)	N/M ^b	N/M ^b	0.01594 ± 0.00110	6.0	N- hydroxydebrisoquine	k	[13]
Human rmARC1	30000 ± 10000	N/M ^b	0.101 ± 0.012 ^c	6.0	TMAO	k	[200]
ZR-75-1 cells	N/M ^b	N/M ^b	0.000069 ± 0.000007	6.0	benzamidoxime	k	[200]
Porcine Liver outer mitochondrial vesicles	N/M ^b	N/M ^b	0.0002816 ± 0.0000069	6.0	benzamidoxime	k	[200]
Porcine Liver cytosol	N/M ^b	N/M ^b	0.00003 ± 0.00006	6.0	benzamidoxime	k	[200]
Porcine Liver microsomal subfraction	N/M ^b	N/M ^b	0.006510 ± 0.000484	6.0	benzamidoxime	k	[200]

Table 1.12 Continued

Enzyme^a	K_m (μM)	K_{cat} (min⁻¹)	Specific Activity (μmol subs/min/mg)	pH	Substrate	Assay Description	Ref.
Human rmARC1	N/M ^b	N/M ^b	0.000174 ± 0.000028	6.0	benzamidoxime	k	[200]
Human rmARC2	N/M ^b	N/M ^b	0.000346 ± 0.000010	6.0	benzamidoxime	k	[200]
ZR-75-1 cells	N/M ^b	N/M ^b	0.0045 ± 0.0002	6.0	TMAO	k	[200]
Porcine Liver outer mitochondrial vesicles	N/M ^b	N/M ^b	0.0007 ± 0.0001	6.0	TMAO	k	[200]
Porcine Liver cytosol	N/M ^b	N/M ^b	t	6.0	TMAO	k	[200]
Porcine Liver microsomal subfraction	N/M ^b	N/M ^b	t	6.0	TMAO	k	[200]
Human rmARC1	N/M ^b	N/M ^b	0.0044 ± 0.0006	6.0	TMAO	k	[200]
Human rmARC2	N/M ^b	N/M ^b	0.0004 ± 0.0001	6.0	TMAO	k	[200]
Human rmARC1	520 ± 140	6.53 ± 0.47 ^d	0.1741 ± 0.0126 ^c	6.0	N4-hydroxycytosine	k	[201]
Human rmARC2	1520 ± 280	2.48 ± 0.17 ^d	0.0653 ± 0.0044 ^c	6.0	N4-hydroxycytosine	k	[201]
Human rmARC1	440 ± 400	4.88 ± 0.12 ^d	0.1302 ± 0.0032 ^c	6.0	N4-hydroxycytidine	k	[201]
Human rmARC2	5650 ± 510	4.22 ± 0.21 ^d	0.1111 ± 0.0054 ^c	6.0	N4-hydroxycytidine	k	[201]
Human rmARC1	770 ± 200	14.07 ± 1.93 ^d	0.3751 ± 0.0515 ^c	6.0	N6-hydroxyadenine	k	[201]
Human rmARC2	720 ± 110	4.57 ± 0.22 ^d	0.1202 ± 0.0057 ^c	6.0	N6-hydroxyadenine	k	[201]
Human rmARC1	980 ± 110	10.49 ± 0.40 ^d	0.2798 ± 0.0108 ^c	6.0	N6- hydroxyadenosine	k	[201]
Human rmARC2	5280 ± 1260	0.68 ± 0.04 ^d	0.0178 ± 0.0011 ^c	6.0	N6- hydroxyadenosine	k	[201]
Human rmARC1 (in presence of NADH, CYB5, CYB5R)	ND ^e	ND ^e	0.1031 ± 0.0387	6.0	N4-hydroxycytidine	k	[201]
Human rmARC1 (in presence of CYB5, CYB5R)	ND ^e	ND ^e	ND ^e	6.0	N4-hydroxycytidine	k	[201]
Human rmARC1 (in presence of NADH, CYB5R)	ND ^e	ND ^e	ND ^e	6.0	N4-hydroxycytidine	k	[201]
Human rmARC1 (in presence of NADH, CYB5)	ND ^e	ND ^e	ND ^e	6.0	N4-hydroxycytidine	k	[201]
NADH, CYB5, CYB5R without mARC1	ND ^e	ND ^e	ND ^e	6.0	N4-hydroxycytidine	k	[201]
Human rmARC1 (in presence of NADH, CYB5, CYB5R)	ND ^e	ND ^e	0.1808 ± 0.0036	6.0	N6-hydroxyadenine	k	[201]
Human rmARC1 (in presence of CYB5, CYB5R)	ND ^e	ND ^e	ND ^e	6.0	N6-hydroxyadenine	k	[201]
Human rmARC1 (in presence of NADH, CYB5R)	ND ^e	ND ^e	ND ^e	6.0	N6-hydroxyadenine	k	[201]

Table 1.12 Continued

Enzyme^a	K_m (μM)	K_{cat} (min⁻¹)	Specific Activity (μmol subs/min/mg)	pH	Substrate	Assay Description	Ref.
Human rmARC1 (in presence of NADH, CYB5)	ND ^e	ND ^e	ND ^e	6.0	N6-hydroxyadenine	k	[201]
NADH, CYB5, CYB5R without mARC1	ND ^e	ND ^e	ND ^e	6.0	N6-hydroxyadenine	k	[201]
Human rmARC1 (in presence of NADH, CYB5, CYB5R)	ND ^e	ND ^e	0.2202 ± 0.026	6.0	N6- hydroxyadenosine	k	[201]
Human rmARC1 (in presence of CYB5, CYB5R)	ND ^e	ND ^e	ND ^e	6.0	N6- hydroxyadenosine	k	[201]
Human rmARC1 (in presence of NADH, CYB5R)	ND ^e	ND ^e	ND ^e	6.0	N6- hydroxyadenosine	k	[201]
Human rmARC1 (in presence of NADH, CYB5)	ND ^e	ND ^e	0.001 ± 0.0001	6.0	N6- hydroxyadenosine	k	[201]
NADH, CYB5, CYB5R without mARC1	ND ^e	ND ^e	ND ^e	6.0	N6- hydroxyadenosine	k	[201]
Human rmARC1 (in presence of NADH, CYB5, CYB5R)	ND ^e	ND ^e	0.1594 ± 0.036	6.0	benzamidoxime	k	[201]
Human rmARC1 (in presence of CYB5, CYB5R)	ND ^e	ND ^e	ND ^e	6.0	benzamidoxime	k	[201]
Human rmARC1 (in presence of NADH, CYB5R)	ND ^e	ND ^e	ND ^e	6.0	benzamidoxime	k	[201]
Human rmARC1 (in presence of NADH, CYB5)	ND ^e	ND ^e	0.0044 ± 0.0004	6.0	benzamidoxime	k	[201]
NADH, CYB5, CYB5R without mARC1	ND ^e	ND ^e	ND ^e	6.0	benzamidoxime	k	[201]
Human rmARC2 (in presence of NADH, CYB5, CYB5R)	ND ^e	ND ^e	0.0502 ± 0.0028	6.0	N4-hydroxycytidine	k	[201]
Human rmARC2 (in presence of CYB5, CYB5R)	ND ^e	ND ^e	ND ^e	6.0	N4-hydroxycytidine	k	[201]
Human rmARC2 (in presence of NADH, CYB5R)	ND ^e	ND ^e	ND ^e	6.0	N4-hydroxycytidine	k	[201]

Table 1.12 Continued

<u>Enzyme^a</u>	<u>K_m (μM)</u>	<u>K_{cat} (min⁻¹)</u>	<u>Specific Activity (μmol subs/min/mg)</u>	<u>pH</u>	<u>Substrate</u>	<u>Assay Description</u>	<u>Ref.</u>
Human rmARC2 (in presence of NADH, CYB5)	ND ^e	ND ^e	ND ^e	6.0	N4-hydroxycytidine	k	[201]
NADH, CYB5, CYB5R without mARC2	ND ^e	ND ^e	ND ^e	6.0	N4-hydroxycytidine	k	[201]
Human rmARC2 (in presence of NADH, CYB5, CYB5R)	ND ^e	ND ^e	0.1335 ± 0.002	6.0	N6-hydroxyadenine	k	[201]
Human rmARC2 (in presence of CYB5, CYB5R)	ND ^e	ND ^e	ND ^e	6.0	N6-hydroxyadenine	k	[201]
Human rmARC2 (in presence of NADH, CYB5R)	ND ^e	ND ^e	ND ^e	6.0	N6-hydroxyadenine	k	[201]
Human rmARC2 (in presence of NADH, CYB5)	ND ^e	ND ^e	ND ^e	6.0	N6-hydroxyadenine	k	[201]
NADH, CYB5, CYB5R without mARC2	ND ^e	ND ^e	ND ^e	6.0	N6-hydroxyadenine	k	[201]
Human rmARC2 (in presence of NADH, CYB5, CYB5R)	ND ^e	ND ^e	0.1053 ± 0.0087	6.0	N6- hydroxyadenosine	k	[201]
Human rmARC2 (in presence of CYB5, CYB5R)	ND ^e	ND ^e	ND ^e	6.0	N6- hydroxyadenosine	k	[201]
Human rmARC2 (in presence of NADH, CYB5R)	ND ^e	ND ^e	ND ^e	6.0	N6- hydroxyadenosine	k	[201]
Human rmARC2 (in presence of NADH, CYB5)	ND ^e	ND ^e	0.0009 ± 0.0001	6.0	N6- hydroxyadenosine	k	[201]
NADH, CYB5, CYB5R without mARC2	ND ^e	ND ^e	ND ^e	6.0	N6- hydroxyadenosine	k	[201]
Human rmARC2 (in presence of NADH, CYB5, CYB5R)	ND ^e	ND ^e	0.1425 ± 0.0244	6.0	benzamidoxime	k	[201]
Human rmARC2 (in presence of CYB5, CYB5R)	ND ^e	ND ^e	ND ^e	6.0	benzamidoxime	k	[201]
Human rmARC2 (in presence of NADH, CYB5R)	ND ^e	ND ^e	ND ^e	6.0	benzamidoxime	k	[201]

Table 1.12 Continued

<u>Enzyme^a</u>	<u>K_m (μM)</u>	<u>K_{cat} (min⁻¹)</u>	<u>Specific Activity (μmol subs/min/mg)</u>	<u>pH</u>	<u>Substrate</u>	<u>Assay Description</u>	<u>Ref.</u>
Human rmARC2 (in presence of NADH, CYB5)	ND ^e	ND ^e	0.0024 ± 0.0002	6.0	benzamidoxime	k	[201]
NADH, CYB5, CYB5R without rmARC2	ND ^e	ND ^e	ND ^e	6.0	benzamidoxime	k	[201]
<i>A. thaliana</i> NR	N/M ^b	N/M ^b	0.02	7.5	Nitrate	n	[202]
<i>A. thaliana</i> rNR	N/M ^b	N/M ^b	0.08	7.5	Nitrate	n	[202]
<i>A. thaliana</i> rNR	15	N/M ^b	36	7.0	Nitrate	n	[203]
<i>A. thaliana</i> rNR	4	N/M ^b	N/M ^b	7.0	NADH	n	[203]
<i>Cucurbita maxima</i> NR	N/M ^b	13920	100	7.0	Nitrate	n	[203, 204, 255]
<i>A. thaliana</i> rNR C191A	N/M ^b	N/M ^b	0	7.0	Nitrate	n	[203]
<i>A. thaliana</i> rNR C191S	N/M ^b	N/M ^b	0	7.0	Nitrate	n	[203]
<i>A. thaliana</i> rNR (deletion of N- terminal amino acids 2-4)	N/M ^b	N/M ^b	82	7.0	Nitrate	n	[203]
<i>A. thaliana</i> NR (substitution of amino acids 2-12 for a His tag)	N/M ^b	N/M ^b	68	7.0	Nitrate	n	[203]
<i>A. thaliana</i> rNR S216A	N/M ^b	N/M ^b	62	7.0	Nitrate	n	[203]
<i>A. thaliana</i> rNR S261A	N/M ^b	N/M ^b	80	7.0	Nitrate	n	[203]
<i>A. thaliana</i> rNR S266A	N/M ^b	N/M ^b	48	7.0	Nitrate	n	[203]
<i>A. thaliana</i> rNR S324A	N/M ^b	N/M ^b	107	7.0	Nitrate	n	[203]
<i>A. thaliana</i> rNR S365A	N/M ^b	N/M ^b	150	7.0	Nitrate	n	[203]
<i>A. thaliana</i> rNR S395A	N/M ^b	N/M ^b	100	7.0	Nitrate	n	[203]
<i>A. thaliana</i> rNR S438A	N/M ^b	N/M ^b	156	7.0	Nitrate	n	[203]
<i>A. thaliana</i> rNR	90 ± 20	12600 ± 1800	N/M ^b	7.0	Nitrate	n	[204]
<i>A. thaliana</i> rNR	0.7 ± 0.3	N/M ^b	N/M ^b	7.0	NADH	n	[204]
<i>Chlorella</i> NR	N/M ^b	10380	N/M ^b	N/M ^b	Nitrate	k	[204, 256]
Maize rNR (small Mo domain-368 residues)	10	N/M ^b	N/M ^b	7.0	NADH	n	[205]

Table 1.12 Continued

Enzyme ^a	K _m (μM)	K _{cat} (min ⁻¹)	Specific Activity (μmol subs/min/mg)	pH	Substrate	Assay Description	Ref.
Maize rNR (small Mo domain-368 residues)	17	138000	69 ^{c, w}	7.0	FeCN	n	[205]
Maize rNR (small Mo domain-368 residues)	6	78000	40 ^{c, w}	7.0	Cyt c	n	[205]
Maize rNR (large Mo domain-595 residues)	10	N/M ^b	N/M ^b	7.0	NADH	n	[205]
Maize rNR (large Mo domain-595 residues)	17	138000	69 ^{c, w}	7.0	FeCN	n	[205]
Maize rNR (large Mo domain-595 residues)	6	78000	40 ^{c, w}	7.0	Cyt c	n	[205]
spinach rNR (Mo domain)	13	N/M ^b	N/M ^b	7.0	NADH	n	[205]
spinach rNR (Mo domain)	32	162000	80 ^{c, w}	7.0	FeCN	n	[205]
spinach rNR (Mo domain)	6	108000	55 ^{c, w}	7.0	Cyt c	n	[205]
<i>Nicotiana tabacum</i> rNR	N/M ^b	N/M ^b	1A ^g	7.5	Nitrate	n	[94]
<i>Nicotiana tabacum</i> rNR	N/M ^b	N/M ^b	1.5	7.5	NADH:cytochrome c	n	[94]
<i>Pichia angusta</i> rNR (S-NaR1)	30 ± 3	9540	N/M ^b	7.5	Nitrate	o	[136]
<i>Pichia angusta</i> rNR (S-NaR1)	ND ^e	124860	N/M ^b	7.5	Nitrate	p	[136]
spinach rNR-Mo domain (GST- tagged)	12 ± 1	10800 ± 6	10.8 ^v	7.6	Nitrate	j	[55]
spinach rNR-Mo domain (His-tagged)	8 ± 1	1500 ± 6	1.5 ^v	7.6	Nitrate	j	[55]
Spinach NR	13	N/M ^b	18 ^s	7.0	Nitrate	n	[55, 257]
<i>A. thaliana</i> rSO	33.8 ± 3.2	N/M ^b	N/M ^b	8.0	Sulfite	i	[209]
tobacco SO	51.4	N/M ^b	N/M ^b	8.0	Sulfite	i	[209]
Chicken Liver SO	33	N/M ^b	N/M ^b	8.0	Sulfite	h	[209],[258]
Human rSO	10.4	1818	994 ^r	8.5	Sulfite	h	[57]
Human rSO (His- tagged) expressed in <i>E. coli</i> TP1000	12.1	1662	731-791 ^r	8.5	Sulfite	h	[57]
Human rSO (His- tagged) expressed in <i>E. coli</i> BL21 DE3	N/M ^b	N/M ^b	113 ^r	8.5	Sulfite	h	[57]

Table 1.12 Continued

<u>Enzyme^a</u>	<u>K_m (μM)</u>	<u>K_{cat} (min⁻¹)</u>	<u>Specific Activity (μmol subs/min/mg)</u>	<u>pH</u>	<u>Substrate</u>	<u>Assay Description</u>	<u>Ref.</u>
Human rSO (His-tagged) expressed in <i>E. coli</i> DH5α	N/M ^b	N/M ^b	467 ^r	8.5	Sulfite	h	[57]
Human rSO (His-tagged) expressed in <i>E. coli</i> MC4100	N/M ^b	N/M ^b	545 ^r	8.5	Sulfite	h	[57]
Human rSO	N/M ^b	N/M ^b	89 ^r	8.5	Sulfite	i	[57]
Human rSO (His-tagged) expressed in <i>E. coli</i> TP1000	N/M ^b	N/M ^b	70 ^r	8.5	Sulfite	i	[57]
Human rSO-Mo domain (His-tagged) expressed in <i>E. coli</i> TP1000	N/M ^b	N/M ^b	104 ^r	8.5	Sulfite	i	[57]
Human rSO	2.4 ± 0.1	2112 ± 24	N/M ^b	8.02	Sulfite	h	[110]
Human rSO	3.8 ± 0.3	1908 ± 114	N/M ^b	8.25	Sulfite	h	[110]
Human rSO	2.4 ± 0.1	1728 ± 66	N/M ^b	8.48	Sulfite	h	[110]
Human rSO Y343F	10.2 ± 2.1	408 ± 18	N/M ^b	8.02	Sulfite	h	[110]
Human rSO Y343F	24.8 ± 7.6	546 ± 60	N/M ^b	8.25	Sulfite	h	[110]
Human rSO Y343F	50.2 ± 9.7	510 ± 48	N/M ^b	8.48	Sulfite	h	[110]
Human rSO	1.29 ± 0.30	792 ± 24	N/M ^b	6.0	Sulfite	h	[111]
Human rSO	1.62 ± 0.14	1062 ± 18	N/M ^b	6.5	Sulfite	h	[111]
Human rSO	2.72 ± 0.23	1452 ± 18	N/M ^b	7.0	Sulfite	h	[111]
Human rSO	3.39 ± 0.35	1482 ± 24	N/M ^b	7.5	Sulfite	h	[111]
Human rSO	4.35 ± 0.11	1554 ± 12	N/M ^b	8.0	Sulfite	h	[111]
Human rSO	8.25 ± 0.44	1614 ± 30	N/M ^b	8.5	Sulfite	h	[111]
Human rSO	22.1 ± 1.6	1542 ± 54	N/M ^b	9.0	Sulfite	h	[111]
Human rSO	67.1 ± 9.0	1578 ± 90	N/M ^b	9.5	Sulfite	h	[111]
Human rSO G473D	1660 ± 324	8.4 ± 0.6	N/M ^b	6.0	Sulfite	h	[111]
Human rSO G473D	990 ± 53	16.8 ± 0.6	N/M ^b	6.5	Sulfite	h	[111]
Human rSO G473D	623 ± 64	30 ± 1.2	N/M ^b	7.0	Sulfite	h	[111]
Human rSO G473D	1063 ± 18	34.2 ± 0.6	N/M ^b	7.5	Sulfite	h	[111]
Human rSO G473D	1223 ± 70	34.8 ± 0.6	N/M ^b	8.0	Sulfite	h	[111]
Human rSO G473D	2040 ± 30	32.4 ± 1.8	N/M ^b	8.5	Sulfite	h	[111]
Human rSO G473D	25878 ± 4825	25.2 ± 0.6	N/M ^b	9.1	Sulfite	h	[111]
Human rSO G473D	ND ^e	ND ^e	N/M ^b	9.6	Sulfite	h	[111]
Human rSO G473A	4.53 ± 1.43	249 ± 30	N/M ^b	6.0	Sulfite	h	[111]
Human rSO G473A	5.36 ± 0.47	954 ± 6	N/M ^b	7.0	Sulfite	h	[111]
Human rSO G473A	17.2 ± 1.6	1296 ± 42	N/M ^b	7.4	Sulfite	h	[111]
Human rSO G473A	48.7 ± 1.1	1572 ± 24	N/M ^b	8.0	Sulfite	h	[111]
Human rSO G473A	107 ± 6	1704 ± 84	N/M ^b	8.5	Sulfite	h	[111]
Human rSO G473A	774 ± 32	1914 ± 18	N/M ^b	9.1	Sulfite	h	[111]
Human rSO G473A	3684 ± 504	906 ± 90	N/M ^b	10.0	Sulfite	h	[111]
Human rSO G473W	1910 ± 238	36 ± 1.2	N/M ^b	6.0	Sulfite	h	[111]
Human rSO G473W	330 ± 41	108 ± 2.4	N/M ^b	7.0	Sulfite	h	[111]
Human rSO G473W	2034 ± 419	148.8 ± 13.8	N/M ^b	8.5	Sulfite	h	[111]

Table 1.12 Continued

<u>Enzyme^a</u>	<u>K_m (μM)</u>	<u>K_{cat} (min⁻¹)</u>	<u>Specific Activity (μmol subs/min/mg)</u>	<u>pH</u>	<u>Substrate</u>	<u>Assay Description</u>	<u>Ref.</u>
Human rSO G473W	10407 ± 4027	81 ± 22.2	N/M ^b	9.0	Sulfite	h	[111]
Human rSO R212A/G473D	ND ^e	ND ^e	N/M ^b	7.0	Sulfite	h	[111]
Human rSO R212A/G473D	ND ^e	ND ^e	N/M ^b	8.5	Sulfite	h	[111]
Human rSO	4.56 ± 0.27	N/M ^b	78.0 ± 1.9 ^{c, r}	7.0	Sulfite	i	[111]
Human rSO	14.9 ± 0.8	N/M ^b	99.8 ± 3.3 ^{c, r}	8.6	Sulfite	i	[111]
Human rSO G473D	26500 ± 1600	N/M ^b	22.1 ± 1.0 ^{c, r}	7.0	Sulfite	i	[111]
Human rSO G473D	41400 ± 7100	N/M ^b	10.2 ± 0.76 ^{c, r}	8.5	Sulfite	i	[111]
Human rSO G473A	6.05 ± 0.46	N/M ^b	29.8 ± 0.5 ^{c, r}	7.0	Sulfite	i	[111]
Human rSO G473A	191 ± 4	N/M ^b	67.8 ± 2.6 ^{c, r}	8.5	Sulfite	i	[111]
Human rSO G473W	21200 ± 900	N/M ^b	70.2 ± 2.8 ^{c, r}	7.0	Sulfite	i	[111]
Human rSO G473W	24000 ± 3600	N/M ^b	28.8 ± 2.7 ^{c, r}	8.5	Sulfite	i	[111]
Human rSO R212A/G473D	ND ^e	N/M ^b	ND ^e	7.0	Sulfite	i	[111]
Human rSO R212A/G473D	ND ^e	N/M ^b	ND ^e	8.5	Sulfite	i	[111]
Human rSO	N/M ^b	N/M ^b	1062 ^r	N/M ^b	Sulfite	h	[109]
Human Apo-rSO + inactive MPT synthase + precursor Z	N/M ^b	N/M ^b	ND ^e	N/M ^b	Sulfite	h	[109]
Human Apo-rSO + active MPT synthase + precursor Z	N/M ^b	N/M ^b	ND ^e	N/M ^b	Sulfite	h	[109]
Human Apo-rSO + active MPT synthase + precursor Z +molybdate	N/M ^b	N/M ^b	552 ^r	N/M ^b	Sulfite	h	[109]
Human Apo-rSO	N/M ^b	N/M ^b	ND ^e	N/M ^b	Sulfite	h	[109]
Human rSO	N/M ^b	N/M ^b	103 ^r	N/M ^b	Sulfite	i	[109]
Human Apo-rSO + inactive MPT synthase + precursor Z	N/M ^b	N/M ^b	ND ^e	N/M ^b	Sulfite	i	[109]
Human Apo-rSO + active MPT synthase + precursor Z	N/M ^b	N/M ^b	ND ^e	N/M ^b	Sulfite	i	[109]
Human Apo-rSO + active MPT synthase + precursor Z +molybdate	N/M ^b	N/M ^b	49 ^r	N/M ^b	Sulfite	i	[109]

Table 1.12 Continued

<u>Enzyme^a</u>	<u>K_m (μM)</u>	<u>K_{cat} (min⁻¹)</u>	<u>Specific Activity (μmol subs/min/mg)</u>	<u>pH</u>	<u>Substrate</u>	<u>Assay Description</u>	<u>Ref.</u>
Human Apo-rSO	N/M ^b	N/M ^b	ND ^e	N/M ^b	Sulfite	i	[109]
human rSO	N/M ^b	N/M ^b	1100 ^f	N/M ^b	Sulfite	N/M ^b	[68]
Rat rSO	N/M ^b	N/M ^b	2000 ^f	N/M ^b	Sulfite	N/M ^b	[68]
human rSO (holo)	21	N/M ^b	N/M ^b	8.0	Sulfite	l	[210]
human rSO (heme free)	41	N/M ^b	N/M ^b	8.0	Sulfite	l	[210]
human rSO (holo)	80000	114	2.04 ^c	7.4	nitrite	m	[212]
human rSO (Mo- domain)	31000	282	6.72 ^c	7.4	nitrite	m	[212]
human rSO	17	960	66 ^f	N/M ^b	sulfite	i	[95]
human rSO-R160Q	1700	144	0.95 ^f	N/M ^b	sulfite	i	[95]
human rSO-R160K	332	288	N/M ^b	N/M ^b	sulfite	i	[95]
Human Hepatic SO	17	N/M ^b	N/M ^a	N/M ^b	Sulfite	N/M ^b	[56, 259]
Maize (<i>Zea mays</i>) rSO	21.4 ± 0.32	N/M ^b	42.56±0.85 ^{c, u}	8.0	Sulfite	i	[56]

a) r- recombinant; b) N/M- Not mentioned; c) specific activity is reported as V_{\max} ; d) value was calculated from data reported; e) ND- not detected; f) NA- negligible activity; g) IA- inactive; h) Monitored the reduction of electron acceptor cytochrome c at 550 nm; i) Monitor reduction of ferrocyanide at 420 nm; j) Monitoring Nitrite/product formation through the Griess colorimetric assay; k) Detection via HPLC of reduction of substrate using NADPH/NADH, cytochrome b5 reductase and cytochrome b5 or b6; l) Protein film Voltammetry (PFV); m) Monitoring oxidation of phenosafranine at 520 nm; n) Monitor reduction of NADH; o) Monitoring the oxidation of electron donor of methyl viologen; p) Monitoring the oxidation of electron donor of bromphenol blue; q) monitor NO production by chemiluminescence in the presence of CYB5, CYB5R, and NADH; r) in U/mg; s) in U; t) active but below assay detection limit; u) in μM/min; v) in μmol nitrate/min/nmol enzyme; w) μmol/min/mol heme; x) in pmol NO produced/s; y) in pmol/min.

Table 1.13: Kinetic parameters for prokaryotic XO family of enzymes.

Enzyme ^a	K _m (μM)	K _{cat} (min ⁻¹)	Specific Activity (μmol subs/min/mg)	pH	Substrate	Assay Description	Ref.
<i>E. coli</i> rAO (with YagQ)	N/M ^b	N/M ^b	27.9 ± 0.2	6.0	Vanillin	l	[120]
<i>E. coli</i> rAO (without YagQ)	N/M ^b	N/M ^b	ND ^e	6.0	Vanillin	l	[120]
<i>E. coli</i> rAO	63 ± 10	5040 ± 300	N/M ^b	6.0	Cinnamaldehyde	l	[120]
<i>E. coli</i> rAO	132 ± 20	7500 ± 120	8.63 ± 0.03	6.0	Vanillin	l	[120]
<i>E. coli</i> rAO	70 ± 7	5820 ± 180	N/M ^b	6.0	Benzaldehyde	l	[120]
<i>E. coli</i> rAO	132 ± 6	420 ± 36	N/M ^b	6.0	Phenylacetic aldehyde	l	[120]
<i>E. coli</i> rAO	428 ± 55	3300 ± 480	N/M ^b	6.0	2,4-Dihydroxybenzaldehyde	l	[120]
<i>E. coli</i> rAO	429 ± 73	408 ± 60	N/M ^b	6.0	Valeraldehyde	l	[120]
<i>E. coli</i> rAO	426 ± 42	660 ± 60	N/M ^b	6.0	Heptaldehyde	l	[120]
<i>E. coli</i> rAO	1150 ± 30	1800 ± 60	N/M ^b	6.0	Acetic aldehyde	l	[120]
<i>E. coli</i> rAO	ND ^e	ND ^e	N/M ^b	6.0	Xanthine	l	[120]
<i>E. coli</i> rAO	ND ^e	ND ^e	N/M ^b	6.0	Hypoxanthine	l	[120]
<i>E. coli</i> rAO	ND ^e	ND ^e	N/M ^b	6.0	Nicotine	l	[120]
<i>E. coli</i> rAO	ND ^e	ND ^e	N/M ^b	6.0	Caffeine	l	[120]
<i>E. coli</i> rAO	ND ^e	ND ^e	N/M ^b	6.0	Pyridoxal	l	[120]
<i>E. coli</i> rAO	ND ^e	ND ^e	N/M ^b	6.0	All-trans-retinaldehyde	l	[120]
<i>E. coli</i> rAO	N/M ^b	N/M ^b	0.27 ± 0.01	6.0	Vanillin	k	[120]
<i>E. coli</i> rAO	N/M ^b	N/M ^b	ND ^e	6.0	Vanillin	s	[120]
<i>E. coli</i> rAO	N/M ^b	N/M ^b	ND ^e	6.0	Vanillin	i	[120]
<i>E. coli</i> rAO	N/M ^b	N/M ^b	ND ^e	6.0	Vanillin	t	[120]
<i>E. coli</i> rAO	N/M ^b	N/M ^b	2.73 ± 0.08	6.0	Vanillin	u	[120]
<i>E. coli</i> rAO	659.3 ± 80.2	65856 ± 2472	N/M ^b	4.0	benzaldehyde	l	[213]
<i>E. coli</i> rAO	306.7 ± 44.21	29160 ± 1170	N/M ^b	4.5	benzaldehyde	l	[213]
<i>E. coli</i> rAO	158.9 ± 35.4	13032 ± 696	N/M ^b	5.0	benzaldehyde	l	[213]
<i>E. coli</i> rAO	129.2 ± 15.5	9042 ± 456	N/M ^b	5.5	benzaldehyde	l	[213]
<i>E. coli</i> rAO	ND ^e	ND ^e	N/M ^b	6.0	benzaldehyde	l	[213]
<i>E. coli</i> rAO	ND ^e	ND ^e	N/M ^b	6.5	benzaldehyde	l	[213]
<i>E. coli</i> rAO	ND ^e	ND ^e	N/M ^b	7.0	benzaldehyde	l	[213]
<i>E. coli</i> rAO	ND ^e	ND ^e	N/M ^b	7.5	benzaldehyde	l	[213]
<i>E. coli</i> rAO	ND ^e	ND ^e	N/M ^b	8.0	benzaldehyde	l	[213]
<i>E. coli</i> rAO (PaoC R440H)	513.9 ± 86.5	24270 ± 1152	N/M ^b	4.0	benzaldehyde	l	[213]
<i>E. coli</i> rAO (PaoC R440H)	395.9 ± 89.0	17580 ± 1044	N/M ^b	4.5	benzaldehyde	l	[213]
<i>E. coli</i> rAO (PaoC R440H)	288.0 ± 60.1	9000 ± 462	N/M ^b	5.0	benzaldehyde	l	[213]
<i>E. coli</i> rAO (PaoC R440H)	59.8 ± 6.7	2922 ± 60	N/M ^b	5.5	benzaldehyde	l	[213]
<i>E. coli</i> rAO (PaoC R440H)	ND ^e	ND ^e	N/M ^b	6.0	benzaldehyde	l	[213]
<i>E. coli</i> rAO (PaoC R440H)	ND ^e	ND ^e	N/M ^b	6.5	benzaldehyde	l	[213]
<i>E. coli</i> rAO (PaoC R440H)	ND ^e	ND ^e	N/M ^b	7.0	benzaldehyde	l	[213]
<i>E. coli</i> rAO (PaoC R440H)	ND ^e	ND ^e	N/M ^b	7.5	benzaldehyde	l	[213]
<i>E. coli</i> rAO (PaoC R440H)	ND ^e	ND ^e	N/M ^b	8.0	benzaldehyde	l	[213]
<i>E. coli</i> rAO (PaoC R440K)	1517.4 ± 252.2	18408 ± 1056	N/M ^b	4.0	benzaldehyde	l	[213]
<i>E. coli</i> rAO (PaoC R440K)	520.1 ± 59.2	19470 ± 540	N/M ^b	4.5	benzaldehyde	l	[213]
<i>E. coli</i> rAO (PaoC R440K)	361.6 ± 96.3	4828.8 ± 288	N/M ^b	5.0	benzaldehyde	l	[213]
<i>E. coli</i> rAO (PaoC R440K)	204.2 ± 45.1	2467.8 ± 102	N/M ^b	5.5	benzaldehyde	l	[213]
<i>E. coli</i> rAO (PaoC R440K)	ND ^e	ND ^e	N/M ^b	6.0	benzaldehyde	l	[213]
<i>E. coli</i> rAO (PaoC R440K)	ND ^e	ND ^e	N/M ^b	6.5	benzaldehyde	l	[213]

Table 1.13 Continued

Enzyme ^a	K _m (μM)	K _{cat} (min ⁻¹)	Specific Activity (μmol subs/min/mg)	pH	Substrate	Assay Description	Ref.
<i>E. coli</i> rAO (PaoC R440K)	ND ^e	ND ^e	N/M ^b	7.0	benzaldehyde	l	[213]
<i>E. coli</i> rAO (PaoC R440K)	ND ^e	ND ^e	N/M ^b	7.5	benzaldehyde	l	[213]
<i>E. coli</i> rAO (PaoC R440K)	ND ^e	ND ^e	N/M ^b	8.0	benzaldehyde	l	[213]
<i>P. furiosus</i> rAO (purified)	N/M ^b	N/M ^b	49	8.0	acetaldehyde	n	[215]
<i>P. furiosus</i> rAO (cell extracts)	N/M ^b	N/M ^b	3.5 ± 1	8.0	acetaldehyde	n	[215]
<i>P. furiosus</i> AO (cell extracts)	N/M ^b	N/M ^b	4.0 ± 0.1	8.0	acetaldehyde	n	[215]
<i>B. diminuta</i> 7 r-Isoquinoline 1- oxidoreductase	N/M ^b	N/M ^b	0.012	8.5	isoquinoline	o	[216]
<i>B. diminuta</i> 7 Isoquinoline 1- oxidoreductase	N/M ^b	N/M ^b	0.04	8.5	isoquinoline	o	[216, 260]
<i>P. putida</i> KT2440 r-nicotinate dehydrogenase	N/M ^b	N/M ^b	1.18	7.0	nicotinate	q	[50]
<i>P. putida</i> KT2440 r-nicotinate dehydrogenase	70	N/M ^b	2.3 ^{c, aa}	8.0	2,5- dihydroxypyridine	v	[217]
<i>P. putida</i> KT2440 r-nicotinate dehydrogenase (O ₂ electron acceptor)	N/M ^b	N/M ^b	1.48	7.5	Nicotinic acid	r	[217]
<i>P. putida</i> KT2440 r-nicotinate dehydrogenase (PMS electron acceptor)	N/M ^b	N/M ^b	5.98	7.5	Nicotinic acid	r	[217]
<i>P. putida</i> KT2440 r-nicotinate dehydrogenase (KCN electron acceptor)	N/M ^b	N/M ^b	ND ^e	7.5	Nicotinic acid	r	[217]
<i>P. putida</i> KT2440 r-nicotinate dehydrogenase (PMS + KCN electron acceptor)	N/M ^b	N/M ^b	5.91	7.5	Nicotinic acid	r	[217]
<i>P. putida</i> KT2440 r-nicotinate dehydrogenase (Anti A electron acceptor)	N/M ^b	N/M ^b	1.35	7.5	Nicotinic acid	r	[217]
<i>P. putida</i> KT2440 r-nicotinate dehydrogenase (PMS + Anti A electron acceptor)	N/M ^b	N/M ^b	5.83	7.5	Nicotinic acid	r	[217]
<i>P. putida</i> KT2440 r-nicotinate dehydrogenase (CytC domain electron acceptor)	N/M ^b	N/M ^b	2.14	7.5	Nicotinic acid	r	[217]
<i>P. putida</i> KT2440 r-nicotinate dehydrogenase (truncated NicB, O ₂ electron acceptor)	N/M ^b	N/M ^b	ND ^e	7.5	Nicotinic acid	r	[217]
<i>P. putida</i> KT2440 r-nicotinate dehydrogenase (truncated NicB, PMS electron acceptor)	N/M ^b	N/M ^b	2.16	7.5	Nicotinic acid	r	[217]
<i>P. putida</i> KT2440 r-nicotinate dehydrogenase (truncated NicB, KCN electron acceptor)	N/M ^b	N/M ^b	ND ^e	7.5	Nicotinic acid	r	[217]

Table 1.13 Continued

Enzyme^a	K_m (μM)	K_{cat} (min⁻¹)	Specific Activity (μmol subs/min/mg)	pH	Substrate	Assay Description	Ref.
<i>P. putida</i> KT2440 r-nicotinate dehydrogenase (truncated NicB, PMS + KCN electron acceptor)	N/M ^b	N/M ^b	1.73	7.5	Nicotinic acid	r	[217]
<i>P. putida</i> KT2440 r-nicotinate dehydrogenase (truncated NicB, Anti A electron acceptor)	N/M ^b	N/M ^b	ND ^e	7.5	Nicotinic acid	r	[217]
<i>P. putida</i> KT2440 r-nicotinate dehydrogenase (truncated NicB, PMS + Anti A electron acceptor)	N/M ^b	N/M ^b	2.07	7.5	Nicotinic acid	r	[217]
<i>P. putida</i> KT2440 r-nicotinate dehydrogenase (truncated NicB, CytC domain electron acceptor)	N/M ^b	N/M ^b	0.04	7.5	Nicotinic acid	r	[217]
<i>P. putida</i> KT2440 r-nicotinate dehydrogenase	19 ± 2	8778 ^d	65.2 ± 2.2 ^c	7.5	piperonal	q	[218]
<i>P. putida</i> KT2440 r-nicotinate dehydrogenase	ND ^e	ND ^e	ND ^e	7.5	Formaldehyde	q	[218]
<i>P. putida</i> KT2440 r-nicotinate dehydrogenase	67.9 ± 14	12222 ^d	97.3 ± 13 ^c	7.5	Acetaldehyde	q	[218]
<i>P. putida</i> KT2440 r-nicotinate dehydrogenase	0.37 ± 0.008	7992 ^d	59.7 ± 4.1 ^c	7.5	Propionaldehyde	q	[218]
<i>P. putida</i> KT2440 r-nicotinate dehydrogenase	0.26 ± 0.04	7956 ^d	58.5 ± 3.2 ^c	7.5	Crotonaldehyde	q	[218]
<i>P. putida</i> KT2440 r-nicotinate dehydrogenase	0.059 ± 0.01	9204 ^d	68.7 ± 3.7 ^c	7.5	Butyraldehyde	q	[218]
<i>P. putida</i> KT2440 r-nicotinate dehydrogenase	1.78 ± 0.45	10680 ^d	79.0 ± 11 ^c	7.5	Isobutyraldehyde	q	[218]
<i>P. putida</i> KT2440 r-nicotinate dehydrogenase	0.05 ± 0.009	8400 ^d	61.3 ± 2.6 ^c	7.5	Valeraldehyde	q	[218]
<i>P. putida</i> KT2440 r-nicotinate dehydrogenase	0.049 ± 0.008	9114 ^d	67.9 ± 3.9 ^c	7.5	Isovaleraldehyde	q	[218]
<i>P. putida</i> KT2440 r-nicotinate dehydrogenase	0.087 ± 0.01	8874 ^d	67.7 ± 3.9 ^c	7.5	1-Hexanal	q	[218]
<i>P. putida</i> KT2440 r-nicotinate dehydrogenase	0.045 ± 0.009	8640 ^d	65.1 ± 4.4 ^c	7.5	Benzaldehyde	q	[218]
<i>P. putida</i> KT2440 r-nicotinate dehydrogenase	0.024 ± 0.003	4032 ^d	29.7 ± 1.4 ^c	7.5	Salicylaldehyde	q	[218]
<i>P. putida</i> KT2440 r-nicotinate dehydrogenase	0.09 ± 0.01	30240 ^d	59.6 ± 1.8 ^c	7.5	3-Hydroxybenzaldehyde	q	[218]
<i>P. putida</i> KT2440 r-nicotinate dehydrogenase	0.024 ± 0.003	1872 ^d	53.0 ± 2.7 ^c	7.5	4-Hydroxybenzaldehyde	q	[218]
<i>P. putida</i> KT2440 r-nicotinate dehydrogenase	0.024 ± 0.004	8928 ^d	66.3 ± 3.7 ^c	7.5	Cinnamaldehyde	q	[218]
<i>P. putida</i> KT2440 r-nicotinate dehydrogenase	0.31 ± 0.04	6696 ^d	49.4 ± 2.1 ^c	7.5	Protocatechualdehyde	q	[218]
<i>P. putida</i> KT2440 r-nicotinate dehydrogenase	0.097 ± 0.006	8730 ^d	64.5 ± 1.1 ^c	7.5	Vanillin	q	[218]

Table 1.13 Continued

Enzyme ^a	K _m (μM)	K _{cat} (min ⁻¹)	Specific Activity (μmol subs/min/mg)	pH	Substrate	Assay Description	Ref.
<i>P. putida</i> KT2440 r-nicotinate dehydrogenase	ND ^e	ND ^e	ND ^e	7.5	Xanthine	q	[218]
<i>A. ilicis</i> Ru ^{61a} r-quinaldine 4-oxidase	35	1764	5 ^y	N/M ^b	quinaldine	o	[219]
Native <i>A. ilicis</i> Ru ^{61a} r-quinaldine 4-oxidase	34	1002	N/M ^b	N/M ^b	quinaldine	o	[219]
<i>A. ilicis</i> Ru ^{61a} r-quinaldine 4-oxidase	17	1494	N/M ^b	N/M ^b	iodonitrotetrazolium chloride	o	[219]
Native <i>A. ilicis</i> Ru ^{61a} r-quinaldine 4-oxidase	19	936	N/M ^b	N/M ^b	iodonitrotetrazolium chloride	o	[219]
<i>P. putida</i> 86 r-quinoline 2-oxidoreductase (pUF1 in strain KT2440)	120	522	2	N/M ^b	quinoline	o	[220]
<i>P. putida</i> 86 r-quinoline 2-oxidoreductase (pUF1 in strain 86-1 Δ <i>qor</i>)	120	5124	17	N/M ^b	quinoline	o	[220]
<i>P. putida</i> 86 quinoline 2-oxidoreductase	180	4440	N/M ^b	N/M ^b	quinoline	N/M ^b	[220, 261]
<i>P. putida</i> 86 r-quinoline 2-oxidoreductase	N/M ^b	N/M ^b	0.37 ^y	N/M ^b	quinoline	p	[221]
<i>P. putida</i> 86 r-quinoline 2-oxidoreductase	N/M ^b	N/M ^b	0.72 ^y	N/M ^b	quinoline	p	[221]
<i>C. acidovorans</i> rXDH (-XdhC), high aeration	66 ± 3	24 ± 60	11.18	7.8	xanthine	m	[69]
<i>C. acidovorans</i> rXDH (-XdhC), low aeration	67 ± 2	1620 ± 60	0.1673	7.8	xanthine	m	[69]
<i>C. acidovorans</i> rXDH (+XdhC), high aeration	85 ± 2	7080 ± 60	46	7.8	xanthine	m	[69]
<i>C. acidovorans</i> rXDH (+XdhC), low aeration	86 ± 5	10740 ± 240	70	7.8	xanthine	m	[69]
<i>C. acidovorans</i> XDH	68 ± 5	7200 ± 180	50	7.8	xanthine	m	[69, 127, 262]
<i>C. acidovorans</i> rXDH (-XdhC)	72 ± 5	1080 ± 60	6.58	7.8	xanthine	m	[127]
<i>C. acidovorans</i> rXDH (+XdhC)	120 ± 5	13200 ± 420	80.00	7.8	xanthine	m	[127]
<i>R. capsulatus</i> rXDH	540 ± 146	33 ± 2	N/M ^b	7.5	benzaldehyde	l	[106]
<i>R. capsulatus</i> rXDH E232V	39.9 ± 7.0	93.5 ± 13.6	N/M ^b	7.5	benzaldehyde	l	[106]
<i>R. capsulatus</i> rXDH R310M	552 ± 188	211 ± 53	N/M ^b	7.5	benzaldehyde	l	[106]
<i>R. capsulatus</i> rXDH E232V/R310M	25.9 ± 15.5	94.2 ± 8.4	N/M ^b	7.5	benzaldehyde	l	[106]
<i>R. capsulatus</i> rXDH	1240 ± 210	2.62 ± 0.06	N/M ^b	7.5	phthalazine	l	[106]
<i>R. capsulatus</i> rXDH E232V	310 ± 80	142.0 ± 27.4	N/M ^b	7.5	phthalazine	l	[106]
<i>R. capsulatus</i> rXDH R310M	ND ^e	ND ^e	N/M ^b	7.5	phthalazine	l	[106]
<i>R. capsulatus</i> rXDH E232V/R310M	420 ± 73	81.0 ± 10.5	N/M ^b	7.5	phthalazine	l	[106]
<i>R. capsulatus</i> rXDH	6.3 ± 1.3	0.39 ± 0.06	N/M ^b	7.5	Retinaldehyde	l	[106]
<i>R. capsulatus</i> rXDH E232V	38.2 ± 10.5	3.3 ± 0.9	N/M ^b	7.5	Retinaldehyde	l	[106]
<i>R. capsulatus</i> rXDH R310M	154.8 ± 7.1	10.9 ± 0.2	N/M ^b	7.5	Retinaldehyde	l	[106]

Table 1.13 Continued

Enzyme ^a	K _m (μM)	K _{cat} (min ⁻¹)	Specific Activity (μmol subs/min/mg)	pH	Substrate	Assay Description	Ref.
<i>R. capsulatus</i> rXDH E232V/R310M	36.6 ± 1.1	3.0 ± 0.2	N/M ^b	7.5	Retinaldehyde	l	[106]
<i>R. capsulatus</i> rXDH	ND ^e	ND ^e	N/M ^b	7.5	acetaldehyde	l	[106]
<i>R. capsulatus</i> rXDH E232V	913 ± 460	88.5 ± 20.1	N/M ^b	7.5	acetaldehyde	l	[106]
<i>R. capsulatus</i> rXDH R310M	6200 ± 1880	110.6 ± 10.9	N/M ^b	7.5	acetaldehyde	l	[106]
<i>R. capsulatus</i> rXDH E232V/R310M	2170 ± 450	56.8 ± 7.6	N/M ^b	7.5	acetaldehyde	l	[106]
<i>R. capsulatus</i> rXDH	59 ± 10	3300 ± 460	N/M ^b	7.5	xanthine	l	[106]
<i>R. capsulatus</i> rXDH E232V	175 ± 7	85.6 ± 15.3	N/M ^b	7.5	xanthine	l	[106]
<i>R. capsulatus</i> rXDH R310M	ND ^e	ND ^e	N/M ^b	7.5	xanthine	l	[106]
<i>R. capsulatus</i> rXDH E232V/R310M	ND ^e	ND ^e	N/M ^b	7.5	xanthine	l	[106]
<i>R. capsulatus</i> rXDH	31.4 ± 1.4	2666 ± 186	N/M ^b	7.5	hypoxanthine	l	[106]
<i>R. capsulatus</i> rXDH E232V	ND ^e	ND ^e	N/M ^b	7.5	hypoxanthine	l	[106]
<i>R. capsulatus</i> rXDH R310M	63.7 ± 10.1	9.0 ± 0.3	N/M ^b	7.5	hypoxanthine	l	[106]
<i>R. capsulatus</i> rXDH E232V/R310M	ND ^e	ND ^e	N/M ^b	7.5	hypoxanthine	l	[106]
<i>R. capsulatus</i> rXDH	31.4 ± 8.3 ^w	N/M ^b	N/M ^b	8.0	Xanthine	h	[222]
<i>R. capsulatus</i> rXDH Q102G	54.5 ± 6.7 ^w	N/M ^b	N/M ^b	8.0	Xanthine	h	[222]
<i>R. capsulatus</i> rXDH Q102A	38.8 ± 3.8 ^w	N/M ^b	N/M ^b	8.0	Xanthine	h	[222]
<i>R. capsulatus</i> rXDH Q197A	38.2 ± 8.4 ^w	N/M ^b	N/M ^b	8.0	Xanthine	h	[222]
<i>R. capsulatus</i> rXDH Q197E	28.4 ± 4.9 ^w	N/M ^b	N/M ^b	8.0	Xanthine	h	[222]
<i>R. capsulatus</i> rXDH	N/M ^b	N/M ^b	16.23	7.5	Xanthine	i	[117]
<i>R. capsulatus</i> rXDH	15	540	N/M ^b	8.0	Xanthine	j	[118]
<i>R. capsulatus</i> rXDH	20	1500	N/M ^b	6.7	Xanthine	j	[118]
<i>R. capsulatus</i> rXDH	23	960	N/M ^b	6.1	Xanthine	j	[118]
<i>R. capsulatus</i> rXDH	54	780	N/M ^b	8.7	Xanthine	j	[118]
<i>R. capsulatus</i> rXDH	62	180	N/M ^b	10.0	Xanthine	j	[118]
<i>R. capsulatus</i> rXDH	64.5 ± 0.9	6480 ± 90	N/M ^b	7.8	Xanthine	i	[119]
<i>R. capsulatus</i> rXDH E232A	163 ± 35	264 ± 32.4	N/M ^b	7.8	Xanthine	i	[119]
<i>R. capsulatus</i> rXDH E730A	ND ^e	ND ^e	N/M ^b	7.8	Xanthine	i	[119]
<i>R. capsulatus</i> rXDH E730D	ND ^e	ND ^e	N/M ^b	7.8	Xanthine	i	[119]
<i>R. capsulatus</i> rXDH E730Q	ND ^e	ND ^e	N/M ^b	7.8	Xanthine	i	[119]
<i>R. capsulatus</i> rXDH E730R	ND ^e	ND ^e	N/M ^b	7.8	Xanthine	i	[119]
<i>R. capsulatus</i> rXDH	N/M ^b	N/M ^b	22.58	8.0	hypoxanthine	i	[47]
<i>R. capsulatus</i> rXDH	58	N/M ^b	115 ^{c, z}	5-10 ^x	xanthine	i	[223]

a) r- recombinant; b) N/M- Not mentioned; c) specific activity is reported as V_{max}; d) value was calculated from data reported; e) ND- not detected; f) NA- negligible activity; g) IA- inactive; h) Monitor Reduction of FAD at 465nm; i) electron acceptor NAD⁺ at 340 nm; j) Protein film voltammetry (PFV); k) Monitored electron acceptor ferredoxin at 420; l) Monitored the reduction of electron acceptor ferricyanide at 420nm; m) Monitored oxidation of xanthine to uric acid by measuring change in absorbance at 295 nm; n) Monitored reduction of electron acceptor benzyl viologen; o) Monitor quinoline-dependent reduction of the artificial electron acceptor, iodonitrotetrazolium chloride; p) monitored reduction of electron acceptor p-iodonitrotetrazolium violet; q) Monitored product formation by HPLC; r) Monitored the formation of product at 295 nm s) monitored cytochrome c reduction at 550nm; t) monitored oxidation of vanillin at 340nm; u) monitored reduction of electron acceptor 2,6-Dichlorophenol-indophenol at 600nm; v) monitored the consumption of substrate (2,5-dihydroxypyridine) at 320nm; w) reported as K_D (unitless); x) apparent K_M and V_{max} determined based on pH dependence in the range of pH 5-10; y) in U/mg; z) in s⁻¹; aa) in μM/(min*mg).

Table 1.14: Kinetic parameters for prokaryotic SO family of enzymes.

Enzyme ^a	K _m (μM)	K _{cat} (min ⁻¹)	Specific Activity (μmol subs/min/mg)	pH	Substrate	Assay Description	Ref.
<i>D. radiodurans</i> rSO	94.5	N/M ^b	N/M ^b	8.0	Sulfite	h	[224]
<i>S. meliloti</i> rSorT (sulfite dehydrogenase)	13.4 ± 0.5	20280 ± 180	N/M ^b	8.0	sulfite	h	[122]
<i>S. meliloti</i> rSorT (sulfite dehydrogenase)	23.4 ± 1.2	N/M ^b	N/M ^b	7.0	sulfite	h	[122]
<i>S. meliloti</i> rSorT (sulfite dehydrogenase)	33.3 ± 6.5	N/M ^b	N/M ^b	6.0	sulfite	h	[122]
<i>S. meliloti</i> SorT (sulfite dehydrogenase)	15.5 ± 1.1	20580 ± 660	N/M ^b	8.0	sulfite	h	[122, 263]
<i>Starkeya novella</i> r-sulphite:cytochrome c oxidoreductase (SorAB)	32 ± 3.8	652500 ± 17280	N/M ^b	8.0	sulfite	i	[171]
<i>Starkeya novella</i> r-sulphite:cytochrome c oxidoreductase (SorAB)	2.3 ± 0.8	N/M ^b	N/M ^b	8.0	cytochrome c	i	[171]
<i>Thiobacillus novellus</i> SorAB	27	706140 ± 38880	N/M ^b	8.0	sulfite	i	[171, 264]
<i>Thiobacillus novellus</i> SorAB	4	706140 ± 38880	N/M ^b	8.0	cytochrome c	i	[171, 264]
<i>T. thermophilus</i> AT62 rSO	10.67 ± 0.51	3199080 ± 49920	11.7 ± 1.0 ^{c, l}	8.0	Sulfite	h	[121]
<i>T. thermophilus</i> AT62 rSO	6.33 ± 0.68	3199080 ± 49920	11.7 ± 1.0 ^{c, l}	8.0	Ferricyanide	h	[121]
<i>E. coli</i> rYedY	12000	289.8	N/M ^b	7.0	DMSO	j	[70]
<i>E. coli</i> rYedY	119000	1536	N/M ^b	7.0	L-methionine sulfoxide	j	[70]
<i>E. coli</i> rYedY	27900	1086	N/M ^b	7.0	tetramethylene sulfoxide	j	[70]
<i>E. coli</i> rYedY	22000	1140	N/M ^b	7.0	TMAO	j	[70]
<i>E. coli</i> rYedY	46400	888	N/M ^b	7.0	TMAO (in 1M Urea)	j	[70]
<i>R. sphaeroides</i> rYedY (C-terminal His-tag)	261000 ± 57000	N/M ^b	30 ± 2 ^c	6.0	DMSO	k	[101]
<i>R. sphaeroides</i> rYedY (N-Termial His-tag without TAT leader sequence)	43000 ± 6000	N/M ^b	49 ± 1 ^c	6.0	DMSO	k	[101]
<i>R. sphaeroides</i> rYedY (N-Termial His-tag with TAT leader sequence)	71000 ± 9000	N/M ^b	49 ± 2 ^c	6.0	DMSO	k	[101]
<i>R. sphaeroides</i> rYedY (with TAT leader sequence; no His-tag)	61000 ± 7000	N/M ^b	56 ± 2 ^c	6.0	DMSO	k	[101]

a) r- recombinant; b) N/M- Not mentioned; c) specific activity is reported as V_{max}; d) value was calculated from data reported; e) ND- note detected; f) NA- negligible activity; g) IA- inactive; h) Monitored reduction of electron acceptor ferricyanide at 420 nm; i) Monitored reduction of cytochrome c at 417-8 nm or 550nm; j) Monitored oxidation of the electron donor benzyl viologen at 570nm; k) Monitored oxidation of the electron donor benzyl viologen at 600nm; l) in μM/min.

Table 1.15: Kinetic parameters for DMSOR family of enzymes.

Enzyme ^a	K _m (μM)	K _{cat} (min ⁻¹)	Specific Activity (μmol subs/min/mg)	pH	Substrate	Assay Description	Ref.
<i>Ralstonia</i> sp. S22 rAio	7 ^{ag}	N/M ^b	140 ^{ag}	8.0	As(III)	u	[99]
<i>Ralstonia</i> sp. S22 rAio	50 ^{ag}	N/M ^b	N/M ^b	8.0	c ₅₅₅ from <i>Aquifex aeolicus</i>	u	[99]
<i>Ralstonia</i> sp. S22 rAio	10 ^{af, ag}	N/M ^b	N/M ^b	6.0	sulfite	u	[99]
<i>Ralstonia</i> sp. S22 rAio without TAT leader sequence	7 ^{ag}	N/M ^b	140 ^{ag}	8.0	As(III)	u	[99]
<i>Ralstonia</i> sp. S22 rAio without TAT leader sequence	70 ^{ag}	N/M ^b	N/M ^b	8.0	c ₅₅₅ from <i>Aquifex aeolicus</i>	u	[99]
<i>Ralstonia</i> sp. S22 rAio without TAT leader sequence	10 ^{af, ag}	N/M ^b	N/M ^b	6.0	sulfite	u	[99]
<i>Ralstonia</i> sp. S22 Aio	6 ^{ag}	N/M ^b	140 ^{ag}	8.0	As(III)	u	[99]
<i>Ralstonia</i> sp. S22 Aio	50 ^{ag}	N/M ^b	N/M ^b	8.0	c ₅₅₅ from <i>Aquifex aeolicus</i>	u	[99]
<i>Ralstonia</i> sp. S22 Aio	10 ^{af, ag}	N/M ^b	N/M ^b	6.0	sulfite	u	[99]
<i>Rhizobium</i> sp. NT-26 rAio	68±4.8	216 ± 15	1.73±0.01 ^c	5.5	arsenite	l	[62]
<i>Rhizobium</i> sp. NT-26 Aio	61	258	2.4 ^c	5.5	arsenite	N/M ^b	[62, 265]
<i>Rhizobium</i> sp. NT-26 rAio	N/M ^b	N/M ^b	1.85	5.5	arsenite	l	[62]
<i>Rhizobium</i> sp. NT-26 rAio S126T	N/M ^b	N/M ^b	0.6	5.5	arsenite	l	[62]
<i>Rhizobium</i> sp. NT-26 rAio F128Y	N/M ^b	N/M ^b	1.5	5.5	arsenite	l	[62]
<i>Rhizobium</i> sp. NT-26 rAio F108C/G123C	N/M ^b	N/M ^b	1.5	5.5	arsenite	l	[62]
<i>Rhizobium</i> sp. NT-26 rAio	9.3 ± 1.5	N/M ^b	120.4 ± 6.0 ^c	8.0	arsenite	u	[82]
<i>Rhizobium</i> sp. NT-26 rAio	0.163 ± 0.008	N/M ^b	0.0184 ± 0.0012 ^c	8.0	antimonite	u	[82]
<i>Shewanella</i> sp. ANA-3 rArr	5	N/M ^b	11,111 ^c	7.0	arsenate	h	[98]
<i>Chrysiogenes arsenatis</i> Arr	300	N/M ^b	7013 ^c	6.5	arsenate	m	[98, 266]
<i>Bacillus selenitireducens</i> Arr	34	N/M ^b	2.5 ^c	8.5	arsenate	h	[98, 267]
<i>Shewanella</i> sp. ANA-3 rArr	44.6 ± 1.6	588600 ± 13200	N/M ^b	7.5	arsenate	h	[225]
<i>Shewanella</i> sp. ANA-3 rArr	325 ^{af}	N/M ^b	N/M ^b	7.5	phosphate	h	[225]
<i>R. sphaeroides</i> rBSOR	15	N/M ^b	11.3 ^c	8.0	BSO	h	[29]
<i>R. sphaeroides</i> rBSOR	20	N/M ^b	11.3 ^c	8.0	Nicotinamide <i>N</i> - oxide	h	[29]
<i>R. sphaeroides</i> rBSOR	807	N/M ^b	11.3 ^c	8.0	<i>L</i> -Methionine sulfoxide	h	[29]
<i>R. sphaeroides</i> rBSOR	850	N/M ^b	11.3 ^c	8.0	<i>d</i> -Methionine sulfoxide	h	[29]
<i>R. sphaeroides</i> rBSOR	11050	N/M ^b	11.3 ^c	8.0	Trimethylamine <i>N</i> - oxide	h	[29]
<i>R. sphaeroides</i> rBSOR	14440	N/M ^b	11.3 ^c	8.0	Dimethyl sulfoxide	h	[29]
<i>R. sphaeroides</i> rBSOR	29	N/M ^b	11.3 ^c	8.0	MV ⁺	i	[29]
<i>R. sphaeroides</i> rBSOR	35	N/M ^b	11.3 ^c	8.0	BV ⁺	i	[29]
<i>R. sphaeroides</i> rBSOR	524	N/M ^b	187.5 ^c	8.0	BSO	j	[29]
<i>R. sphaeroides</i> rBSOR	414	N/M ^b	123.8 ^c	8.0	Nicotinamide <i>N</i> - oxide	j	[29]

Table 1.15 Continued

Enzyme ^a	K _m (μM)	K _{cat} (min ⁻¹)	Specific Activity (μmol subs/min/mg)	pH	Substrate	Assay Description	Ref.
<i>R. sphaeroides</i> rBSOR	10000	N/M ^b	38.8 ^c	8.0	<i>L</i> -Methionine sulfoxide	j	[29]
<i>R. sphaeroides</i> rBSOR	10070	N/M ^b	38.1 ^c	8.0	<i>d</i> -Methionine sulfoxide	j	[29]
<i>R. sphaeroides</i> rBSOR	482000	N/M ^b	192.5 ^c	8.0	Trimethylamine <i>N</i> -oxide	j	[29]
<i>R. sphaeroides</i> rBSOR	207000	N/M ^b	60 ^c	8.0	Dimethyl sulfoxide	j	[29]
<i>R. sphaeroides</i> rBSOR	662	N/M ^b	21.3 ^c	8.0	Ferricyanide	j	[29]
<i>R. sphaeroides</i> rBSOR	269	N/M ^b	375 ^c	8.0	NADPH	i	[29]
<i>R. sphaeroides</i> rBSOR	394	N/M ^b	35 ^c	8.0	NADH	i	[29]
<i>R. sphaeroides</i> rBSOR	N/M ^b	N/M ^b	N/M ^b	9.6	biotin	k	[73]
<i>E. coli</i> rDMSOR (isolated from DMSOR knockout)	N/M ^b	N/M ^b	8.5	7.0	DMSO	m	[229]
<i>E. coli</i> rDMSOR C102W (isolated from DMSOR knockout)	N/M ^b	N/M ^b	8.1	7.0	DMSO	m	[229]
<i>E. coli</i> rDMSOR C102S (isolated from DMSOR knockout)	N/M ^b	N/M ^b	9.7	7.0	DMSO	m	[229]
<i>E. coli</i> rDMSOR C102W	N/M ^b	N/M ^b	17.8	7.0	DMSO	m	[229]
<i>E. coli</i> rDMSOR C102S	N/M ^b	N/M ^b	15.4	7.0	DMSO	m	[229]
<i>E. coli</i> rDMSOR C102F	N/M ^b	N/M ^b	17.8	7.0	DMSO	m	[229]
<i>E. coli</i> rDMSOR C102Y	N/M ^b	N/M ^b	10.8	7.0	DMSO	m	[229]
<i>E. coli</i> rDMSOR	N/M ^b	N/M ^b	10.4	7.0	DMSO	m	[229]
<i>E. coli</i> rDMSOR (isolated from DMSOR knockout)	N/M ^b	N/M ^b	69.1	7.0	TMAO	m	[229]
<i>E. coli</i> rDMSOR C102W (isolated from DMSOR knockout)	N/M ^b	N/M ^b	60.5	7.0	TMAO	m	[229]
<i>E. coli</i> rDMSOR C102S (isolated from DMSOR knockout)	N/M ^b	N/M ^b	85.2	7.0	TMAO	m	[229]
<i>E. coli</i> rDMSOR C102W	N/M ^b	N/M ^b	172.8	7.0	TMAO	m	[229]
<i>E. coli</i> rDMSOR C102S	N/M ^b	N/M ^b	147.9	7.0	TMAO	m	[229]
<i>E. coli</i> rDMSOR C102F	N/M ^b	N/M ^b	162.1	7.0	TMAO	m	[229]
<i>E. coli</i> rDMSOR C102Y	N/M ^b	N/M ^b	117.4	7.0	TMAO	m	[229]
<i>E. coli</i> rDMSOR	N/M ^b	N/M ^b	92.9 ^{ac}	7.0	TMAO	m	[229]
<i>E. coli</i> rDMSOR	N/M ^b	N/M ^b	736	7.0	TMAO	m	[75]
<i>R. capsulatus</i> rDMSOR	9.7 ± 1.2	2574 ± 36	N/M ^b	8.0	DMSO	h	[166]
<i>R. capsulatus</i> rDMSOR	193.8 ± 9.8	8070 ± 294	N/M ^b	8.0	TMAO	h	[166]
<i>R. capsulatus</i> rDMSOR	ad	168 ± 12	N/M ^b	8.0	DMS	l	[166]
<i>R. capsulatus</i> rDMSOR Y114F	185.5 ± 10.3	4884 ± 144	N/M ^b	8.0	DMSO	h	[166]
<i>R. capsulatus</i> rDMSOR Y114F	811.8 ± 24.6	22722 ± 1650	N/M ^b	8.0	TMAO	h	[166]
<i>R. capsulatus</i> rDMSOR Y114F	ad	42 ± 6	N/M ^b	8.0	DMS	l	[166]
<i>R. sphaeroides</i> rDMSOR	7	N/M ^b	42.4	7.5	DMSO	h	[54]
<i>R. sphaeroides</i> rDMSOR	N/M ^b	N/M ^b	211.8	7.5	TMAO	h	[54]
<i>R. sphaeroides</i> rDMSOR	N/M ^b	N/M ^b	50.6	7.5	methionine sulfoxide	h	[54]
<i>R. sphaeroides</i> rDMSOR	N/M ^b	N/M ^b	64.7	7.5	Chlorate	h	[54]
<i>R. sphaeroides</i> rDMSOR	N/M ^b	N/M ^b	56.5	7.5	BSO	h	[54]
<i>R. sphaeroides</i> rDMSOR	20	N/M ^b	83.5	7.5	adenosine <i>N</i> -oxide	h	[54]
<i>R. sphaeroides</i> rDMSOR S147C	1000	N/M ^b	16.5	7.5	DMSO	h	[54]
<i>R. sphaeroides</i> rDMSOR S147C	N/M ^b	N/M ^b	43.5	7.5	TMAO	h	[54]

Table 1.15 Continued

<u>Enzyme^a</u>	<u>K_m (μM)</u>	<u>K_{cat} (min⁻¹)</u>	<u>Specific Activity (μmol subs/min/mg)</u>	<u>pH</u>	<u>Substrate</u>	<u>Assay Description</u>	<u>Ref.</u>
<i>R. sphaeroides</i> rDMSOR S147C	N/M ^b	N/M ^b	0.046	7.5	methionine sulfoxide	h	[54]
<i>R. sphaeroides</i> rDMSOR S147C	N/M ^b	N/M ^b	2.24	7.5	Chlorate	h	[54]
<i>R. sphaeroides</i> rDMSOR S147C	N/M ^b	N/M ^b	0.306	7.5	BSO	h	[54]
<i>R. sphaeroides</i> rDMSOR S147C	800	N/M ^b	423.5	7.5	adenosine <i>N</i> ¹ - oxide	h	[54]
<i>R. sphaeroides</i> rDMSOR	68000 ± 5000	138000 ± 3000	N/M ^b	7.5	TMAO	h	[97]
<i>R. sphaeroides</i> rDMSOR Y114F	88000 ± 5000	258000 ± 4800	N/M ^b	7.5	TMAO	h	[97]
<i>R. sphaeroides</i> rDMSOR Y114A	2300 ± 400	114000 ± 6000	N/M ^b	7.5	TMAO	h	[97]
<i>E. coli</i> rTMAOR	210 ± 100	150000 ± 12000	1158 ^{aa}	7.5	TMAO	h	[97]
<i>E. coli</i> rTMAOR + Y	10000 ± 3000	150000 ± 18000	N/M ^b	7.5	TMAO	h	[97]
<i>R. sphaeroides</i> rDMSOR	7 ± 1	3000 ± 120	N/M ^b	7.5	DMSO	h	[97]
<i>R. sphaeroides</i> rDMSOR Y114F	180 ± 60	10800 ± 1200	N/M ^b	7.5	DMSO	h	[97]
<i>R. sphaeroides</i> rDMSOR Y114A	400 ± 20	4020 ± 120	N/M ^b	7.5	DMSO	h	[97]
<i>E. coli</i> rTMAOR	6000 ± 300	780 ± 12	N/M ^b	7.5	DMSO	h	[97]
<i>E. coli</i> rTMAOR + Y	6300 ± 500	144 ± 36	N/M ^b	7.5	DMSO	h	[97]
<i>R. sphaeroides</i> rDMSOR	330 ± 30	3480 ± 120	N/M ^b	7.5	methionine sulfoxide	h	[97]
<i>R. sphaeroides</i> rDMSOR Y114F	19000 ± 3000	10800 ± 1200	N/M ^b	7.5	methionine sulfoxide	h	[97]
<i>R. sphaeroides</i> rDMSOR Y114A	16000 ± 1000	5520 ± 300	N/M ^b	7.5	methionine sulfoxide	h	[97]
<i>E. coli</i> rTMAOR	7100 ± 700	2400 ± 120	N/M ^b	7.5	methionine sulfoxide	h	[97]
<i>E. coli</i> rTMAOR + Y	12000 ± 2000	1200 ± 240	N/M ^b	7.5	methionine sulfoxide	h	[97]
<i>R. sphaeroides</i> rDMSOR	20 ± 4	6600 ± 420	N/M ^b	7.5	adenosine- ¹ N-oxide	h	[97]
<i>R. sphaeroides</i> rDMSOR Y114F	520 ± 50	132000 ± 4200	N/M ^b	7.5	adenosine- ¹ N-oxide	h	[97]
<i>R. sphaeroides</i> rDMSOR Y114A	80 ± 10	72000 ± 6000	N/M ^b	7.5	¹ N-oxide	h	[97]
<i>E. coli</i> rTMAOR	260 ± 20	84000 ± 120	N/M ^b	7.5	adenosine- ¹ N-oxide	h	[97]
<i>E. coli</i> rTMAOR + Y	280 ± 80	49800 ± 4800	N/M ^b	7.5	¹ N-oxide	h	[97]
<i>H. influenzae</i> rTMAOR	6700 ± 2000	26082 ± 3126	N/M ^b	6.8	TMAO	m	[79]
<i>H. influenzae</i> rTMAOR	140 ± 50	5124 ± 546	N/M ^b	6.8	DMSO	m	[79]
<i>H. influenzae</i> rTMAOR	410 ± 80	5502 ± 264	N/M ^b	6.8	methionine sulfoxide	m	[79]
<i>H. influenzae</i> rTMAOR	1520 ± 280	10956 ± 654	N/M ^b	6.8	BSO	m	[79]
<i>E. coli</i> FDH (-O ₂)	N/M ^b	N/M ^b	0.09	N/M ^b	formate	l	[60]
<i>E. coli</i> fdhf mutant (-O ₂)	N/M ^b	N/M ^b	0.09	N/M ^b	formate	l	[60]

Table 1.15 Continued

Enzyme ^a	K _m (μM)	K _{cat} (min ⁻¹)	Specific Activity (μmol subs/min/mg)	pH	Substrate	Assay Description	Ref.
<i>E. coli</i> FDH <i>fdnG</i> mutant (-O ₂)	N/M ^b	N/M ^b	<0.01	N/M ^b	formate	l	[60]
<i>E. coli</i> <i>fdhf</i> & <i>fdnG</i> double mutant (-O ₂)	N/M ^b	N/M ^b	<0.01	N/M ^b	formate	l	[60]
<i>E. coli</i> FDH (-O ₂ , +NO ₃ ⁻)	N/M ^b	N/M ^b	0.27	N/M ^b	formate	l	[60]
<i>E. coli</i> <i>fdhf</i> mutant (-O ₂ , +NO ₃ ⁻)	N/M ^b	N/M ^b	0.48	N/M ^b	formate	l	[60]
<i>E. coli</i> FDH <i>fdnG</i> mutant (-O ₂ , +NO ₃ ⁻)	N/M ^b	N/M ^b	<0.01	N/M ^b	formate	l	[60]
<i>E. coli</i> <i>fdhf</i> & <i>fdnG</i> double mutant (-O ₂ , +NO ₃ ⁻)	N/M ^b	N/M ^b	<0.01	N/M ^b	formate	l	[60]
<i>E. coli</i> rFDH	800	N/M ^b	N/M ^b	7.0	formate	s	[234]
<i>E. coli</i> rFDH	2500	N/M ^b	N/M ^b	7.0	CO ₂	s	[234]
<i>E. coli</i> FDH	26000	N/M ^b	N/M ^b	N/M ^b	formate	N/M ^b	[234]
<i>E. coli</i> rFDH	N/M ^b	N/M ^b	0.2	7.4	formate	m	[232]
<i>E. coli</i> rFDH	N/M ^b	240	N/M ^b	7.5	formate	h	[233]
<i>E. coli</i> rFDH	N/M ^b	9600	N/M ^b	7.5	formate	m	[233]
<i>E. coli</i> rFDH	N/M ^b	<60	N/M ^b	7.5	CO ₂	h	[233]
<i>E. coli</i> rFDH	N/M ^b	180 ^{ah}	N/M ^b	7.5	formate	s	[233]
<i>E. coli</i> rFDH	N/M ^b	80 ^{ah}	N/M ^b	7.5	CO ₂	s	[233]
<i>Syntrophobacter fumaroxidans</i> FDH	N/M ^b	90000	N/M ^b	7.5-8	formate	h	[233, 268]
<i>Syntrophobacter fumaroxidans</i> FDH	N/M ^b	66000	N/M ^b	8.0	formate	m	[233, 269]
<i>Syntrophobacter fumaroxidans</i> FDH	N/M ^b	30000	N/M ^b	7.5-8	CO ₂	h	[233, 268]
<i>Syntrophobacter fumaroxidans</i> FDH	N/M ^b	160 ^{ah}	N/M ^b	6.5	formate	s	[233, 268]
<i>Syntrophobacter fumaroxidans</i> FDH	N/M ^b	5 ^{ah}	N/M ^b	6.5	CO ₂	s	[233, 268]
<i>R. capsulatus</i> rFDH	281 ± 10	2189 ± 38	N/M ^b	9.0	formate	v	[89]
<i>R. capsulatus</i> rFDH	278 ± 29	2380 ± 64	N/M ^b	9.0	formate	w	[88]
<i>R. capsulatus</i> rFDH	277 ± 43	1918 ± 82	N/M ^b	9.0	formate	l	[88]
<i>R. capsulatus</i> rFDH	ND ^e	89 ± 1.0	N/M ^b	6.8	NADH	x	[88]
<i>R. capsulatus</i> rFDH	173 ± 19	N/M ^b	N/M ^b	9.0	NAD+	y	[88]
<i>R. capsulatus</i> rFDH	349 ± 41	9781 ± 310	N/M ^b	9.0	NAD+	z	[88]
<i>R. capsulatus</i> rFDH	ND ^e	3566 ± 133	N/M ^b	8.0	NADH	aa	[88]
<i>R. capsulatus</i> rFdsGB	1050 ± 148	1916 ± 110	N/M ^b	9.0	NAD+	z	[88]
<i>R. capsulatus</i> rFdsGB	129 ± 15	413 ± 10	N/M ^b	8.0	NADH	aa	[88]
<i>R. capsulatus</i> rFDH	190	2124	N/M ^b	9.0	formate	v	[91]
<i>R. sphaeroides</i> rNapAB	170	N/M ^b	25 ^c U/mg ^{ac}	7.0	nitrate	h	[168]
<i>R. sphaeroides</i> rNapA	45	N/M ^b	5.9 ^c U/mg ^{ac}	7.0	nitrate	h	[168]
<i>C. necator</i> rNap	N/M ^b	N/M ^b	0.73	6.5	nitrate	m	[170]
<i>C. necator</i> rNap K85R	N/M ^b	N/M ^b	0.17	6.5	nitrate	m	[170]
<i>C. necator</i> rNap K85M	N/M ^b	N/M ^b	1A ^g	6.5	nitrate	m	[170]
<i>C. necator</i> rNap	120	N/M ^b	29	5.5	nitrate	m	[93]
<i>D. desulfuricans</i> Nap	32-116	N/M ^b	18.6	8-9	nitrate	t	[168, 270]
<i>R. sphaeroides</i> rNap	120	N/M ^b	38.9 ^c	7.0	nitrate	m	[167]
<i>R. sphaeroides</i> rNap	600	N/M ^b	0.97 ^c	7.0	tellurite	m	[167]
<i>R. sphaeroides</i> rNap	270	N/M ^b	0.27 ^c	7.0	selenate	m	[167]

Table 1.15 Continued

Enzyme ^a	K _m (μM)	K _{cat} (min ⁻¹)	Specific Activity (μmol subs/min/mg)	pH	Substrate	Assay Description	Ref.
<i>Synechococcus</i> sp. rNarB	50	4800	N/M ^b	8.0	nitrate	h	[84]
<i>Synechococcus</i> sp. rNarB	2500	300	N/M ^b	8.0	chlorate	h	[84]
<i>Synechococcus</i> sp. rNarB	2500	60	N/M ^b	8.0	selenate	h	[84]
<i>Synechococcus</i> sp. rNarB	13000 ^{af}	N/M ^b	N/M ^b	8.0	Nitrate, azide as inhibitor	h	[84]
<i>Synechococcus</i> sp. rNarB	80	N/M ^b	N/M ^b	8.0	Nitrate	s	[84]
<i>Synechococcus</i> sp. rNarB	350	N/M ^b	N/M ^b	8.0	Nitrate	s	[84]
<i>E. coli</i> rNarGHI	N/M ^b	N/M ^b	48 ± 14	8.0	nitrate	m	[238]
<i>E. coli</i> rNarGHI S719A	N/M ^b	N/M ^b	54 ± 11	8.0	nitrate	m	[238]
<i>E. coli</i> rNarGHI H1163A	N/M ^b	N/M ^b	23 ± 4	8.0	nitrate	m	[238]
<i>E. coli</i> rNarGHI H1184A	N/M ^b	N/M ^b	36 ± 1	8.0	nitrate	m	[238]
<i>E. coli</i> rNarGHI H1092A	N/M ^b	N/M ^b	1 ± 0	8.0	nitrate	m	[238]
<i>E. coli</i> rNarGHI H1092R	N/M ^b	N/M ^b	8.6 ± 1	8.0	nitrate	m	[238]
<i>E. coli</i> rNarGHI H1098A	N/M ^b	N/M ^b	16 ± 2	8.0	nitrate	m	[238]
<i>E. coli</i> NR-A (membrane fraction)	N/M ^b	N/M ^b	100	6.8	nitrate	m	[243]
<i>E. coli</i> NR-A (soluble fraction)	N/M ^b	N/M ^b	74	6.8	nitrate	m	[243]
<i>E. coli</i> rNR-A (membrane fraction)	N/M ^b	N/M ^b	100	6.8	nitrate	m	[243]
<i>E. coli</i> rNR-A (soluble fraction)	N/M ^b	N/M ^b	65	6.8	nitrate	m	[243]
<i>E. coli</i> rNR-A (membrane fraction) C26A	N/M ^b	N/M ^b	90	6.8	nitrate	m	[243]
<i>E. coli</i> rNR-A (soluble fraction) C26A	N/M ^b	N/M ^b	84	6.8	nitrate	m	[243]
<i>E. coli</i> rNR-A (membrane fraction) C196A	N/M ^b	N/M ^b	<0.3	6.8	nitrate	m	[243]
<i>E. coli</i> rNR-A (soluble fraction) C196A	N/M ^b	N/M ^b	<0.3	6.8	nitrate	m	[243]
<i>E. coli</i> rNR-A (membrane fraction) C227A	N/M ^b	N/M ^b	<0.3	6.8	nitrate	m	[243]
<i>E. coli</i> rNR-A (soluble fraction) C227A	N/M ^b	N/M ^b	<0.3	6.8	nitrate	m	[243]
<i>E. coli</i> rNR-A (membrane fraction) C263A	N/M ^b	N/M ^b	6	6.8	nitrate	m	[243]
<i>E. coli</i> rNR-A (soluble fraction) C263A	N/M ^b	N/M ^b	6	6.8	nitrate	m	[243]
<i>E. coli</i> NR-A	N/M ^b	N/M ^b	5.5	6.8	nitrate	n	[243]
<i>E. coli</i> NR-A	N/M ^b	N/M ^b	14	6.8	nitrate	o	[243]
<i>E. coli</i> NR-A	N/M ^b	N/M ^b	59	6.8	nitrate	p	[243]
<i>E. coli</i> rNR-A	N/M ^b	N/M ^b	5.4	6.8	nitrate	n	[243]
<i>E. coli</i> rNR-A	N/M ^b	N/M ^b	14	6.8	nitrate	o	[243]
<i>E. coli</i> rNR-A	N/M ^b	N/M ^b	55	6.8	nitrate	p	[243]
<i>E. coli</i> rNR-A, C26A	N/M ^b	N/M ^b	1.2	6.8	nitrate	n	[243]
<i>E. coli</i> rNR-A, C26A	N/M ^b	N/M ^b	3.7	6.8	nitrate	o	[243]
<i>E. coli</i> rNR-A, C26A	N/M ^b	N/M ^b	25	6.8	nitrate	p	[243]
<i>E. coli</i> rNR-A, C196A	N/M ^b	N/M ^b	0	6.8	nitrate	n	[243]
<i>E. coli</i> rNR-A, C196A	N/M ^b	N/M ^b	0	6.8	nitrate	o	[243]
<i>E. coli</i> rNR-A, C196A	N/M ^b	N/M ^b	0	6.8	nitrate	p	[243]
<i>E. coli</i> rNR-A, C227A	N/M ^b	N/M ^b	0	6.8	nitrate	n	[243]
<i>E. coli</i> rNR-A, C227A	N/M ^b	N/M ^b	0	6.8	nitrate	o	[243]
<i>E. coli</i> rNR-A, C227A	N/M ^b	N/M ^b	0	6.8	nitrate	p	[243]
<i>E. coli</i> rNR-A, C263A	N/M ^b	N/M ^b	3.9	6.8	nitrate	n	[243]
<i>E. coli</i> rNR-A, C263A	N/M ^b	N/M ^b	0	6.8	nitrate	o	[243]
<i>E. coli</i> rNR-A, C263A	N/M ^b	N/M ^b	18	6.8	nitrate	p	[243]
<i>E. coli</i> rNR (narGH +J)	243	15.6 ± 0.36	49	6.5	nitrate	m	[242]
<i>E. coli</i> rNR (narGH +J)	571	7.08 ± 2.34	N/M ^b	6.5	nitrate	m	[242]

Table 1.15 Continued

Enzyme ^a	K _m (μM)	K _{cat} (min ⁻¹)	Specific Activity (μmol subs/min/mg)	pH	Substrate	Assay Description	Ref.
<i>E. coli</i> rNR (narGH +J) C16A	80.3	2.604 ± 0.204	8.5	6.5	nitrate	m	[242]
<i>E. coli</i> rNR (narGH +J) C19A	140	2.01 ± 0.204	6.9	6.5	nitrate	m	[242]
<i>E. coli</i> rNR (narGH +J) W220C	179	8.34 ± 0.6	27	6.5	nitrate	m	[242]
<i>E. coli</i> rNR (narGH +J) W220F	345	17.34 ± 4.02	56	6.5	nitrate	m	[242]
<i>E. coli</i> rNR (narGH +J) C244A	N/M ^b	N/M ^b	<0.1	6.5	nitrate	m	[242]
<i>E. coli</i> NR	N/M ^b	N/M ^b	49	6.5	nitrate	m	[242]
<i>E. coli</i> NR knock out strain	N/M ^b	N/M ^b	<0.1	6.5	nitrate	m	[242]
<i>E. coli</i> NR <i>moa</i> mutant	N/M ^b	N/M ^b	<0.1	6.5	nitrate	m	[242]
<i>E. coli</i> NR <i>mob</i> mutant	N/M ^b	N/M ^b	<0.1	6.5	nitrate	m	[242]
<i>E. coli</i> rNR (narGHIJ)	N/M ^b	N/M ^b	7	8.3	nitrate	m	[248]
<i>E. coli</i> rNR (narZYWV)	N/M ^b	N/M ^b	0.43	8.3	nitrate	m	[248]
<i>E. coli</i> Nar membrane fraction	N/M ^b	N/M ^b	1.80	N/M ^b	nitrate	m	[248]
<i>E. coli</i> Nar soluble fraction	N/M ^b	N/M ^b	0.08	N/M ^b	nitrate	m	[247]
<i>E. coli</i> Nar knockout strain membrane fraction	N/M ^b	N/M ^b	<0.02	N/M ^b	nitrate	m	[247]
<i>E. coli</i> Nar knockout strain soluble fraction	N/M ^b	N/M ^b	<0.02	N/M ^b	nitrate	m	[247]
<i>E. coli</i> rNarGHJI membrane fraction	N/M ^b	N/M ^b	9.0	N/M ^b	nitrate	m	[247]
<i>E. coli</i> rNarGHJI soluble fraction	N/M ^b	N/M ^b	0.6	N/M ^b	nitrate	m	[247]
<i>E. coli</i> rNarGH membrane fraction	N/M ^b	N/M ^b	<0.02	N/M ^b	nitrate	m	[247]
<i>E. coli</i> rNarGH soluble fraction	N/M ^b	N/M ^b	<0.02	N/M ^b	nitrate	m	[247]
<i>E. coli</i> rNarGH +NarJI membrane fraction	N/M ^b	N/M ^b	7.0	N/M ^b	nitrate	m	[247]
<i>E. coli</i> rNarGH +NarJI soluble fraction	N/M ^b	N/M ^b	0.44	N/M ^b	nitrate	m	[247]
<i>E. coli</i> rNarGH +NarJ membrane fraction	N/M ^b	N/M ^b	2.0	N/M ^b	nitrate	m	[247]
<i>E. coli</i> rNarGH +NarJ soluble fraction	N/M ^b	N/M ^b	2.0	N/M ^b	nitrate	m	[247]
<i>E. coli</i> rNarGH +NarI membrane fraction	N/M ^b	N/M ^b	<0.02	N/M ^b	nitrate	m	[247]
<i>E. coli</i> rNarGH +NarI soluble fraction	N/M ^b	N/M ^b	<0.02	N/M ^b	nitrate	m	[247]
<i>E. coli</i> rNarGH + NarWV membrane fraction	N/M ^b	N/M ^b	4.6	N/M ^b	nitrate	m	[247]
<i>E. coli</i> rNarGH + NarWV soluble fraction	N/M ^b	N/M ^b	0.9	N/M ^b	nitrate	m	[247]
<i>E. coli</i> rNarGH + NarW membrane fraction	N/M ^b	N/M ^b	1.64	N/M ^b	nitrate	m	[247]
<i>E. coli</i> rNarGH + NarW soluble fraction	N/M ^b	N/M ^b	1.60	N/M ^b	nitrate	m	[247]
<i>E. coli</i> rNarGH + NarV membrane fraction	N/M ^b	N/M ^b	<0.02	N/M ^b	nitrate	m	[247]
<i>E. coli</i> rNarGH + NarV soluble fraction	N/M ^b	N/M ^b	<0.02	N/M ^b	nitrate	m	[247]
<i>E. coli</i> Nar	N/M ^b	N/M ^b	0.098	N/M ^b	nitrate	m	[247]
<i>E. coli</i> Nar knock out strain	N/M ^b	N/M ^b	0.001-0.003	N/M ^b	nitrate	p	[247]
<i>E. coli</i> rNarGH +NarJI	N/M ^b	N/M ^b	0.079	N/M ^b	nitrate	p	[247]
<i>E. coli</i> rNarGH +NarWV	N/M ^b	N/M ^b	0.037	N/M ^b	nitrate	p	[247]
<i>E. coli</i> rNarGH +NarJ	N/M ^b	N/M ^b	0.001-0.003	N/M ^b	nitrate	p	[247]
<i>E. coli</i> rNarGH +NarW	N/M ^b	N/M ^b	0.001-0.003	N/M ^b	nitrate	p	[247]
<i>E. coli</i> rNarGH +NarI	N/M ^b	N/M ^b	0.001-0.003	N/M ^b	nitrate	p	[247]
<i>E. coli</i> rNarGH +NarV	N/M ^b	N/M ^b	0.001-0.003	N/M ^b	nitrate	p	[247]
<i>E. coli</i> rNarGYWV	300	N/M ^b	58	6.8	nitrate	m	[87]
<i>E. coli</i> rNarGYWV	N/M ^b	N/M ^b	93	6.8	Chlorate	m	[87]
<i>E. coli</i> rNarGYWV	N/M ^b	N/M ^b	1.2	6.8	TMAO	m	[87]
<i>E. coli</i> rNarGYWV	N/M ^b	N/M ^b	28.2	6.8	nitrate	h	[87]
<i>E. coli</i> rNarGYWV	N/M ^b	N/M ^b	0.1	6.8	nitrate	p	[87]
<i>E. coli</i> rNarGYWV	N/M ^b	N/M ^b	0.2	6.8	nitrate	q	[87]
<i>E. coli</i> rNarGYWV	N/M ^b	N/M ^b	5.9	6.8	nitrate	r	[87]

Table 1.15 Continued

Enzyme ^a	K _m (μM)	K _{cat} (min ⁻¹)	Specific Activity (μmol subs/min/mg)	pH	Substrate	Assay Description	Ref.
<i>E. coli</i> NR membranes	N/M ^b	N/M ^b	1.85	6.8	nitrate	m	[87]
<i>E. coli</i> NR knock out strain membranes	N/M ^b	N/M ^b	<0.02	6.8	nitrate	m	[87]
<i>E. coli</i> rNarGHJI membranes	N/M ^b	N/M ^b	6.80	6.8	nitrate	m	[87]
<i>E. coli</i> rNarG + NarHJI membranes	N/M ^b	N/M ^b	4.60	6.8	nitrate	m	[87]
<i>E. coli</i> rNarZYWV membranes	N/M ^b	N/M ^b	1	6.8	nitrate	m	[87]
<i>E. coli</i> rNarZ + NarYWV membranes	N/M ^b	N/M ^b	0.80	6.8	nitrate	m	[87]
<i>E. coli</i> rNarGYWV membranes	N/M ^b	N/M ^b	3.50	6.8	nitrate	m	[87]
<i>E. coli</i> rNarG + NarYWV membranes	N/M ^b	N/M ^b	1.60	6.8	nitrate	m	[87]
<i>E. coli</i> rNarZ + NarHJI membranes	N/M ^b	N/M ^b	0.60	6.8	nitrate	m	[87]
<i>E. coli</i> NR membranes	N/M ^b	N/M ^b	85	6.8	nitrate	p	[87]
<i>E. coli</i> NR knock out strain membranes	N/M ^b	N/M ^b	<1	6.8	nitrate	p	[87]
<i>E. coli</i> rNarGHJI membranes	N/M ^b	N/M ^b	69	6.8	nitrate	p	[87]
<i>E. coli</i> rNarG + NarHJI membranes	N/M ^b	N/M ^b	68	6.8	nitrate	p	[87]
<i>E. coli</i> rNarZYWV membranes	N/M ^b	N/M ^b	72	6.8	nitrate	p	[87]
<i>E. coli</i> rNarZ + NarYWV membranes	N/M ^b	N/M ^b	28	6.8	nitrate	p	[87]
<i>E. coli</i> rNarGYWV membranes	N/M ^b	N/M ^b	14	6.8	nitrate	p	[87]
<i>E. coli</i> rNarG + NarYWV membranes	N/M ^b	N/M ^b	12	6.8	nitrate	p	[87]
<i>E. coli</i> rNarZ + NarHJI membranes	N/M ^b	N/M ^b	9	6.8	nitrate	p	[87]
<i>E. coli</i> rNR-Z	3900	N/M ^b	N/M ^b	6.8	nitrate	m	[249]
<i>E. coli</i> rNR-A	3100	N/M ^b	N/M ^b	6.8	nitrate	m	[249]
<i>E. coli</i> NR-Z strain MC4100 (-O ₂ , +KNO ₃)	N/M ^b	N/M ^b	0.746	6.8	nitrate	m	[249]
<i>E. coli</i> NR-Z strain MC4100 (-O ₂ , -KNO ₃)	N/M ^b	N/M ^b	0.029	6.8	nitrate	m	[249]
<i>E. coli</i> NR-Z strain MC4100 (-O ₂ , +TMAO)	N/M ^b	N/M ^b	0.020	6.8	nitrate	m	[249]
<i>E. coli</i> NR-Z strain MC4100 (+O ₂)	N/M ^b	N/M ^b	0.010	6.8	nitrate	m	[249]
<i>E. coli</i> NR knockout strain (-O ₂ , +KNO ₃)	N/M ^b	N/M ^b	0.011	6.8	nitrate	m	[249]
<i>E. coli</i> NR knockout strain (-O ₂ , -KNO ₃)	N/M ^b	N/M ^b	0.009	6.8	nitrate	m	[249]
<i>E. coli</i> NR knockout strain (-O ₂ , +TMAO)	N/M ^b	N/M ^b	0.007	6.8	nitrate	m	[249]
<i>E. coli</i> NR knockout strain (+O ₂)	N/M ^b	N/M ^b	0.015	6.8	nitrate	m	[249]
<i>E. coli</i> rNR-Z (-O ₂ , +KNO ₃)	N/M ^b	N/M ^b	0.221	6.8	nitrate	m	[249]
<i>E. coli</i> rNR-Z (-O ₂ , -KNO ₃)	N/M ^b	N/M ^b	0.197	6.8	nitrate	m	[249]
<i>E. coli</i> rNR-Z (-O ₂ , +TMAO)	N/M ^b	N/M ^b	0.242	6.8	nitrate	m	[249]
<i>E. coli</i> rNR-Z (+O ₂)	N/M ^b	N/M ^b	0.215	6.8	nitrate	m	[249]
<i>E. coli</i> NR-Z strain MC4100 (-O ₂ , +KNO ₃)	N/M ^b	N/M ^b	2.8	6.8	chlorate	m	[249]
<i>E. coli</i> NR-Z strain MC4100 (-O ₂ , -KNO ₃)	N/M ^b	N/M ^b	0.083	6.8	chlorate	m	[249]
<i>E. coli</i> NR-Z strain MC4100 (-O ₂ , +TMAO)	N/M ^b	N/M ^b	0.080	6.8	chlorate	m	[249]
<i>E. coli</i> NR-Z strain MC4100 (+O ₂)	N/M ^b	N/M ^b	IA ⁹	6.8	chlorate	m	[249]
<i>E. coli</i> NR knockout strain (-O ₂ , +KNO ₃)	N/M ^b	N/M ^b	0.035	6.8	chlorate	m	[249]
<i>E. coli</i> NR knockout strain (-O ₂ , -KNO ₃)	N/M ^b	N/M ^b	0.09	6.8	chlorate	m	[249]
<i>E. coli</i> NR knockout strain (-O ₂ , +TMAO)	N/M ^b	N/M ^b	0.04	6.8	chlorate	m	[249]
<i>E. coli</i> NR knockout strain (+O ₂)	N/M ^b	N/M ^b	IA ⁹	6.8	chlorate	m	[249]
<i>E. coli</i> rNR-Z (-O ₂ , +KNO ₃)	N/M ^b	N/M ^b	0.64	6.8	chlorate	m	[249]
<i>E. coli</i> rNR-Z (-O ₂ , -KNO ₃)	N/M ^b	N/M ^b	0.71	6.8	chlorate	m	[249]
<i>E. coli</i> rNR-Z (-O ₂ , +TMAO)	N/M ^b	N/M ^b	0.53	6.8	chlorate	m	[249]
<i>E. coli</i> rNR-Z (+O ₂)	N/M ^b	N/M ^b	IA ⁹	6.8	chlorate	m	[249]
<i>E. coli</i> NR-Z strain MC4100 (-O ₂ , +KNO ₃)	N/M ^b	N/M ^b	0.024	6.8	TMAO	m	[249]
<i>E. coli</i> NR-Z strain MC4100 (-O ₂ , -KNO ₃)	N/M ^b	N/M ^b	0.026	6.8	TMAO	m	[249]

Table 1.15 Continued

Enzyme ^a	K _m (μM)	K _{cat} (min ⁻¹)	Specific Activity (μmol subs/min/mg)	pH	Substrate	Assay Description	Ref.
<i>E. coli</i> nitrate reductase Z strain MC4100 (-O ₂ , +TMAO)	N/M ^b	N/M ^b	1.098	6.8	TMAO	m	[249]
<i>E. coli</i> NR-Z strain MC4100 (+O ₂)	N/M ^b	N/M ^b	IA ^a	6.8	TMAO	m	[249]
<i>E. coli</i> NR knockout strain (-O ₂ , +KNO ₃)	N/M ^b	N/M ^b	0.017	6.8	TMAO	m	[249]
<i>E. coli</i> NR knockout strain (-O ₂ , -KNO ₃)	N/M ^b	N/M ^b	0.027	6.8	TMAO	m	[249]
<i>E. coli</i> NR knockout strain (-O ₂ , +TMAO)	N/M ^b	N/M ^b	0.956	6.8	TMAO	m	[249]
<i>E. coli</i> NR knockout strain (+O ₂)	N/M ^b	N/M ^b	IA ^a	6.8	TMAO	m	[249]
<i>E. coli</i> rNR-Z (-O ₂ , +KNO ₃)	N/M ^b	N/M ^b	0.004	6.8	TMAO	m	[249]
<i>E. coli</i> rNR-Z (-O ₂ , -KNO ₃)	N/M ^b	N/M ^b	0.031	6.8	TMAO	m	[249]
<i>E. coli</i> rNR-Z (-O ₂ , +TMAO)	N/M ^b	N/M ^b	0.865	6.8	TMAO	m	[249]
<i>E. coli</i> rNR-Z (+O ₂)	N/M ^b	N/M ^b	IA ^a	6.8	TMAO	m	[249]
<i>E. coli</i> NR-Z strain MC4100	N/M ^b	N/M ^b	0.0749	6.8	nitrate	p	[249]
<i>E. coli</i> NR knockout strain	N/M ^b	N/M ^b	0.0027	6.8	nitrate	p	[249]
<i>E. coli</i> rNR-Z	N/M ^b	N/M ^b	0.0517	6.8	nitrate	p	[249]
<i>E. coli</i> NR-Z strain MC4100 (anaerobic, +nitrate)	N/M ^b	N/M ^b	0.730	6.8	nitrate	m	[249]
<i>E. coli</i> rNR, <i>fnr</i> mutant strain (anaerobic, +nitrate)	N/M ^b	N/M ^b	0.018	6.8	nitrate	m	[249]
<i>E. coli</i> rNR, <i>fnr</i> mutant strain (anaerobic, +nitrate)	N/M ^b	N/M ^b	0.193	6.8	nitrate	m	[249]
<i>E. coli</i> NR-Z strain MC4100 (aerobic, +nitrate)	N/M ^b	N/M ^b	0.016	6.8	nitrate	m	[249]
<i>E. coli</i> rNR, <i>fnr</i> mutant strain (aerobic, +nitrate)	N/M ^b	N/M ^b	0.014	6.8	nitrate	m	[249]
<i>E. coli</i> rNR, <i>fnr</i> mutant strain (aerobic, +nitrate)	N/M ^b	N/M ^b	0.201	6.8	nitrate	m	[249]
<i>B. megaterium</i> NCT-2 rNas	670	N/M ^b	0.058	7.1	nitrate	t	[53]
<i>H. mediterranei</i> Nar	820	N/M ^b	N/M ^b	8.0	nitrate	t	[53, 271]
<i>O. anthropic</i> Nar	340	N/M ^b	N/M ^b	7.0	nitrate	t	[53, 272]
<i>N. agilis</i> Nar	40	N/M ^b	N/M ^b	6.0	nitrate	t	[53, 273]
<i>P. aerophilum</i> Nar	58	N/M ^b	N/M ^b	N/M ^b	nitrate	N/M ^b	[53, 274]
<i>D. desulfuricans</i> Nap	32	N/M ^b	N/M ^b	8-9	nitrate	t	[53, 270]
<i>A. chroococcum</i> Nas	250	N/M ^b	N/M ^b	7.0	nitrate	t	[53, 275]
<i>A. halophytica</i> Nas	460	N/M ^b	N/M ^b	7.5	nitrate	t	[53, 276]
<i>R. capsulatus</i> Nas	96	N/M ^b	N/M ^b	N/M ^b	nitrate	N/M ^b	[53, 277]
<i>H. mediterranei</i> Nas	950	N/M ^b	N/M ^b	9.0	nitrate	t	[53, 278]
<i>S. denitrificans</i> S25DH ₁	N/M ^b	N/M ^b	0.00187	7.0	Cholest-4-en-3-one	ab	[226]
<i>S. denitrificans</i> rS25DH ₁	390 ± 80	66.6 ± 4.8	0.395	7.0	Cholest-4-en-3-one	ab	[226]
<i>S. denitrificans</i> rS25DH ₁	290 ± 90	13.8 ± 0.6	N/M ^b	7.0	Vitamin D ₃	ab	[226]
<i>S. denitrificans</i> rS25DH ₂	124 ± 20	17.4 ± 0.6	0.151	7.0	Cholest-4-en-3-one	ab	[226]
<i>S. denitrificans</i> rS25DH ₂	123 ± 20	19.8 ± 0.6	N/M ^b	7.0	7-Dehydrocholesterol	ab	[226]
<i>S. denitrificans</i> rS25DH ₃	1840 ± 800	1.08 ± 0.6	0.0046	7.0	Campest-4-en-3-one	ab	[226]

Table 1.15 Continued

<u>Enzyme^a</u>	<u>K_m (μM)</u>	<u>K_{cat} (min⁻¹)</u>	<u>Specific Activity (μmol subs/min/mg)</u>	<u>pH</u>	<u>Substrate</u>	<u>Assay Description</u>	<u>Ref.</u>
<i>S. denitrificans</i> rS25DH ₄	450 ± 13	12.6 ± 1.2	0.097	7.0	Cholest-4-en-3-one	ab	[226]
<i>S. denitrificans</i> rS25DH ₄	340 ± 90	10.2 ± 1.2	N/M ^b	7.0	Campest-4-en-3-one	ab	[226]
<i>S. denitrificans</i> rS25DH ₄	120 ± 10	8.4 ± 0.18	N/M ^b	7.0	β-Sitost-4-en-3-one	ab	[226]

a) r- recombinant; b) N/M- Not mentioned; c) specific activity is reported as V_{max} ; d) value was calculated from data reported; e) ND- not detected; f) NA- negligible activity; g) IA- inactive; h) Monitored oxidation of electron donor reduced methyl viologen; i) BSO reduction to biotin was monitored at 533 nm using the colorimetric reagent, p-dimethylaminocinnamaldehyde; j) Monitored oxidation of electron donor NADPH/NADH at 340nm; k) disk biological assay, growth on biotin; l) Monitored the phenazine methosulfate (PMS) mediated reduction of 2,6-dichlorophenolindophenol (DCPIP); m) Monitored oxidation of electron donor reduced benzyl viologen; n) Monitored duroquinol-nitrate reductase activity by measuring the oxidation of duroquinol; o) Monitored menaquinol-nitrate reductase activity by measuring the oxidation of menaquinol; p) Monitored product formation utilizing formate as an electron donor; q) Monitored oxidation of reduced benzyl viologen, in the prescence of inhibitor cyanide; r) Monitored oxidation of reduced benzyl viologen, in the prescence of inhibitor zinc; s) protein film voltammetry (PFV); t) monitored nitrite formaiton utilizing diazo coupling and coloumetric determination; u) Monitoted the reduction of cytochromes as electron acceptors; v) Monitored change in NADH absorption at 340 nm using NAD⁺ as electron acceptor; w) monitored the reduction of artificial electron acceptor, ferricyanide at 420nm; x) Used CO₂ as electron acceptor. Monitored change in NADH absorption at 340 nm; y) Used NAD⁺ as electron acceptor and formate as electron donor. Monitored change in NADH absorption at 340 nm; z) Used NAD⁺ as electron acceptor and MV as electron donor. Monitored the oxidation of MV at 600nm; aa) Used Ferricyanide as electron acceptor and NADH as electron donor. Monitored change in NADH absorption at 340 nm; ab) monitoring product formation by ultra high-performance liquid chromatography; ac) in U/mg; ad) beleow detection limit and could not be determined; ae) specific activity determine in pH 8.0; af) reported as K_i for inhibitor; ag) no units reported; ah) in μA/cm².

Table 1.16: Known REMP chaperones for molybdopterins enzymes.

Name of REMP	Chaperone for	Proposed Roles/Functions	Ref.
TorD	TorA, TMAO reductase	Stabilization/maturation; binds TAT leader sequence and the core of apo-TorA; prevents proteolysis; TorD binds MGD and is required for Moco insertion; TorD interacts with MobA for bis-MGD formation	[63, 131, 279]
DmsD	DmsA, DMSO reductase; YnfEF, selenite reductase	DmsD binds TAT leader sequence; DmsD is necessary for activity of protein partners; it is proposed DmsD may be involved in bis-MGD insertion like TorD; no interaction between DmsD and the target core has been observed thus the role in maturation is unclear	[131, 280]
SerD	SerA, selenate reductase	SerD has not been investigated but sequence and operon structure suggest SerD to function as a chaperone similar to NarJ	[281, 282]
PcrD	PcrA, perchlorate reductase	PcrD has not been investigated but sequence similarity to SerD, DhD, EbdD, and NarJ suggest PcrD is a chaperone involved in the assembly of a mature molybdenum enzyme, in this case PcrA	[283]
ClrD	ClrA, chlorate reductase	ClrD has not been investigated but sequence similarity to SerD, EbdD, and DhD suggest ClrD is a chaperone involved in the assembly of a mature molybdenum enzyme, in this case ClrA	[284]
ArxD	ArxA, arsenite oxidase	ArxD has not been investigated but sequence similarity to TorD suggests ArxD is a chaperone involved in maturation of the molybdenum enzyme ArxA	[285]
ArrD	ArrA, Arsenate reductase	ArrD has not been investigated but sequence similarity to TorD suggests ArrD is a chaperone involved in maturation of the molybdenum enzyme ArrA	[286]
DdhD	DdhA, DMS dehydrogenase	DdhD has not been investigated but sequence similarity to SerD and NarJ suggest DdhD is a chaperone involved in the assembly of a mature molybdenum enzyme, in this case DdhA	[287]
EbdD	EbdA, ethylbenzene dehydrogenase	EbdD has not been investigated but sequence similarity to SerD, TorD, and NarJ suggest EbdD is a chaperone involved in the assembly of a mature molybdenum enzyme, in this case EbdA	[288]
PaoD	PaoC, periplasmic aldehyde oxidase	PaoD is essential for the maturation of the periplasmic aldehyde oxidase, PaoC; PaoD binds Moco; PaoD is involved in insertion of the MCD cofactor into PaoC; PaoD binds the sulfated form of MCD and may be involved in cofactor sulfuration	[120, 289, 290]
NarJ	NarG, Nitrate reductase	Stabilization/maturation; binds N-terminal region and the core of apo-NarG; may be involved in cofactor insertion; provides stability and is involved in anchoring NarGH complex to NarI in the membrane	[131, 291]
NarW	NarZ, Nitrate reductase	NarW is in the <i>narZYWV</i> operon but can be exchanged for NarJ thus both are believed to perform the same roles/functions; NarW is involved in stabilization and maturation similar to NarJ	[131, 291]
NapD	NapA, Nitrate reductase	Activity depends on the presence of NapD; NapD binds the TAT leader sequence but does not bind the core of NapA; the exact role of NapD is unclear but there is evidence NapD may have a role in stabilization and NapA folding	[131, 292]
NapF	NapA, Nitrate reductase	NapF is not present in all <i>nap</i> operon; NapF is involved in the transfer of the [4Fe4S] cluster to NapA	[131, 292]
NapL	NapA, Nitrate reductase	NapL is not present in all <i>nap</i> operons; NapL's role is unknown; NapA activity is reduced in the absence of NapL	[293, 294]
XdhC	XdhB, Xanthine dehydrogenase	XdhC binds Moco, stabilizing it and protecting it until the insertion of the terminal sulfur ligand; XdhC interacts with L-cysteine desulfurase; XdhC inserts the sulfated Moco into XdhB; may assist in enzyme folding after Moco insertion	[131, 295]
Moco Sulfurase (ABA3 in <i>Arbidopsis</i> , HMCS in humans)	Eukaryotic XO family members (XO and AO for example)	Functional homology to XdhC; responsible for the sulfuration step of Moco maturation in the eukaryotic XO family; L-cysteine desulfurase domain and a Moco binding domain present in Moco sulfurase	[131, 177]
FdhD	FdhF/FdnG/FdoG, Formate dehydrogenase	FdhD binds bis-MGD and is required for Moco insertion; FdhD interacts with sulfur transferase, IscS, and is believed to transfer sulfur to the Mo center of Moco	[131, 296]
FdhE	FdhF/FdnG/FdoG, Formate dehydrogenase	FdhE is not present in all formate dehydrogenase operons; FdhE's role is unknown; FdhF activity is reduced in the absence of FdhE	[296]
FdsC	FdsA, Formate dehydrogenase	FdsC binds bis-MGD and is required for Moco insertion; Mo center coordination changes from a terminal ligand of sulfido to oxo in the presence and absence of FdsC respectively; maturation heavy role	[88, 131, 296]

Table 1.16 Continued

Name of REMP	Chaperone for	Proposed Roles/Functions	Ref.
FdsD	FdsA, Formate dehydrogenase	Unclear role; FdsD interacts with FdsC and MobA; it has been proposed that FdsD may have a role in protection of bis-MGD while bound to FdsC, or to facilitate the specific transfer of bis-MGD from MobA to FdsC.; Moco insertion/stabilization heavy role	[88, 296]
SdhD	SdhA (alpha subunit), steroid C-25 dehydrogenase	Unclear role; SdhD is required for active enzyme; SdhD is proposed to have a role in protein folding and Moco insertion	[226]

CHAPTER 2. MOLECULAR CLONING, EXPRESSION, AND PURIFICATION OF PERIPLASMIC NITRATE REDUCTASE

2.1 Introduction

In order to understand how the molybdenum cofactor is tuned in various enzymes to perform the diverse chemistry achieved in nature, investigations have been initiated in the enzyme periplasmic nitrate reductase (Nap). This enzyme has significant consequences on the nitrogen cycle, microbial metabolism, and human health. Nitrate reduction occurs in three processes: denitrification, assimilatory nitrate reduction to ammonia (ANRA), and dissimilatory nitrate reduction to ammonia (DNRA) (Figure 2.1) [16]. Microbes are the driving force behind the global nitrogen cycle as they use an assortment of redox reactions to metabolize nitrogen for energy transduction, detoxification, or assimilation [16]. Among the enzymes responsible for these processes are the nitrite reductases (NiRs) and nitrate reductases (NRs). NiRs reduce NO_2^- to either ammonia (NH_4^+) or nitric oxide (NO) (and ultimately N_2) while NRs catalyze the reduction of nitrate (NO_3^-) to nitrite (NO_2^-) [16].

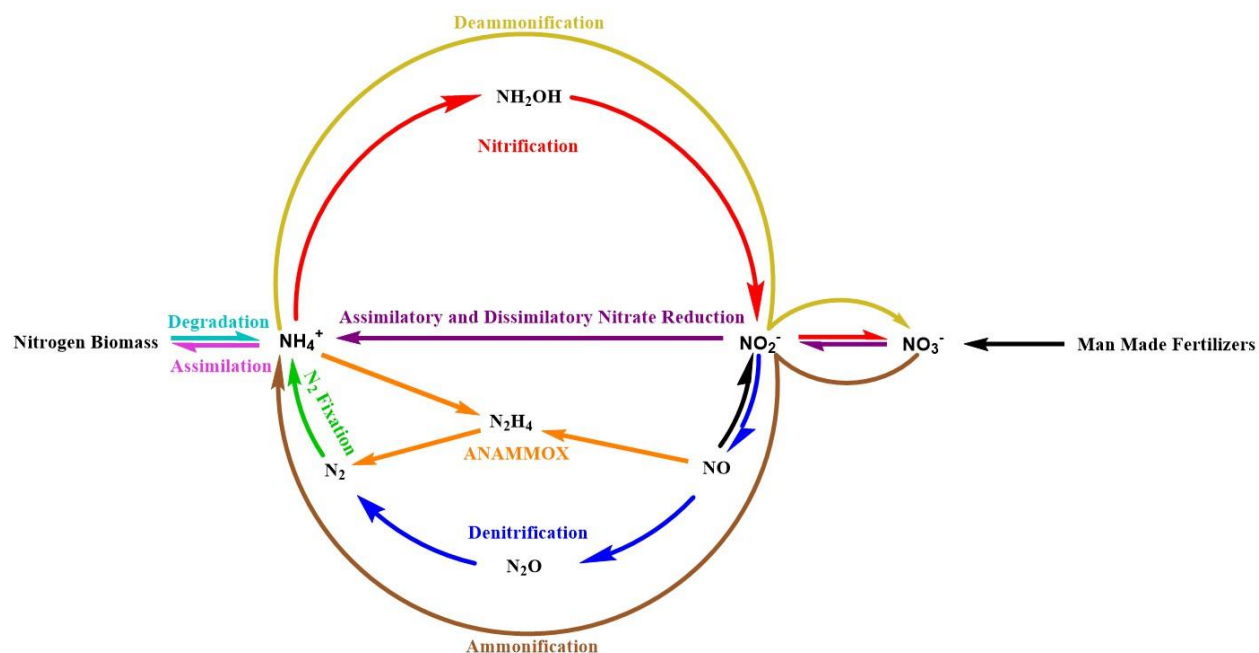


Figure 2.1: Diagram of the biological nitrogen cycle. Reactions are color coded by process.

Nitrate has typically held a bad reputation for many decades, mainly because of its proposed association with formation of toxic nitrosyl compounds and carcinogenic nitrosamines. The nitrate ion itself is not considered to be toxic. Investigations into the relationship between nitrates and tumors have shown no clear evidence that dietary nitrate could increase the occurrence of tumors [297]. However, when nitrate is converted into nitrite by commensal bacteria, the nitrite ion can be converted into carcinogenic nitrosamines under certain conditions such as those found in the acidic stomach environment [297, 298]. Nitrosamines were reported to be related to tumor formation and several cancers such as esophageal, gastric, and colon cancers.

Nitrite produced from nitrates in drinking water can bind to hemoglobin to form methemoglobin. Methemoglobin interferes with the oxygen capacity of the blood resulting in methemoglobinemia, which is a life-threatening disease when methemoglobin levels exceed about 10% of the total hemoglobin count [299]. Patients exhibit symptoms of cyanosis, developing an unusual blue-gray skin color and are often described as irritable or lethargic. Infants are particularly susceptible during their first six months of life as they lack an efficient mechanism to convert methemoglobin back to hemoglobin. When methemoglobin levels pass 50%, the patient can quickly become comatose and even die if the condition is not recognized and treated [300]. Approximately 40,000 infants below six months of age are expected to be members of homes that have nitrate-contaminated private water supplies [300]. In recent years, medical and physiological benefits of dietary nitrate have been explored. Nitrate benefits physiological functions including cardiovascular protection such as blood pressure reduction, prevention of platelet aggregation, and vasodilation effects similar to those of NO [297, 298]. The exact molecular mechanisms of how nitrate elicits such effects are still not fully understood. Considering the many functions impacted by nitrate, it is likely that several mechanisms are involved [301].

In humans, nitrate reduction is dependent on the microbial community living in the body. Nitrate reductases (NRs) are molybdenum-containing enzymes that reduce nitrate to nitrite. These NRs have been categorized based on function, structure of the active site, and cellular location (Figure 2.2). Prokaryotic NRs have been divided into three categories: periplasmic (Nap), respiratory (Nar), and assimilatory (Nas) [12]. Nas proteins are located in the cytoplasm and are involved in nitrate assimilation. Nar proteins are membrane bound but oriented toward the cytoplasm. These proteins participate in the generation of energy by coupling proton transfer with

the reduction of nitrate. Nap proteins are located in the periplasm or periplasmic membrane, and are generally involved in redox balancing, respiration, and nitrate-scavenging.

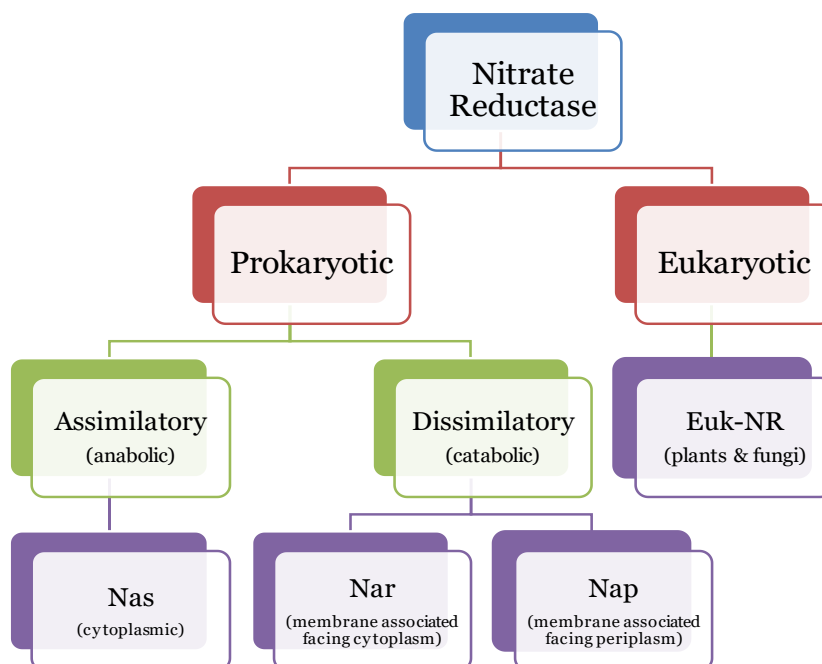


Figure 2.2: Nitrate reductase classification flow chart. Nitrate reductases are divided into four general categories: eukaryotic nitrate reductases (Euk-NR), periplasmic nitrate reductases (Nap), respiratory nitrate reductases (Nar), and assimilatory nitrate reductases (Nas).

Nap will be the focus of this project. Nap is a dissimilatory protein, *i.e.* it is an enzyme involved in a catabolic pathway that reduces nitrate and excretes the end products as either N_2 or NH_4^+ . The reduction of nitrate by Nap can be coupled to the production of ATP. There are multiple Nap subunits including those that are involved in electron transport and those involved in maturation [16]. The *nap* operon (Figure 2.3) has combinations of the 12 known *nap* genes: A, B, C, D, E, F, G, H, K, L, M, S with four distinct operon structures (EDABC, DAGHBC, CMADGH and AGHBFLD). Of the different proteins NapB, NapC, NapG and NapH are redox-active partner subunits while NapL, NapD and NapF are thought to be involved in maturation and cofactor insertion. NapA is the catalytic subunit, while proteins encoded by genes such as *napE*, *napK*, *napM* and *napS* are rare with unknown function [16].

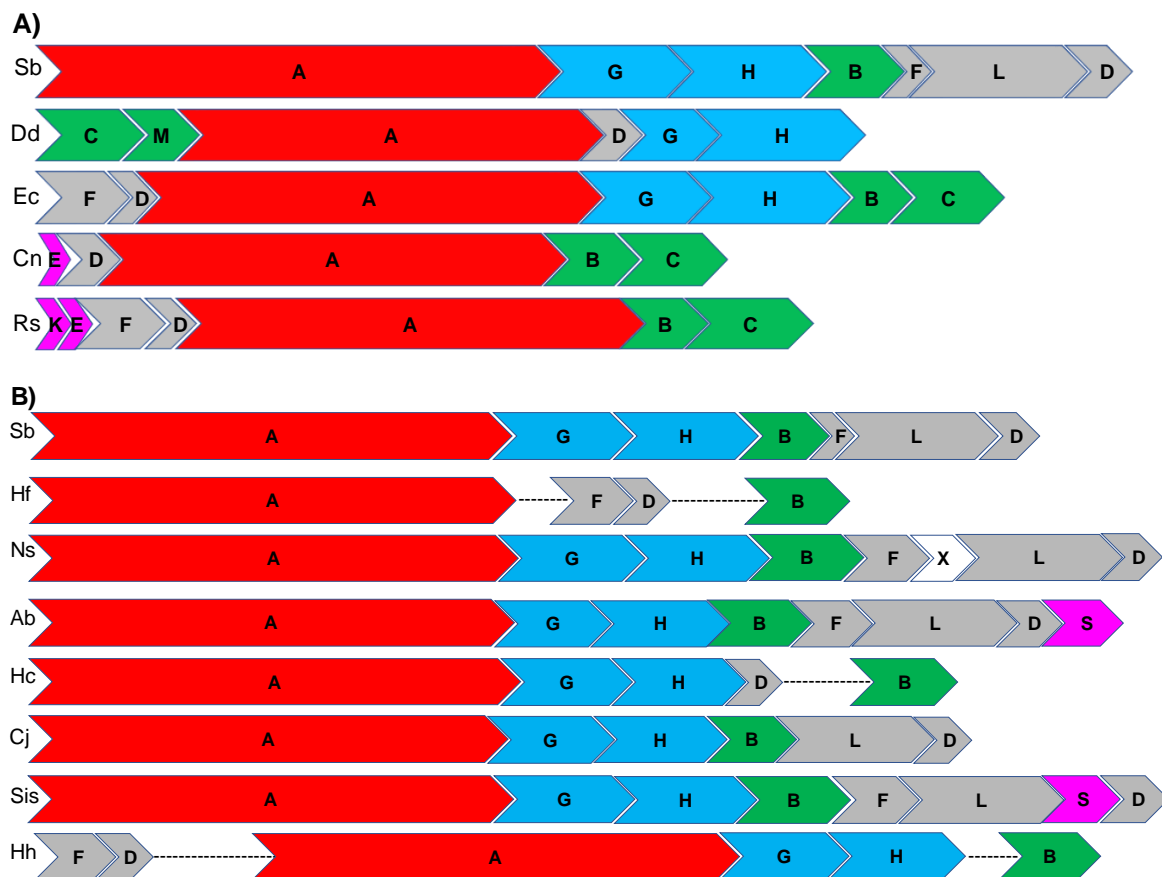


Figure 2.3: The operon structures of *nap* A) between Proteobacterial classes and B) within Epsilonproteobacteria. From the top down in A) *S. barnesii* (ϵ), *D. desulfuricans* (δ), *E. coli* (γ), *C. necator* (β), and *R. sphaeroides* (α). From the top down in B) *S. barnesii* SES-3, *H. felis* ATCC 49179, *N. salsuginis* DSM 16511, *A. butzleri* JV22, *H. cetorum* MIT 007128, *C. jejuni* 51494, *Sulfurimonas* sp. AST-10, *H. heilmannii* ASB 1.4. Genes are labelled by subunit letter and color coded by subunit. X is a hypothetical protein that is not a confirmed component of the *nap* operon. The dashed lines between genes represents the various amounts of DNA that separates the *nap* genes in that genome.

This project focuses on NapA, the 70-110 kDa Moco-containing catalytic subunit. Most studies on NapA have focused on alpha, beta, gamma, and deltaproteobacteria, not the epsilonproteobacteria, therefore little is known about *Epsilonproteobacterial* NapA. The *Epsilonproteobacteria* are significant because their genome contain only one type of NR, Nap, and they can respire on nitrate [16]. *Campylobacter jejuni* NapA has been chosen to study the *Epsilonproteobacterial* Nap given its importance to nitrate reduction and its influence on the virulence factors of *Campylobacter*. While fundamental biochemical information is lacking for an in depth understanding of nitrate reduction by *C. jejuni*, an extensive bioinformatics analysis of

the *Epsilonproteobacterial C. jejuni* Nap has been conducted previously [16, 302]. *Epsilonproteobacteria* such as *Campylobacter*, *Helicobacter*, and *Wollinella* have a highly conserved *napAGHBFLD* operon. Interestingly, the *C. jejuni nap* operon does not contain *napF*.

In order to understand nitrate reduction in *C. jejuni*, and to investigate the factors that influence the tuning of the molybdenum center, a *C. jejuni* NapA functional investigation was spearheaded through NapA expression and biochemical characterization. As a class B microaerophilic pathogen, *C. jejuni* requires a specific atmosphere of 5% O₂, 10% CO₂, and 85% N₂ [303]. In addition, *C. jejuni* has a large doubling time of 90-200 min depending on the strain [304]. Due to the general inconvenience for protein production, a heterologous expression system in *E. coli* was developed for *C. jejuni* NapA [302, 305].

As described in Chapter 1, overexpression of a moco-containing enzyme has several challenges. A general understanding of Nap expression and maturation in *C. jejuni* is necessary for designing an efficient expression system for active NapA enzyme. The *nap* operon (Figure 2.3) has combinations of the 12 known *nap* genes with four distinct operon structures where *C. jejuni* Nap has the *napAGHBLD* operon. NapA is the catalytic subunit; NapG, NapH, and NapB are electron transfer partners; and NapL and NapD are maturation proteins. Of these partners, the small *c*-type cytochrome NapB is the most studied. NapB is approximately 16-18 kDa and contains two *c*-type heme cofactors [16, 306]. Electrons are transferred from NapB to NapA to reduce nitrate. Studies of *P. pantotrophus* NapAB indicate both hemes are low-spin and have histidine as the axial ligand [307]. The protein sequence and crystal structure of *Haemophilus influenzae* NapB suggest NapB belongs to a new class of cytochrome *c*. The conserved residues among the NapB family are lining the heme pockets or are found in the vicinity of the heme groups suggesting the protein-protein interfaces and NapB interactions may vary between organisms attenuating the electron transfer properties [306]. Additionally Simpson *et al.* determined residues in both NapA and NapB that form a salt bridge responsible for the strong interaction at the NapAB interface [308].

NapA has been isolated in both monomeric and heteromeric forms [61, 130, 168, 309, 310]. Whether the Nap is monomeric or heterodimeric depends on its ability to form salt bridges at the NapA:NapB interface [308, 311]. Two residues E47 and S772 (in *Rhodobacter sphaeroides*) have been identified as critical for the formation of the NapAB heterodimer. The sequence alignment of *C. jejuni* NapA with *R. sphaeroides* NapA (Figure 2.4) shows the presence of a proline (P70)

instead of a glutamate precluding the formation of the salt bridge, and thus *C. jejuni* NapA is expected to purify as a monomer due to a weakened NapA:NapB interface. For this reason, NapB was excluded from the heterologous construct.

The NapGH complex is proposed to act as a quinol oxidase that enables direct electron transport to NapB [306]. NapG contains four iron-sulfur clusters and has a putative Twin Arginine Translocase (TAT) leader sequence. Kern demonstrated that NapG is located at the periplasmic side of the membrane and that NapH is required to bind NapG to the membrane [312]. NapH has four transmembrane helices and contains two iron-sulfur binding motifs on its cytoplasmic C-terminus [16, 312]. NapG and NapH are both required for rapid electron transfer from ubiquinol via NapC to the NapB–NapA complex [313]. In organisms which do not encode a NapC homologue such as *C. jejuni*, NapGH anchors the NapAB complex to the periplasmic membrane and supplies electrons directly from the quinone pool to the active site in NapA via the diheme NapB [16, 314]. In order to study the free soluble NapA and simplify the expression system, the membrane anchor of NapGH was not included in the heterologous expression system.

In addition to the electron transfer partners NapG, NapH, and NapB, the *C. jejuni nap* operon contains two genes encoding maturation chaperones NapL and NapD. NapL is a ~35 kDa protein with unknown function. Bioinformatic analysis has provided some information on NapL. NapL is annotated as a tryptophan-aspartic acid (WD) repeat protein. The WD repeat domain has a conserved sequence of approximately 40–60 amino acids. The domain starts with a glycine histidine (GH) dipeptide near the N-terminus and ends with a tryptophan-aspartic acid (WD) dipeptide at the C-terminus. WD proteins typically have seven or more of the WD repeats present [315].

There is also a putative Secretion Translocase (SecT) leader sequence of MKKFLFILSLFCVLSYA (as predicted by Phobius and SignalP webserver, <http://phobius.sbc.su.se/> and <http://www.cbs.dtu.dk/services/SignalP/> respectively) on the N-terminus of NapL implying that NapL is a periplasmic protein that is translocated into the periplasm unfolded utilizing the SecT translocation pathway [312]. Whether or not it associates with the membrane or simply just interacts with the NapA subunit free in the periplasm is unknown. NapL has never been isolated and tertiary structural information has not been experimentally determined. Despite all the speculations, very little experimental information is available concerning NapL's function. However, mutations in two Epsilonproteobacteria, *W.*

succinogenes [293] and *C. jejuni* [294], revealed the absence of NapL impacts NapA activity and overall cell growth. This result suggests that NapL has a role in NapA maturation.

NapD is a Redox Enzyme Maturation Protein (REMP) chaperone as mentioned in Chapter 1. Like TorD and several other REMPs, NapD binds the TAT signal peptide. The TAT system transports fully folded proteins across the membrane from the cytoplasm to the periplasm [160, 316, 317]. The TAT enzyme complex recognizes a unique peptide leader sequence, S/TRRXFLK [160]. Once bound, the folded target protein is transferred across the membrane by the TAT complex to be released into the periplasm. NapD binds to the TAT signal peptide of the catalytic subunit NapA to prevent premature enzyme from transferring into the periplasm before it is fully folded with cofactors inserted [318]. This process is referred to as “TAT proofreading.” The NapD chaperone is directly involved with TAT system through this TAT proofreading process, and NapD adopts a ferredoxin-type fold when bound with NapA [160]. This ferredoxin-type fold differs from the all-helical protein folding of the TorD family of proteins, and thus became known as a new family of twin-arginine signal-peptide binding proteins [160]. Recently, it was discovered that the binding of NapD to NapA results in a small conformational change to NapA, and that this interaction points toward a role for NapD in the process of inserting the molybdenum cofactor into NapA [316].

Successful heterologous production of a metalloprotein like NapA often requires the coexpression of genes encoding dedicated chaperones, such as NapL and NapD, to ensure proper folding and metal center insertion. Expression of *Pseudomonas* strain G-179 NapA in *E. coli*, without the cognate maturation proteins, resulted in non-functional NapA found in inclusion bodies [319]. Genetic experiments with *Wolinella succinogenes* show *napL* and *napD* to be critical for full activity in a similar Nap system [293]. These studies emphasize the importance of maturation proteins in obtaining functional enzyme. To maximize heterologous production of active NapA containing both a molybdenum cofactor and a [4Fe4S] cluster, the maturation proteins NapL and NapD were coexpressed in this study. In addition, the TAT leader sequence on NapA was not modified to preserve the possible interactions with these maturation proteins.

Dd	MSTSRRDFLK YFMSAAVAAASGAGFGSLAL----AADNRPEKWKVGVCRYCTGCGVLVGVKDGKAVAIQGD PNN--HNAGLLQLKGSLL	85
Cj	--MNRDFIKNTAIASAASVA--GLSVPSSML----GAQEEDWKWDKAVCRFCGTGCGIMIAKDKGKIVATKGDPAAPVNRGLNCKIKGYFN	83
Ec	MKLSRRSFMKANAVAAAAA--GLSVPGVARAVVGQEE--AIKWDKAPCRFCGTGCGVLVGTQQGRVVACQGDPAFVNRGLNCKIKGYFL	87
Rs	MTLTRDLIKAQAAATAAAAA--GLPVSALAQPVTGGAEALRIWRSKAPCRFCGTGCGVMVGTDRDQVAVATHGDTQAEVNRGLNCKIKGYFL	89
Cn	MKISRRDFIKQTAITATASVA--GVTLPAGAANFVTDSEVTKLWRSKAPCRFCGTGCGVTAVKDNKVVATQGDPAFVNRGLNCKIKGYFL	89
	. ** : : * * : : : : * * . . : : * * . ** : : : : : : : : : : * * : : * * : : * * : : *	
Dd	IPVLNSKERVTPQLVRRH-----KGGKLEPVSWDEALDLMASRFRSSIDMYGPNSVAWYGGSGCLTEESYVANKIFKGGFGTNNVDGNP	169
Cj	AKIMYGEDRLVMPLLRMNEKEGFDDKKGKQQVSWQRAFDMEKQFKKAYNELVGTGIGIFGSGQYTIQEGYAALKLAKAGFRTNNIDPNA	173
Ec	PKIMYGKDRLTQPLLRMK--NGKYDKEGEFTPTWQAFDVMEEKFKTALKEKGPESIGMFGSGQWTIWEGYAASKLKFAGFRSNNIDPNA	176
Rs	SKIMYGEDRLTTPLLRMK--DGVYHKEGEFAPVSWDEAFDMAAKRVLKEKGPKAVGMFGSGQWTIWEGYAASKLMRAGFRSNNIDPNA	178
Cn	SKIMYGQDRLTRPLMRMK--NGKYDKNGDFAPVTDQAFDEMERQFKRVLKEKGPATAVACSAPAQWTVWEGYAAAKLYKAGFRSNNIDPNA	178
	: : : : : : * : * . * * : : : : * : : : . * : : . * * * * : : * : * : * : * : *	
Dd	RHCMAVGGYVTSFGKDEPMGTADIDQATCFIIGSNTSEAHFVLFRRRIARRKQVEP--GVKIIIVADPRRTNTSRIADMHVAFRPGTDL	258
Cj	RHCMAVVGFMQTFGVDEPSGCYDDIELTDITITWGANMAEMHPILWSRVSDRKLSNLDKVKVNLSTFSNRTSNIADIEIIFKPNTDL	263
Ec	RHCMAVVGFMRTFGMDEPMGCYDDIEQADAFVLWGANMAEMHPILWSRTNRRLSNQ--NVTVAVLSTYQHRSEFELADNGIIFTFQSDL	265
Rs	RHCMAAATAFMRTFGMDEPMGCYDDFEAADAFVLWGSNMAEMHPILWSRLTDRRLSHE--HVRVAVLSTFTHRSMDLADTPIIFRPGTDL	267
Cn	RHCMAAAGFMRTFGMDEPMGCYDDFEAADAFVLWGSNMAEMHPILWTRVTDRLSHP--KTRVVVLSTFTHRCFDLADIGIIFKPQTDL	267
	* * * * * . : : : * * * * * * * : : : : : * * : * * * * : * : * : * : * : * * : * * : *	
Dd	AFMHSMWVIINEE--LDNPRFWQRYVNFN-----	286
Cj	AIWNYIAREIVYNHPEAMD MKFIKDHCVFATGYADIGYGMRRNPNHPKFKESEKDTVEKENVITLDDEEATSLSYLGVKAGDKFEMKHQG	353
Ec	VILNYIANYIIQNN--AINQDFFSKHVNLRKGATDIGYGLRPTHLEK--AA-----KNPG	317
Rs	AILNYIAHHIISTG--RVNRDFVDRHTNFALGATDIGYGLRPEHQLQL--AA-----KGAA	319
Cn	AMLNYIANYIIRNN--KVNKDFVNKHTVFKEGVTDIGYGLRDPHPLQK--AA-----KNAS	319
	. : . : * * : : * : *	
Dd	-DAEGKPSDFEGYKAFLENYRPEKVAEICRV-----PVEQIYGAARAFAE--SAATMSLWCMGINQRVQGVFANNLIHNLHLITGQIC	366
Cj	VADKNWEISFDEFKKG LAPYTLEYTARVAKGDDNESLED FKKKLQELANLYIEKNRKVVSFWTMGFNQHTRGSWVNEQAYMVHFLLGKQA	443
Ec	S-DASEPMSFEDYKAFVAEYTLKTAEMTG-----PKDQLEQLAQLYADPNKKVISYWTMGFNQHTRGVWANNLVYNLHLLTGKIS	398
Rs	DAGAMTPTDFETFAALVSEYTLKAAEISGV-----EPALLEELAELYADPDRKVMSLWTMGFNQHVGVWANNMVYNLHLLTGKIS	401
Cn	DPGAAKVITFDEFKFKVSKYDADYVSKLSAV-----PKAKLDQLAELYADPNIKVMSLWTMGFNQHTRGTWANNMVYNLHLLTGKIA	401
	* : : : * : : : : : : : : : : * . : : . : * * * : : : * : * . : : : * : .	
Dd	RPGATSFSLTGQPNACGGVRDGGALSHLLPAGRAIPNAKHRAEMEKLWGLPEGRIAPEPGYHTVALFEALGRGDVKCMII CETNPAHTLP	456
Cj	KPGSGAFSLTGQPSACGTAREVGTFSHRLPADMVVANPKHREISEKIWKVPKTIINPKPGSPYLNIMRDLEDGKIKFAWVQVNNPWQNTA	533
Ec	QPGCGPFSLTGQPSACGTAREVGTFAHRLPADMVVTNEKHRDICEKKWNIPSGTIPAKIGLHAVAQDRALKDGLNLYWTMCTNNMQAGP	488
Rs	EPGNSPFSLTGQPSACGTAREVGTFAHRLPADMVVTNPEHRAHAEIWKLPAGLLPDWVGAAHAVEQDRKLHDGEINFYWVQVNNMQAAP	491
Cn	TPGNSPFSLTGQPSACGTAREVGTFSHRLPADMVVTNPKHREAEERIWKLPAGTIPDKPGYDAVLQNRMLKDGLNAYWVQVNNMQAAA	491
	** * * * * . * * : : : * * * : : * : * : * * . * : * : : * : : : * : *	

Figure 2.4: Amino acid sequence alignment of NapA from *Desulvibrio desulfuricans* (Dd), *Campylobacter jejuni* (Cj), *E. coli* (Ec), *Rhodobacter sphaeroides* (Rs), and *Cuprividicus necator* (Cn). The highly conserved residues are highlighted in grey and important residues are in color. The cysteines coordinating the [4Fe4S] cluster are green and the Mo-coordinating cysteine is highlighted in yellow. Two residues proposed to be critical for the NapAB interface by reference [308] are highlighted in red.

Figure 2.4 continued

Dd	NLNK-VHKAMSHPEFIVCIEAFDAVTLEYADLVLPFAFWCERDGVYGCGERRRSLTEKAVDPFGQCRPTVNTLVEFARRAGVDPQL--	543
Cj	NANH-WIAAAREMDNFIVVSDCYPGI-SAKVADLILPSAMIYEKYGAYGNAERRTQHWKQQVLPVGAAMSDTWQILEFAKRFLKEVWKE	621
Ec	NINEERMPGWRDPRNFIIVSDPYPTV-SALAADLILPTAMWVEKEGAYGNAERRTQFWRQQVQAPGEAKSDLWQLVQFSRRFKTEEVWPE	577
Rs	NIDQETYPGYRNPENFIVVSDAYPTV-TGRCADLVLPAMWVEKEGAYGNAERRTHFWHQLVEAPGEARSDLWQLMEFSKRFTTDEVWPE	580
Cn	NLMEEGLPGYRNPANFIVVSDAYPTV-TALAADLVLPAMWVEKEGAYGNAERRTQFWHQLVDAPGEARSDLWQLVEFAKRFKVEEVWPP	580
	****: : : * : ***:*** *: *: *.** .*** .: * * . : : : : *	
Dd	-----VNFRNAEDVWNEWRMVSK	561
Cj	QKVDNKLTLPSVLEEAKAMGYSEDDTLFDVLFANKEAKSFNPNDIAKGFNDTDVKGDERKIQGSDDGKEFTGYGFFVQKYLWEEYRKFGFL	711
Ec	ELLAKKPE-----LRGKTLYEVLATPEVSKFPVSELAKD-----QLNDESRELGFYLOKGLFEEYAWFGR	638
Rs	EILSAAPA-----YRGKTLFEVLFANGSVDRFPASDVNPD-----HANHEAALFGFYPQKGLFEEYAAFGR	641
Cn	ELIAKKPE-----YKGKTLYDVLRYNGQVDKFLKDVNAE-----YHNAEAKAFGFYLOKGLFEEYATFGR	641
	* : : : : *	
Dd	GTTYDFWGMTRERLRKESGLIWPCPSEDHPGTSRLRYVRGQDPCVPADHP-DRFFFFYGKP-----DGRAVIWMRPA	630
Cj	GHGHDLDAD--FDTYHKVRGLRWPVVNG--KETQWRFNTKFDYYAKKAAPNSDFAFYGDFNKMLTNGDLIAPKDEKEHSIKNKAKIFFRPF	797
Ec	GHGHDLDAP--FDDYHKARGLRWPVVNG--KETQWRYSEGNDPYVKA---GEGYKFYGKP-----DGKAVIFALPF	701
Rs	GHGHDLDAP--FDTYHEVRGLRWPVVEG--EETRWRRYREGFDPYVKP---GEGLRFYGKP-----DGRAVILGVPI	704
Cn	GHGHDLDAP--FDAYHEARGLRWPVVNG--KETRWRYREGSDPYVKA---GTGFQFYGNP-----DGKAVIFALPY	704
	* : : : : * * * * . * * : * . * * * . * * *	
Dd	KGAAEEDPAEYPLYLTSMRVIDHWHATMTGKVPQLKANPIAFVEINEEDAARTGIKHGDSVIVETRRDAMELP--ARVSDVCRPGLIA	718
Cj	MKAPERPSKEYPFWLATGRVLEHWHSGTMTMRVPELYRAVPEALCYMSEKDGEKLGGLNQGLVWVESRRGKVKARVDMRGRNKPVGGLVY	887
Ec	EPAAEAPDEEYDLWLSTGRVLEHWHGSMTRRVPELHRAFPPEAVLFHPLDAKARDLRRGDKVKVVSRRGEVISIVETRGRNRPPQGLVY	791
Rs	EPPAESPDDEFGFWLVTGRVLEHWHSGSMTLRVPELYKAFFGAVCFMHPEDARSRLNRGSEVRVISRRGEIRTRLETRGRNRMPRGVVF	794
Cn	EPPAESPDKEYPYWLVTGRVLEHWHSGSMTLRVPELYRSFPNAVVMHPEDAKALGLRRGVEVEVVSRRGRMRSRIETRGRDAPPRGLVF	794
	* * . *: : * : * : * : * : * : * : * : * : * : * : * : * : * : *	
Dd	VPFFDPKKLVNKLFLDADPVSREPEYKICARVRKA	755
Cj	VPWFDEVYINKVTLDATCPLSKQTDFFKKCAVKIYKA	924
Ec	MPFFDAAQLVNKLTLDATDPLSKETDFFKKCAVKLEKV	828
Rs	VPWFDAQLINKVTLDANDPISRQTDFFKKCAVKIEAV	831
Cn	VPWFDAQLINKVTLDATCPLSLQTDFFKKCAVKIVKV	831
	:*: ** :*: *** :*: * : :*: ** : : *	

In summary, the molybdenum cofactor containing enzyme periplasmic nitrate reductase (Nap) impacts the nitrogen cycle, microbial metabolism, and human health. Thus, the biochemical properties and function of Nap are essential in understanding the nuances of Moco and the fundamental implications those properties have on various areas of life. Nap exists as an enzyme complex in pathogen *C. jejuni* consisting of NapA, the catalytic subunit, NapB, the heme containing electron transfer partner, and NapGH, the membrane associated iron sulfur cluster containing electron transfer partners. Additionally, present in the operon are *napLD* genes that encode maturation proteins NapL and NapD. NapLD proteins are necessary for full nitrate reductase activity in *C. jejuni*. In this chapter, the molecular cloning and expression of the *napALD* genes as well as the purification of recombinant *C. jejuni* NapA will be discussed. The procedures developed in this chapter will provide an optimal isolation method for obtaining active NapA enzyme for further study.

2.2 Materials and Methods

Bacto yeast extract of autolyzed yeast cells was purchased from Becton, Dickinson and Company (Sparks, MD, USA) and peptone was purchased from Research Products International (Mt. Prospect, IL, USA). His-Trap HP and HiPrep Sephacryl S-200 HR columns were purchased from GE Healthcare Biosciences (Uppsala, Sweden). The Pierce Coomassie Plus (Bradford) Protein Assay Kit, trypsin, chymotrypsin, and His-Pur Ni-NTA Superflow Agarose Resin were purchased from Thermo Scientific (Rockford, IL, USA). The Qubit Assay Kit was purchased from Invitrogen Life Technologies Corporation (Eugene, OR, USA). Buffers and other reagents were purchased at the highest available grade from either Sigma-Aldrich (St. Louis, MO, USA) or Fisher Scientific (Pittsburg, PA, USA).

Genomic DNA from *C. jejuni* RM1221 was generously supplied by Dr. William Miller. *E. coli* strains, DNA polymerase, and restriction enzymes were purchased from New England Biolabs (Ipswich, MA, USA). Primers were synthesized by Integrated DNA Technologies (Coralville, IA, USA). DNA sequencing was carried out at ACGT Inc. (Germantown, MD, USA).

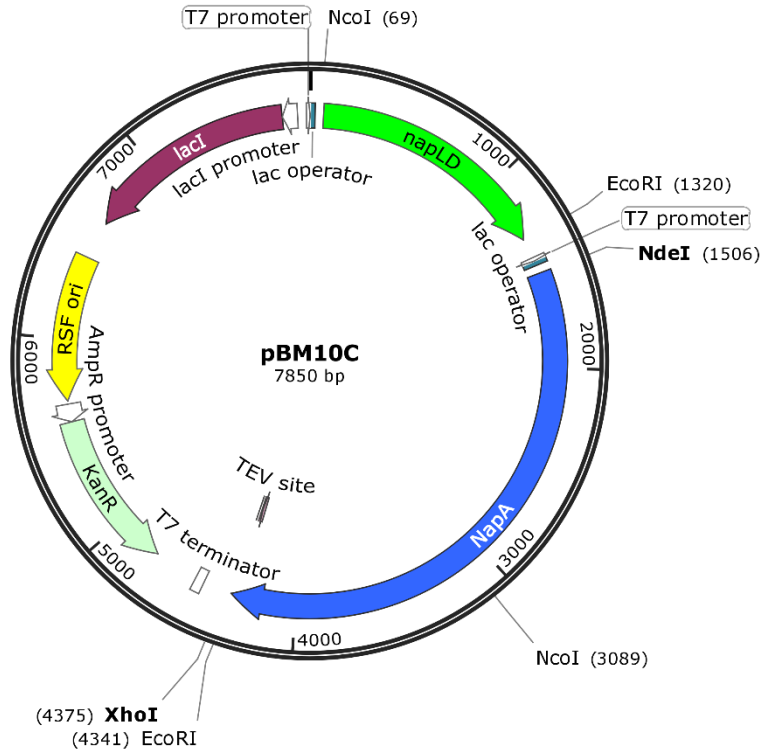


Figure 2.5: Plasmid map of pBM10C. Construct pBM10C contains the *C. jejuni napLD* genes inserted between the NcoI and EcoRI endonuclease sites and the *C. jejuni* His-tagged *napA* gene inserted between the NdeI and XhoI endonuclease sites of the pRSF-Duet-1 expression vector.

2.2.1 Molecular Cloning of the *C. jejuni nap* Genes

All molecular cloning primers were designed according to common microbiological methods, and synthesized by Integrated DNA Technologies (Coralville, IA, USA). Plasmids and oligonucleotides utilized in this endeavor are listed in Table 2.1. Polymerase Chain Reaction (PCR) mixtures and thermocycler parameters are listed in Appendix B. The pCnapA and pCnapLD constructs [302] were utilized as the source of *C. jejuni napA*, *napL* and *napD* genes. PCR was used to amplify *napLD* maturation genes (YP 178877 and YP 178878) and the DNA fragment was inserted into the pTZS7R/T TA cloning vector (Thermo Fisher) yielding plasmid pBM8A. The *napLD* genes were excised using NcoI and EcoRI and then inserted into the pRSFDuet-1 expression vector (Novagen) to yield plasmid pBM9A. The *napA* gene (YP 178873) was amplified using PCR and the restriction enzyme-digested fragment was inserted into the pMCSG32 vector (DNASU) using NdeI and XmaI upstream from the TEV cleavable C-terminal hexa-histidine coding sequence, yielding the pMCSG32_*napA* plasmid. The *napA* gene was excised with NdeI

and XhoI taking the tagged gene and inserting it into the same sites of pBM9A containing the maturation genes *napLD* to yield plasmid pBM10C. Thus, pBM10C (Figure 2.5) allows coexpression of His-tagged *napA* with untagged *napLD* in *E. coli* from separate T7 promoters. All DNA constructs were confirmed by sequencing (ACGT Inc) [305].

Table 2.1: Summary of plasmids and oligonucleotides used in the cloning of *C. jejuni napALD*.

Plasmid or Oligonucleotide	Description	Source
pTZS7R/T	TA cloning vector (Amp ^R)	Thermo Scientific
pRSF-Duet-1	Plasmid for coexpression of two target orfs (Kan ^R)	Novagen
pMCSG32	Plasmid encoding TEV-cleavable C-terminal hexa-histidine coding sequence (Amp ^R)	DNASU
pBM8A	1.25 kbp PCR amplified fragment including the <i>napLD</i> genes cloned into pTZS7R/T (Amp ^R)	This work
pBM9A	1.25 kbp NcoI-EcoRI restriction fragment from pBM8A including the <i>napLD</i> genes cloned into pRSF-Duet-1 at the corresponding restriction sites (Kan ^R)	This work
pMCSG32_ <i>napA</i>	NdeI-XmaI digested PCR amplified 2.8 kbp fragment including the <i>napA</i> gene cloned into pMCSG32 at the corresponding restriction sites upstream from the TEV-cleavable C-terminal hexa-histidine coding sequence (Amp ^R)	This work
pBM10C	NdeI-XhoI digested 2.8 kbp fragment including the <i>napA</i> gene and TEV-cleavable C-terminal hexa-histidine coding sequence from pMCSG32_ <i>napA</i> cloned into pBM9A at the corresponding restriction sites (Kan ^R)	This work
<i>napA</i> -NdeI	5'-AAG AAG GAG ATA TAC ATA TGA ATA GAA GGG ATT TTA TTA AAA ATA CCG C-3'	This work
<i>napA</i> -XmaI	5'-GGT GGT GCT CGA GCC CGG GAG CCT TAT AAA TTT TTA CAG C-3'	This work
<i>napLD</i> -NcoI	5'- GAT TAG CCA TGG GGA AAA AAT TTC TTT TTA TTT T-3'	This work
<i>napLD</i> -EcoRI	5'- GCT GCG GAA TTC TTA AGA AAA TTG ATT AAA TA-3'	This work

2.2.2 Bacterial Strains and Growth Conditions

Escherichia coli K12 (New England Biolabs Shuffle T7 *lysY* #C3027) cells containing the pBM10C plasmid were maintained on LB medium supplemented with 30 µg/mL kanamycin. Inoculated cultures were grown overnight at 37°C, then unless otherwise stated the cells were

transferred to 1 L of fresh auto-induction medium [320] containing 12 g/L peptone, 24 g/L yeast extract, 1 g/L glucose, 2 g/L lactose, 0.50% (v/v) glycerol and 90 mM potassium phosphate buffer pH 7.00. The cultures were supplemented with kanamycin (30 μ g/mL) and Na₂MoO₄ (1 mM), then incubated at room temperature for 48 h [305]. NapA (~108 kDa) expression was induced by the lactose present in the medium. Cells were collected by centrifugation at 4400 \times g at 4°C.

2.2.3 Expression Optimization Experiments

Traditional isopropyl- β -D-thiogalactopyranoside (IPTG) induction started with a small-scale culture of the pBM10C K12 strain in Luria-Bertani broth (LB) media. The small-scale culture was diluted 1:50 in the nutrient-rich terrific broth (TB) media and supplemented with molybdate and iron. The optical density (OD) was monitored regularly at 600 nm, and when the OD reached ~0.4-0.6 A.U., then NapA expression was induced by the addition of IPTG. IPTG binds the *lac* repressor protein, lacI, reducing its affinity for the operator enabling the T7 RNA polymerase to bind at the promoter site and begin transcription [321]. The induced cells were then allowed to grow and express NapA for a set time before being harvested. For these expression experiments, NapA was purified by an Immobilized Metal Affinity Chromatography (IMAC) spin column (Section 2.2.5.1) and then analyzed by SDS-PAGE. Prior to the development of the nitrate reductase assay, most expression experiments were analyzed by measuring the intensities of the NapA band in the denaturing SDS-PAGE gel. Each of the individual experiments optimizing several expression parameters are described in detail in the sections below.

2.2.3.1 IPTG Optimization

Four TB cultures were inoculated with the same small-scale culture. Each TB culture was induced with the addition of IPTG at a different concentration i.e. 0 mM, 1 mM, 10 mM, 100 mM IPTG final concentrations. The cells grew overnight at room temperature (~24°C) for a set induction time. NapA was purified by an IMAC spin column (Section 2.2.5.1) for each separate culture. NapA expression was compared determining the intensity of the NapA band using SDS-PAGE.

2.2.3.2 Glucose Optimization

Glucose addition was tested to reduce pBM10C plasmid leakiness. Again, four TB cultures were inoculated by the same small scale pBM10C *E. coli* K12 culture. A control TB culture was inoculated with the untransformed *E. coli* K12 strain. Of the four *napA*-containing cultures, one was untreated while IPTG was added to the second (1 mM final concentration of IPTG), glucose was added to the third (1% (w/v) final concentration of glucose) and both IPTG and glucose was added to the final culture. The cells were harvested and NapA expression was probed by SDS-PAGE as discussed above. Then, glucose concentration was optimized. Four TB cultures were inoculated by the same small scale pBM10C *E. coli* K12 culture and the concentrations of glucose tested were 0.5%, 1%, 2%, 4% (w/v). Utilizing the optimal glucose concentration, the IPTG concentration was reexamined. IPTG concentrations of 0.1, 1, 10, and 100 mM were tested during this optimization procedure. All cultures were harvested and NapA expression was probed by SDS-PAGE as discussed above.

2.2.3.3 Optimization of Induction Temperature

Similar to the experiments described above, four TB cultures were prepared. All cultures were supplemented with 0.5% (w/v) of glucose and inoculated with the same small scale pBM10C *E. coli* K12 culture. When an OD₆₀₀ of 0.4-0.6 AU was reached, 0.1 mM IPTG was added to induce NapA expression. The cultures were then transferred to different temperatures (16°C, ~24°C, 37°C, or 42°C) but were all terminated at the same time. All cultures were harvested and NapA expression was probed by SDS-PAGE as discussed above.

2.2.3.4 Optimization of Induction Time

One 450 mL TB culture was prepared and supplemented with 0.5% (w/v) of glucose before being inoculated with a small-scale pBM10C *E. coli* K12 culture. When an OD₆₀₀ of 0.4-0.6 AU was reached, 0.1 mM IPTG was added to induce NapA expression. The cells were grown at room temperature (~24°C) for up to 24 hours. Approximately 50 mL aliquots were taken and harvested at various times to obtain samples with induction times of 2, 4, 6, 8, 12, 16, 20, 24 hours. All cultures were harvested and NapA expression was probed by SDS-PAGE as discussed above.

2.2.3.5 Optimized IPTG Method

The optimized traditional IPTG induction method for NapA expression was determined to be as follows. First, a small-scale culture of the pBM10C K12 strain in LB media in grown overnight (~16 h). The small-scale culture was diluted 1:50 in the nutrient-rich TB media and supplemented with molybdate and glucose (final concentrations of 1.1 mM and 0.5% (w/v), respectively). The OD was monitored regularly at 600 nm, and when the OD reached ~0.4-0.6 AU, then NapA expression was induced by the addition of IPTG (final concentration 0.1 mM). Cultures grew at room temperature (~24°C) for 12-16 hours. Growth was terminated by harvesting the cells via centrifugation @ 4400 x g at 4°C.

2.2.3.6 Auto-induction Method

A small-scale culture of the pBM10C K12 strain in LB media was grown overnight (~16 h) at 37°C. The small-scale culture was diluted 1:50 in the nutrient-rich auto-induction media. The auto-induction medium recipe was supplied by Dr. Alex Latta [320]. For a 1 L batch of auto-induction media, the solution contained 12 g/L peptone, 24 g/L yeast extract, 1 g/L glucose, 2 g/L lactose, 0.50% (v/v) glycerol and 90 mM potassium phosphate buffer pH 7.00. The cultures were supplemented with kanamycin (30 µg/mL) and Na₂MoO₄ (1 mM), then incubated at room temperature for 48 h. NapA (~108 kDa) expression was induced by the present lactose and growth was terminated by harvesting the cells via centrifugation @ 4400 x g at 4°C.

2.2.4 Anaerobic versus Aerobic Expression Comparison

Batches of 1-2 L of NapA expression strain (pBM10C in *E. coli* K12) in auto-induction media were grown under several conditions: 1) aerobic growth for 24 h with agitation; 2) aerobic growth for 48 h with agitation; 3) anaerobic growth for 24 h with agitation; 4) anaerobic growth for 48 h with agitation; 5) anaerobic growth for 24 h without agitation; 6) anaerobic growth for 48 h without agitation. Anaerobically grown cells were additionally supplemented with 0.4% (v/v) DMSO, an alternative electron acceptor to replace oxygen. All cultures were harvested and NapA expression and Moco insertion was probed by SDS-PAGE and metal analysis, respectively.

2.2.5 Purification Optimization Experiments

2.2.5.1 IMAC Spin Columns

For expression optimization studies, partially purified samples enriched with NapA were compared by SDS-PAGE. To obtain the partially purified NapA enriched samples, cells were lysed by ultrasonication using 30-s pulses in 45-s intervals over 10 min in an ice bath. The lysate was centrifuged at $7100 \times g$ for 1 h at 4°C. The clarified lysate was loaded onto a homemade spin column containing His-Pur Ni-NTA Superflow Agarose Resin.

Briefly, the spin columns were prepared by adding approximately 2 mL of resin to a 15 mL conical tube to act as the affinity column. Resin settled by gravity and excess solution was removed. The resin was equilibrated by addition of 2-3 mL Tris-HCl Lysis buffer (10 mM Imidazole, 300 mM NaCl, 50 mM Tris-HCl pH 8.0). Resin was mixed with the newly added buffer and settled by gravity before excess solution was removed. This process was repeated three times to equilibrate the resin in Tris-HCl Lysis buffer. Approximately 10 mL of clarified lysate was loaded onto the makeshift column and the column was rotated on a test tube orbit shaker at 4°C for ~1 h. After this binding phase, the columns were centrifuged at $7100 \times g$ for ~10-15 min to pellet the resin. The unbound protein was siphoned off the resin.

Loosely bound undesirable contaminant proteins were washed from the column with wash buffer (30 mM imidazole 300 mM, NaCl 50 mM, Tris-HCl pH 7.0). About 2-3 mL of wash buffer was added to the resin and the column was mixed by the orbit shaker for ~15-30 min at 4°C. The columns were centrifuged at $7100 \times g$ for ~10-15 min to pellet the resin and the washed off protein was siphoned off the resin. The procedure was repeated for a total of three times. NapA was eluted by the addition of 2 mL elution buffer (400 mM Imidazole, 300 mM NaCl, 50 mM Tris-HCl pH 7.5). The column was mixed by the orbit shaker for 30 min at 4°C, then centrifuged at $7100 \times g$ for ~10-15 min to pellet the resin. The eluted NapA solution was siphoned off the resin and concentrated in a 30-kDa Amicon centrifugal filter until the final volume was under 500 μ L. This partially purified NapA enriched sample was then analyzed by SDS-PAGE.

2.2.5.2 Addition of Protease inhibitors:

Batches of 1 L of NapA expression strain (pBM10C in *E. coli* K12) were grown and harvested as in Section 2.2.3.6. Cells were harvested via centrifugation at $4400 \times g$ at 4°C. A

control sample with no additives was purified as above in Section 2.2.5.1. The control sample was compared to a sample containing the serine protease inhibitor, phenylmethylsulfonyl fluoride (PMSF), at a final concentration of 1 mM and to a sample containing the commercial protease inhibitor cocktail, Bacterial ProteaseArrest (G Biosciences Inc.), diluted 1:1000. Protease inhibitors were added to cells during lysis and then samples were purified and analyzed by SDS-PAGE as above in Section 2.2.5.1.

2.2.5.3 *Periplasmic Isolation*

Four methods of periplasmic isolation were tested and compared to a control where the cells were broken by sonication. The results of this experiment are discussed later in Section 2.3.3.1 Periplasmic Isolation. The four protocols are listed in detail below.

Method 1 was a lysozyme and ethylenediaminetetraacetic acid (EDTA) treatment incubated at 4°C. The cells were resuspended in sucrose buffer. Lysozyme and EDTA were added to a final concentration of 0.6 mg/mL and 5 mM respectively. The protein solution rotated on the orbit shaker for 1 h at 4°C. The solution was centrifuged at 3000 x g to pellet the spheroplasts. The periplasmic fraction in the supernatant was collected and purified further by using a Ni-NTA spin column as described above in Section 2.2.5.1.

Method 2 was identical to method 1 except the cells were incubated at 30°C in an incubator shaker at 175 rpm and Method 3 was a chloroform treatment incubated at room temperature. In method, 3 the cells were resuspended in Tris-HCl lysis buffer. Chloroform was added to a final concentration of 2% (v/v). The solution was incubated at room temperature (~24°C) in an incubator shaker at 175 rpm for ~15 min. Then 10 times more chloroform was added to the solution and centrifuged at 5800 x g at 4°C for 30 min. The periplasmic fraction in the supernatant was collected and purified further by using a Ni-NTA spin column as described above in Section 2.2.5.1.

Method 4 was the osmotic method which alters the salinity of the solution to use the osmotic pressure to disrupt the membrane. The cells were resuspended in 20 mM phosphate buffer pH 8.0 with 2% (w/v) sucrose. EDTA was added to a final concentration of 16 mM and then the cells incubated at room temperature (~24°C) for 10 min. The solution was centrifuged at 3000 x g 4°C for 10 min. The supernatant was removed, and the pellet was washed with 5 mL cold Millipore water then centrifuged at 3000 x g 4°C for 20 min. The supernatant was removed, and the pellet

was resuspended in phosphate-sucrose buffer. Lysozyme was added to a final concentration of 1 mg/mL, and the solution was incubated at room temperature (~24°C) 175 rpm for 1 h. The solution was centrifuged at 3000 x g 4°C for 20 min. The periplasmic fraction in the supernatant was collected and purified further by using a Ni-NTA spin column as described above in Section 2.2.5.1.

2.2.5.4 Affinity Chromatography

Liquid chromatography steps were conducted on an Äkta Prime Plus LC system (GE Healthcare). Sample was loaded onto a HisTrap HP 5 mL prepacked column (GE Life Sciences) at 5 mL/min. Initially, a linear gradient was utilized. The gradient started from 0% Buffer A (50 mM HEPES, 300 mM NaCl, 10 mM imidazole pH 7.0) to 100% Buffer B (50 mM HEPES, 300 mM NaCl, 250 mM imidazole pH 7.0) over a volume of 400 mL. Later, an optimized step gradient was introduced. The step gradient washed the column first with 5 column volumes of 4% buffer B (~20 mM imidazole), then a second step of 5 column volumes of 17% buffer B (~50 mM imidazole), and finally eluting NapA with 5 column volumes of 100% buffer B (250 mM imidazole).

2.2.5.5 Size Exclusion Chromatography

Liquid chromatography steps were conducted on an Äkta Prime Plus LC system (GE Healthcare) with either the SEC buffer (150 mM NaCl, 50 mM HEPES pH 7.0) or the NaCl-free SEC buffer (50 mM HEPES pH 7.0). Sample was loaded onto a HiPrep 16/60 Sephacryl S-200 size exclusion column (GE Healthcare) at 0.2 mL/min. Fractions were collected overnight at 4°C in a chromatography cabinet. Elution of the complete NapA peak(s) took approximately 6.5 h. The eluted fractions were tested for activity and the active fractions were pooled and concentrated as isolated NapA. NapA was eluted too close to the exclusion limit of the HiPrep 16/60 Sephacryl S-200 column to calibrate the column for the purpose of determining NapA's molecular weight empirically. With the assistance of Dr. Millie Georgiadis, a Superdex-200 column (GE Healthcare) was calibrated and utilized to determine NapA's molecular weight (flow rate: 0.5 mL/min). The average distribution constant (K_{av}) and elution data from proteins ribonuclease A (13,700 Da), carbonic anhydrase (28,000 Da), ovalbumin (43,000 Da), bovine serum albumin (67,000 Da),

catalase (232,000 Da), ferritin (440,000 Da), thyroglobulin (669,000 Da), and blue dextran (2,000,000 Da) were used to construct a calibration curve for elution from the Superdex-200 column.

2.2.5.6 Final Optimized Protocol for Purification of Recombinant *C. jejuni* NapA

The final procedure for purification of recombinant *C. jejuni* NapA has been recently published [305]. The cell pellet was resuspended in ice cold buffer containing 50 mM HEPES, 300 mM sodium chloride, and 10 mM imidazole at pH 7.00. Cells were lysed by ultrasonication using 30 s pulses in 45 s intervals over 10 min in an ice bath. The lysate was centrifuged at $7100 \times g$ for 1 h at 4°C. The soluble fraction was loaded on a HisTrap HP 5 mL prepacked column (GE Life Sciences), and separation was conducted with an ÄKTA Prime Plus (GE Life Sciences) system. The column was washed with a step gradient of 20 mM and 50 mM imidazole. NapA was eluted with 250 mM imidazole. The fractions were pooled and concentrated using 30-kDa cutoff centrifugal filters (Millipore). The concentrated protein was loaded onto a HiPrep 16/60 Sephacryl S-200 size exclusion column (GE Healthcare). The resulting NapA fractions were pooled, concentrated and stored in buffer containing 50 mM HEPES pH 7.00 at –80°C.

2.2.6 SDS-PAGE

SDS-PAGE gels were poured in house composed of 10% acrylamide resolving and 4% acrylamide stacking gels. The complete recipe is listed in Appendix C. SDS-PAGE gels were inserted into the Bio-Rad Mini-Protean Tetra System and submerged in 1X TG-SDS buffer (VWR Chemicals LLC, Solon, OH, USA). Protein samples were normalized to total protein concentration of 0.4 µg/mL and prepared in Laemmli Sample Buffer (Bio-Rad). SDS-PAGE samples were mixed and briefly centrifuged before being heated at 95°C for 5 min. Approximately 5 µL of sample was loaded per lane and 5 µL of PageRuler Plus Prestained Protein Ladder (Thermo Scientific, Rockford, IL, USA) was loaded to a single lane. Electrophoresis was run at 121 V until the dye front reached the bottom of the gel without running off the gel. The gels were stained in Coomassie Quick Stain (recipe in Appendix C) and then destained overnight in 10% (v/v) acetic acid. The gels were imaged utilizing a Bio-Rad Gel Doc EZ system. Image Lab 4.1 software was used to determine the density of protein bands in addition to editing the gel images.

2.2.7 Activity Assays

NR activity was measured spectrophotometrically by monitoring oxidation of reduced methyl viologen at 630 nm or 600 nm. Methyl viologen was reduced electrochemically in an inert atmosphere glovebox using a Metrohm PGASTAT204 potentiostat in a three-electrode system with an Ag/AgCl reference electrode, a platinum wire auxiliary electrode and platinum mesh as the working electrode. The potential was held at -500 mV vs SHE (midpoint potential of methyl viologen is -449 mV vs SHE at pH 7.00; [322]) until methyl viologen was reduced. Assays were conducted in an inert atmosphere glove box at 25°C using a Bio-Tek ELx808 Absorbance Microplate Reader or a Bio-Tek EPOCH 2 Absorbance Microplate Reader. Nitrate addition initiated the reaction which was monitored for 5 min. The rate of methyl viologen oxidation was calculated using the Beer-Lambert law given the extinction coefficient of reduced methyl viologen ($7800\text{ M}^{-1}\text{ cm}^{-1}$ at 630 nm; $11407\text{ M}^{-1}\text{ cm}^{-1}$ at 600 nm). These rates were analyzed using OriginPro 2016-2018 (OriginLab Inc.). Protein concentrations were determined using the Pierce Coomassie Plus (Bradford) Protein Assay Kit (Thermo Scientific) with bovine serum albumin standard (Thermo Scientific) [305].

2.2.8 Mass Spectrometry

2.2.8.1 *Digested Peptide Analysis*

Mass spectrometry was conducted with the assistance of Dr. Jennifer McGarry. Protein samples were digested with trypsin/chymotrypsin [323] and loaded onto a $100\text{ }\mu\text{m} \times 2\text{ cm}$ Acclaim PepMap 100 C_{18} nano trap column ($5\text{ }\mu\text{m}$, $100\text{ }\text{\AA}$) (Thermo Scientific) with an Ultimate 3000 liquid chromatograph (Thermo Scientific) at $3\text{ }\mu\text{l/min}$. The peptides were separated on a silica capillary column that was custom packed with C_{18} reverse phase material (Halo peptide, $2.7\text{ }\mu\text{M}$, $160\text{ }\text{\AA}$). The samples were run at $0.3\text{ }\mu\text{l/min}$ starting with 96% solvent A (100% water, 0.1% formic acid) and 4% solvent B (100% acetonitrile, 0.1% formic acid) over 25 minutes followed by a 45-minute gradient from 10% to 90% solvent B. The column effluent was directly coupled to the Q-Exactive orbitrap mass spectrometer using a Flex ion source (Thermo-Fisher). The mass spectrometer was controlled by Xcalibur 2.2 software and operated in data-dependent acquisition mode. Spectra of peptide mass were acquired from an m/z range of 300-2000 at a high mass resolving power. The top 25 most abundant charged ions were subjected to higher-energy collisional dissociation (HCD)

with an m/z range of 300-2000 with intensity threshold of $3.3e^4$, charge states less than 7 and unassigned charge states were excluded [305].

The higher-energy collisional dissociated data were extracted using Proteome Discoverer (Thermo Fisher) using Sequest version 1.4.1.14 (Thermo Fisher). The files were searched against the Uniprot *E. coli* K12 database which contains 4313 proteins. The database also contained *C. jejuni* proteins of interest (NapA, NapD, and NapL). Sequest was searched with a fragment ion tolerance of 0.020 Da and a parent ion tolerance of 10 pm. Carbamidomethylation of cysteine was specified as a fixed modification. The enzyme specificity was set to trypsin/chymotrypsin with missed cleavage of 3. A target decoy data base search was performed. Peptide identifications were accepted with a target false discovery rate (FDR) between 0.05 (relaxed, moderate confidence) and 0.01 (strict, high confidence). The validation was based on the q-value which is the minimal FDR at which the ID is considered correct. A post database search filter was applied with an Xcorr value greater than 2 for high peptide confidence [305].

2.2.8.2 Intact Protein Analysis by Ion Mobility Mass Spectrometry

NapA samples were measured by ion mobility mass spectrometry by Dr. Jared Shaw at the Department of Energy on a Q Exactive UHMR Orbitrap mass spectrometer (Thermo Fisher Scientific). All samples were prepared and analyzed by Dr. Jennifer McGarry and Dr. Ian Webb. The NapA enzyme was expressed and purified according to the optimal purification method in Section 2.2.5.6 except that the sample was buffer exchanged into 100 mM ammonium acetate during the sSEC step. A sample of as-isolated protein concentration 14 mg/mL in 100 mM ammonium acetate pH 7.00 was diluted 10X and loaded into nanoelectrospray borosilicate capillaries and ionized with a platinum wire inserted into the sample solution. The charge state for the complex NapAD in the as-isolated protein mixture was isolated and 100 V of collisional energy applied to dissociate the complex in order to determine the molecular weights of the free NapD and free NapA. The mass spectrometric data was fit using UniDec1 where all charge states for a species were fit simultaneously to obtain the uncharged mass of NapA.

2.2.8.3 Metal Analysis by Inductively Coupled Plasma Mass Spectrometry (ICP-MS)

Metal analysis was conducted at the University of Pittsburgh with the assistance of Dr. Daniel Bain. Protein samples were measured by mass, then digested by the addition of concentrated sub-boil distilled trace metal grade nitric acid. The nitric acid/sample mix was evaporated to dryness. The residue was additionally digested by aqua regia and evaporated to dryness again. The doubly digested residue was diluted 100-fold with 2% nitric acid prior to measurement. In cases where organic materials were not completely dissolved, 30% hydrogen peroxide was added to the 2% nitric acid and the solution dried down again. This digestate was diluted 100-fold with 2% nitric acid as before. Dilutions were measured by mass. Internal standard spikes of beryllium, germanium and thallium were added to the diluted solution to assess instrument drift during analysis. Metal concentrations in these diluted solutions were measured on a PerkinElmer NexION 300X (Waltham, MA) inductively coupled plasma mass spectrometer. The instrument was calibrated before each run utilizing a five-point concentration curve. Drift was assessed by re-measuring samples along with blanks every ten samples. Diluted solution concentrations were transformed to actual concentrations using the mass measurements recorded during dilution [305].

2.3 Results

The *C. jejuni nap* genes were successfully cloned into the pBM10C construct (Figure 2.5). The pBM10C construct, containing the His-tagged *C. jejuni napA* with untagged *C. jejuni napLD* genes, was transformed into *E. coli* K12 (New England Biolabs Shuffle T7 lysY #C3027) cells. *C. jejuni* NapA overexpression was optimized for the parameters of IPTG concentration, induction temperature, induction time, and media composition. NapA expression was first optimized for the traditional IPTG induction media. This optimized method was then compared to an auto-induction media that utilized the presence of glucose and lactose to slowly initiate gene expression. NapA purification was optimized utilizing affinity chromatography and size exclusion chromatography. The following sections describe in detail experiments conducted to obtain the optimized expression and purification methods (Sections 2.2.3.6 and 2.2.5.6 respectively) for isolating *C. jejuni* NapA.

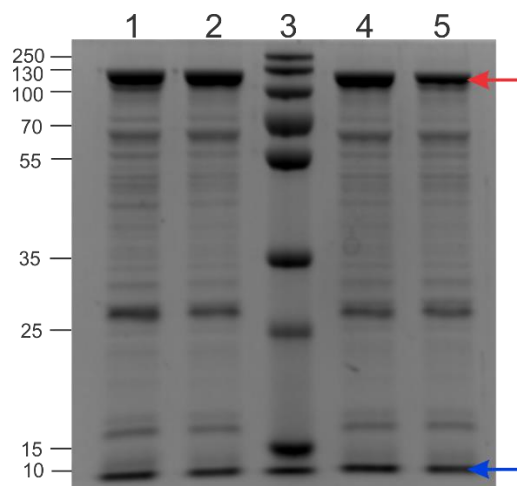


Figure 2.6: SDS-PAGE gel of enriched NapA (~108 kDa) samples where NapA was expressed under various IPTG concentrations. Lane 1- NapA expressed in the prescence of 0 mM IPTG, Lane 2- NapA expressed in the prescence of 1 mM IPTG, Lane 3- PageRuler Plus prestained protein ladder (kDa), Lane 4- NapA expressed in the prescence of 10 mM IPTG, Lane 5- NapA expressed in the prescence of 100 mM IPTG. The ~ 108-kDa NapA bands are denoted by the red arrow and the ~12 kDa NapD bands are denoted by the blue arrow.

2.3.1 Optimizing NapA Expression

NapA expression was optimized by determining the best conditions for enzyme expression. The optimal condition was established by determining the intensity of the NapA band in SDS-PAGE. The first expression parameter optimized was the concentration of IPTG used to induce NapA expression. (Figure 2.6). NapA yield was approximately 0.23 mg, 0.27 mg, 0.25 mg, and 0.24 mg for 0 mM, 1 mM, 10 mM, and 100 mM concentrations of IPTG respectively. As observed by lane 2 in Figure 2.6, an IPTG concentration of 1 mM is optimal. The higher IPTG concentration (lane 5, Figure 2.6) decreased NapA expression. Interestingly, NapA was expressed without the addition of IPTG suggesting that pBM10C had a leaky promoter. Upon further research into the *lac* operon, the *lac* promoter was reported as notorious for leaky expression in *E. coli* [324]. High expression occurs in the absence of the inducer due to low levels of the *lac* promoter repressor protein LacI, which relies on the expression of the single chromosomal gene compared to the multiple copies of the *lac* controlled expression vector [324]. Grossman *et al.* reported the addition of glucose reduced leaky expression [325]. Expression is not fully induced until all the glucose has been depleted [324].

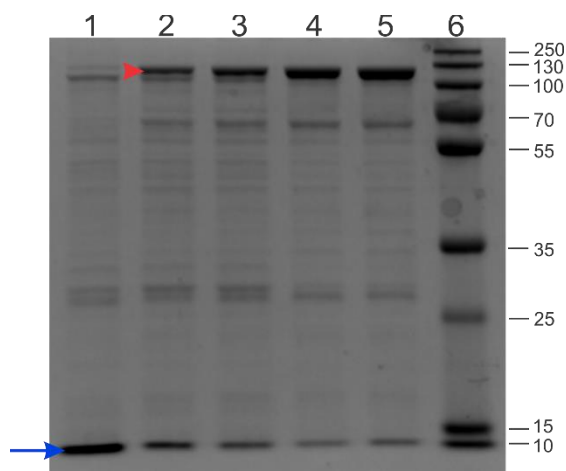


Figure 2.7: SDS-PAGE gel of enriched NapA (~108 kDa) samples where NapA was expressed under various conditions testing for leaky expression. Lane 1-Empty *E. coli* K12 strain expressed as a negative control, Lane 2- NapA expressed in the prescence of 0 mM IPTG and 0% (w/v) glucose, Lane 3- NapA expressed in the prescence of 1 mM IPTG and 0% (w/v) glucose, Lane 4- NapA expressed in the prescence of 0 mM IPTG and 1% (w/v) glucose, Lane 5- NapA expressed in the prescence of 1 mM IPTG and 1% (w/v) glucose, Lane 6- PageRuler Plus prestained protein ladder (kDa). The ~ 108-kDa NapA bands are denoted by the red arrowhead and the ~12 kDa NapD bands are denoted by the blue arrow.

Leaky expression was unfavorable for optimal cell growth and expression of active NapA due to the slight toxicity of enzyme in the host. Therefore, the amount of glucose added was the next expression parameter optimized. First, glucose was tested for the ability to reduce leaky expression. As depicted in Figure 2.7, the control did not produce a NapA band (Lane 1). As observed previously in Figure 2.7, the culture containing only pBM10C plasmid is leaky and produces a NapA band (Figure 2.7, Lane 2). Surprisingly, the culture with plasmid plus glucose (Figure 2.7, Lane 4) expressed a similar yield of NapA at 1.13 mg than the culture with plasmid plus IPTG at 1.18 mg of NapA (Figure 2.7, Lane 3). This is most likely due to the fact that glucose can be used as a carbon source by the cell increasing growth and thus expression. Glucose is reported to reduce leakiness but does not stop it entirely, so the optimal amount of glucose must be determined. The combination of IPTG and glucose addition (Figure 2.7, Lane 5) produced the most NapA as expected. From this experiment, it was determined that both the addition of glucose and IPTG needed to be optimized.

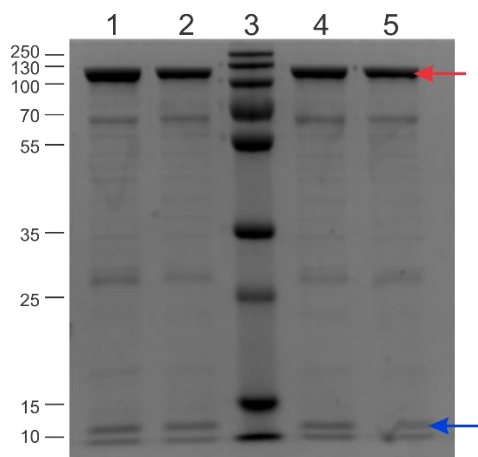


Figure 2.8: SDS-PAGE gel of enriched NapA (~108 kDa) samples where NapA was expressed under various glucose concentrations. Lane 1- NapA expressed in the presence of 0.5% (w/v) glucose, Lane 2- NapA expressed in the presence of 1% (w/v) glucose, Lane 3- PageRuler Plus prestained protein ladder (kDa), Lane 4- NapA expressed in the presence of 2% (w/v) glucose, Lane 5- NapA expressed in the presence of 4% (w/v) glucose. The ~ 108-kDa NapA bands are denoted by the red arrow and the ~12 kDa NapD bands are denoted by the blue arrow.

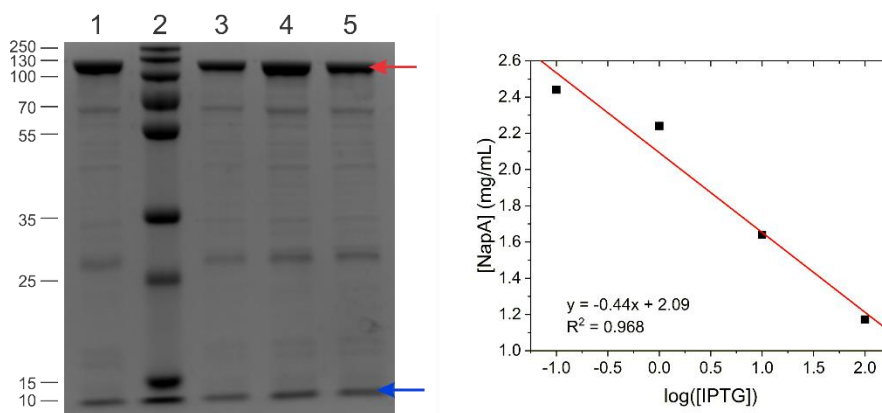


Figure 2.9: Left panel: SDS-PAGE gel of enriched NapA (~108 kDa) samples where NapA was expressed under various IPTG concentrations in the presence of 0.5% (w/v) glucose. Lane 1- NapA expressed in the presence of 0.1 mM IPTG, Lane 2- PageRuler Plus prestained protein ladder (kDa), Lane 3- NapA expressed in the presence of 1 mM IPTG, Lane 4- NapA expressed in the presence of 10 mM IPTG, Lane 5- NapA expressed in the presence of 100 mM IPTG. The ~ 108-kDa NapA bands are denoted by the red arrow and the ~12 kDa NapD bands are denoted by the blue arrow. Right panel: NapA expression plotted as a function of the logarithmic IPTG concentration. NapA expression decreases with increasing IPTG concentration.

Glucose concentrations were tested first, then IPTG was retested to see if the combination of glucose and IPTG shifted the optimal concentration for NapA expression. The glucose concentrations tested were 0.5%, 1%, 2%, and 4% (w/v) with NapA yields of 1.21 mg, 0.80 mg,

1.11 mg, and 1.00 mg respectively. As observed in Figure 2.8, the optimal glucose concentration was 0.5% (w/v) (Lane 1). Utilizing the optimal glucose concentration, the IPTG concentration was reexamined. IPTG concentrations of 0.1, 1, 10, and 100 mM were tested and depicted in Figure 2.9 with yields of 1.22 mg, 1.12 mg, 0.86 mg, and 0.82 mg of NapA respectively. The yield of NapA decreased with increasing IPTG concentration which may reflect the increased cellular toxicity as a result of NapA expression. The cells may increase protease production to reduce the concentration of the toxic protein at higher IPTG concentrations. The optimal concentration of IPTG, when 0.5% glucose is used in the media, is 0.1 mM IPTG (Figure 2.9, Lane 1).

NapA contains molybdenum cofactor (Moco) that is required for activity. The molybdenum enzyme literature mostly reports that lower temperatures and longer induction times increase Moco incorporation [57, 72]. There are a few exceptions [67, 96, 127] to this rule that can produce active enzyme at higher temperatures in shorter growth periods, for example Ivanov *et al.* reported 89% molybdenum incorporation in xanthine dehydrogenase (XDH) when the enzyme was expressed at 37°C for 4-5 hours [127]. Induction temperature and time were tested for NapA expression to ensure the optimal production of NapA. NapA yields of 0.39 mg, 0.56, 0.29 mg, and 0.14 mg were obtained for induction temperature of 16°C, 24°C, 37°C, and 42°C respectively. The optimal NapA expression temperature was determined to be room temperature (~24°C) as displayed in Figure 2.10, Lane 3. Finally, the optimal induction time was determined in a similar fashion. Illustrated in Figure 2.11, induction times from 12-24 hours (Lanes 6-9 respectively) gave reasonably close expression amounts of NapA with yields of 0.12 mg, 0.22 mg, 0.50 mg, 0.43 mg, 0.97 mg, 0.85 mg, 0.69 mg, and 0.58 mg for 2 h, 4 h, 6 h, 8 h, 12 h, 16 h, 20 h, and 24 h induction times respectively. The 12 h sample (Lane 6) had the most NapA expression.

The optimized traditional method of IPTG induction was compared to an auto-induction method. The auto-induction method uses set concentrations of glucose and lactose to slowly initiate NapA expression by depending on bacterial energy source regulation mechanisms. The cell will utilize glucose first because catabolite repression and inducer exclusion prevent the uptake of lactose by lactose permease. Then once glucose is absent, it will start to use lactose. Lactose will be converted to allolactose, the natural inducer of the *lac* operon, which initiates NapA expression via interaction with the *lac* repressor [100]. The cells grow ~48 h to enable slow protein expression as well as applicable time for Moco incorporation.

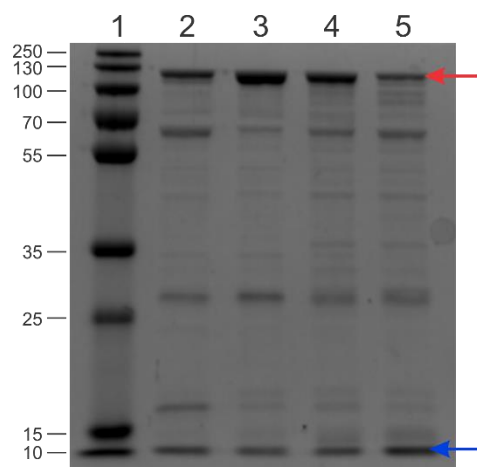


Figure 2.10: SDS-PAGE gel of enriched NapA (~108 kDa) samples where NapA was expressed at various temperatures. Lane 1- PageRuler Plus prestained protein ladder (kDa), Lane 2- NapA expressed at 16°C, Lane 3- NapA expressed at room temperature (~24°C), Lane 4- NapA expressed at 37°C, Lane 5- NapA expressed at 42°C. The ~ 108-kDa NapA bands are denoted by the red arrow and the ~12 kDa NapD bands are denoted by the blue arrow.

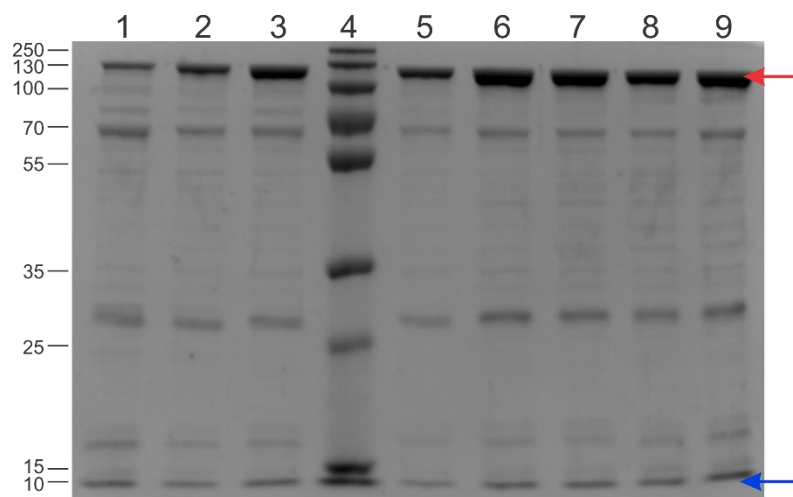


Figure 2.11: SDS-PAGE gel of enriched NapA (~108 kDa) samples where NapA was expressed at various induction times. Lane 1- NapA expressed for 2 h, Lane 2- NapA expressed for 4 h, Lane 3- NapA expressed for 6 h, Lane 4- PageRuler Plus prestained protein ladder (kDa) Lane 5- NapA expressed for 8 h, Lane 6- NapA expressed for 12 h, Lane 7- NapA expressed for 16 h, Lane 8- NapA expressed for 20 h, Lane 9- NapA expressed for 24 h. The ~ 108-kDa NapA bands are denoted by the red arrow and the ~12 kDa NapD bands are denoted by the blue arrow.

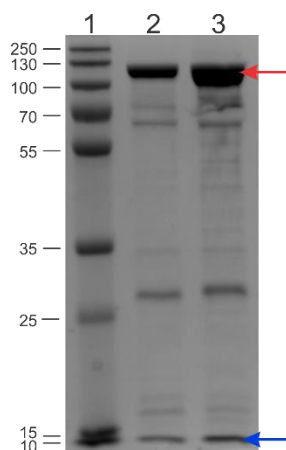


Figure 2.12: Traditional induction versus auto-induction. Lane 1- PageRuler Plus prestained protein ladder (kDa), Lane 2- NapA expressed by the optimized traditional induction method, Lane 3- NapA expressed by auto-induction. The ~ 108-kDa NapA bands are denoted by the red arrow and the ~12 kDa NapD bands are denoted by the blue arrow.

Comparison of the two expression methods revealed that the auto-induction method produces more NapA as observed in Figure 2.12 with a NapA yield of 0.41 mg for traditional IPTG induction and 0.88 mg for the auto-induction method. Auto-induction media is richer with additional carbon sources which boost *E. coli* growth. Higher yields of *E. coli* produce more NapA. According to the molybdenum enzyme literature (refer to Chapter 1 Section 1.4.2.1b), lower temperatures and longer growth periods aid in the successful production and insertion of the Moco. Specific activities of the two NapA samples expressed by the two methods discussed above confirmed the NapA produced by the auto-induction method was 2.5 times more active than the NapA produced by the traditional IPTG induction method, which agrees with the current literature (Chapter 1). Thus, the final optimized expression method utilized for NapA expression was the auto-induction method.

2.3.2 Anaerobic Expression of NapA

NapA has an iron-sulfur cluster that is close to the surface of the enzyme and is prone to oxidative damage [130, 326, 327]. Most iron-sulfur enzymes are expressed and purified anaerobically to reduce oxidative damage. At this time, aerobic purification was the focus of this project and anaerobic purification was not attempted but it will be explored in the future. Anaerobic expression was tested regardless.

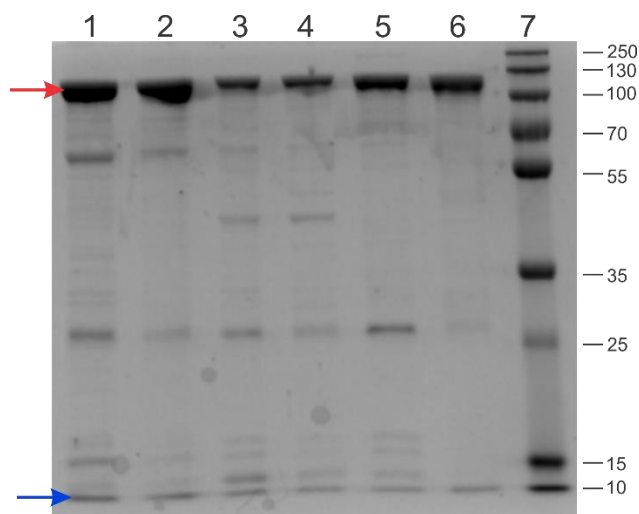


Figure 2.13: SDS-PAGE of anaerobically expressed NapA versus aerobically expressed NapA. Lane 1-NapA aerobically expressed for 24 h with agitation, Lane 2- NapA aerobically expressed for 48 h with agitaiton, Lane 3- NapA anaerobically expressed for 24 h without agitation, Lane 4- NapA anaerobically expressed for 48 h without agitation, Lane 5- NapA anaerobically expressed for 24 h with agitation, Lane 6- NapA anaerobically expressed for 48 h with agitation, Lane 7- PageRuler Plus prestained protein ladder (kDa). The ~ 108-kDa NapA bands are denoted by the red arrow and the ~12 kDa NapD bands are denoted by the blue arrow.

Aerobically grown cells grew better with a greater overall cell yield compared to the anaerobically grown cells (32 g/L vs 18 g/L). As observed by SDS-PAGE (Figure 2.13), the anaerobic cells without agitation produced less NapA than anaerobic/aerobic cells with agitation. Aerobic cells with agitation produced slightly higher amounts of NapA than anaerobic cells with agitation. Metal analysis of the NapA samples revealed that the 24-h expressed NapA had less molybdenum incorporation than the 48-h expressed NapA. Interestingly, NapA expressed aerobically had similar molybdenum incorporation as the anaerobically expressed enzyme. NapA expressed from both methods was very similar, and no improvement on iron-sulfur incorporation was observed in the metal analysis data. Thus, for convenience and a slight increase in protein yield, aerobic expression was preferred.

2.3.3 Optimizing NapA Purification

Once NapA expression had been optimized, NapA purification procedures were improved through similar experiments with the purification parameters. Purification parameters such as

fractionation method and supplements, as well as chromatography methods were investigated to optimize the quantity of active NapA purified from the heterologous system. The results of these investigations are discussed in the sections below.

2.3.3.1 Periplasmic Isolation

NapA is a periplasmic enzyme and thus a periplasmic isolation step would be ideal for purifying the enzyme and removing a bulk number of contaminants. Four methods of periplasmic isolation were tested and compared to a control where the cells were broken by sonication. The four protocols are listed in detail in Section 2.2.5.3. Briefly, method 1 was a lysozyme and EDTA treatment incubated at 4°C. Method 2 was identical to method 1 except the cells were incubated at 30°C. Method 3 was a chloroform treatment incubated at room temperature. Method 4 was the osmotic method which alters the salinity of the solution to use osmotic pressure to disrupt the membrane.

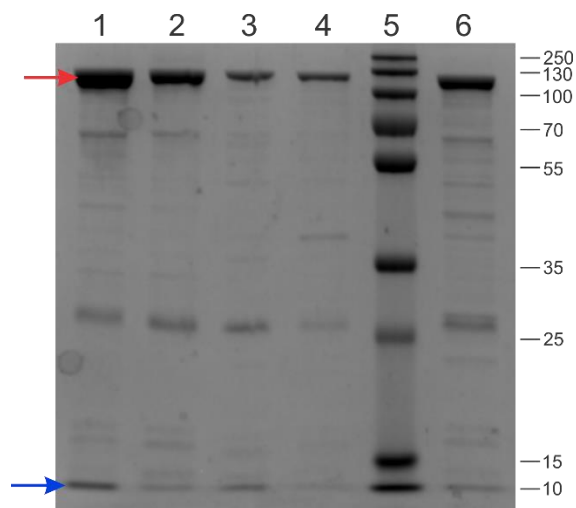


Figure 2.14: SDS-PAGE of periplasmic isolated NapA with various methods. Lane 1- NapA from sonicated control containing both cytoplasmic and periplasmic proteins, Lane 2- NapA isolated from method #1, Lane 3- NapA isolated from method #2, Lane 4- NapA isolated from method #3, Lane 5- PageRuler Plus prestained protein ladder (kDa), Lane 6- NapA isolated from method #4. The ~108-kDa NapA bands are denoted by the red arrow and the ~12 kDa NapD bands are denoted by the blue arrow.

Comparison of the four periplasmic isolation methods revealed that methods 1 (0.33 mg NapA) and 4 (0.36 mg NapA) were better than methods 2 (0.08 mg NapA) and 3 (0.23 mg NapA)

at producing the most NapA as observed in Figure 2.14. However, the periplasmic extraction did not produce more NapA than complete cell disruption by sonication (1.37 mg NapA). Metal analysis of method 1 and method 4 NapA compared to the control NapA isolated by sonication disclosed reasonable Mo incorporation for the control (50-90%) while the periplasmic extracted samples were below the detection limit. The overall yield of NapA extracted from the periplasm was less than 1/3 of that isolated by complete cell disruption. Periplasm isolation produced less NapA, and the enzyme was less active than compared to the complete cell disruption by sonication. Thus, sonication was used for complete cell disruption from this point on.

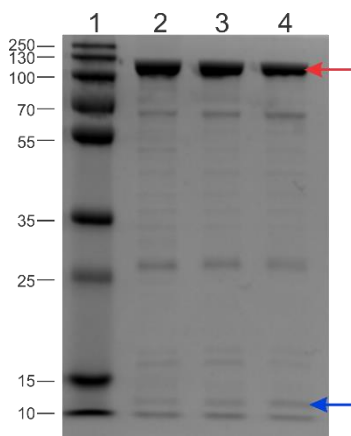


Figure 2.15: SDS-PAGE of NapA purified in the presence and absence of protease inhibitors. Lane 1- PageRuler Plus prestained protein ladder (kDa), Lane 2- NapA purified in the absence of the protease inhibitor cocktail and PMSF, Lane 3- NapA purified in the presence of the protease inhibitor cocktail and the absence of PMSF, Lane 4- NapA purified in the absence of the protease inhibitor cocktail and the presence of PMSF. The ~ 108-kDa NapA bands are denoted by the red arrow and the ~12 kDa NapD bands are denoted by the blue arrow.

2.3.3.2 Addition of Protease Inhibitors

NapA purification involved multiple steps over several hours and eventually over two days. Thus, the addition of protease inhibitors was tested to ensure the highest quantities of NapA could be obtained. The protease inhibitors were intended to prevent proteolytic degradation of NapA over the extended time for NapA isolation. However, no difference was observed between the control and the samples with protease inhibitor (Figure 2.15). The same approximate quantity of NapA was isolated (0.64 mg, 0.63 mg, and 0.53 mg for Figure 2.15 lanes 2, 3, and 4 respectively). As a result, the expensive protease inhibitors were not added in the optimized purification protocol to reduce the cost of NapA purification.

2.3.3.3 Affinity Chromatography

NapA was cloned with a C-terminal His-tag for purification by affinity chromatography. After cell disruption by sonication, the clarified lysate was loaded onto a HisTrap HP 5 mL prepacked column (GE Life Sciences). NapA was eluted by increasing the concentration of imidazole in the mobile phase. Various linear gradients were attempted. Initiating a gradient over 400 mL from 0% buffer B (~10 mM imidazole) to 85% buffer B (~340 mM imidazole) worked the best resulting in the cleaner fractions. (Figure 2.16) NapA begins to elute ~ 55 mM imidazole but is still fairly dirty. The elution of the majority of higher quality NapA fractions was around ~80-100 mM imidazole.

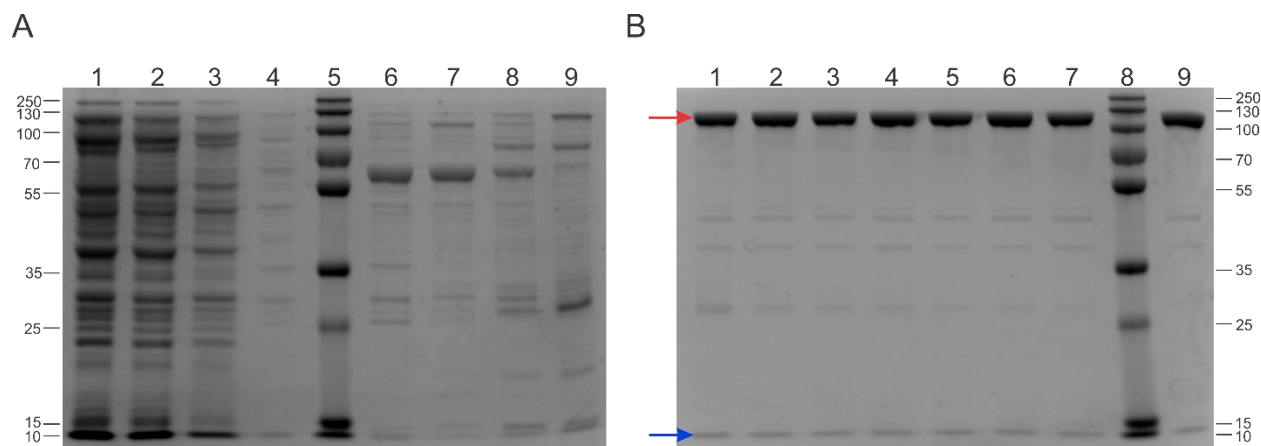


Figure 2.16: SDS-PAGE of NapA purification utilizing a linear imidazole gradient during the affinity chromatography step. A) Lane 1-clarified lysate, Lane 2-His-trap column flow through (non-binding proteins), Lane 3-washing with buffer A (wwbA) fraction #1, Lane 4-wwbA fraction #2, Lane 5- PageRuler Plus prestained protein ladder (kDa), Lane 6- linear imidazole gradient (lig) fraction # 12, Lane 7- lig fraction # 15, Lane 8- lig fraction # 19, Lane 9- lig fraction # 24. B) Lane 1- lig fraction # 34, Lane 2- lig fraction # 36, Lane 3- lig fraction # 37, Lane 4- lig fraction # 38, Lane 5- lig fraction # 39, Lane 6- lig fraction # 40, Lane 7- lig fraction # 41, Lane 8- PageRuler Plus prestained protein ladder (kDa), Lane 9- lig fraction # 42. The ~ 108-kDa NapA bands are denoted by the red arrow and the ~12 kDa NapD bands are denoted by the blue arrow.

The combination of a step and linear gradient was attempted to reduce the time constraints and lower the length of the gradient needed to purify NapA. Steps of 20 mM, 30 mM, 50 mM and 60 mM imidazole were introduced to wash the column at the respective imidazole concentrations eluting undesirable protein contaminants from the affinity column. An 80 mL linear gradient was initiated from 60 mM to 240 mM imidazole. The step gradient worked well, and no visible

difference was observed for the fractions over the linear gradient. Therefore, for convenience a quick protocol was developed that only required the use of a step gradient. This protocol reduced the wash steps to include a 10 mM, 20 mM and 50 mM imidazole wash steps. The elution step was set at 250 mM imidazole immediately after all the wash steps were complete (Figure 2.17). This step gradient was incorporated into the final optimized NapA purification protocol. Although NapA purified by affinity chromatography was purified to 80-90% homogeneity, there was still an unknown band at ~25 kDa that could possibly be peptidyl-prolyl cis-trans isomerase SlyD from *E. coli*, a probable NapD band at ~10-13 kDa and occasionally some light bands between 30-70 kDa (Figure 2.17).

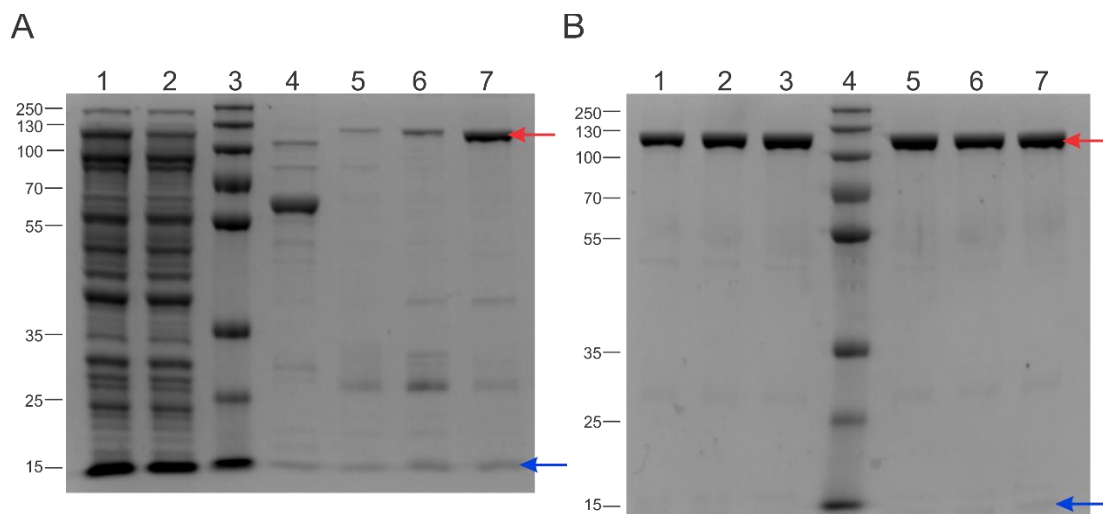


Figure 2.17: SDS-PAGE of NapA purified by a step gradient during the affinity chromatography step. A) Lane 1- clarified lysate, Lane 2-His-trap column flow through (non-binding proteins), Lane 3- PageRuler Plus prestained protein ladder (kDa), Lane 4- 20 mM imidazole wash step, Lane 5- 50 mM imidazole wash step, Lane 6- His-trap fraction #1-3, Lane 7- His-trap fraction #7-9. B) Lane 1- His-trap fraction #22, Lane 2- His-trap fraction #23, Lane 3- His-trap fraction #24, Lane 4- PageRuler Plus prestained protein ladder (kDa), Lane 5- His-trap fraction #25, Lane 6- His-trap fraction #26, Lane 7- His-trap fraction #27. The ~ 108-kDa NapA bands are denoted by the red arrow and the ~12 kDa NapD bands are denoted by the blue arrow. NapD is faint and running at the dye front.

2.3.3.4 Size Exclusion Chromatography

Further purification was achieved through size exclusion chromatography (SEC). After NapA was purified by affinity chromatography, the NapA fractions were pooled and concentrated under 2 mL to be loaded on a HiPrep 16/60 Sephacryl S-200 size exclusion column (GE

Healthcare). The sample was run initially in a mobile phase of Tris-HCl pH 7 at 0.2 mL/min overnight at 4°C. Size exclusion resulted in a loss of total protein but the NapA fractions were cleaner with a smaller percentage of the 25-30-kDa band (Figure 2.18). Concentration and buffer exchange of pure NapA for kinetic analysis was problematic. The NR assay was buffered in HEPES and the switch from Tris to HEPES often led to protein precipitation. The most likely reason for the precipitation is a change in ionic strength or pH when switching buffers. The ionic Tris-HCl buffer system has a higher ionic strength than the zwitterionic HEPES buffer. Zwitterions have been shown to not influence ionic strength directly [328]. Additionally, the Tris-HCl buffer is more temperature and concentration dependent when maintain the correct pH. To avoid precipitation of protein in the future the buffer system for the purification of NapA was switched from Tris to HEPES. Concentrating in HEPES without switching buffers was more effective at keeping the protein solubilized and more protein was retained in the soluble fraction. The ‘as isolated’ NapA eluted from the SEC column frequently as two peaks sometimes only partially resolved (Figure 2.19).

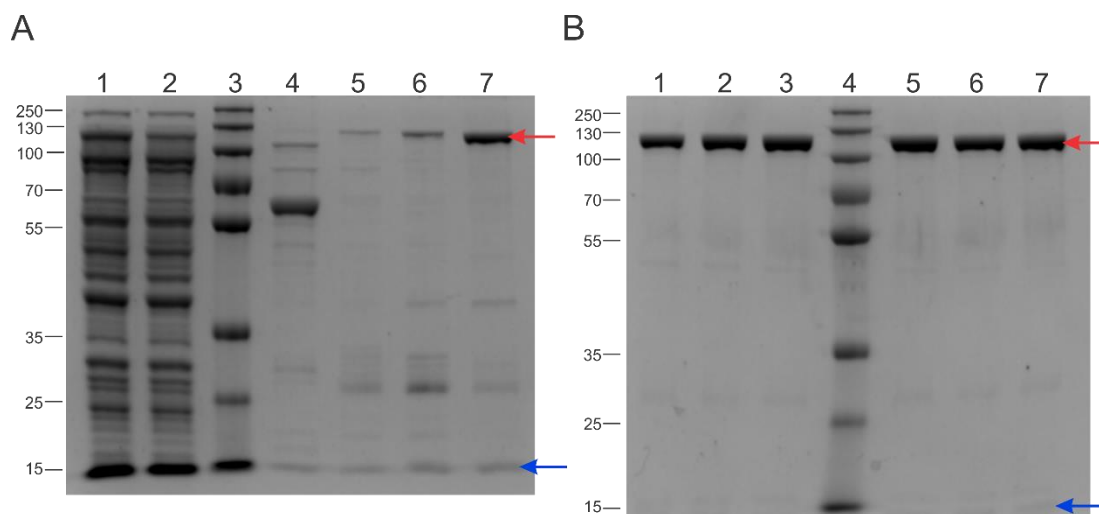


Figure 2.18: SDS-PAGE examples of Size Exclusion Chromatography (SEC) fractions. A) SEC resulted in a single peak. Lane 1- SEC fraction # 9, Lane 2- SEC fraction # 10, Lane 3- SEC fraction # 11, Lane 4- SEC fraction # 12, Lane 5- SEC fraction # 13, Lane 6- SEC fraction # 14, Lane 7- PageRuler Plus prestained protein ladder (kDa), Lane 8- Pure NapA. B) SEC resulted in two peaks. Lane 1- SEC peak #1 (eluted first), Lane 2- SEC peak #2 (eluted second), Lane 3- PageRuler Plus prestained protein ladder (kDa). The ~ 108-kDa NapA bands are denoted by the red arrow and the ~12 kDa NapD bands are denoted by the blue arrow.

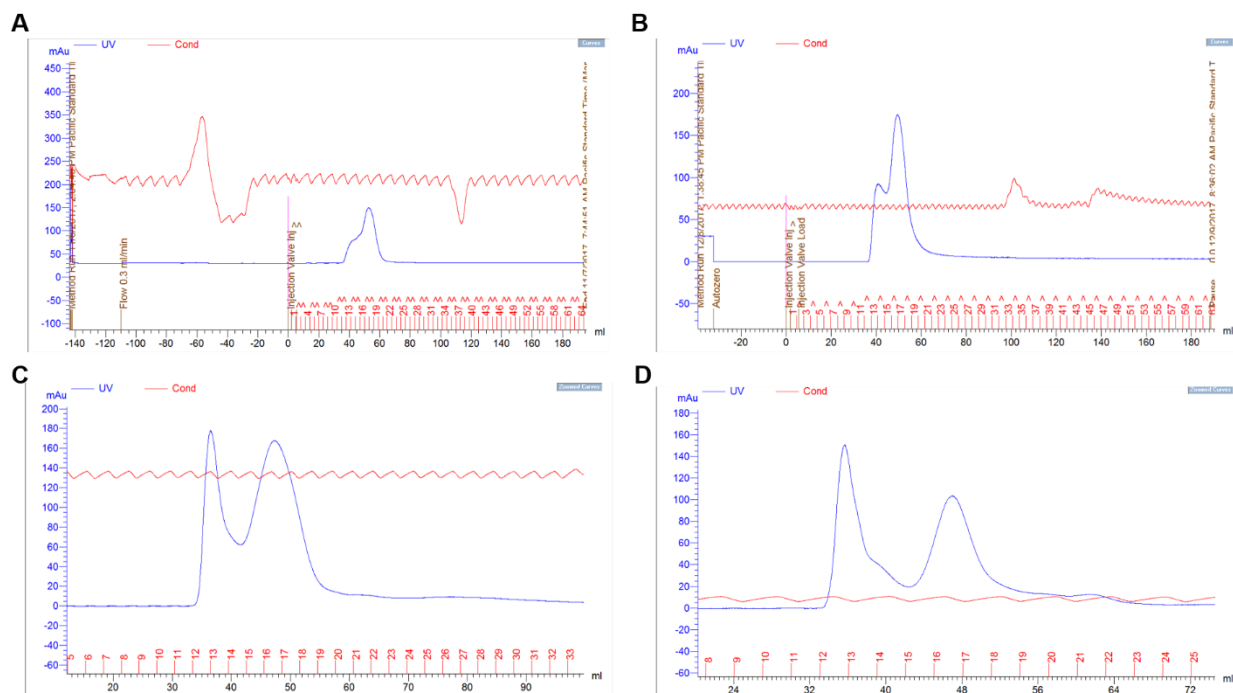


Figure 2.19: Example chromatograms of NapA as-isolated samples during SEC on the HiPrep 16/60 Sephacryl S-200 column when the two peaks are resolved differently at a flow rate of 0.2 mL/min. A) Native NapA isolated 11-7-17. B) Native NapA isolated 12-9-17. C) Native NapA isolated 3-23-18. D) Native NapA isolated 5-16-18.

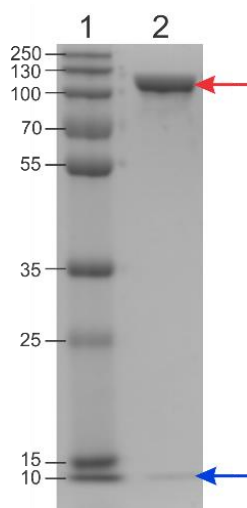


Figure 2.20: SDS-PAGE of NapA purified via the optimized protocol previously published [329]. Lane 1- PageRuler Plus prestained protein ladder (kDa), Lane 2- Pure NapA. The ~ 108-kDa NapA band is denoted by the red arrow and the ~12 kDa NapD band is denoted by the blue arrow.

1	MNRRDFIKNT	AIASAASVAG	LSVPSSMLGA	QEEDWKWDKA	VCRFCGTGCG
51	IMIARKDGKI	VATKGDPAAP	VNRGLNCIKG	YFNAKIMYGE	DRLVMPLLRM
101	NEKGEFDKKG	KFQQVSWQRA	FDMEKQFKK	AYNELGVTGI	GIFGSGQYTI
151	QEGYAALKLA	KAGFRTNNID	PNARHCMASA	VVGFMQTFGV	DEPSGCYDDI
201	ELTDTIITWG	ANMAEMHPIL	WSRVSDRKLS	NLDKVKVVNL	STFSNRTSNI
251	ADIEIIFKPN	TDLAIWNYIA	REIVYNHPEA	MDMKFIKDHC	VFATGYADIG
301	YGMRNNPNHP	KFKESEKDTV	EKENVITLDD	EEATSLSYLG	VKAGDKFEMK
351	HQGVADKNWE	ISFDEFKKGL	APYTLEYTAR	VAKGDDNESL	EDFKKKLQEL
401	ANLYIEKNRK	VVSFWTMGFN	QHTRGSWVNE	QAYMVHFLLG	KQAKPGSGAF
451	SLTGQPSACG	TAREVGTFSH	RLPADMVVAN	PKHREISEKI	WKVPAKTINP
501	KPGSPYLNIM	RDLEDGKIKF	AWVQVNNPWQ	NTANANHWIA	AAREMDNFIV
551	VSDCYPGISA	KVADLILPSA	MIYEKWGAYG	NAERRTQHWK	QQVLPVGAAM
601	SDTWQILEFA	KRFKLKEVWK	EQKVDNKLTL	PSVLEEAKAM	GYSEDDTLFD
651	VLFANKEAKS	FNPNDIAIKG	FDNTDVKGDE	RKIQGS DGKE	FTGYGFFVQK
701	YLWEEYRKFG	LGHGHDLADF	DTYHKVRGLR	WPVVNGKETQ	WRFNTKFDYY
751	AKKAAPNSDF	AFYGDFNKML	TNGDLIAPKD	EKEHSIKNKA	KIFFRPFMKA
801	PERPSKEYPF	WLATGRVLEH	WHSGMTMRV	PELYRAVPEA	LCYMSEKDGE
851	KLGLNQGDIV	WVESRRGKVK	ARVDMRGRNK	PPVGLVYVPW	FDENVYINKV
901	TLDATCPLSK	QTDFKKCAVK	IYKAPGENLY	FQSAGHHHHH	H

Figure 2.21: Mass spectrometry coverage map of *C. jejuni* NapA overexpressed in *E. coli* K12. The identified peptides are highlighted in red. A 73% coverage was obtained.

2.3.3.5 Optimized NapA Purification

Under the optimized conditions, as specified in Section 2.2.5.6, (Figure 2.20), approximately 15-20 mg of pure NapA is obtained from 10 L of culture resulting in a total yield of ~1.5-2 mg/L of culture. Mass spectrometry was utilized to confirm the observed band was in fact *C. jejuni* NapA (Figure 2.21). Interestingly, NapD was present in every NapA in-solution digest analyzed. Regardless, the isolated NapA was determined to be active and has high Mo incorporation as well (greater than 90% Mo incorporation on average).

2.3.3.6 Molecular Size Determination of NapA

Due to the elution of multiple peaks in the SEC column (Figure 2.19), as-isolated NapA's molecular weight was determined from a calibrated SEC column. The eluted NapA peak (Figure 2.22A) was eluted from the calibrated SEC column at ~12.5 mL. The eluted volume of NapA was used to calculate the average distribution constant, K_{av} , from equation (2.1) where V_e is the elution volume of the target protein, V_0 is the void volume, and V_c is the geometrical bed volume. For the

calibration of NapA on the Superdex 200 10/300 GL column, the parameters for calculating K_{av} are as follows: $V_0 = 7.65$ mL, the $V_c = 24$ mL, and $V_e = 12.5$ mL. The calibration curve in Figure 2.22B revealed that the as-isolated NapA enzyme elutes as one peak at approximately 127 kDa and the shoulder eluting at ~10 mL may represent a multimer of NapA with an estimated molecular weight of ~386 kDa, which are both higher than the expected ~108 kDa molecular weight of *C. jejuni* NapA.

$$K_{av} = \frac{V_e - V_0}{V_c - V_0} \quad (2.1)$$

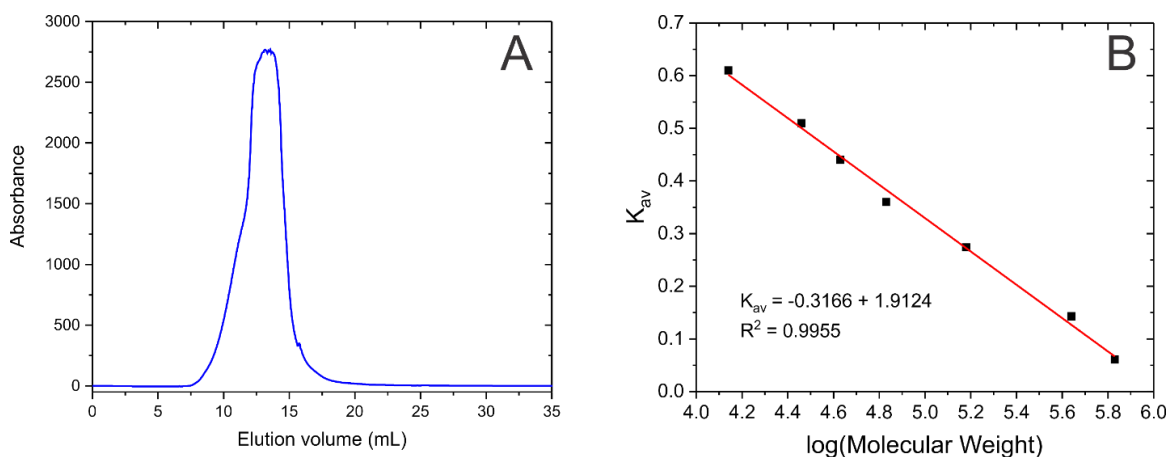


Figure 2.22: Size exclusion chromatography calibration for molecular weight determination. A) chromatogram of the eluted NapA peak. B) calibration curve for the Superdex-200 column at flow rate of 0.5 mL/min.

To confirm the molecular size of NapA and explore the reason NapD is present in the sample after size exclusion, as-isolated NapA was subjected to intact mass spectrometry. The as-isolated NapA enzyme exists mostly in a NapAD complex (Figure 2.23). NapAD (+22) complex mass in the full spectrum data was found to be 121,717 Da. When the charge state for the complex NapAD was isolated and 100 V of collisional energy applied, the complex mass was again 121,717 Da and the separated proteins free NapD and NapA were also identified. The NapD mass was calculated at 12,843.85 Da with a +7 charge. The NapA at a +15 charge state was calculated at 108,873 Da. The theoretical masses of NapD and NapA calculated from sequence are 12,844 Da and 108,871.33 Da, respectively, for the NapA Mo center with terminal oxo ligand.

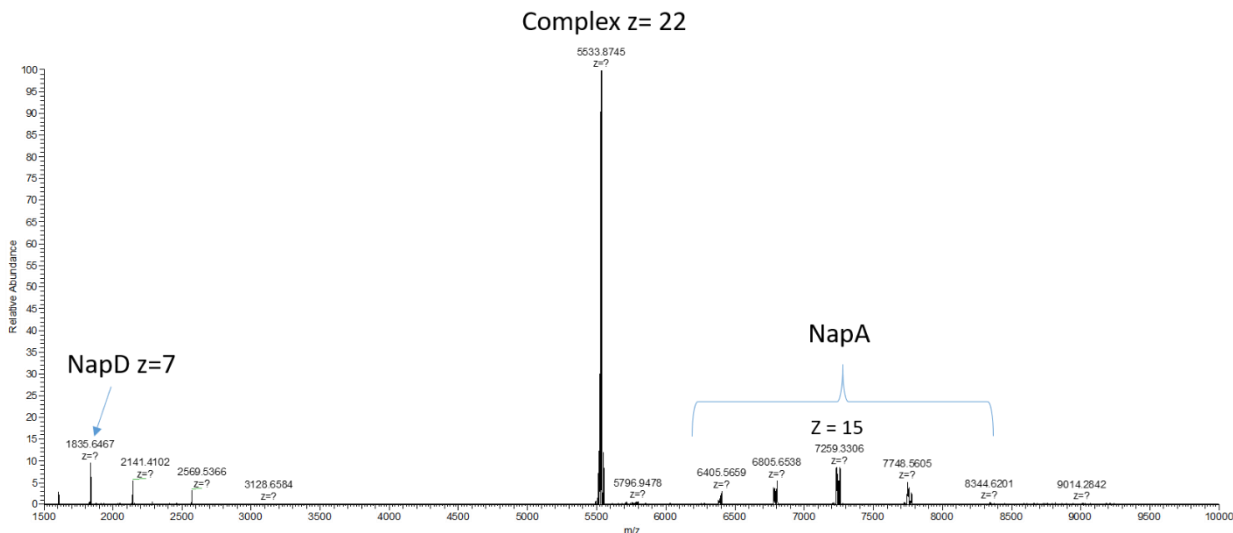


Figure 2.23: Intact mass spectrum of as-isolated NapA revealing the presence of a NapAD complex. This spectrum is the isolated m/z 5533 peak representing the complex and its CID fragments. Free NapA and free NapD were obtained with CID of the NapAD complex peak at ~100 V of collisional energy. Data was collected by Dr. Jared Shaw and the data analyzed by Dr. Ian Webb and Dr. Jennifer McGarry.

2.4 Discussion

C. jejuni NapA has been successfully cloned and expressed in *E. coli*. NapA was coexpressed with the maturation proteins NapL and NapD in *E. coli* K12. Expression experiments have confirmed literature precedent that low temperatures and longer growth periods produce more molybdopterin holoenzymes. Unexpectedly, the auto-induction media was superior in both protein yield and Moco incorporation as compared to the traditional IPTG induction method. The additional carbon sources as well as the slow transition to initiate translation of *nap* sequences significantly increased the yield of holo NapA.

NapA contains both a molybdopterin cofactor and a [4Fe4S] cluster, the latter of which is sensitive to oxidative damage. Since the [4Fe4S] cluster could be degraded by excess oxygen and nitrate respiration is naturally an anaerobic process, anaerobic expression of *C. jejuni* NapA in *E. coli*, where the cellular environment is naturally reducing, was investigated to increase holo enzyme isolated. However, only a slight difference in yield was observed. Anaerobic expression yielded slightly less NapA with similar molybdenum incorporation suggesting that the media may need additional nutrients to support anaerobic growth and that the electron acceptor DMSO may

not be the best choice due its formation of DMS, which may impact the cell negatively in high concentrations.

Expressing NapA with its natural TAT leader sequence was ideally designed to streamline purification procedures by isolating the mature enzyme from the periplasm where there are fewer protein contaminants. The periplasmic isolated NapA should have been more active based on reports that only mature NapA should collect in the periplasm especially since the cell has developed proofreading mechanisms to prevent early transport [330-332]. The opposite effect was observed. Most of the NapA produced was remaining in the cytoplasm in mature form. It's not impossible for the TAT complex to transport misfolded or unfolded proteins [332, 333] but it seems unlikely when NapD is still bound to the TAT (in a 1:1 ratio of NapD:NapA) as observed by mass spectrometry. The low NapA transportation observed may be due to inefficient TAT processing as a result of the differences between the *E. coli* and *C. jejuni* TAT machinery. Maillard *et al.* reported a strong anti-transport activity as a result of the tight binding of NapD to NapA [160]. Maillard further suggests NapD bound to the signal sequence could adopt a different conformation from free NapD that would allow it to “talk” to the NapA mature enzyme or to a second accessory protein [160]. The question, then is whether NapA is not fully mature thus NapD is still bound or whether the mechanism that triggers NapD release is missing.

This expression system uses the TAT leader sequence from *C. jejuni* to preserve the interaction with *C. jejuni* NapD while relying on the *E. coli* TAT enzyme complex to recognize the *C. jejuni* leader sequence for transport across the membrane. Poor TAT processing, which may be the result of poor compatibility or a completely missing accessory protein that interacts with NapD, would explain the low quantity of active NapA extracted from the periplasm. As observed by Hilton *et al.*, the TAT signal peptide can influence the yield of recombinant enzyme. Hilton *et al.* reported the *R. sphaeroides* DMSOR was inactive with the native signal sequence while activity was partially restored when an *E. coli* TAT signal sequence was used. However, the best expression of active recombinant *R. sphaeroides* DMSOR was observed when no signal peptide was present [54]. For the heterologous expression of *C. jejuni* NapA in *E. coli*, the *C. jejuni* TAT signal sequence or the NapD chaperone may be causing problems for the *E. coli* TAT complex resulting in inefficient *C. jejuni* NapA translocation, which is supported by the presence of TAT signal peptide in the mass spectrometrically analyzed samples. At this time, for this heterologous expression system in *E. coli*, a complete cell disruption method is the best method for obtaining

high quantities of active *C. jejuni* NapA. The impact this decision will have on the quality of NapA and the possibility of a heterogeneous mixture of NapA forms will be discussed in more detail in the characterization of NapA in Chapter 4. Since a periplasmic isolation step was no longer feasible due to the low enzyme yield and low activity, the bulk impurities were removed with chromatography. The *napA* gene was cloned with a cleavable His-tag for use in affinity chromatography. Affinity chromatography worked well with NapA purified to 80-90% homogeneity. The remaining impurities included an unknown band at ~25 kDa, a probable NapD band at ~10-13 kDa and occasionally some light bands between 30-70 kDa. SEC was employed as a final step to remove the lower molecular weight impurities. While SEC did remove the majority of remaining contaminants, multiple peaks eluted containing nitrate reductase activity.

Size exclusion would often result in a single peak with a shoulder or two resolved NapA peaks eluting from the Sephacryl S-200 column (Figure 2.19). ICP-MS analysis and specific activity of the two peaks revealed the first eluted peak (starting to elute at ~35 mL) had less activity and less Mo content than the second eluted peak (starting to elute at ~40-50 mL). Interestingly, when the SEC column was attempted to be calibrated for molecular weight determination of the peaks it was revealed that NapA which is expected to be ~108 kDa and easily resolved by the Sephacryl S-200 column was actually starting to elute in the void volume (~35-40 mL). Thus, the two peaks could represent some form of NapA that is on the edge of the resolution of the column, which may represent protein aggregation or the formation of a multimer. To test this theory NapA was run on a calibrated SEC column. Remarkably, NapA eluted as a single peak and a slight shoulder with determined molecular weights of ~127 and ~386 kDa for the peak and shoulder respectively (Figure 2.22A). It is possible that NapA is aggregating or forming a multimer in the form of $(\alpha\beta)_n$. From this point on, the two resolved NapA peaks are kept separated and the second eluted peak is used for NapA characterization due to the higher metal incorporation as seen in ICP-MS experiments.

The mixture of NapA states observed could be a result of incomplete maturation in *E. coli* and thus the protein is unstable and begins to aggregate over the 6.5 h time frame of NapA elution from the Sephacryl S-200 column. As a heterologous expression system, *C. jejuni* NapA relies on the protein production and Moco biosynthetic machinery of the host *E. coli*. The host produces a functional enzyme, but it may not produce the enzyme as efficiently as *C. jejuni*. For example, *C. jejuni* and *E. coli* use different codons and thus translation may be less efficient as a result. In

fact, several groups have utilized either codon-optimized genes or “codon plus” *E. coli* strains [30, 55, 180]. The two NapA forms could also represent a recognition problem between the NapA chaperone, NapD, the *C. jejuni* TAT leader sequence, and the *E. coli* TAT complex. The *E. coli* TAT leader sequence is different from the *C. jejuni* sequence (Figure 2.4) and as observed during the periplasmic isolation experiments, most of the active protein does not get exported as mentioned above. Furthermore, the process of concentrating the protein sample before it can be loaded onto the SEC column could also cause the protein to aggregate and start to precipitate out of solution. The aggregation could possibly result in partial denaturation of the enzyme and loss of Moco which would support the observation of the enzyme in the first eluted SEC peak containing less Mo.

Mass spectrometry has confirmed both SEC elution peaks to contain *C. jejuni* NapA and in every NapA in-solution digest analyzed by mass spectrometry, *C. jejuni* NapD has also been present. This suggests NapD is tightly bound to NapA in agreement with Maillard [160]. Intact mass spectrometry revealed the as-isolated NapA enzyme is isolated as a complex of NapA and NapD with a molecular weight of 121,717 Da (Figure 2.23). This observation is in agreement with the SEC calibration which revealed a peak of ~127 kDa for isolated NapA in the more active eluted peak. The first elute peak was much larger but at ~386 kDa this protein sample could represent aggregation and a multimer of the three NapAD complexes. The intact NapAD complex isolated in the mass spectrometer was further scrutinized by collision-induced dissociation (CID) and the NapAD complex was dissociated into free NapD and NapA proteins. The mass was determined to be 12,844 Da and 108,871. Da for free NapD and free NapA, respectively. The latter molecular weight is in good agreement with the expected molecular weight of the NapA enzyme.

Despite the observed presence of NapD, NapL has never been identified by mass spectrometry. This is not surprising as NapL is expected to be secreted to the periplasm prior to being folded by the SecT transport system [293, 312]. NapL has no tag in this expression system and if it is present in the periplasm, it cannot interact with NapA which, in this case, is mostly isolated from the cytoplasm as shown in Figure 2.14. The complete cell disruption method produced three times as much NapA as the periplasmic isolation methods. While NapL does influence NapA activity [293], active NapA is still produced despite the high probability that NapL is unable to perform its function in this heterologous system. NapL is mostly found in ϵ -proteobacteria [293, 312] and thus its function is highly specific to *C. jejuni* NapA compared to

previously isolated Naps. NapL's role and an improved expression system where NapA is transported to the periplasm and can interact with NapL is a project that should be pursued in the future.

The transport problem is not simple. To transport NapA effectively, the host strain would either need to be engineered to incorporate the *C. jejuni* TAT complex or *C. jejuni* NapA would need to be cloned with the *E. coli* TAT leader sequence. The former is a difficult project with no guarantee for success because the TAT enzymes are complex and imbedded in the membrane which could prove problematic in a foreign host. Utilizing the *E. coli* TAT leader sequence is an option with one caveat: Is the *E. coli* TAT sequence able to interact with *C. jejuni* NapD? If *C. jejuni* NapD cannot interact, then will NapA be inactive or will *E. coli* NapD be able to fill in? The answers to these questions are unclear and such aspects will need to be explored in the future. One experiment, described below, examines the necessity of *C. jejuni* NapD to NapA maturation and full activity.

NapA expression in the absence of *C. jejuni napLD* genes was conducted to reaffirm the necessity of using NapD and to demonstrate that *E. coli napD* still present in the host genome is not sufficient to produce mature *C. jejuni* NapA. The pMCSG32_napA expression construct was expressed in *E. coli* in the absence of *C. jejuni napLD* genes. Minimal NapA enzyme was purified from this system which may be a result of NapA being degraded by proteases in the absence of *C. jejuni* NapD. The isolated NapA was mostly in an immature form with low Mo incorporation (<10%) and very low activity indistinguishable from the background rates of the assay suggesting inactive NapA was isolated. While the functionality of NapL in the *E. coli* host is questionable, the absence of both maturation genes severely reduces NapA production and significantly reduces activity suggesting that the *E. coli* host is unable to supply alternative chaperones to efficiently mature *C. jejuni* NapA.

In addition to a maturation problem, the other possible reason for the two NapA forms observed in SEC could be the degradation of the enzyme during purification. As mentioned before, iron-sulfur clusters are prone to oxidative damage. Another possible reason for degradation of the NapA enzyme could be caused by the His-tag. Iron-sulfur cluster integrity and cleavage of the His-tag will be discussed in Chapters 3 and 4 respectively. Regardless, one form of NapA (the second SEC eluted peak) appears to have high Mo incorporation and high activity suggesting that although

there may be a TAT processing dilemma occurring, there is active NapA in the cytoplasm that can successfully be isolated and characterized.

2.5 Summary

C. jejuni NapA has been successfully heterologously expressed for the first time. Optimizations of expression revealed the expression construct is leaky and for an optimized IPTG induction NapA should be expressed with 0.1 mM IPTG and 0.5% glucose at room temperature for approximately 12-16 h. Periplasmic isolation of the expressed NapA enzyme revealed a TAT processing dilemma where very little active NapA was exported to the periplasm. An optimized method of expression and purification has been developed where cells are completely disrupted, and the crude enzyme is purified by affinity chromatography and SEC. The optimized method has a final yield of ~2 mg of active NapA per liter of culture.

Although 2 mg NapA/ L of culture is plenty for kinetic analysis and is a fair yield for the overexpression of a Moco enzyme, the NapA yield is still less than ideal for characterization techniques that require >30 mg/mL enzyme concentrations. The high demand of protein can be met by purifying multiple batchings and pooling the enzyme fractions. The current methods are successful but inconvenient in that a large amount of time and effort is still required to obtain the necessary quantities for spectroscopic characterization of the Mo center. Regardless, the project was able to move forward and NapA was investigated.

The isolated enzyme has high molybdenum incorporation but is isolated as a mixture of states as revealed by SEC and intact mass spectrometry. The functionality of NapL is questionable but the importance of NapD has been confirmed. NapD appears to be tightly bound to NapA and the isolated NapA enzyme is in reality a mixture of isolated free NapA enzyme and a NapAD complex. The intact mass spectrometry determined the as-isolated NapA sample is isolated predominantly in the NapAD complex form with a ratio of 1:1 of NapA:NapD. Despite the presence of NapD, NapA is still highly active. While the current expression system has introduced new questions about the maturation and processing of the heterologous enzyme in *E. coli*, the current expression system provides sufficient amounts of active NapA enzyme for biochemical characterization and investigations into *C. jejuni* NapA's structure and function.

CHAPTER 3. ACTIVITY AND CHARACTERIZATION OF RECOMBINANT PERIPLASMIC NITRATE REDUCTASE

A version of this chapter has been published as cited in reference [329]. Adapted by permission from Oxford University Press, FEMS Microbiology Letters, Copyright Liscence 4844410603268.

3.1 Introduction

Campylobacter jejuni has been classified as an emerging antibiotic-resistant pathogen that infects 400-500 million people annually across the globe [334-336]. Currently nearly 1% of Europe's population is infected [337]. The cost of these infections worldwide is close to ~\$8 billion [338] with ~\$1.7 billion being incurred in the U.S. alone [334]. *Campylobacter jejuni* is commonly present in the gastrointestinal tract (GIT) of chickens and can be transmitted to humans via contaminated food or water [339]. In infants, *C. jejuni* infection causes severe diarrhea in 6–12% of cases. This is a serious problem as diarrhea is the second leading cause of mortality in children globally [340]. Infection may also be detrimental to children as it is suggested to be an important contributor to growth defects, especially in low-resource settings [341]. Due to the increased antibiotic resistance of *C. jejuni* and the impact on human health, specifically infants and children, physiological understanding of *C. jejuni* and development of new therapeutic strategies are crucial.

Aside from gastroenteritis infections, pathogens like *C. jejuni* have been attributed to causing methemoglobinemia, a disease where methemoglobin is produced by the oxidation of the heme iron in hemoglobin Fe(III) preventing O₂ from binding [342]. Methemoglobinemia has also been linked to well water with high concentrations of nitrate [300]. However, re-evaluation of these studies indicates that the cases of incidence occurred with well water that was contaminated with feces [342]. Due to fecal contamination, the water contained appreciable amounts of bacterial pathogens such as *C. jejuni* as well as nitrate, implying methemoglobinemia may be induced by bacterial nitrate reduction producing NO that converts hemoglobin to methemoglobin. The nitrate reduction by *C. jejuni* has not been fully investigated despite a potential correlation between excess nitrate in well water, the presence of *C. jejuni* and methemoglobinemia. Therefore, there is a need to understand nitrate reduction in *C. jejuni* at the molecular level.

Nitrate reduction in *C. jejuni*, like in other bacteria, is catalyzed by a class of pterin-containing molybdenum enzymes called nitrate reductase. There are three subclasses of prokaryotic nitrate reductases: periplasmic (Nap), respiratory (Nar) and assimilatory (Nas) [12]. Of these, *C. jejuni* only harbors the *nap* genes [343]. Nap is a dissimilatory enzyme complex, i.e. it is a catabolic complex that reduces nitrate. When Nap is coupled to the oxidation of formate or NADH, a proton gradient is generated enabling the production of ATP. Moreover, Nap can generate energy through nitrate respiration as part of the denitrification and dissimilatory nitrate reduction to ammonia pathways in bacteria [12, 344].

Unlike many pathogens, *C. jejuni* has no defining toxins and relies on other mechanisms for infection [345]. The key metabolic pathways, like nitrate metabolism, that boost colonization may be one such mechanism. To this end, the oxidation of various electron donors such as FADH₂, H₂, formate, lactate or succinate can be coupled with nitrate (NO₃⁻) reduction. Succinate is readily available in the host's GIT [303] where NO₃⁻ reduction has been recognized as an influential factor during *C. jejuni* host colonization [339, 346]. Under inflammatory conditions the concentration of formate is increased and formate oxidation has been shown to be influenced by elevated nitrate levels [347].

During colonization in chickens, *C. jejuni* induces expression of the *napAGHBLD* operon [348] and during *C. jejuni* infection of mammalian cells, the expression of the catalytic subunit, NapA, is increased [339]. A *napA* deletion decreased the adhesion of *C. jejuni* to human INT-407 cells and impacted motility and biofilm formation [349]. Recently, Nap has been shown to be important in the pathogenesis of the intestinal pathogen *Salmonella typhimurium* that is also passed by poultry reservoirs to humans [350]. It has been demonstrated that a *napA* deletion reduces the ability to infect host cells signifying Nap influences pathogenesis [350]. This result may indicate a common mechanism for intestinal pathogen survival via nitrate respiration using Nap in the GIT when the human host consumes 30-130 mg of nitrate daily [299].

Campylobacter jejuni NapA has not been biochemically characterized despite the significance of NO₃⁻ reduction by this pathogen. It has also been reported that there is a potential use of nitrate reductase genes for differentiating *Campylobacter* species [351]. Given the paucity of biochemical characterization of *C. jejuni*, fundamental information to understand nitrate reduction by *C. jejuni* is lacking. The following study will aid in the understanding of the

fundamental properties of Nap from a pathogen, leading to a better appreciation of nitrogen metabolism in *C. jejuni*, ultimately gaining insight on a target of promising therapeutic potential.

The catalytic subunit of Nap, NapA, has been isolated from native organisms as a heterodimer with the electron transfer partner diheme c-type cytochrome NapB, from *E. coli* [61], *R. sphaeroides* [168], *Achromobacter fischeri* [352], *Cupriavidus necator* [353], and *Thiosphaera pantotropha* [354], or as a monomer from *D. desulfuricans* [355]. Whether the Nap is monomeric or heterodimeric depends on its ability to form salt bridges at the NapA:NapB interface [308, 311]. Two residues E47 and S772 (in *R. sphaeroides* Figure 3.1) have been identified as critical for the formation of the NapAB heterodimer [308]. The sequence alignment (Figure 2.4) of *C. jejuni* NapA with *R. sphaeroides* NapA shows the presence of a proline (P70) instead of a critical glutamate precluding the formation of the salt bridge. In light of this substitution, *C. jejuni* NapA was expected to be a monomer or a weak dimer in solution. *E. coli* NapA also contains this proline substitution and Jepson *et al.* reported that although NapA and NapB interact, the NapAB complex is not tight and the subunits purify independently [61]. NapA representatives from each class of gram negative *proteobacteria* have been isolated except the *Epsilonproteobacteria*. The class of *Epsilonproteobacteria* includes notable human pathogens like *Helicobacter* and *Campylobacter*. To date, *C. jejuni* NapA is the first active *Epsilonproteobacterial* NapA to be isolated and have its enzymatic properties explored.

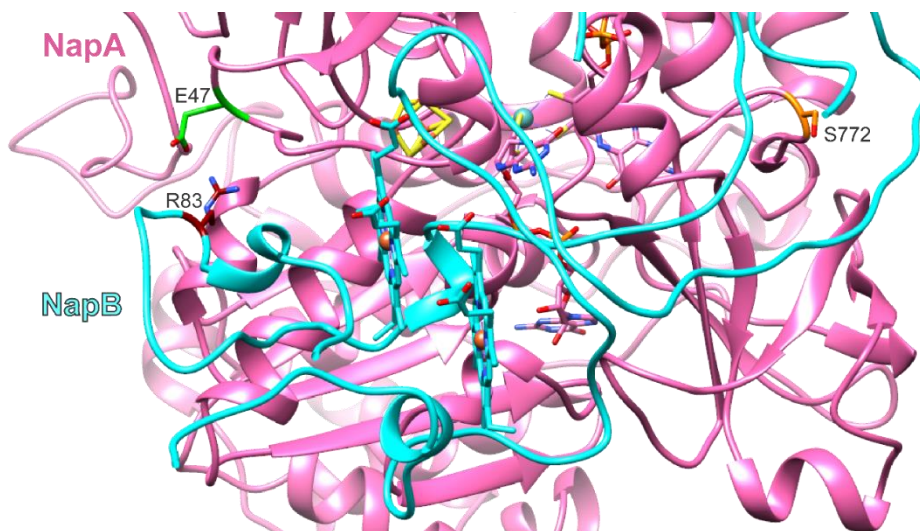


Figure 3.1: Interface of *R. sphaeroides* NapAB (PDB 1OGY) with NapA in pink and NapB in cyan. The essential residues reported by Simpson *et al.* [308] are highlighted as E47 in green, S772 in orange, and R83 in dark red. The image was created with Chimera and Corel Draw.

In summary, nitrate metabolism has been implicated in the virulence of pathogen *C. jejuni*, the leading cause of gastroenteritis. While there have been significant developments in the genetic and physiological knowledge on *C. jejuni*, fundamental information at the molecular level is necessary to fully understand nitrate reduction in this pathogen. In this chapter, the *C. jejuni* NapA enzyme will be biochemically characterized and kinetically analyzed to lay the foundation for probing the mechanism of this enzyme and for increasing the understanding of nitrate reduction in *C. jejuni*. The biochemical properties of NapA will be discussed in context of *C. jejuni* physiology.

3.2 Materials and Methods for Biochemical Characterization of NapA

Buffers and other reagents were purchased at the highest available grade from either Sigma-Aldrich (St. Louis, MO, USA) or Fisher Scientific (Pittsburg, PA, USA). The Pierce Coomassie Plus (Bradford) Protein Assay Kit, trypsin, and chymotrypsin were purchased from Thermo Scientific (Rockford, IL, USA).

3.2.1 UV-Vis Spectroscopy

UV-Vis spectra were collected on various protein concentrations in 50 mM HEPES pH 7.00 using an Agilent 8453 spectrophotometer scanning from 200-800 nm.

3.2.2 Protein Concentration Determination

Protein concentrations were determined using the Coomassie Plus (Bradford) Protein Assay Kit (Thermo Scientific) with bovine serum albumin as a standard (Pierce).

3.2.3 Mass Spectrometry

Mass spectrometry was conducted as described in Chapter 2 Section 2.2.8.1.

3.2.4 Metal Analysis

Metal Analysis was conducted at the University of Pittsburgh with the assistance of Dr. Daniel Bain as described in Chapter 2 Section 2.2.8.3.

3.2.5 Enzyme Kinetics

Nitrate reductase activity was measured spectrophotometrically by monitoring oxidation of reduced methyl viologen at 630 nm (ELx808) or 600 nm (Epoch2). Methyl viologen (MV) was reduced electrochemically in an inert atmosphere glovebox using a Metrohm PGASTAT204 potentiostat in a three-electrode system with an Ag/AgCl reference electrode, a platinum wire auxiliary electrode and platinum mesh as the working electrode. The potential was held at -550 mV vs SHE (midpoint potential of MV is -449 mV vs SHE at pH 7.00; [322]) until MV was reduced. Assays were conducted in an inert atmosphere glove box at 25°C using a Bio-Tek ELx808 Absorbance Microplate Reader or a Bio-Tek Epoch2 Absorbance Microplate Reader. Assays were conducted with a total reaction volume of 250-300 μL . Nitrate addition initiated the reaction which was monitored for 5 min (for native NapA). The rate of MV oxidation was calculated using the Beer-Lambert law given the extinction coefficient of reduced MV ($7800\text{ M}^{-1}\text{cm}^{-1}$ at 630 nm; $11407\text{ M}^{-1}\text{cm}^{-1}$ at 600 nm). The nitrate reduction rates were corrected for the concentration of active NapA in the as-isolated samples by utilizing the molybdenum content determine through ICP-MS to calculate the approximate concentration of holo active NapA in the total protein concentrations. These corrected rates were then analyzed with a non-linear Michaelis–Menten model using OriginPro 9 (OriginLab Inc.) [305].

For pH experiments, MV was prepared as above in the appropriate pH with the exception of pH 5.5 which would not stay reduced in multiple buffer systems. NapA was pre-reduced by treatment with the appropriate pH MV solution for approximately 30-60 minutes (pH 5.5 was pre-reduced with pH 6.0 MV). The enzyme was further buffer exchanged in the appropriate pH buffer. Substrate was also diluted in the proper pH buffer. Assays were conducted with a total reaction volume of 250 μL . The reaction was initiated, monitored and analyzed as described above. The reactions in pH 5.5 used a minimum volume of pH 6 MV replacing the pH 5.5 MV solution. The reaction mixture's pH was tested to confirm minimal shift in pH. Each pH curve was produced with one biological replicate with three technical replicates for each substrate concentration.

3.2.6 Homology Model

A three-dimensional model of the *C. jejuni* NapA structure was created by Dr. Courtney Sparacino-Watkins using the structure of *Rhodobacter sphaeroides* (PDB: 1OGY) NapA as the

template [302, 305]. The electrostatic potentials of NapA from *C. jejuni*, *D. desulfuricans*, *E. coli*, and *R. sphaeroides* were calculated in Pymol at pH 7.00 using the APBS plugin with the default settings. The images are colored where red is acidic, blue is basic, and white is neutral (-10 kT =red; 10 kT =blue; 0 kT =white). *D. desulfuricans* (2NAP), *E. coli* (2NYA), and *R. sphaeroides* (1OGY) structure data was downloaded from PDB.org database.

3.3 Results

3.3.1 NapA Characterization

The UV-Vis spectrum of *C. jejuni* NapA (Figure 3.2) shows a band at 400 nm similar to the band observed in the spectrum of *Desulfovibrio desulfuricans* NapA, indicating the presence of a $[4\text{Fe}_4\text{S}]$ cluster [355]. The metal (Mo and Fe) content in the enzyme was determined by inductively coupled plasma mass spectrometry (ICP-MS). The metal analyses indicate 92% Mo incorporation in active *C. jejuni* NapA. The Fe:Mo ratio was slightly higher than the theoretical value of 4:1 suggesting complete iron incorporation. Furthermore, the high molybdenum incorporation confirms an effective expression system for active *C. jejuni* NapA has been achieved. This represents the first example of a heterologously expressed functional periplasmic nitrate reductase.

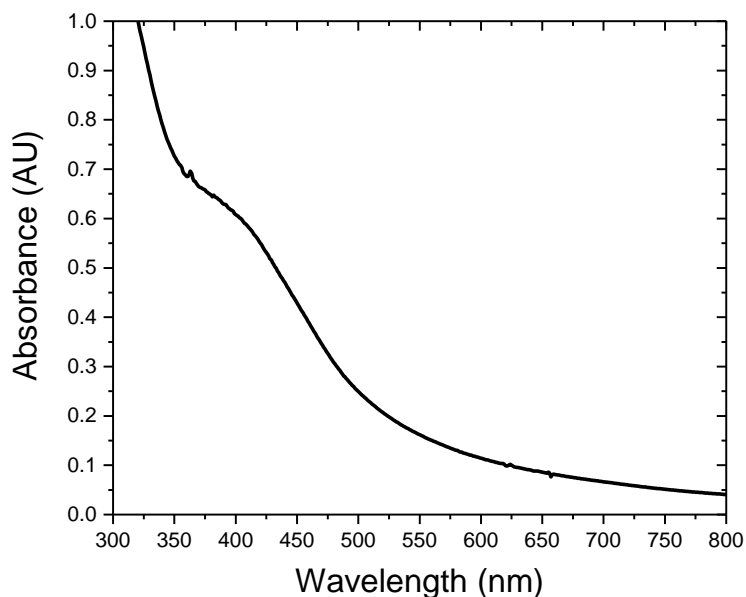


Figure 3.2: UV-Vis spectrum of as-isolated *C. jejuni* NapA in 50 mM HEPES pH 7.0.

The electrostatic potential was calculated for *C. jejuni* NapA, and, for comparison, the *R. sphaeroides*, *D. desulfuricans*, and *E. coli* NapA structures (Figure 3.3). In all structures, a dense region of positive charge is localized in the active site funnel, possibly used to facilitate the transport of NO_3^- into the cavity for catalytic transformation. The homology model [302, 305] suggests the substrate channel and catalytic pocket are more basic than other NapA proteins, which may influence the substrate binding as well as product release.

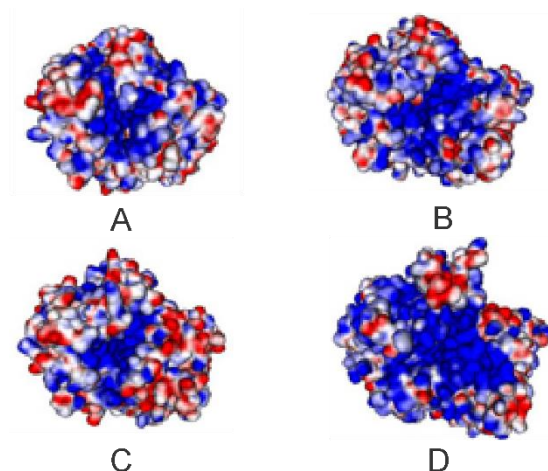


Figure 3.3: The electrostatic potential plots for NapA showing the active site face of (a) *D. desulfuricans*, (b) *E. coli*, (c) *R. sphaeroides* and (d) *C. jejuni*, *D. desulfuricans*, *E. coli* and *R. sphaeroides* (PDB codes 2NAP, 2NYA, and 1OGY, respectively) structure data were downloaded from PDB.org database. Comparison of the electrostatic maps reveals that NapA from *C. jejuni* is the most basic, as indicated by the blue color, while *R. sphaeroides* is the most acidic (red). *D. desulfuricans* and *E. coli* electrostatic potential maps are intermediate. The NapA structures were aligned and the electrostatic potentials were calculated in Pymol ($-10 \text{ kT} = \text{red}$; $10 \text{ kT} = \text{blue}$; $0 \text{ kT} = \text{white}$).

3.3.2 Nitrate Reductase Activity of NapA

Campylobacter jejuni NapA displays Michaelis-Menten kinetics (Figure 3.4), with a calculated maximum velocity (V_{\max}) of $3.40 \pm 0.10 \mu\text{moles min}^{-1} \text{ mg protein}^{-1}$ and a K_M for NO_3^- of $3.40 \pm 0.44 \mu\text{M}$. The determined k_{cat} was $5.91 \pm 0.18 \text{ s}^{-1}$ and the calculated kinetic putative second-order rate (k_{cat}/K_M) constant was $1.74 \times 10^6 \text{ M}^{-1} \text{ s}^{-1}$. A comparison of the K_M and V_{\max} values with those reported for other characterized NapA (Table 3.1) reveals important differences in the kinetic properties. The major difference is the low K_M of the heterologously produced *C. jejuni* NapA which indicates a high binding affinity for NO_3^- [305].

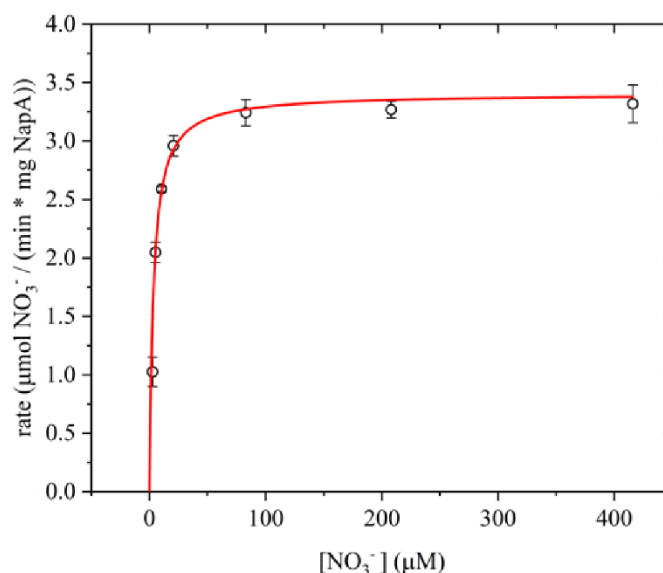


Figure 3.4: Steady-state kinetic analysis using the Michaelis-Menten model of the reduction of nitrate by *C. jejuni* NapA. The solid lines represent Michaelis-Menten fit. The data was analyzed, and the graph produced in Origin. This kinetics curve was reproduced by at least ten biological replicates. Each curve contained three technical replicates for each substrate concentration.

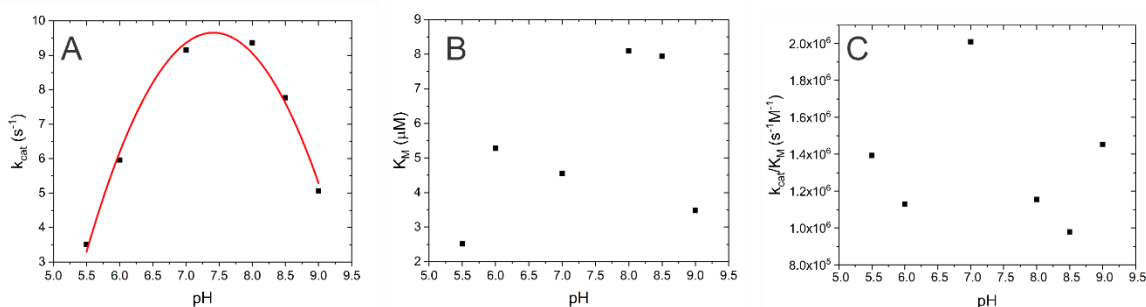


Figure 3.5: The effect of pH on *C. jejuni* NapA nitrate reductase activity with respect to A) k_{cat} , B) K_M , and C) k_{cat}/K_M . *C. jejuni* NapA has a pH optimum of 7.4 but is most efficient at pH 7.

3.3.3 The pH Effect on *C. jejuni* NapA Activity

The pH optimum was also determined for *C. jejuni* NapA with a calculated maximum turnover at pH 7.4 while the maximum efficiency was observed at pH 7.0 (Figure 3.5). The change in k_{cat} due to pH was small shifting $\sim 6 \text{ s}^{-1}$ from the least active pH to the most active pH. Similarly, the impact on K_M displayed no obvious pattern and the change in K_M ranged from 2.5 to 8.1 μM (Table 3.2). Interestingly, a decline in reaction velocity was observed at high nitrate concentration in some instances (Figure 3.6). This decline in reaction velocity has been observed at pH 7.0

consistently above nitrate concentrations of 400 μM and occasionally occurring as low as 200 μM . The same decline in reaction velocity was observed at the nitrate concentrations of 200-400 μM for every pH examined between pH 5.5-9.0 except at pH 6.0 (Figure 3.6).

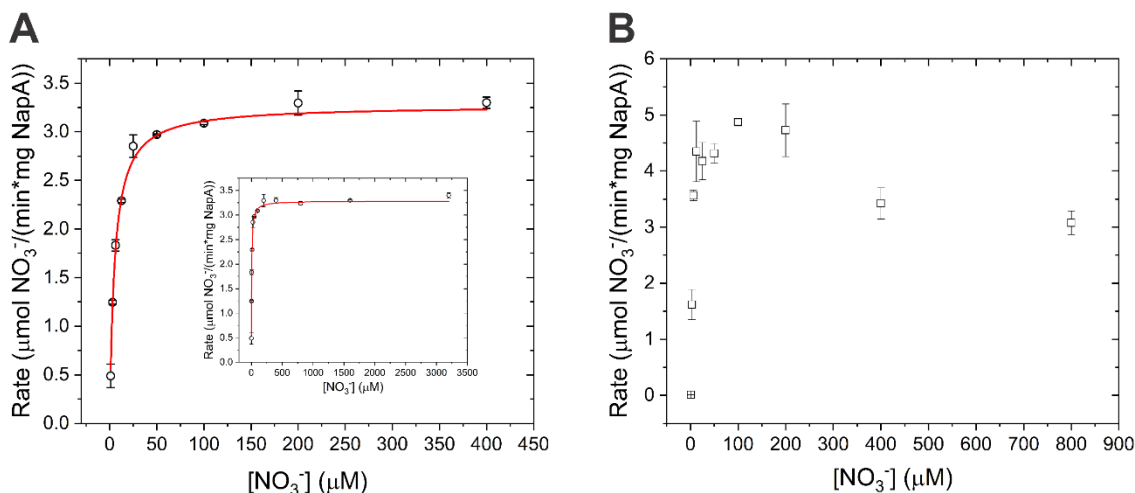


Figure 3.6: Observed pattern in the velocity of nitrate reduction at excess $[\text{NO}_3^-]$ by NapA at A) pH 6.0 (inset shows the extended concentration range tested) B) pH 7.0. The observed decline in velocity depicted in (B) has been observed at excess $[\text{NO}_3^-]$ in all pH conditions investigated except pH 6.0 (A).

Table 3.1: Kinetic parameters reported for NapA (A) or NapAB (AB) in various organisms using the methyl/benzyl viologen solution assay.

Organism	pH	K_M (μM)	k_{cat} (s^{-1})	V_{max} ($\mu\text{moles nitrate min}^{-1} \text{mg}^{-1}$)	k_{cat}/K_M ($\text{M}^{-1} \text{s}^{-1}$)	Reference
<i>Campylobacter jejuni</i> (A)	7.00	3.40 ± 0.44	5.91 ± 0.18	3.40 ± 0.10	1.74×10^6	This work
<i>Rhodobacter sphaeroides</i> (A)	7.00	120.00	70.20*	39.00	5.85×10^5	[167]
<i>Paracoccus pantotrophus</i> (AB)	7.00	112.00	58.00		5.18×10^5	[356]
<i>Paracoccus pantotrophus</i> (AB)	7.20	1300.00	240.00		1.85×10^5	[357]
<i>Magnetospirillum magnetotacticum</i> (AB)	7.00	3.20	2.50		7.81×10^5	[358]
<i>Aliivibrio fischeri</i> (AB)	7.50	65.00	10.00*	1.50	1.54×10^5	[352]

*Values calculated from kinetic parameters using the reported protein concentrations.

3.4 Discussion

C. jejuni NapA is a very efficient NO_3^- reducing enzyme with a high k_{cat}/K_M value and low K_M . The low K_M indicates a high binding affinity for NO_3^- (Table 3.1), which is consistent with the electrostatic potential calculations (Figure 3.3). The low K_M could prove useful to the pathogen when competing for nitrate with the commensal nitrate utilizing organisms of the host microflora. Nitrate metabolism has been positively associated with colonization by *Salmonella* [350], *E. coli* [359], and *C. jejuni* [349].

Both solution-based assay and protein film voltammetry (PFV) have been used in understanding the kinetic properties of Nap, although they exhibit some differences. In solution assays are homogenous and obey the steady-state approximation while PFV assays are heterogeneous and the electroactive enzyme coverage of the electrode is often unknown thus making it impossible to obtain turnover frequency (specific activity) [360]. For example, *R. sphaeroides* NapAB has a reported K_M of 7.50 μM , which is similar to the *C. jejuni* NapA K_M of 3.40 μM [361]. However, Bertrand *et al.* [362] argued the K_M measured in solution assays potentially depends on all rates in the catalytic cycle and will depart from the K_M determined by PFV, if intermolecular electron transfer is the rate-determining step in solution assays. Thus, the K_M values determined in solution may be higher than those determined by PFV. For this reason, we only discuss solution-based parameters obtained by using reduced MV as an electron donor (Table 3.1).

Compared to other Nap proteins in Table 3.1, *C. jejuni* NapA has the second highest substrate affinity, second only to *Magnetospirillum magnetotacticum*. Interestingly, *M. magnetotacticum* prefers microaerobic environments like *C. jejuni* [363]. Although *M. magnetotacticum* is not known to be pathogenic, its *nap* operon does appear to be phylogenetically closer to *C. jejuni nap* than its fellow *alphaproteobacteria* [344]. Furthermore, *C. jejuni* NapA appears to be a more efficient NO_3^- reducer than NapA from *M. magnetotacticum* as well as all other reported Nap proteins (Table 3.1) by approximately 2-12 times in the k_{cat}/K_M . Although the k_{cat}/K_M is higher, k_{cat} itself is lower than the homologously expressed Naps in Table 3.1. A lower k_{cat} may be attributable to substrate/product inhibition, attenuated electron transfer or conformational change. However, the exact reason for a lower k_{cat} remains an open question.

Campylobacter jejuni NapA exhibits a higher affinity towards NO_3^- . We suggest this is because it encounters low concentrations of NO_3^- under physiological conditions [350, 359].

Although the inflammatory response increases nitrate concentration in the GIT of the host [347, 350, 359], the concentration of NO_3^- is still below 1 mM [350, 359]. Nap is expressed maximally at 1 mM NO_3^- and does not express above 6 mM NO_3^- . In contrast, Nar expresses maximally at 10 mM NO_3^- and does not express below 1 mM NO_3^- . This NO_3^- regulated expression pattern suggests that Nap will be the primary nitrate reductase expressed at a low NO_3^- concentration [364]. Therefore, a pathogen that uses Nap may have an advantage under these conditions [350].

As Nap does not depend on NO_3^- uptake and transport across the membrane, it has been suggested that Nap faces the periplasm and acts as a NO_3^- scavenger [365]. Genetic experimentation suggests that NO_3^- metabolism is important in the physiology of *C. jejuni* [339, 348, 349]. The high efficiency of this enzyme compared to Nap proteins from non-pathogenic organisms suggests nitrate metabolism is important to this intestinal pathogen, but its role in pathogenicity is not completely clear. We suggest that NO_3^- is one of the metabolites or substrates that the pathogen relies on to ensure proper colonization into the gut of its host. The high substrate affinity of *C. jejuni* NapA suggests the Nap system has a role in scavenging for NO_3^- which has a relatively low concentration in the GIT with NO_3^- concentrations under 1 mM. Even during inflammation, when nitric oxide synthase is overexpressed leading to a higher production of NO_3^- , the NO_3^- concentration does not exceed 1 mM [350, 359]. These findings are in agreement with Lopez *et al.* [350] and underscore the importance of Nap in the physiology of pathogens such as *C. jejuni*.

As a possible NO_3^- scavenger in the GIT, *C. jejuni* cells expressing Nap may be exposed to various pH conditions. The GIT can range from a pH of 5.7 in the caecum to pH 6-7.4 in the small intestine [366]. The pH in the periplasm of gram negative bacteria often reflects the external pH conditions [367]. The pH profile of *C. jejuni* NapA reveals that NapA is indeed active in the range of pH 6-8 as is expected of most enzymes (Figure 3.5, Table 3.2). The pH optimum of *C. jejuni* NapA was determined to be 7.4 which is the same pH in the small intestine where *C. jejuni* prefers to colonize in the GIT [303, 368]. Interestingly, *C. jejuni* NapA's k_{cat} and K_M do not vary significantly with pH (Table 3.2, K_M shifts at most by 6 μM and k_{cat} shifts at most by 6 s^{-1}). While pH dependence has been reported for other Nap enzymes [270, 352, 354, 369, 370], the majority of reports present the data as percent activity of Nap at various pH conditions [270, 352, 354] or are conducted as part of PFV study [356]. In most cases, these reports unfortunately do not provide

enough information to calculate the kinetic parameters as a function of pH. As a result, comparing the range of change on kinetic parameters due to pH conditions is difficult.

However, a recent study on *R. sphaeroides* Nap reports the pH dependence data in a form that an estimated range for the variability of both K_M and k_{cat} can be determined over a pH range of 5.0-8.0 [370]. Zeamari and coworkers [370] observed a change in K_M of 50 μM to 250 μM , which is significantly different than *C. jejuni* NapA's range of 6 μM . Furthermore, Zeamari *et al.* [370] report a change in k_{cat} of $\sim 50 s^{-1}$ as compared to the $6 s^{-1}$ difference in *C. jejuni* NapA. Interestingly, *R. sphaeroides* is a free-living microbe often found in soil or aquatic environments [371]. Perhaps the general resistance to pH changes observed in *C. jejuni* NapA is in part aiding in the virulence of the pathogen. The pH resistance may be a mechanism to confront the physiological pH equilibria in the GIT of the hosts that *C. jejuni* tends to colonize.

Table 3.2: Kinetic parameters reported for recombinant *C. jejuni* NapA at various pH.

pH	K_M (μM)	k_{cat} (1/s)	V_{max} ($\mu mol NO_3^- / (min * mg NapA)$)	k_{cat}/K_M ($s^{-1} M^{-1}$)
5.5	2.52 ± 0.56	3.51 ± 0.05	1.93 ± 0.03	1.39×10^6
6.0	5.28 ± 0.15	5.96 ± 0.02	3.28 ± 0.01	1.13×10^6
7.0	4.55 ± 1.60	9.14 ± 0.69	5.04 ± 0.38	2.01×10^6
8.0	8.10 ± 3.90	9.36 ± 1.10	5.16 ± 0.61	1.16×10^6
8.5	7.94 ± 2.80	7.77 ± 0.73	4.29 ± 0.40	9.78×10^5
9.0	3.48 ± 0.56	5.06 ± 0.14	2.79 ± 0.08	1.45×10^6

In addition to the pH profile, a slight decline was observed in the velocity of the nitrate reduction rate of *C. jejuni* NapA at high NO_3^- concentrations (Figure 3.6). The observed decline in reaction velocity could be the result of substrate and/or product inhibition. Fourmond *et al.* observed in PFV (corroborated in solution assays) of nitrate reduction by *R. sphaeroides* NapA that a dead-end inactive enzyme species accumulates under specific conditions as a result of substrate inhibition. *R. sphaeroides* NapAB appears to slowly and reversibly convert to an inactive form at high potential and high substrate concentrations assayed by PFV. The inactive form slowly

appears in solution assays at high substrate concentrations if a high potential electron donor is utilized. Furthermore, the inactive enzyme species is very pronounced at low pH conditions but is also observed in the more alkaline pH where the value of K_i increases with pH [372]. Fourmond hypothesizes the inhibition is uncompetitive where the inactivation is a) an oxidation or b) a chemical step coupled to an oxidation and it is further proposed that the inactive form is created by the addition of a second nitrate molecule binding to the enzyme-substrate complex (Figure 3.7) [372].

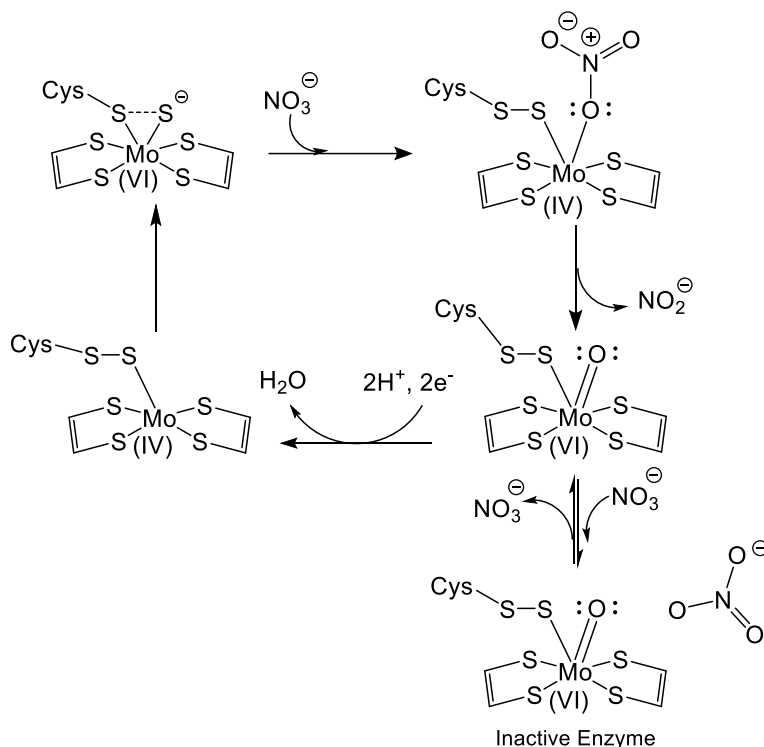


Figure 3.7: Proposed mechanism for substrate inhibition of *R. sphaeroides* NapAB. A second nitrate molecule binds in a reversible process in the active site preventing the regeneration of the reduced free enzyme state and reversibly inactivating the enzyme.

When the second inhibiting nitrate molecule is released or not present, the enzyme is activated and the activation is coupled to the reduction of the oxidized inactive form of the enzyme [372]. Further investigation by Jacques *et al.* revealed that the inhibiting nitrate molecule binds to three redox states, the Mo(IV), Mo(V), and Mo(VI) states [373]. The inhibiting nitrate has a higher affinity for the Mo(VI) state than either the Mo(IV) or the Mo(V) state and thus the inactive form accumulates mostly in the Mo(VI) state [373]. Jacques proposes that due to the small size of the

active site pocket, the inhibiting nitrate molecule enters the pocket after product release but before the transferred oxygen atom has been detached from the molybdenum center. The inhibition is a result of the nitrate molecule preventing the transferred oxo group at the molybdenum center from being released which forces the enzyme into a dead-end inactive species that cannot bind nitrate [373].

Interestingly, Fourmond observed a substrate inhibition under different conditions than the reaction velocity decline noted in *C. jejuni* NapA. Fourmond observed in pH 6.0 solution assays with MV (mid-point potential -449 mV [322]) as an electron donor that the inactive species did not form, nor was substrate inhibition observed at a nitrate concentration step from 4 mM to 40 mM. Meanwhile, assays with methylene blue (mid-point potential -70 mV) observed a rate decrease of approximately 8-fold indicating formation of the inactive substrate inhibited enzyme [372]. For *C. jejuni* NapA, the inactivation process is different as the decrease in rate is observed despite the use of a low potential electron donor (MV). The overall nitrate concentration range is lower as well since the declining rate is observed between 200-400 μ M while Fourmond observed substrate inhibition with a K_i of 4 mM. *C. jejuni* NapA may be more readily inhibited by substrate than the *R. sphaeroides* enzyme due to its higher affinity for nitrate. The observation that *C. jejuni* NapA activity at pH 6.0 does not show a declining reaction velocity at high NO_3^- concentration (Figure 3.6) when the *R. sphaeroides* enzyme inhibition is most significant at the same pH has significant implications. This observation could be a result of the different charge distribution between the *R. sphaeroides* and *C. jejuni* enzymes (Figure 3.3). *R. sphaeroides* Nap has a more acidic pI as compared to *C. jejuni* NapA [305, 344]. However, the active sites of both enzymes are densely positively charged (Figure 3.8) suggesting the interior of the enzymes is similarly charged. Alternatively, a specific protonation state of the nearby residues could be required to stabilize the inhibiting nitrate molecule and the pKa of the catalytic pockets for both enzymes may be different. Further investigation into the declining reaction velocity of *C. jejuni* NapA and the possibility of substrate inhibition in *C. jejuni* NapA using both PFV and solution assays is necessary to explore these hypotheses.

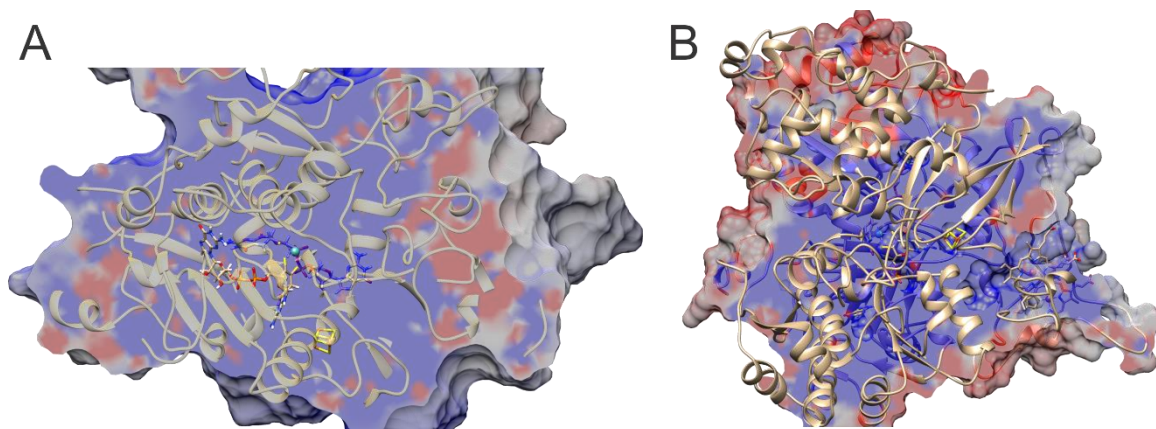


Figure 3.8: Electrostatic charges of the active site pockets of A) *C. jejuni* NapA and B) *R. sphaeroides* NapAB (PDB 1OGY). The electrostatic potentials were calculated in Chimera using the APBS plugin (−10 kT = red; 10 kT = blue; 0 kT = white).

3.5 Summary

The recombinant *C. jejuni* NapA has been biochemically characterized. This is the first example of a functional NapA from an *Epsilonproteobacterium* that has been overexpressed, purified, and biochemically characterized. Kinetic analysis of *C. jejuni* NapA revealed a high substrate-binding affinity and kinetic efficiency. The high substrate affinity of *C. jejuni* NapA suggests the Nap system has a role in scavenging for NO_3^- , which has a relatively low concentration in the GIT with NO_3^- concentrations under 1 mM. Even during inflammation when nitric oxide synthase is overexpressed leading to a higher production of nitrate, the nitrate concentration does not exceed 1 mM [350, 359]. These findings are in agreement with Lopez *et al.* [350] and underscore the importance of Nap in the physiology of pathogens such as *C. jejuni*. Additionally, the pH optimum of *C. jejuni* NapA of 7.4 is similar to the pH of the small intestine where *C. jejuni* prefers to colonize in the GIT [303, 368]. *C. jejuni* NapA exhibits a general resistance to pH changes which may be a mechanism to confront the physiological pH equilibria in the GIT of the hosts that *C. jejuni* tends to colonize. This foundational knowledge of *C. jejuni* NapA will serve as a basis and first step in investigating the chemistry occurring at the Mo center in the active site in NapA. The structure and mechanism of the Mo center will be discussed in Chapter 4.

CHAPTER 4. THE MOLYBDENUM CENTER AND ACTIVE SITE OF PERIPLASMIC NITRATE REDUCTASE

4.1 Introduction

NapA, the periplasmic nitrate reductase (NR), uses a molybdenum center to catalyze the reduction of nitrate to nitrite. The molybdenum center is coordinated by four sulfur atoms from two pyranopterin cofactors, another sulfur atom from a cysteine residue (C176 in *C. jejuni* NapA), and a terminal ligand, which is also suggested to be a sulfur atom (Figure 4.1) [374, 375]. In addition to the molybdenum center, sequence analysis suggests that *C. jejuni* NapA harbors a [4Fe4S] cluster due to the presence of a CXXCXXXC motif in the N-terminus. *C. jejuni* NapA has a calculated molecular weight of ~108 kDa, making it the largest among all Nap proteins isolated (Figure 2.4). As suggested in structurally homologous *E. coli* formate dehydrogenase (FDH) and in *R. sphaeroides* NapAB (PDB: 1FDO for FDH and 1OGY for Nap), a lysine (K79) residue in *C. jejuni* NapA is involved in hydrogen bonding between the [4Fe4S] cluster and the pterin moiety for efficient electron transfer [370, 376].

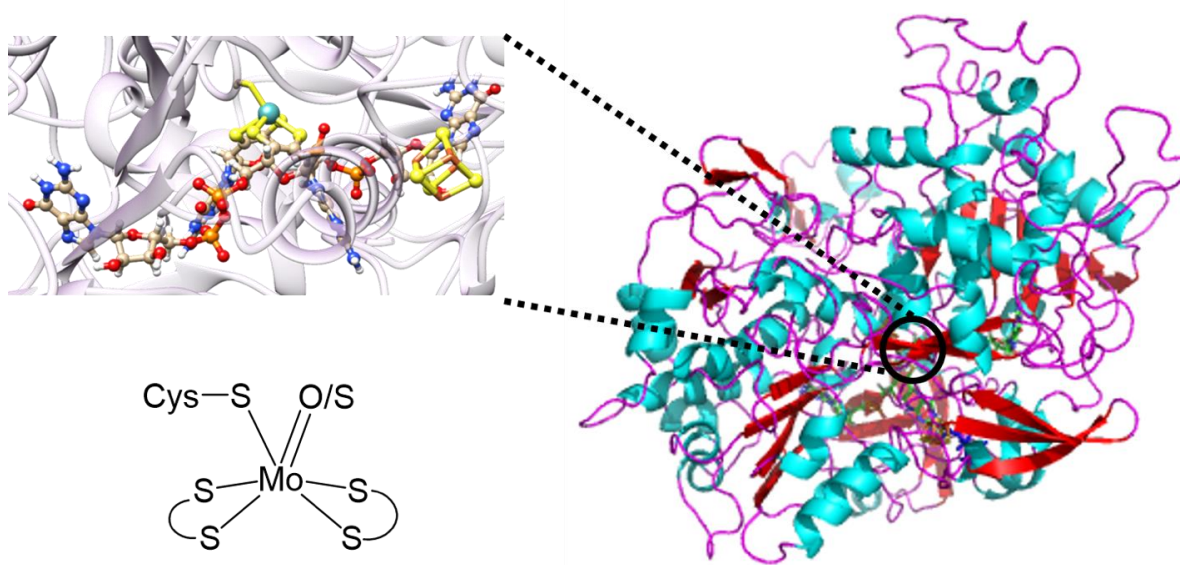


Figure 4.1: Homology model of *C. jejuni* NapA created in MOE by Courtney Sparacino-Watkins [329]. Full model depicted in the right panel and a zoomed in view of the molybdenum center in the upper left panel. The first coordination sphere of molybdenum is depicted as a line drawing in the lower left panel. The terminal ligand in the sixth position is unassigned in *C. jejuni* NapA and may be occupied by either an oxygen or a sulfur atom.

The reduction of NO_3^- is a two-electron process that oxidizes the molybdenum center. To reduce the molybdenum cofactor back to an active state following substrate oxidation, electrons are taken from a quinone pool by NapH and transferred to NapG through multiple iron sulfur clusters. The electrons move from NapG to the heme of NapB before being transferred to the molybdenum center via the [4Fe4S] cluster and the pyranopterin cofactor to reduce the NapA enzyme from the Mo(VI) state to the Mo(IV) state (Figure 4.2). These structural features of *C. jejuni* NapA have been defined by previous studies on Nap enzymes from various organisms [130, 168, 309, 377] and corroborated by a *C. jejuni* NapA homology model (Figure 4.1).

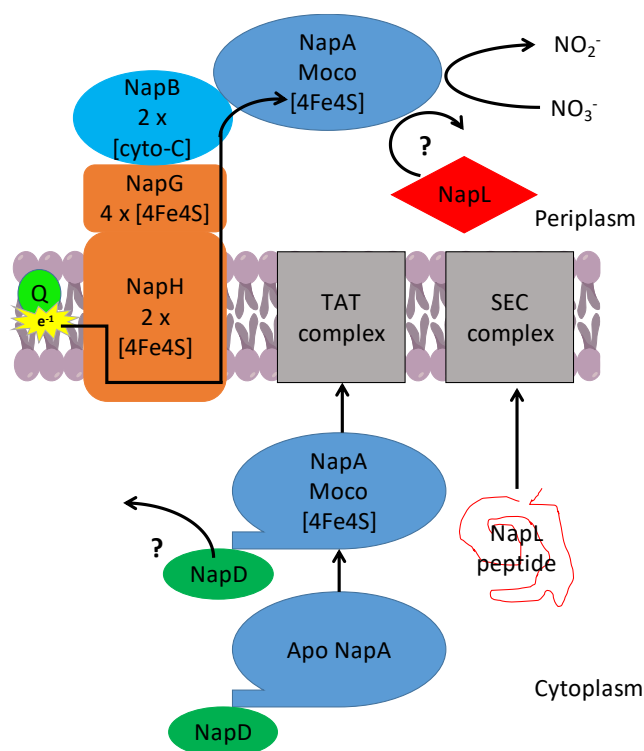


Figure 4.2: Diagram of the Nap enzyme complex depicting electron transfer in Nap and the possible roles of chaperones, NapD and NapL, in the maturation and transport of NapA. Q represents the quinone pool and question marks represent unclear mechanisms.

The first crystal structure of the catalytic subunit of any NR was reported for the monomeric NapA from *Desulfovibrio desulfuricans* [309]. The structure (PDB: 2NAP, 1.9 Å resolution) showed the presence of two prosthetic groups, [4Fe4S] and Moco, within 14 Å of each other. The molybdenum center is deeply buried in the protein, ~15 Å from the surface, and is coordinated by two ene-dithiolates from the MPT cofactors and C140 (*D. desulfuricans* numbering). The fifth

coordination position had originally been assigned as a terminal oxo-group, but recently it has been revised to a sulfido group [310]. The terminal sulfur is proposed to form a partial persulfide bond with the cysteine sulfur as the S—S bond distance of ~ 2.2 Å is shorter than the sum of the van der Waals radii, 3.6 Å [310, 375].

A new structure of NapAB from *Cupriavidus necator* (PDB: 3ML1, 1.6 Å resolution) from the same group, solved by the molecular replacement method, showed a very similar molybdenum coordination sphere [130]. The active site surrounding the molybdenum center is comprised residues that are highly conserved in *C. jejuni* NapA (e.g., *C. necator* NapA: R400, R392, E168, D167, and R150) (Figure 2.4). R392 and D167 form a salt bridge and are directed towards the active site, and mutation of D167A abolishes catalytic activity [378].

An initial catalytic mechanism for the Nap enzymes has been proposed based on the crystal structure of *D. desulfuricans* NapA, in which NO_3^- binds to the five-coordinate Mo-center via one oxygen atom to give a six-coordinate center [309]. The NO_3^- is reduced to nitrite and the coordinated oxygen is transferred to Mo, becoming a terminal oxo group of the now oxidized Mo(VI) center. Reduction of the Mo with reducing equivalents from menaquinol results in protonation of the Mo=O to water, leading to its dissociation to regenerate the penta-coordinate Mo(IV) center. This mechanism is consistent with the oxygen atom transfer (OAT) reaction mode of action proposed for DMSOR and ArrAB (Figure 4.3).

This mechanism was revised due to the finding that the terminal ligand to Mo in oxidized NapA of both *D. desulfuricans* [310] and *Cupriavidus necator* [130] is a sulfido rather than an oxo group [375]. Specifically, migration of the cysteine S from Mo occurs in the presence of substrate and the cysteine S forms a disulfide bond with the terminal sulfido moiety. Substrate binds to the vacant site and OAT commences. Product is released leaving an oxidized Mo center coordinated by terminal disulfide species and an oxo group. The reduced Mo center is regenerated after $2e^-/\text{H}^+$ coupled steps. The change in the coordination of cysteine and the formation of the disulfide bond is termed as a sulfur shift event (Figure 4.4) [375]. Support for this mechanism has been provided by density functional theory (DFT) calculations [326, 379], but no direct experimental proof has been reported. It is not clear how the disulfide bond remains intact during the reductive regeneration steps.

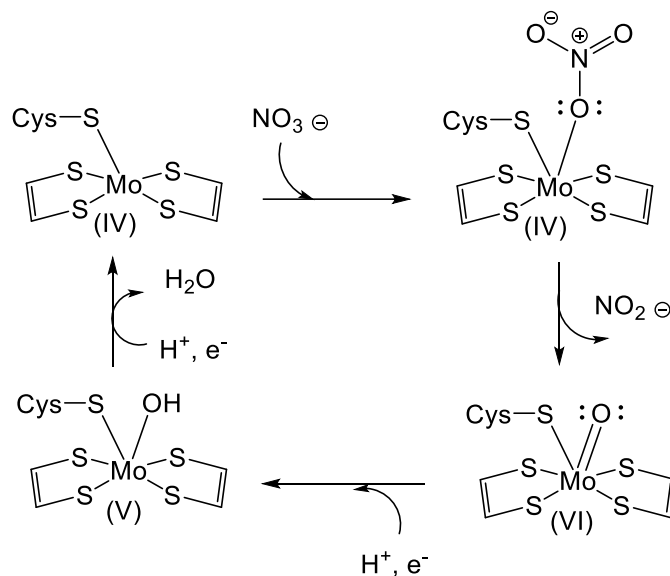


Figure 4.3: The proposed OAT mechanism for Nap where Mo is coordinated by a terminal oxo ligand in which NO_3^- binds to the five-coordinate Mo-center via one oxygen atom to give a six-coordinate center. NO_3^- is reduced to nitrite and oxygen is transferred to Mo, becoming a terminal oxo group of the oxidized Mo(VI) center. The resting Mo(IV) state is regenerated by reduction of the Mo via protonation of the Mo=O to water leading to its dissociation.

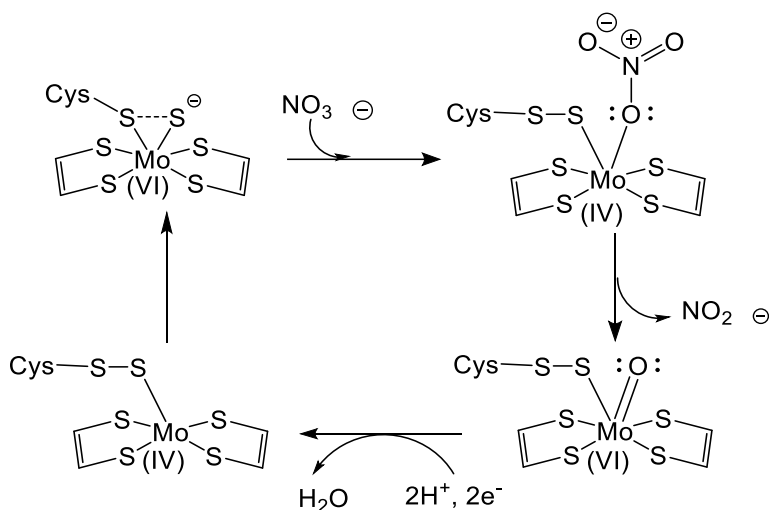


Figure 4.4: The sulfur shift mechanism as proposed in reference [375]. The initial resting state of the enzyme is proposed to have a Mo—S- as opposed to the Mo=S moiety. Thus, the terminal sulfido group can undergo internal redox with the cysteine sulfur forming a disulfide bond. The disulfide bond has been proposed to form in the presence of substrate, with migration of the cysteine S from Mo in the sulfur shift. Nitrate binds to the vacant site on the Mo center, transfers an oxygen atom to the Mo, and product nitrite is released. The resting state is then regenerated by proton-coupled electron transfer, the formation and departure of a water molecule, and the internal redox of the terminal sulfide with cysteine sulfur.

In summary, the following hypothesis can be made: the fifth and sixth coordinating ligands to the Mo center influence substrate preference and a set of amino acid residues in the catalytic pocket and the substrate channel have evolved to optimize the selectivity within a class of substrates (e.g., smaller oxyanions vs larger neutral substrates). Furthermore, the presence of analogous residues is suggestive of similar mechanistic paths. In this chapter, the NapA enzyme will be further characterized through a combination of spectroscopic and kinetic experiments in order to study the structure and function of the molybdenum active site as a method for initial investigations into the catalytic mechanism.

4.2 Materials and Methods

Buffers and other reagents were purchased at the highest available grade from either Sigma-Aldrich (St. Louis, MO, USA) or Fisher Scientific (Pittsburgh, PA, USA). The Pierce Coomassie Plus (Bradford) Protein Assay Kit, was purchased from Thermo Scientific (Rockford, IL, USA). The Pro-TEV Plus Kit was purchased from Promega Corporation (Madison, WI, USA).

4.2.1 Protein Concentration Determination

Protein concentrations were determined using the Coomassie Plus (Bradford) Protein Assay Kit (Thermo Scientific) with bovine serum albumin standard (Pierce).

4.2.2 SDS-PAGE

SDS-PAGE was performed as described in Chapter 2 Section 2.2.6.

4.2.3 Metal Analysis

Metal analysis was conducted at the University of Pittsburgh with the assistance of Dr. Daniel Bain as described in Chapter 2 Section 2.2.8.3.

4.2.4 Enzyme Kinetics

Nitrate reductase activity was measured spectrophotometrically by monitoring oxidation of reduced methyl viologen as described in Chapter 2 Section 2.2.7. Sulfate inhibition experiments

were conducted as in Section 2.2.7 with sulfate present in the reaction buffer at concentrations of 0 mM, 0.1 mM, and 1 mM. The resulting data was used to produce a Lineweaver-Burke plot in order to determine the inhibition mode of sulfate. Once sulfate was determined not to be an inhibitor, NaCl effects on nitrate activity were determined by removing all NaCl from the protein via buffer exchange or desalting column and by preparing NaCl free reaction solutions. MV solutions were prepared electrochemically as in Section 2.2.7; however, sodium sulfate was utilized at a concentration of 150 mM to maintain the salt bridge during electrolysis instead of NaCl. NaCl dependence experiments were conducted as above with NaCl introduced into the reaction buffer at final concentrations of 0 M, 0.1 M, 0.2 M, 0.3 M, 0.4 M, 0.5 M, 0.6 M, 0.7 M, 0.8 M, 0.9 M, and 1 M. All data were analyzed as previously mentioned in Section 2.2.7. Each curve was produced with one biological replicate and three technical replicates for each substrate concentration.

4.2.5 Tobacco Etch Virus (TEV) Protease Cleavage

Cells containing *C. jejuni* NapA enzyme were lysed and purified by affinity chromatography as previously discussed in Section 2.3.3.3. The affinity chromatography fractions containing NapA were pooled and buffered exchanged into 50 mM Hepes 0.2 mM MgCl₂ pH 7.00. The Tobacco Etch Virus (TEV) protease reaction consisted of 0.2 mM MgCl₂, 1 mM DTT, 10 mM imidazole, 300 mM NaCl, 50 mM HEPES pH 7.00 and 85.5 µg NapA/µL TEV (~5 units of protease). The reactions were incubated at room temperature for approximately 1.5 h. Protein samples were concentrated, and excess salt was removed via centrifugal filter. The buffer-exchanged sample was purified by affinity chromatography utilizing a HisTrap HP 5 mL prepac column (GE Life Sciences) as before. The tagged protease and the cleaved tag will bind to the column while the cleaved NapA enzyme (untagged) will elute immediately in a purified form.

4.2.6 X-ray Absorption Spectroscopy (XAS)

Mo K-edge X-ray absorption spectroscopic (XAS) measurements and the corresponding data analyses were conducted by collaborators Dr. Jing Yang and Prof. Martin Kirk from the Department of Chemistry and Chemical Biology at The University of New Mexico. All XAS data for the *wt*-NapA enzyme and variants were collected at beamline 7-3 (BL7-3) of the Stanford

Synchrotron Radiation Light source (SSRL) under storage ring (SPEAR3) conditions with an energy of 3 GeV and a current of ~500 mA in top-off mode. Approximately ~150 μL of the NapA enzyme sample in two different concentrations (35.5 and 49 mg/mL, 50 mM HEPES pH 7.00) were loaded into DelrinR sample cells that were subsequently sealed with thin Kapton tape and then quickly frozen in liquid nitrogen. XAS data were collected in the energy range from 19,692 eV to 21,261 eV ($k = 18 \text{ \AA}^{-1}$) using an unfocused beam in a liquid He cryostat stabilized at ~10 K. The Mo K_{α} fluorescence signal was collected using a 30-element Ge array detector with a Soller slit and a Z-2 (Zr) filter that functions to minimize unwanted light sources including incident scattering and non-Mo K_{α} emission. Eight data scans were obtained for each sample. The energy was calibrated to a Mo foil reference sample, which was collected simultaneously with the protein sample. Energy calibration, background correction, data averaging, and data normalization were all performed using the program ATHENA, which is part of the Demeter software package version 0.9.18.2.5

Gas-phase geometry optimizations and electronic structure calculations for various NapA computationally were performed at the density functional level of theory (DFT) using the Gaussian 09 revision C.01 software package. The calculations utilized the B3LYP exchange-correlation functional with 6-31g* basis set for all light atoms, and a LAN2DZ basis set with a LANL2 effective core potential for Mo.

4.3 Results

4.3.1 The Influence of NaCl and Sulfate on *C. jejuni* NapA Activity

The effect of NaCl was investigated to determine ionic strength effects before additional salts could be tested as possible substrates. Remarkably, NaCl seems to impact K_M while hardly showing any significant effect on k_{cat} (Figure 4.5). The K_M shifts by an order of magnitude ranging from 3 to 30 μM while k_{cat} changes at the most by 8 s^{-1} (Table 4.1). While no obvious pattern is observed between k_{cat} and NaCl concentration, the K_M has a moderate positive linear correlation with the NaCl concentration (Figure 4.5).

Additionally, NapA was probed for inhibition by the larger oxyanion, sulfate. The Lineweaver-Burke plot (Figure 4.6) of NapA activity in the presence of 0 mM, 0.1 mM, and 1 mM sulfate reveals no inhibition pattern. The data for all conditions is within error thus producing

three linear fits that are essentially the same line. Thus, inhibition studies of sulfate show no effect on K_M or turnover implying sulfate does not interfere in the catalytic pocket. Figure 4.6 shows a slight curvature suggesting there maybe some impact on the activity. However, the error suggests that the impact is small and negligible for the purpose of this study.

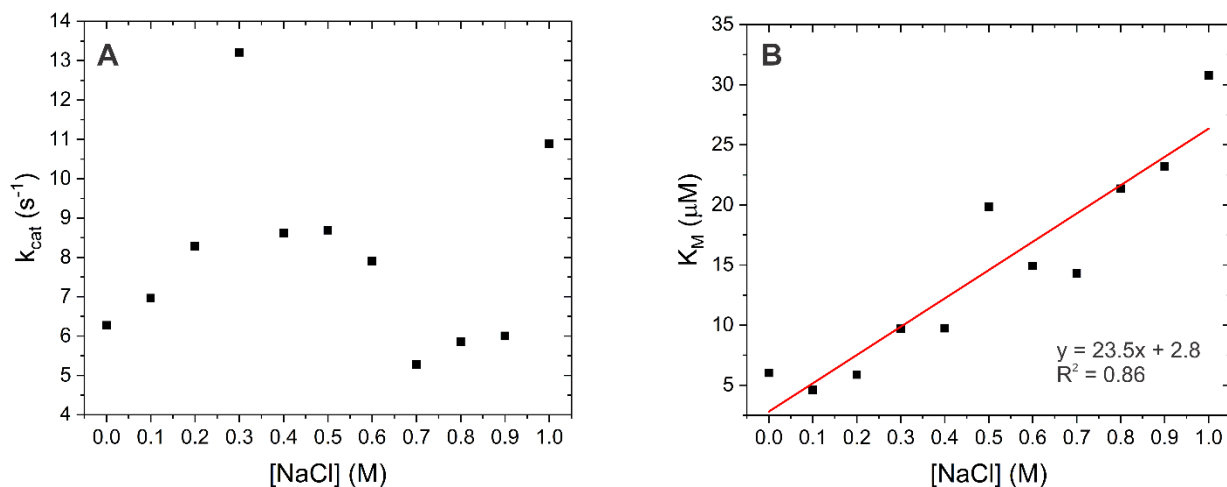


Figure 4.5: The impact of NaCl on the nitrate reductase activity of *C. jejuni* NapA with respect to A) k_{cat} and B) K_M . The ionic strength ranged from 0.13 M in the 0 M NaCl sample to 1.13 M in the 1.0 M NaCl sample.

Table 4.1: Kinetic parameters reported for recombinant *C. jejuni* NapA in the prescence of various NaCl concentrations.

[NaCl] (M)	K_m (μM)	k_{cat} (s^{-1})	k_{cat}/K_m ($1/s \cdot M$)
0.0	3.67 ± 1.49	5.17 ± 0.36	1.41×10^6
0.1	4.61 ± 0.87	6.96 ± 0.08	1.51×10^6
0.2	5.88 ± 0.60	8.28 ± 0.08	1.41×10^6
0.3	9.70 ± 2.71	13.21 ± 0.60	1.36×10^6
0.4	9.72 ± 1.31	8.61 ± 0.38	8.86×10^5
0.5	19.85 ± 6.31	8.69 ± 0.74	4.38×10^5
0.6	14.92 ± 0.70	7.90 ± 0.03	5.29×10^5
0.7	14.30 ± 1.66	5.28 ± 0.24	3.69×10^5
0.8	21.34 ± 1.61	5.86 ± 0.13	2.75×10^5
0.9	23.21 ± 2.94	6.00 ± 0.20	2.59×10^5
1	30.79 ± 2.27	10.89 ± 0.21	3.54×10^5

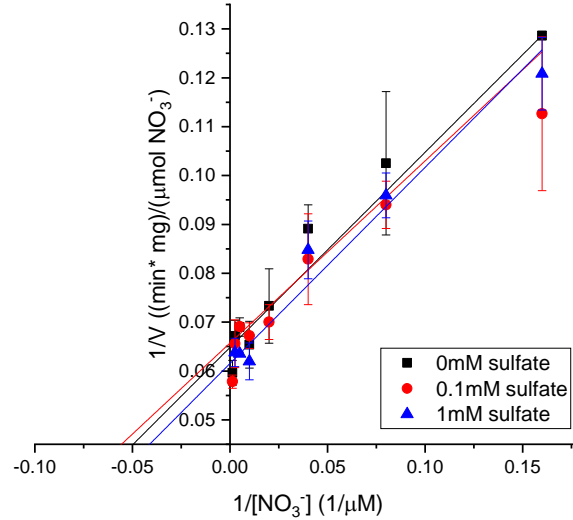


Figure 4.6: Lineweaver-Burke plot of the inhibition of *C. jejuni* NapA by sulfate. Nitrate reduction rates of *C. jejuni* NapA in the presence of 0 mM sulfate, 0.1 mM sulfate, and 1 mM sulfate are depicted by the black squares, red circles, and the blue triangles, respectively. The data of all three conditions is within error of each other resulting in three lines that are essentially the same suggesting sulfate is not an inhibitor of *C. jejuni* NapA. Curvature of the data may suggest a small impact, but this impact is minimal and may be beyond the detection limit of the enzyme assay.

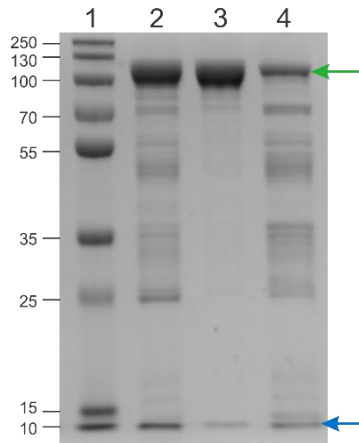


Figure 4.7: SDS-PAGE gel of TEV cleaved NapA. Lane 1- PageRuler Plus prestained protein ladder (kDa), Lane 2-TEV protease + NapA reaction mixture, Lane 3-NapA cleaved by TEV protease and purified by a second run on the HisTrap column, Lane 4-TEV protease + bound His-tagged NapA + contaminant proteins eluted from the HisTrap column after TEV cleavage. The NapA band at ~108-kDa is denoted by the green arrow and the NapD band is denoted by the blue arrow. Bands below the NapA band in lanes 2 and 4 are affinity column contaminants normally removed by SEC.

4.3.2 Impact of the His-tag on Metal Loading and Nitrate Reductase Activity

The mixture of NapA states observed during elution from the size-exclusion column could be a result of incomplete maturation in *E. coli* or could be the result of metal stripping which has been reported in some cases when a His-tag is used [128]. A TEV cleavage site was cloned into the NapA construct (Figure 2.5) and was used to determine if the His-tag was detrimental to the metal loading and the activity of the purified NapA enzyme. While it is unlikely that the His-tag would strip Mo, the tag may adjust the overall folded structure of the enzyme and the stability of the Moco. Additionally, the [4Fe4S] cluster is on the surface and may be prone to metal stripping by the tag. Both possibilities would negatively impact nitrate reductase activity. TEV cleavage of the His-tag was only ~ 76% effective leaving some portion (~24%) of the enzyme His-tagged as evidenced by the ~108 kDa band in lane 4 of Figure 4.7. Despite this loss in yield, the cleaved enzyme was purified to greater than 90% homogeneity (lane 3, Figure 4.7).

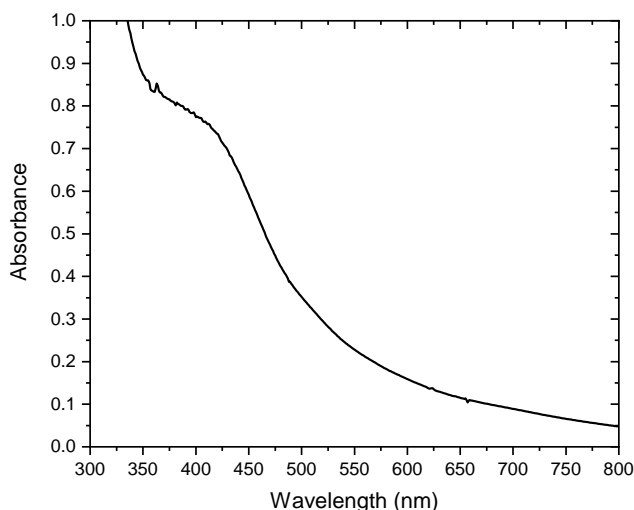


Figure 4.8: UV-Vis spectrum of as-isolated *C. jejuni* NapA cleaved by TEV protease in 50 mM HEPES pH 7.0.

The UV-Vis spectrum of the cleaved enzyme was akin to the UV-Vis spectrum of the His-tagged NapA (Figure 4.8) with a band at 400 nm indicating the presence of the [4Fe4S] cluster. The molybdenum incorporation was also very similar with approximately 90% Mo incorporated on average after TEV cleavage. Thus, the His-tag is not detrimental to metal loading and stabilization of the cofactors in recombinant *C. jejuni* NapA. Additionally, the TEV-cleaved enzyme exhibited similar nitrate reactivity as its His-tagged counterpart suggesting the His-tag

does not interfere with catalysis (Figure 4.9). The cleaved enzyme had a K_M of $5.8 \pm 2.5 \mu\text{M}$ and a k_{cat} of $4.81 \pm 0.35 \text{ s}^{-1}$, which is very similar to the His-tagged enzyme's K_M for NO_3^- of $3.40 \pm 0.44 \mu\text{M}$ and k_{cat} of $5.91 \pm 0.18 \text{ s}^{-1}$.

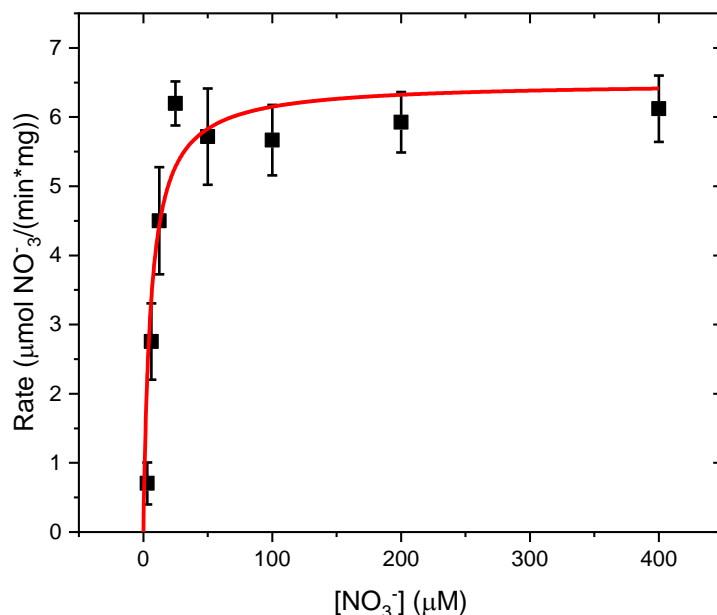


Figure 4.9: Steady-state kinetic analysis using the Michaelis-Menten model of the reduction of nitrate by *C. jejuni* NapA with the His-tag cleaved by TEV protease. The solid line represents the Michaelis-Menten fit. The data was analyzed, and the graph produced in Origin. This kinetic curve was reproduced by at least ten biological replicates. Each curve contained three technical replicates for each substrate concentration.

4.3.3 XAS of Recombinant *C. jejuni* NapA

The X-ray absorption near-edge structure (XANES) spectra for the as-isolated *C. jejuni* NapA samples are presented in Figure 4.10. The molybdenum K-edge energy of the two batches of as-isolated enzyme revealed the as-isolated enzyme may be a heterogeneous mixture of enzyme states. The extended X-ray absorption fine structure (EXAFS) data (Figure 4.11) have been used to provide information about the first coordination sphere of the molybdenum center in the active site of *C. jejuni* NapA. Analysis of the EXAFS data resulted in the best fit of the 35.5 mg/mL sample as a mixture of 1:0.9 (fit to $k=12$) to 1:1.2 (fit to $k=14$) of Mo(VI) with a coordination sphere consisting of (1) 1 terminal oxo + 5 S thiol scatterers and (2) Mo(IV) with 1 hydroxido + 5 S thiol scatterers (Figure 4.11). Additional fits to the EXAFS data are listed in Table 4.2.

Table 4.2: EXAFS fits for as-isolated *C. jejuni* NapA (35.5 mg/mL) XAS data. The data were fit in k space in a k range of 2.4-12 with R range of 1.15-3. $E_0=20016$ eV. Mo-S phase correction applied. Fits 8-9 are the best fits analyzed and are depicted in Figure 4.11.

Mo-O (Å)			Mo-S (Å)			So ²	ΔE ₀ (eV)	R (%)
Fit 1. use model 1, Oxidized form, with 1oxo+5S								
1 (fix)	1.700/1.720	0.0087	5 (fix)	2.378/2.464	0.0070	1 (fix)	-2.537	5.93
Fit 2. use model 1, Oxidized form, with 1oxo+5S								
1 (fix)	2.061/1.720	-0.0025	3 (fix) 2 (fix)	3.043/2.464 2.751/2.547	0.023 0.015	1 (fix)	67.84	56.59
Fit 3. use model 2, Oxidized form, with 1sulfido+5S								
			1 (fix) 5 (fix)	2.206/2.170 2.366/2.447	0.0019 0.0047	1 (fix)	-7.734	13.60
Fit 4. use model 3, Oxidized form, with 1water+5S								
1 (fix)	2.269/2.265	0.016	5 (fix)	2.377/2.352	0.0070	1 (fix)	-2.270	7.67
Fit 5. use model 4, Reduced form, with 1OH+5S								
1 (fix)	2.236/2.022	0.014	5 (fix)	2.378/2.402	0.0070	1 (fix)	-2.348	7.52

Table 4.2 Continued

Mo-O (Å)			Mo-S (Å)			S ₀ ²	ΔE ₀ (eV)	R (%)
Fit 6. use model 5, Reduced form, with 1SH+5S								
			6 (fix)	2.374/2.409	0.0083	1 (fix)	-4.065	10.89
Fit 7. use model 5, Reduced form, with 1SH+5S, allow N of Mo-S to vary								
			4.95	2.375/2.409	0.0069	1 (fix)	-3.519	7.56
Fit 8. use model 1, Oxidized form, with 1oxo+5S, and add a long Mo-O path, k=2.4-12								
1 (fix) 0.9	1.722/1.720 2.040/1.900	0.0083 0.0046	5 (fix)	2.375/2.464	0.0067	1 (fix)	-3.660	5.82
Fit 9. use model 1, Oxidized form, with 1oxo+5S, and add a long Mo-O path, k=2.4-14								
1 (fix) 1.2	1.738/1.720 2.050/1.900	0.0094 0.0033	5 (fix)	2.379/2.464	0.0064	1 (fix)	-3.538	10.54

* S_0^2 - amplitude reduction term, ΔE_0 - energy shift relative to the threshold E_0 , R - weighted factor that gives the fractional misfit of theoretical model (i.e. the lower the value then the better the model fits the data).

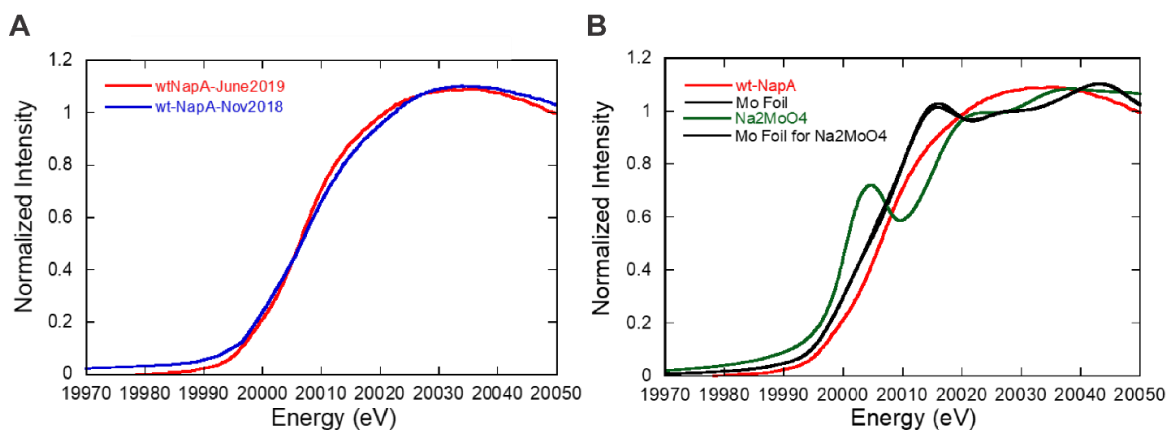


Figure 4.10: XANES spectra of two batches of WT *C. jejuni* NapA at 49 mg/mL (isolated November 2018) and 35.5 mg/mL (isolated June 2019). A) the Mo K-edge of WT NapA isolated in November 2018 in blue (edge energy of 20013.68 eV) and WT NapA isolated in June 2019 in red (edge energy of 20012.12 eV). B) XANES spectra of the 35.5-mg/mL NapA sample isolated in June 2019 compared to the reference Mo foil. NapA sample is in red, Mo foil is in black, and sodium molybdate is in green.

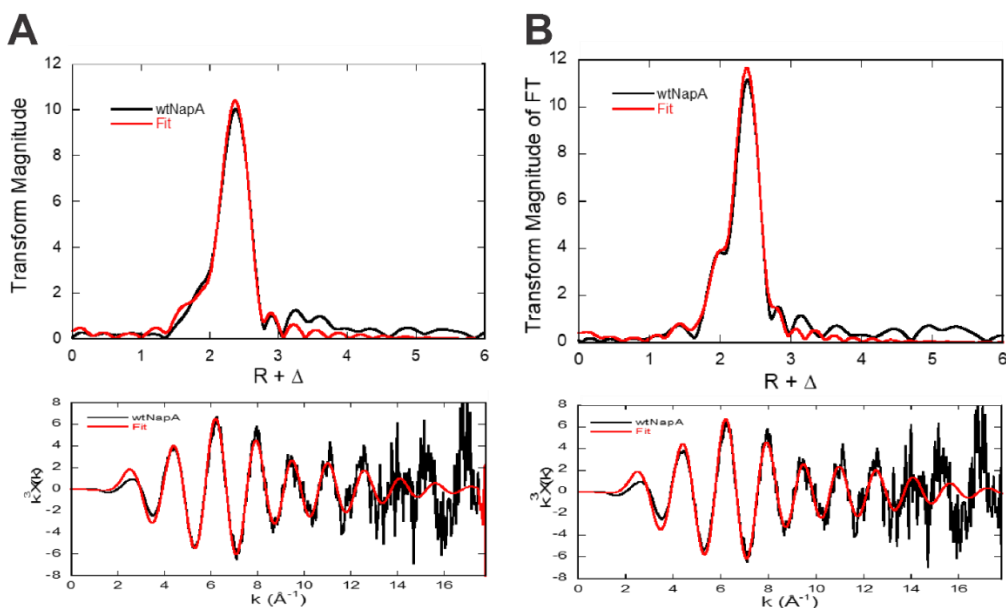


Figure 4.11: EXAFS Spectra for WT NapA (isolated June 2019, 35.5 mg/mL sample). A) WT NapA fit to 1 Mo=O + 5 Mo-S + 0.9 Mo-O active site model. Top panel is the Fourier transform of EXAFS data and the bottom panel is the k-space data. B) WT NapA fit to 1 Mo=O + 5 Mo-S + 1.2 Mo-O active site model. Top panel is the Fourier transform of EXAFS data and the bottom panel is the k-space data. Experimental data is the black line and the fit is the red line.

An additional sample of as-isolated NapA in the presence of 450 mM NaCl was examined using XAS to determine if the ionic strength affect in Figure 4.5 where the ions impact K_M but not

k_{cat} is due to a Cl^- induced perturbation in the molybdenum first coordination sphere. The XANES spectra of the NaCl-treated sample as compared to the untreated as-isolated NapA sample is depicted in Figure 4.12. The rising edge of the NaCl-treated NapA sample is found to occur at a higher energy than the untreated as-isolated NapA. The overall patterns in the XANES spectra of the untreated NapA and NaCl-treated samples are observed to be significantly different. Thus, Cl^- appears to be perturbing the molybdenum center in a manner, however, the exact nature of this perturbation is unclear at this point.

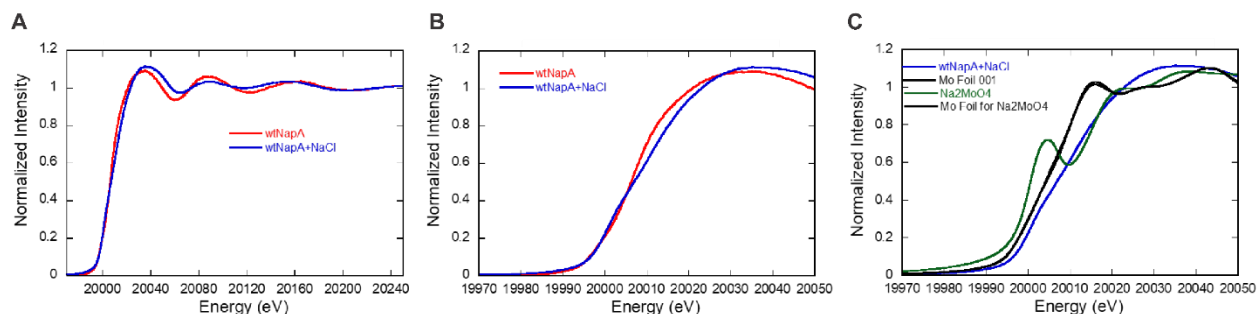


Figure 4.12: XANES spectra of two batches of WT *C. jejuni* NapA treated with 450 mM NaCl. A) Full XANES spectra depicting the difference in oscillation patterns of WT NapA (red) and NaCl-treated NapA (blue). B) the Mo K-edge of WT NapA isolated in June 2019 in blue (edge energy of 20012.12 eV) and WT NapA treated with NaCl in red (edge energy of 20015.24 eV). C) XANES spectra of the NaCl-treated NapA sample compared to the reference Mo foil. NaCl-treated NapA sample is in blue, Mo foil is in black, and sodium molybdate is in green.

The EXAFS data for NaCl-treated NapA (Figure 4.13) can be fitted with several different models (Table 4.3). The combination of 2 long Mo-S/Cl with 3 short Mo-S/Cl bonds, 3 long Mo-S/Cl with 2 short Mo-S/Cl bonds, 4 long Mo-S/Cl with 2 short Mo-S/Cl bonds, and 3 long Mo-S/Cl with 3 short Mo-S/Cl bonds provide similar quality fits to the data. The only discernable difference for the 5S/Cl and 6S/Cl fits come in at the $k=16$ area; however, in this area the data set is very noisy. Thus, it cannot be determined with confidence if the Mo ion is coordinated by a 5S or 5S+1Cl donor ligand set. If purely based on the R factor, then Fit 6 represents the best fit where the Mo ion is coordinated with one terminal oxo, one shorter sulfur/chloride shell (2 Mo-S/Cl), and one long sulfur/chloride shell (3 Mo-S/Cl). However, Fit 5 is also a reasonably good fit and results in a markedly smaller Debye-Waller factor for the Mo-S/Cl shells. Thus, based on all these analyses, these two sulfur/chloride shells may contain between 2-3 Mo-S/Cl bonds in each shell, resulting in a possible total approximately 5-6 Mo-S/Cl bonds.

Table 4.3: EXAFS fits for as-isolated *C. jejuni* NapA treated with 450 mM NaCl XAS data. The data were fit in k space in a k range of 2.4-12 with R range of 1.15-3. $E_0=20016$ eV. Mo-S phase correction applied. Fits 5-6 are the best fits analyzed and are depicted in Figure 4.13.

Mo-O (Å)			Mo-S/Cl (Å)			S ₀ ²	ΔE ₀ (eV)	R (%)
use model 1, Oxidized form, with 1oxo+5S by varying the combination of number of S/Cl atoms								
Fit1 1 (fix)	1.736/1.720	0.00073	5 (fix) 1 (fix)	2.361/2.464 10.533/2.547	0.0098 0.38	1 (fix)	-7.322	27.86
Fit2 1 (fix)	1.758/1.720	0.0011	4 (fix) 2 (fix)	2.504/2.464 2.360/2.547	0.013 0.0035	1 (fix)	1.533	15.55
Fit3 1 (fix)	1.757/1.720	0.0011	3 (fix) 3 (fix)	2.532/2.464 2.367/2.547	0.0091 0.0047	1 (fix)	1.111	16.91
Fit4 1 (fix)	1.731/1.720	0.00083	2 (fix) 4 (fix)	2.805/2.464 2.349/2.547	0.021 0.0080	1 (fix)	-9.807	18.24
Fit5 1 (fix)	1.756/1.720	0.0012	2 (fix) 3 (fix)	2.535/2.464 2.371/2.547	0.0056 0.0042	1 (fix)	0.789	12.72
Fit6 1 (fix)	1.758/1.720	0.0012	3 (fix) 2 (fix)	2.502/2.464 2.358/2.547	0.0094 0.0030	1 (fix)	1.398	11.83
Fit7 1 (fix)	1.735/1.720	0.00082	4 (fix) 1 (fix)	2.355/2.464 2.367/2.547	0.0079 0.0089	1 (fix)	-7.924	19.03

* S_0^2 - amplitude reduction term, ΔE_0 - energy shift relative to the threshold E_0 , R - weighted factor that gives the fractional misfit of theoretical model (i.e. the lower the value then the better the model fits the data).

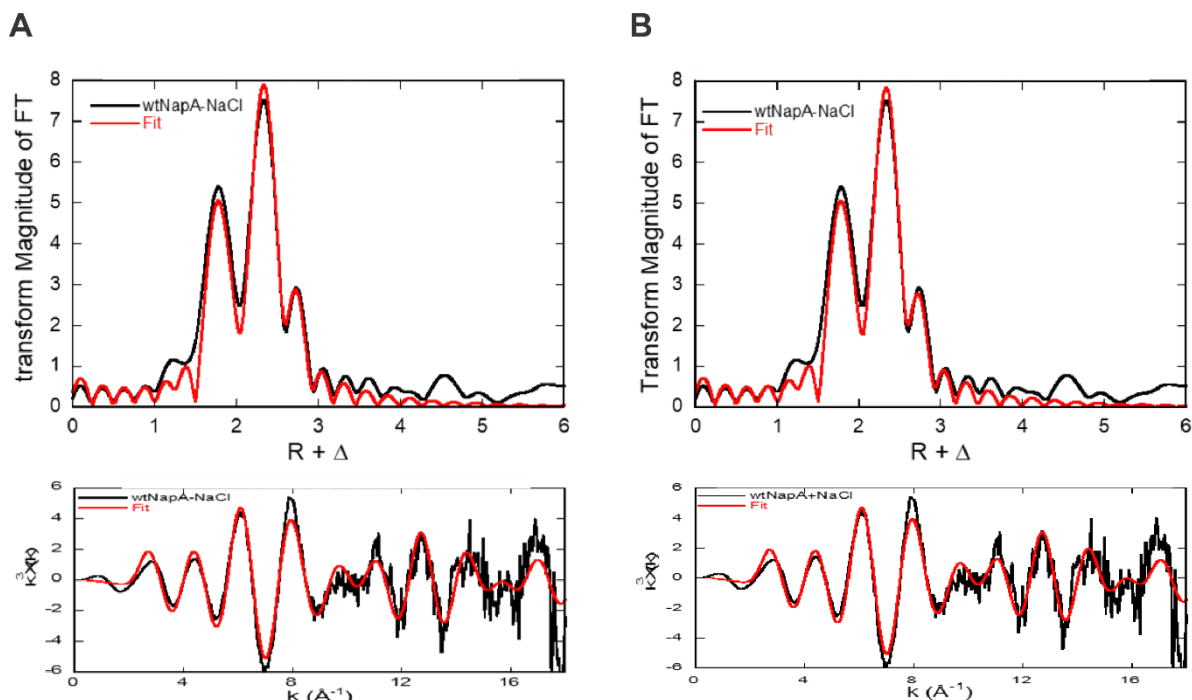


Figure 4.13: EXAFS Spectra for WT NapA treated with 450 mM NaCl. A) NaCl-treated WT NapA fit to 1 Mo=O + 2 Mo-S (long) + 3 Mo-S (short) active site model. Top panel is the Fourier transform of EXAFS data and the bottom panel is the k-space data. B) NaCl-treated WT NapA fit to 1 Mo=O + 3 Mo-S (long) + 2 Mo-S (short) active site model. Top panel is the Fourier transform of EXAFS data and the bottom panel is the k-space data. Experimental data is the black line and the fit is the red line.

4.4 Discussion

The effect of NaCl concentration on NapA NR activity was investigated for the recombinant *C. jejuni* enzyme. In *C. jejuni* NapA the presence of chloride seems to impact binding affinity (K_M) while hardly showing any significant effect on turnover (Figure 4.5). The K_M for nitrate moderately increases with NaCl concentration and thus we propose that chloride may be bound in some form to NapA such that nitrate entrance and docking to the molybdenum center are hindered as is the case for sulfite oxidase (SO).

While the impact of chloride has not been investigated in structural studies of NapA, it has been observed in the crystal structure of a similar MPT enzyme, SO. Chloride inhibits molybdenum enzyme SO by creating a blocked species where substrate and/or product is sterically hindered preventing entrance or departure from the catalytic pocket [4]. In SO, chloride was previously suggested to be directly bound to Mo as suggested by EPR [4, 380]. However, XAS

and X-ray crystallography suggest the chloride is bound in the pocket interacting with R190 and W204 (Figure 4.14). The bound chloride ion disrupts substrate access and product departure from the active site by somehow promoting hydrolysis of the Mo-OSO_3^- bond of the reduced enzyme-product complex leaving a Mo-OH ligand in its place [4, 381-383]. In *C. jejuni* NapA, NaCl impacts K_M while the turnover rate is virtually unaffected, which agrees with the latter position. The chloride ion may hinder substrate binding resulting in an increase in K_M ; however, the turnover is not significantly affected suggesting that substrate binding to Mo is not the rate-limiting step in the reduction of nitrate.

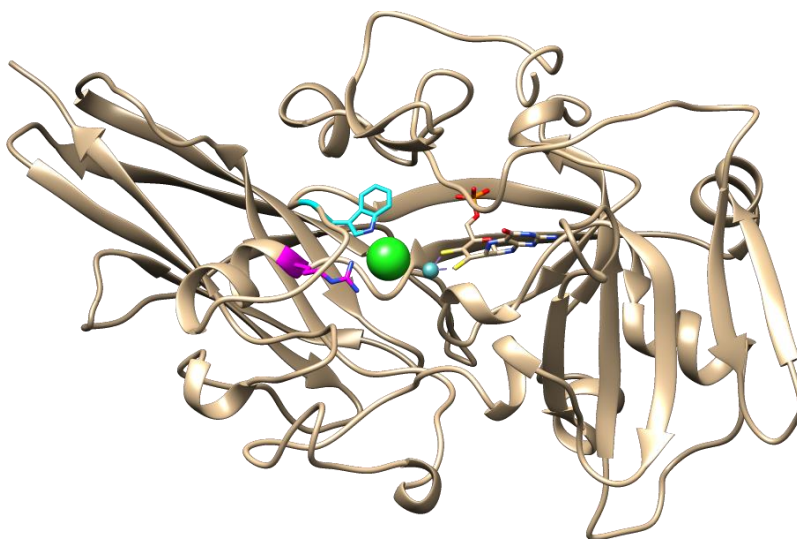


Figure 4.14: Crystal structure of sulfite oxidase (PDB 2A99, 42% identity with *C. jejuni* NapA) with chloride ion bound in the active site. Molybdenum ion depicted as blue sphere, chloride ion as green sphere, W204 in cyan, and R190 in magenta. Image visualized in Chimera.

The larger oxyanion sulfate, however, does not impact NapA activity nor nitrate binding. While chloride is probably present in the active site pocket impacting substrate affinity, sulfate shows no effect on affinity or turnover (Figure 4.6) implying this large anion does not interfere in the catalytic pocket. Sulfate has been shown to exhibit activation effects on *D. desulfuricans* NapA, but only in phosphate buffer suggesting a dependence on ionic strength not a specific interaction with sulfate [270]. Bursakov [270] suggests the enzyme may suffer changes in the surface charge modifying the structure and making the molybdenum site more accessible, justifying in this way the higher activities for high salt concentration.

C. jejuni NapA activity does not significantly change in the presence of sulfate and the higher NaCl concentration does not significantly impact activity either suggesting the *C. jejuni* enzyme may be more resistant to ionic changes than the *D. desulfuricans* enzyme. The size and surface charge of *C. jejuni* NapA is larger and the surface is more basic than other Naps including *D. desulfuricans* NapA (Figure 3.3) [305, 344]. These different properties associated with *C. jejuni* NapA may be responsible for the resistant behavior to ionic strength as compared to other nitrate reductases.

Further structural information regarding the nature of the ligand set around the molybdenum center of NapA was gathered from XAS experiments of recombinant *C. jejuni* NapA in order to better understand the activity and mechanistic transitions of the NR. The XANES spectra for as-isolated *C. jejuni* NapA samples (Figure 4.10) revealed the possibility of NapA being isolated as a heterogeneous mixture of enzyme states. As previously mentioned in Chapter 2, the SEC fractionation of NapA into two eluted peaks suggested multiple forms of NapA were isolated. However, the XAS samples were prepared from only the second eluted peak of SEC purified enzyme, suggesting that even within the two eluted peaks the isolated enzyme is a heterogeneous mixture of enzyme states. SEC suggests NapA is isolated as different molecular sizes or a possible difference in folded/maturity states of the enzyme and XAS spectra reveal the as-isolated NapA exists as a heterogeneous mixture of either molybdenum oxidation states and/or different molybdenum coordination geometries. The heterogeneous mixture could be inherent to the as-isolated sample and reflect the natural mixture of states, or it could represent a mishandling of the enzyme where the Mo center is oxidatively damaged resulting in a mixture of oxidation states.

Despite the discovery of the heterogeneity of as-isolated NapA enzyme, the EXAFS data (Figure 4.11) were fit to determine the structural details concerning the nature of the first coordination sphere of the molybdenum ion. The as-isolated NapA enzyme was fitted to a model containing a mixture of 1.0:0.9 (Fit 8: fit to $k=12 \text{ \AA}^{-1}$) to 1.0:1.2 (Fit 9: fit to $k=14 \text{ \AA}^{-1}$) of Mo(VI) with 1 Mo=O + 5 Mo-S bonds and Mo(IV) with 1 Mo-OH + 5 Mo-S bonds (Table 4.2). This fit was the best among those tested in Table 4.2 with a reasonable weighted R factor giving a fractional misfit between the data and the model of 5.82% for Fit 8 and 10.54% for Fit 9. The most important result from the models fit to these data is the fact that a terminal sulfido group (=S) does not appear to be coordinated to the Mo center as has been established for the *D. desulfuricans* Nap

[310] and the *C. necator* Nap enzyme [130]. This result has profound implications for the mechanism of *C. jejuni* NapA.

The currently accepted mechanism for Nap is the sulfur shift mechanism proposed in 2013 (Figure 4.4) [375]. Briefly, a persulfide bond between the terminal sulfido and ligating cysteine sulfur forms in the presence of substrate, with decoordination of the cysteine sulfur from Mo. Nitrate now binds to the vacant site and OAT commences. The change in the coordination of cysteine sulfur to a terminal persulfide is thus termed the ‘sulfur shift’ (Figure 4.4) [375]. Without a terminal inorganic sulfur donor (*i.e.* sulfide) bound to Mo in *C. jejuni* NapA, a sulfur shift cannot occur. Thus, *C. jejuni* NapA most likely follows a mechanism similar to that originally proposed for *D. desulfuricans* Nap (Figure 4.3) [309].

It is strange that one Nap enzyme would have a terminal sulfido and another would replace it with a terminal oxo group. Thus, it is possible that Nap really should be coordinated by a terminal sulfido, and the sulfido has been oxidized to a terminal oxo during the aerobic expression and purification of recombinant *C. jejuni* NapA. Oxidative degradation of a terminal sulfido has been previously proposed for aerobically purified TMAOR by Kaufmann *et al.* [384]. However, the evidence provided by Kaufmann *et al.* that a terminal sulfido naturally occurs in TMAOR is lacking as well as evidence to support their proposal of oxidative degradation [384]. Thus, there exists great controversy over the assignment of sulfido or oxo as the sixth terminal ligand in this family of enzyme.

Chemically, it would be expected that the resonance forms of the sulfido bond proposed during the sulfur shift in Nap would be preferentially protonated instead of the terminal oxo as has been discussed in small molecule systems [385-389]. For example, when water was introduced to solutions of $[L^*MoS(S_2PR_2)]^+$ ($L^* = HB(3-Pr^i pz)_2(5-Pr^i pz)^-$; $R = Pr^i, Ph$), the initial product was short-lived and was suggested to likely be $L^*Mo^V S(OH)(S_2PR_2)$. The short-lived species was rapidly transformed to a more thermodynamically favored form of $L^*Mo^V O(SH)(S_2PR_2)$. The Mo=S moiety was thus concluded to undergo decomposition and/or dinucleation in the presence of water unless actively stabilized [385]. Additionally, in the selenido-bis(dithiolene)-molybdenum(IV) and -tungsten(IV) complex model system the formation of a $M^{VI}O(Se)$ species was unconfirmed; however, the results obtained from OAT experiments suggest that the $M^{VI}O(Se)$ species might be generated once by initial OAT. Before successive turnover can commence, Se is reductively eliminated from the $M^{VI}O(Se)$ unit to give the observed reduced $M^{IV}O$ complex [387].

Doonan *et al.* [386] conducted an extensive investigation combining computations and spectroscopic studies on small molecule mimics of the Moco in XO. The vibrational Raman results indicated the terminal sulfido ligand has little effect on the nature of the apical $M\equiv O$ bond and that the out-of-plane sulfido orbital does not compete favorably with the oxo ligand for the $\psi_{xz,yz}$ orbitals. The Mulliken population analysis shows the sulfido and oxo donors possess net negative charges, with a more ionic Mo-O_{oxo} bond as compared with Mo-S_{sulfido}. The results were consistent with the sulfido being a more efficient charge donor to Mo when compared with the O_{oxo} donor. Furthermore, if the sulfido ligand lies in the equatorial plane of the active site under turnover conditions, then this geometric arrangement was suggested to control the reactivity of the active site regarding reaction mechanisms involving the sulfido as an electrophile. The sulfido ligand was proposed as a potential conduit for electron flow from substrate to the oxidized molybdenum site. The large Mo-S_{sulfido} covalency results in the S_{sulfido} being considerably more electrophilic than the terminal oxo. With respect to the O_{oxo} donor, the more electrophilic nature of S_{sulfido} in the [MoOS]²⁺ unit is consistent with the $\psi_{xy}\pi^*$ orbital acting as the two electron acceptor orbital in either a hydride or coupled $2e^-/H^+$ transfer mechanism [386].

Sproules *et al.* [389] observed similar trends in W-complexes where the sulfido-W(V) complexes have lower energy electronic transitions, lower g_{iso} , larger $A_{iso}(^{183}W)$ values, and more positive reduction potentials compared with their oxo-W(V) counterparts. Upon exchanging a terminal oxo for a sulfido ligand the HOMO–LUMO gap is lowered by $\sim 5000\text{ cm}^{-1}$, which leads to lower g-values as a result of the reduced ligand field splitting [389]. Similarly, Doonan and coworkers [388] also reported that the frontier orbitals of oxosulfido-Mo(V) compounds are dominated by contributions from the Mo=S unit, with significant covalency and extensive spin delocalization across the whole unit.

Therefore, due to the increased electrophilicity of the sulfido compared to the oxo group we predict the sulfido electrons donated to Moco would reside in the sulfur orbitals resulting in reactivity similar to that proposed for xanthine oxidase (XO) in either a hydride or coupled $2e^-/H^+$ transfer mechanism. Either way, S_{sulfido} would be reductively eliminated before oxygen during the regeneration of the Mo(IV) center in Nap. This would effectively inactivate the enzyme after a single turnover if the sulfur shift theory were true. In addition, Nap has no role for the sulfido group in catalysis. In FDH the sulfido is proposed to be the hydride acceptor after C-H bond cleavage in substrate formate [91, 390, 391]. Nitrate reduction is an OAT reaction without a formal

C-H bond to be broken and thus no hydride to participate in this role for the sulfido group that is suspected to be present in Nap. It is tempting to suggest that the reason FDH can turn over nitrate but Nap cannot turnover formate is linked to the absence of sulfido or an alternative partner that can cleave the C-H bond and accept the hydride to be transferred. Although we can conclude that the as-isolated *C. jejuni* NapA enzyme does not have a terminal sulfido coordinated to its Mo center, whether the sulfido or oxo terminal group is physiologically native to Nap and the implications to its mechanism cannot be determined at this time.

Furthermore, the XAS data of the as-isolated NapA compared to a sample treated with NaCl has a k space oscillation pattern and a Fourier Transform in R space that is significantly different (Figure 4.13). Their differing oscillation patterns suggest a different first coordination sphere around the Mo ion in the active site. Thus, it strongly implies that the added high concentration of Cl⁻ does impact the first coordination sphere of the Mo ion. However, as noted by George *et al.* [392], EXAFS is incapable of distinguishing between atom scatters of similar atomic number such as sulfur and chlorine. Thus, if Cl⁻ does in fact bind to Mo, then it will manifest as an apparent increase in the Mo-S/Cl coordination number because the Mo-Cl and Mo-S bond lengths are different by less than the EXAFS resolution [392].

Therefore, what we concluded regarding Cl⁻ treatment is that it changes the first sphere coordination of Mo. The EXAFS data analysis of the as-isolated NapA sample compared to the Cl⁻ treated sample reveal a change in the Mo-S(/Cl) bond lengths. The untreated enzyme has five identical Mo-S bond (2.379 Å) distances while the Cl⁻ treated enzyme has two different Mo-S/Cl bond distances. The best fit to the data revealed the Cl⁻ treated enzyme has a Mo ion coordinated with one oxygen shell (1 oxo bond; Fit 5-1.756 Å, Fit 6-1.758 Å), one shorter sulfur shell (2-3 Mo-S(/Cl); Fit 5-2.371 Å, Fit 6-2.358 Å), and one long sulfur shell (2-3 Mo-S(/Cl); Fit 5-2.535 Å, Fit 6-2.502 Å). From the XAS measurements alone it is not possible to determine if the Cl⁻ is binding to Mo or simply interacting with one of the dithiolene units creating the observed asymmetry. The only discernable difference in the models is apparent in the k=16 region, but the data set is very noisy at high k. As a result, the distinction between a Mo ion coordinated by 5S or 5S+1Cl cannot be determined.

Since the kinetic investigation of the impact of NaCl on NapA activity revealed no influence on k_{cat} but a moderate positive correlation with K_M (Figure 4.5), then Cl⁻ is most likely not bound as an axial ligand to Mo, which has been shown in small molecule mimics to inactivate the catalysis

at the Mo center [393]. The EXAFS data cannot confirm this assumption due to the high level of noise in the area around $k=16$, however, the EXAFS data are consistent with two alternative possibilities. First, the Cl^- may be situated in the catalytic pocket as in SO [4, 381-383], where it interferes with substrate binding. Second, the Cl^- could be interacting with one of the dithiolene units coordinating to Mo resulting in a shift of substrate affinity. It is possible that one sulfur from a dithiolene unit dissociates from the Mo and is replaced by a Cl^- ligand since dithiolene dissociation has been previously observed in DMSOR [394-396] and NR [357].

XAS measurements have revealed recombinant NapA is isolated as a mixture of coordination geometries, and chloride specifically influences the first coordination sphere of Mo. As mentioned previously, the exact reason NapA is isolated in a heterogenous mixture is not clear. Since NapA is purified via a His-tag, interference from the affinity tag must be excluded. While His-tags are an extremely common method for purifying overexpressed enzyme, they are notorious for interfering with enzyme activity particularly by extracting metals [128] and can cause protein characterization challenges [55, 101]. While Mo is unlikely to be stripped by the His-tag, Fe could be. In addition, any protein tag may interfere with protein folding and stability which could also impact Moco stability and thus activity. For example, Temple *et al.* observed untagged SO had higher molybdenum incorporation (80%) than the His-SO (62%) but the kinetic parameters were not significantly different (Table 1.12) [57]. The effect of the His-tag is enzyme-specific and does not appear to result in molybdenum loss or impact activity in every case, as in the case of YedY where a C-terminal His-tag was detrimental to the activity of YedY due to the His-tag interfering in YedY folding [101]. So, in order to test whether the *C. jejuni* NapA His-tag could be responsible for the heterogenous mixture observed in the as-isolated enzyme or impact activity, the His-tag was cleaved. The cleaved enzyme had similar activity and metal content as the tagged enzyme, thus demonstrating that the *C. jejuni* NapA His-tag is not responsible for metal loss or negative activity effects. Unfortunately, it is still unclear what phenomena is causing the heterogenous mixture of as-isolated NapA.

4.5 Summary

The recombinant *C. jejuni* NapA has been structurally characterized by XAS. The as-isolated NapA enzyme is a heterogenous mixture of either Mo oxidation states or Mo coordination geometries, as evidenced by XAS measurements. The most notable feature is the fact that a

terminal sulfido donor (=S) is not coordinated to the Mo center, which has significant implications for the mechanism of *C. jejuni* NapA. EXAFS in combination with kinetic experiments suggests that Cl⁻ impacts the active site of NapA. The data may represent a structural change that impacts substrate affinity due to an increase in ionic strength. Two possibilities by which Cl⁻ may impact the active site are: first, the Cl⁻ may be situated in the catalytic pocket as in SO [4, 381-383] interfering with substrate binding or second, the Cl⁻ could be interacting with one of the dithiolene units coordinating Mo resulting in a shift of substrate affinity. It is possible that one or more sulfur atoms from a dithiolene unit dissociates from the Mo and is replaced by a Cl ligand; however, at the current resolution of the EXAFS data this possibility cannot be confirmed. The resolution in EXAFS represents how reliable the distances obtained from the EXAFS fit are. To improve the resolution in the future, EXAFS samples must contain higher concentrations of Mo to improve the signal quality. Sampling a longer k space oscillation range would also improve the resolution. The k space oscillation range depends on the quality of the sample (i.e. concentration of intact Mo centers) and the experimental conditions of the SSRL. Specifically, a higher energy beam may increase sensitivity. This foundational knowledge of *C. jejuni* NapA will serve as a basis and first step in investigating the efficacy of substrate selection by the members of the DMSOR family specifically focusing on the role of the Mo coordinating residue as will be discussed in detail in Chapter 5.

CHAPTER 5. ROLE OF THE MOLYBDENUM-COORDINATING RESIDUE IN PERIPLASMIC NITRATE REDUCTASE

A version of this chapter has been submitted to the Journal of Biological Inorganic Chemistry.

5.1 Introduction

The MPT-containing enzymes have been contributing to life for millennia, dating as far back as 3.5–3.8 billion years. Furthermore, the Moco, determined to be present in LUCA, the last universal common ancestor [23, 397]. Today there are over 50 different molybdopterin enzymes known to catalyze a variety of chemistries in the cycling of C, N, S, As, and Se, all relying on the Moco (Figure 5.1A). The biochemical efficacy among the molybdopterin enzymes depends on the variations in the enzyme structure, particularly on the molybdenum coordination environments. However, the extent to which the structural variation impacts the kinetic proficiency remains unclear. To evaluate these variations, the role of the coordinating amino acid in the dimethyl sulfoxide reductase (DMSOR) family of molybdopterin enzymes was investigated.

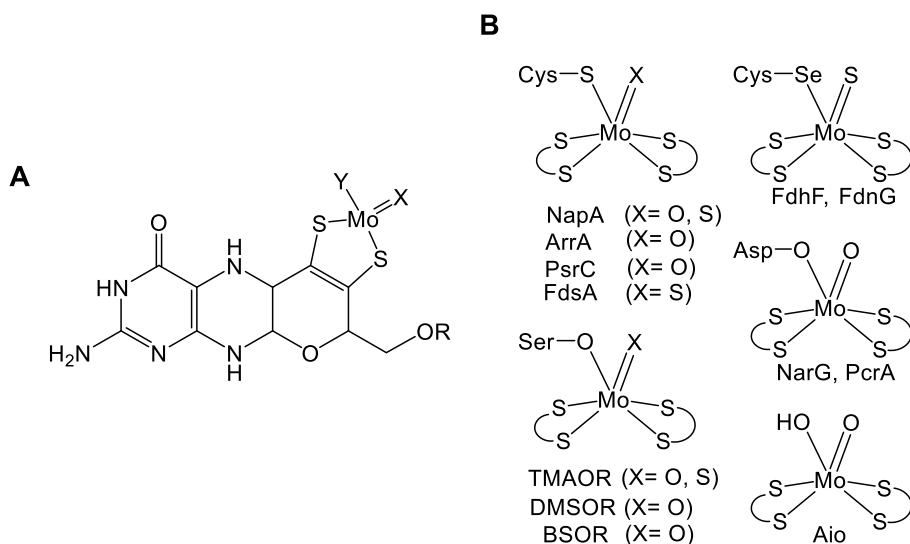


Figure 5.1: A) a partial structure of Moco as in Nap, consists of the Mo metal coordinated by two molybdopterin (MPT) molecules (only one is displayed here). The Mo metal is coordinated to four dithiolene sulfurs that are appended to a pyranopterin heterocycle. The generic R group is guanine dinucleotide in Nap. (B) The first coordination sphere of Mo in several members of the DMSOR family.

The extensive array of respiratory enzymes encoded by bacterial genomes enables a diverse metabolism. Of these respiratory enzymes, members of the DMSOR family such as nitrate reductase (NR), dimethyl sulfoxide reductase (DMSOR), trimethylamine N-oxide reductase (TMAOR), and formate dehydrogenase (FDH), contribute to this broad diversity. Many enzymes in the DMSOR family use oxygen atom transfer (OAT) reactions for substrate transformation, e.g., periplasmic nitrate reductase (Nap) and respiratory nitrate reductase (Nar) reduce nitrate to nitrite, TMAOR reduces TMAO to TMA, and DMSOR reduces DMSO to DMS.

The basic structure of Moco is depicted in Figure 5.1A, where the trigonal prismatic molybdenum center in DMSOR family members is coordinated by four sulfur donors from two molybdopterin (MPT) cofactors. The 5th and 6th positions vary depending on the enzyme (Figure 1). The 5th position (Y in Figure 5.1A) is occupied by a coordinated amino acid residue and the 6th position is defined as the terminal position (X in Figure 5.1). Thus, the DMSOR family of enzymes has diverse active sites that vary in the first coordination sphere of the molybdenum center (Figure 5.1B). Interestingly, enzymes that catalyze the same reaction, such as Nap and Nar, have different molybdenum coordination spheres. In NapA, for instance, molybdenum is coordinated by a cysteine residue in the 5th position and an oxo or a sulfido group in the 6th position while in NarG the 5th position is held by an aspartate residue and the 6th position is an oxo group. Despite the variations at the molybdenum center, both NapA and NarG enzymes can reduce nitrate to nitrite (Figure 5.1B).

The coordinating residue has been hypothesized to tune the substrate preference through the adjustment of chemical properties of the molybdenum center [398]. Expression of functional MPT enzymes has been challenging (Chapter 1; [1]); however, progress in this area has been made [1, 54, 67, 90, 97, 135, 167, 369, 378, 384, 399-404]. These pursuits have revealed the coordinating residue is critical in the physiological function of the DMSOR family of enzymes while not required for Moco insertion and stability [135]. However, the substrate profile of these variants has been limited to the natural substrates of the native enzyme. The consequences of exchanging the coordinating amino acid on the activities of various substrates have not been fully explored. Thus, the mode of action of the coordinating residue in this family of enzymes is not completely understood.

Herein, we examine the role of the coordinating residue through a kinetic and energetic perspective. The goal of this work is to develop a fundamental understanding of the extent that

perturbations at the molybdenum center, specifically the coordinating amino acid residue, influence the function of members of the DMSOR family. To this end, we have selected periplasmic nitrate reductase (NapA) from *Campylobacter jejuni* [329] as a model system. Alanine, serine, and aspartate variants of the coordinating cysteine in *C. jejuni* NapA have been produced and analyzed in this study. Steady-state kinetic profiles for nitrate, TMAO, and DMSO for each variant have been determined to develop a quantitative picture. The data are presented and discussed in the context of current knowledge of how molybdenum coordination influences the activity of the DMSOR family of enzymes.

5.2 Materials and Methods

The QuikChange II Mutagenesis Kit was purchased from Agilent (Cedar Creek, TX, USA). Mutagenesis primers were designed according to Agilent's QuikChange method, and synthesized by Integrated DNA Technologies (Coralville, IA, USA). DNA sequencing was carried out at ACGT Inc. (Germantown, MD, USA).

5.2.1 Protein Concentration Determination

Protein concentrations were determined using the Coomassie Plus (Bradford) Protein Assay Kit (Thermo Scientific) with bovine serum albumin as a standard (Pierce).

5.2.2 SDS-PAGE

SDS-PAGE was performed as described in Chapter 2 Section 2.2.6.

5.2.3 Metal Analysis

Metal analysis was conducted at the University of Pittsburgh with the assistance of Dr. Daniel Bain as described in Chapter 2 Section 2.2.8.3.

5.2.4 UV-Vis Spectroscopy

UV-Vis spectra were collected on various protein concentrations in 50 mM HEPES pH 7.00 using an Agilent 8453 spectrophotometer scanning from 200-800 nm.

Table 5.1: Reported variations of the molybdenum-coordinating residue in various mononuclear molybdenum enzymes.

Enzyme	Variant	Specific Activity ($\mu\text{mol}/\text{min} \cdot \text{mg}$)	Substrate	Percent of WT	pH	Reference
<i>Cj</i> NapA	C176	3.40	Nitrate	100%	7.0	[329]
<i>Cj</i> NapA	C176S	0.026	Nitrate	0.76%	7.0	[329]
<i>Cj</i> NapA	C176D	0.58	Nitrate	17%	7.0	This work
<i>Cj</i> NapA	C176A	inactive	Nitrate	0%	7.0	This work
<i>Cj</i> NapA	C176	0.053	TMAO	100%	7.0	This work
<i>Cj</i> NapA	C176S	0.063	TMAO	119%	7.0	This work
<i>Cj</i> NapA	C176D	inactive	TMAO	0%	7.0	This work
<i>Cj</i> NapA	C176A	inactive	TMAO	0%	7.0	This work
<i>Cj</i> NapA	C176	inactive	DMSO	0%	7.0	This work
<i>Cj</i> NapA	C176S	inactive	DMSO	0%	7.0	This work
<i>Cj</i> NapA	C176D	0.009	DMSO	0.26%	7.0	This work
<i>Cj</i> NapA	C176A	inactive	DMSO	0%	7.0	This work
<i>Cn</i> Nap	C181	0.73	Nitrate	100%	6.5	[378]
<i>Cn</i> Nap	C181S	inactive	Nitrate	0%	6.5	[378]
<i>An</i> Nas	C150	103000	Nitrate	100%	6.8	[399]
<i>An</i> Nas	C150A	inactive	Nitrate	0%	6.8	[399]
<i>Ec</i> Fdh-H	U140	2800 ^d	Formate	100%	7.5	[400]
<i>Ec</i> Fdh-H	U140C	9 ^d	Formate	0.32%	7.5	[400]
<i>Rc</i> FDH	C386	Not reported	Formate	100%	9.0	[90]
<i>Rc</i> FDH	C386S	inactive	Formate	0%	9.0	[90]
<i>Rc</i> FDH	C386	Not reported	Formate	88%	8.0	[90]
<i>Rc</i> FDH	C386S	inactive	Formate	0%	8.0	[90]
<i>Rc</i> FDH	C386	Not reported	Formate	6%	7.0	[90]
<i>Rc</i> FDH	C386S	inactive	Formate	0%	7.0	[90]
<i>Rs</i> BSOR ^a	S121	375	BSO	100%	8.0	[135]
<i>Rs</i> BSOR ^a	S121A	0.06 ^b	BSO	0.02% ^b	8.0	[135]
<i>Rs</i> BSOR ^a	S121T	0.63 ^b	BSO	0.17% ^b	8.0	[135]

Table 5.1 Continued

Enzyme	Variant	Specific Activity ($\mu\text{mol}/\text{min}\cdot\text{mg}$)	Substrate	Percent of WT	pH	Reference
<i>R_S</i> BSOR ^a	S121C	0.38 ^b	BSO	0.1% ^b	8.0	[135]
<i>R_S</i> BSOR ^a	S121	21.3	Ferricyanide	100%	8.0	[135]
<i>R_S</i> BSOR ^a	S121A	inactive	Ferricyanide	0%	8.0	[135]
<i>R_S</i> BSOR ^a	S121T	0.63 ^b	Ferricyanide	2.9% ^b	8.0	[135]
<i>R_S</i> BSOR ^a	S121C	0.5 ^b	Ferricyanide	2.4% ^b	8.0	[135]
<i>R_S</i> BSOR ^a	S121	385	TMAO	100%	8.0	[135]
<i>R_S</i> BSOR ^a	S121A	inactive	TMAO	0%	8.0	[135]
<i>R_S</i> BSOR ^a	S121T	0.13 ^b	TMAO	0.03% ^b	8.0	[135]
<i>R_S</i> BSOR ^a	S121C	0.13 ^b	TMAO	0.03% ^b	8.0	[135]
<i>R_S</i> BSOR ^a	S121	248	NNO	100%	8.0	[135]
<i>R_S</i> BSOR ^a	S121A	0.04 ^b	NNO	0.02% ^b	8.0	[135]
<i>R_S</i> BSOR ^a	S121T	0.75 ^b	NNO	0.30% ^b	8.0	[135]
<i>R_S</i> BSOR ^a	S121C	0.13 ^b	NNO	0.05% ^b	8.0	[135]
<i>R_S</i> BSOR ^a	S121	319	ANO	100%	8.0	[135]
<i>R_S</i> BSOR ^a	S121A	inactive	ANO	0%	8.0	[135]
<i>R_S</i> BSOR ^a	S121T	0.63 ^b	ANO	0.20% ^b	8.0	[135]
<i>R_S</i> BSOR ^a	S121C	0.13 ^b	ANO	0.04% ^b	8.0	[135]
<i>R_S</i> BSOR ^a	S121	76.3	MSO	100%	8.0	[135]
<i>R_S</i> BSOR ^a	S121A	inactive	MSO	0%	8.0	[135]
<i>R_S</i> BSOR ^a	S121T	inactive	MSO	0%	8.0	[135]
<i>R_S</i> BSOR ^a	S121C	inactive	MSO	0%	8.0	[135]
<i>R_S</i> BSOR ^a	S121	120	DMSO	100%	8.0	[135]
<i>R_S</i> BSOR ^a	S121A	inactive	DMSO	0%	8.0	[135]
<i>R_S</i> BSOR ^a	S121T	inactive	DMSO	0%	8.0	[135]
<i>R_S</i> BSOR ^a	S121C	inactive	DMSO	0%	8.0	[135]
<i>R_S</i> DMSOR ^a	S147	42.4	DMSO	100%	7.5	[54]
<i>R_S</i> DMSOR ^a	S147C	16.5	DMSO	39%	7.5	[54]
<i>R_S</i> DMSOR ^a	S147	212	TMAO	100%	7.5	[54]
<i>R_S</i> DMSOR ^a	S147C	44	TMAO	21%	7.5	[54]

Table 5.1 Continued

Enzyme	Variant	Specific Activity ($\mu\text{mol}/\text{min}\cdot\text{mg}$)	Substrate	Percent of WT	pH	Reference
<i>Rs</i> DMSOR ^a	S147	51	MSO	100%	7.5	[54]
<i>Rs</i> DMSOR ^a	S147C	0.05	MSO	0.09%	7.5	[54]
<i>Rs</i> DMSOR ^a	S147	65	Chlorate	100%	7.5	[54]
<i>Rs</i> DMSOR ^a	S147C	2.2	Chlorate	3.5%	7.5	[54]
<i>Rs</i> DMSOR ^a	S147	56	BSO	100%	7.5	[54]
<i>Rs</i> DMSOR ^a	S147C	0.31	BSO	0.54%	7.5	[54]
<i>Rs</i> DMSOR ^a	S147	84	ANO	100%	7.5	[54]
<i>Rs</i> DMSOR ^a	S147C	424	ANO	507%	7.5	[54]
<i>Ec</i>	control	1.5	DMSO	15%	7.0	[401]
<i>Ec</i> DMSOR	S176	10	DMSO	100%	7.0	[401]
<i>Ec</i> DMSOR	S176A	0.4 ^b	DMSO	4% ^b	7.0	[401]
<i>Ec</i> DMSOR	S176C	0.36 ^b	DMSO	3.6% ^b	7.0	[401]
<i>Ec</i> DMSOR	S176H	0.29 ^b	DMSO	2.9% ^b	7.0	[401]
<i>Ec</i>	control	16	TMAO	17%	7.0	[401]
<i>Ec</i> DMSOR	S176	96	TMAO	100%	7.0	[401]
<i>Ec</i> DMSOR	S176A	3.6 ^b	TMAO	3.8% ^b	7.0	[401]
<i>Ec</i> DMSOR	S176C	3.1 ^b	TMAO	3.2% ^b	7.0	[401]
<i>Ec</i> DMSOR	S176H	2.8 ^b	TMAO	2.9% ^b	7.0	[401]
Anaerobic <i>Ec</i> TMAOR	S191	Not reported	TMAO	100% ^e	6.5	[384]
Anaerobic <i>Ec</i> TMAOR	S191C	Not reported	TMAO	~40% ^e	6.5	[384]
Aerobic <i>Ec</i> TMAOR	S191	Not reported	TMAO	~40% ^e	6.5	[384]
Aerobic <i>Ec</i> TMAOR	S191C	Not reported	TMAO	~40% ^e	6.5	[384]
Chicken SO	C185	Not reported	Sulfite	100%	8.5	[402]
Chicken SO	C185S	inactive	Sulfite	<1% ^b	8.5	[402]
Chicken SO	C185A	inactive	Sulfite	<1% ^b	8.5	[402]

Table 5.1 Continued

Enzyme	Variant	Specific Activity ($\mu\text{mol/min}\cdot\text{mg}$)	Substrate	Percent of WT	pH	Reference
Human SO	C207	Not reported	Sulfite	100%	8.5	[67]
Human SO	C207S	inactive	Sulfite	~0.0005%	8.5	[67]
Human SO ^c	C207	9.4 ^d	Sulfite	100%	6.0	[403]
Human SO ^c	C207U	26.1 ^d	Sulfite	278%	6.0	[403]
Human SO ^c	C207	19.8 ^d	Sulfite	100%	7.1	[403]
Human SO ^c	C207U	46.6 ^d	Sulfite	235%	7.1	[403]
Human SO ^c	C207	19.8 ^d	Sulfite	100%	7.9	[403]
Human SO ^c	C207U	37.7 ^d	Sulfite	190%	7.9	[403]
Human SO ^c	C207	25.8 ^d	Sulfite	100%	8.4	[403]
Human SO ^c	C207U	41.2 ^d	Sulfite	160%	8.4	[403]
Human SO ^c	C207	36.2 ^d	Sulfite	100%	8.9	[403]
Human SO ^c	C207U	31.8 ^d	Sulfite	88%	8.9	[403]

^acalculated from reported values and assay information; ^bbelow assay background, essentially inactive, ^cSO was modified exchanging four Cys residues to Ser to facilitate the exchange of C207 with U; ^dvalue reported as k_{cat} in s^{-1} ; ^evalues estimated based on graphic representations published; ^fSO-sulfite oxidase, DMSOR-dimethyl sulfoxide reductase, BSOR-biotin sulfoxide reductase, Nas-assimilatory nitrate reductase, Nap-periplasmic nitrate reductase, WT-wildtype, TMAO- trimethyl amine N-oxide, NNO- nicotinamide-N-oxide, ANO-adenosine N^1 -oxide, MSO- methionine sulfoxide, *Cj*- *C. jejuni*, *Cn*- *Cuprividas necator*, *An*-*Aspergillus nidulans*, *Ec*-*E. coli*, *Rc*- *Rhodobacter capsulatus*, *Rs*- *R. sphaeroides*, U-selenocysteine.

5.2.5 Site-Directed Mutagenesis

Mutagenesis of *C. jejuni napA* was conducted using the QuikChange II Site-Directed Mutagenesis Kit (Qiagen) with the pBM10C plasmid as template according to the manufacturer's protocol. The primers designed for the *napA-C176S/A/D* mutations are listed in Table 5.2. The PCR product was sequenced at ACGT Inc. Plasmids pBM10C_C176S, pBM10C_C176D, and pBM10C_C176A were expressed to produce the C176S, C176D, and C176A NapA variants, respectively.

Table 5.2: Summary of plasmids and oligonucleotides used in this study.

Plasmid or Oligonucleotide	Description	Source
pBM10C	NdeI-XhoI digested 2.8 Kbp fragment including the <i>napA</i> gene and TEV-cleavable C-terminal hexa-histidine coding sequence from pMCSG32_ <i>napA</i> cloned into pBM9A at the corresponding restriction sites (Kan ^R)	This Work
pBM10C_C176S	Site-directed mutagenesis of pBM10C with <i>napA-C176S</i> (Kan ^R)	This Work
pBM10C_C176D	Site-directed mutagenesis of pBM10C with <i>napA-C176D</i> (Kan ^R)	This Work
pBM10C_C176A	Site-directed mutagenesis of pBM10C with <i>napA-C176A</i> (Kan ^R)	This Work
<i>napA-C176S</i> -forward	5'-AAT GCA AGA CAT <u>T</u> CT ATG GCC TCT GCA-3'	This Work
<i>napA-C176S</i> -reverse	5'-TGC AGA GGC CAT <u>A</u> GA ATG TCT TGC ATT-3'	This Work
<i>napA-C176D</i> -forward	5'-AAT GCA AGA CAT <u>G</u> AT ATG GCC TCT GCA-3'	This Work
<i>napA-C176D</i> -reverse	5'- TGC AGA GGC CAT <u>A</u> TC ATG TCT TGC ATT-3'	This Work
<i>napA-C176A</i> -forward	5'-AAT GCA AGA CAT <u>G</u> CT ATG GCC TCT G-3'	This Work
<i>napA-C176A</i> -reverse	5'-CAG AGG CCA TAG <u>C</u> AT GTC TTG CAT T-3'	This Work

* Amp^R indicates resistance to ampicillin, and Kan^R resistance to kanamycin; bp, basepair. Mutated bases are underlined.

5.2.6 Production and Purification of Recombinant Proteins

NapA (~108 kDa) and its variants (C176S/D/A NapA) were expressed and purified as discussed in Chapter 2.

5.2.7 Steady-State Kinetics

Nitrate reductase activity was measured spectrophotometrically by monitoring oxidation of reduced methyl viologen as described in Chapter 2 Section 2.2.7. TMAO, and DMSO reductase activities were measured spectrophotometrically by monitoring oxidation of reduced methyl viologen at 600 nm in the same manner as nitrate reductase activity with a few differences. Assays were conducted with a total reaction volume of 250 μ L (NapA) or 100 μ L (variants). Substrate addition initiated the reaction which was monitored for 5 minutes (NapA) or 15 min (NapA-C176S/A/D). Again, all rates were corrected for the concentration of active NapA in as-isolated samples by using the determined Mo concentrations for each sample. For pH experiments, methyl viologen was prepared and nitrate reduction rates were measured as previously described in Chapter 3 Section 3.2.5.

5.3 Results

5.3.1 Variants of NapA and their Characterization

In NapA, the coordinating residue to molybdenum is a Cys. In the case of *C. jejuni* NapA, it is Cys176, which was successfully exchanged for Ser, Asp, and Ala. The Ser variant emulates the first coordination sphere of molybdenum in TMAO reductase (TMAOR), and DMSOR (Figure 5.1B). The identity of both the native NapA and the C176S NapA variant have been confirmed by LC-MS and isolated previously [329]. The Asp variant mimics the first molybdenum coordination sphere of NarG, while the Ala variant was produced as control where no amino acid residue is coordinated to the Mo-center. Such a center has been found in arsenite oxidase (Aio) where molybdenum is not coordinated by a protein residue (Figure 5.1B) [405, 406].

The purity of each protein preparation was monitored by SDS-PAGE (Figure 5.2). The integrity of the [4Fe-4S] cluster was observed by UV-Vis spectrometry with a band 400 nm (Figure 5.3) similar to *Desulfovibrio desulfuricans* NapA [355] and cofactor incorporation was measured via inductively coupled plasma mass spectrometry (ICP-MS) (Table 5.3). The Ser and Ala variants have reasonable molybdenum incorporation of 70-80% which is comparable to the native NapA enzyme (Table 5.3) while the Asp variant has significantly lower molybdenum incorporation. On average, the amount of holo C176D NapA isolated is 14-28 times lower than the yield of holoenzyme isolated for native NapA or the C176S/A NapA variants. While native recombinant

NapA was on average isolated with a yield of 2.3 mg/L of culture, the C176S/A variants typically purified in higher yields of 3.7 and 4 mg/L of culture respectively. The C176D variant; however, had a significantly lower yield of 0.72 mg/L of culture.

Table 5.3: Metal analysis of *C. jejuni* NapA variants.

Enzyme Variant	Average Moles of Mo per Mole of Enzyme	Average Moles of Fe per Mole of Enzyme	Average Moles of Fe per Mole of Mo
<i>Cj</i> NapA	$0.92 \pm 0.1^*$	$5.0 \pm 1.2^*$	$5.4 \pm 0.3^*$
<i>Cj</i> C176S NapA	$0.74 \pm 0.1^*$	$3.8 \pm 1.1^*$	$5.1 \pm 0.3^*$
<i>Cj</i> C176D NapA	0.15 ± 0.03	1.2 ± 0.4	8 ± 0.4
<i>Cj</i> C176A NapA	0.79 ± 0.1	3.4 ± 1.1	4.3 ± 0.3

*Value represents what is incorporated in NapA assuming a NapA:NapD ratio of 1;1.

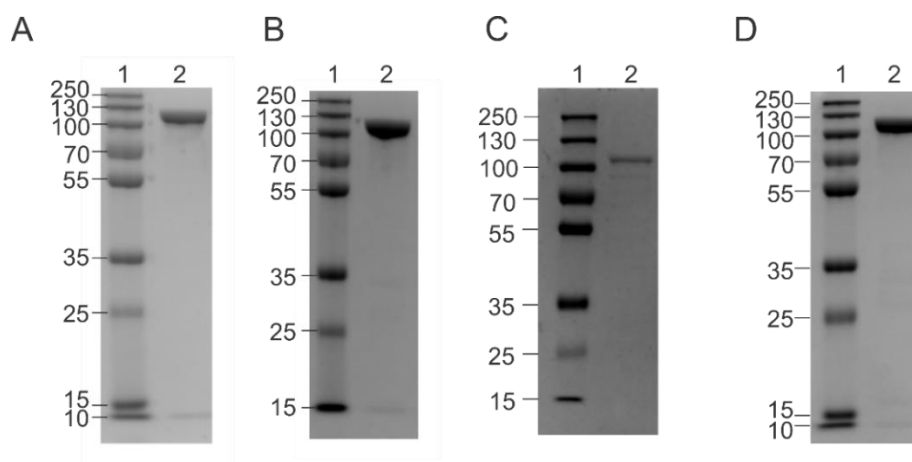


Figure 5.2: Purity and integrity of C176 NapA variants. SDS-PAGE of A) native *C. jejuni* NapA, B) C176S NapA, C) C176D NapA, and D) C176A NapA. The NapA variants are ~108 kDa.

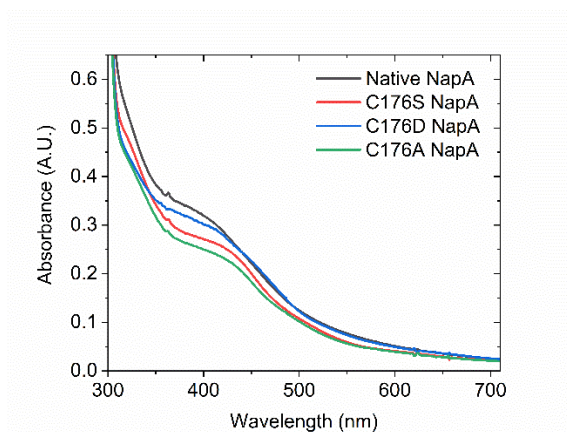


Figure 5.3: UV-Visible Spectra of the C176 NapA variants in 50 mM HEPES pH 7.00.

Table 5.4: Kinetic parameters of *C. jejuni* NapA and C176S/D/A variants compared to similar DMSOR family enzymes

Enzyme ^a	Substrate	K _m (μM)	k _{cat} (s ⁻¹)	k _{cat} /K _m (1/s* ^a M)	Reference
<i>Cj</i> WT rNapA	Nitrate	3.4 ± 0.44	5.91 ± 0.176	1.74 x 10 ⁶	[329]
<i>Cj</i> C176S rNapA	Nitrate	307 ± 16	0.045 ± 0.001	1.47 x 10 ²	[329]
<i>Cj</i> C176D rNapA	Nitrate	462 ± 66	0.339 ± 0.012	7.34 x 10 ²	This work
<i>Cj</i> C176A rNapA	Nitrate	Inactive	Inactive	Inactive	This work
<i>Cj</i> WT rNapA	TMAO	161 ± 20	0.092 ± 0.0026	5.71 x 10 ²	This work
<i>Cj</i> C176S rNapA	TMAO	205 ± 7	0.109 ± 0.0015	5.33 x 10 ²	This work
<i>Cj</i> C176D rNapA	TMAO	Inactive	Inactive	Inactive	This work
<i>Cj</i> C176A rNapA	TMAO	Inactive	Inactive	Inactive	This work
<i>Cj</i> WT rNapA	DMSO	Inactive	Inactive	Inactive	This work
<i>Cj</i> C176S rNapA	DMSO	Inactive	Inactive	Inactive	This work
<i>Cj</i> C176D rNapA	DMSO	28.2 ± 4.5	0.023 ± 0.001	8.16 x 10 ²	This work
<i>Cj</i> C176A rNapA	DMSO	Inactive	Inactive	Inactive	This work
<i>Rs</i> rNapAB	Nitrate	120	70.2	5.9 x 10 ⁵	[167]
<i>Pp</i> NapAB	Nitrate	112	58	5.2 x 10 ⁵	[356]
<i>Ec</i> rTMAOR	TMAO	210 ± 100	2500 ± 200	1.2 x 10 ⁷	[97]
<i>Rs</i> rDMSOR	DMSO	7 ± 1	50 ± 2	7.1 x 10 ⁶	[97]
<i>Ec</i> NarG	Nitrate	2	7.2	3.63 x 10 ⁶	[404]

^a*Cj*-*Campylobacter jejuni*, WT- wildtype, *Rs*- *Rhodobacter sphaeroides*, *Pp*- *Paracoccus pantotrophus*, *Ec*- *Escherichia coli*, r-recombinant enzyme

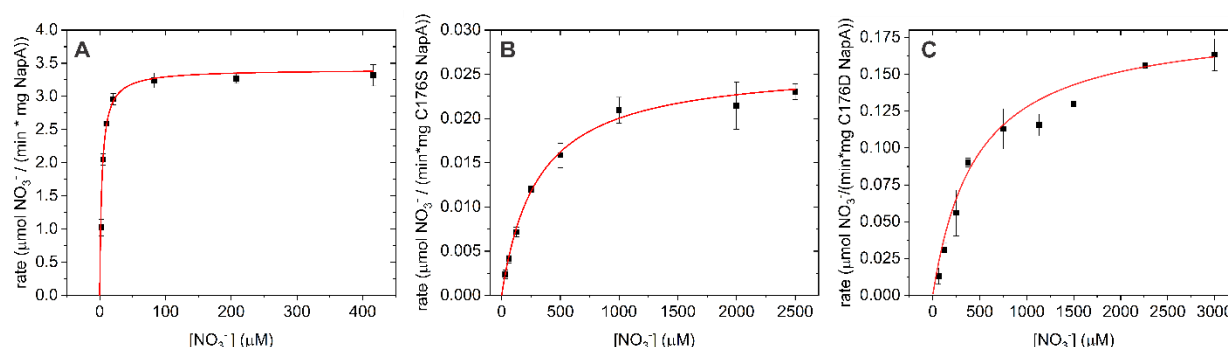


Figure 5.4: Steady-state kinetic data following the Michaelis-Menten model using nitrate as a substrate for (A) native *C. jejuni* NapA (B) C176S *C. jejuni* NapA variant (C) C176D *C. jejuni* NapA variant. These kinetics curves were reproduced by at least four biological replicates. Each data point in the curves contained three technical replicates for each substrate concentration.

5.3.2 Steady-State Kinetics of NapA Variants using Nitrate as a Substrate

Steady-state kinetic analysis of native NapA revealed an approximate K_M for nitrate of 3.4 μM and k_{cat} of 5.91 s^{-1} (using methyl viologen as a colorimetric electron donor) suggesting the enzyme has a high affinity for nitrate and is efficient at reducing nitrate as previously reported in Chapter 3 (Table 5.4). Compared to the native NapA, the K_M in C176S NapA has increased 100-fold and k_{cat} has decreased by 2 orders of magnitude (Figure 5.4AB, Table 5.4). The C176D NapA variant shows attenuated nitrate reductase activity with a k_{cat} 17 times lower than the native NapA enzyme and a K_M for nitrate that is 1.5 times higher than the K_M for nitrate reduction by the C176S NapA variant (Figure 5.4C, Table 5.4). Unlike the C176S/D NapA variants, C176A NapA is inactive towards nitrate. Exchanging the sulfur donor from Cys for an oxygen donor from either Asp or Ser decreases k_{cat} and increases K_M for nitrate while the uncoordinated variant completely abolishes nitrate activity and thus underscores the importance of a coordinated amino acid residue.

5.3.3 TMAO and DMSO Reductase Activity

Both native NapA and C176S NapA reduce TMAO, with C176S NapA having a slightly higher k_{cat} by 0.017 s^{-1} for reduction of TMAO; both enzymes have similar k_{cat}/K_M for TMAO reduction. (Figure 5.5, Table 5.4) The K_M of native NapA increased by 50 times when nitrate is substituted with TMAO as the substrate, and the k_{cat} for nitrate is 64 times higher than the k_{cat} for TMAO. The opposite effect was observed for C176S NapA. Here, the K_M for C176S NapA with TMAO as substrate decreased by a factor of 1.5 compared to the K_M of nitrate for C176S NapA. The k_{cat} of C176S NapA for TMAO reduction increased 2-fold as compared to C176S NapA nitrate reduction k_{cat} (Table 5.4). Interestingly, C176D NapA does not reduce TMAO unlike the native NapA enzyme that readily reduces TMAO. In contrast, DMSO reductase activity was nonexistent in both native NapA and C176S NapA, while C176D NapA is active, albeit marginally (Figure 5.6, Table 5.4). The K_M of the C176D NapA for DMSO decreased 16.5 times and the k_{cat} decreased by ~15 times when compared to C176D NapA towards nitrate activity (Table 5.4). Unlike the C176S/D variants, C176A NapA is inactive toward nitrate, DMSO, and TMAO.

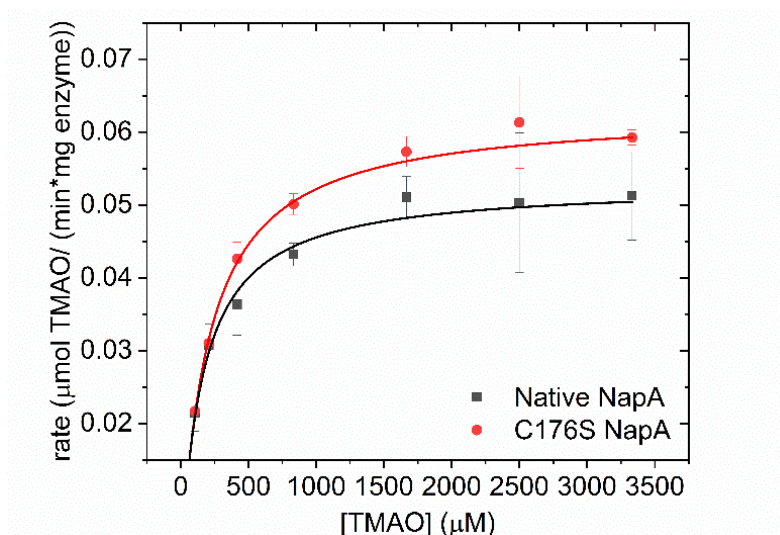


Figure 5.5: Steady-state kinetic data following the Michaelis-Menten model using TMAO as a substrate for native *C. jejuni* NapA (black squares) and C176S NapA (red circles). These kinetics curves were reproduced by one biological replicate. Each data point contained three technical replicates for each substrate concentration.

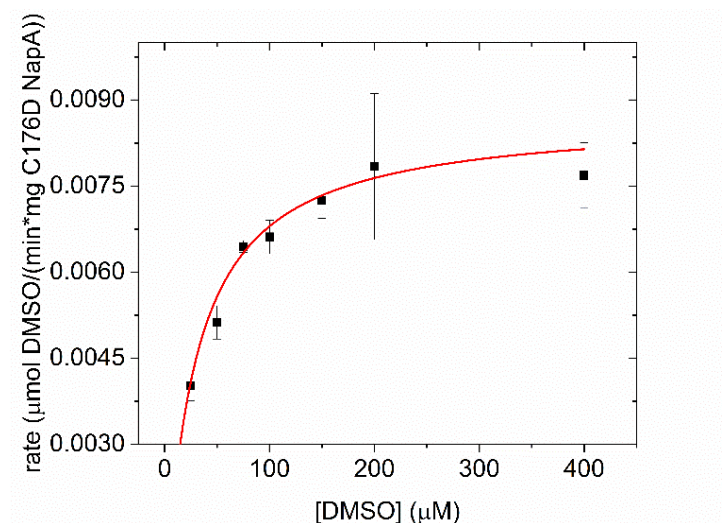


Figure 5.6: Steady-state kinetic data using DMSO as a substrate for C176D NapA fit to the Michaelis-Menten model. This kinetics curve was reproduced by at least five biological replicates. Each data point contained three technical replicates for each substrate concentration.

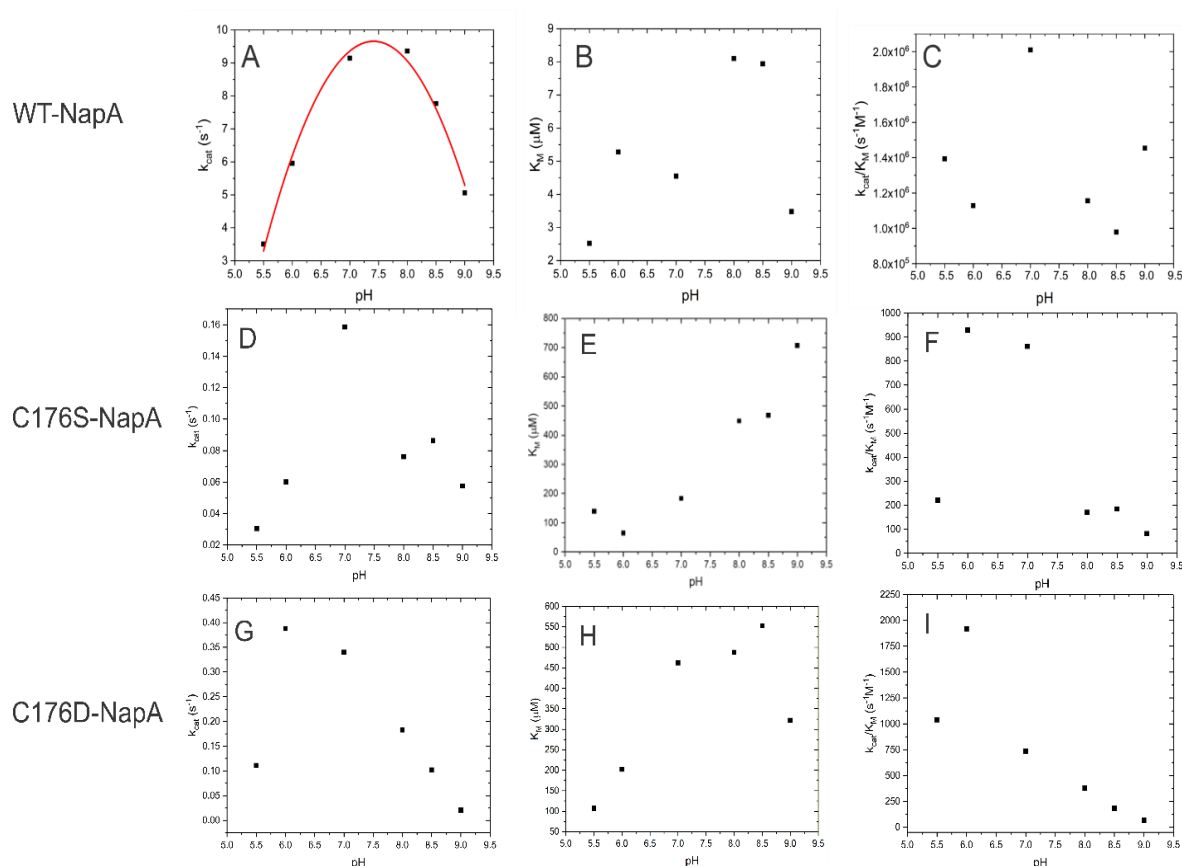


Figure 5.7: The pH profile for the NapA variants with nitrate as substrate. Top panel: native NapA pH dependence of A) k_{cat} , B) K_M , and C) k_{cat}/K_M . Middle panel: C176S NapA pH dependence of D) k_{cat} , E) K_M , and F) k_{cat}/K_M . Bottom panel: C176D NapA pH dependence of G) k_{cat} , H) K_M , and I) k_{cat}/K_M .

5.3.4 Nitrate Activity Dependence on pH

A pH profile of the nitrate reductase activity was developed for all active variants. The pH optimum was determined for *C. jejuni* NapA with a calculated maximum k_{cat} at pH 7.4 (Figure 5.7) while the maximum efficiency (k_{cat}/K_M) was observed at pH 7.0. The change in k_{cat} due to pH was small, a difference of $\sim 6 \text{ s}^{-1}$ at a pH where the enzyme is most active versus a pH where the enzyme is least active. The impact on K_M displayed no obvious pattern and the change in K_M ranged from 2.5 to 8.1 μM (Table 5.5). The C176A NapA variant was inactive toward nitrate, therefore pH studies were not conducted. C176S NapA has a pH optimum at pH ~ 7.0 (Figure 5.7). The change in k_{cat} due to pH was small, shifting $< 1 \text{ s}^{-1}$ but still larger than the standard error associated with k_{cat} . However, K_M increases linearly with pH ranging from 65 μM to 700 μM over the pH range of 5.5-9.0 (Table 5.5). The C176D NapA variant has a pH optimum of ~ 6.3 (Figure

5.7). The K_M of C176D NapA increases with pH similar to C176S NapA. In addition, C176D NapA's k_{cat}/K_M decreases with increasing pH. The trends for all three of the kinetic parameters suggest C176D NapA prefers slightly acidic conditions for optimal activity.

Table 5.5: Kinetic parameters for NapA variants at various pH conditions

Enzyme	pH	K_M (μM)	k_{cat} (1/s)	V_{max} ($\mu mol NO_3^- / (min * mg NapA)$)	k_{cat}/K_M ($s^{-1} M^{-1}$)
WT NapA	5.5	2.52 ± 0.56	3.51 ± 0.05	1.93 ± 0.03	1.39×10^6
WT NapA	6.0	5.28 ± 0.15	5.96 ± 0.02	3.28 ± 0.01	1.13×10^6
WT NapA	7.0	4.55 ± 1.60	9.14 ± 0.69	5.04 ± 0.38	2.01×10^6
WT NapA	8.0	8.10 ± 3.90	9.36 ± 1.10	5.16 ± 0.61	1.16×10^6
WT NapA	8.5	7.94 ± 2.80	7.77 ± 0.73	4.29 ± 0.40	9.78×10^5
WT NapA	9.0	3.48 ± 0.56	5.06 ± 0.14	2.79 ± 0.08	1.45×10^6
C176S NapA	5.5	139 ± 17	0.031 ± 0.0007	0.017 ± 0.0004	2.23×10^2
C176S NapA	6.0	65 ± 13	0.060 ± 0.0011	0.033 ± 0.0006	9.23×10^2
C176S NapA	7.0	184 ± 23	0.159 ± 0.0090	0.087 ± 0.0232	8.64×10^2
C176S NapA	8.0	449 ± 28	0.076 ± 0.0029	0.042 ± 0.0016	1.69×10^2
C176S NapA	8.5	468 ± 47	0.086 ± 0.0022	0.048 ± 0.0012	1.84×10^2
C176S NapA	9.0	707 ± 91	0.058 ± 0.0031	0.032 ± 0.0017	8.20×10^1
C176D NapA	5.5	107 ± 11	0.151 ± 0.007	0.083 ± 0.004	1.41×10^3
C176D NapA	6.0	202 ± 28	0.530 ± 0.039	0.292 ± 0.022	2.62×10^3
C176D NapA	7.0	462 ± 66	0.339 ± 0.012	0.187 ± 0.007	7.34×10^2
C176D NapA	8.0	488 ± 48	0.249 ± 0.019	0.137 ± 0.011	5.10×10^2
C176D NapA	8.5	553 ± 47	0.139 ± 0.005	0.077 ± 0.003	2.51×10^2
C176D NapA	9.0	322 ± 50	0.011 ± 0.0006	0.006 ± 0.0003	3.42×10^1

5.4 Discussion

5.4.1 Nitrate Reduction by the C176 Nap Variants

The enzymes in the DMSOR family can utilize a wide variety of substrates, and the molybdenum coordination site exhibits the most diversity among the MPT enzyme families. Focusing on coordination environments of DMSOR/TMAOR, Nar, and the no protein-based ligand as control, respectively, the C176S/D/A NapA variants were prepared, and their kinetic properties were determined. The C176D NapA has a slightly k_{cat}/K_M for nitrate reduction but has a lower molybdenum incorporation than the C176S NapA variant. There are a variety of possible reasons for the lower Mo incorporation and low production of C176D NapA. For example, the variant could increase cellular toxicity diminishing the total protein yield of C176D NapA, or cofactor transfer and/or insertion into the C176D variant could be limited. The most likely possibility; however, is that the Asp ligand impacts folding of this enzyme which may result in a reduction in the stabilization of Moco in the active site.

The Moco is held in place in the active sites of Mo enzymes through a network of hydrogen-bonding interactions with the nearby residues [4]. The C176A NapA variant has high Mo incorporation without a protein ligand coordinating to Mo suggesting the interactions holding Moco in place are minimally disturbed and that a coordinating residue is not an obligatory requirement for securely anchoring Moco in the active site but may reflect a role in Mo positioning or a more chemical role in catalysis. This observation is consistent with the S121A mutation in *R. sphaeroides* BSOR which was reported to have 84.8% of the Mo content compared to native BSOR [135]. The C176S NapA variant and the native NapA have comparable molybdenum incorporation, however, the C176D NapA has significantly lower Mo content. It is tempting to suggest that due to the shorter Mo—O bond in C176D NapA compared to the Mo—S bond in native NapA, the oxygen donor in C176D NapA could induce a structural rearrangement, which results in a disruption of the interactions holding Moco securely in place. However, the oxygen donor in the Ser ligand leads to a shorter oxygen bond compared to the Mo—S bond in native NapA without a significant loss in Mo incorporation.

An Asp residue has a longer and bulkier side chain than a Ser residue. Although reports of cofactor and/or Mo content in studies of molybdenum coordinating residue variants are limited, a correlation can be made between the size of the side chain and metal content from two independent studies on *E. coli* DMSOR [401] and *R. sphaeroides* BSOR [135] respectively. The *E. coli*

DMSOR variants S176A, S176C, and S176H showed molybdenum incorporation of 0.44, 0.32, 0.27 nmol/mg protein, respectively, decreasing in Mo content with an increasing size of the amino acid side chain of the coordinating residue [401]. Similarly, in *R. sphaeroides* BSOR molybdenum incorporation decreased with the size of the amino acid side chain of the coordinating residue where S121A, S121C, and S121T, had 84.8, 84.6, and 71.8 % of the native BSOR's molybdenum content [135].

In addition to the size of the Asp side chain, there is also the possibility of bidentate coordination by the C176D NapA Asp ligand during catalysis, similar to *Azospira suillum* PcrA [407]. It is tempting to suggest that a combination of the shorter Mo-O bond, the larger side chain, and the possibility of a bidentate carboxylate coordination in C176D NapA could induce a structural rearrangement, which can result in a disruption of the interactions holding Moco securely in place potentially instigating loss of Moco during enzyme isolation. A quantum mechanics/molecular mechanics (QM/MM) study is ongoing in our laboratory that will address how the Asp ligand and the other mutations structurally perturb the structure of *C. jejuni* NapA. Thus, the possibility of a structural rearrangement in C176D NapA will be tested in future studies. While the geometry of the Mo center in the variants is not expected to shift due to the exchanging coordinating residue, it is reasonable to expect some rearrangement of the catalytic pocket due to the expected shorter O-Mo bond as compared to the S-Mo bond of the coordinating residue. For example, in *R. sphaeroides* NapA (PDB: 1OGY) the Cys-S-Mo bond is approximately 2.089 Å while the Ser-O-Mo bond in TMAOR (PDB 1TMO) is approximately 1.730 Å. However, these bond distances may be unreliable due to the quality and resolution of the crystal structures at 2.5 Å and 3.2 Å, respectively. Small molecule mimics of the Mo center in Moco-containing enzymes reveal the Ser-O-Mo bond is closer to 2.1 Å while the Cys-S-Mo bond is closer to 2.4 Å [408]. Regardless of whether there is a structural perturbation caused by the mutation, the C176D variant is produced in a significant lower yield (0.72 mg C176D NapA/L culture vs 2.3 mg native NapA/L culture) and with lower Mo content (15% in C176D NapA vs 92% in native NapA) than the native enzyme discussed in Chapter 2 suggesting the mutation impacts production of the variant in some fashion.

5.4.2 Alternative Substrates of the C176 Nap Variants

The main mode of action for the NapA, DMSOR, and TMAOR enzymes is believed to be through OAT reactions where oxygen is transferred from the substrate to the Mo center during catalysis. [374]. Schultz *et al.* [409] have demonstrated the OAT reaction in *R. sphaeroides* DMSOR utilizing ^{18}O isotope studies and computational studies support the claim for both DMSOR [410, 411] and Nap function via OAT reactions [379, 412]. OAT reactivity has also been observed in many discrete inorganic molecules [408, 413-441]. Thus, it is reasonable to anticipate that *C. jejuni* NapA and the C176 NapA variants utilize an OAT reaction as a mode of action.

NapA reduces nitrate to nitrite and the ability to reduce S or N-oxides has not been reported. While exchange of the S donor Cys ligand for an oxygen donor ligand such as Ser or Asp does impact nitrate reductase activity, whether these variants could reduce substrates such as TMAO and DMSO was unexplored. The reduction of DMSO and TMAO is naturally conducted by DMSOR and TMAOR, where both enzymes have a Ser coordinated Mo-center (Figure 5.1B) [442]. Therefore, the substrate selectivity of NapA was initiated with TMAO and DMSO as alternative substrates (Figure 5.8). This marks the first example of an investigation where these variants have been studied with substrates that were not known to be turned over by the native enzyme.

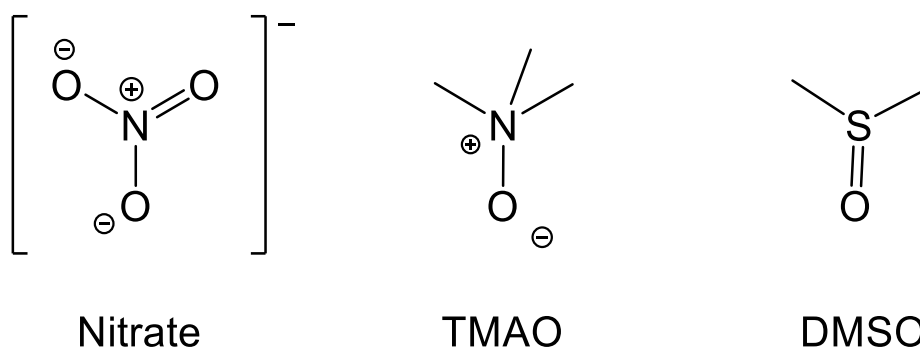


Figure 5.8: Chemical structures of the substrates explored in this study with nitrate on the left, TMAO in the center, and DMSO on the right.

Remarkably, both native *C. jejuni* NapA and C176S NapA reduce TMAO. The K_M values are similar to *E. coli* TMAOR (Table 5.4) while the turnover is severely diminished, and the TMAO reduction efficiencies of the two Nap variants are similar to each other (Figure 5.5, Table

5.4). The C176D/A NapA variants, however, are completely inactive toward TMAO. Surprisingly, C176D NapA cannot turnover TMAO, but can turn over DMSO.

DMSO reductase activity was nonexistent in the native enzyme and in the C176S/A variants, while the C176D NapA variant was active albeit with a slow turnover rate (Figure 5.6, Table 5.4). This suggests the Asp substitution was able to tune substrate specificity toward a previously inactive substrate similar to the increased activity of *R. sphaeroides* S147C DMSOR variant for adenosine-¹N-oxide (ANO) reduction [54]. In the present case, the Asp ligand seems to impact the substrate affinity and/or the binding process. The Asp ligand could impact binding directly if the carboxylate ligand interacts with the substrate or indirectly by modulating a chemical property of the active site. The K_M of DMSO was 28.2 μ M compared to that of nitrate at 462 μ M for C176D NapA suggesting the Asp residue may be stabilizing a DMSO bound form.

It is curious that the native NapA enzyme can turnover TMAO but not DMSO. DMSO reductases can reduce both S and N-oxides while TMAO reductases are generally more selective and can only efficiently reduce N-oxides [97]. Kaufmann *et al.* [384] reported a TMAOR variant where the molybdenum-coordinating residue Ser is exchanged for a Cys has approximately 40% TMAO specific activity compared to the native TMAOR enzyme. Similarly, Hilton *et al.* [54] observed 21% TMAO specific activity in the *R. sphaeroides* S147C DMSOR variant. Thus, it is not surprising the *C. jejuni* NapA, where molybdenum is naturally coordinated by Cys, has residual TMAO activity. Hilton *et al.* [54] observed 39% DMSO specific activity in the *R. sphaeroides* S147C DMSOR variant and so it was unexpected for native NapA to be unable to turnover DMSO while it can turnover TMAO.

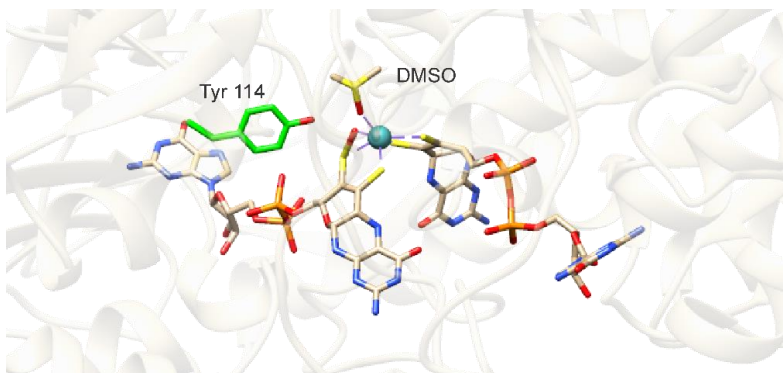


Figure 5.9: Influential tyrosine in DMSOR. Chimera image of the DMSOR crystal structure PDB 4DMR depicting the molybdopterin active site with bound DMSO molecule and influential Tyr 114 in green.

Johnson *et al.* [97] suggested that the presence of a Tyr residue in *R. sphaeroides* DMSOR preferentially selects for S-oxides over N-oxides and this Tyr is absent in both *E. coli* TMAOR and Nap. The presence of Tyr114 in *R. sphaeroides* DMSOR increases the catalytic efficiency of DMSOR for S-oxides as compared to N-oxides (Figure 5.9). Insertion of a Tyr residue in TMAOR mimicking Tyr114 increases the efficiency of the TMAOR reduction of S-oxides [97]. Ridge *et al.* [166] noted that Tyr114 in *R. sphaeroides* DMSOR is in close proximity to the sulfur atom of the bound DMSO (~ 3.3 Å) which led them to propose that the Tyr may have a role in weakening the S-O bond in bound DMSO through an interaction between the sulfur atom and the hydroxy side chain of Tyr. The inability of the *R. sphaeroides* Y114F DMSOR variant to produce the enzyme-substrate complex by adding DMS, the product, which is accomplished in the native enzyme [166], supports this notion. Cobb *et al.* demonstrated with electron paramagnetic resonance spectroscopy (EPR) that Tyr114 in *R. capsulatus* DMSOR does not significantly interact with the Mo(V) state [443] further corroborating the hypothesis that Tyr114 has a role in stabilizing the enzyme-substrate complex. Thus, it is clear that the Tyr114 plays an important role in catalyzing DMSO reduction.

Secondary structure matching (SSM) analysis shows that in place of Tyr114 of *R. capsulatus* DMSOR, *C. jejuni* NapA has Gly144 [444]. We hypothesize that NapA cannot bind DMSO readily without the stabilization of the intermediate provided by Tyr114. Interestingly, C176D NapA can turnover DMSO but the native NapA enzyme cannot. We suggest that the single change of the Cys-S ligand to an Asp-O ligand enables C176D NapA to stabilize the DMSO bound form via interaction with the carboxylate side chain of Asp where the native NapA cannot. In this model, the carboxylate side chain of Asp provides one oxygen donor to molybdenum and the second oxygen may interact with DMSO stabilizing the enzyme-substrate complex in a similar fashion to Tyr114 (Figure 5.10). Stabilization of a DMSO bound intermediate in this variant compared to the native enzyme would thus enable turnover. Further investigation is necessary to determine the exact characteristic(s) that the mutation influences that may be responsible for the DMSO activity observed for the C176D NapA variant. Modeling study of the *C. jejuni* NapA active sites in all four variants is ongoing.

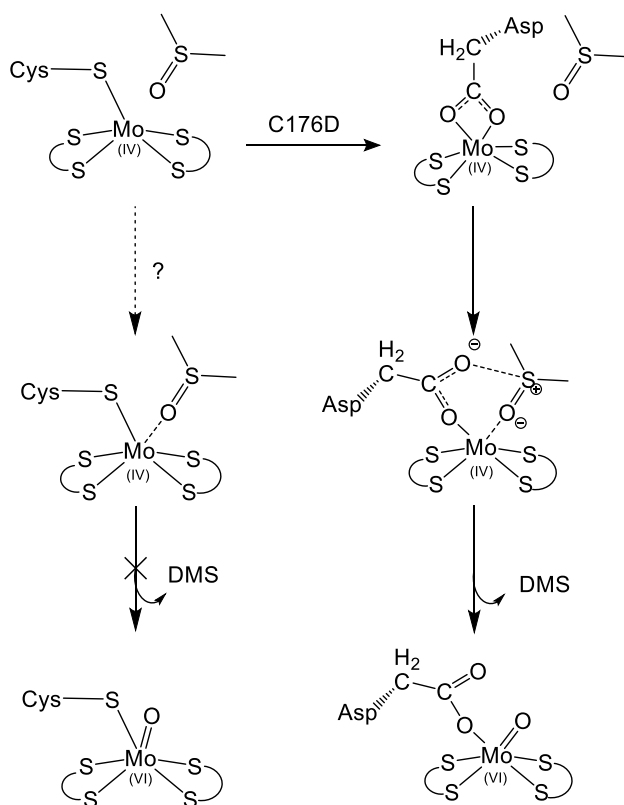


Figure 5.10: Proposed interaction of the Asp ligand with bound DMSO compared to a Cys ligand at the active site in NapA variants. The native Nap interaction with DMSO is shown in the left panel and C176D NapA interaction is shown in the right panel. It is unclear if DMSO binds in native NapA but DMSO is not turned over. C176D NapA can stabilize DMSO binding to molybdenum through a proposed electrostatic interaction between the partially positive sulfur atom in DMSO and the partially negative carboxylate oxygen atom. The stabilized enzyme-substrate complex in the C176D variant enable DMSO turnover.

5.4.3 Implications of Mo Ligand Exchange in Energetics

The elementary steps involved in nitrate reduction by NapA are schematically shown in Figure 5.11. In this figure, as isolated enzyme in the oxo-Mo(VI) state, denoted as E^0 , is reduced by two coupled electron proton transfer processes to generate the reactive Mo(IV) state (E). Under the assay condition this process is accomplished by reduced methyl viologen. The substrate nitrate, denoted as S, binds to this E state forming the enzyme-substrate (ES) complex which goes through a transition state denoted $[ES^\ddagger]$. The transition state, $[ES^\ddagger]$, is proposed to be a structure where the enzyme is bound to a form of nitrate where the N-O bond is weakened and the Mo=O moiety begins to form (Figure 5.11). Nitrite is released regenerating the oxo-Mo(VI) state, E^0 . Thus, substrate transformation is completed, and enzyme regeneration begins again.

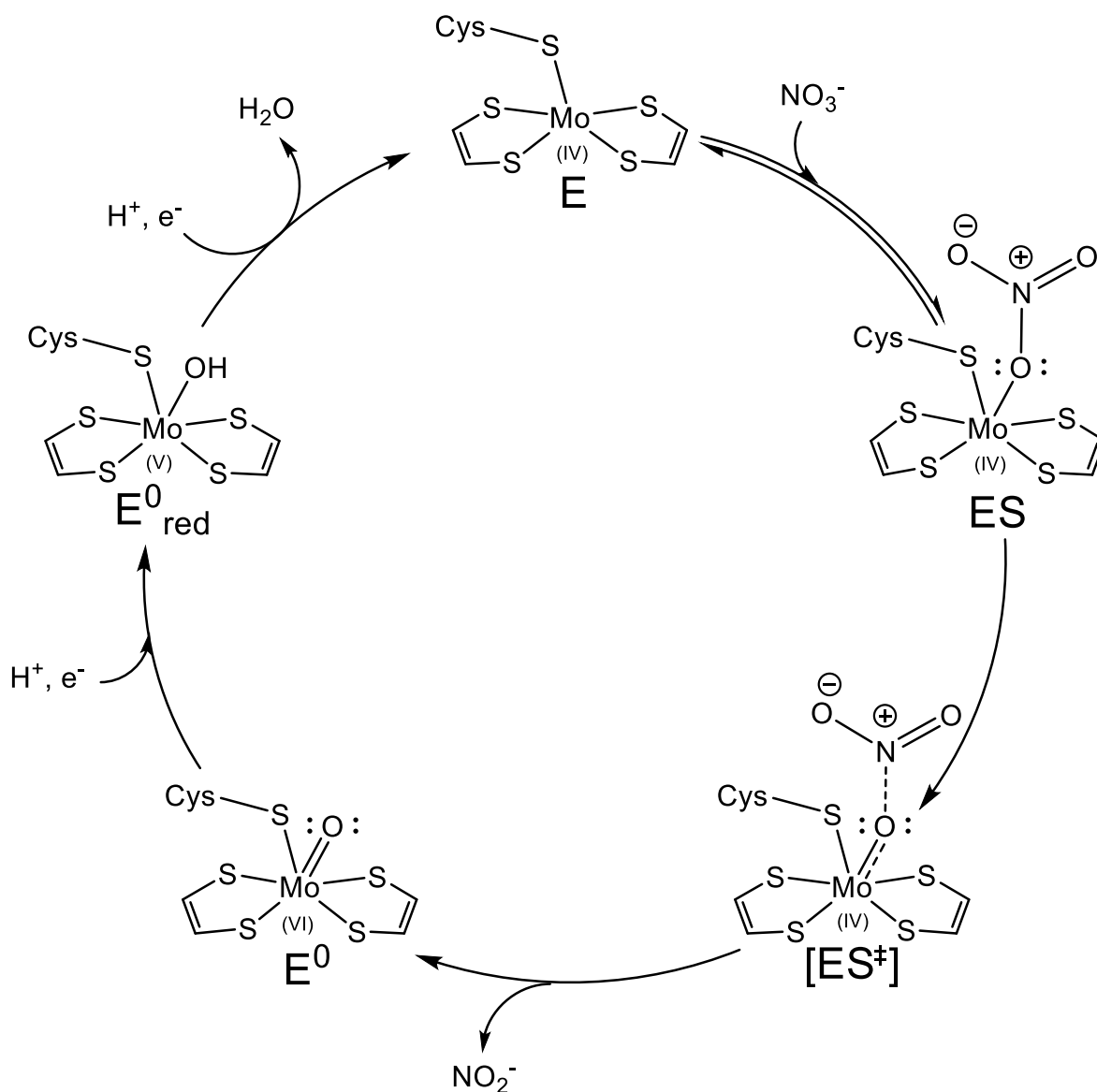


Figure 5.11: Catalytic scheme proposed for *C. jejuni* NapA. The reduced molybdenum (IV) state of the enzyme (denoted E) binds reversibly to substrate nitrate (denoted S) in the first step forming the ES complex where nitrate is coordinated to the Mo(IV) metal center. As catalysis proceeds, the O-N bond weakens and the Mo=O bond begins to form in the proposed transition state (denoted [ES ‡]). Nitrate is reduced to nitrite transferring an oxygen atom to the oxidized Mo(VI) center (denoted E 0). The enzyme is regenerated from the oxidized E 0 state to the fully reduced E state in two proton coupled electron transfer steps with an intermediate Mo(V) state of the enzyme denoted E $^0_{\text{red}}$. The terminal oxo moiety transferred from the original substrate is protonated to produce water. Water diffuses from the active site enabling another substrate molecule to bind to the fully reduced Mo(IV) state (E).

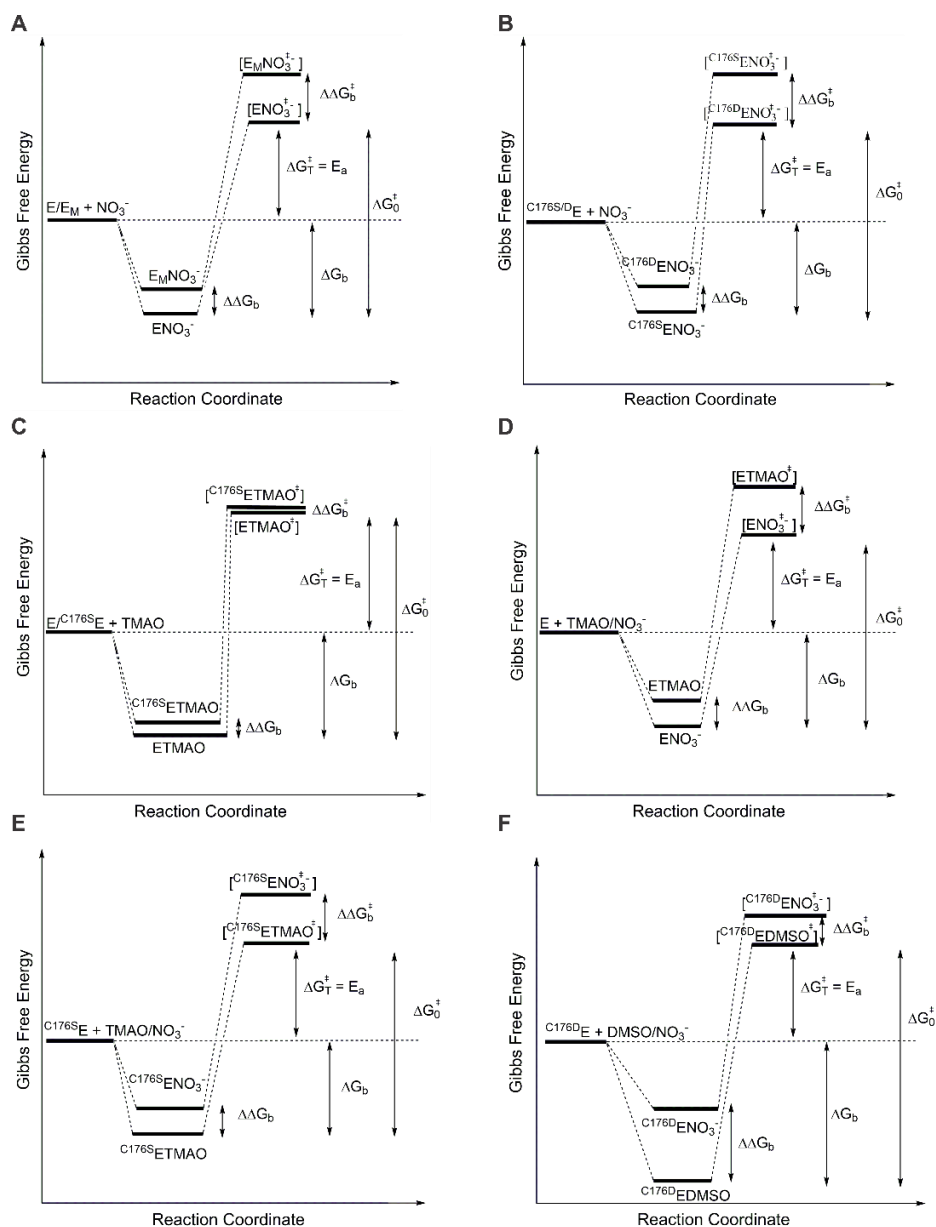


Figure 5.12: Schematic diagrams depicting energy changes due to the effect of mutation or substrate. The activation energy of nitrate reduction calculated from k_{cat}/K_M is ΔG_T^\ddagger and is composed of two terms: the energetically unfavorable term ΔG_0^\ddagger , which represents the activation energy of the chemical steps where bonds are broken and created (i.e. for k_{cat}), and the energetically favorable term ΔG_b , which represents the realization of binding energy (i.e. from the K_D or estimated from K_M). (A) Diagram comparing the reaction of native NapA enzyme, E, with substrate nitrate to the reaction of C176S/D variant enzymes, E_M , with substrate nitrate. (B) Diagram comparing the reaction of the C176S NapA, ($C^{176S}E$) and C176D NapA ($C^{176D}E$) with substrate nitrate. (C) Diagram comparing the reaction of the E and $C^{176S}E$ with substrate TMAO. (D) Diagram comparing the reaction of the E with substrates nitrate and TMAO. (E) Diagram comparing the reaction of the $C^{176S}E$ with substrates nitrate and TMAO (F) Diagram comparing the reaction of the $C^{176D}E$ with substrates nitrate and DMSO.

In several molybdopterin enzymes such as XO [445], DMSOR [446], and Nap [372, 447], it has been demonstrated that the electron transfer steps involved in the regeneration of the enzyme are not rate-limiting. The electron transfer during the regeneration of the reduced Mo(IV) state from the oxidized Mo(VI) state of Nap enzymes is faster than the catalytic turnover [372, 447]. Thus, the effect on the catalysis on different variants is a result of an energetic change at the molybdenum center rather than as a change in the redox potential in the Mo(VI)/(V) or the Mo(V)/(IV) couples. Thus, here we focus on the substrate transformation steps probing the energetics of the ES complex and $[ES^\ddagger]$ during the course of the reaction.

Kinetic values can be used to approximate the incremental binding energy between two conditions (i.e. relative differences between two substrates, or amino acid mutations) to reveal useful information about energy states of the enzyme during substrate transformations [448]. The pseudo second-order rate constant, k_{cat}/K_M , can be used to determine the activation energy for nitrate reduction by NapA denoted as ΔG_T^\ddagger . This energy value is composed of two terms: the energetically unfavorable term ΔG_0^\ddagger , which represents the activation energy of the chemical steps where bonds are broken and created (i.e., representing k_{cat}), and the energetically favorable term ΔG_b , which represents the realization of binding energy (i.e., from the K_D or estimated from K_M when S binds to E). As such, differences in these parameters induced by amino acid exchange or altering substrates can be a useful tool in determining how and why the energetics of the reaction are changing.

Transition state theory in combination with the enzymatic kinetic model (e.g., Michaelis-Menten) can be utilized for calculating $\Delta\Delta G_b$, the incremental or change in the binding energy of the enzyme and substrate as well as $\Delta\Delta G_b^\ddagger$ the incremental or change in the binding energy of the enzyme and the substrate in the transition state [448] as given below in equations (5.1) and (5.2).

$$\Delta\Delta G_b = -RT \ln \left[\frac{(1/K_M)_A}{(1/K_M)_B} \right] \quad (5.1)$$

$$\Delta\Delta G_b^\ddagger = -RT \ln \left[\frac{(k_{cat}/K_M)_A}{(k_{cat}/K_M)_B} \right] \quad (5.2)$$

The constant R represents the gas constant and T is the temperature in Kelvin. The term $(k_{cat}/K_M)_{A/B}$ represents the specificity constant under conditions A and B, respectively, while $(1/K_M)_{A/B}$ estimates the association constant of enzyme and substrate under conditions A and B, respectively. For analysis of the NapA variants, two sets of conditions were analyzed to determine the $\Delta\Delta G_b$ and the $\Delta\Delta G_b^\ddagger$ (Table 5.6). The effect of the mutation while keeping the substrate (i.e., nitrate and TMAO) constant is represented in the first set of conditions. The second set of conditions represents the different substrates for the same variant; and all three variants were analyzed.

Table 5.6: Calculated $\Delta\Delta G_b$ and $\Delta\Delta G_b^\ddagger$ values comparing the effects of mutation and substrate for the enzyme-substrate complex and the enzyme-bound transition state, respectively.

Enzyme A ^a	Substrate A ^a	Enzyme B ^b	Substrate B ^b	$\Delta\Delta G_b$ (kJ/mol) ^c	$\Delta\Delta G_b^\ddagger$ (kJ/mol) ^d
WT NapA	Nitrate	C176S NapA	Nitrate	$-11.2 \pm 2 \times 10^{-6}$	$-23.2 \pm 3 \times 10^{-12}$
WT NapA	Nitrate	C176D NapA	Nitrate	$-12.2 \pm 1 \times 10^{-6}$	$-19.3 \pm 8 \times 10^{-11}$
C176D NapA	Nitrate	C176S NapA	Nitrate	$1.0 \pm 2 \times 10^{-4}$	$-4.0 \pm 4 \times 10^{-8}$
WT NapA	TMAO	C176S NapA	TMAO	$-0.6 \pm 1 \times 10^{-4}$	$-0.2 \pm 2 \times 10^{-7}$
WT NapA	Nitrate	WT NapA	TMAO	$-9.5 \pm 4 \times 10^{-6}$	$-19.9 \pm 7 \times 10^{-11}$
C176S NapA	TMAO	C176S NapA	Nitrate	$-1.0 \pm 4 \times 10^{-5}$	$-3.2 \pm 2 \times 10^{-8}$
C176D NapA	DMSO	C176D NapA	Nitrate	$-6.9 \pm 1 \times 10^{-5}$	$-0.3 \pm 3 \times 10^{-7}$

^aenzyme type and substrate for condition A in equations (5.1)-(5.2), ^benzyme type and substrate for condition B in equations (5.1)-(5.2), ^ccalculated $\Delta\Delta G_b$ values utilizing equation (5.1) under the conditions A and B specified, ^dcalculated $\Delta\Delta G_b^\ddagger$ values utilizing equation (5.2) under the conditions A and B specified.

The $\Delta\Delta G_b$ values represent the difference in the binding energy of the substrate or alternate substrate and the native enzyme or its variants. If the $\Delta\Delta G_b$ value is negative, then condition A lowers the energy level of the ES complex by $\Delta\Delta G_b$ compared to the energy level of the ES complex under condition B. Similarly, the $\Delta\Delta G_b^\ddagger$ value represents the difference in the binding energy of the enzyme or its variants with the substrate in the transition state, $[ES^\ddagger]$. Thus, the change in binding energy reveals that the native NapA enzyme has a lower $[ES^\ddagger]$ free energy with nitrate as substrate by approximately 23.2 kJ/mol ($\Delta\Delta G_b^\ddagger$) and 19.3 kJ/mol ($\Delta\Delta G_b^\ddagger$) than the C176S and C176D variants, respectively. Additionally, the native NapA enzyme has lower energy for the ES complex by approximately 11.2 kJ/mol ($\Delta\Delta G_b$) and 12.2 kJ/mol ($\Delta\Delta G_b$) than the C176S and C176D variants, respectively.

The impact of the Ser mutation on the energetics of nitrate reduction by NapA is depicted in Figure 5.12A. The differential energy changes in ES and [ES[‡]] reveal an incongruent energetic pattern where the mutation influences both states to different degrees. A similar pattern is observed for the impact the Asp mutation has on NapA nitrate reduction (Figure 5.12A). This result suggests the coordinating Cys residue is involved in stabilizing the ES and [ES[‡]] states during the catalytic cycle when nitrate is reduced resulting in a lower activation energy barrier for nitrate reduction for the native enzyme compared to the C176S/D NapA variants. C176D NapA has a lower [ES[‡]] free energy than C176S NapA by ~4 kJ/mol ($\Delta\Delta G_b^\ddagger$) and a higher ES energy level by ~1 kJ/mol ($\Delta\Delta G_b$) (Figure 5.12B, Table 5.6) suggesting the oxygen donor to the molybdenum center may not be the only factor influencing the driving force.

Remarkably, the change in binding energy for the mutation of Ser on TMAO reduction was less significant than previously mentioned binding energies. Native NapA had a ~0.6 kJ/mol ($\Delta\Delta G_b$) lower energy for the ES state and a ~0.2 kJ/mol ($\Delta\Delta G_b^\ddagger$) lower energy for the [ES[‡]] state compared to C176S NapA with TMAO as substrate (Figure 5.12C) implying that the activation energies of these variants for the reduction of TMAO are very similar and may be responsible for the similar efficiencies. The [ES[‡]] states are essentially the same resulting in a minimal shift in activation energies consistent with the almost identical k_{cat} values for the two variants. Although both the [ES[‡]] and the ES states are almost isoenergetic between the two Nap variants, the larger magnitude in energy differences is observed in the ES state. Such a result suggests the Ser residue is impacting the binding energy by destabilizing the ES state. Thus, the destabilized ES state increases K_M which may result in a small increase in k_{cat} . As a result, the slightly higher increase in the native NapA enzyme's TMAO reduction efficiency can be attributed to the lower ES binding energy and thus a lower K_M for the native NapA enzyme.

The impact of substrate for a particular variant on incremental binding energy was also analyzed. For the native NapA enzyme which can turnover both nitrate and TMAO, the energy for the reduction of nitrate for the ES state and the [ES[‡]] state respectively was ~9.5 kJ/mol ($\Delta\Delta G_b$) and ~19.9 kJ/mol ($\Delta\Delta G_b^\ddagger$) lower than that of reducing TMAO. The energy values suggest reduction of TMAO has a higher activation energy barrier than that of nitrate for the native NapA enzyme (Figure 5.12D). The incremental binding energy comparing native NapA to C176S NapA is very similar at ~19.2 kJ/mol ($\Delta\Delta G_b^\ddagger$) suggesting there is a small difference between substrates for C176S NapA. This observation was corroborated by ~3.2 kJ/mol ($\Delta\Delta G_b^\ddagger$) lower [ES[‡]] energy

and ~ 1 kJ/mol ($\Delta\Delta G_b$) lower ES energy for TMAO versus nitrate reduction by C176S NapA (Figure 5.12E).

The change in the ES binding energy for C176S NapA going from nitrate to TMAO was a smaller magnitude than it was in native NapA where the latter enzyme favored nitrate and the C176S variant favored TMAO. While the kinetic efficiencies revealed no impact of the Ser residue on TMAO turnover, the energy calculations indicate the Ser ligand tunes substrate selectivity. The substrate preference is adjusted by essentially lowering the activation energy barrier through destabilization of the ES and $[ES^\ddagger]$ states of C176S NapA with nitrate instead of stabilizing the states in the reaction with TMAO. This result is supported by the fact that the native NapA enzyme and C176S NapA TMAO energy states are so similar. Likewise, the C176D mutation lowers the ES and the $[ES^\ddagger]$ energies for DMSO versus nitrate reduction by ~ 6.9 kJ/mol ($\Delta\Delta G_b$) and ~ 0.3 kJ/mol ($\Delta\Delta G_b^\ddagger$), respectively (Table 5.6, Figure 5.12F). The Asp mutation impacts the ES state to a greater degree supporting the previous hypothesis that the Asp ligand can stabilize the DMSO binding to the enzyme while the other variants cannot.

5.4.4 The Impact of pH on Nitrate Reduction Catalyzed by the C176 NapA Variants

The coordinating residue appears to impact binding and may impact the stabilization of the ES and $[ES^\ddagger]$ complexes thus impacting the driving force and kinetic rate of the reaction in order to tune substrate selectivity. The exact mechanism of action for this stabilization of ES and/or $[ES^\ddagger]$ is unclear. The coordinating residue has been reported to interact directly with the substrate for formate dehydrogenase, FDH. Specifically, the coordinating residue had been hypothesized to influence the proton shuttling capability of the enzyme [398]. Exchanging the coordinating residue could impact the proton shuttle pathway directly as seems to be the case for *E. coli* FDH where the SeCys is suggested to abstract the α proton from formate after C-H bond cleavage [398]. The coordinating amino acid could also have an indirect role in which it is possible that the pK_a of individual amino acids of the catalytic pocket has been altered by exchanging coordinating residues. The exchanged residue could shift the hydrophobicity, change the electrostatics, or alter the hydrogen-bond networks of nearby residues in the catalytic pocket [449]. This could in turn impact the formation of the ES complex or the stabilization of the transition state, $[ES^\ddagger]$, thus altering the energetics of the enzyme and tuning substrate preference. pH profiles of each nitrate

active variant have been examined to explore the impact the coordinating residue may have on the pK_a of the residues forming the active site of Nap and possibly the proton shuttling process.

Interestingly, *C. jejuni* NapA's k_{cat} and K_M do not vary significantly with pH (Table 5.5, maximum shift in K_M is 6 μ M and that for is k_{cat} 6 s^{-1}). While pH dependence has been reported for other Nap enzymes [270, 352, 354, 369, 450], the majority of reports present the data as percent activity of Nap at various pH conditions [270, 352, 354]. As a result, comparing the pH effect on kinetic parameters is difficult. However, a recent study by Zeamri *et al.* on *R. sphaeroides* Nap reported the pH dependence of both K_M and k_{cat} over a pH range of 5.0-8.0 [450]. They [450] observed a change in K_M of 50 μ M to 250 μ M, which is significantly different than *C. jejuni* NapA's range of 6 μ M. Furthermore, Zeamari *et al.* [450] reported a change in k_{cat} of $\sim 50 s^{-1}$ as compared to the 6 s^{-1} difference in *C. jejuni* NapA. Interestingly, *R. sphaeroides* is a free-living microbe often found in soil or aquatic environments [371]. Perhaps the insensitivity to pH observed in *C. jejuni* NapA is in part aiding in the virulence of the pathogen as compared to the free-living microbe, *R. sphaeroides*. In fact, pH has been reported to impact the expression of several virulence factors, and pH conditions significantly impact biofilm formation, a common factor that prevents the efficient treatment of several pathogens [451-455]. The effect of pH displayed by *C. jejuni* NapA may be a mechanism to confront the physiological pH equilibria in the GI tract of the hosts that *C. jejuni* colonizes enabling this key metabolic enzyme to keep functioning as conditions change during colonization.

The C176S and C176D NapA variants have similar pH optima of 7.0 and 6.3, respectively (Figure 5.7). The most notable feature of these pH profiles is the impact the coordinating residue seems to have on K_M and effectively on substrate affinity. The K_M of both variants increases with more alkaline pH while no obvious pattern is observed for the native NapA's K_M value over the same pH range (Figure 5.7, Table 5.5). This data suggests that the oxygen donor provided by both Ser and Asp ligands impacts the pK_a of the Nap active site and is influencing the protonation state of residues that stabilize substrate binding. The differential pH effect of the variants compared to the native enzyme may explain the difference in (de)stabilization of the ES and $[ES^\ddagger]$ states by the altered coordinating residues.

Further analysis of the pH data was conducted utilizing the methods of Dixon [456, 457] and Fersht [448] where the kinetic rate parameters are derived as a function of $[H^+]$ and the dissociation constants of protonation forms (K_a). The data for the native NapA were fit to equation (5.3), where

$$\log(k_{obs}) = \frac{k_{max}}{1+10^{(pH-pK_1)}+10^{(pK_2-pH)}} \quad (5.3)$$

k_{obs} is the observed kinetic parameter over the examined pH range, k_{max} is the pH corrected theoretical maximal value of the kinetic parameter being fit, and pK_1 and pK_2 are relevant pK_a values being fit. This approach has successfully been applied in understanding the pH effect in arylsulphatase [458] and SO [459]. The native NapA pH data was successfully fit to equation (5.3) where pK_a values were determined to be 5.44 and 9.38 (Figure 5.13A).

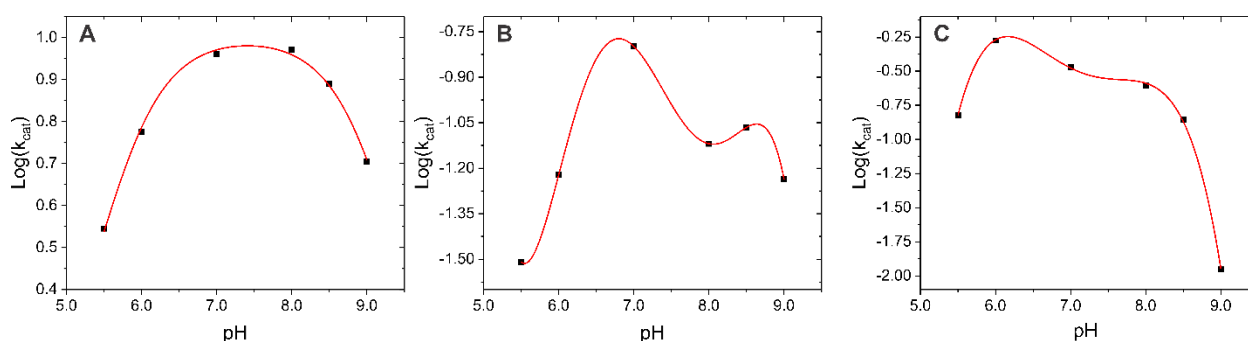
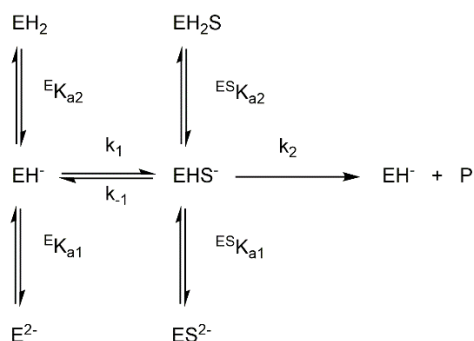


Figure 5.13: The double logarithmic plot of $\log(k_{cat})$ vs pH for nitrate reduction by A) native NapA, B) C176S NapA, C) C176D NapA represents the pH dependence of the turnover number, k_{cat} , for each of the C176 Nap variants. The data in (A) was fit to equation (3) in the text and revealed two catalytically important ionizations in NapA with pK_a of 5.44 and 9.38. The data in (B) and (C) did not converge to equation (3) and thus were fit to higher polynomials to qualitatively determine information about the catalytically important ionizations in the C176S/D variants. Based on the shape of the fitted curve, the C176S/D variants are proposed to form products from multiple protonic states of the ES complex.

The double logarithm plot of $\log(k_{cat})$ as a function of pH for native NapA (Figure 5.13A) where k_{cat} is equal to k_2 in the enzyme equations in Figure 5.13A reveals information on the ionization of only the ES complex. As such, there are two possible ionizations in the ES complex that impact catalysis. The first pK_a represents an ionization where the deprotonated form is necessary for activity. The second pK_a represents ionization of a separate entity where deprotonation inactivates the enzyme and thus the protonated form of this residue is necessary for optimal activity. Thus, equation (5.3) assumes the single protonated form (EHS^-) is the only catalytically active form (Figure 5.14A). The pK_a of 5.44 represents the residue in the enzyme that is catalytically important in its deprotonated form. While residue pK_a values can shift significantly

in the protein environment, many residues have a typical range for their pK_a values that can be used as a starting point [448]. This residue could be an Asp or Glu whose usual pK_a range is 2-5.5 in proteins or it could be a His, which has a pK_a range of 5-8 [448]. There is also the possibility that the pK_a of 5.44 represents the ionization of an α -CO₂H group from the residue at the C-terminus since the ionization of the α -CO₂H group also has a pK_a range of 2-5.5 in proteins [448].

A



B

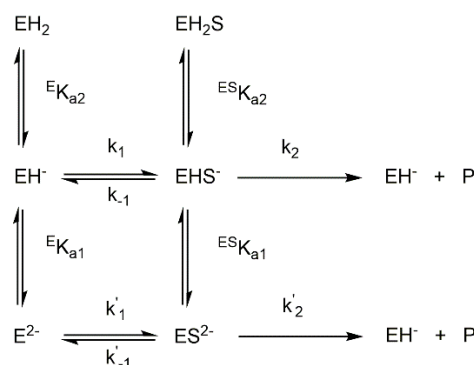


Figure 5.14: Diagrams of the enzyme equations involved in the protonation states of the NapA enzyme. The free enzyme and enzyme-substrate complex have in a simplified form three protonation forms representing protonation of residues that are catalytically important. The biomolecule can be fully deprotonated, monoprotated, or diprotonated: A) where only one protonated state, i.e. the monoprotontated state (EHS^-), is catalytically active and B) where two protonic states, i.e. the monoprotated (EHS^-) and the fully deprotonated (ES^{2-}) states, produce products.

According to a homology model of *C. jejuni* NapA [329], there are no Asp or Glu residues within hydrogen bonding distance to the molybdenum center. There are a few instances of Asp or Glu residues nearby the MPT components of Moco, and so it is possible the protonation state of a

residue hydrogen-bonding to one of the MPT molecules could influence catalysis. The importance of the MPT group in catalysis has been the focus of several recent investigations [80, 238, 460]; however, the exact manner in which the MPT influences catalysis is unclear.

The other possible residue that the pK_a of 5.44 could represent is a His residue. There are two His residues in close proximity to the molybdenum center. Residue H822 is positioned slightly under the molybdenum center in between the two MPT molecules and thought to interact in the hydrogen-bonding network of the MPT molecules. Residue H175 is directly next to the coordinating C176 residue and positioned above the molybdenum center in the catalytic pocket. The hydrogen-bonding residues to the Moco may impact catalysis, by influencing the redox state of the MPT molecule which in turn can impact the potential of the molybdenum center. The residue H175 however is in the pocket and can influence the stabilization of the ES complex or be involved in proton shuttling during catalysis. Both His candidates, His175 and His822, in NapA are prime targets and will be investigated with additional mutagenesis studies in the future.

The second pK_a of 9.38 represents the deprotonation of a residue that inactivates the enzyme. This residue could be a Tyr which usually has a pK_a range of 9-12 or it could be a Cys which has a pK_a range of 8-11 [448]. At this time, we hypothesize that deprotonation of either a crucial Tyr or Cys would result in the loss of a crucial hydrogen bonding interaction that impacts the structural integrity of the enzyme resulting in the decreased activity. A few possibilities include Y81, C459, C554, and Y887. Y81 is positioned between the NapA [4Fe4S] cluster and the NapAB interface. While C459, C554, and Y887 are in the catalytic pocket of NapA. Specifically, C554 is approximately 2.6 Å from the guanine nucleotide of one MGD molecule while Y887 is positioned similarly within 3.1 Å of the phosphate on the other MGD molecule. Further investigation is needed to determine if any of the potential candidates correspond to this crucial ionization.

The C176S/D NapA variants exhibit a more complicated profile as the plots of $\log(k_{cat})$ as a function of pH (Figure 5.13BC) cannot be fit with equation (5.3). The data were fit to high order polynomials and the shape of the fit suggests that two protonic states (EHS^- and ES^{2-}) can yield products as shown in the enzyme reaction diagram in Figure 5.14B [457]. The observation of the higher of the two maxima at low pH (Figure 5.13BC) further suggests the deprotonation diminishes the rate of nitrate reduction and further deprotonation may even inactivate the enzyme [457]. The difference in the two maxima is larger in C176S NapA (Figure 5.13B) suggesting the diminishing rate effect on catalysis at higher pH may be more significant in this variant, which is supported by

the kinetic data where k_{cat} for C176S NapA at optimal pH is 0.159 s^{-1} and k_{cat} for C176D NapA at optimal pH is 0.530 s^{-1} (Table 5.5).

Through determination of the inflection points of the polynomial fits in Figure 5.12B and C, we can estimate that the pK_a for the ionization step that diminishes the rate of nitrate reduction may be between 6.6 and 7.7 for C176D NapA and between 7.1 and 8.3 for C176S NapA. However, the pK_a estimates are inexact for complex ionization patterns especially when multiple pK_a values are close together as they are in this case. The main result of the pH profile of the coordinating residue variants indicates that the coordinating residue does impact key ionizations during catalysis. It is tempting to suggest that the change in protonation states and proton shuttling in the C176 Nap variants may cause the energetic changes discussed above. However, further investigation is needed to confirm how the mutation is impacting pK_a and which partner residues in the pocket are affected.

5.5 Summary

DMSOR family enzymes can transform different substrates, and the coordinated amino acid residues influence the enzyme efficiency as well as the substrate affinity. The Asp variant of Nap, reported for the first time, has a low yield and low Mo incorporation. This is the first investigation into the TMAO and DMSO activities of any Nap variants and is also the first documentation of TMAOR activity by a Nap enzyme. Remarkably, the C176D NapA variant reduces DMSO but not TMAO, when the other variants can only reduce TMAO. This investigation represents a detailed kinetic and energetic perspective of the Mo-coordinating residues as recorded by determining the incremental binding energies of the ES and $[\text{ES}^\ddagger]$ states of the Nap C176 variants. Determination of the binding energies suggest:

- The coordinating Cys residue is involved in stabilizing the ES and $[\text{ES}^\ddagger]$ states during the catalysis of nitrate reduction.
- The activation energy for nitrate reduction is lower for the native NapA compared to the C176S/D NapA variants.
- The coordinated Ser residue impacts the binding energy by destabilizing the ES state in TMAO reduction and thus increasing K_M compared to native NapA that results in a small increase in k_{cat} . Consequently, the slightly higher increase in the native enzyme's TMAO

reduction efficiency can be attributed to the lowering of the ES binding energy and lowering of K_M in native NapA.

- TMAO reduction has a higher activation energy barrier than nitrate reduction for native NapA.
- The Ser ligand does indeed tune substrate selectivity by essentially lowering the activation energy barrier by destabilizing the ES and $[ES^\ddagger]$ states of C176S NapA and nitrate instead of stabilizing the states in the reaction with TMAO.
- The Asp mutation impacts the ES state to a greater degree than the $[ES^\ddagger]$ which supports the hypothesis that the Asp ligand can stabilize the DMSO binding to the enzyme when the other variants cannot.

Additionally, the pH profiles of the C176 variants were investigated to see if the differences in energetics and kinetics were related to proton shuttling. The insensitivity to pH observed in *C. jejuni* NapA may in part be aiding in the virulence of the pathogen as compared to free-living microbes. Native NapA, C176S NapA, and C176D NapA have pH optima at 7.4, 7.0, 6.3, respectively, but the most notable feature of these pH profiles is the impact the coordinating residue seems to have on K_M and effectively on substrate affinity. The K_M of both C176S/D variants increases with more alkaline pH while no obvious pattern is observed for the native NapA's K_M value over the same pH range. The main finding of the pH profile of the coordinating residue variants indicates that the coordinating residue does impact key ionizations during catalysis.

Under the assumption that the majority of the DMSOR family follow OAT reaction as the *modus operandi* regardless of the substrate, then the differences lie in Nature's way of selecting the most efficient conditions to turnover a specific substrate. The coordinating residue is one component that nature has accomplished this goal to tune substrate selectivity as highlighted by the efficiencies of the TMAO and DMSO activity of these Nap variants, the coordinating residue is not the only factor. Thus, there is still much to learn about the mechanisms of the DMSOR family and the role of the coordinating residue.

CHAPTER 6. CONCLUSIONS

6.1 Overview and Conclusions

The molybdenum cofactor (Moco) has persisted in life forms for 3 billion years and was among one of the essential cofactors that were present in the last universal common ancestor, LUCA [23, 397]. As such, Moco is present in all life and plays an essential role in the cycling of C, S, N, As, and Se. Moco is composed of three components: the pyranopterin heterocycle, a dithiolene unit appended to the pyran ring, and the Mo metal center coordinated by the dithiolene sulfurs (Figure 1.1). All three components are redox-active, but it is unclear how they function in concert to tune substrate specificity and catalysis [4]. Additionally, many of these enzyme contain additional cofactors, such as a [4Fe4S] cluster, which are essential for electron transfer to the Mo center. Therefore, cofactor content and in this case full metal content are essential for full activity in this class of enzymes.

The main objective of this study was to focus on the molybdenum center and determine how molybdenum coordination impacts catalysis, specifically the role of the coordinating residue was the central target for investigation. In order to probe the molybdenum center, a molybdenum enzyme must be isolated in an active form. For this study, the DMSOR family of molybdenum enzymes was chosen for study due to its high diversity in molybdenum coordination in the active site (Figure 5.1B). The DMSOR family enzyme periplasmic nitrate reductase (NapA) was selected as the model enzyme to investigate the molybdenum center coordination for multiple reasons.

First, nitrate reductases have significant impacts on society. Nitrate reductases are involved in the nitrogen cycle, nitrate specifically is important to agriculture and has been a pollutant of water supplies [344]. Nitrate and nitrogen species produced from nitrate (i.e. nitrite and nitric oxide) have been linked to several health benefits and serious diseases [344]. Second, of the nitrate reductase types Nap in particular has been linked to the pathogenicity of intestinal pathogens such as *Salmonella*, *E. coli*, and *C. jejuni* [339, 349, 350, 359]. Third, there exist ambiguities in the molybdenum coordination sphere and currently proposed mechanism of the catalytic subunit NapA. Thus, NapA is a reasonable choice for the member of the DMSOR family to focus on during the investigation of the molybdenum center.

In order to study NapA, large quantities of active enzyme are necessary therefore we chose to heterologously over express *C. jejuni* NapA in *E. coli* to produce an efficient expression system capable of producing high quantities of active enzyme. In Chapter 1, we explored the literature to best prepare efficient expression of high quantities of an active Moco-containing enzyme in the *E. coli* host. From literature precedent, we optimized the expression and purification method for isolating *C. jejuni* NapA in an *E. coli* host (Chapter 2). NapA was successfully cloned and expressed marking this work as the first heterologously expressed Nap enzyme and the first Nap isolated from an Epsilonproteobacteria. The successful expression demonstrated that *E. coli* is fully capable of inserting the proper form of Moco (i.e. bis-MGD) and folding of the enzyme.

An optimized IPTG induction method was determined in Chapter 2 (Section 2.2.3.5) and compared to an auto-induction method (Section 2.2.3.6). The auto-induction method produced a higher yield of enzyme, and the enzyme was more active than the IPTG method of induction. This result agrees with the literature reviewed in Chapter 1 that reported higher yields of active protein when the enzyme is expressed at low temperatures for longer growth times. The slower expression appears to keep the host cells healthier, prevent target enzyme from being degraded, and proper insertion of Moco resulting in high cofactor loading.

Unexpectedly, periplasmic isolation of the periplasmic protein, NapA, was insufficient in producing large quantities of active enzyme as compared to complete cell disruption suggesting there is a TAT processing issue in *E. coli*. We suspect that the *E. coli* TAT machinery has either reached its capacity and is saturated resulting in little to no NapA transport or that the *E. coli* TAT machinery has difficulties recognizing and processing the *C. jejuni* TAT leader sequence. Due to the low yield of enzyme isolated from the periplasmic space, NapA purification was optimized with complete cell disruption by sonication prior to purification by affinity and size exclusion chromatography. Under the optimized method, NapA was purified to 90% homogeneity where 1.5-2 mg/L of culture was obtained with 90% or higher Mo incorporation.

Two peaks eluted during where the first eluted peak has lower Mo content than the second peak. This phenomenon may be due to peak broadening and the isolated enzyme eluting very close to the void volume for the Sephacryl S-200 column. The second eluted peak had higher Mo incorporation and thus was more active than the first peak. After calibration on the Sephadex S-200, NapA emerged as one peak with a molecular weight of ~ 100kDa. However, this observation contradicts the mass spectrometric analysis of as-isolated NapA. Trypsin-digested samples of both

SEC peaks isolated from the Sephacryl S-200 column contain both NapA and NapD proteins. Additionally, NapD can be seen in the SDS-PAGE gels. Intact mass spectrometry of the as-isolated NapA enzyme revealed the protein exists mostly as a NapAD complex. CID of the NapAD complex peak from the intact mass spectrometry spectrum was able to dissociate the complex into free NapA and NapD components matching the predicted molecular weights of the free enzymes. NapD appears to be tightly bound to NapA yet NapA is still active.

NapL, however, has never been observed in any mass spectrometry samples. NapL is an untagged periplasmic protein that is suspected to fold in the periplasm and thus it is possible that NapL is possibly being degraded before it can interact with NapA. Furthermore, NapL could be expressed and transported to the periplasm efficiently while NapA is not and thus NapL would be unable to accomplish its function. It is also possible that NapL has not properly been expressed in *E. coli*. While NapL has never been observed during protein expression, DNA sequencing confirms it is positioned upstream of NapD in the pBM10C construct (Appendix D). NapL and NapD have been demonstrated to be essential for full activity but not essential for nitrate reduction in both *Wolinella succinogenes* [293] and *C. jejuni* [294]. *C. jejuni* NapA expression without *napLD* genes in the current study resulted in low enzyme yield with low Mo incorporation and low activity which at least shows in the current expression system that NapD is necessary for NapA activity. Until it can be confirmed that NapL and NapA are interacting in this system, little can be stated about the importance or role of NapL.

Despite the presence of NapD and possibility that a key function of NapL was unfulfilled, the NapA enzyme was still active with high Mo incorporation and an intact [4Fe4S] cluster and thus biochemical characterization of the native NapA enzyme was explored in Chapters 3 and 4. *C. jejuni* NapA was modelled previously [302, 344] and an electrostatic potential diagram shows that the pocket and substrate are positively charged where *C. jejuni* NapA has the most basic surface compared to previously isolated Nap enzymes. The observed rate of nitrate reduction was plotted as a function of substrate concentration and fit to the Michaelis-Menten model. The K_M was determined to be 3.40 μM and the k_{cat} was 5.91 s^{-1} . As compared to previously isolated Nap enzymes, *C. jejuni* NapA is a more efficient nitrate reducer as indicated by the k_{cat}/K_M . The low K_M is particularly noteworthy and may suggest *C. jejuni* Nap is used for nitrate scavenging.

The pH dependence of nitrate activity of native *C. jejuni* NapA was also analyzed (Chapter 3). The optimum pH was determined to be 7.4, and NapA appeared to be pH resistant over the

range of pH 5.5-9.0. The dependence on k_{cat} shows a shift of 6 s^{-1} , and dependence on K_{M} shows a change of $6 \text{ }\mu\text{M}$ over the examined pH range. However, NapA isolated from *R. sphaeroides* demonstrated a change of 50 s^{-1} and $200 \text{ }\mu\text{M}$ in k_{cat} and K_{M} , respectively [370]. Interestingly, *C. jejuni* NapA also showed a decline in reaction velocity at substrate concentrations higher than 200-400 μM and is suspected of representing a substrate-inhibited form of NapA similar to the inhibited form of *R. sphaeroides* NapA [372]. The pH dependence and kinetic parameters of the *C. jejuni* NapA enzyme suggest NapA acts as a nitrate scavenger in *C. jejuni* and may play an important role in metabolism that supports the growth and infection of this bacterium.

The nitrate activity dependence on NaCl was investigated in Chapter 4 along with the impact of the His-tag on metal content and enzyme activity. While the His-tag was demonstrated to not strip metal or impact catalysis, NaCl did influence the kinetic parameters. The concentration of NaCl impacts K_{M} not k_{cat} . The K_{M} for nitrate increases with salt concentration suggesting Cl^- may be binding in the catalytic pocket of NapA influencing substrate binding. There is also the possibility the change in ionic strength is impacting solubility.

The molybdenum center of NapA in the absence and presence of NaCl was probed by X-ray absorption spectroscopy. XAS spectra of as-isolated NapA in the absence of Cl^- revealed that NapA is isolated as a heterogeneous mixture. The mixture could represent either variation in the oxidation state of Mo or variation in the coordination sphere of Mo. The EXAFS spectrum of the mixture was fit to 5 Mo-S bonds assigned to the four dithiolene sulfurs and the coordinating Cys sulfur and a 1:0.9-1.2 ratio of Mo=O to Mo-OH for the 6th and final ligand. The most notable observation is that *C. jejuni* NapA has no sulfido ligand present in the first coordination sphere of molybdenum which has serious implications on the mechanism for NapA. However, currently we are unsure whether the sulfido is missing because it is physiologically not present or for some other unknown reason. Still we are inclined to support the former claim due to the reactivity of sulfido ligands in small molecules and the high probability that upon regeneration of the MoIV resting state that the sulfido ligand will most likely be reductively eliminated before the terminal oxo moiety (as discussed in detail in Chapter 4). In fact, it may be possible that the sulfido is not physiologically present in Nap but is being introduced into the enzyme due to the methods used to isolate or crystallize it in *C. necator* NapA [130].

The Cl^- treated NapA sample had a more positive edge energy in the XAS spectra as compared to the untreated as-isolated NapA in addition to a significantly different oscillation

pattern. The data suggest Cl^- treatment perturbs the active site but the mode of action is unclear. The resolution of the XAS data is not high enough to distinguish S and Cl atoms. All that can be confidently stated is that there are 5-6 S/Cl bonds possible in total and 2-3 bonds are longer than the remaining 2-3 bonds. The Cl^- does not appear to be bound to Mo in a manner that impact catalysis since the turnover number is unaffected by Cl^- concentration. However, Cl^- could be bound in the pocket interfering with substrate binding or possibly interacting pyranopterin molecule and perhaps perturbing dithiolene coordination.

Finally, the main objective of this study was investigated in Chapter 5 where the coordinating Cys (C176) was exchanged for Ser, Asp, and Ala to probe the role of the coordinating residue in activity and substrate selectivity. The C176 residue is coordinating Mo and its presence is essential for proper function of NapA. The variants C176S/D/A have been confirmed by sequencing and metal analysis revealed the presence of Mo while UV-Vis spectroscopy suggests the $[\text{4Fe4S}]$ cluster is intact. Variant C176S and C176D NapA are active towards nitrate albeit far less effective than the wild type. Both K_M and k_{cat} are impacted in these variants, suggesting not only the expected redox potential but also the binding of the substrate is influenced.

The C176S mutation does not appear to impact the rate of TMAO reduction but did significantly reduce NR activity. Remarkably, the C176D NapA variant reduces DMSO but not TMAO, when the other variants can only reduce TMAO. C176D can reduce DMSO suggesting a shift in substrate specificity. C176A is an inactive variant of NapA for all three substrates suggesting the redox potential may have shifted resulting in an enzyme incapable of reducing alternative substrates. This investigation represents a detailed kinetic and energetic perspective of the Mo-coordinating residues that has been recorded by determining the incremental binding energies of the ES and $[\text{ES}^\ddagger]$ states of the Nap C176 variants. Determination of the binding energies suggest:

The results revealed that NapA has a significantly lower activation energy barrier compared to the C176S/D variants for nitrate reduction. Interestingly, the C176D variant has a lower ES^\ddagger free energy than the C176S variant by ~ 4 kJ/mol suggesting the oxygen ligand to the molybdenum center is not the only factor influencing the drive force of the reaction. The native NapA had a ~ 178 J/mol lower energy for ES^\ddagger compared to the C176S variant for TMAO reduction implying that the activation energies of these variants for the reduction of TMAO are very similar and may be responsible for the observed similar efficiencies during kinetic analysis.

From this energetic study, we can conclude that the coordinating Cys residue is involved in stabilizing the ES and $[ES^\ddagger]$ states during the catalysis of nitrate reduction. Furthermore, the activation energy for nitrate reduction is lower for the native NapA compared to the C176S/D NapA variants. TMAO reduction has a higher activation energy barrier than nitrate reduction for native NapA. The coordinated Ser residue impacts the binding energy by destabilizing the ES state in TMAO reduction and thus increasing K_M compared to native NapA that results in a small increase in k_{cat} . Consequently, the slightly higher increase in the native enzyme's TMAO reduction efficiency can be attributed to the lowering of the ES binding energy and lowering of K_M in native NapA. The Ser ligand does indeed tune substrate selectivity by essentially lowering the activation energy barrier by destabilizing the ES and $[ES^\ddagger]$ states of C176S NapA and nitrate instead of stabilizing the states in the reaction with TMAO. The Asp mutation impacts the ES state to a greater degree than the $[ES^\ddagger]$ which supports the hypothesis that the Asp ligand can stabilize the DMSO binding to the enzyme when the other variants cannot.

While there have been several studies on the impact of the coordinating residue in molybdenum enzymes (Table 5.1), no Asp mutation has ever been investigated. All Ala variants ever made to investigate the coordinating residue in Mo enzymes have been inactive (Table 5.1). However, few examples of a native Cys to Ser mutation at the Mo center of this family of enzymes are reported, but they all report the mutation to inactivate the enzyme [67, 90, 378, 402]. However, mutating a native Ser to a Cys in the active site gives mixed results. *R. sphaeroides* DMSOR where Ser was exchanged for Cys modifies the reactivity of the molybdenum center where both decreases and increases in specific activity for various substrates are observed. Reduction activities for DMSO and TMAO decrease by 60-80% and MetSO/BSO/chlorate activities are essentially non-existent while adenosine N^1 -oxide (ANO) activity increases by 400% [54]. In contrast, a Cys substituted for Ser in BSOR resulted in an inactive variant [135]. Thus, this study has significantly added to the knowledge about the role of the Mo coordinating residue by investigating this essential residue in a more detailed kinetic and energetic perspective.

Additionally, the pH profiles of the C176 variants were investigated to see if the differences in energetics and kinetics were related to proton shuttling. The pH dependence of WT and C176S/D NapA reveal the variants shift the optimal pH more toward acidic pH. The variants induce an increase in K_M , effectively decreasing affinity with more alkaline pH suggesting the Ser and Asp residues shift the pK_a of a nearby residue in the pocket that is involved in substrate

binding. Further analysis of the pH data indicates, a residue with pK_a of ~ 5.44 in the native NapA enzyme must be deprotonated for optimal activity of NapA. The residue in question could possibly be His175 or His822 which are in the pocket close to the Mo center. Additionally, deprotonation of a residue with pK_a of ~ 9.38 deactivates the enzyme which could represent a crucial Tyr or Cys residue that is essential for the structural integrity of the enzyme or in maintaining the proper conformation of the cofactors. The pK_a determination of the C176S/D variants is more complex. The main finding of the pH profile of the coordinating residue variants indicates that the coordinating residue does impact key ionizations during catalysis.

Under the assumption that the majority of the DMSOR family follow an OAT reaction regardless of the substrate, then the differences lie in nature's way of selecting the most efficient conditions to turnover a specific substrate. The coordinating residue is one component that nature has accomplished this goal to tune substrate selectivity as highlighted by the efficiencies of the TMAO and DMSO activity of these Nap variants, the coordinating residue is not the only factor. Thus, there is still much to learn about the mechanisms of the DMSOR family and the role of the coordinating residue.

6.2 Significance

Understanding the role of the coordinating residue in the DMSOR family of molybdenum enzymes is essential to comprehend the catalytic process at the molybdenum center in this family of enzymes. DMSOR family enzymes can transform different substrates many of which are involved in the metabolism of microbes that form essential processes in the cycling of C, S, N, As, and Se [4]. Additionally, some of these key metabolic enzymes may impact the virulence of pathogens as seems to be the case for Nap in *C. jejuni*, *Salmonella*, and *E. coli* [339, 349, 350, 359]. The coordinated amino acid residues influence the enzyme efficiency as well as the substrate affinity and the information gathered in this work will be the foundation to understanding the redox properties of the Moco and how catalysis is tuned in this family of enzymes. Thus, this knowledge can be applied in the future to those targeting these Moco-containing enzymes for various reasons such as bioremediation, health, and more.

6.3 Future Work

The work presented here is just the foundation for investigation in NapA and the functioning of Moco enzymes in general. As with all well-designed experimentation, this work has generated many new questions about NapA and its molybdenum enzyme family. Thus, there is a variety of directions this work could pursue in the future. Outlined below are a few areas of interest this work has illuminated during the past several years that have yet to be fully explored.

First, the enzyme formate dehydrogenase (FDH) is a member of the DMSOR family with remarkable structural similarity to Nap. Both enzymes have very similar folds and active sites except for a few key residues in the pocket [91]. In FDH, there is a key His residue (H141) that is essential to the hydride transfer mechanism of formate oxidation [91, 376]. This residue is exchanged for a Met in Nap enzymes. Interestingly, FDH can turn over nitrate but Nap is unable to turn over formate. Thus, it would be interesting to introduce a His residue in this position in Nap and see if the presence of this key His can enable formate activity in NapA. Similarly, it would be interesting to insert the crucial Tyr114 from DMSOR [97] into Nap to see if the Tyr residue can enable Nap to turn over DMSO.

Second, the pH study of *C. jejuni* NapA revealed that the reaction velocity of nitrate reduction decreased at nitrate concentrations greater than 200-400 μM (Chapter 3). A similar pattern was observed in *R. sphaeroides* NapA but under different conditions [372]. At this time, we are unsure why this observation is made under different conditions for the two enzymes. Thus, in the future it would be noteworthy to investigate the possibility of substrate inhibition more closely. Specifically, both PFV and MV solution assays must be conducted under the same conditions as the *R. sphaeroides* enzyme. Additionally, this enzyme is a heterodimer of NapAB and thus it would be prudent to clone and isolate NapB so that a comparison can be made between the complex and free NapA enzyme.

Third, the pH study also revealed the pK_a of a crucial residue in NapA required to be in its deprotonated form for optimal activity (Chapter 5). A possible candidate for this H175 that is located in the pocket next to the coordinating Cys. A mutagenesis study where this residue is exchanged with Ala, Tyr, and Trp would elucidate the possible role this residue has in the pocket and may confirm if this His is indeed the residue with the crucial pK_a determined in the pH study.

Fourth, it would be prudent to expand the substrate profile for the C176 variants. Specifically, the focus should be shifted to small oxyanions that are similar in size and shape to

nitrate. Preliminary enzyme dependence data suggests that perchlorate, arsenate, and selenate may be prime candidates. Additionally, the C176A variant was inactive for all substrates tested. The current hypothesis is that the uncoordinated site may have tuned redox activity to prefer the oxidation of substrates instead of reduction. Therefore, C176A should be tested for oxidase activities starting with the ability to oxidize arsenite. Preliminary enzyme dependence data suggest arsenite can be turned over, but this result needs to be confirmed and a full kinetic curve should be obtained.

Fifth, the periplasmic isolation in addition to mass spectrometry experiments introduced several questions about maturation and transport of *C. jejuni* NapA in its *E. coli* host. Why is NapA not being efficiently transported? Would using the *E. coli* TAT leader sequence help? What is happening to NapL? Is it being degraded before it performs its role? What is its unknown role? Does the presence of NapD influence the activity of NapA? Answering each of these questions is a highly involved process. Several microbiological paths lie ahead. The TAT leader sequence could be changed or removed all together to see if that boosts production of active enzyme and/or alters the amount transported across the membrane. NapD and NapL could be purified and isolated independently to explore their structure and function. The NapL SecT leader sequence could be removed to possibly enable the formation of a NapAL complex in the cytoplasm. With the proper collaboration, NapA could be isolated natively from *C. jejuni* and compared to the heterologously isolated enzyme. Thus, the maturation and transport of NapA in this expression system is a sensible direction to travel in the future.

Sixth, the major hypothesis in the molybdenum enzyme field for the role of the coordinating residue was implied by Boyington [376] where redox potential or pKa could be shifted to tune substrate preference. Having already initiated investigations in pH dependence (Chapter 5), the remaining route to test in the future would be to measure the redox potentials of the Mo center in the C176 variants. One way to determine these potentials is to use EPR to follow the Mo(V) signal and titrate samples with dyes of known redox potential. This experiment would confirm if the coordinating residue does indeed shift the Mo redox potential in NapA. In addition, structural characterization must be conducted on these variants to see if conformation changes could be responsible for the observed activity. The structural characterizations would include XAS, X-ray crystallography, and circular dichroism spectroscopy.

Seventh, in Chapter 5 the variation in the first coordination sphere of DMSOR family of enzymes was discussed where the coordinating residue varies as well as a terminal ligand. The obvious next step to this work would be to probe the role of the terminal ligand. In Chapter 4, we proposed that the sulfido terminal ligand in Nap may not be physiologically relevant and in reality, the terminal group is an oxo moiety. An excellent path for this project in the future would be to test this hypothesis. It is not an easy thing to prove or disprove, but we can begin by taking all measures to ensure oxidative degradation does not occur, i.e. expression and purify the enzyme anaerobically. The cells could be expressed anaerobically using fumarate as an alternative electron acceptor to oxygen. The anaerobic purification could be achieved using the combination of reducing agents such as DTT and facilities such as a glove bag that are under an inert atmosphere while purifying.

In addition, there have been reports of chemical sulfuration where the terminal sulfido is reconstituted. Sulfur reconstitution and then removal by CN^- would be an excellent way to see the effect of the terminal sulfur on nitrate activity. However, it would also need to be verified that the CN^- treatment did not impact the $[\text{4Fe4S}]$ cluster as well. Such experiments would lead into investigations into the validity of the sulfur shift mechanism. If the terminal sulfido could be replaced with a heavier isotope of sulfur perhaps the sulfur shift event could be traced with spectroscopic techniques. XAS could provide snapshots of the active site before and after substrate addition for example. Kinetic isotope studies should reveal a slower activation step for a Nap enzyme with the heavier sulfur atom compared to the lighter sulfur center as the sulfur shift occurs initially. This experiment would require a pre-steady state approach of stopped flow or freeze-quench techniques.

Finally, the recent direction in the Moco enzyme field has been to explore the role of the other redox active components of Moco, i.e. the pyranopterin molecule and dithiolene unit. The conformation, redox state, and whether the pyran ring is closed or open all have been shown to influence the activity of the enzyme possibly through redox potential changes [8, 80, 238, 461-463]. The next step for this investigation would be to explore the MPT ligand of molybdenum. Specifically, how coordination impacts activity by altering the redox state and/or conformation of the pyranopterin molecule. There are a few residues that have been proposed to influence the redox state as well as residues proposed to stabilize the ring open versus the ring closed form of the pyran ring. Additionally, several examples based on crystallographic studies have provided the hydrogen

bond network that holds the cofactor in place but could also influence pyranopterin conformation. All of these residues would also make prime targets for mutagenesis studies to induce changes in the pyranopterin group that can be examined for the effects on activity and redox potential.

In conclusion, the NapA project and investigation of structure and function of the Moco active site has a bright future with many avenues that should be explored. The knowledge gained from such future studies will not only impact studies on nitrate metabolism but also will elucidate key mechanistic methods this fascinating class of enzymes utilizes to do a variety of different chemistries.

APPENDIX A. BUFFERS

All buffers were prepared as follows unless otherwise stated. The buffer components were dissolved in 80% of the total volume of millipore water and titrated to the correct pH with appropriate amounts of strong acid (HCl) or strong base (NaOH). Once the buffer pH had been adjusted, the solution was diluted to the desired final volume.

Spin Column and Periplasmic Isolation Buffers (Chapter 2 Section 2.2.5)

Lysis Buffer (Chapter 2 Section 2.2.5.1)

10 mM imidazole, 300 mM NaCl, and 50 mM Tris-HCl pH 8.0

Wash Buffer (Chapter 2 Section 2.2.5.1)

30 mM imidazole, 300 mM NaCl, and 50 mM Tris-HCl pH 7.0

Elution Buffer (Chapter 2 Section 2.2.5.1)

400 mM imidazole, 300 mM NaCl, and 50 mM Tris-HCl pH 7.5

Sucrose Buffer (Chapter 2 Section 2.2.5.3)

500 mM sucrose, 50 mM Tris-HCl pH 7.6

Purification Buffers (Chapter 2 Section 2.2.5)

Affinity Chromatography Buffer A (Lysis Buffer; Chapter 2 Section 2.2.5.4)

300 mM NaCl, 10 mM imidazole, and 50 mM HEPES pH 7.0

Affinity Chromatography Buffer B (Chapter 2 Section 2.2.5.4)

300 mM NaCl, 250 mM imidazole, and 50 mM HEPES pH 7.0

Size Exclusion Chromatography Buffer (no salt) (Chapter 2 Section 2.2.5.5)

50 mM HEPES pH 7.0

Size Exclusion Chromatography Buffer (with salt) (Chapter 2 Section 2.2.5.5)

150 mM NaCl and 50 mM HEPES pH 7.0

DNA Extraction Buffers (discussed in Appendix B)

TGE Buffer

10 mM EDTA, 50 mM glucose, 25 mM Tris-HCl pH 8.0

TE Buffer

1 mM EDTA, 10 mM Tris-HCl pH 8.0

Electrophoresis Buffers (discussed in Chapter 2 Section 2.2.5 and Appendix B)

SDS-PAGE Resolving Buffer

0.4% (w/v) SDS, 1.5 M Tris-HCl pH 8.8

SDS-PAGE Stacking Buffer

0.4% (w/v) SDS, 1.5 M Tris-HCl pH 6.8

50X TAE Buffer

242 g Tris

18.61 g EDTA

57.1 mL glacial acetic acid

Fill to 1 L with distilled water

Kinetics Buffers (Chapter 2 Section 2.2.5.7 and Chapter 3 Section 3.2.5)

pH 9.0 Buffer

50 mM Tris-HCl pH 9.0

pH 8.5 Buffer

50 mM Tris-HCl pH 8.5

pH 8.0 Buffer

50 mM Tris-HCl pH 8.0

pH 7.0 Buffer

50 mM HEPES pH 7.0

pH 6.0 Buffer

50 mM BisTris pH 6.0

pH 5.5 Buffer

50 mM citrate pH 5.5

APPENDIX B. MOLECULAR CLONING RECIPES AND METHODS

For constructs in Chapter 2

PCR Reaction Mixtures

napLD genes:

2 μ L template DNA (pCnapLD plasmid created by Courtney Sparacino-Watkins)

1 μ L primer napLD_NcoI_Fwd

1 μ L primer napLD_EcoRI_Rvs

25 μ L Taq Master Mix

21 μ L nuclease free water

50 μ L Total

napA gene:

1 μ L template DNA (pCnapA plasmid created by Courtney Sparacino-Watkins)

3 μ L primer napA_XmaI_Fwd

3 μ L primer napA_XmaI_Rvs

25 μ L Taq Master Mix

18 μ L nuclease free water

50 μ L Total

Thermocycler Parameters

Table B.1: Thermocycler Parameters for PCR of the *napLD* genes.

<u>Temperature (°C)</u>	<u>Time</u>	<u>Cycles</u>
95	30 s	1
95	30 s	30
56	1 min	
68	2 min	
68	5 min	1
4	hold	1

Table B.2: Thermocycler Parameters for PCR of the *napA* gene.

<u>Temperature (°C)</u>	<u>Time</u>	<u>Cycles</u>
95	30 s	1
95	30 s	30
60	1 min	
68	4 min	
68	5 min	1
4	hold	1

Ligation Methods

Thermo Fisher Scientific TA Cloning Kit: creation of construct pBM8A

3 μ L pTZS7R/T vector
6 μ L 5X ligation buffer
9.5 μ L PCR sample A (amplified *napLD* genes)
10.5 μ L nuclease free water
1 μ L T4 DNA Ligase
30 μ L Total

Ligation occurred at 16°C for 16 h, enzyme inactivated at 65°C for 5 min and held at 4°C

Thermo Fisher Scientific TA Cloning Kit: creation of construct pTZS7R/T-NapA

3 μ L pTZS7R/T vector
6 μ L 5X ligation buffer
16.5 μ L PCR sample (amplified *napA* gene)
3.5 μ L nuclease free water
1 μ L T4 DNA Ligase
30 μ L Total

Ligation occurred at 22°C for 16 h, enzyme inactivated at 65°C for 5 min and held at 4°C

Creation of construct pMCSG32-NapA

The pMCSG32 vector was dephosphorylated to prevent closure of the vector without the inserted DNA fragment containing the *nap* genes. To ~600 μ L of digested vector add 60 μ L NEB phosphatase buffer, and 5 μ L phosphatase enzyme (NEB commercial enzyme). Incubate reaction at 37°C for 1-5h then heat inactivate the enzyme at 80°C for 5-10 min.

Ligation Mixture

6 μ L dephosphorylated NdeI and XmaI digested pMCSG32 vector

4 μ L 5X ligation buffer

18 μ L NdeI and XmaI digested *napA* gene (extracted from pTZS7R/T-NapA)

3.5 μ L nuclease free water

2 μ L T4 DNA Ligase

30 μ L Total

Ligation occurred at 16°C for 16 h, enzyme inactivated at 65°C for 20 min and held at 4°C

Creation of construct pBM9A

The pRSF vector was dephosphorylated to prevent closure of the vector without the inserted DNA fragment containing the *nap* genes. To the bulk digest (~400 μ L) add 1 μ L nuclease free water, 4 μ L NEB phosphatase buffer, and 5 μ L phosphatase enzyme (NEB commercial enzyme). Incubate reaction at 37°C for 1-5h then heat inactivate the enzyme at 80°C for 5-10 min.

Ligation Mixture

1 μ L NcoI and EcoRI digested and dephosphorylated pRSF Duet vector (Novagen)

2 μ L 5X ligation buffer

0-5 μ L NcoI and EcoRI digested *napLD* genes (extracted from pBM8A)

X μ L nuclease free water

1 μ L T4 DNA Ligase

20 μ L Total

Ligation occurred at 16°C for 16 h, enzyme inactivated at 65°C for 5 min and held at 4°C

Creation of construct pBM10C

The pBM9A vector was dephosphorylated to prevent closure of the vector without the inserted DNA fragment containing the *nap* genes. To the bulk digest (~400 μ L) add 1 μ L nuclease free

water, 4 μ L NEB phosphatase buffer, and 5 μ L phosphatase enzyme (NEB commercial enzyme). Incubate reaction at 37°C for 1-5h then heat inactivate the enzyme at 80°C for 5-10 min.

Ligation Mixture

1 μ L NdeI and XhoI digested and dephosphorylated pBM9A vector

2 μ L 5X ligation buffer

0-5 μ L NdeI and XhoI digested *napA* gene (extracted from pMCSG32-NapA)

X μ L nuclease free water

1 μ L T4 DNA Ligase

20 μ L Total

Ligation occurred at 16°C for 16 h, enzyme inactivated at 65°C for 5 min and held at 4°C

Phenol/Chloroform DNA Extraction Protocol

1. Grow a 50 mL culture containing the DNA to be extracted
2. Centrifuge the culture at 7000 rpm 4°C for 30 min
3. Resuspend the pellet in 1.2 mL TGE buffer and let solution incubate at room temperature for ~5 min
4. Prepare fresh the NaOH/SDS solution as 1.2 mL 1M NaOH, 600 µL 10% (w/v) SDS, and 4.2 mL of Millipore water (all solution components should be sterile before mixing)
5. Add 2.5 mL of the sterile NaOH/SDS solution to the cell solution and invert 3 times to mix
6. Incubate the cell solution on ice for ~ 5 min
7. Add 1.9 mL of sterile 3 M potassium acetate (KOAc) and invert to mix
8. Incubate the cell solution on ice for ~ 5 min
9. Centrifuge the cells at 5000 rpm 4°C for ~40 min
10. Remove supernatant and store the supernatant in the freezer ~1-2 h
11. Add 3 mL phenol and 3 mL chloroform to the supernatant
12. Vortex solution for ~1 min until uniform
13. Centrifuge the solution at 5000 rpm 4°C for ~5 min
14. Extract the aqueous phase (Top layer) and added it to another mixture of 3 mL phenol and 3 mL chloroform
15. Vortexed solution for 1-2 min
16. Centrifuge the solution at 5000 rpm 4°C for ~5 min
17. Removed supernatant and added it to 6 mL 100% ethanol
18. Vortexed briefly and incubated solution in the -80°C freezer for 15 min
19. Centrifuge the solution at 5000 rpm 4°C for ~10 min
20. Remove and discard supernatant
21. Wash the pellet with 75-100% ethanol by pipetting without disturbing the pellet
22. Remove all traces of ethanol and let the pellet air dry 10-15 min ensuring all ethanol has evaporated
23. Dissolved pellet in 200 µL of TE buffer
24. Add 10 µL RNaseA and transfer solution to a clean sterile tube
25. Store isolated DNA in the -20°C freezer

Restriction Digestion Protocols

Followed NEB Biolabs manufacturers protocols for each enzyme. Briefly, us the general protocol below.

Digestion (small scale)

2 μ L Restriction Enzyme

1 μ g DNA sample to be digested

5 μ L 10X NEB Cutsmart buffer (unless otherwise stated by NEB protocol)

X μ L nuclease free water

50 μ L Total

Digestion (bulk)

10 μ L Restriction Enzyme

5-10 μ g DNA sample to be digested

40 μ L 10X NEB Cutsmart buffer (unless otherwise stated by NEB protocol)

X μ L nuclease free water

400 μ L Total

Reaction is run at 37°C (unless otherwise stated by NEB protocol), digest for 1-16 h, enzyme can be inactivated by optimal inactivation temperature and duration for the specified enzyme as noted by NEB protocol.

Chemically Competent Cell Production and DNA Transformation Protocols

Production of Chemically Competent Cells

1. Prepare sterile solutions of 0.1 M CaCl_2 and 0.1 M CaCl_2 + 15% glycerol (keep cold)
2. Grow a starter culture of the cell line the night before
3. Inoculate a 50 mL culture with the overnight starter culture and let it grow at 37°C until an OD_{600} of 0.2-0.3 was reached
4. Place cells on ice for ~15 min
5. Centrifuge cells at 4000 rpm 4°C for 10 min
6. Discard media and resuspend cell pellet in 30 mL 0.1 M CaCl_2
7. Let cells incubate on ice for ~30 min
8. Centrifuge cells at 4000 rpm 4°C for 10 min
9. Discard supernatant and resuspend cell pellet in 2-3 mL 0.1 M CaCl_2 + 15% glycerol
10. Aliquot out cells in aliquots of 50 μL per microfuge tube
11. Freeze cells slowly on dry ice and store in the -80°C freezer

DNA Transformation

1. Add 1-20 μL DNA sample to chemically competent cells, use 0 μL DNA for a negative control and 1-10 μL of pUC19 for a positive control
2. Mix by gentle pipetting
3. Let cells incubate on ice ~30 min
4. Heat shock 30 s- 2 min at 42°C
5. Place cells on ice for 2 min
6. Add ~ 1 mL of sterile LB media to each sample
7. Let cells grow for 1 h at 37°C
8. Plate cells on appropriate antibiotic LB agar plates (negative control is plated on LB agar which should grow as a lawn and is also plated on any antibiotic plates used for the experiment which should show no growth)
9. Let plates grow at 37°C for ~16-18 h

APPENDIX C. ADDITIONAL PROTOCOLS

Electrophoresis Protocols (Ch. 2 Section 2.2.5 & Appendix B, buffers from Appendix A)

DNA Electrophoresis

Prepare the agarose gel as described below. Once the gel is solid, remove the comb and fill the apparatus to the full line (buffer in both trays and submerging the gel) with running buffer (1X TAE buffer). Run the gel at 100-115 V making sure the lanes start near the negative end since negatively charged DNA will run to the positive end. Allow the gel to run until the dye front is three quarters of the way down the gel. Carefully remove the gel from the apparatus to image it. Wear proper PPE due to the mutagenic effects of the ethidium bromide in the gel. Image the gel using a UV light source. Discard the gel in the proper waste container.

0.8% Agarose Gel (double recipe for thicker gel i.e. deeper sample wells)

Dilute 20 mL 50X TAE Buffer into 1 L to prepare 1X TAE buffer

Add 0.4 g agarose to 50 mL 1X TAE buffer

Heat solution in microwave for 10-30 s pulses, swirl to mix as needed

Let solution cool to touch without solidifying

Added 5 μ L of 5 mg/mL ethidium bromide (mutagen) and swirl to mix

Pour solution into gel apparatus, eliminate any bubbles, and insert comb

Wait until solid (gel should look opaque and cloudy)

SDS-PAGE

Prepare the resolving gel first. Mix the water, acrylamide and buffer solutions in a tube and vortex briefly to mix. Assemble the glass plates in the gel pouring apparatus and make sure there is no leaking. Quickly add the catalysts ammonium persulfate and TEMED to the solution and vortex to mix. Quickly transfer the solution in between the short plate and the long plate in the pouring apparatus. Leave room (a few cm) for the stacking gel and the comb. Place a thin layer of water or isopropanol on top of the resolving gel to remove bubbles and prevent an uneven edge. Wait until the resolving gel is solidified before preparing the stacking gel. There should be a few milliliters of gel solution left in the tube to assist in determining when the gel solution is solid. Remove the isopropanol layer using capillary action of a Kimwipe. Prepare the stacking gel in the

same manner as the resolving gel. Have the comb nearby before adding the catalysts. Transfer the catalyzed reaction solution to directly on top of the resolving gel. Fill the apparatus to the top so that it is on the verge of overflowing. Carefully insert the comb in between the two glass plates.

Wait until the gel is completely solidified as gauged by the remaining reaction solution still in the tube. Carefully remove the glass plates (with solid gel in between) from the pouring station. Insert the glass plates with gel in the Biorad mini gel electrophoresis apparatus. Make sure the short plate is facing in toward the wire. Make sure there are two gels facing each other in the apparatus or one gel and a buffer dam. Pour 1X running buffer (commercial TGS, Tris-Glycine-SDS buffer from VWR) in between the two short plates or the short plate and the buffer dam. Make sure the apparatus is not leaking (reassemble if it is leaking). Pour the rest of the running buffer in the outer container to the appropriate level as marked. Carefully remove the comb and load samples. Run the gels at ~121 V until the dye front is at the bottom of the gel but do not let the dye front run off the gel. Remove the gel from between the two glass plates and discard the stacking gel portion. Keep track of directionality so that the lanes can be properly identified. Place the gel in a small container and cover the gel with Coomassie Quick Stain. Let the gel stain on a shake plate or rotator platform for ~20-30 min. Remove the stain and save it as it can be reused multiple times. Cover the gel in destain solution and let it shake/rock overnight until protein bands are visible compared to the gel background. Image accordingly.

10 % Acrylamide Resolving Gel (makes 2.5 mini gels)

7.6 mL DI water

4 mL 40% acrylamide/bis-acrylamide

4.16 mL SDS-PAGE Resolving Buffer

160 μ L 10% (w/v) ammonium persulfate (make fresh each time)

16 μ L TEMED

4% Acrylamide Stacking Gel (makes 2.5 mini gels)

6.2 mL DI water

1 mL 40% acrylamide/bis-acrylamide

2.6 mL SDS-PAGE Resolving Buffer

100 μ L 10% (w/v) ammonium persulfate (make fresh each time)

10 μ L TEMED

Coomassie Quick Stain

20 mL glacial acetic acid

180 mL distilled water

0.012% (w/v) Coomassie G-250 dye

Coomassie Destain

10% (v/v) Acetic acid

Kinetics Protocols (Chapter 2 Section 2.2.5.7 and Chapter 3 Section 3.2.5)

Preparing the Reaction Solution and Measuring Initial Rates

Enzyme was degassed into the glovebox while frozen and thawed in the glovebox fridge at 4°C. The enzyme was titrated with reduced methyl viologen until it stayed dark purple and then the enzyme was incubated in the fridge for 10-60 min or overnight in cases with excessive background rates (most likely due to dissolved oxygen). The enzyme was buffer exchanged with centrifugal filter microfuge tubes (10 kDa) with more reduced methyl viologen or buffer depending on how potent (darkly colored) the methyl viologen solution was. The enzyme was concentrated to under 100 µL. The enzyme was diluted appropriately so that there was a reasonable signal during the enzyme reaction that was above the background rate but slow enough to measure the initial rate accurately and reproducibly. The reaction mixture varied for each prep of enzyme. Typically for WT NapA 30-100 ng of enzyme was present in a well of 250-300 µL. Minimal methyl viologen is added to the reaction to obtain an absorbance of 0.8-1.0 A.U. in the absence of substrate. Buffer was added to the reaction mixture to 240 µL and then a blank measurement was taken to ensure the well/reaction mixture was not contaminated with a competing substrate that would react with methyl viologen or the enzyme. The reaction was initiated with 10 µL of substrate and the rate monitored at 600 or 630 nm for a set time (5-15 min). Once a reliable reaction mixture composition had been determined by trial and error, the reaction mixture was prepared in bulk and supplied to multiple wells so that whole rows of the 96 well plate could be monitored at once.

APPENDIX D. SEQUENCING AND MASS SPECTROMETRIC CONFIRMATION OF PERIPLASMIC NITRATE REDUCTASE PROTEINS

NapD Coverage Map

NapD was observed in the SDS-PAGE gels as an unresolved band in the dye front smaller than the resolved 15-kDa standard band (refer to Chapter 2). The NapD suspected band was confirmed to be NapD after the trypsin digested band was subjected to LC-MS/MS analysis as discussed in Chapter 2. The peptide coverage map of the NapD band is given in Figure A.5.1. In addition, *C. jejuni* NapD peptides were identified in every in-solution NapA digest ever measured. NapD was present in both SEC peaks as discussed in Chapter 2. The *E. coli* NapD and NapA sequences are significantly different and the peptides identified are unique to *C. jejuni* NapD.

```
1  MNNLSSVLIL  AKEEYINDLK  KAISEIPFCS  VELCENEKII  VVIESENLED
51  ELNSYKMLEK  LPNIISINMV  FSYQDLNDDI  QKAINGAIE  TIEKNENAEN
101 I RYYGSVFNQ  FS
```

Figure D.1: Mass spectrometric analysis of *C. jejuni* NapD expressed in *E. coli* K12. The identified peptides are highlighted in red. A 34% coverage was obtained.

Sequencing Confirmation of C176 Variants

Below are the DNA sequence alignments of the *nap* genes in the various constructs produced to create the C176 Nap variants.

Figure D.2: The *napLD* sequence alignment utilizing Clustal OMEGA Alignment Tool. The *napLD* sequence in construct pBM10C is compared to the *napLD* gene sequence in *C. jejuni* RM1221. The insertion of the codon GGG for a glycine residue at position 4-6 was intentional to keep the genes in frame in the desired construct.

pBM10C	ATGGGGAAAAAATTTCTTTTATTTTGTAGTCTTTTTTGTGTTTTGTCTTATGCTTATGAG	60
napLD	atg--AAATAATTTCTTTTATTTTGTAGTCTTTTTTGTGTTTTGTCTTATGCTTATGAG	57

pBM10C	CTGAAATTAAATGCCAATATAACAGCTTTAAAGCTTGATAAGCAAACTTATATATAGGC	120
napLD	CTGAAATTAAATGCCAATATAACAGCTTTAAAGCTTGATAAGCAAACTTATATATAGGC	117

pBM10C	ACTGATAAAGGTGAAATTTTGCAATATAACATTAAGATAAAAGTTTAAAAGAACTTTTA	180
napLD	ACTGATAAAGGTGAAATTTTGCAATATAACATTAAGATAAAAGTTTAAAAGAACTTTTA	177

pBM10C	TCTTTGCCAAAGATTAAAAATTATTATGGTGATGATTTTGCTAAAATTACAACATTGAT	240
napLD	TCTTTGCCAAAGATTAAAAATTATTATGGTGATGATTTTGCTAAAATTACAACATTGAT	237

pBM10C	ATTTTAAACATACACTTTTAATACTTAGCGAGGGTGATTTTGGTGCTAAAAATTTAAGT	300
napLD	ATTTTAAACATACACTTTTAATACTTAGCGAGGGTGATTTTGGTGCTAAAAATTTAAGT	297

pBM10C	TTTATAAGGAAAAATTACAAATCAAAAAGCTCGAAGAAAATAGCATAATAAAAGCATTT	360
napLD	TTTATAAGGAAAAATTACAAATCAAAAAGCTCGAAGAAAATAGCATAATAAAAGCATTT	357

pBM10C	TTTATCAATGAAATACTTATCTTTTGATTTCTATTGGTCTGAAATAGAATTGATTGAT	420
napLD	TTTATCAATGAAATACTTATCTTTTGATTTCTATTGGTCTGAAATAGAATTGATTGAT	417

pBM10C	AAAAGTTTAAAAAATATAAAAAAATTTAATTTTCCCATTCCTAGTCTTAATGATGCAGTT	480
napLD	AAAAGTTTAAAAAATATAAAAAAATTTAATTTTCCCATTCCTAGTCTTAATGATGCAGTT	477

pBM10C	TTAAATGAAGATAAGAGTAGACTAATTGCAGGTTTTGAGAGTGGCGAAGTAGAACTTTTT	540
napLD	TTAAATGAAGATAAGAGTAGACTAATTGCAGGTTTTGAGAGTGGCGAAGTAGAACTTTTT	537

pBM10C	GATTTGAAAAATTGGAAGATGTTGAAAACTATGATAAAATGCATAAAGATAATATCTAT	600
napLD	GATTTGAAAAATTGGAAGATGTTGAAAACTATGATAAAATGCATAAAGATAATATCTAT	597

pBM10C	CAAGTAGATTTTAAAAAATATGTTATTTAAGTTGTGGAACGGATAGGCGTATAGGAGTT	660
napLD	CAAGTAGATTTTAAAAAATATGTTATTTAAGTTGTGGAACGGATAGGCGTATAGGAGTT	657

pBM10C	GTAATAAATGAAGAACAAAATTTTTTACAAAAGATTTTTTGATATATACTTGTGCTTTA	720
napLD	GTAATAAATGAAGAACAAAATTTTTTACAAAAGATTTTTTGATATATACTTGTGCTTTA	717

pBM10C	AGTCTTAATGGAGAATTGGCTGTTTATAGCGATAATGAAGCTGGAGTTAGTGAAGTTTTT	780
napLD	AGTCTTAATGGAGAATTGGCTGTTTATAGCGATAATGAAGCTGGAGTTAGTGAAGTTTTT	777

pBM10C	AGCACAAGTGATTTTAAGCCTGTTAAAACTTTTAATAATGAAAATTTGATGAGTGAGTTT	840
napLD	AGCACAAGTGATTTTAAGCCTGTTAAAACTTTTAATAATGAAAATTTGATGAGTGAGTTT	837

pBM10C	ATTATTTTTTTAAACAATAAAGATTTTATCGTTTCAGGCTTTGGTGATAGTATAATGTTT	900
napLD	ATTATTTTTTTAAACAATAAAGATTTTATCGTTTCAGGCTTTGGTGATAGTATAATGTTT	897

pBM10C	AGGAGTATTGATGAATAATCTTTCTAGTGTTTTGATTTAGCAAAAGAAGAATATATAAA	960
napLD	AGGAGTATTGATGAATAATCTTTCTAGTGTTTTGATTTAGCAAAAGAAGAATATATAAA	957

pBM10C	TGATTTAAAAAAGGCTATATCTGAAATTCCTTTTTGTTCTGTAGAAGTTTGTGAAAATGA	1020
napLD	TGATTTAAAAAAGGCTATATCTGAAATTCCTTTTTGTTCTGTAGAAGTTTGTGAAAATGA	1017

pBM10C	AAAGATTATAGTTGTGATTGAAAGTGAAAATTTAGAAGATGAATTAACTCTTATAAAAT	1080
napLD	AAAGATTATAGTTGTGATTGAAAGTGAAAATTTAGAAGATGAATTAACTCTTATAAAAT	1077

pBM10C	GCTTGAGAAATTGCCAATATTATCAGCATTAATATGGTTTTTCTTATCAAGATTTAAA	1140
napLD	GCTTGAGAAATTGCCAATATTATCAGCATTAATATGGTTTTTCTTATCAAGATTTAAA	1137

pBM10C	TGATGATATCCAAAAAGCAATCAATAGCGGCGCAATAGAAACGATAGAAAAAATGAAAA	1200
napLD	TGATGATATCCAAAAAGCAATCAATAGCGGCGCAATAGAAACGATAGAAAAAATGAAAA	1197

pBM10C	TGCTGAGAATATTCGCTACTATGGTAGTGATTTAATCAATTTTCTTAA	1249
napLD	TGCTGAGAATATTCGCTACTATGGTAGTGATTTAATCAATTTTCTTAA	1246

Figure D.3: The *napA* sequence alignment utilizing Clustal OMEGA Alignment Tool. The *napA* sequence in construct pBM10C is compared to the *napA* gene sequence in *C. jejuni* RM1221. The mutation of the base A1506 to T1506 is a silent mutation in the protein sequence and was ignored. The mismatch at the end represents the insertion of the TEV cleavage site and the histidine tag cloned onto the C-terminus of the protein.

pBM10C napA	ATGAATAGAAGGGATTTTATTAATAACCGCTATTGCAAGTGCCTAGTGTTCAGGG ATGAATAGAAGGGATTTTATTAATAACCGCTATTGCAAGTGCCTAGTGTTCAGGG *****	60 60
pBM10C napA	CTTAGTGTTCAGCTCTATGCTTGGCGCGCAAGAAGAAGATTGGAATGGGATAAAGCT CTTAGTGTTCAGCTCTATGCTTGGCGCGCAAGAAGAAGATTGGAATGGGATAAAGCT *****	120 120
pBM10C napA	GTTTGTAGATTTTGTGGAAGTGGCTGTGGAATTATGATAGCTAGAAAAGATGGCAAAATC GTTTGTAGATTTTGTGGAAGTGGCTGTGGAATTATGATAGCTAGAAAAGATGGCAAAATC *****	180 180
pBM10C napA	GTAGCAACAAAAGGTGATCCTGCAGCACCCGTAAATCGCGGACTTAATTGTATCAAAGGT GTAGCAACAAAAGGTGATCCTGCAGCACCCGTAAATCGCGGACTTAATTGTATCAAAGGT *****	240 240
pBM10C napA	TATTTTAATGCTAAGATCATGTATGGTGAAGATCGTCTTGTATTGCCTTTCGCTCGCATG TATTTTAATGCTAAGATCATGTATGGTGAAGATCGTCTTGTATTGCCTTTCGCTCGCATG *****	300 300
pBM10C napA	AATGAAAAAGGCGAATTGATAAAAAAGGCAAAATTCACAAAGTTTCTTGGCAAAGAGCC AATGAAAAAGGCGAATTGATAAAAAAGGCAAAATTCACAAAGTTTCTTGGCAAAGAGCC *****	360 360
pBM10C napA	TTTGATGAAATGGAAAAACAATTTAAAAAGCCTACAATGAACTCGGCGTTACAGGTATA TTTGATGAAATGGAAAAACAATTTAAAAAGCCTACAATGAACTCGGCGTTACAGGTATA *****	420 420
pBM10C napA	GGGATTTTGGTAGTGGGCAATATACTATCCAAGAAGTTATGCTGCTTTAAAGCTTGCA GGGATTTTGGTAGTGGGCAATATACTATCCAAGAAGTTATGCTGCTTTAAAGCTTGCA *****	480 480
pBM10C napA	AAAGCGGGTTTGAACAATAATATCGATCCAAATGCAAGACATTGTATGGCCTCTGCA AAAGCGGGTTTGAACAATAATATCGATCCAAATGCAAGACATTGTATGGCCTCTGCA *****	540 540
pBM10C napA	GTGGTTGGTTTATGCAAACTTTGGTGTAGATGAGCCATCAGGCTGTTATGATGATATA GTGGTTGGTTTATGCAAACTTTGGTGTAGATGAGCCATCAGGCTGTTATGATGATATA *****	600 600
pBM10C napA	GAGCTTACAGATACTATTATCACTTGGGAGCTAATATGGTGAAATGCACCAATCCTT GAGCTTACAGATACTATTATCACTTGGGAGCTAATATGGTGAAATGCACCAATCCTT *****	660 660
pBM10C napA	TGGTCAAGAGTAAGTGATAGAAAATAAGCAATCTTGATAAGGTTAAAGTTGTTAATCTA TGGTCAAGAGTAAGTGATAGAAAATAAGCAATCTTGATAAGGTTAAAGTTGTTAATCTA *****	720 720
pBM10C napA	AGCACTTTTCTAACCGTACTTCAAATATTGCTGATATTGAAATTATTTTAAACCAAAT AGCACTTTTCTAACCGTACTTCAAATATTGCTGATATTGAAATTATTTTAAACCAAAT *****	780 780
pBM10C napA	ACAGATTTGGCTATTGGAATTACATAGCAAGAGAGATTGTTTATAATCATCCAGAGGCT ACAGATTTGGCTATTGGAATTACATAGCAAGAGAGATTGTTTATAATCATCCAGAGGCT *****	840 840
pBM10C napA	ATGGATATGAAATTTATCAAAGATCACTGCGTATTGCAACTGGTTATGCTGATATTGGT ATGGATATGAAATTTATCAAAGATCACTGCGTATTGCAACTGGTTATGCTGATATTGGT *****	900 900
pBM10C napA	TATGGTATGAGAAATAATCCAAATCATCCAAATTTAAGAAAGTGAAAAAGATACGGTT TATGGTATGAGAAATAATCCAAATCATCCAAATTTAAGAAAGTGAAAAAGATACGGTT *****	960 960
pBM10C napA	GAAAAAGAAAATGTAATCACTTTAGACGATGAAGAGGCTACTTCTTTATCTTATCTTGGC GAAAAAGAAAATGTAATCACTTTAGACGATGAAGAGGCTACTTCTTTATCTTATCTTGGC *****	1020 1020
pBM10C napA	GTTAAAGCGGGTGATAAATTGAAATGAAACATCAAGGTGTGGCTGATAAAACTGGGAA GTTAAAGCGGGTGATAAATTGAAATGAAACATCAAGGTGTGGCTGATAAAACTGGGAA *****	1080 1080
pBM10C napA	ATTTCTTTTGACGAATTTAAAAAGGTTTAGCCCTTATACCTTTAGAATACACTGCAAGA ATTTCTTTTGACGAATTTAAAAAGGTTTAGCCCTTATACCTTTAGAATACACTGCAAGA *****	1140 1140
pBM10C napA	GTAGCCAAAGGTGATGATAATGAGTCTTTGGAAGATTTAAGAAAAACTTCAAGAATTA GTAGCCAAAGGTGATGATAATGAGTCTTTGGAAGATTTAAGAAAAACTTCAAGAATTA *****	1200 1200

Figure D.3 Continued

pBM10C	GCTAATCTTTACATAGAGAAAAATCGCAAAGTCGTAAGTTTTTGGACTATGGGCTTTAAT	1260
napA	GCTAATCTTTACATAGAGAAAAATCGCAAAGTCGTAAGTTTTTGGACTATGGGCTTTAAT	1260

pBM10C	CAACACACAAGAGGTTCTTGGGTAAATGAACAAGCTTATATGGTACATTTTTTGCTAGGA	1320
napA	CAACACACAAGAGGTTCTTGGGTAAATGAACAAGCTTATATGGTACATTTTTTGCTAGGA	1320

pBM10C	AAGCAAGCTAAACCAGGTAGTGGAGCCTTTTCTTTAACAGGACAGCCAAGTGCCTGTGGA	1380
napA	AAGCAAGCTAAACCAGGTAGTGGAGCCTTTTCTTTAACAGGACAGCCAAGTGCCTGTGGA	1380

pBM10C	ACAGCTAGGGAAGTAGGAACCTTCTCACATCGTTTGCCTGCAGATATGGTTGTAGCCAAT	1440
napA	ACAGCTAGGGAAGTAGGAACCTTCTCACATCGTTTGCCTGCAGATATGGTTGTAGCCAAT	1440

pBM10C	CCAAAACACAGAGAAATTTCTGAAAAAATTTGGAAGTTCCTGCAAAGACTATCAACCCA	1500
napA	CCAAAACACAGAGAAATTTCTGAAAAAATTTGGAAGTTCCTGCAAAGACTATCAACCCA	1500

pBM10C	AAACCTGGTTCTCCTTATCTTAATATCATGAGAGATTTAGAAGATGAAAAATTAAATTT	1560
napA	AAACCTGGTTCTCCTTATCTTAATATCATGAGAGATTTAGAAGATGAAAAATTAAATTT	1560

pBM10C	GCATGGGTGCAAGTGAATAATCCATGGCAAAACACTGCAAAATGCAAACTACTGGATTGCA	1620
napA	GCATGGGTGCAAGTGAATAATCCATGGCAAAACACTGCAAAATGCAAACTACTGGATTGCA	1620

pBM10C	GCAGCAAGAGAAATGGATAATTTTATGTTGTAAGTGATTGTTATCCTGGAATTCAGCA	1680
napA	GCAGCAAGAGAAATGGATAATTTTATGTTGTAAGTGATTGTTATCCTGGAATTCAGCA	1680

pBM10C	AAAGTAGCTGATCTTATTTTACCAAGCGCTATGATTTATGAAAAATGGGGTGCTTATGGT	1740
napA	AAAGTAGCTGATCTTATTTTACCAAGCGCTATGATTTATGAAAAATGGGGTGCTTATGGT	1740

pBM10C	AATGCTGAAAGAAGAACTCAACATTGGAAACAACAAGTCTTACCTGTAGGTGCTGCCATG	1800
napA	AATGCTGAAAGAAGAACTCAACATTGGAAACAACAAGTCTTACCTGTAGGTGCTGCCATG	1800

pBM10C	AGTGATACTTGGCAAATTTTGAATTTGCAAAACGCTTTAAGCTTAAAGAAGTTTGAAAA	1860
napA	AGTGATACTTGGCAAATTTTGAATTTGCAAAACGCTTTAAGCTTAAAGAAGTTTGAAAA	1860

pBM10C	GAGCAAAAAGTGGATAATAAGCTTACCTTGCCAAGCGTTTTAGAAGAGGCAAAAGCTATG	1920
napA	GAGCAAAAAGTGGATAATAAGCTTACCTTGCCAAGCGTTTTAGAAGAGGCAAAAGCTATG	1920

pBM10C	GGTTATAGCGAAGATGATACACTTTTGTATGTGCTATTTGCCAATAAAGAAGCAAAAAGC	1980
napA	GGTTATAGCGAAGATGATACACTTTTGTATGTGCTATTTGCCAATAAAGAAGCAAAAAGC	1980

pBM10C	TTTAATCCAAACGATGCCATCGCAAAAGGCTTTGATAATACCGATGTTAAAGGTGATGAG	2040
napA	TTTAATCCAAACGATGCCATCGCAAAAGGCTTTGATAATACCGATGTTAAAGGTGATGAG	2040

pBM10C	AGAAAAATTCAGGCAGTGATGGAAAAGAATTTACAGGCTATGGCTTTTTCGTTCAAAAA	2100
napA	AGAAAAATTCAGGCAGTGATGGAAAAGAATTTACAGGCTATGGCTTTTTCGTTCAAAAA	2100

pBM10C	TATCTTTGGGAAGAATATCGTAAATTTGGCTTAGGGCACGGACATGATTAGCGGATTTT	2160
napA	TATCTTTGGGAAGAATATCGTAAATTTGGCTTAGGGCACGGACATGATTAGCGGATTTT	2160

pBM10C	GATACCTATCATAAAGTAAGGGGTTAAGATGGCCTGTGGTTAATGGCAAGGAAACACAG	2220
napA	GATACCTATCATAAAGTAAGGGGTTAAGATGGCCTGTGGTTAATGGCAAGGAAACACAG	2220

pBM10C	TGGAGATTTAACTAAATTTGATTATTATGCTAAAAAGCGGCTCCAAATTCAGATTTT	2280
napA	TGGAGATTTAACTAAATTTGATTATTATGCTAAAAAGCGGCTCCAAATTCAGATTTT	2280

pBM10C	GCTTTTTATGGTGATTTTAAACAAATGCTTACAAATGGGGATTTAATAGCTCCTAAAGAT	2340
napA	GCTTTTTATGGTGATTTTAAACAAATGCTTACAAATGGGGATTTAATAGCTCCTAAAGAT	2340

Figure D.3 Continued

pBM10C	GAAAAAGAGCACAGTATTAAAAATAAGGCTAAAATTTCTTTAGGCCATTTATGAAAGCA	2400
napA	GAAAAAGAGCACAGTATTAAAAATAAGGCTAAAATTTCTTTAGGCCATTTATGAAAGCA	2400

pBM10C	CCTGAAAGACCAAGTAAAGAGTATCCATTCTGGCTTGCAACAGGAAGGGTTTATGAGCAT	2460
napA	CCTGAAAGACCAAGTAAAGAGTATCCATTCTGGCTTGCAACAGGAAGGGTTTATGAGCAT	2460

pBM10C	TGGCATAGTGGAAGTATGACTATGCGTGTGCCTGAGCTTTATCGCGCTGTGCCTGAAGCA	2520
napA	TGGCATAGTGGAAGTATGACTATGCGTGTGCCTGAGCTTTATCGCGCTGTGCCTGAAGCA	2520

pBM10C	CTTTGCTATATGAGTGAGAAAGATGGAGAGAAATTAGGCTTAAATCAAGGTGATTGGTT	2580
napA	CTTTGCTATATGAGTGAGAAAGATGGAGAGAAATTAGGCTTAAATCAAGGTGATTGGTT	2580

pBM10C	TGGGTGGAATCTCGTCGCGGTAAAGTAAAAGCAAGAGTAGATATGCGCGGAAGAAACAAA	2640
napA	TGGGTGGAATCTCGTCGCGGTAAAGTAAAAGCAAGAGTAGATATGCGCGGAAGAAACAAA	2640

pBM10C	CCGCCTGTAGGACTTGTGTATGTGCCGTGGTTTGATGAGAATGTATATCAATAAAGTT	2700
napA	CCGCCTGTAGGACTTGTGTATGTGCCGTGGTTTGATGAGAATGTATATCAATAAAGTT	2700

pBM10C	ACTTTGGATGCGACTTGTCCACTTTCAAACAAACTGACTTTAAAAATGCGCTGTAAAA	2760
napA	ACTTTGGATGCGACTTGTCCACTTTCAAACAAACTGACTTTAAAAATGCGCTGTAAAA	2760

pBM10C	ATTTATAAGGCTCCCGGGAGAACCTGTACTTCCAATCCGCCGGGCACCACCATCATCAT	2820
napA	ATTTATAAGGCTTAA-----	2775

pBM10C	CATTAA	2826
napA	-----	2775

Figure D.4: The *napA* sequence alignment utilizing Clustal OMEGA Alignment Tool. The *napA* sequence in construct C176S-pBM10C is compared to the *napA* gene sequence in template pBM10C that was previously confirmed to be the correct *C. jejuni* RM1221 *napA* gene sequence. The mutation of the base G527 to C527 is the desired mutation in the DNA sequence creating the Cys to Ser exchange at position 176 in the NapA protein sequence.

C176S pBM10C	ATGAATAGAAAGGATTTTATTAAAAATACCGCTATTGCAAGTGCTGCTAGTGTTCAGGG ATGAATAGAAAGGATTTTATTAAAAATACCGCTATTGCAAGTGCTGCTAGTGTTCAGGG *****	60 60
C176S pBM10C	CTTAGTGTTCAGCTCTATGCTTGGCGCGCAAGAAGAAGATTGGAAATGGGATAAAGCT CTTAGTGTTCAGCTCTATGCTTGGCGCGCAAGAAGAAGATTGGAAATGGGATAAAGCT *****	120 120
C176S pBM10C	GTTTGTAGATTTTGTGGAAGTGGCTGTGGAATTATGATAGCTAGAAAAGATGGCAAAATC GTTTGTAGATTTTGTGGAAGTGGCTGTGGAATTATGATAGCTAGAAAAGATGGCAAAATC *****	180 180
C176S pBM10C	GTAGCAACAAAAGGTGATCCTGCAGCACCCGTAAATCGCGGACTTAATTGTATCAAAGGT GTAGCAACAAAAGGTGATCCTGCAGCACCCGTAAATCGCGGACTTAATTGTATCAAAGGT *****	240 240
C176S pBM10C	TATTTTAATGCTAAGATCATGTATGGTGAAGATCGTCTTGTATTGCCTTGTCTCGCATG TATTTTAATGCTAAGATCATGTATGGTGAAGATCGTCTTGTATTGCCTTGTCTCGCATG *****	300 300
C176S pBM10C	AATGAAAAAGGCGAATTGATAAAAAAGGCAAAATTCACAAAGTTTCTTGGCAAAGAGCC AATGAAAAAGGCGAATTGATAAAAAAGGCAAAATTCACAAAGTTTCTTGGCAAAGAGCC *****	360 360
C176S pBM10C	TTTGATGAAATGGAAAAACAATTTAAAAAGCCTACAATGAACTCGGCGTTACAGGTATA TTTGATGAAATGGAAAAACAATTTAAAAAGCCTACAATGAACTCGGCGTTACAGGTATA *****	420 420
C176S pBM10C	GGGATTTTGGTAGTGGGCAATATACTATCCAAGAAGTTATGCTGCTTTAAAGCTTGCA GGGATTTTGGTAGTGGGCAATATACTATCCAAGAAGTTATGCTGCTTTAAAGCTTGCA *****	480 480
C176S pBM10C	AAAGCGGGTTTGAACAAATAATATCGATCCAAATGCAAGACATTCATGGCCTCTGCA AAAGCGGGTTTGAACAAATAATATCGATCCAAATGCAAGACATTCATGGCCTCTGCA *****	540 540
C176S pBM10C	GTGGTTGGTTTATGCAAACTTTGGTGTAGATGAGCCATCAGGCTGTTATGATGATATA GTGGTTGGTTTATGCAAACTTTGGTGTAGATGAGCCATCAGGCTGTTATGATGATATA *****	600 600
C176S pBM10C	GAGCTTACAGATACTATTATCACTTGGGAGCTAATATGGTGAAATGCACCAATCCTT GAGCTTACAGATACTATTATCACTTGGGAGCTAATATGGTGAAATGCACCAATCCTT *****	660 660
C176S pBM10C	TGGTCAAGAGTAAGTGATAGAAAATAAGCAATCTTGATAAGGTTAAAGTTGTTAATCTA TGGTCAAGAGTAAGTGATAGAAAATAAGCAATCTTGATAAGGTTAAAGTTGTTAATCTA *****	720 720
C176S pBM10C	AGCACTTTTCTAACCGTACTTCAAATATTGCTGATATTGAAATTATTTTAAACCAAAT AGCACTTTTCTAACCGTACTTCAAATATTGCTGATATTGAAATTATTTTAAACCAAAT *****	780 780
C176S pBM10C	ACAGATTTGGCTATTGGGAATTACATAGCAAGAGAGATTGTTTATAATCATCCAGAGGCT ACAGATTTGGCTATTGGGAATTACATAGCAAGAGAGATTGTTTATAATCATCCAGAGGCT *****	840 840
C176S pBM10C	ATGGATATGAAATTTATCAAAGATCACTGCGTATTGCAACTGGTTATGCTGATATTGGT ATGGATATGAAATTTATCAAAGATCACTGCGTATTGCAACTGGTTATGCTGATATTGGT *****	900 900
C176S pBM10C	TATGGTATGAGAAATAATCCAAATCATCCAAATTTAAGAAAGTGAAAAAGATACGGTT TATGGTATGAGAAATAATCCAAATCATCCAAATTTAAGAAAGTGAAAAAGATACGGTT *****	960 960
C176S pBM10C	GAAAAAGAAAATGTAATCACTTTAGACGATGAAGAGGCTACTTCTTTATCTTATCTTGGC GAAAAAGAAAATGTAATCACTTTAGACGATGAAGAGGCTACTTCTTTATCTTATCTTGGC *****	1020 1020
C176S pBM10C	GTTAAAGCGGGTGATAAATTTGAAATGAAACATCAAGGTGTGGCTGATAAAACTGGGAA GTTAAAGCGGGTGATAAATTTGAAATGAAACATCAAGGTGTGGCTGATAAAACTGGGAA *****	1080 1080
C176S pBM10C	ATTTCTTTTGACGAATTTAAAAAGGTTTAGCCCCCTATACCTTTAGAATACACTGCAAGA ATTTCTTTTGACGAATTTAAAAAGGTTTAGCCCCCTATACCTTTAGAATACACTGCAAGA *****	1140 1140
C176S pBM10C	GTAGCCAAAGGTGATGATAATGAGTCTTTGGAAGATTTTAAAGAAAACTTCAAGAATTA GTAGCCAAAGGTGATGATAATGAGTCTTTGGAAGATTTTAAAGAAAACTTCAAGAATTA *****	1200 1200

Figure D.4 Continued

C176S	GCTAATCTTTACATAGAGAAAAATCGCAAAGTCGTAAGTTTTTGGACTATGGGCTTTAAT	1260
pBM10C	GCTAATCTTTACATAGAGAAAAATCGCAAAGTCGTAAGTTTTTGGACTATGGGCTTTAAT	1260

C176S	CAACACACAAGAGGTTCTTTGGGTAAATGAACAAGCTTATATGGTACATTTTTTGCTAGGA	1320
pBM10C	CAACACACAAGAGGTTCTTTGGGTAAATGAACAAGCTTATATGGTACATTTTTTGCTAGGA	1320

C176S	AAGCAAGCTAAACCAGGTAGTGGAGCCTTTTCTTTAACAGGACAGCCAAGTGCCTGTGGA	1380
pBM10C	AAGCAAGCTAAACCAGGTAGTGGAGCCTTTTCTTTAACAGGACAGCCAAGTGCCTGTGGA	1380

C176S	ACAGCTAGGGAAGTAGGAACCTTCTCACATCGTTTGCCTGCAGATATGGTTGTAGCCAAT	1440
pBM10C	ACAGCTAGGGAAGTAGGAACCTTCTCACATCGTTTGCCTGCAGATATGGTTGTAGCCAAT	1440

C176S	CCAAAAACACAGAGAAATTTCTGAAAAAATTTGGAAAGTTCCTGCAAAGACTATCAACCCA	1500
pBM10C	CCAAAAACACAGAGAAATTTCTGAAAAAATTTGGAAAGTTCCTGCAAAGACTATCAACCCA	1500

C176S	AAACCTGGTTCTCCTTATCTTAATATCATGAGAGATTTAGAAGATGAAAAATTAAATTT	1560
pBM10C	AAACCTGGTTCTCCTTATCTTAATATCATGAGAGATTTAGAAGATGAAAAATTAAATTT	1560

C176S	GCATGGGTGCAAGTGAATAATCCATGGCAAAACACTGCAATGCAAACTACTGGATTGCA	1620
pBM10C	GCATGGGTGCAAGTGAATAATCCATGGCAAAACACTGCAATGCAAACTACTGGATTGCA	1620

C176S	GCAGCAAGAGAAATGGATAATTTTATGTTGTAAGTGATTGTTATCCTGGAATTTAGCA	1680
pBM10C	GCAGCAAGAGAAATGGATAATTTTATGTTGTAAGTGATTGTTATCCTGGAATTTAGCA	1680

C176S	AAAGTAGCTGATCTTATTTTACCAAGCGCTATGATTTATGAAAAATGGGGTGCTTATGGT	1740
pBM10C	AAAGTAGCTGATCTTATTTTACCAAGCGCTATGATTTATGAAAAATGGGGTGCTTATGGT	1740

C176S	AATGCTGAAAGAAGAACTCAACATTGGAAACAACAAGTCTTACCTGTAGGTGCTGCCATG	1800
pBM10C	AATGCTGAAAGAAGAACTCAACATTGGAAACAACAAGTCTTACCTGTAGGTGCTGCCATG	1800

C176S	AGTGATACTTGGCAAATTTTGAATTTGCAAAACGCTTTAAGCTTAAAGAAGTTTGAAAA	1860
pBM10C	AGTGATACTTGGCAAATTTTGAATTTGCAAAACGCTTTAAGCTTAAAGAAGTTTGAAAA	1860

C176S	GAGCAAAAAGTGGATAATAAGCTTACCTTGCCAAGCGTTTGAAGAGGCAAAAGCTATG	1920
pBM10C	GAGCAAAAAGTGGATAATAAGCTTACCTTGCCAAGCGTTTGAAGAGGCAAAAGCTATG	1920

C176S	GGTTATAGCGAAGATGATACACTTTTGTATGTGCTATTTGCCAATAAAGAAGCAAAAAGC	1980
pBM10C	GGTTATAGCGAAGATGATACACTTTTGTATGTGCTATTTGCCAATAAAGAAGCAAAAAGC	1980

C176S	TTTAATCCAAACGATGCCATCGCAAAAGGCTTTGATAATACCGATGTTAAAGGTGATGAG	2040
pBM10C	TTTAATCCAAACGATGCCATCGCAAAAGGCTTTGATAATACCGATGTTAAAGGTGATGAG	2040

C176S	AGAAAAATTCAAGGCAGTGATGGAAAAGAATTTACAGGCTATGGCTTTTTCGTTCAAAAA	2100
pBM10C	AGAAAAATTCAAGGCAGTGATGGAAAAGAATTTACAGGCTATGGCTTTTTCGTTCAAAAA	2100

C176S	TATCTTTGGGAAGAATATCGTAAATTTGGCTTAGGGCACGGACATGATTAGCGGATTTT	2160
pBM10C	TATCTTTGGGAAGAATATCGTAAATTTGGCTTAGGGCACGGACATGATTAGCGGATTTT	2160

C176S	GATACCTATCATAAAGTAAGGGGTTTAAGATGGCCTGTGGTTAATGGCAAGGAAACACAG	2220
pBM10C	GATACCTATCATAAAGTAAGGGGTTTAAGATGGCCTGTGGTTAATGGCAAGGAAACACAG	2220

C176S	TGGAGATTTAATACTAAATTTGATTATTATGCTAAAAAGCGGCTCCAAATTCAGATTTT	2280
pBM10C	TGGAGATTTAATACTAAATTTGATTATTATGCTAAAAAGCGGCTCCAAATTCAGATTTT	2280

C176S	GCTTTTTATGGTGATTTTAAACAAAATGCTTACAAATGGGGATTTAATAGCTCCTAAAGAT	2340
pBM10C	GCTTTTTATGGTGATTTTAAACAAAATGCTTACAAATGGGGATTTAATAGCTCCTAAAGAT	2340

Figure D.4 Continued

C176S	GAAAAAGAGCACAGTATTAAAAATAAGGCTAAAATTTTCTTTAGGCCATTTATGAAAGCA	2400
pBM10C	GAAAAAGAGCACAGTATTAAAAATAAGGCTAAAATTTTCTTTAGGCCATTTATGAAAGCA	2400

C176S	CCTGAAAGACCAAGTAAAGAGTATCCATTCTGGCTTGCAACAGGAAGGGTTTATAGAGCAT	2460
pBM10C	CCTGAAAGACCAAGTAAAGAGTATCCATTCTGGCTTGCAACAGGAAGGGTTTATAGAGCAT	2460

C176S	TGGCATAGTGGAACATGACTATGCGTGTGCCTGAGCTTTATCGCGCTGTGCCTGAAGCA	2520
pBM10C	TGGCATAGTGGAACATGACTATGCGTGTGCCTGAGCTTTATCGCGCTGTGCCTGAAGCA	2520

C176S	CTTTGCTATATGAGTGAGAAAGATGGAGAGAAATTAGGCTTAAATCAAGGTGATTGGTT	2580
pBM10C	CTTTGCTATATGAGTGAGAAAGATGGAGAGAAATTAGGCTTAAATCAAGGTGATTGGTT	2580

C176S	TGGGTGGAATCTCGTCGCGGTAAAGTAAAAGCAAGAGTAGATATGCGCGGAAGAAACAAA	2640
pBM10C	TGGGTGGAATCTCGTCGCGGTAAAGTAAAAGCAAGAGTAGATATGCGCGGAAGAAACAAA	2640

C176S	CCGCCTGTAGGACTTGTGTATGTGCCGTGGTTTGATGAGAATGTATATATCAATAAAGTT	2700
pBM10C	CCGCCTGTAGGACTTGTGTATGTGCCGTGGTTTGATGAGAATGTATATATCAATAAAGTT	2700

C176S	ACTTTGGATGCGACTTGTCCACTTTCAAACAAACTGACTTTAAAAAATGCGCTGTAAAA	2760
pBM10C	ACTTTGGATGCGACTTGTCCACTTTCAAACAAACTGACTTTAAAAAATGCGCTGTAAAA	2760

C176S	ATTTATAAGGCTCCCGGGGAGAACCTGTACTTCCAATCCGCCGGGCACCACCATCATCAT	2820
pBM10C	ATTTATAAGGCTCCCGGGGAGAACCTGTACTTCCAATCCGCCGGGCACCACCATCATCAT	2820

C176S	CATTAA 2826	
pBM10C	CATTAA 2826	

Figure D.5: The *napA* sequence alignment utilizing Clustal OMEGA Alignment Tool. The *napA* sequence in construct C176S-pBM10C is compared to the *napA* gene sequence in template pBM10C that was previously confirmed to be the correct *C. jejuni* RM1221 *napA* gene sequence. The mutation of the bases T526 and G527 to G526 and A527 respectively are the desired mutations in the DNA sequence creating the Cys to Asp exchange at position 176 in the NapA protein sequence.

C176D pBM10C	ATGAATAGAAAGGATTTTATTAATAACCGCTATTGCAAGTGCTGCTAGTGTGCAGGG ATGAATAGAAAGGATTTTATTAATAACCGCTATTGCAAGTGCTGCTAGTGTGCAGGG *****	60 60
C176D pBM10C	CTTAGTGTTCGAAGCTCTATGCTTGGCGCGCAAGAAGAAGATTGGAAATGGGATAAAGCT CTTAGTGTTCGAAGCTCTATGCTTGGCGCGCAAGAAGAAGATTGGAAATGGGATAAAGCT *****	120 120
C176D pBM10C	GTTTGTAGATTTTGTGGAAGTGGCTGTGGAATTATGATAGCTAGAAAAGATGGCAAAATC GTTTGTAGATTTTGTGGAAGTGGCTGTGGAATTATGATAGCTAGAAAAGATGGCAAAATC *****	180 180
C176D pBM10C	GTAGCAACAAAAGGTGATCCTGCAGCACCCGTAAATCGCGGACTTAATTGTATCAAAGGT GTAGCAACAAAAGGTGATCCTGCAGCACCCGTAAATCGCGGACTTAATTGTATCAAAGGT *****	240 240
C176D pBM10C	TATTTTAATGCTAAGATCATGTATGGTGAAGATCGTCTTGTATTGCCTTTCGCTTCGCATG TATTTTAATGCTAAGATCATGTATGGTGAAGATCGTCTTGTATTGCCTTTCGCTTCGCATG *****	300 300
C176D pBM10C	AATGAAAAAGGCGAATTGATAAAAAAGGCAAAATTCACAAGTTTCTTGGCAAAGAGCC AATGAAAAAGGCGAATTGATAAAAAAGGCAAAATTCACAAGTTTCTTGGCAAAGAGCC *****	360 360
C176D pBM10C	TTTGATGAAATGGAAAAACAATTTAAAAAGCCTACAATGAACTCGGCGTTACAGGTATA TTTGATGAAATGGAAAAACAATTTAAAAAGCCTACAATGAACTCGGCGTTACAGGTATA *****	420 420
C176D pBM10C	GGGATTTTGGTAGTGGGCAATATACTATCCAAGAAGGTTATGCTGCTTTAAAGCTTGCA GGGATTTTGGTAGTGGGCAATATACTATCCAAGAAGGTTATGCTGCTTTAAAGCTTGCA *****	480 480
C176D pBM10C	AAAGCGGGTTTGAACAATAATATCGATCCAAATGCAAGACATGATATGGCCTCTGCA AAAGCGGGTTTGAACAATAATATCGATCCAAATGCAAGACATGATATGGCCTCTGCA *****	540 540
C176D pBM10C	GTGGTTGGTTTATGCAAACTTTGGTGTAGATGAGCCATCAGGCTGTTATGATGATATA GTGGTTGGTTTATGCAAACTTTGGTGTAGATGAGCCATCAGGCTGTTATGATGATATA *****	600 600
C176D pBM10C	GAGCTTACAGATACTATTATCACTTGGGAGCTAATATGGTGAAATGCACCAATCCTT GAGCTTACAGATACTATTATCACTTGGGAGCTAATATGGTGAAATGCACCAATCCTT *****	660 660
C176D pBM10C	TGGTCAAGAGTAAGTGATAGAAAATAAGCAATCTTGATAAGGTTAAAGTTGTTAATCTA TGGTCAAGAGTAAGTGATAGAAAATAAGCAATCTTGATAAGGTTAAAGTTGTTAATCTA *****	720 720
C176D pBM10C	AGCACTTTTCTAACCGTACTTCAAATATTGCTGATATTGAAATTATTTTAAACCAAAT AGCACTTTTCTAACCGTACTTCAAATATTGCTGATATTGAAATTATTTTAAACCAAAT *****	780 780
C176D pBM10C	ACAGATTTGGCTATTGGAATTACATAGCAAGAGAGATTGTTTATAATCATCCAGAGGCT ACAGATTTGGCTATTGGAATTACATAGCAAGAGAGATTGTTTATAATCATCCAGAGGCT *****	840 840
C176D pBM10C	ATGGATATGAAATTTATCAAAGATCACTGCGTATTGCAACTGGTTATGCTGATATTGGT ATGGATATGAAATTTATCAAAGATCACTGCGTATTGCAACTGGTTATGCTGATATTGGT *****	900 900
C176D pBM10C	TATGGTATGAGAAATAATCCAAATCATCCAAATTTAAGAAAGTGAAAAAGATACGGTT TATGGTATGAGAAATAATCCAAATCATCCAAATTTAAGAAAGTGAAAAAGATACGGTT *****	960 960
C176D pBM10C	GAAAAAGAAAATGTAATCACTTTAGACGATGAAGAGGCTACTTCTTTATCTTATCTTGGC GAAAAAGAAAATGTAATCACTTTAGACGATGAAGAGGCTACTTCTTTATCTTATCTTGGC *****	1020 1020
C176D pBM10C	GTTAAAGCGGGTGATAAATTTGAAATGAAACATCAAGGTGTGGCTGATAAAACTGGGAA GTTAAAGCGGGTGATAAATTTGAAATGAAACATCAAGGTGTGGCTGATAAAACTGGGAA *****	1080 1080
C176D pBM10C	ATTTCTTTTGACGAATTTAAAAAGGTTTAGCCCTTATACCTTTAGAATACACTGCAAGA ATTTCTTTTGACGAATTTAAAAAGGTTTAGCCCTTATACCTTTAGAATACACTGCAAGA *****	1140 1140
C176D pBM10C	GTAGCCAAAGGTGATGATAATGAGTCTTTGGAAGATTTTAAAGAAAACTTCAAGAATTA GTAGCCAAAGGTGATGATAATGAGTCTTTGGAAGATTTTAAAGAAAACTTCAAGAATTA *****	1200 1200

Figure D.5 Continued

C176D	GCTAATCTTTACATAGAGAAAAATCGCAAAGTCGTAAGTTTTTGGACTATGGGCTTTAAT	1260
pBM10C	GCTAATCTTTACATAGAGAAAAATCGCAAAGTCGTAAGTTTTTGGACTATGGGCTTTAAT	1260

C176D	CAACACACAAGAGGTTCTTTGGGTAAATGAACAAGCTTATATGGTACATTTTTTGCTAGGA	1320
pBM10C	CAACACACAAGAGGTTCTTTGGGTAAATGAACAAGCTTATATGGTACATTTTTTGCTAGGA	1320

C176D	AAGCAAGCTAAACCAGGTAGTGGAGCCTTTTCTTTAACAGGACGCCAAGTGCCTGTGGA	1380
pBM10C	AAGCAAGCTAAACCAGGTAGTGGAGCCTTTTCTTTAACAGGACGCCAAGTGCCTGTGGA	1380

C176D	ACAGCTAGGGAAGTAGGAACCTTCTCACATCGTTTGCCTGCAGATATGGTTGTAGCCAAT	1440
pBM10C	ACAGCTAGGGAAGTAGGAACCTTCTCACATCGTTTGCCTGCAGATATGGTTGTAGCCAAT	1440

C176D	CCAAAACACAGAGAAATTTCTGAAAAAATTTGGAAGTTCCTGCAAAGACTATCAACCCA	1500
pBM10C	CCAAAACACAGAGAAATTTCTGAAAAAATTTGGAAGTTCCTGCAAAGACTATCAACCCA	1500

C176D	AAACCTGGTTCTCCTTATCTTAATATCATGAGAGATTTAGAAGATGAAAAATTAAATTT	1560
pBM10C	AAACCTGGTTCTCCTTATCTTAATATCATGAGAGATTTAGAAGATGAAAAATTAAATTT	1560

C176D	GCATGGGTGCAAGTGAATAATCCATGGCAAAACACTGCAATGCAAACTACTGGATTGCA	1620
pBM10C	GCATGGGTGCAAGTGAATAATCCATGGCAAAACACTGCAATGCAAACTACTGGATTGCA	1620

C176D	GCAGCAAGAGAAATGGATAATTTTATGTTGTAAGTGATTGTTATCCTGGAATTCAGCA	1680
pBM10C	GCAGCAAGAGAAATGGATAATTTTATGTTGTAAGTGATTGTTATCCTGGAATTCAGCA	1680

C176D	AAAGTAGCTGATCTTATTTTACCAAGCGCTATGATTTATGAAAAATGGGGTGCTTATGGT	1740
pBM10C	AAAGTAGCTGATCTTATTTTACCAAGCGCTATGATTTATGAAAAATGGGGTGCTTATGGT	1740

C176D	AATGCTGAAAGAAGAACTCAACATTGGAAACAACAAGTCTTACCTGTAGGTGCTGCCATG	1800
pBM10C	AATGCTGAAAGAAGAACTCAACATTGGAAACAACAAGTCTTACCTGTAGGTGCTGCCATG	1800

C176D	AGTGATACTTGGCAAATTTTGAATTTGCAAAACGCTTTAAGCTTAAAGAAGTTTGAAA	1860
pBM10C	AGTGATACTTGGCAAATTTTGAATTTGCAAAACGCTTTAAGCTTAAAGAAGTTTGAAA	1860

C176D	GAGCAAAAAGTGGATAATAAGCTTACCTTGCCAAGCGTTTGAAGAGGCAAAAGCTATG	1920
pBM10C	GAGCAAAAAGTGGATAATAAGCTTACCTTGCCAAGCGTTTGAAGAGGCAAAAGCTATG	1920

C176D	GGTTATAGCGAAGATGATACACTTTTGTATGTGCTATTTGCCAATAAAGAAGCAAAAAGC	1980
pBM10C	GGTTATAGCGAAGATGATACACTTTTGTATGTGCTATTTGCCAATAAAGAAGCAAAAAGC	1980

C176D	TTTAATCCAAACGATGCCATCGCAAAAGGCTTTGATAATACCGATGTTAAAGGTGATGAG	2040
pBM10C	TTTAATCCAAACGATGCCATCGCAAAAGGCTTTGATAATACCGATGTTAAAGGTGATGAG	2040

C176D	AGAAAAATTCAAGGCAGTGATGGAAAAGAATTTACAGGCTATGGCTTTTTCGTTCAAAAA	2100
pBM10C	AGAAAAATTCAAGGCAGTGATGGAAAAGAATTTACAGGCTATGGCTTTTTCGTTCAAAAA	2100

C176D	TATCTTTGGGAAGAATATCGTAAATTTGGCTTAGGGCACGGACATGATTAGCGGATTTT	2160
pBM10C	TATCTTTGGGAAGAATATCGTAAATTTGGCTTAGGGCACGGACATGATTAGCGGATTTT	2160

C176D	GATACCTATCATAAAGTAAGGGGTTAAGATGGCCTGTGGTTAATGGCAAGGAAACACAG	2220
pBM10C	GATACCTATCATAAAGTAAGGGGTTAAGATGGCCTGTGGTTAATGGCAAGGAAACACAG	2220

C176D	TGGAGATTTAATACTAAATTTGATTATTATGCTAAAAAGCGGCTCCAAATTCAGATTTT	2280
pBM10C	TGGAGATTTAATACTAAATTTGATTATTATGCTAAAAAGCGGCTCCAAATTCAGATTTT	2280

C176D	GCTTTTATGGTGATTTTAAACAAATGCTTACAAATGGGGATTTAATAGCTCCTAAAGAT	2340
pBM10C	GCTTTTATGGTGATTTTAAACAAATGCTTACAAATGGGGATTTAATAGCTCCTAAAGAT	2340

C176D	GAAAAAGAGCACAGTATTAATAAATAAGGCTAAAATTTCTTTAGGCCATTTATGAAAGCA	2400
pBM10C	GAAAAAGAGCACAGTATTAATAAATAAGGCTAAAATTTCTTTAGGCCATTTATGAAAGCA	2400

Figure D.5 Continued

C176D	CCTGAAAGACCAAGTAAAGAGTATCCATTCTGGCTTGCAACAGGAAGGGTTT	2460
pBM10C	CCTGAAAGACCAAGTAAAGAGTATCCATTCTGGCTTGCAACAGGAAGGGTTT	2460

C176D	TGGCATAGTGGAAGTATGACTATGCGTGTGCCTGAGCTTTATCGCGCTGTGCCTGAAGCA	2520
pBM10C	TGGCATAGTGGAAGTATGACTATGCGTGTGCCTGAGCTTTATCGCGCTGTGCCTGAAGCA	2520

C176D	CTTTGCTATATGAGTGAGAAAGATGGAGAGAAATTAGGCTTAAATCAAGGTGATTGGTT	2580
pBM10C	CTTTGCTATATGAGTGAGAAAGATGGAGAGAAATTAGGCTTAAATCAAGGTGATTGGTT	2580

C176D	TGGGTGGAATCTCGTCGCGGTAAAGTAAAGCAAGAGTAGATATGCGCGGAAGAAACAAA	2640
pBM10C	TGGGTGGAATCTCGTCGCGGTAAAGTAAAGCAAGAGTAGATATGCGCGGAAGAAACAAA	2640

C176D	CCGCCTGTAGGACTTGTGTATGTGCCGTGGTTTGATGAGAATGTATATATCAATAAAGTT	2700
pBM10C	CCGCCTGTAGGACTTGTGTATGTGCCGTGGTTTGATGAGAATGTATATATCAATAAAGTT	2700

C176D	ACTTTGGATGCGACTTGTCCACTTTCAAAACAACTGACTTTAAAAAATGCGCTGTAAAA	2760
pBM10C	ACTTTGGATGCGACTTGTCCACTTTCAAAACAACTGACTTTAAAAAATGCGCTGTAAAA	2760

C176D	ATTTATAAGGCTCCCGGGGAGAACCTGTACTTCCAATCCGCCGGGCACCACCATCATCAT	2820
pBM10C	ATTTATAAGGCTCCCGGGGAGAACCTGTACTTCCAATCCGCCGGGCACCACCATCATCAT	2820

C176D	CATTAA 2826	
pBM10C	CATTAA 2826	

Figure D.6: The *napA* sequence alignment utilizing Clustal OMEGA Alignment Tool. The *napA* sequence in construct C176A-pBM10C is compared to the *napA* gene sequence in template pBM10C that was previously confirmed to be the correct *C. jejuni* RM1221 *napA* gene sequence. The mutation of the base T526 and G527 to G526 and C527 respectively are the desired mutations in the DNA sequence creating the Cys to Ala exchange at position 176 in the NapA protein sequence.

C176A pBM10C	ATGAATAGAAGGGATTTTATTAAAAATACCGCTATTGCAAGTGCTGCTAGTGTTCAGGG ATGAATAGAAGGGATTTTATTAAAAATACCGCTATTGCAAGTGCTGCTAGTGTTCAGGG *****	60 60
C176A pBM10C	CTTAGTGTTCAGCTCTATGCTTGGCGCGCAAGAAGAAGATTGGAAATGGGATAAAGCT CTTAGTGTTCAGCTCTATGCTTGGCGCGCAAGAAGAAGATTGGAAATGGGATAAAGCT *****	120 120
C176A pBM10C	GTTTGTAGATTTTGTGGAAGTGGCTGTGGAATTATGATAGCTAGAAAAGATGGCAAAATC GTTTGTAGATTTTGTGGAAGTGGCTGTGGAATTATGATAGCTAGAAAAGATGGCAAAATC *****	180 180
C176A pBM10C	GTAGCAACAAAAGGTGATCCTGCAGCACCCGTAAATCGCGGACTTAATTGTATCAAAGGT GTAGCAACAAAAGGTGATCCTGCAGCACCCGTAAATCGCGGACTTAATTGTATCAAAGGT *****	240 240
C176A pBM10C	TATTTTAATGCTAAGATCATGTATGGTGAAGATCGTCTTGTATTGCCTTTCGCTTCGCATG TATTTTAATGCTAAGATCATGTATGGTGAAGATCGTCTTGTATTGCCTTTCGCTTCGCATG *****	300 300
C176A pBM10C	AATGAAAAAGGCGAATTGATAAAAAAGGCAAAATTCACAAAGTTTCTTGGCAAAGAGCC AATGAAAAAGGCGAATTGATAAAAAAGGCAAAATTCACAAAGTTTCTTGGCAAAGAGCC *****	360 360
C176A pBM10C	TTTGATGAAATGGAAAAACAATTTAAAAAGCCTACAATGAACTCGGCGTTACAGGTATA TTTGATGAAATGGAAAAACAATTTAAAAAGCCTACAATGAACTCGGCGTTACAGGTATA *****	420 420
C176A pBM10C	GGGATTTTGGTAGTGGGCAATATACTATCCAAGAAGGTTATGCTGCTTTAAAGCTTGCA GGGATTTTGGTAGTGGGCAATATACTATCCAAGAAGGTTATGCTGCTTTAAAGCTTGCA *****	480 480
C176A pBM10C	AAAGCGGGTTTGAACAAATAATATCGATCCAAATGCAAGACATGCTATGGCCTCTGCA AAAGCGGGTTTGAACAAATAATATCGATCCAAATGCAAGACATGCTATGGCCTCTGCA *****	540 540
C176A pBM10C	GTGGTTGGTTTATGCAAACTTTGGTGTAGATGAGCCATCAGGCTGTTATGATGATATA GTGGTTGGTTTATGCAAACTTTGGTGTAGATGAGCCATCAGGCTGTTATGATGATATA *****	600 600
C176A pBM10C	GAGCTTACAGATACTATTATCACTTGGGAGCTAATATGGTGAAATGCACCAATCCTT GAGCTTACAGATACTATTATCACTTGGGAGCTAATATGGTGAAATGCACCAATCCTT *****	660 660
C176A pBM10C	TGGTCAAGAGTAAGTGATAGAAAATAAGCAATCTTGATAAGGTTAAAGTTGTTAATCTA TGGTCAAGAGTAAGTGATAGAAAATAAGCAATCTTGATAAGGTTAAAGTTGTTAATCTA *****	720 720
C176A pBM10C	AGCACTTTTCTAACCGTACTTCAAATATTGCTGATATTGAAATTATTTTAAACCAAAT AGCACTTTTCTAACCGTACTTCAAATATTGCTGATATTGAAATTATTTTAAACCAAAT *****	780 780
C176A pBM10C	ACAGATTTGGCTATTGGAATTACATAGCAAGAGAGATTGTTTATAATCATCCAGAGGCT ACAGATTTGGCTATTGGAATTACATAGCAAGAGAGATTGTTTATAATCATCCAGAGGCT *****	840 840
C176A pBM10C	ATGGATATGAAATTTATCAAAGATCACTGCGTATTGCAACTGGTTATGCTGATATTGGT ATGGATATGAAATTTATCAAAGATCACTGCGTATTGCAACTGGTTATGCTGATATTGGT *****	900 900
C176A pBM10C	TATGGTATGAGAAATAATCCAAATCATCCAAATTTAAGAAAGTGAAAAAGATACGGTT TATGGTATGAGAAATAATCCAAATCATCCAAATTTAAGAAAGTGAAAAAGATACGGTT *****	960 960
C176A pBM10C	GAAAAAGAAAATGTAATCACTTTAGACGATGAAGAGGCTACTTCTTTATCTTATCTTGGC GAAAAAGAAAATGTAATCACTTTAGACGATGAAGAGGCTACTTCTTTATCTTATCTTGGC *****	1020 1020
C176A pBM10C	GTTAAAGCGGGTGATAAAATTGAAATGAAACATCAAGGTGTGGCTGATAAAACTGGGAA GTTAAAGCGGGTGATAAAATTGAAATGAAACATCAAGGTGTGGCTGATAAAACTGGGAA *****	1080 1080
C176A pBM10C	ATTTCTTTTGACGAATTTAAAAAGGTTTAGCCCCTTATACTTTGAATACACTGCAAGA ATTTCTTTTGACGAATTTAAAAAGGTTTAGCCCCTTATACTTTGAATACACTGCAAGA *****	1140 1140
C176A pBM10C	GTAGCCAAAGGTGATGATAATGAGTCTTTGGAAGATTTTAAAGAAAACTTCAAGAATTA GTAGCCAAAGGTGATGATAATGAGTCTTTGGAAGATTTTAAAGAAAACTTCAAGAATTA *****	1200 1200

Figure D.6 Continued

C176A pBM10C	GCTAATCTTTACATAGAGAAAAATCGCAAAGTCGTAAGTTTTTGGACTATGGGCTTTAAT GCTAATCTTTACATAGAGAAAAATCGCAAAGTCGTAAGTTTTTGGACTATGGGCTTTAAT *****	1260 1260
C176A pBM10C	CAACACACAAGAGGTTCTTTGGGTAAATGAACAAGCTTATATGGTACATTTTTTGCTAGGA CAACACACAAGAGGTTCTTTGGGTAAATGAACAAGCTTATATGGTACATTTTTTGCTAGGA *****	1320 1320
C176A pBM10C	AAGCAAGCTAAACCAGGTAGTGGAGCCTTTTCTTTAACAGGACAGCCAAGTGCCTGTGGA AAGCAAGCTAAACCAGGTAGTGGAGCCTTTTCTTTAACAGGACAGCCAAGTGCCTGTGGA *****	1380 1380
C176A pBM10C	ACAGCTAGGGAAGTAGGAACCTTCTCACATCGTTTGCCTGCAGATATGGTTGTAGCCAAT ACAGCTAGGGAAGTAGGAACCTTCTCACATCGTTTGCCTGCAGATATGGTTGTAGCCAAT *****	1440 1440
C176A pBM10C	CCAAAACACAGAGAAATTTCTGAAAAAATTTGGAAAGTTCCTGCAAAGACTATCAACCCA CCAAAACACAGAGAAATTTCTGAAAAAATTTGGAAAGTTCCTGCAAAGACTATCAACCCA *****	1500 1500
C176A pBM10C	AAACCTGGTTCTCCTTATCTTAATATCATGAGAGATTTAGAAGATGAAAAATTAAATTT AAACCTGGTTCTCCTTATCTTAATATCATGAGAGATTTAGAAGATGAAAAATTAAATTT *****	1560 1560
C176A pBM10C	GCATGGGTGCAAGTGAATAATCCATGGCAAAACACTGCAAAATGCAAACTACTGGATTGCA GCATGGGTGCAAGTGAATAATCCATGGCAAAACACTGCAAAATGCAAACTACTGGATTGCA *****	1620 1620
C176A pBM10C	GCAGCAAGAGAAATGGATAATTTTATGTTGTAAGTGATTGTTATCCTGGAATTTAGCA GCAGCAAGAGAAATGGATAATTTTATGTTGTAAGTGATTGTTATCCTGGAATTTAGCA *****	1680 1680
C176A pBM10C	AAAGTAGCTGATCTTATTTTACCAAGCGCTATGATTTATGAAAAATGGGGTGCTTATGGT AAAGTAGCTGATCTTATTTTACCAAGCGCTATGATTTATGAAAAATGGGGTGCTTATGGT *****	1740 1740
C176A pBM10C	AATGCTGAAAGAAGAACTCAACATTGGAAACAACAAGTCTTACCTGTAGGTGCTGCCATG AATGCTGAAAGAAGAACTCAACATTGGAAACAACAAGTCTTACCTGTAGGTGCTGCCATG *****	1800 1800
C176A pBM10C	AGTGATACTTGGCAAATTTTGAATTTGCAAAACGCTTTAAGCTTAAAGAAGTTTGAAA AGTGATACTTGGCAAATTTTGAATTTGCAAAACGCTTTAAGCTTAAAGAAGTTTGAAA *****	1860 1860
C176A pBM10C	GAGCAAAAAGTGGATAATAAGCTTACCTTGCCAAGCGTTTGAAGAGGCAAAAGCTATG GAGCAAAAAGTGGATAATAAGCTTACCTTGCCAAGCGTTTGAAGAGGCAAAAGCTATG *****	1920 1920
C176A pBM10C	GGTTATAGCGAAGATGATACACTTTTGTATGTGCTATTTGCCAATAAAGAAGCAAAAAGC GGTTATAGCGAAGATGATACACTTTTGTATGTGCTATTTGCCAATAAAGAAGCAAAAAGC *****	1980 1980
C176A pBM10C	TTTAATCCAAACGATGCCATCGCAAAAGGCTTTGATAATACCGATGTTAAAGGTGATGAG TTTAATCCAAACGATGCCATCGCAAAAGGCTTTGATAATACCGATGTTAAAGGTGATGAG *****	2040 2040
C176A pBM10C	AGAAAAATTCAAGGCAGTGATGGAAAAGAATTTACAGGCTATGGCTTTTTCGTTCAAAAA AGAAAAATTCAAGGCAGTGATGGAAAAGAATTTACAGGCTATGGCTTTTTCGTTCAAAAA *****	2100 2100
C176A pBM10C	TATCTTTGGGAAGAATATCGTAAATTTGGCTTAGGGCACGGACATGATTAGCGGATTTT TATCTTTGGGAAGAATATCGTAAATTTGGCTTAGGGCACGGACATGATTAGCGGATTTT *****	2160 2160
C176A pBM10C	GATACCTATCATAAAGTAAGGGGTTAAGATGGCCTGTGGTTAATGGCAAGGAAACACAG GATACCTATCATAAAGTAAGGGGTTAAGATGGCCTGTGGTTAATGGCAAGGAAACACAG *****	2220 2220
C176A pBM10C	TGGAGATTTAATACTAAATTTGATTATTATGCTAAAAAGCGGCTCCAAATTCAGATTTT TGGAGATTTAATACTAAATTTGATTATTATGCTAAAAAGCGGCTCCAAATTCAGATTTT *****	2280 2280
C176A pBM10C	GCTTTTTATGGTGATTTTAAACAAATGCTTACAAATGGGGATTTAATAGCTCCTAAAGAT GCTTTTTATGGTGATTTTAAACAAATGCTTACAAATGGGGATTTAATAGCTCCTAAAGAT *****	2340 2340
C176A pBM10C	GAAAAAGAGCACAGTATTAATAAAGGCTAAATTTTCTTTAGGCCATTTATGAAAGCA GAAAAAGAGCACAGTATTAATAAAGGCTAAATTTTCTTTAGGCCATTTATGAAAGCA *****	2400 2400

Figure D.6 Continued

C176A	CCTGAAAGACCAAGTAAAGAGTATCCATTCTGGCTTGCAACAGGAAGGGTTT	2460
pBM10C	CCTGAAAGACCAAGTAAAGAGTATCCATTCTGGCTTGCAACAGGAAGGGTTT	2460

C176A	TGGCATAGTGGAAGTATGACTATGCGTGTGCCTGAGCTTTATCGCGCTGTGCCTGAAGCA	2520
pBM10C	TGGCATAGTGGAAGTATGACTATGCGTGTGCCTGAGCTTTATCGCGCTGTGCCTGAAGCA	2520

C176A	CTTTGCTATATGAGTGAGAAAGATGGAGAGAAATTAGGCTTAAATCAAGGTGATTGGTT	2580
pBM10C	CTTTGCTATATGAGTGAGAAAGATGGAGAGAAATTAGGCTTAAATCAAGGTGATTGGTT	2580

C176A	TGGGTGGAATCTCGTCGCGGTAAAGTAAAGCAAGAGTAGATATGCGCGGAAGAAACAAA	2640
pBM10C	TGGGTGGAATCTCGTCGCGGTAAAGTAAAGCAAGAGTAGATATGCGCGGAAGAAACAAA	2640

C176A	CCGCCTGTAGGACTTGTGTATGTGCCGTGGTTTGATGAGAATGTATATATCAATAAAGTT	2700
pBM10C	CCGCCTGTAGGACTTGTGTATGTGCCGTGGTTTGATGAGAATGTATATATCAATAAAGTT	2700

C176A	ACTTTGGATGCGACTTGTCCACTTTCAAAACAACTGACTTTAAAAAATGCGCTGTAAAA	2760
pBM10C	ACTTTGGATGCGACTTGTCCACTTTCAAAACAACTGACTTTAAAAAATGCGCTGTAAAA	2760

C176A	ATTTATAAGGCTCCCGGGGAGAACCTGTACTTCCAATCCGCCGGGCACCACCATCATCAT	2820
pBM10C	ATTTATAAGGCTCCCGGGGAGAACCTGTACTTCCAATCCGCCGGGCACCACCATCATCAT	2820

C176A	CATTAA 2826	
pBM10C	CATTAA 2826	

Mass Spectrometry Confirmation of the C176S NapA Variant

1	MNRRDFIKNT	AIASAASVAG	LSVPSSMLGA	QEEDWKWDKA	VCRFCGTGCG
51	IMIARKDGKI	VATKGDPAAP	VNRGLNCIKG	YFNAKIMYGE	DRLVMPLLRM
101	NEKGEFDKKG	KFQQVSWQRA	FDEMEKQFKK	AYNELGVTGI	GIFGSGQYTI
151	QEGYAALKLA	KAGFRTNNID	PNARHSMASA	VVGFMQTFGV	DEPSGCYDDI
201	ELTDTIITWG	ANMAEMHPIL	WSRVSDRKLS	NLDKVKVVNL	STFSNRTSNI
251	ADIEIIFKPN	TDLAIWNYIA	REIVYNHPEA	MDMKFIKDHC	VFATGYADIG
301	YGMRNNPNHP	KFKESEKDTV	EKENVITLDD	EEATSLSYLG	VKAGDKFEMK
351	HQGVADKNWE	ISFDEFKKGL	APYTLEYTAR	VAKGDDNESL	EDFKKKLQEL
401	ANLYIEKNRK	VVSFWTMGFN	QHTRGSWVNE	QAYMVHFLLG	KQAKPGSGAF
451	SLTGQPSACG	TAREVGTFSH	RLPADMVVAN	PKHREISEKI	WKVPAKTINP
501	KPGSPYLNIM	RDLEDGKIKF	AWVQVNNPWQ	NTANANHWIA	AAREMDNFIV
551	VSDCYPGISA	KVADLILPSA	MIYEKWGAYG	NAERRTQHWK	QQVLPVGAAM
601	SDTWQILEFA	KRFKLKEVWK	EQKVDNKLTL	PSVLEEAKAM	GYSEDDTLFD
651	VLFANKEAKS	FNPNDIAIKG	FDNTDVKGDE	RKIQGS DGKE	FTGYGFFVQK
701	YLWEEYRKFG	LGHGHDADF	DTYHKVRGLR	WPVVNGKETQ	WRFNTKFDYY
751	AKKAAPNSDF	AFYGDFNKML	TNGDLIAPKD	EKEHSIKNKA	KIFFRPFMKA
801	PERPSKEYPF	WLATGRVLEH	WHS GTMTMRV	PELYRAVPEA	LCYMSEKDGE
851	KLGLNQGD LV	WVESRRGKVK	ARVDMRGRNK	PPVGLVYVPW	FDENVYINKV
901	TLDATCPLSK	QTDFKKCAVK	IYKAPGENLY	FQSAGHHHHH	H

Figure D.7 Mass spectrometric analysis of *C. jejuni* NapA-C176S expressed in *E. coli* K12. The identified peptides are highlighted in red. A 32% coverage was obtained. The amino acid altered in NapA-C176S is underlined.

APPENDIX E. PERIPLASMIC NITRATE REDUCTASE ACTIVITY AS A FUNCTION OF TIME

The activity of isolated *C. jejuni* NapA was determined as a function of storage time (Table E.1). The enzyme was isolated over two days as described in Chapter 2. The isolated enzyme was aliquoted and stored in a liquid nitrogen dewar for a span of 1 day to 3 months. The data was collected one independent sample and must be reproduced in the future. Some of the data was collected prior to the purchase of a quartz 96 well plate and may reflect error associated with contaminated buffer and plastic 96 well plates. The data suggest k_{cat} does diminish with time but after 3 months the enzyme still had 90% of the activity initially measured 1 day after purification. The decrease observed in K_M may represent the diminishing rate component of the Michaelis constant or could represent the improved assay conditions and or technique with time. The study is inconclusive and will need to be repeated in the future for an accurate gauge of the storage lifetime of the recombinant NapA. It is also suggested that metal content be determined if possible, to determine the storage stability of the cofactors.

Table E.1: NapA Activity Over Three Months.

Enzyme	Storage Time	K_M (μM)	k_{cat} (s^{-1})	k_{cat}/K_M ($s^{-1} \cdot M^{-1}$)
WT NapA	1 day	86 ± 23	5.03 ± 0.61	5.85×10^4
WT NapA	2 weeks	21 ± 3.4	5.71 ± 0.16	2.72×10^5
WT NapA	1.5 months	10.1 ± 1.0	5.57 ± 0.18	5.51×10^5
WT NapA	3 months	5.78 ± 2.5	4.81 ± 0.35	8.32×10^5

APPENDIX F. PRELIMINARY INVESTIGATION OF ARSENITE ACTIVITY

C176A Arsenite Activity Preliminary Data

Methods

Arsenite oxidase activity was measured spectrophotometrically by monitoring reduction of 2,4-dichlorophenolindophenol (DCPIP) at 600 nm. Assays were conducted in an inert atmosphere glove box at 25°C using a Bio-Tek EPOCH 2 Absorbance Microplate Reader. Arsenite addition initiated the reaction which was monitored for 15 min. The rate of DCPIP reduction was calculated using the Beer-Lambert law given the extinction coefficient of DCPIP ($23 \text{ mM}^{-1} \text{ cm}^{-1}$, 600 nm [464]). These rates were analyzed using OriginPro 9. Protein concentrations were determined using the Pierce Coomassie Plus (Bradford) Protein Assay Kit (Thermo Scientific) with bovine serum albumin standard (Thermo Scientific).

Results and Discussion

Enzyme dependence was measured to determine if arsenite was a viable substrate before a full curve of dependence on substrate concentration was determined. The total volume in the well was held constant at 100 μL and DCPIP concentration was $\sim 4 \text{ mM}$ in 50 mM HEPES pH 7.00 to obtain an absorbance reading of 0.8-1 A.U. before the reaction was initiated. Figure F.1 depicts the arsenite oxidation rate's dependence on enzyme concentration. The rate roughly quadruples with enzyme concentration suggesting the enzyme can oxidize arsenite. A full profile changing arsenite concentration while holding enzyme concentration constant was attempted. However, the rate was extremely slow and the signal to noise ratio was not high enough to get a viable signal to measure an accurate rate. The DCPIP/arsenite activity assay must be optimized in the future to obtain more kinetic information. Although the enzyme dependence suggests activity, it was only conducted once and without further confirmation that arsenite was oxidized must be viewed skeptically until future experiments can be conducted to confirm arsenite is a viable substrate for the C176A enzyme.

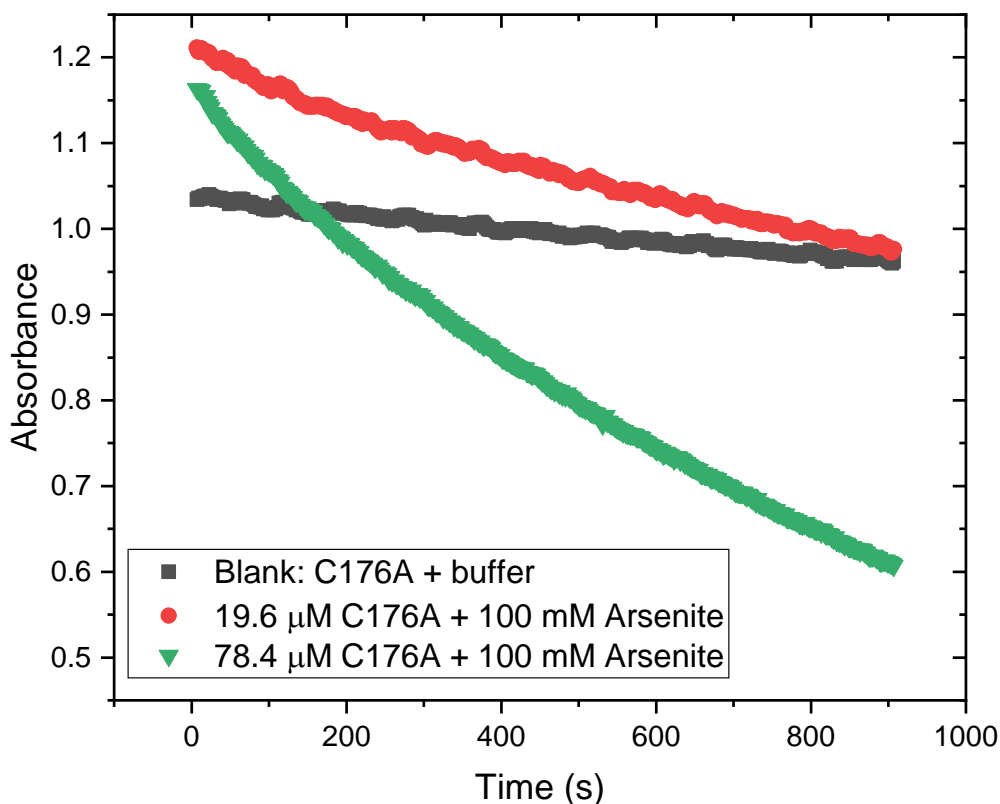


Figure F.1: Enzyme dependence of the arsenite oxidation rate by the C176A NapA variant. The background rate was determined by a blank measurement of C176A enzyme, buffer, and DCPIP (black squares). The reaction was initiated with addition of buffer to simulate substrate addition. Two enzyme concentrations were tested at 19.6 μ M (red circles) and the four-fold higher concentration of 78.4 μ M C176A (green triangles). The reaction of both samples was initiated with the addition of arsenite (final concentration of 100 mM). The blank had a minimal observed background rate and the higher concentration of enzyme was determined to have a rate approximately four times larger than the lower concentration of enzyme.

APPENDIX G. MUTATION OF A CRITICAL LYSINE RESIDUE IN THE ELECTRON TRANSFER PATHWAY OF PERIPLASMIC NITRATE REDUCTASE

K79G NapA Variant

Methods

Mutagenesis of *C. jejuni napA* was conducted using the QuikChange II Site-Directed Mutagenesis Kit (Qiagen) with the pBM10C plasmid as template as in Chapter 5. The primers designed for the napA-K79G mutation are 5'-GGA CTT AAT TGT ATC GGA GGT TAT TTT-3' and 5'-AGC ATT AAA ATA ACC TCC GAT ACA ATT-3'. The PCR product was sequenced at ACGT Inc. Plasmid pBM10C_K79G was expressed to produce the K79G NapA variant in the same fashion as the native enzyme discussed in Chapter 2. The K79G variant was purified by the optimized protocol in Chapter 2. SDS-PAGE was used to screen fractions for NapA content and purity using standard protocols as previously discussed. Nitrate activity assays were conducted as described in Chapter 2 and the electronic spectrum was measured as described in Chapter 3.

Results and Discussion

The K79G variant of NapA was designed to probe the role of Lys79 in electron transfer from the [4Fe4S] cluster to the PDT molecule of Moco which would eventually travel to the Mo center to reduce the metal to the Mo(IV) resting state thus regenerating the enzyme for another catalytic cycle. The mutation was confirmed at the DNA level via sequencing conducted by ACGT Inc (Figure G.1). The variant was successfully purified to greater than 90% homogeneity (Figure G.2). The electronic spectrum indicated an intact [4Fe4S] cluster (Figure G.3) and metal analysis revealed molybdenum incorporation to be approximately ~37%. Kinetic analysis of the K79G variant revealed nitrate can be turned over by the variant. A V_{\max} of 0.004 ± 0.0004 $\mu\text{mol nitrate}/(\text{min} \cdot \text{mg enzyme})$, K_M for nitrate of 178 ± 103 μM , and k_{cat} of 0.008 ± 0.0007 s^{-1} were determined by fitting the nitrate activity data to the Michaelis-Menten Model (Figure G.4). As indicated by the error on K_M , the experiment needs to be repeated and more substrate concentrations below 150 μM must be investigated to obtain more accurate and reproducible data to fit in order to determine accurate kinetic parameters. Despite the unreliability of the kinetic parameters, we can conclude the variant is active and the electron transfer pathway has not been

completely blocked but it is premature to ascertain why electrons are still being transferred. It is tempting to say that reduced methyl viologen may donate electrons directly to the metal center and not solely through the physiologically determined electron transfer pathway. Further investigation is needed to fully understand what is happening in the K79G variant and what exactly the role of Lys79 is in NapA *in vivo*.

Figure G.1: The *napA* sequence alignment utilizing Clustal OMEGA Alignment Tool. The *napA* sequence in construct K79G-pBM10C is compared to the *napA* gene sequence in template pBM10C that was previously confirmed to be the correct *C. jejuni* RM1221 *napA* gene sequence. The mutation of the base A235 and A236 to G235 and G236 respectively are the desired mutations in the DNA sequence creating the Lys to Gly exchange at position 79 in the NapA protein sequence.

K79G	ATGAATAGAAAGGATTTTATTAATAACCGCTATTGCAAGTGCTGCTAGTGTTCAGGG	60
pBM10C	ATGAATAGAAAGGATTTTATTAATAACCGCTATTGCAAGTGCTGCTAGTGTTCAGGG	60
K79G	CTTAGTGTTCAGCTCTATGCTTGGCGCGCAAGAAGAAGATTGGAATGGGATAAAGCT	120
pBM10C	CTTAGTGTTCAGCTCTATGCTTGGCGCGCAAGAAGAAGATTGGAATGGGATAAAGCT	120
K79G	GTTTGTAGATTTTGTGGAAGTGGCTGTGGAATTATGATAGCTAGAAAAGATGGCAAAATC	180
pBM10C	GTTTGTAGATTTTGTGGAAGTGGCTGTGGAATTATGATAGCTAGAAAAGATGGCAAAATC	180
K79G	GTAGCAACAAAAGGTGATCCTGCAGCACCCGTAAATCGCGGACTTAATTGTATCGGAGGT	240
pBM10C	GTAGCAACAAAAGGTGATCCTGCAGCACCCGTAAATCGCGGACTTAATTGTATCAAGGT	240
K79G	TATTTTAATGCTAAGATCATGTATGGTGAAGATCGTCTTGTATTGCCTTTCGCTCGCATG	300
pBM10C	TATTTTAATGCTAAGATCATGTATGGTGAAGATCGTCTTGTATTGCCTTTCGCTCGCATG	300
K79G	AATGAAAAAGGCGAATTGATAAAAAAGGCAAAATTCACAAAGTTTCTTGGCAAAGAGCC	360
pBM10C	AATGAAAAAGGCGAATTGATAAAAAAGGCAAAATTCACAAAGTTTCTTGGCAAAGAGCC	360
K79G	TTTGATGAAATGGAAAAACAATTTAAAAAGCCTACAATGAACTCGGCGTTACAGGTATA	420
pBM10C	TTTGATGAAATGGAAAAACAATTTAAAAAGCCTACAATGAACTCGGCGTTACAGGTATA	420
K79G	GGGATTTTGGTAGTGGGCAATATACTATCCAAGAAGGTTATGCTGCTTTAAAGCTTGCA	480
pBM10C	GGGATTTTGGTAGTGGGCAATATACTATCCAAGAAGGTTATGCTGCTTTAAAGCTTGCA	480
K79G	AAAGCGGGTTTTAGAACAAATAATATCGATCCAAATGCAAGACATTGTATGGCCTCTGCA	540
pBM10C	AAAGCGGGTTTTAGAACAAATAATATCGATCCAAATGCAAGACATTGTATGGCCTCTGCA	540
K79G	GTGGTTGGTTTTATGCAAACTTTTGGTGTAGATGAGCCATCAGGCTGTTATGATGATATA	600
pBM10C	GTGGTTGGTTTTATGCAAACTTTTGGTGTAGATGAGCCATCAGGCTGTTATGATGATATA	600
K79G	GAGCTTACAGATACTATTATCACTTGGGAGCTAATATGGTGAAATGCACCAATCCTT	660
pBM10C	GAGCTTACAGATACTATTATCACTTGGGAGCTAATATGGTGAAATGCACCAATCCTT	660
K79G	TGGTCAAGAGTAAGTGATAGAAAATAAGCAATCTTGATAAGGTTAAAGTTGTTAATCTA	720
pBM10C	TGGTCAAGAGTAAGTGATAGAAAATAAGCAATCTTGATAAGGTTAAAGTTGTTAATCTA	720
K79G	AGCACTTTTCTAACCGTACTTCAAATATTGCTGATATTGAAATTATTTTAAACCAAAT	780
pBM10C	AGCACTTTTCTAACCGTACTTCAAATATTGCTGATATTGAAATTATTTTAAACCAAAT	780
K79G	ACAGATTTGGCTATTGGAATTACATAGCAAGAGAGATTGTTTATAATCATCCAGAGGCT	840
pBM10C	ACAGATTTGGCTATTGGAATTACATAGCAAGAGAGATTGTTTATAATCATCCAGAGGCT	840
K79G	ATGGATATGAAATTTATCAAAGATCACTGCGTATTGCAACTGGTTATGCTGATATTGGT	900
pBM10C	ATGGATATGAAATTTATCAAAGATCACTGCGTATTGCAACTGGTTATGCTGATATTGGT	900
K79G	TATGGTATGAGAAATAATCCAAATCATCCAAATTTAAGAAAGTGAAAAAGATACGGTT	960
pBM10C	TATGGTATGAGAAATAATCCAAATCATCCAAATTTAAGAAAGTGAAAAAGATACGGTT	960
K79G	GAAAAAGAAAATGTAATCACTTTAGACGATGAAGAGGCTACTTCTTTATCTTATCTTGGC	1020
pBM10C	GAAAAAGAAAATGTAATCACTTTAGACGATGAAGAGGCTACTTCTTTATCTTATCTTGGC	1020
K79G	GTTAAAGCGGGTGATAAATTGAAATGAAACATCAAGGTGTGGCTGATAAAACTGGGAA	1080
pBM10C	GTTAAAGCGGGTGATAAATTGAAATGAAACATCAAGGTGTGGCTGATAAAACTGGGAA	1080
K79G	ATTTCTTTTGACGAATTTAAAAAGGTTTAGCCCCTTATACTTTGAATACACTGCAAGA	1140
pBM10C	ATTTCTTTTGACGAATTTAAAAAGGTTTAGCCCCTTATACTTTGAATACACTGCAAGA	1140
K79G	GTAGCCAAAGGTGATGATAATGAGTCTTTGGAAGATTTAAGAAAAACTTCAAGAATTA	1200
pBM10C	GTAGCCAAAGGTGATGATAATGAGTCTTTGGAAGATTTAAGAAAAACTTCAAGAATTA	1200

Figure G.1 Continued

K79G	GCTAATCTTTACATAGAGAAAAATCGCAAAGTCGTAAGTTTTTGGACTATGGGCTTTAAT	1260
pBM10C	GCTAATCTTTACATAGAGAAAAATCGCAAAGTCGTAAGTTTTTGGACTATGGGCTTTAAT	1260

K79G	CAACACACAAGAGGTTCTTTGGGTAAATGAACAAGCTTATATGGTACATTTTTTGCTAGGA	1320
pBM10C	CAACACACAAGAGGTTCTTTGGGTAAATGAACAAGCTTATATGGTACATTTTTTGCTAGGA	1320

K79G	AAGCAAGCTAAACCAGGTAGTGGAGCCTTTTCTTTAACAGGACAGCCAAGTGCCTGTGGA	1380
pBM10C	AAGCAAGCTAAACCAGGTAGTGGAGCCTTTTCTTTAACAGGACAGCCAAGTGCCTGTGGA	1380

K79G	ACAGCTAGGGAAGTAGGAACCTTCTCACATCGTTTGCCTGCAGATATGGTTGTAGCCAAT	1440
pBM10C	ACAGCTAGGGAAGTAGGAACCTTCTCACATCGTTTGCCTGCAGATATGGTTGTAGCCAAT	1440

K79G	CCAAAACACAGAGAAATTTCTGAAAAAATTTGAAAAGTTCCTGCAAAGACTATCAACCCA	1500
pBM10C	CCAAAACACAGAGAAATTTCTGAAAAAATTTGAAAAGTTCCTGCAAAGACTATCAACCCA	1500

K79G	AAACCTGGTTCTCCTTATCTTAATATCATGAGAGATTTAGAAGATGAAAAATTAAATTT	1560
pBM10C	AAACCTGGTTCTCCTTATCTTAATATCATGAGAGATTTAGAAGATGAAAAATTAAATTT	1560

K79G	GCATGGGTGCAAGTGAATAATCCATGGCAAAACACTGCAATGCAAACTACTGGATTGCA	1620
pBM10C	GCATGGGTGCAAGTGAATAATCCATGGCAAAACACTGCAATGCAAACTACTGGATTGCA	1620

K79G	GCAGCAAGAGAAATGGATAATTTTATGTTGTAAGTGATTGTTATCCTGGAATTCAGCA	1680
pBM10C	GCAGCAAGAGAAATGGATAATTTTATGTTGTAAGTGATTGTTATCCTGGAATTCAGCA	1680

K79G	AAAGTAGCTGATCTTATTTTACCAAGCGCTATGATTTATGAAAAATGGGGTGCTTATGGT	1740
pBM10C	AAAGTAGCTGATCTTATTTTACCAAGCGCTATGATTTATGAAAAATGGGGTGCTTATGGT	1740

K79G	AATGCTGAAAGAAGAACTCAACATTGGAAACAACAAGTCTTACCTGTAGGTGCTGCCATG	1800
pBM10C	AATGCTGAAAGAAGAACTCAACATTGGAAACAACAAGTCTTACCTGTAGGTGCTGCCATG	1800

K79G	AGTGATACTTGGCAAATTTTGAATTTGCAAAACGCTTTAAGCTTAAAGAAGTTTGAAA	1860
pBM10C	AGTGATACTTGGCAAATTTTGAATTTGCAAAACGCTTTAAGCTTAAAGAAGTTTGAAA	1860

K79G	GAGCAAAAAGTGGATAATAAGCTTACCTTGCCAAGCGTTTGAAGAGGCAAAAGCTATG	1920
pBM10C	GAGCAAAAAGTGGATAATAAGCTTACCTTGCCAAGCGTTTGAAGAGGCAAAAGCTATG	1920

K79G	GGTTATAGCGAAGATGATACACTTTTGTATGTGCTATTTGCCAATAAAGAAGCAAAAAGC	1980
pBM10C	GGTTATAGCGAAGATGATACACTTTTGTATGTGCTATTTGCCAATAAAGAAGCAAAAAGC	1980

K79G	TTTAATCCAACGATGCCATCGCAAAAGGCTTTGATAATACCGATGTTAAAGGTGATGAG	2040
pBM10C	TTTAATCCAACGATGCCATCGCAAAAGGCTTTGATAATACCGATGTTAAAGGTGATGAG	2040

K79G	AGAAAAATTCAAGGCAGTGATGGAAAAGAATTTACAGGCTATGGCTTTTTCGTTCAAAAA	2100
pBM10C	AGAAAAATTCAAGGCAGTGATGGAAAAGAATTTACAGGCTATGGCTTTTTCGTTCAAAAA	2100

K79G	TATCTTTGGGAAGAATATCGTAAATTTGGCTTAGGGCACGGACATGATTAGCGGATTTT	2160
pBM10C	TATCTTTGGGAAGAATATCGTAAATTTGGCTTAGGGCACGGACATGATTAGCGGATTTT	2160

K79G	GATACCTATCATAAAGTAAGGGGTTAAGATGGCCTGTGGTTAATGGCAAGGAAACACAG	2220
pBM10C	GATACCTATCATAAAGTAAGGGGTTAAGATGGCCTGTGGTTAATGGCAAGGAAACACAG	2220

K79G	TGGAGATTTAATACTAAATTTGATTATTATGCTAAAAAGCGGCTCCAAATTCAGATTTT	2280
pBM10C	TGGAGATTTAATACTAAATTTGATTATTATGCTAAAAAGCGGCTCCAAATTCAGATTTT	2280

K79G	GCTTTTATGGTGATTTTAAACAAATGCTTACAAATGGGGATTTAATAGCTCCTAAAGAT	2340
pBM10C	GCTTTTATGGTGATTTTAAACAAATGCTTACAAATGGGGATTTAATAGCTCCTAAAGAT	2340

K79G	GAAAAAGAGCACAGTATTAATAAATAAGGCTAAAATTTCTTTAGGCCATTTATGAAAGCA	2400
pBM10C	GAAAAAGAGCACAGTATTAATAAATAAGGCTAAAATTTCTTTAGGCCATTTATGAAAGCA	2400

Figure G.1 Continued

K79G	CCTGAAAGACCAAGTAAAGAGTATCCATTCTGGCTTGCAACAGGAAGGGTTT	2460
pBM10C	CCTGAAAGACCAAGTAAAGAGTATCCATTCTGGCTTGCAACAGGAAGGGTTT	2460

K79G	TGGCATAGTGGAAGTATGACTATGCGTGTGCCTGAGCTTTATCGCGCTGTGCCTGAAGCA	2520
pBM10C	TGGCATAGTGGAAGTATGACTATGCGTGTGCCTGAGCTTTATCGCGCTGTGCCTGAAGCA	2520

K79G	CTTTGCTATATGAGTGAGAAAGATGGAGAGAAATTAGGCTTAAATCAAGGTGATTGGTT	2580
pBM10C	CTTTGCTATATGAGTGAGAAAGATGGAGAGAAATTAGGCTTAAATCAAGGTGATTGGTT	2580

K79G	TGGGTGGAATCTCGTCGCGGTAAAGTAAAGCAAGAGTAGATATGCGCGGAAGAAACAAA	2640
pBM10C	TGGGTGGAATCTCGTCGCGGTAAAGTAAAGCAAGAGTAGATATGCGCGGAAGAAACAAA	2640

K79G	CCGCCTGTAGGACTTGTGTATGTGCCGTGGTTTGATGAGAATGTATATATCAATAAAGTT	2700
pBM10C	CCGCCTGTAGGACTTGTGTATGTGCCGTGGTTTGATGAGAATGTATATATCAATAAAGTT	2700

K79G	ACTTTGGATGCGACTTGTCCACTTTCAAAACAACTGACTTTAAAAAATGCGCTGTAAAA	2760
pBM10C	ACTTTGGATGCGACTTGTCCACTTTCAAAACAACTGACTTTAAAAAATGCGCTGTAAAA	2760

K79G	ATTTATAAGGCTCCCGGGGAGAACCTGTACTTCCAATCCGCCGGGCACCACCATCATCAT	2820
pBM10C	ATTTATAAGGCTCCCGGGGAGAACCTGTACTTCCAATCCGCCGGGCACCACCATCATCAT	2820

K79G	CATTAA	2826
pBM10C	CATTAA	2826

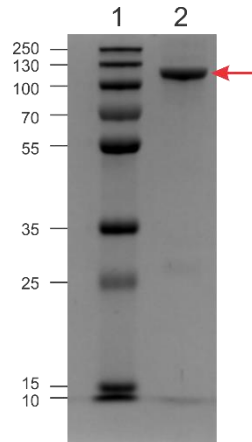


Figure G.2: SDS-PAGE of K79G-NapA purified via the optimized protocol discussed in Chapter 2. Lane 1- PageRuler Plus Prestained Protein Ladder (kDa), Lane 2- Pure K79G-NapA. The ~ 108 kDa NapA band is denoted by the red arrow.

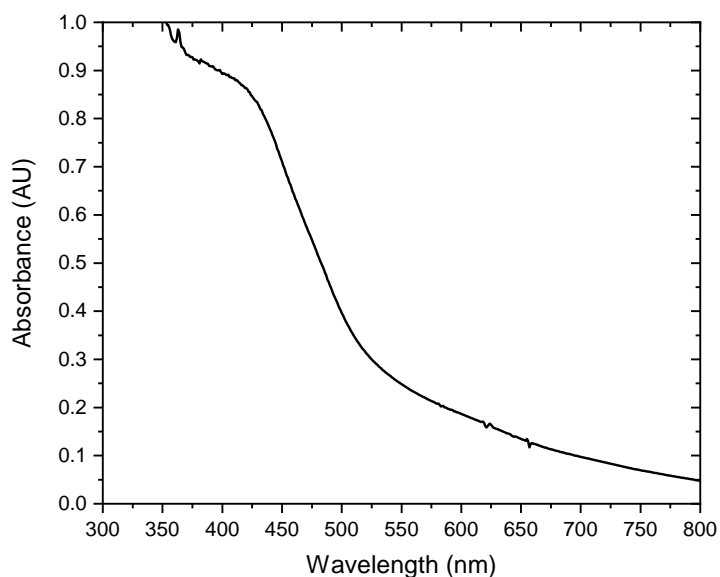


Figure G.3: UV-Vis spectrum of as-isolated *C. jejuni* K79G-NapA in 50 mM HEPES pH 7.00.

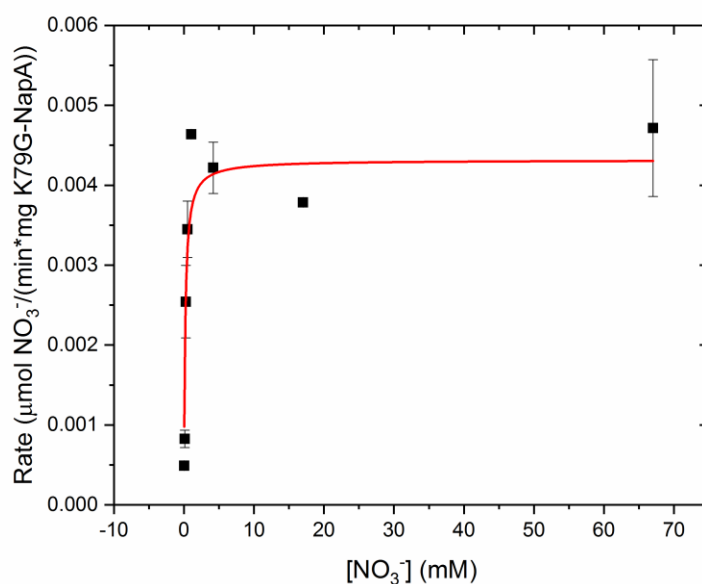


Figure G.4: Steady-state kinetic analysis using the Michaelis-Menten model of the reduction of nitrate by *C. jejuni* K79G-NapA. The solid lines represent Michaelis-Menten fit. The data was analyzed, and the graph produced in Origin. A V_{\max} of 0.004 ± 0.0004 $\mu\text{mol nitrate}/(\text{min} \cdot \text{mg enzyme})$, K_M for nitrate of 178 ± 103 μM , and k_{cat} of 0.008 ± 0.0007 s^{-1} were determined from the fit. This kinetics curve was reproduced by only one biological replicate. Each curve contained 1-3 technical replicates for each substrate concentration.

REFERENCES

1. B. Mintmier, S. Nassif, J. F. Stolz and P. Basu (2020) *J Biol Inorg Chem*, doi 10.1007/s00775-020-01787-y;10.1007/s00775-00020-01787-y.
2. P. Basu and S. J. N. Burgmayer (2011) *Coord Chem Rev* 255:1016-1038.
3. G. Schwarz (2005) *Cell Mol Life Sci* 62:2792-2810.
4. R. Hille, J. Hall and P. Basu (2014) *Chem Rev (Washington, DC, U S)* 114:3963-4038.
5. H. Dobbek (2011) *Coord Chem Rev* 255:1104-1116.
6. P. J. Gonzalez, M. G. Rivas, C. S. Mota, C. D. Brondino, I. Moura and J. J. G. Moura (2013) *Coord Chem Rev* 257:315-331.
7. C. E. M. Stevenson, F. Sargent, G. Buchanan, T. Palmer and D. M. Lawson (2000) *Structure* 8:1115-1125.
8. R. A. Rothery, B. Stein, M. Solomonson, M. L. Kirk and J. H. Weiner (2012) *Proc Natl Acad Sci U S A* 109:14773-14778, S14773/14771-S14773/14775.
9. H. Dobbek, L. Gremer, R. Kiefersauer, R. Huber and O. Meyer (2002) *Proc Natl Acad Sci U S A* 99:15971-15976.
10. A. Magalon, J. G. Fedor, A. Walburger and J. H. Weiner (2011) *Coord Chem Rev* 255:1159-1178.
11. R. R. Mendel and T. Kruse (2012) *Biochim Biophys Acta, Mol Cell Res* 1823:1568-1579.
12. J. F. Stolz and P. Basu (2002) *ChemBioChem* 3:198-206.
13. S. Gruenewald, B. Wahl, F. Bittner, H. Hungeling, S. Kanzow, J. Kotthaus, U. Schwering, R. R. Mendel and B. Clement (2008) *J Med Chem* 51:8173-8177.
14. C. E. Sparacino-Watkins, J. Tejero, B. Sun, M. C. Gauthier, J. Thomas, V. Ragireddy, B. A. Merchant, J. Wang, I. Azarov, P. Basu and M. T. Gladwin (2014) *J Biol Chem* 289:10345-10358.
15. R. Hille (1996) *Chem Rev (Washington, D C)* 96:2757-2816.
16. C. Sparacino-Watkins, J. F. Stolz and P. Basu (2014) *Chem Soc Rev* 43:676-706.
17. G. Schwarz, R. R. Mendel and M. W. Ribbe (2009) *Nature (London, U K)* 460:839-847.
18. S. Leimkuhler, M. M. Wuebbens and K. V. Rajagopalan (2011) *Coord Chem Rev* 255:1129-1144.

19. C. Iobbi-Nivol and S. Leimkuhler (2013) *Biochim Biophys Acta*, Bioenerg 1827:1086-1101.
20. R. R. Mendel and S. Leimkuehler (2015) *JBIC, J Biol Inorg Chem* 20:337-347.
21. S. Leimkuehler (2017) *Biol Chem* 398:1009-1026.
22. R. R. Mendel (2013) *J Biol Chem* 288:13165-13172.
23. B. Schoepp-Cothenet, R. van Lis, P. Philippot, A. Magalon, M. J. Russell and W. Nitschke (2012) *Sci Rep* 2:263-263.
24. G. Schwarz (2016) *Curr Opin Chem Biol* 31:179-187.
25. A. Veldman, J. A. Santamaria-Araujo, S. Sollazzo, J. Pitt, R. Gianello, J. Yapliito-Lee, F. Wong, C. A. Ramsden, J. Reiss, I. Cook, J. Fairweather and G. Schwarz (2010) *Pediatrics* 125:e1249-1254.
26. J. Sambrook and D. W. Russell (2001) *Molecular cloning: A laboratory manual*. Cold Spring Harbor Laboratory Press, .
27. C. Pinske, M. Boenn, S. Krueger, U. Lindenstrauss and R. G. Sawers (2011) *PLoS One* 6:e22830.
28. S. Carneiro, E. C. Ferreira and I. Rocha (2013) *J Biotechnol* 164:396-408.
29. V. V. Pollock and M. J. Barber (1997) *J Biol Chem* 272:3355-3362.
30. G. D'Errico, S. A. Di, C. F. La, M. Rossi and R. Cannio (2006) *J Bacteriol* 188:694-701.
31. J. A. Vasina and F. Baneyx (1997) *Protein Expression Purif* 9:211-218.
32. W. H. Brondyk (2009) *Methods Enzymol* 463:131-147.
33. H. P. Sorensen and K. K. Mortensen (2005) *J Biotechnol* 115:113-128.
34. C. Kinsland (2010) *Comprehensive natural products ii*. Elsevier, Oxford, pp. 695-721.
35. P. Kaufmann, S. Leimkuhler and C. Iobbi-Nivol (2019) *Methods Mol Biol* 1876:141-152.
36. R. Soyka and W. Pfeiderer (1990) *Pteridines* 2:63-74.
37. R. Soyka, W. Pfeiderer and R. Prewo (1990) *Helv Chim Acta* 73:808-826.
38. R. S. Pilato, K. A. Eriksen, M. A. Greaney, E. I. Stiefel, S. Goswami, L. Kilpatrick, T. G. Spiro, E. C. Taylor and A. L. Rheingold (1991) *J Am Chem Soc* 113:9372-9374.
39. R. S. Pilato, K. Eriksen, M. A. Greaney, Y. Gea, E. C. Taylor, S. Goswami, L. Kilpatrick, T. G. Spiro, A. L. Rheingold and E. I. Stiefel (1993) *ACS Symp Ser* 535:83-97.

40. B. Bradshaw, A. Dinsmore, W. Ajana, D. Collison, C. D. Garner and J. A. Joule (2001) *J Chem Soc, Perkin Trans 1*, doi 10.1039/b108579b:3239-3244.
41. L. Marbella, B. Serli-Mitasev and P. Basu (2009) *Angew Chem, Int Ed* 48:3996-3998.
42. K. Clinch, D. K. Watt, R. A. Dixon, S. M. Baars, G. J. Gainsford, A. Tiwari, G. Schwarz, Y. Saotome, M. Storek, A. A. Belaidi and J. A. Santamaria-Araujo (2013) *J Med Chem* 56:1730-1738.
43. I. V. Pimkov, A. A. Peterson, D. N. Vaccarello and P. Basu (2014) *RSC Adv* 4:19072-19076.
44. I. V. Pimkov, B. Serli-Mitasev, A. A. Peterson, S. C. Ratvasky, B. Hammann and P. Basu (2015) *Chemistry* 21:17057-17072.
45. A. Magalon and R. R. Mendel (2015) *EcoSal Plus* 6:1-31.
46. S. Leimkühler and R. R. Mendel (2017) *Molybdenum and tungsten enzymes: Biochemistry*. The Royal Society of Chemistry, pp. 100-116.
47. S. Leimkuhler, M. Kern, P. S. Solomon, A. G. McEwan, G. Schwarz, R. R. Mendel and W. Klipp (1998) *Mol Microbiol* 27:853-869.
48. S. Leimkuhler, S. Angermuller, G. Schwarz, R. R. Mendel and W. Klipp (1999) *J Bacteriol* 181:5930-5939.
49. S. Leimkuhler and W. Klipp (1999) *J Bacteriol* 181:2745-2751.
50. Y. Yang, S. Yuan, T. Chen, P. Ma, G. Shang and Y. Dai (2009) *Biodegradation* 20:541-549.
51. A. Hochheimer, R. A. Schmitz, R. K. Thauer and R. Hedderich (1995) *Eur J Biochem* 234:910-920.
52. J. A. Vorholt, M. Vaupel and R. K. Thauer (1996) *Eur J Biochem* 236:309-317.
53. S. Chu, D. Zhang, D. Wang, Y. Zhi and P. Zhou (2017) *Int J Biol Macromol* 101:1019-1028.
54. J. C. Hilton, C. A. Temple and K. V. Rajagopalan (1999) *J Biol Chem* 274:8428-8436.
55. V. V. Pollock, R. C. Conover, M. K. Johnson and M. J. Barber (2002) *Arch Biochem Biophys* 403:237-248.
56. Z. Xia, K. Sun, M. Wang, K. Wu, H. Zhang and J. Wu (2012) *PLoS One* 7:e37383.
57. C. A. Temple, T. N. Graf and K. V. Rajagopalan (2000) *Arch Biochem Biophys* 383:281-287.

58. M. Ibdah, Y.-T. Chen, C. G. Wilkerson and E. Pichersky (2009) *Plant Physiol* 150:416-423.
59. D. Y. Huang, A. Furukawa and Y. Ichikawa (1999) *Arch Biochem Biophys* 364:264-272.
60. B. L. Berg and V. Stewart (1990) *Genetics* 125:691-702.
61. B. J. N. Jepson, S. Mohan, T. A. Clarke, A. J. Gates, J. A. Cole, C. S. Butler, J. N. Butt, A. M. Hemmings and D. J. Richardson (2007) *J Biol Chem* 282:6425-6437.
62. T. P. Warelow, M. Oke, B. Schoepp-Cothenet, J. U. Dahl, N. Bruselat, G. N. Sivalingam, S. Leimkuhler, K. Thalassinou, U. Kappler, J. H. Naismith and J. M. Santini (2013) *PLoS One* 8:e72535.
63. V. Mejean, C. Iobbi-Nivol, M. Lepelletier, G. Giordano, M. Chippaux and M. C. Pascal (1994) *Mol Microbiol* 11:1169-1179.
64. C. A. Temple and K. V. Rajagopalan (2000) *J Biol Chem* 275:40202-40210.
65. D. Sambasivarao, R. J. Turner, J. L. Simala-Grant, G. Shaw, J. Hu and J. H. Weiner (2000) *J Biol Chem* 275:22526-22531.
66. Y. Yamaguchi, T. Matsumura, K. Ichida, K. Okamoto and T. Nishino (2007) *J Biochem* 141:513-524.
67. R. M. Garrett and K. V. Rajagopalan (1996) *J Biol Chem* 271:7387-7391.
68. R. M. Garrett, D. B. Bellissimo and K. V. Rajagopalan (1995) *Biochim Biophys Acta, Gene Struct Expression* 1262:147-149.
69. N. V. Ivanov, F. Hubalek, M. Trani and D. E. Edmondson (2003) *Eur J Biochem* 270:4744-4754.
70. L. Loschi, S. J. Brokx, T. L. Hills, G. Zhang, M. G. Bertero, A. L. Lovering, J. H. Weiner and N. C. J. Strynadka (2004) *J Biol Chem* 279:50391-50400.
71. S. J. Brokx, R. A. Rothery, G. Zhang, D. P. Ng and J. H. Weiner (2005) *Biochemistry* 44:10339-10348.
72. C. A. Temple, G. N. George, J. C. Hilton, M. J. George, R. C. Prince, M. J. Barber and K. V. Rajagopalan (2000) *Biochemistry* 39:4046-4052.
73. V. V. Pollock and M. J. Barber (1995) *Arch Biochem Biophys* 318:322-332.
74. D. E. Pierson and A. Campbell (1990) *J Bacteriol* 172:2194-2198.
75. R. Cammack and J. H. Weiner (1990) *Biochemistry* 29:8410-8416.

76. R. A. Rothery, J. L. Simala Grant, J. L. Johnson, K. V. Rajagopalan and J. H. Weiner (1995) *J Bacteriol* 177:2057-2063.
77. R. A. Rothery and J. H. Weiner (1996) *Biochemistry* 35:3247-3257.
78. K. Heffron, C. Leger, R. A. Rothery, J. H. Weiner and F. A. Armstrong (2001) *Biochemistry* 40:3117-3126.
79. R. Dhouib, D. S. M. P. Othman, V. Lin, X. J. Lai, H. G. S. Wijesinghe, M. Nasreen, P. V. Bernhardt, A. G. McEwan, U. Kappler, A.-T. Essilfie, P. M. Hansbro and A. Davis (2016) *Front Microbiol* 7:1743.
80. S. Duval, J. M. Santini, D. Lemaire, F. Chaspoul, M. J. Russell, S. Grimaldi, W. Nitschke and B. Schoepp-Cothenet (2016) *Biochim Biophys Acta, Bioenerg* 1857:1353-1362.
81. T. P. Warelow, J. M. Santini, M. J. Pushie, M. J. Pushie, J. J. H. Cotelesage, G. N. George and G. N. George (2017) *Sci Rep* 7:1757.
82. Q. Wang, T. P. Warelow, Y.-S. Kang, C. Romano, T. H. Osborne, C. R. Lehr, B. Bothner, T. R. McDermott, J. M. Santini and G. Wang (2015) *Appl Environ Microbiol* 81:1959-1965.
83. L. M. Rubio, E. Flores and A. Herrero (2002) *Photosynth Res* 72:13-26.
84. B. J. N. Jepson, L. J. Anderson, L. M. Rubio, C. J. Taylor, C. S. Butler, E. Flores, A. Herrero, J. N. Butt and D. J. Richardson (2004) *J Biol Chem* 279:32212-32218.
85. M. G. Bertero, R. A. Rothery, M. Palak, C. Hou, D. Lim, F. Blasco, J. H. Weiner and N. C. Strynadka (2003) *Nature structural biology* 10:681-687.
86. R. A. Rothery, F. Blasco and J. H. Weiner (2001) *Biochemistry* 40:5260-5268.
87. F. Blasco, F. Nunzi, J. Pommier, R. Brasseur, M. Chippaux and G. Giordano (1992) *Mol Microbiol* 6:209-219.
88. T. Hartmann and S. Leimkuehler (2013) *FEBS J* 280:6083-6096.
89. N. Bohmer, T. Hartmann and S. Leimkuhler (2014) *FEBS Lett* 588:531-537.
90. P. Schrapers, T. Hartmann, R. Kositzki, H. Dau, S. Reschke, C. Schulzke, S. Leimkuehler and M. Haumann (2015) *Inorg Chem* 54:3260-3271.
91. T. Hartmann, S. Leimkuhler, P. Schrapers, H. Dau, M. Haumann, T. Utesch, Y. Rippers, M. A. Mrogiński and M. Nimtz (2016) *Biochemistry* 55:2381-2389.
92. J. C. Hilton and K. V. Rajagopalan (1996) *Biochim Biophys Acta, Protein Struct Mol Enzymol* 1294:111-114.

93. R. A. Siddiqui, U. Warnecke-Eberz, A. Hengsberger, B. Schneider, S. Kostka and B. Friedrich (1993) *J Bacteriol* 175:5867-5876.
94. H. N. Truong, C. Meyer and F. Daniel-Vedele (1991) *Biochem J* 278:393-397.
95. R. M. Garrett, J. L. Johnson, T. N. Graf, A. Feigenbaum and K. V. Rajagopalan (1998) *Proc Natl Acad Sci U S A* 95:6394-6398.
96. R. M. Garrett and K. V. Rajagopalan (1994) *J Biol Chem* 269:272-276.
97. K. E. Johnson and K. V. Rajagopalan (2001) *J Biol Chem* 276:13178-13185.
98. D. Malasarn, J. R. Keefe and D. K. Newman (2008) *J Bacteriol* 190:135-142.
99. R. van Lis, W. Nitschke, T. P. Warelow, L. Capowiez, J. M. Santini and B. Schoepp-Cothenet (2012) *Biochim Biophys Acta, Bioenerg* 1817:1701-1708.
100. F. W. Studier (2005) *Protein Expression and Purification* 41:207-234.
101. M. Sabaty, S. Grosse, G. Adryanczyk, S. Boiry, F. Biaso, P. Arnoux and D. Pignol (2013) *BMC Biochem* 14:28.
102. T. Palmer, C.-L. Santini, C. Iobbi-Nivol, D. J. Eaves, D. H. Boxer and G. Giordano (1996) *Mol Microbiol* 20:875-884.
103. J. F. Alfaro, C. A. Joswig-Jones, W. Ouyang, J. Nichols, G. J. Crouch and J. P. Jones (2009) *Drug Metab Dispos* 37:2393-2398.
104. T. Hartmann, M. Terao, E. Garattini, C. Teutloff, J. F. Alfaro, J. P. Jones and S. Leimkuhler (2012) *Drug Metab Dispos* 40:856-864.
105. M. Mahro, C. Coelho, J. Trincão, D. Rodrigues, M. Terao, E. Garattini, M. Saggi, F. Lendzian, P. Hildebrandt, M. J. Romão and S. Leimkuehler (2011) *Drug Metab Dispos* 39:1939-1945.
106. S. Schumann, M. Terao, E. Garattini, M. Saggi, F. Lendzian, P. Hildebrandt and S. Leimkuhler (2009) *PLoS One* 4:e5348.
107. Z. Marelja, M. Dambowsky, M. Bolis, M. L. Georgiou, E. Garattini, F. Missirlis and S. Leimkuehler (2014) *J Exp Biol* 217:2201-2211.
108. J. M. Klein and G. Schwarz (2012) *J Cell Sci* 125:4876-4885.
109. S. Leimkuhler and K. V. Rajagopalan (2001) *J Biol Chem* 276:1837-1844.
110. C. Feng, H. L. Wilson, J. K. Hurley, J. T. Hazzard, G. Tollin, K. V. Rajagopalan and J. H. Enemark (2003) *J Biol Chem* 278:2913-2920.
111. H. L. Wilson, S. R. Wilkinson and K. V. Rajagopalan (2006) *Biochemistry* 45:2149-2160.

112. N. Schrader, K. Fischer, K. Theis, R. R. Mendel, G. Schwarz and C. Kisker (2003) *Structure* 11:1251-1263.
113. B. Wahl, D. Reichmann, D. Nicks, N. Krompholz, A. Havemeyer, B. Clement, T. Messerschmidt, M. Rothkegel, H. Biester, R. Hille, R. R. Mendel and F. Bittner (2010) *J Biol Chem* 285:37847-37859.
114. J. Kotthaus, B. Wahl, A. Havemeyer, J. Kotthaus, D. Schade, D. Garbe-Schoenberg, R. Mendel, F. Bittner and B. Clement (2011) *Biochem J* 433:383-391.
115. J. Yang, L. J. Giles, C. Ruppelt, R. R. Mendel, F. Bittner and M. L. Kirk (2015) *J Am Chem Soc* 137:5276-5279.
116. J. J. Truglio, K. Theis, S. Leimkuhler, R. Rappa, K. V. Rajagopalan and C. Kisker (2002) *Structure* 10:115-125.
117. S. Leimkuehler, R. Hodson, G. N. George and K. V. Rajagopalan (2003) *J Biol Chem* 278:20802-20811.
118. K. F. Aguey-Zinsou, P. V. Bernhardt and S. Leimkuehler (2003) *J Am Chem Soc* 125:15352-15358.
119. S. Leimkuhler, A. L. Stockert, K. Igarashi, T. Nishino and R. Hille (2004) *J Biol Chem* 279:40437-40444.
120. M. Neumann, G. Mittelstaedt, C. Iobbi-Nivol, M. Saggu, F. Lendzian, P. Hildebrandt and S. Leimkuehler (2009) *FEBS J* 276:2762-2774.
121. A. Di Salle, G. D'Errico, F. La Cara, R. Cannio and M. Rossi (2006) *Extremophiles* 10:587-598.
122. L. Low, K. J. Ryan, V. B. Paul and K. Ulrike (2011) *Front Microbiol* 2:58.
123. S. Robin, M. Arese, E. Forte, P. Sarti, A. Giuffre and T. Soulimane (2011) *J Bacteriol* 193:3988-3997.
124. K. G. V. Havelius, S. Reschke, S. Horn, A. Doring, D. Nicks, R. Hille, C. Schulzke, S. Leimkuhler and M. Haumann (2011) *Inorg Chem* 50:741-748.
125. Y. Zhang, S. Rump and V. N. Gladyshev (2011) *Coord Chem Rev* 255:1206-1217.
126. P. Kaufmann, B. R. Duffus, B. Mitrova, C. Iobbi-Nivol, C. Teutloff, M. Nimtz, L. Jaensch, U. Wollenberger and S. Leimkuehler (2018) *Biochemistry* 57:1130-1143.
127. N. V. Ivanov, M. Trani and D. E. Edmondson (2004) *Protein Expression Purif* 37:72-82.
128. J. Arnau, C. Lauritzen, G. E. Petersen and J. Pedersen (2006) *Protein Expression Purif* 48:1-13.

129. H. Yu, H. Tang, Y. Li and P. Xu (2015) *Appl Environ Microbiol* 81:8330-8338.
130. C. Coelho, P. J. Gonzalez, J. G. Moura, I. Moura, J. Trincao and M. J. Romao (2011) *J Mol Biol* 408:932-948.
131. S. Leimkühler, O. N. Lemaire and C. Iobbi-Nivol (2017) *Molybdenum and tungsten enzymes: Biochemistry. The Royal Society of Chemistry*, pp. 117-142.
132. O. Genest, M. Neumann, F. Seduk, W. Stoecklein, V. Mejean, S. Leimkuehler and C. Iobbi-Nivol (2008) *J Biol Chem* 283:21433-21440.
133. J. M. Dow, F. Gabel, F. Sargent and T. Palmer (2013) *Biochem J* 452:57-66.
134. M. Neumann and S. Leimkuehler (2008) *FEBS J* 275:5678-5689.
135. V. V. Pollock and M. J. Barber (2000) *J Biol Chem* 275:35086-35090.
136. G. G. Barbier, R. C. Joshi, E. R. Campbell and W. H. Campbell (2004) *Protein Expression Purif* 37:61-71.
137. S.-A. Freibert, B. D. Weiler, U. Muhlenhoff, E. Bill, A. J. Pierik and R. Lill (2018) *Methods Enzymol* 599:197-226.
138. D. P. Barupala, S. P. Dzul, P. J. Riggs-Gelasco and T. L. Stemmler (2016) *Arch Biochem Biophys* 592:60-75.
139. D. C. Johnson, D. R. Dean, A. D. Smith and M. K. Johnson (2005) *Annu Rev Biochem* 74:247-281.
140. M. Buehning, A. Valleriani and S. Leimkuehler (2017) *Biochemistry* 56:1987-2000.
141. N. Tanaka, M. Kanazawa, K. Tonosaki, N. Yokoyama, T. Kuzuyama and Y. Takahashi (2016) *Mol Microbiol* 99:835-848.
142. J. N. Agar, C. Krebs, J. Frazzon, B. H. Huynh, D. R. Dean and M. K. Johnson (2000) *Biochemistry* 39:7856-7862.
143. H. Huang, L. Hu, W. Yu, H. Li, F. Tao, H. Xie and S. Wang (2016) *Protein Expression Purif* 121:1-8.
144. Y. Takahashi and M. Nakamura (1999) *J Biochem* 126:917-926.
145. M. Nakamura, K. Saeki and Y. Takahashi (1999) *J Biochem* 126:10-18.
146. J. Liu, S. Chakraborty, P. Hosseinzadeh, Y. Yu, S. Tian, I. Petrik, A. Bhagi and Y. Lu (2014) *Chem Rev (Washington, DC, U S)* 114:4366-4469.
147. H. Sjuts, K. Fisher, M. S. Dunstan, S. E. Rigby and D. Leys (2012) *Protein Expression Purif* 85:224-229.

148. C. Wachnowsky, B. Rao, S. Sen, B. Fries, C. J. Howard, J. J. Ottesen and J. A. Cowan (2019) *JBIC, J Biol Inorg Chem* 24:1035-1045.
149. H. A. Dailey, T. A. Dailey, S. Gerdes, D. Jahn, M. Jahn, M. R. O'Brian and M. J. Warren (2017) *Microbiol Mol Biol Rev* 81:e00048-00016/00041-e00048-00016/00062.
150. K. Fiege, C. J. Querebillo, P. Hildebrandt and N. Frankenberg-Dinkel (2018) *Biochemistry* 57:2747-2755.
151. F. W. Krainer, S. Capone, M. Jäger, T. Vogl, M. Gerstmann, A. Glieder, C. Herwig and O. Spadiut (2015) *Microbial Cell Factories* 14:4.
152. A. F. Verissimo and F. Daldal (2014) *Biochim Biophys Acta* 1837:989-998.
153. R. K. J. Olsen, E. Konarikova, T. Schwarzmayr, T. B. Haack, T. Meitinger, T. M. Strom, H. Prokisch, T. A. Giancaspero, P. Leone, S. Mosegaard, J. Palmfeldt, N. Gregersen, V. Boczonadi, A. Pyle, R. Horvath, L. Matakovic, R. G. Feichtinger, J. A. Mayr, A. Veauville-Merllie, C. Vianey-Saban, C. Acquaviva, C. Terrile, E. Graf, M. Auranen, M. Galluccio, A. Imbard, P. Gutierrez-Rios, M. Oppenheim, M. Schiff, S. Pichard, O. Rigal, P. F. Chinnery, V. Konstantopoulou, D. Moslinger, B. Talim, S. Gucer, H. Topaloglu, T. Coskun, A. Botta, E. Pegoraro, A. Malena, L. Vergani, D. Mazza, M. Zollino, D. Ghezzi, T. Tyni, A. Boneh and M. Barile (2016) *Am J Hum Genet* 98:1130-1145.
154. C. A. Abbas and A. A. Sibirny (2011) *Microbiol Mol Biol Rev* 75:321-360.
155. V. Y. Yatsyshyn, D. V. Fedorovych and A. A. Sibirny (2009) *Appl Biochem Microbiol* 45:115-124.
156. C. S. Chan, D. C. Bay, T. G. H. Leach, T. M. L. Winstone, L. Kuzniatsova, V. A. Tran and R. J. Turner (2014) *Biochim Biophys Acta, Biomembr* 1838:2971-2984.
157. I. J. Oresnik, C. L. Ladner and R. J. Turner (2001) *Mol Microbiol* 40:323-331.
158. K. Hatzixanthis, T. A. Clarke, A. Oubrie, D. J. Richardson, R. J. Turner and F. Sargent (2005) *Proc Natl Acad Sci U S A* 102:8460-8465.
159. C. S. Chan, T. M. L. Winstone, L. Chang, C. M. Stevens, M. L. Workentine, H. Li, Y. Wei, M. J. Ondrechen, M. Paetzel and R. J. Turner (2008) *Biochemistry* 47:2749-2759.
160. J. Maillard, C. A. E. M. Spronk, G. Buchanan, V. Lyall, D. J. Richardson, T. Palmer, G. W. Vuister and F. Sargent (2007) *Proc Natl Acad Sci U S A* 104:15641-15646.
161. R. Freudl and R. Freudl (2018) *Microb Cell Fact* 17:52.
162. P. Natale, T. Brueser and A. J. M. Driessen (2008) *Biochim Biophys Acta, Biomembr* 1778:1735-1756.
163. K. Segers and J. Anne (2011) *Chem Biol (Cambridge, MA, U S)* 18:685-698.

164. P. A. Lee, D. Tullman-Ercek and G. Georgiou (2006) *Annu Rev Microbiol* 60:373-395.
165. J. H. Choi and S. Y. Lee (2004) *Appl Microbiol Biotechnol* 64:625-635.
166. J. P. Ridge, K.-F. Aguey-Zinsou, P. V. Bernhardt, I. M. Brereton, G. R. Hanson and A. G. McEwan (2002) *Biochemistry* 41:15762-15769.
167. M. Sabaty, C. Avazeri, D. Pignol and A. Vermeglio (2001) *Appl Environ Microbiol* 67:5122-5126.
168. P. Arnoux, M. Sabaty, J. Alric, B. Frangioni, B. Guigliarelli, J.-M. Adriano and D. Pignol (2003) *Nat Struct Biol* 10:928-934.
169. J. Grove, S. Tanapongpipat, G. Thomas, L. Griffiths, H. Crooke and J. Cole (1996) *Mol Microbiol* 19:467-481.
170. T. Hettmann, R. A. Siddiqui, J. von Langen, C. Frey, M. J. Romao and S. Diekmann (2003) *Biochem Biophys Res Commun* 310:40-47.
171. U. Kappler and A. G. McEwan (2002) *FEBS Lett* 529:208-214.
172. C. Peng, C. Shi, X. Cao, Y. Li, F. Liu and F. Lu (2019) *Frontiers in Bioengineering and Biotechnology* 7.
173. A. Karyolaimos, H. Ampah-Korsah, T. Hillenaar, A. Mestre Borrás, K. M. Dolata, S. Sievers, K. Riedel, R. Daniels and J.-W. de Gier (2019) *Frontiers in Microbiology* 10.
174. S. MacIntyre, R. Freudl, M. Degen, I. Hindennach and U. Henning (1987) *J Biol Chem* 262:8416-8422.
175. J. Frobel, P. Rose and M. Muller (2012) *Philos Trans R Soc Lond B Biol Sci* 367:1029-1046.
176. F. J. M. Mergulhão, D. K. Summers and G. A. Monteiro (2005) *Biotechnology Advances* 23:177-202.
177. F. Bittner, M. Oreb and R. R. Mendel (2001) *J Biol Chem* 276:40381-40384.
178. M. Zarepour, K. Simon, M. Wilch, U. Nielaender, T. Koshiba, M. Seo, T. Lindel and F. Bittner (2012) *Plant Mol Biol* 80:659-671.
179. H. Koiwai, S. Akaba, M. Seo, T. Komano and T. Koshiba (2000) *J Biochem* 127:659-664.
180. A. Foti, T. Hartmann, C. Coelho, T. Santos-Silva, M. J. Romao and S. Leimkuehler (2016) *Drug Metab Dispos* 44:1277-1285.
181. T. Asakawa, K. Itoh, M. Adachi, K. Hoshino, N. Watanabe and Y. Tanaka (2008) *Biol Pharm Bull* 31:380-385.

182. K. Hoshino, K. Itoh, A. Masubuchi, M. Adachi, T. Asakawa, N. Watanabe, T. Kosaka and Y. Tanaka (2007) *Biol Pharm Bull* 30:1191-1198.
183. K. Itoh, T. Asakawa, K. Hoshino, M. Adachi, K. Fukiya, N. Watanabe and Y. Tanaka (2009) *Biol Pharm Bull* 32:31-35.
184. K. Fukiya, K. Itoh, S. Yamaguchi, A. Kishiba, M. Adachi, N. Watanabe and Y. Tanaka (2010) *Drug Metab Dispos* 38:302-307.
185. M. Terao, M. Kurosaki, G. Saltini, S. Demontis, M. Marini, M. Salmona and E. Garattini (2000) *J Biol Chem* 275:30690-30700.
186. M. Kurosaki, M. Terao, M. M. Barzago, A. Bastone, D. Bernardinello, M. Salmona and E. Garattini (2004) *J Biol Chem* 279:50482-50498.
187. M. Kurosaki, S. Demontis, M. M. Barzago, E. Garattini and M. Terao (1999) *Biochem J* 341 (Pt 1):71-80.
188. P. Mu, M. Zheng, M. Xu, Y. Zheng, X. Tang, Y. Wang, K. Wu, Q. Chen, L. Wang and Y. Deng (2014) *Drug Metab Dispos* 42:511-519, 519 pp..
189. M. Adachi, K. Itoh, A. Masubuchi, N. Watanabe and Y. Tanaka (2007) *J Biochem Mol Biol* 40:1021-1027.
190. C. Hesberg, R. Haensch, R. R. Mendel and F. Bittner (2004) *J Biol Chem* 279:13547-13554.
191. Y. Kuwabara, T. Nishino, K. Okamoto, T. Matsumura, B. T. Eger, E. F. Pai and T. Nishino (2003) *Proc Natl Acad Sci U S A* 100:8170-8175.
192. B. Adams, D. J. Lowe, A. T. Smith, C. Scazzocchio, S. Demais and R. C. Bray (2002) *Biochem J* 362:223-229.
193. M. Saksela and K. O. Raivio (1996) *Biochem J* 315:235-239.
194. S. G. Kozmin, P. Leroy, Y. I. Pavlov and R. M. Schaaper (2008) *Mol Microbiol* 68:51-65.
195. M. A. Fini, D. Orchard-Webb, B. Kosmider, J. D. Amon, R. Kelland, G. Shibao and R. M. Wright (2008) *J Cell Biochem* 105:1008-1026.
196. C. Chen, G. Cheng, H. Hao, M. Dai, X. Wang, L. Huang, Z. Liu and Z. Yuan (2013) *PLoS One* 8:e73912.
197. T. Nishino, Y. Amaya, S. Kawamoto, Y. Kashima, K. Okamoto and T. Nishino (2002) *J Biochem* 132:597-606.
198. T. Nishino, K. Okamoto, Y. Kawaguchi, H. Hori, T. Matsumura, B. T. Eger, E. F. Pai and T. Nishino (2005) *J Biol Chem* 280:24888-24894.

199. A. Chamizo-Ampudia, A. Galvan, E. Fernandez and A. Llamas (2017) *Int J Mol Sci* 18:670/671-670/618.
200. J. Schneider, U. Girreser, A. Havemeyer, F. Bittner and B. Clement (2018) *Chem Res Toxicol* 31:447-453.
201. N. Krompholz, C. Krischkowski, D. Reichmann, D. Garbe-Schoenberg, R.-R. Mendel, F. Bittner, B. Clement and A. Havemeyer (2012) *Chem Res Toxicol* 25:2443-2450.
202. W. Su, S. C. Huber and N. M. Crawford (1996) *Plant Cell* 8:519-527.
203. W. Su, J. A. Mertens, K. Kanamaru, W. H. Campbell and N. M. Crawford (1997) *Plant Physiol* 115:1135-1143.
204. L. Skipper, W. H. Campbell, J. A. Mertens and D. J. Lowe (2001) *J Biol Chem* 276:26995-27002.
205. J. A. Mertens, N. Shiraishi and W. H. Campbell (2000) *Plant Physiol* 123:743-756.
206. C. M. Pieterse, K. J. van't, d. B.-V. G. C. van and F. Govers (1995) *Curr Genet* 27:359-366.
207. K. Fischer, G. G. Barbier, H.-J. Hecht, R. R. Mendel, W. H. Campbell and G. Schwarz (2005) *Plant Cell* 17:1167-1179.
208. G. G. Barbier and W. H. Campbell (2005) *J Biol Chem* 280:26049-26054.
209. T. Eilers, G. Schwarz, H. Brinkmann, C. Witt, T. Richter, J. Nieder, B. Koch, R. Hille, R. Hansch and R. R. Mendel (2001) *J Biol Chem* 276:46989-46994.
210. P. Kalimuthu, A. A. Belaidi, G. Schwarz and P. V. Bernhardt (2017) *ChemElectroChem* 4:947-956.
211. B. Preuss, C. Berg, F. Altenberend, M. Gregor, S. Stevanovic and R. Klein (2007) *Clin Exp Immunol* 150:312-321.
212. J. Wang, J. Tejero, C. Sparacino-Watkins, L. Wang, V. Ragireddy, S. Frizzell, E. E. Kelley, M. T. Gladwin, J. Wang, J. Tejero, C. Sparacino-Watkins, L. Wang, V. Ragireddy, S. Frizzell, Y. Zhang, M. T. Gladwin, S. Krizowski, K. Fischer-Schrader, G. Schwarz, D. Nicks, R. Hille, E. E. Kelley and P. Basu (2015) *Antioxid Redox Signal* 23:283-294.
213. M. A. S. Correia, A. R. Otrelo-Cardoso, V. Schwuchow, K. G. V. Sigfridsson Clauss, M. Haumann, M. J. Romao, S. Leimkuhler and T. Santos-Silva (2016) *ACS Chem Biol* 11:2923-2935.
214. A. Yasuhara, M. Akiba-Goto and K. Aisaka (2005) *Biosci, Biotechnol, Biochem* 69:2435-2438.

215. I. M. Scott, G. M. Rubinstein, G. L. Lipscomb, M. Basen, G. J. Schut, A. M. Rhaesa, W. A. Lancaster, F. L. Poole, 2nd, M. W. W. Adams and R. M. Kelly (2015) *Appl Environ Microbiol* 81:7339-7347.
216. I. Israel, M. Sohni and S. Fetzner (2002) *FEMS Microbiol Lett* 210:123-127.
217. J. I. Jimenez, A. Canales, J. Jimenez-Barbero, K. Ginalski, L. Rychlewski, J. L. Garcia and E. Diaz (2008) *Proc Natl Acad Sci U S A* 105:11329-11334.
218. S. Doi, Y. Hashimoto, C. Tomita, T. Kumano and M. Kobayashi (2016) *Sci Rep* 6:38021.
219. K. Parschat, B. Hauer, R. Kappl, R. Kraft, J. Huttermann and S. Fetzner (2003) *J Biol Chem* 278:27483-27494.
220. U. Frerichs-Deeken, B. Goldenstedt, R. Gahl-Janssen, R. Kappl, J. Huttermann and S. Fetzner (2003) *Eur J Biochem* 270:1567-1577.
221. M. Blase, C. Bruntner, B. Tshisuaka, S. Fetzner and F. Lingens (1996) *J Biol Chem* 271:23068-23079.
222. C. Dong, J. Yang, M. L. Kirk, S. Reschke and S. Leimkuhler (2017) *Inorg Chem* 56:6830-6837.
223. S. Reschke, S. Mebs, K. G. V. Sigfridsson-Clauss, R. Kositzki, S. Leimkuehler and M. Haumann (2017) *Inorg Chem* 56:2165-2176.
224. G. D'Errico, A. Di Salle, F. La Cara, M. Rossi and R. Cannio (2006) *J Bacteriol* 188:694-701.
225. N. R. Glasser, D. K. Newman, P. H. Oyala, T. H. Osborne, J. M. Santini and D. K. Newman (2018) *Proc Natl Acad Sci U S A*, .
226. C. Jacoby, J. Eipper, M. Warnke, O. Tiedt, M. Mergelsberg, M. Boll, H.-J. Stark, B. Daus, Z. Martin-Moldes, M. T. Zamarro and E. Diaz (2018) *MBio* 9.
227. J. H. Weiner, G. Shaw, R. J. Turner and C. A. Trieber (1993) *J Biol Chem* 268:3238-3244.
228. R. A. Rothery and J. H. Weiner (1993) *Biochemistry* 32:5855-5861.
229. R. A. Rothery and J. H. Weiner (1991) *Biochemistry* 30:8296-8305.
230. P. A. Cotter and R. P. Gunsalus (1989) *J Bacteriol* 171:3817-3823.
231. S. Witthoff, L. Eggeling, M. Bott and T. Polen (2012) *Microbiology (Reading, U K)* 158:2428-2439.
232. M. Ihara, Y. Kawano, Y. Fujiwara, T. Kodo, M. Mizuguchi, Y. Mochiduki, K. Kodoh, A. Okabe and I. Matsuno (2015) *J Photochem Photobiol, A* 313:154-162.

233. A. Bassegoda, C. Madden, D. W. Wakerley, E. Reisner and J. Hirst (2014) *J Am Chem Soc* 136:15473-15476.
234. W. E. Robinson, A. Bassegoda, E. Reisner and J. Hirst (2017) *J Am Chem Soc* 139:9927-9936.
235. F. Zinoni, A. Birkmann, T. C. Stadtman and A. Boeck (1986) *Proc Natl Acad Sci U S A* 83:4650-4654.
236. A. P. Shuber, E. C. Orr, M. A. Recny, P. F. Schendel, H. D. May, N. L. Schauer and J. G. Ferry (1986) *J Biol Chem* 261:12942-12947.
237. M. Bokranz, M. Gutmann, C. Kortner, E. Kojro, F. Fahrenholz, F. Lauterbach and A. Kroger (1991) *Arch Microbiol* 156:119-128.
238. S.-Y. Wu, R. A. Rothery and J. H. Weiner (2015) *J Biol Chem* 290:25164-25173.
239. M. Seif Eddine, F. Biaso, R. Arias-Cartin, E. Pilet, J. Rendon, S. Lyubenova, F. Seduk, B. Guigliarelli, A. Magalon and S. Grimaldi (2017) *ChemPhysChem*, doi 10.1002/cphc.201700571: Ahead of Print.
240. J. Rendon, F. Biaso, P. Ceccaldi, R. Toci, F. Seduk, A. Magalon, B. Guigliarelli and S. Grimaldi (2017) *Inorg Chem*, doi 10.1021/acs.inorgchem.6b03129: Ahead of Print.
241. R. Arias-Cartin, P. Ceccaldi, J.-M. Blanc, A. Walburger, A. Magalon, P. Ceccaldi, B. Schoepp-Cothenet, B. Guigliarelli, S. Grimaldi, K. Frick, T. Friedrich and V. Receveur-Brechot (2016) *Sci Rep* 6:37743.
242. J. Buc, C. L. Santini, F. Blasco, R. Giordani, M. L. Cardenas, M. Chippaux, A. Cornish-Bowden and G. Giordano (1995) *Eur J Biochem* 234:766-772.
243. B. Guigliarelli, A. Magalon, M. Asso, P. Bertrand, C. Frixon, G. Giordano and F. Blasco (1996) *Biochemistry* 35:4828-4836.
244. P. Lanciano, A. Magalon, P. Bertrand, B. Guigliarelli and S. Grimaldi (2007) *Biochemistry* 46:5323-5329.
245. R. A. Rothery, M. G. Bertero, R. Cammack, M. Palak, F. Blasco, N. C. Strynadka and J. H. Weiner (2004) *Biochemistry* 43:5324-5333.
246. A. Magalon, D. Lemesle-Meunier, R. A. Rothery, C. Frixon, J. H. Weiner and F. Blasco (1997) *J Biol Chem* 272:25652-25658.
247. F. Blasco, J. Pommier, V. Augier, M. Chippaux and G. Giordano (1992) *Mol Microbiol* 6:221-230.
248. B. Guigliarelli, M. Asso, C. More, V. Augier, F. Blasco, J. Pommier, G. Giordano and P. Bertrand (1992) *Eur J Biochem* 207:61-68.

- 249. C. Iobbi, C. L. Santini, V. Bonnefoy and G. Giordano (1987) *Eur J Biochem* 168:451-459.
- 250. K. Itoh, A. Masubuchi, T. Sasaki, M. Adachi, N. Watanabe, K. Nagata, Y. Yamazoe, M. Hiratsuka, M. Mizugaki and Y. Tanaka (2007) *Drug Metab Dispos* 35:734-739.
- 251. W. A. Doyle, J. F. Burke, A. Chovnick, F. L. Dutton, J. R. S. Whittle and R. C. Bray (1996) *Eur J Biochem* 239:782-795.
- 252. T. A. Krenitsky, T. Spector and W. W. Hall (1986) *Arch Biochem Biophys* 247:108-119.
- 253. V. Massey, P. E. Brumby and H. Komai (1969) *J Biol Chem* 244:1682-1691.
- 254. T. Saito and T. Nishino (1989) *J Biol Chem* 264:10015-10022.
- 255. M. G. Redinbaugh and W. H. Campbell (1985) *J Biol Chem* 260:3380-3385.
- 256. L. P. Solomonson, G. H. Lorimer, R. L. Hall, R. Borchers and J. L. Bailey (1975) *J Biol Chem* 250:4120-4127.
- 257. M. J. Barber and B. A. Notton (1990) *Plant Physiol* 93:537-540.
- 258. M. S. Brody and R. Hille (1995) *Biochim Biophys Acta, Protein Struct Mol Enzymol* 1253:133-135.
- 259. H. J. Cohen and I. Fridovich (1971) *J Biol Chem* 246:359-366.
- 260. M. Lehmann, B. Tshisuaka, S. Fetzner, P. Roeger and F. Lingens (1994) *J Biol Chem* 269:11254-11260.
- 261. R. Bauder, B. Tshisuaka and F. Lingens (1990) *Biol Chem Hoppe-Seyler* 371:1137-1144.
- 262. Q. Xiang and D. E. Edmondson (1996) *Biochemistry* 35:5441-5450.
- 263. J. J. Wilson and U. Kappler (2009) *Biochim Biophys Acta, Bioenerg* 1787:1516-1525.
- 264. U. Kappler, B. Bennett, J. Rethmeier, G. Schwarz, R. Deutzmann, A. G. McEwan and C. Dahl (2000) *J Biol Chem* 275:13202-13212.
- 265. J. M. Santini and R. N. vanden Hoven (2004) *J Bacteriol* 186:1614-1619.
- 266. T. Krafft and J. M. Macy (1998) *Eur J Biochem* 255:647-653.
- 267. E. Afkar, J. Lisak, C. Saltikov, P. Basu, R. S. Oremland and J. F. Stolz (2003) *FEMS Microbiol Lett* 226:107-112.
- 268. T. Reda, C. M. Plugge, N. J. Abram and J. Hirst (2008) *Proc Natl Acad Sci U S A* 105:10654-10658.

269. F. A. M. de Bok, P.-L. Hagedoorn, P. J. Silva, W. R. Hagen, E. Schiltz, K. Fritsche and A. J. M. Stams (2003) *Eur J Biochem* 270:2476-2485.
270. S. A. Bursakov, C. Carneiro, M. J. Almendra, R. O. Duarte, J. Caldeira, I. Moura and J. J. G. Moura (1997) *Biochem Biophys Res Commun* 239:816-822.
271. B. Lledo, R. M. Martinez-Espinosa, F. C. Marhuenda-Egea and M. J. Bonete (2004) *Biochim Biophys Acta, Gen Subj* 1674:50-59.
272. S. H. Kim, S. H. Song and Y. J. Yoo (2006) *Biotechnol Bioprocess Eng* 11:32-37.
273. P. A. Straat and A. Nason (1965) *J Biol Chem* 240:1412-1426.
274. S. Afshar, E. Johnson, S. De Vries and I. Schroder (2001) *J Bacteriol* 183:5491-5495.
275. M. G. Guerrero, J. M. Vega, E. Leadbetter and M. Losada (1973) *Arch Mikrobiol* 91:287-304.
276. S. Thaivanich and A. Incharoensakdi (2007) *World J Microbiol Biotechnol* 23:85-92.
277. R. Blasco, F. Castillo and M. Martinez-Luque (1997) *FEBS Lett* 414:45-49.
278. R. M. Martinez-Espinosa, F. C. Marhuenda-Egea and M. J. Bonete (2001) *FEMS Microbiol Lett* 204:381-385.
279. J.-P. Dos Santos, C. Iobbi-Nivol, C. Couillault, G. Giordano and V. Mejean (1998) *J Mol Biol* 284:421-433.
280. P. T. Bilous and J. H. Weiner (1988) *J Bacteriol* 170:1511-1518.
281. E. J. Dridge and C. S. Butler (2010) *Biochimie* 92:1268-1273.
282. A. Bowen, F. Theis and J. M. Macy (2000) *DNA Sequence* 10:365-377.
283. K. S. Bender, C. Shang, R. Chakraborty, S. M. Belchik, J. D. Coates and L. A. Achenbach (2005) *J Bacteriol* 187:5090-5096.
284. H. D. Thorell, K. Stenklo, J. Karlsson and T. Nilsson (2003) *Appl Environ Microbiol* 69:5585-5592.
285. K. Zargar, A. Conrad, D. L. Bernick, T. M. Lowe, V. Stolc, S. Hoeft, R. S. Oremland, J. Stolz and C. W. Saltikov (2012) *Environ Microbiol* 14:1635-1645.
286. C. Richey, P. Chovanec, S. Hoeft McCann, R. Oremland, P. Basu and J. Stolz (2009) *Biochemical and Biophysical Research Communications* 382:298-302.
287. C. A. McDevitt, P. Hugenholtz, G. R. Hanson and A. G. McEwan (2002) *Mol Microbiol* 44:1575-1587.

288. R. Rabus, M. Kube, A. Beck, F. Widdel and R. Reinhardt (2002) *Arch Microbiol* 178:506-516.
289. M. Neumann, F. Seduk, C. Iobbi-Nivol and S. Leimkuhler (2011) *J Biol Chem* 286:1400-1408.
290. A. R. Otrelo-Cardoso, V. Schwuchow, D. Rodrigues, E. J. Cabrita, S. Leimkuhler, M. J. Romao and T. Santos-Silva (2014) *PLoS One* 9:e87295.
291. F. Blasco, C. Iobbi, J. Ratouchniak, V. Bonnefoy and M. Chippaux (1990) *MGG, Mol Gen Genet* 222:104-111.
292. G. Thomas, L. Potter and J. A. Cole (1999) *FEMS Microbiol Lett* 174:167-171.
293. M. Kern, A. M. Mager and J. Simon (2007) *Microbiology* 153:3739–3747.
294. M. S. Pittman, K. T. Elvers, L. Lee, M. A. Jones, R. K. Poole, S. F. Park and D. J. Kelly (2007) *Molecular Microbiology* 63:575-590.
295. R. K. Thauer, K. Jungermann and K. Decker (1977) *Bacteriol Rev* 41:100-180.
296. T. Hartmann, N. Schwanhold and S. Leimkuehler (2015) *Biochim Biophys Acta, Proteins Proteomics* 1854:1090-1100.
297. L. Ma, L. Hu, X. Feng and S. Wang (2018) *Aging Dis* 9:938-945.
298. Z. Kalaycioglu and F. B. Erim (2019) *J Agric Food Chem* 67:7205-7222.
299. M. H. Ward, R. R. Jones, J. D. Brender, K. T. M. de, B. S. G. van, P. J. Weyer, B. T. Nolan, C. M. Villanueva, C. M. Villanueva, C. M. Villanueva and C. M. Villanueva (2018) *Int J Environ Res Public Health* 15.
300. L. Knobeloch, B. Salna, A. Hogan, J. Postle and H. Anderson (2000) *Environ Health Perspect* 108:675-678.
301. J. O. Lundberg, M. Carlstrom and E. Weitzberg (2018) *Cell Metab* 28:9-22.
302. C. Sparacino-Watkins (2011) *Chemistry and Biochemistry*. Duquesne University, Pittsburgh, PA, pp. 252.
303. D. Hofreuter (2014) *Front Cell Infect Microbiol* 4:137.
304. M. E. Konkel, J. E. Christensen, A. S. Dhillon, A. B. Lane, R. Hare-Sanford, D. M. Schaberg and C. L. Larson (2007) *Applied and environmental microbiology* 73:2297-2305.
305. B. Mintmier, J. M. McGarry, P. Basu, C. Sparacino-Watkins, J. Sallmen, J. R. McCormick, J. F. Stolz, K. Fischer-Schrader, G. Schwarz, A. Magalon and D. J. Bain (2018) *FEMS Microbiol Lett*, .

306. A. Brige, D. Leys, T. E. Meyer, M. A. Cusanovich and J. J. Van Beeumen (2002) *Biochemistry* 41:4827-4836.
307. C. S. Butler, S. J. Ferguson, B. C. Berks, A. J. Thomson, M. R. Cheesman and D. J. Richardson (2001) *FEBS Lett* 500:71-74.
308. P. J. L. Simpson, A. A. McKinzie and R. Codd (2010) *Biochem Biophys Res Commun* 398:13-18.
309. J. Dias, M. Than, A. Humm, G. P. Bourenkov, H. D. Bartunik, S. Bursakov, J. Calvete, J. Caldeira, C. Carneiro, J. J. Moura, I. Moura and M. J. Romao (1999) *Structure (London)* 7:65-79.
310. S. Najmudin, P. J. Gonzalez, J. Trincao, C. Coelho, A. Mukhopadhyay, N. M. F. S. A. Cerqueira, C. C. Romao, I. Moura, J. J. G. Moura, C. D. Brondino and M. J. Romao (2008) *JBIC, J Biol Inorg Chem* 13:737-753.
311. P. J. L. Simpson, D. J. Richardson and R. Codd (2010) *Microbiology (Reading, U K)* 156:302-312.
312. M. Kern and J. Simon (2009) *Biochim Biophys Acta, Bioenerg* 1787:646-656.
313. T. H. C. Brondijk, A. Nilavongse, N. Filenko, D. J. Richardson and J. A. Cole (2004) *Biochem J* 379:47-55.
314. J. Simon, M. Saenger, S. C. Schuster and R. Gross (2003) *Mol Microbiol* 49:69-79.
315. D. Li and R. Roberts (2001) *Cell Mol Life Sci* 58:2085-2097.
316. J. M. Dow, S. Grahl, R. Ward, R. Evans, O. Byron, D. G. Norman, T. Palmer and F. Sargent (2014) *FEBS J* 281:246-260.
317. S. Grahl, J. Maillard, C. A. E. M. Spronk, G. W. Vuister and F. Sargent (2012) *Mol Microbiol* 83:1254-1267.
318. K. Hatzixanthis, T. A. Clarke, A. Oubrie, D. J. Richardson, R. J. Turner and F. Sargent (2005) *Proceedings of the National Academy of Sciences of the United States of America* 102:8460-8465.
319. L. Bedzyk, T. Wang and R. W. Ye (1999) *Journal of Bacteriology* 181:2802-2806.
320. A. Latta (2019) *Chemistry and Chemical Biology*. Indiana University-Purdue University Indianapolis, Indianapolis, IN, pp. 150.
321. M. Lewis (2011) *J Mol Biol* 409:14-27.
322. T. Watanabe and K. Honda (1982) *J Phys Chem* 86:2617-2619.
323. J. A. Thomas (2016) *Chemistry and Biochemistry*. Duquesne University, Pittsburgh, .

324. G. L. Rosano and E. A. Ceccarelli (2014) *Front Microbiol* 5:172.
325. T. H. Grossman, E. S. Kawasaki, S. R. Punreddy and M. S. Osburne (1998) *Gene* 209:95-103.
326. N. M. Cerqueira, P. J. Gonzalez, C. D. Brondino, M. J. Romao, C. C. Romao, I. Moura and J. J. Moura (2009) *J Comput Chem* 30:2466-2484.
327. Y. Nicolet, R. Rohac, L. Martin and J. C. Fontecilla-Camps (2013) *Proc Natl Acad Sci U S A* 110:7188-7192, S7188/7181-S7188/7186.
328. E. Stellwagen, J. D. Prantner and N. C. Stellwagen (2008) *Anal Biochem* 373:407-409.
329. B. Mintmier, J. M. McGarry, C. E. Sparacino-Watkins, J. Sallmen, K. Fischer-Schrader, A. Magalon, J. R. McCormick, J. F. Stolz, G. Schwarz, D. J. Bain and P. Basu (2018) *FEMS Microbiol Lett* 365:fny151.
330. R. J. Turner, A. L. Papish and F. Sargent (2004) *Can J Microbiol* 50:225-238.
331. F. Sargent, B. C. Berks and T. Palmer (2006) *FEMS Microbiol Lett* 254:198-207.
332. B. Hou and T. Brueser (2011) *Biomol Concepts* 2:507-523.
333. F. Sargent (2007) *Microbiology* (Reading, U K) 153:633-651.
334. T. J. Johnson, J. M. Shank and J. G. Johnson (2017) *Front Microbiol* 8:487.
335. W. C. L. Fischer, D. Sack and R. E. Black (2010) *PLoS Negl Trop Dis* 4:e768.
336. S. Backert and D. Hofreuter (2013) *J Microbiol Methods* 95:8-23.
337. S. V. R. Epps, R. B. Harvey, M. E. Hume, T. D. Phillips, R. C. Anderson and D. J. Nisbet (2013) *Int J Environ Res Public Health* 10:6292-6304, 6213 pp..
338. J. C. Buzby, B. M. Allos and T. Roberts (1997) *The Journal of infectious diseases* 176 Suppl 2:S192-197.
339. X. Liu, B. Gao, V. Novik and J. E. Galan (2012) *PLoS Pathog* 8:e1002562.
340. J. Liu, J. A. Platts-Mills, J. Juma, F. Kabir, J. Nkeze, C. Okoi, D. J. Operario, J. Uddin, S. Ahmed, P. L. Alonso, M. Antonio, S. M. Becker, W. C. Blackwelder, R. F. Breiman, A. S. G. Faruque, B. Fields, J. Gratz, R. Haque, A. Hossain, M. J. Hossain, S. Jarju, F. Qamar, N. T. Iqbal, B. Kwambana, I. Mandomando, T. L. McMurphy, C. Ochieng, J. B. Ochieng, M. Ochieng, C. Onyango, S. Panchalingam, A. Kalam, F. Aziz, S. Qureshi, T. Ramamurthy, J. H. Roberts, D. Saha, S. O. Sow, S. E. Stroup, D. Sur, B. Tamboura, M. Taniuchi, S. M. Tennant, D. Toema, Y. Wu, A. Zaidi, J. P. Nataro, K. L. Kotloff, M. M. Levine and E. R. Houpt (2016) *Lancet* 388:1291-1301.

341. C. Amour, E. Mduma, J. Gratz, E. Svensen, E. T. Rogawski, R. L. Guerrant, E. R. Houpt, J. A. Platts-Mills, M. McGrath, J. C. Seidman, B. J. J. McCormick, S. Shrestha, L. Bodhidatta, A. Samie, P. Bessong, M. Mahfuz, T. Ahmed, S. Qureshi, A. Hotwani, S. Shakoor, S. Babji, G. Kang, D. R. Trigos, A. A. M. Lima, M. Kosek, D. Lang and M. Gottlieb (2016) *Clin Infect Dis* 63:1171-1179.
342. D. S. Powlson, T. M. Addiscott, N. Benjamin, K. G. Cassman, K. T. M. de, G. H. van, J.-L. L'Hirondel, A. A. Avery and K. C. van (2008) *J Environ Qual* 37:291-295.
343. B. M. Pearson, D. J. H. Gaskin, R. P. A. M. Segers, J. M. Wells, P. J. M. Nuijten and A. H. M. van Vliet (2007) *J Bacteriol* 189:8402-8403.
344. C. Sparacino-Watkins, J. F. Stolz and P. Basu (2014) *Chem Soc Rev* 43:676-706.
345. A. A. Crofts, F. M. Poly, C. P. Ewing, J. M. Kuroiwa, J. E. Rimmer, C. Harro, D. Sack, K. R. Talaat, C. K. Porter, R. L. Gutierrez, B. DeNearing, J. Brubaker, R. M. Laird, A. C. Maue, K. Jaep, A. Alcala, D. R. Tribble, M. S. Riddle, A. Ramakrishnan, A. J. McCoy, B. W. Davies, P. Guerry and M. S. Trent (2018) *Nat Microbiol* 3:494-502.
346. R. A. Weingarten, J. L. Grimes and J. W. Olson (2008) *Appl Environ Microbiol* 74:1367-1375.
347. E. R. Hughes, M. G. Winter, B. A. Duerkop, L. Spiga, T. Furtado de Carvalho, W. Zhu, C. C. Gillis, L. Buttner, M. P. Smoot, C. L. Behrendt, S. Cherry, R. L. Santos, L. V. Hooper and S. E. Winter (2017) *Cell Host Microbe* 21:208-219.
348. C. A. Woodall, M. A. Jones, P. A. Barrow, J. Hinds, G. L. Marsden, D. J. Kelly, N. Dorrell, B. W. Wren and D. J. Maskell (2005) *Infect Immun* 73:5278-5285.
349. I. I. Kassem, M. Khatri, M. A. Esseili, Y. M. Sanad, Y. M. Saif, J. W. Olson and G. Rajashekara (2012) *BMC Microbiol* 12:258.
350. C. A. Lopez, F. Rivera-Chavez, M. X. Byndloss and A. J. Baumler (2015) *Infect Immun* 83:3470-3478.
351. W. G. Miller, C. T. Parker, S. Heath and A. J. Lastovica (2007) *BMC Microbiol* 7:11.
352. J. C. Sadana and W. D. McElroy (1957) *Arch Biochem Biophys* 67:16-34.
353. C. Coelho, P. J. Gonzalez, J. Trincao, A. L. Carvalho, S. Najmudin, T. Hettman, S. Dieckman, J. J. G. Moura, I. Moura and M. J. Romao (2007) *Acta Crystallogr, Sect F: Struct Biol Cryst Commun* 63:516-519.
354. B. C. Berks, D. J. Richardson, C. Robinson, A. Reilly, R. T. Aplin and S. J. Ferguson (1994) *Eur J Biochem* 220:117-124.
355. S. Bursakov, M.-Y. Liu, W. J. Payne, J. LeGall, I. Moura and J. J. G. Moura (1995) *Anaerobe* 1:55-60.

356. A. J. Gates, D. J. Richardson and J. N. Butt (2008) *Biochem J* 409:159-168.
357. C. S. Butler, J. M. Charnock, B. Bennett, H. J. Sears, A. J. Reilly, S. J. Ferguson, C. D. Garner, D. J. Lowe, A. J. Thomson, B. C. Berks and D. J. Richardson (1999) *Biochemistry* 38:9000-9012.
358. A. Taoka, K. Yoshimatsu, M. Kanemori and Y. Fukumori (2003) *Can J Microbiol* 49:197-206.
359. S. E. Winter, M. G. Winter, M. N. Xavier, P. Thiennimitr, V. Poon, A. M. Kestra, R. C. Laughlin, G. Gomez, J. Wu, S. D. Lawhon, I. E. Popova, S. J. Parikh, L. G. Adams, R. M. Tsolis, V. J. Stewart and A. J. Bäumler (2013) *Science (Washington, DC, U S)* 339:708-711.
360. M. del Barrio and V. Fourmond (2019) *ChemElectroChem* 6:4949-4962.
361. B. Frangioni, P. Arnoux, M. Sabaty, D. Pignol, P. Bertrand, B. Guigliarelli and C. Leger (2004) *J Am Chem Soc* 126:1328-1329.
362. P. Bertrand, B. Frangioni, S. Dementin, M. Sabaty, P. Arnoux, B. Guigliarelli, D. Pignol and C. Leger (2007) *J Phys Chem B* 111:10300-10311.
363. D. Maratea and R. P. Blakemore (1981) *International Journal of Systematic and Evolutionary Microbiology* 31:452-455.
364. H. Wang, C.-P. Tseng and R. P. Gunsalus (1999) *J Bacteriol* 181:5303-5308.
365. L. C. Potter and J. A. Cole (1999) *Biochemical Journal* 344:69-76.
366. J. Fallingborg (1999) *Danish medical bulletin* 46:183-196.
367. J. C. Wilks and J. L. Slonczewski (2007) *Journal of Bacteriology* 189:5601.
368. G. D. Inglis, L. D. Kalischuk, H. W. Busz and J. P. Kastelic (2005) *Applied and Environmental Microbiology* 71:5145.
369. A. J. Gates, D. J. Richardson and J. N. Butt (2008) *Biochem J* 409:159-168.
370. K. Zeamari, G. Gerbaud, V. Fourmond, F. Biaso, B. Guigliarelli, S. Grosse, P. Arnoux, M. Sabaty, D. Pignol, F. Chaspoul and B. Burlat (2019) *Biochim Biophys Acta Bioenerg.*
371. S. J. Callister, C. D. Nicora, X. Zeng, J. H. Roh, M. A. Dominguez, C. L. Tavano, M. E. Monroe, S. Kaplan, T. J. Donohue, R. D. Smith and M. S. Lipton (2006) *J Microbiol Methods* 67:424-436.
372. V. Fourmond, M. Sabaty, P. Arnoux, P. Bertrand, D. Pignol and C. Leger (2010) *J Phys Chem B* 114:3341-3347.

373. J. G. J. Jacques, B. Burlat, B. Guigliarelli, C. Leger, P. Arnoux, M. Sabaty, D. Pignol and V. Fourmond (2014) *Biochim Biophys Acta*, .
374. R. Hille, J. Hall and P. Basu (2014) *Chem Rev* 114:3963-4038.
375. N. M. F. S. A. Cerqueira, P. A. Fernandes, P. J. Gonzalez, J. J. G. Moura and M. J. Ramos (2013) *Inorg Chem* 52:10766-10772.
376. J. C. Boyington, V. N. Gladyshev, S. V. Khangulov, T. C. Stadtman and P. D. Sun (1997) *Science (Washington, D C)* 275:1305-1308.
377. B. J. N. Jepson, A. Marietou, S. Mohan, J. A. Cole, C. S. Butler and D. J. Richardson (2006) *Biochem Soc Trans* 34:122-126.
378. T. Hettmann, R. A. Siddiqui, C. Frey, T. Santos-Silva, M. J. Romao and S. Diekmann (2004) *Biochem Biophys Res Commun* 320:1211-1219.
379. M. Hofmann (2009) *JBIC, J Biol Inorg Chem* 14:1023-1035.
380. C. J. Doonan, H. L. Wilson, B. Bennett, R. C. Prince, K. V. Rajagopalan and G. N. George (2008) *Inorg Chem* 47:2033-2038.
381. E. Karakas, H. L. Wilson, T. N. Graf, S. Xiang, S. Jaramillo-Busquets, K. V. Rajagopalan and C. Kisker (2005) *J Biol Chem* 280:33506-33515.
382. E. L. Klein, A. V. Astashkin, D. Ganyushin, C. Riplinger, K. Johnson-Winters, F. Neese and J. H. Enemark (2009) *Inorg Chem* 48:4743-4752.
383. M. J. Pushie, C. J. Doonan, H. L. Wilson, K. V. Rajagopalan and G. N. George (2011) *Inorg Chem* 50:9406-9413.
384. P. Kaufmann, B. R. Duffus, B. Mitrova, C. Iobbi-Nivol, C. Teutloff, M. Nimtz, L. Jansch, U. Wollenberger and S. Leimkuhler (2018) *Biochemistry* 57:1130-1143.
385. C. G. Young, L. J. Laughlin, S. Colmanet and S. D. B. Scrofani (1996) *Inorg Chem* 35:5368-5377.
386. C. J. Doonan, N. D. Rubie, K. Peariso, H. H. Harris, S. Z. Knottenbelt, G. N. George, C. G. Young and M. L. Kirk (2008) *J Am Chem Soc* 130:55-65.
387. H. Tano, R. Tajima, H. Miyake, S. Itoh and H. Sugimoto (2008) *Inorg Chem* 47:7465-7467.
388. C. J. Doonan, C. Gourlay, D. J. Nielsen, V. W. L. Ng, P. D. Smith, D. J. Evans, G. N. George, J. M. White and C. G. Young (2015) *Inorg Chem* 54:6386-6396.
389. S. Sproules, A. A. Eagle, G. N. George, J. M. White and C. G. Young (2017) *Inorg Chem* 56:5189-5202.

390. D. Nicks and R. Hille (2019) *Protein Sci* 28:111-122.
391. D. Nicks, J. Duvvuru, M. Escalona and R. Hille (2016) *J Biol Chem* 291:1162-1174.
392. G. N. George, C. A. Kipke, R. C. Prince, R. A. Sunde, J. H. Enemark and S. P. Cramer (1989) *Biochemistry* 28:5075-5080.
393. K. Pal and S. Sarkar (2008) *European Journal of Inorganic Chemistry* 2008:5338-5349.
394. R. C. Bray, B. Adams, A. T. Smith, B. Bennett and S. Bailey (2000) *Biochemistry* 39:11258-11269.
395. F. Schneider, J. Loewe, R. Huber, H. Schindelin, C. Kisker and J. Knaeblein (1996) *J Mol Biol* 263:53-69.
396. H. Schindelin, C. Kisker, J. Hilton, K. V. Rajagopalan and D. C. Rees (1996) *Science (Washington, D C)* 272:1615-1621.
397. M. C. Weiss, F. L. Sousa, N. Mrnjavac, S. Neukirchen, M. Roettger, S. Nelson-Sathi and W. F. Martin (2016) *Nature microbiology* 1:16116.
398. J. C. Boyington, V. N. Gladyshev, S. V. Khangulov, T. C. Stadtman and P. D. Sun (1997) *Science* 275:1305-1308.
399. J. Garde, J. R. Kinghorn and A. B. Tomsett (1995) *J Biol Chem* 270:6644-6650.
400. M. J. Axley, A. Boeck and T. C. Stadtman (1991) *Proc Natl Acad Sci U S A* 88:8450-8454.
401. C. A. Trieber, R. A. Rothery and J. H. Weiner (1996) *J Biol Chem* 271:27339-27345.
402. J. A. Qiu, H. L. Wilson, M. J. Pushie, C. Kisker, G. N. George and K. V. Rajagopalan (2010) *Biochemistry* 49:3989-4000.
403. S. Reschke, D. Nicks, H. Wilson, K. G. V. Sigfridsson, M. Haumann, K. V. Rajagopalan, R. Hille and S. Leimkuhler (2013) *Biochemistry* 52:8295-8303.
404. F. F. Morpeth and D. H. Boxer (1985) *Biochemistry* 24:40-46.
405. P. J. Ellis, T. Conrads, R. Hille and P. Kuhn (2001) *Structure* 9:125-132.
406. T. P. Warelow, M. Oke, B. Schoepp-Cothenet, J. U. Dahl, N. Bruselat, G. N. Sivalingam, S. Leimkuhler, K. Thalassinou, U. Kappler, J. H. Naismith and J. M. Santini (2013) *PLoS One* 8:e72535.
407. M. D. Youngblut, C.-L. Tsai, I. C. Clark, H. K. Carlson, A. P. Maglaqui, P. S. Gau-Pan, S. A. Redford, A. Wong, J. A. Tainer and J. D. Coates (2016) *J Biol Chem* 291:9190-9202.
408. P. Basu, V. N. Nemykin and R. S. Sengar (2009) *Inorg Chem* 48:6303-6313.

409. B. E. Schultz, R. Hille and R. H. Holm (1995) *J Am Chem Soc* 117:827-828.
410. C. E. Webster and M. B. Hall (2001) *J Am Chem Soc* 123:5820-5821.
411. J. Li and U. Ryde (2014) *Inorganic Chemistry* 53:11913-11924.
412. H. Xie and Z. Cao (2010) *Organometallics* 29:436-441.
413. P. Basu, B. W. Kail, A. K. Adams and V. N. Nemykin (2013) *Dalton Trans* 42:3071-3081.
414. P. Basu, B. W. Kail and C. G. Young (2010) *Inorg Chem* 49:4895-4900.
415. V. N. Nemykin and P. Basu (2005) *Inorg Chem* 44:7494-7502.
416. V. N. Nemykin, J. Laskin and P. Basu (2004) *J Am Chem Soc* 126:8604-8605.
417. V. N. Nemykin, S. R. Davie, S. Mondal, N. Rubie, M. L. Kirk, A. Somogyi and P. Basu (2002) *J Am Chem Soc* 124:756-757.
418. B. S. Lim and R. H. Holm (2001) *J Am Chem Soc* 123:1920-1930.
419. M. Ahmadi, C. Fischer, A. C. Ghosh and C. Schulzke (2019) *Front Chem* 7:486.
420. T. Schindler, A. Sauer, T. P. Spaniol and J. Okuda (2018) *Organometallics* 37:4336-4340.
421. F. Li, M. R. Talipov, C. Dong, S. Bali and K. Ding (2018) *J Biol Inorg Chem* 23:193-207.
422. A. C. Ghosh, P. P. Samuel and C. Schulzke (2017) *Dalton Trans* 46:7523-7533.
423. H. Sugimoto and H. Tsukube (2008) *Chem Soc Rev* 37:2609-2619.
424. R. S. Sengar, V. N. Nemykin and P. Basu (2008) *J Inorg Biochem* 102:748-756.
425. B. W. Kail, L. M. Perez, S. D. Zaric, A. J. Millar, C. G. Young, M. B. Hall and P. Basu (2006) *Chem - Eur J* 12:7501-7509.
426. J. Jiang and R. H. Holm (2005) *Inorg Chem* 44:1068-1072.
427. J.-J. Wang, O. P. Kryatova, E. V. Rybak-Akimova and R. H. Holm (2004) *Inorg Chem* 43:8092-8101.
428. J. T. Hoffman, S. Einwaechter, B. S. Chohan, P. Basu and C. J. Carrano (2004) *Inorg Chem* 43:7573-7575.
429. P. D. Smith, A. J. Millar, C. G. Young, A. Ghosh and P. Basu (2000) *J Am Chem Soc* 122:9298-9299.
430. C. Lorber, M. R. Plutino, L. I. Elding and E. Nordlander (1997) *J Chem Soc, Dalton Trans*:3997-4004.

431. L. T. Elrod and E. Kim (2018) *Inorg Chem* 57:2594-2602.
432. A. Dupe, M. E. Judmaier, F. Belaj, K. Zangger and N. C. Moesch-Zanetti (2015) *Dalton Trans* 44:20514-20522.
433. J. Leppin, C. Foerster and K. Heinze (2014) *Inorg Chem* 53:12416-12427.
434. M. Volpe and N. C. Moesch-Zanetti (2012) *Inorg Chem* 51:1440-1449.
435. D. Wallace, L. T. Gibson, J. Reglinski and M. D. Spicer (2007) *Inorg Chem* 46:3804-3806.
436. R. S. Sengar and P. Basu (2007) *Inorg Chim Acta* 360:2092-2099.
437. A. J. Millar, C. J. Doonan, P. D. Smith, V. N. Nemykin, P. Basu and C. G. Young (2005) *Chem - Eur J* 11:3255-3267.
438. V. N. Nemykin and P. Basu (2004) *Dalton Trans*, doi 10.1039/b403964e:1928-1933.
439. G. C. Tucci, J. P. Donahue and R. H. Holm (1998) *Inorg Chem* 37:1602-1608.
440. L. J. Laughlin and C. G. Young (1996) *Inorg Chem* 35:1050-1058.
441. R. H. Holm (1990) *Coord Chem Rev* 100:183-221.
442. V. W. T. Cheng and J. H. Weiner (2014) *EcoSal Plus*, doi 10.1128/ecosalplus.3.2.8:1-32.
443. N. Cobb, C. Hemann, G. A. Polsinelli, J. P. Ridge, A. G. McEwan and R. Hille (2007) *J Biol Chem* 282:35519-35529.
444. E. Krissinel and K. Henrick (2004) *Acta Crystallogr, Sect D: Biol Crystallogr* D60:2256-2268.
445. S. T. Smith, K. V. Rajagopalan and P. Handler (1967) *J Biol Chem* 242:4108-4117.
446. N. Cobb, T. Conrads and R. Hille (2005) *J Biol Chem* 280:11007-11017.
447. V. Fourmond, B. Burlat, S. Dementin, M. Sabaty, P. Arnoux, E. Etienne, B. Guigliarelli, P. Bertrand, D. Pignol and C. Leger (2010) *Biochemistry* 49:2424-2432.
448. A. Fersht, U. A. Fersht, W. H. Freeman and Company (1999). W. H. Freeman, New York, pp. 324-400.
449. B. M. Tynan-Connolly and J. E. Nielsen (2007) *Protein Sci* 16:239-249.
450. K. Zeamari, G. Gerbaud, S. Grosse, V. Fourmond, F. Chaspoul, F. Biaso, P. Arnoux, M. Sabaty, D. Pignol, B. Guigliarelli and B. Burlat (2019) *Biochim Biophys Acta Bioenerg* 1860:402-413.
451. N. John, V. B. Vidyalakshmi and A. A. M. Hatha (2019) *J Food Sci* 84:2250-2255.

- 452. H. Do, N. Makthal, A. R. VanderWal, M. O. Saavedra, R. J. Olsen, J. M. Musser and M. Kumaraswami (2019) *Nat Commun* 10:2586.
- 453. A.-M. Israil, C. Delcaru and M.-C. Balotescu Chifiriuc (2009) *Rom Biotechnol Lett* 14:4545-4559.
- 454. B. House, J. V. Kus, N. Prayitno, R. Mair, L. Que, F. Chingcuanco, V. Gannon, D. G. Cvitkovitch and D. B. Foster (2009) *Microbiology* 155:2907-2918.
- 455. F. De Bernardis, F. A. Mühlischlegel, A. Cassone and W. A. Fonzi (1998) *Infect Immun* 66:3317-3325.
- 456. M. Dixon (1953) *Biochem J* 55:161-170.
- 457. K. F. Tipton and H. B. F. Dixon (1979) *Methods Enzymol* 63:183-234.
- 458. C. O'Fagain, B. M. Butler and T. J. Mantle (1983) *Biochem J* 213:603-607.
- 459. M. S. Brody and R. Hille (1999) *Biochemistry* 38:6668-6677.
- 460. R. A. Rothery, B. Stein, M. Solomonson, M. L. Kirk and J. H. Weiner (2012) *Proc Natl Acad Sci U S A* 109:14773-14778.
- 461. R. A. Rothery and J. H. Weiner (2015) *J Biol Inorg Chem* 20:349-372.
- 462. S. J. Nieter Burgmayer and M. L. Kirk (2019) *Struct Bonding (Berlin, Ger)* 179:101-151.
- 463. D. R. Gisewhite, J. Yang, B. R. Williams, A. Esmail, B. Stein, M. L. Kirk and S. J. N. Burgmayer (2018) *J Am Chem Soc* 140:12808-12818.
- 464. G. L. Anderson, J. Williams and R. Hille (1992) *J Biol Chem* 267:23674-23682.